



## Polymer Solar Cells – Non Toxic Processing and Stable Polymer Photovoltaic Materials

**Søndergaard, Roar R.; Krebs, Frederik C**

*Publication date:*  
2012

*Document Version*  
Publisher's PDF, also known as Version of record

[Link back to DTU Orbit](#)

*Citation (APA):*  
Søndergaard, R., & Krebs, F. C. (2012). Polymer Solar Cells – Non Toxic Processing and Stable Polymer Photovoltaic Materials. Department of Energy Conversion and Storage, Technical University of Denmark. (Risø-PhD; No. 82(EN)).

### DTU Library

Technical Information Center of Denmark

---

#### General rights

Copyright and moral rights for the publications made accessible in the public portal are retained by the authors and/or other copyright owners and it is a condition of accessing publications that users recognise and abide by the legal requirements associated with these rights.

- Users may download and print one copy of any publication from the public portal for the purpose of private study or research.
- You may not further distribute the material or use it for any profit-making activity or commercial gain
- You may freely distribute the URL identifying the publication in the public portal

If you believe that this document breaches copyright please contact us providing details, and we will remove access to the work immediately and investigate your claim.

# Polymer Solar Cells – Non Toxic Processing and Stable Polymer Photovoltaic Materials

Risø-PhD-Report

Roar Søndergaard  
Risø-PhD-82

Risø DTU  
National Laboratory for Sustainable Energy

---



**Author:** Roar Søndergaard  
**Title:** Polymer solar cells – Non Toxic Processing and Stable  
Polymer Photovoltaic Materials

**Division:** Solar Energy Programme

**Academic advisor:**

Professor Frederik C. Krebs  
Risø National Laboratory for Sustainable Energy  
Technical University of Denmark

**Report number:** Risø-PhD-82  
(EN)

**ISBN 978-87-550-3929-2**

**Sponsorship:** The project was  
financed by the Danish Strategic  
Research Council (DSF: 2104-07-  
0022)

Information Service Department  
Risø National Laboratory for  
Sustainable Energy  
Technical University of Denmark  
P.O.Box 49  
DK-4000 Roskilde  
Denmark  
Telephone +45 46774005  
[bibl@risoe.dtu.dk](mailto:bibl@risoe.dtu.dk)  
Fax +45 46774013  
[www.risoe.dtu.dk](http://www.risoe.dtu.dk)

# Preface

This PhD thesis presents the main results of my work carried out at Risø National Laboratory for Sustainable Energy, Technical University of Denmark, representing three years of work with final submission of the thesis in September 2011, as part of the Danish research program to obtain the degree as PhD. The work has been financed by the Danish Strategic Research Council (DSF: 2104-07-0022) with supervision by Professor Frederik C. Krebs. The thesis is based on a number of papers which I have authored/co-authored during the project. Most of these are published while others have been submitted for publication. These can be found in Appendix 2 along with further published papers which are not described in the thesis.

Although my background is within organic synthesis I have had the opportunity to work with numerous tasks and challenges that are generally not included in the work day of an organic chemist (among many can be mentioned device building, device characterization, testing of alternative electrodes and fabrication of solar panels). Such diversity is for me an ideal way of working, and for that I am very thankful.

There is no doubt that the main reason that the above has been possible is my supervisor Frederik C. Krebs. Your energy, passion and enthusiasm are highly contagious and you have an amazing ability to be present for questions and discussion without interfering in the actual work process. Such trust gives an incredible freedom. Thank you.

I would also like to thank Mikkel Jørgensen for always taking the time to discuss a scientific question or problem. For comments on my thesis I would like to thank Frederik, Mikkel and Søren.

Special thanks to all on the 'Synthesis team': Eva, Martin, Jon and Ole. You are extremely good colleagues and a pleasure to work with. More generally I would like to thank the Solar Cell Group for the last three years. It has been a pleasure to be here, and I have enjoyed your company both in the scientific discussions but just as important on a more social basis when drinking afternoon coffee or enjoying a glass of champagne.

Finally I would like to thank my wife Karin and my two children Sigrun and Aksel for the support and understanding I have received during this thesis. You mean everything to me and I could never have done this without you.



## Abstract

The field of polymer solar cell has experienced enormous progress in the previous years, with efficiencies of small scale devices ( $\sim 1 \text{ mm}^2$ ) now exceeding 8%. However, if the polymer solar cell is to achieve success as a renewable energy resource, mass production of sufficiently stable and efficient cell must be achieved. For a continuous success it is therefore essential to transfer the accomplishments from the laboratory to large scale facilities for actual production. In order to do so, several issues have to be approached. Among these are more environmentally friendly processing and development of more stable materials.

The field of polymer solar cells has evolved around the use of toxic and carcinogenic solvents like chloroform, benzene, toluene, chlorobenzene, dichlorobenzene and xylene. As large scale production of organic solar cells is envisaged to production volumes corresponding to several  $\text{GW}_{\text{peak}}$ , this is not a suitable approach from neither a production nor environmental point of view. As a consequence new materials, which can be processed from more environmentally friendly solvents (preferably water), need to be developed.

In this thesis, the issue has been approached through synthesis of polymers carrying water coordinating side chains which allow for processing from semi-aqueous solution. A series of different side chains were synthesized and incorporated into the final polymers as thermocleavable tertiary esters. Using a cleavable side chain induces stability to solar cells as it slows down diffusion through the active layer, but just as important it renders the layer insoluble. This allows for further processing, using the same solvent, without dissolving already processed layers, and resulted in the first ever reported solar cells where all layers are processed from aqueous or semi-aqueous solution.

As previously mentioned many advantages can be achieved by use of thermocleavable materials.

Unfortunately the cleavage temperatures are too high to allow processing on flexible substrates like PET. As a final result, the reduction in cleavage temperature of thermocleavable thiophene polymers with ester side chains, through acid catalysis have been examined. The study shows that substantial lowering of the temperatures can be obtained for tertiary, secondary and primary esters, but further research needs to be performed in order to transfer the reaction to solar cells.

From a stability point of view, the current state of the art polymers are not stable enough to be processed by large area processing methods like roll-to-roll (R2R) coating techniques, as this has to be performed in air. This calls for the development of new materials, which can endure such processing conditions, and in this context it would be preferable to have a guideline towards which properties of a polymer that either induces stability or causes it to degrade. As part of a larger study, aiming at mapping the relative stability influence of different donors and acceptors in low-band-gap polymers, four polymers were synthesized for examination of their photochemical stabilities. Two of these were furthermore optimized for R2R processing and were tested together with other cells, in an outdoor study involving 8 countries. Panels containing the cells encapsulated in polyurethane were manufactured, measured and installed by travelling between the different locations. Following 4½ months outdoor exposure the trip was done again in order to dismount the panels for shipment back to Denmark, where final characterization was made. The use of polyurethane for encapsulation showed improved conservations of the cells compared to previous studies.

## Resumé

Plast-solcelle forskningen har i de senere år set en enorm udvikling, og effektiviteter på mere end 8 % er opnået for små celler (~1 mm<sup>2</sup>). Det sagt, står forskningsområdet over for en enorm udfordring, hvis den ønskede realisering af plast-solceller som alternativ energikilde skal opnås. Det overordnede succes-kriterium står og falder med hvorvidt det er muligt at fremstille stabile, effektive plast-solceller ved massefremstilling. Mange problemer skal i den forbindelse løses. Blandt disse er mere miljørigtig fremstilling af plast-solceller samt udvikling af mere stabile materialer.

Udviklingen af plast-solceller er i høj grad sket omkring brugen af toksiske og kræftfremkaldende solventer som kloroform, benzen, klorbenzen, diklorbenzen og xylene. Disse solventer er ikke kompatible med masseproduktion hverken fra et miljø- eller arbejdsmiljø-mæssigt synspunkt. Som konsekvens heraf er det nødvendigt at udvikle nye materialer som kan processeres fra mere miljøvenlige solventer, som bio-nedbrydelige alkoholer eller i bedste fald vand.

Dette er i denne afhandling gjort ved fremstilling af polymerer med polære sidekæder der kan koordinere til polære solventer, hvilket gør det muligt at processere fra semi-vandig opløsning. En serie sidekæder blev fremstillet og inkorporeret i de endelige polymerer som thermokløvbare tertiære estere. Brugen af sidekæder som efterfølgende kan fjernes giver flere fordele. For det første øger det stabiliteten af det aktive lag, men ligeså vigtigt gør det det aktive lag uopløseligt, hvilket gør det muligt at processere ovenpå laget med samme solvent uden at det genopløses. Dette er vigtigt da plast-solceller har en multi-lagsstruktur. Som overordnet resultat er det lykkedes at fremstille den første plast-solcelle nogensinde, hvor alle lag, inklusiv den bagerste elektrode, var processeret fra vand eller semi-vandige opløsninger.

Som nævnt ovenfor er der flere fordele ved brugen af thermokløvbare materialer. Desværre er kløvningstemperaturerne for høje til at kunne anvendes på fleksible substrater som PET, og et studie blev derfor udført med henblik på at reducere kløvningstemperaturen ved syre katalyse af thermokløvbare thiophen-polymerer med ester sidekæder. Studiet viste at kløvningstemperaturen kan reduceres kraftigt ved brug af katalytiske mængder syre for både tertiære, sekundære og primære estere. Yderligere forskning er dog nødvendig før reaktionen kan overføres til plast solceller.

Set ud fra et stabilitet synspunkt er de nuværende 'top-materialer' inden for plast-solceller ikke egnede til fremstilling af større solceller i en industrisammenhæng (ved for eksempel rulle-til-rulle coating). Dette

skyldes at de anvendte polymerer er følsomme over for ilt og vand, hvilket ikke passer med storskala processering, da det rent praktisk er nødvendigt at udføre sådanne processer i luft. Det er derfor nødvendigt med fremstilling af nye materialer, som er mindre følsomme over for luft, og i den forbindelse vil det være praktisk med en guideline, til hvilke egenskaber i en polymer som gør den enten mere eller mindre stabil. Som del af et større studie, hvor det er forsøgt at kortlægge den relative indflydelse, af forskellige donor og acceptor enheder, på stabiliteten af low-band-gap polymerer, blev fire polymer fremstillet og undersøgt. To af disse blev optimeret ved rulle-til-rulle processering og indgik sammen med andre typer celler ydermere i et udendørs stabilitets studie i 8 lande hvor polyuretans egenskab som indkapsling blev undersøgt. Paneler indeholdende cellerne i polyuretan blev fremstillet, karakteriseret og til sidst installeret ved at rejse mellem de forskellige test lokaliteter. Efter ca. 4½ måned udendørs eksponering gennemførtes rejsen igen for at nedtage panelerne og sende dem tilbage til Danmark for endelig karakterisering af nedbrydningen. Indkapsling i polyuretan viste sig som en forbedret metode til indkapsling af solceller sammenlignet med tidligere studier.

<b>CHAPTER 1</b>	<b>2</b>
<b>Introduction</b>	<b>2</b>
1.1 Background	2
1.2 Polymer Solar cells	4
1.3 Device characteristics and general definitions	9
1.4 State of the art materials	12
1.5 Key issues for future OPV success which has been approached in this thesis	17
1.5.1 Introduction – Roll-to-roll processing of organic solar cells	17
1.5.2 Substitution of toxic solvents for more environmentally friendly processing	20
1.6 Aim and scope of this thesis	23
1.7 References	25
<b>CHAPTER 2</b>	<b>34</b>
<b>Synthesis of side chains for water processable polymers and fullerene for all water processed solar cells</b>	<b>34</b>
2.1 Introduction	34
2.2 Synthesis of polymer side chains with potential for good coordination with polar solvents	37
2.2.1 Synthesis of 1-(2,3-bis(( <i>tert</i> -butyldimethylsilyl)oxy)propoxy)-2-methylpropan-2-ol	38
2.2.2 Synthesis of 4-(2,3-bis(( <i>tert</i> -butyldimethylsilyl)oxy)propoxy)-2-methylbutan-2-ol	40
2.2.3 Synthesis of 3,4-bis(( <i>tert</i> -butyldimethylsilyl)oxy)-2-methylbutan-2-ol	41
2.2.4 Synthesis of 4-(2-(( <i>tert</i> -butyldimethylsilyl)oxy)ethoxy)-2-methylbutan-2-ol	42
2.2.5 Synthesis of 4-(2-methoxyethoxy)-2-methylbutan-2-ol	43
2.3 Synthesis of monomers and polymers	44
2.3.1 Synthesis of monomers	44
2.3.2 Synthesis of polymers and solubility tests	45
2.3.3 Synthesis of fullerenes for processing of solar cells	47
2.3.4 General discussion of the observed solubilities	49
2.4 Device fabrication of all water processed solar cells	51
2.5 Conclusion	53
2.6 Experimental	53
2.6.1 Synthesis	53
2.6.2 Device preparation	69
2.7 References	70
<b>CHAPTER 3</b>	<b>72</b>
<b>Synthesis of new LBG polymers for analysis of photochemical stability and R2R processed solar cells</b>	<b>72</b>
3.1 Introduction	72
3.2 Synthesis of polymers	74
3.2.1 Synthesis of cBDT-BTBT	75
3.2.2 Synthesis of tBDT-BTBT	76
3.2.3 Synthesis of DTTI-BT	77
3.2.4 Synthesis of Cbz-DTDP	78
3.2.4 Optical properties of the polymers	80
3.3 Photochemical stability analysis	81
3.4 Optimization of R2R processing of polymer cBDT-BTBT and cBDT-BTBT	83
3.5 Conclusion	87
3.6 Experimental section	88

3.6.1 Synthesis	88
2.6.2 Device preparation and testing	100
2.7 Reference list	101
<b>CHAPTER 4</b>	<b>103</b>
<b>The use of polyurethane as encapsulation method for organic solar cells – an outdoor field study on the influence of local climate on device stability.</b>	<b>103</b>
4.1 Introduction	104
4.2 Preparation of the solar panels	106
4.2.1 Type of cells used	106
4.2.2 Assembly of the solar panels	108
4.3 Measuring and installing the panels	111
4.4 Results and discussion	112
4.4.1 Outdoor $V_{oc}$ and $I_{sc}$ measurements	113
4.4.2 Overall performance after outdoor exposure	117
4.4.3 Evaluation of the panel design	120
4.5 Conclusion	121
4.6 References	122
<b>CHAPTER 5</b>	<b>124</b>
<b>Acid catalyzed thermocleavage of thiophene polymers with ester side chains</b>	<b>124</b>
5.1 Introduction	124
5.2 Thermocleavage of P3MHOCT in the presence of strong acid	125
5.2.1 Examination of the cleavage temperatures of the tertiary ester moiety in the polymer P3MHOCT in the presence of catalytic amounts of different strong acids	127
5.3 Examination of the influence of catalytic amounts of strong acid on the thermocleavage of polymers carrying secondary and primary ester side groups.	131
5.3.1 Synthesis of secondary and primary ester analogues to P3MHOCT	131
5.3.2 Examination of the cleavage temperatures for thiophene polymers with secondary and primary side chains	132
5.5 Experimental section	134
5.6 References	137
<b>APPENDIX 1</b>	<b>138</b>
<b>Non successful synthesis</b>	<b>138</b>
<b>APPENDIX 2</b>	<b>143</b>
<b>Publication list:</b>	<b>143</b>



# Chapter 1

## Introduction

### 1.1 Background

Looking at the energy supplies available for man in the modern world they almost all originate from the sun. Fossil fuels are the remains of biomaterials that have slowly been transformed with time into the forms (oil, coal and gas) that we can exploit. Wind energy, one of the most exploited renewable energies, is the result of the rotation of earth in combination with heating from the sun which creates air currents, and biofuels are produced as a result of photosynthesis. None of these however can provide a direct transformation of sunlight into the form of energies that we use every day. Only two such direct conversions exist today: solar heating systems, which are mainly used for heating houses and for hot water, and photovoltaic devices (solar cells) which are capable of the direct transformation of sunlight into electricity.

When looking at the emerging photo-catalysis for direct transformation of sunlight into electricity, the prospects are immense as the world total energy consumption only corresponds to a very small fraction of the energy of the light hitting the earth's surface (0.02%). This stands in contrast to the amount of energy actually being produced by photovoltaics (PV) which according to 'Renewable Energy Policy Network for the 21st Century' (REN21) corresponded to 0.5% of the worlds energy consumption (when including 'off-grid PVs').<sup>[1]</sup> While our environment is surrounded with abundant solar power, the PV technology is still too expensive to become a primary energy source. Therefore, the main task of the solar cell field is to develop a technology, which can provide cheap PV products and make the photo-conversion of sunlight into electrical power cost efficient.

The conversion of absorbed photons directly into electrical energy, also called the photovoltaic effect, was first discovered in 1839 by the French physicist Alexandre-Edmond Becquerel. Studying platinum electrodes, covered with silver bromide or silver chloride, he found that a photocurrent emerged when these were illuminated in aqueous solution.<sup>[2,3]</sup> It took more than a century though before the first commercialisation of the PV technology was attempted, when the first crystalline silicon p-n junction solar cell was developed at Bell Laboratories in 1954.<sup>[4]</sup> The reported device could convert solar radiation into electrical power with an efficiency of 6%. The field of photovoltaics have gone through several stages



since then. These are generally categorized as ‘generations’ according to the time sequence where they started to play a serious role within the solar cell field.<sup>[5]</sup> The *first generation* (1G) solar cells are large scale, single junction devices. Most of the production is based on silicon wafers including single crystal and multi-crystalline silicon, and accounts for nearly 90 % of the current photovoltaic production. The efficiency of the single junction cells has a theoretical limit of about 30% (the Shockley – Queisser limit)<sup>[6,7]</sup> and currently the common silicon wafer based devices show nearly 20% efficiency in general and has reached efficiencies of up to 25%.<sup>[8]</sup> Yet, the cost per produced 1 Watt of power is nearly 3-4 times higher than the cost of electricity produced by conventional means due to the high cost of the material (half of the cost of first generation devices is the silicon wafer) and production technology. Even though the price continuously decreases along with the progress of the technology, the 1G technology will possibly reach their price limit before achieving the competitive level in the market. The *second generation* (2G) solar cells have been under intense development through the 1990’s and 2000’s. These cells address the cost issue and the primary task is to decrease the amount of expensive material used in the production process while keeping the efficiency of the device high. The foremost approach is producing thin film solar cells on low cost substrates (such as glass or copper foil). Different techniques are used in the production processes (solution deposition, vapor deposition, electroplating etc.) and the most successful materials for 2G are amorphous silicon, CuIn(Ga)Se<sub>2</sub> (CIGS), CdTe/CdS, which are being deposited on thin substrates. Single cell devices based on these materials can deliver laboratory power conversion efficiencies up to 20% while module efficiencies are a little more moderate at 16% due to the large difficulties that lies in producing large scale uniform films.<sup>[8]</sup> Although thin film technology can significantly decrease the cost of PV compared to those of 1G, 2G solar cells will probably approach a cost minimum per Watt that is still relatively high compared with ‘conventional energy’ due to efficiency limits combined with material and processing costs. The *third generation* (3G) is the alternative approach to cost reduction through usage of unconventional low cost materials and by increasing the efficiency by multiple stacking of solar cells. 3G solar cells introduce the idea of multi junction solar cells, which can drastically increase the efficiency by improving the harvesting of photons and even overcome the theoretical limit of 30 %. Currently the highest efficiencies reported for multijunction solar cells are at 32 % and up to 42 % when using high concentration.<sup>[8]</sup> 3G utilizes new concepts in terms of device architectures and materials. Among the more atypical approaches are the organic photovoltaics where organic material is used in the light absorption process. Although still in the developing stage organic PVs seems a promising low cost alternative to the more expensive inorganic counterpart. Organic PVs are particularly interesting because these offer the potential of very low cost and fast processing in large area production.

The field of organic PVs can generally be divided into three classes; Small molecule,<sup>[9,10]</sup> dye-sensitized,<sup>[11-13]</sup> and Polymer Solar Cells. Especially the use of conjugated polymers in PVs is an attractive alternative to the traditional silicon based solar cells. The mechanical flexibility of these materials allows for deposition on flexible substrates, they are strong absorbers of visible light thus reducing the amount of material necessary (down to 100 nm layers) keeping the cost of the final device down and finally polymers can be made soluble in various solvents allowing the usage of high throughput production methods using wet-processing, which literally means printing or coating of solar cells using roll-to-roll (R2R) machinery similar to the way in which news papers are made.<sup>[14-26]</sup> This thesis will focus exclusively on the fabrication of polymer based solar cells, and the use of the term 'organic solar cell' will refer only to polymer solar cell unless stated otherwise.

### 1.2 Polymer Solar cells

Since the discovery of organic materials with conductive properties in 1906<sup>[27]</sup> they have been the subject of studies for their potential use in various electronic applications. Especially during the last 10-20 years the development of organic semiconducting materials have advanced very rapidly. This has led to the demonstration and optimization of a range of organic based solid state devices, including organic light-emitting diodes (OLEDs),<sup>[28]</sup> field-effect transistors (FETs),<sup>[29]</sup> photodiodes,<sup>[9]</sup> and photovoltaic cells. Within the field of organic solar cells enormous progress has been achieved over the last 4-5 years. Numerous reviews and special issues have been published on the subject during the same period, including types of solar cells that span a variety of active layer compositions such as all-polymer, polymer-fullerene, small molecules and hybrid solar cells.<sup>[21,30-56]</sup> The polymer-fullerene solar cells, which are based on an electron donating polymer and an electron accepting fullerene, have so far proven to be the most successful and the first steps towards commercialization have been initiated.

The general organic solar cell architecture is comprised of a multilayer stack, with the active layer sandwiched between the two electrodes (Figure 1.1). One of the electrodes needs to be transparent in order to allow illumination of the photoactive layer, and often buffer layers are applied between the active material and the electrodes in order to ensure a selective charge transport. A typical laboratory buildup of

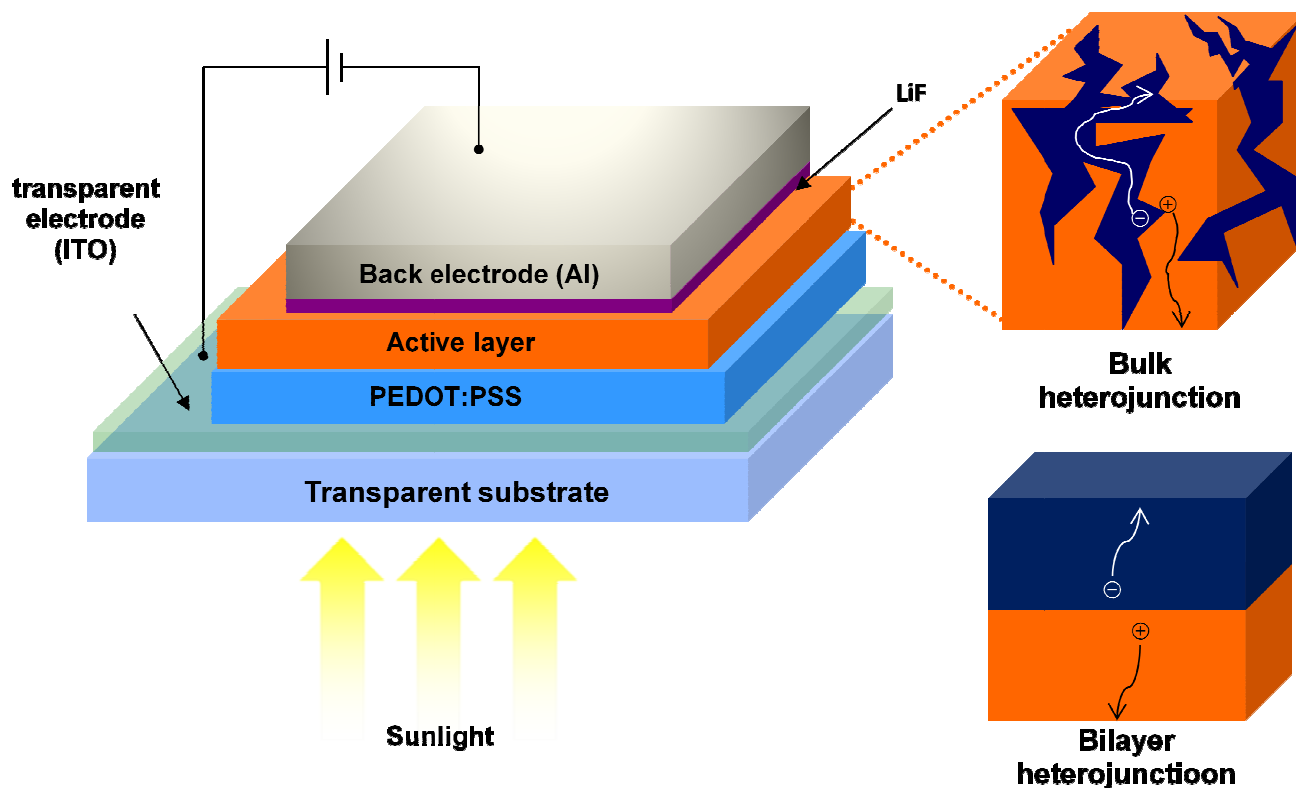


**Figure 1.1** Schematic illustration of the layered architecture in a typical OPV device. This is accompanied with a close-up of the photoactive layer of a bulk heterojunction, showing the interpenetrating network of donor and acceptor material, and a bilayer heterojunction where donor and acceptor are placed on top of each other. In both cases the pathway of the free charge carriers are shown.

an organic solar cell would be to start with a pre-prepared substrate coated with the transparent electrode indium tin oxide (ITO). On top of this is spin coated a very thin layer of poly(3,4-ethylenedioxythiophene)-poly-(styrenesulfonate)(PEDOT:PSS), which smoothes out the surface roughness and acts a buffer layer which facilitates hole transfer and blocks electrons transport between the active layer and the ITO. Subsequently a mixture of the donor and acceptor material is spin coated from an appropriate organic solvent. As the solvent evaporates the donor and acceptor material will phase separate creating an interpenetrating network inside the photoactive layer. Finally, by evaporative vacuum deposition first a thin hole blocking layer of lithium fluoride (LiF) followed by a layer of aluminum (Al) as the back electrode, is evaporated on top.

There is a main difference in the working principle of the organic PVs as compared to inorganic PVs. Where absorption of a photon by an inorganic material creates free charge carriers upon excitation of electrons from the valence band to the conduction band (the two electronic bands are so close in energy

that they practically form a continuum), free carriers are not created so easily in organic PV. Because of the relative low dielectric constants of organic materials, excitation of organic semiconductors leads to a bound state, a so-called 'exciton', of an electron and a positive charge carrier called a 'hole'.<sup>[57,58]</sup> In order to be able to extract a current, this bound state needs to be dissociated into free charge carriers that can be collected at the electrodes. The problem is that polymers generally exhibit high hole mobility but a low electron mobility, and if only pure polymer is used this will generally lead to recombination of the charge carriers. This intrinsic carrier mobility imbalance in the polymer can be overcome by incorporation of an *n*-type semiconductor, like the fullerenes, to act as an electron acceptor and a pathway for electron transport as shown in Figure 1.1. By use of materials with an energy offset in the molecular orbitals of the polymer (donor) and the *n*-type semiconductor (acceptor) it is possible to separate the charge carriers. In other words a material that willingly gives up electrons is brought into contact with a material with strong electron accepting properties, which forces the exciton to split into free charge carriers. This is commonly known as the donor-acceptor heterojunction approach.<sup>[59-62]</sup>

The photoactive layer can in principle consist of any two components that have the right energy alignment to allow the photo-induced charge transfer between donor and acceptor to take place. In reality there are very few good acceptor materials available, and although efforts have been made in order to find suitable polymers with high electron affinity and good conductance,<sup>[59,62-66]</sup> the by far most commonly used acceptor materials in OPVs are fullerenes. Soluble Buckminster fullerene derivatives like [6,6]-phenyl C<sub>61</sub> butyric acid methyl ester (PCBM) or its 'big brother' [6,6]-phenyl C<sub>71</sub> butyric acid methyl ester (C<sub>70</sub>-PCBM) have several properties that make them very attractive for use in solar cells (Figure 1.2). From a practical point of view

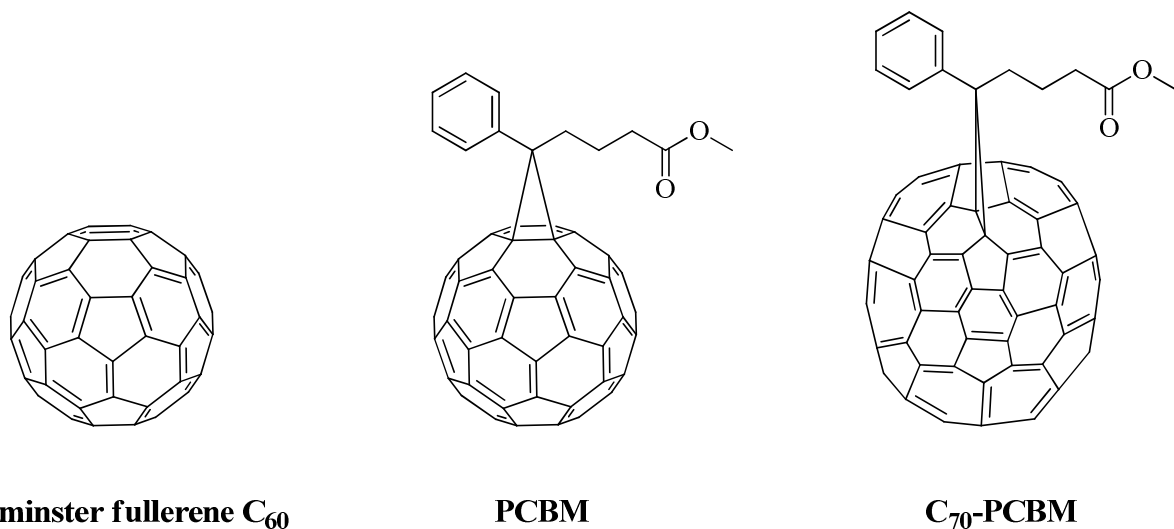


**Figure 1.2** Molecular structure of buckminsterfullerene C<sub>60</sub> and the soluble fullerene derivatives [6,6]-phenyl C<sub>61</sub>-butyric acid methyl ester (PCBM) and the larger and more oval shaped [6,6]-phenyl C<sub>71</sub> butyric acid methyl ester (C<sub>70</sub>-PCBM).

they are easily processed from almost all solvents that are used in OPV fabrications, but more importantly the molecules have a very high electron affinity relative to the various potential organic donors because of an energetically deep-lying LUMO.<sup>[67]</sup> Combined with the fact that photo induced charge transfer from the excited state of a conjugated polymer to a fullerene is known to be very fast ( $\sim 45$  fs) while the reversible transfer is orders of magnitude slower,<sup>[68]</sup> this ensures good charge separation of the exciton. The fullerenes furthermore show very high electron mobility<sup>[69]</sup> and have an ability to pack effectively in crystalline structures that favour transport of the electrons to the cathode.<sup>[70]</sup>  $C_{70}$ -PCBM have a slight advantage to  $C_{60}$ -PCBM when used in OPVs, as low energy transitions are allowed in the former which makes it possible for the  $C_{70}$ -PCBM itself to absorb visible light, thus aiding in the overall absorption of photons.<sup>[71]</sup>  $V_{oc}$  also tend to be slightly higher when using  $C_{70}$ -PCBM because of more favorable energy levels.

The mechanism by which light is converted to electric power in organic photovoltaics (OPVs) consists of four basic steps which are illustrated in Figure 1.3. 1) The photon is absorbed by the active material, which promotes the electron to the lowest unoccupied molecular orbital (LUMO), while leaving the positive charge carrier in the highest occupied molecular orbital (HOMO). The excited pair is still bound by

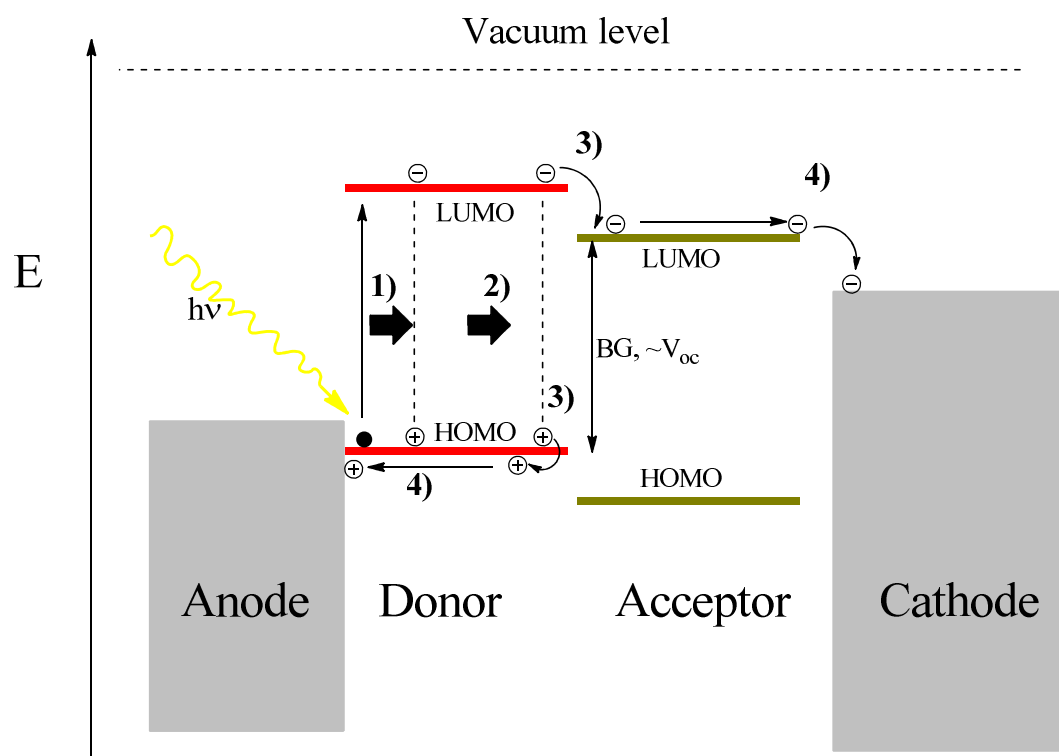


**Figure 1.3** Schematic illustration of the photoelectric conversion mechanism.

coulomb attraction forces forming an exciton; 2) The exciton diffuses to the interface of the donor and acceptor; 3) The exciton is dissociated into free carriers at the interface between donor and acceptor. One of the main reasons that the efficiency of OPVs is considerably lower compared to inorganic solar cells is because the charge carriers lose energy during separation of the excited pair; 4) Finally the free carriers are transported and collected at the opposite electrodes. The collection is assured by the asymmetric ionization energy or work function of the electrodes.

Generally it should be stated that each of the four steps is crucial for efficient power generation and there are many loss mechanisms involved in this sequence. First of all, the efficiency of the heterojunction is limited by the exciton diffusion length (typically  $\sim 3\text{-}10$  nm in most organic semiconductors).<sup>[9,72,73]</sup>

Excitons formed at positions further than this have a lower probability of efficient charge separation and harvesting. Efficient charge separation can only occur at the  $p\text{-}n$  interface and ideally the heterojunction should be constructed in manner such that the excitons are generated in the vicinity of the interface. At the same time the constructed heterojunction should insure a direct or percolating pathway of the charge carriers to the relevant electrodes in order to effectively transport and collect the charges. The initial use of heterojunctions in solar cells were prepared as bilayer junctions (see Figure 1.1).<sup>[74]</sup> This was a major improvement, compared to the very first solar cells where the active layer only consisted of pure polymer.<sup>[75-77]</sup> However, as the separation of charges is limited by the exciton diffusion length, only photons absorbed in the near vicinity of the  $p\text{-}n$  interface will contribute to the photocurrent while the rest is lost through recombination processes. The major breakthrough came with the introduction of the bulk hetero junction (BHJ),<sup>[59,62,78]</sup> in which the photoactive layer consists of a heterogenic blend of the donor and acceptor material. This led to a major increase in generated free charge carriers upon light absorption. In the ideal situation the heterojunction should consist of a nanoscale interpenetrating bicontiguous network of donor and acceptor material, which ensures that all excitons are generated in the vicinity of the  $p\text{-}n$  interface, thus leading to maximum charge separation.

Although the performance of polymer solar cells have continued to increase, with power conversion efficiencies (PCE) now reaching 8.3%,<sup>[79]</sup> they are still generally inferior to the traditional silicon solar cell with respect to PCE and more importantly with respect to stability. As illustrated in Figure 1.4 the ideal photovoltaic device is cheap to produce and will have a high efficiency and a long lifetime. Status so far is that the organic PVs can only compete with the inorganic PVs when looking at the estimated final production cost of large area solar cells, but with continuous improvements in efficiency and stability of the organic PVs, there is reason to believe that the technology will someday reach a level where it can compete with the inorganic PVs.

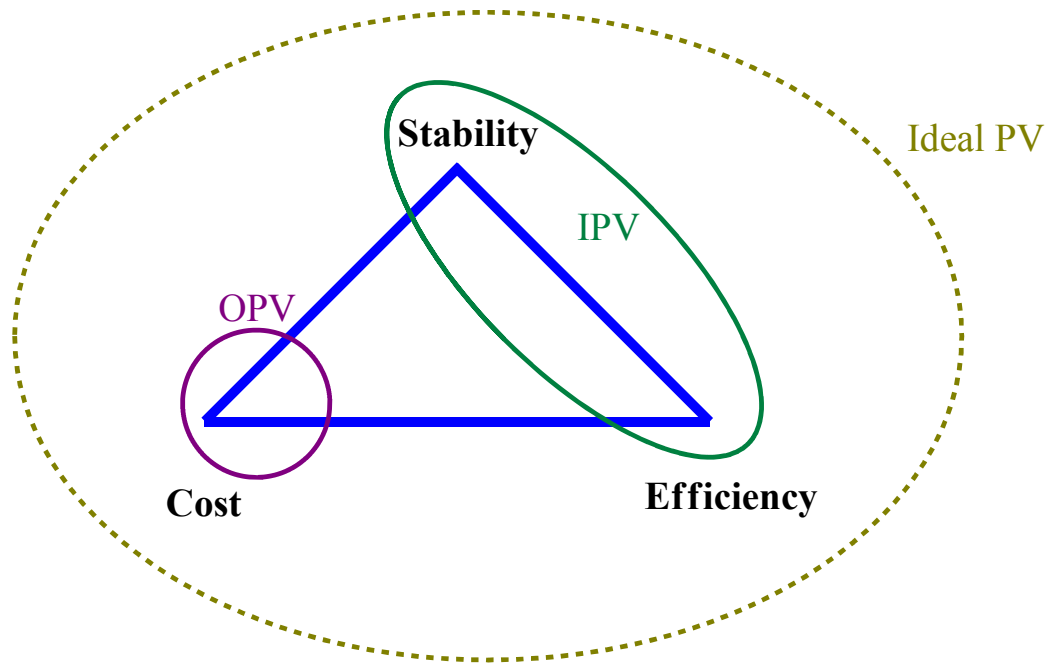


**Figure 1.4:** The critical triangle for PV devices visualizing the three key aspects for success. The ideal PV device simultaneously fulfills the demands of low cost, high efficiency and high stability. Organic PVs (OPV) have a potentially very low production cost, but still lacks improvement in both stability and efficiency. As for the inorganic PV (IPV) the situation is the opposite. Due to the expensive materials and very high thermal budget of the IPV it is very improbable that the technology will reach ‘ideal’ conditions. The cheap OPV technology on the other hand still has the potential to reach such a state.

### 1.3 Device characteristics and general definitions

The solar cell in the dark acts as a simple diode. When exposed to sunlight the electric circuit becomes more complex. The simplest model that approximates the circuitry of a performing organic solar cell is illustrated in Figure 1.5. The circuitry is constituted of 1) A diode with ideality factor  $n$  and saturation current  $I_0$  (current in the dark at reverse bias), 2) A source to provide current that corresponds to photocurrent  $I_L$  generated during illumination, 3)  $R_s$  series resistance, which takes into account all the resistances at interfaces in the layers, the conductivity of the semiconductors and the electrodes, 4) Shunt resistance  $R_{sh}$ , which takes into account the leakage of the current through shunts due to the defects in the films. For good performance of the device  $R_s$  needs to be low and  $R_{sh}$  has to have high values.

Figure 1.6 shows the current voltage characteristics (IV curves) for a typical solar cell. The figure also shows the key parameters that define the performance of the cell. These are the open circuit voltage  $V_{OC}$ , short circuit current  $I_{SC}$ , fill factor  $FF$ , the maximum power  $P_{max}$ , and the corresponding voltage and the

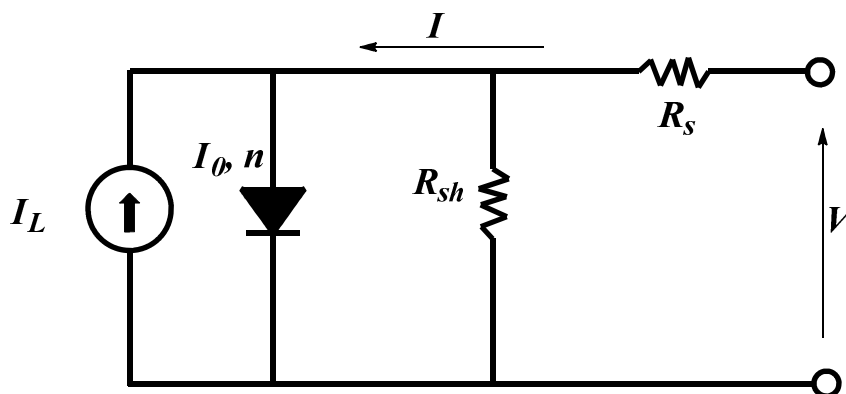


**Figure 1.5** Simplest model of the electric circuit of an organic solar cell.

current at the maximum power point  $V_{max}$  and  $I_{max}$ . As a general rule the following expression can be used to estimate the voltage of an organic heterojunction solar cell using PCBM as acceptor:

$$V_{oc} = E_{HOMO,D} - E_{LUMO,A} - 0.4 V \quad (1)$$

where  $E_{HOMO,D}$  is the oxidation potential of the polymer (donor),  $E_{LUMO,A}$  is the reduction potential of PCBM and the value 0.4 V is the approximate voltage loss at the electrodes.<sup>[80,81]</sup>

Equation (2) show the definition of the power conversion efficiency (PCE) of the solar cell, which is a measure of the ratio between maximum electric power produced ( $P_{out}$ ) by the cell and the power of the incident light on the cell ( $P_{in}$ ):

$$\eta = \frac{P_{out}}{P_{in}} = \frac{I_{max}V_{max}}{P_{in}} = FF \frac{I_{sc}V_{oc}}{P_{in}} \quad (2)$$

where the  $FF$  is defined as:

$$FF = \frac{I_{max}V_{max}}{I_{sc}V_{oc}} \quad (3)$$

The  $FF$  shows how much power is produced in practice by the cell with given  $I_{sc}$  and  $V_{oc}$  compared to the theoretically possible value. The  $FF$  is significantly affected by the parasitic resistances  $R_s$  and  $R_{sh}$ .

Typically, good operating organic solar cell delivers  $FF$  values in the range of 60 – 65 %.

Another important quantity that defines the quality of energy conversion is the quantum efficiency (QE) of a solar cell. The QE defines the number of charge carriers collected at the electrodes per number of incident photons on the solar cell area at a given wavelength. If every incident photon results in one collected charge carrier then the QE is equal to unity (no recombination losses). There are two ways of



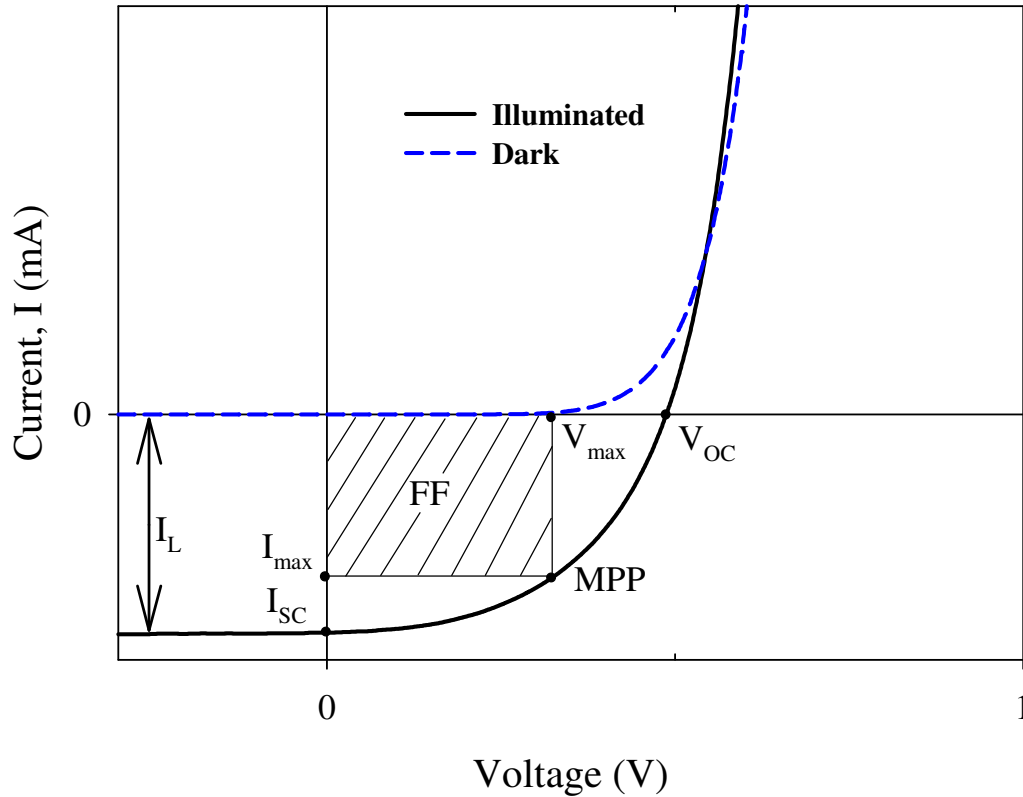


**Figure 1.6:** Dark and light IV characteristics of an OPV. The short circuit current ( $I_{sc}$ ) and the open circuit voltage ( $V_{oc}$ ), can be read directly as the intersections with the ordinate and the abscissa respectively. The maximum power point (MPP,  $P_{max} = I_{max} \times V_{max}$ ) is the point on the curve where the product of  $I$  and  $V$  reaches maximum. The relative ratio between the maximum power and the product of  $I_{sc}$  and  $V_{oc}$  then defines what is called the fill factor (FF).  $FF = (I_{max} \times V_{max}) / (I_{sc} \times V_{oc})$ .  $I_L$  is the photocurrent generated under illumination.

defining the QE: The 'External Quantum Efficiency' (EQE) is the ratio between number of collected carriers and number of all **incident** photons on the cell at a given wavelength (EQE is also sometimes called **IPCE**, which stands for **I**ncident-**P**hoton-to-**e**lectron **C**onversion **E**fficiency). The 'Internal Quantum Efficiency' (IQE) is the ratio between the number of collected carriers and number of all **absorbed** photons by the cell at a given wavelength (in the IQE the light transmitted through and reflected from the cell is excluded).

## 1.4 State of the art materials

The ‘kick-off’ for polymer based solar cells happened in 1992 with the first results of photo induced charge transfer from a conjugated polymer to a buckminster fullerene ( $C_{60}$ ) reported by Sariciftci *et al.*<sup>[60]</sup> Since then the field of polymer/fullerene solar cells has been through a continuous evolution. From an active layer materials point of view, the state of the art was until recently dominated by the bulk heterojunctions prepared from poly(3-hexylthiophene) (P3HT) and the fullerenes PCBM and  $C_{70}$ -PCBM. An enormous amount of research has been dedicated to this system and efficiencies in the range of 4-5 % have been achieved.<sup>[82-86]</sup> In many ways the P3HT polymer is very advantageous for use in solar cells. It is easy processable, it is fairly simple to produce and it is relatively stable towards degradation. The main disadvantage of P3HT is the poor matching of its absorption spectrum with the solar emission spectrum. Figure 1.7 shows the solar spectrum with the curve of the integrated photon flux. The band gap, also called the energy gap ( $E_g$ ), of P3HT is around 1.9 eV, limiting the absorbance to wavelengths below 650 nm.

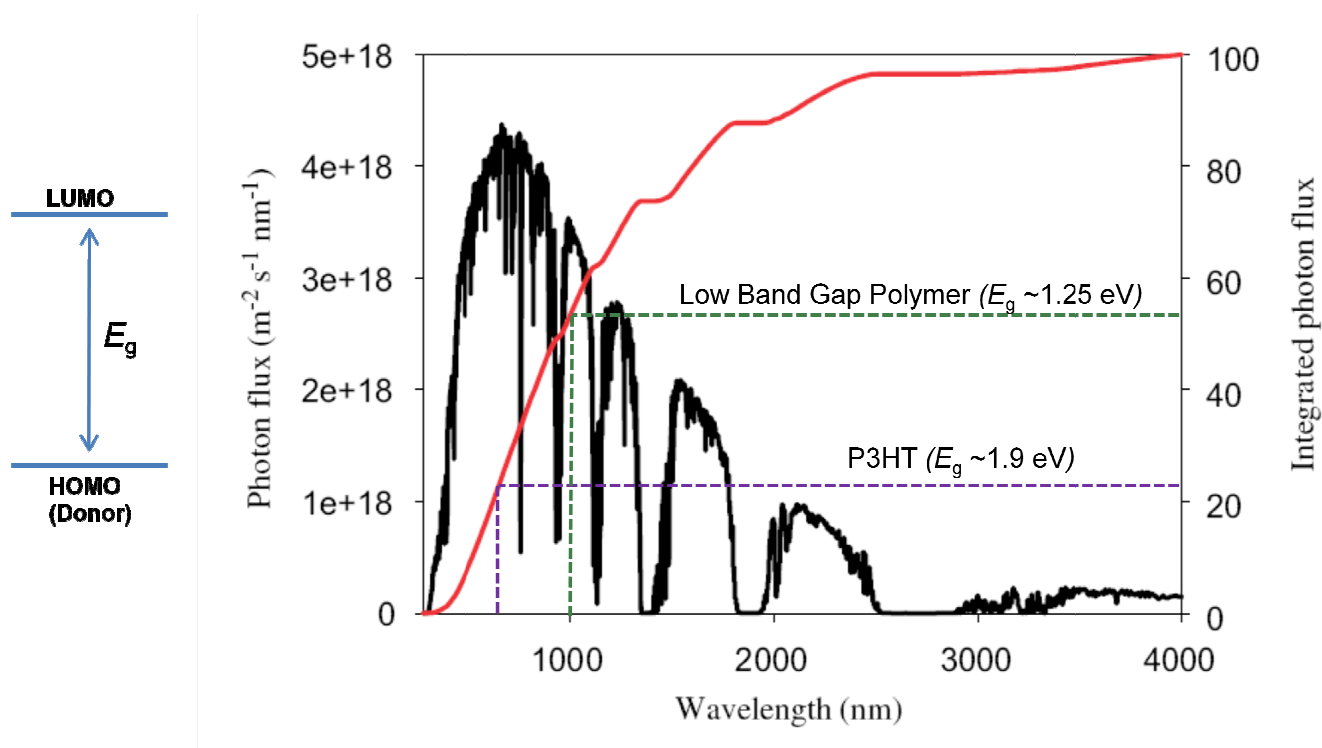


**Figure 1.7:** Photon flux from the sun at the earth's surface ( $1000 \text{ W m}^{-2}$ , AM1.5G) as a function of wavelength. The integral of the curve is shown on the right  $y$ -axis as a percentage of the total number of photons (Modified Figure from reference [30]). P3HT, which only absorbs photons with wavelengths below 650 nm, only have the potential to harvest up to 22.4% of the available solar photons, while a Low Band Gap Polymer, assuming absorption up to around 1000 nm, would have the potential to extract more than 50%.

Since the photon flux reaching the surface of earth from the sun has a maximum at approximately 1.8 eV (700 nm) P3HT is only able to harvest up to 22.4% of the available solar photons.<sup>[30,87]</sup> In order to increase the efficiency of OPVs to their optimal value the band gap of the polymer has to be tuned to the light spectrum to collect a higher number of photons. Simultaneously it is necessary to take into account that the alignment of the bands of donor and acceptor must be favorable for good charge separation. The offset of HOMO and LUMO levels between the two materials needs to be at least a few hundred meV in order to efficiently separate the excitons to free carriers with a minimum loss of  $V_{OC}$ .<sup>[88]</sup> Often this offset is called the exciton binding energy. The voltage of the device is defined by the difference between the energy level of the HOMO in the donor and the energy level for the LUMO in the acceptor. The number of absorbed photons and consequently also the maximum possible current is defined by the lowest band gap of two materials. Decreasing the band gap of the active material allows for absorption of a larger amount of photons with potentially higher power conversion efficiencies as a benefit as illustrated in Figure 1.7. It should be emphasized though that a continuous increase in the potential amount of harvested photons

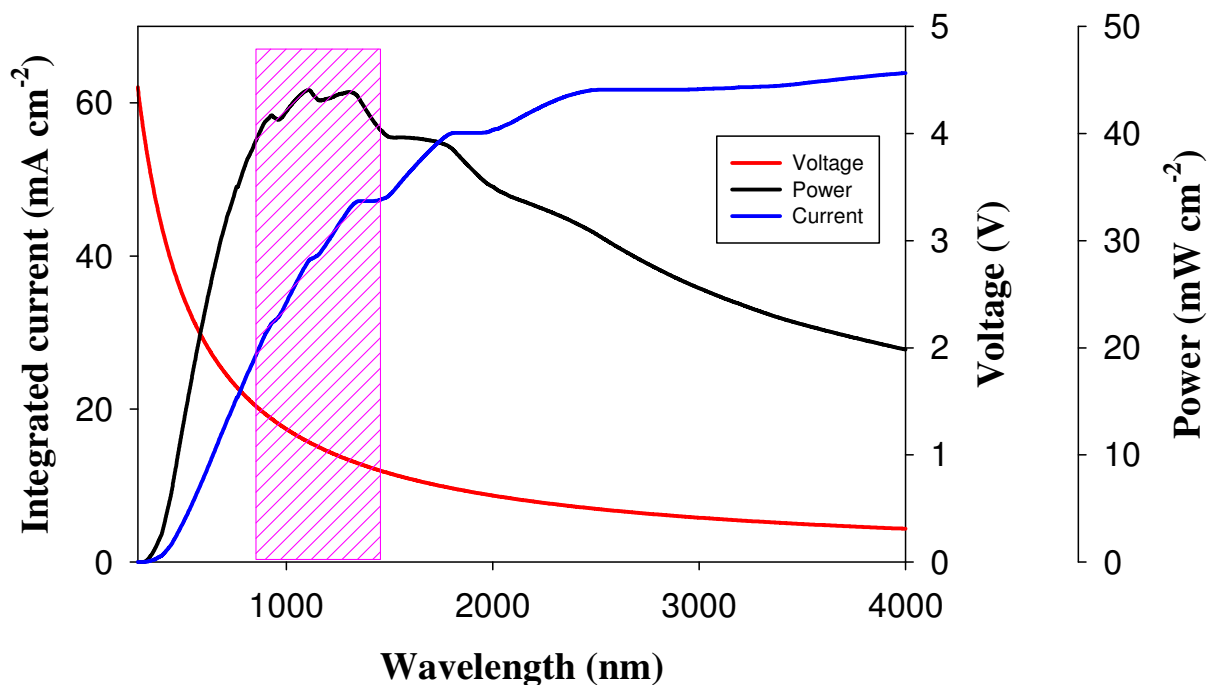


**Figure 1.8:** Maximum power obtainable in OPVs based on AM 1.5G emission spectrum. The power is calculated as the product of the integrated current (assuming an EQE of 100%) and the voltage of a device taken as the value of the bandgap. The power is thus the maximum theoretical value, neglecting thermodynamic effects and losses as well as the influence of the fill factor of the final solar cell. The purple box is the range of bandgaps where the most efficient devices can be found.<sup>[89]</sup> © Society of Photo-Optical Instrumentation Engineers.

(increase in the theoretical obtainable current) by lowering the band-gap does not lead to a continuous increase the PCE. As shows in equation (2) the PCE is proportional to  $V_{oc}$  which then again is proportional with  $E_g$ , and a lowering of the bandgap thus also have a factor opposing an increase in PCE. As illustrated in Figure 1.8 the maximum theoretical PCE can be obtained for polymers absorbing up to 900-1500 nm.<sup>[89]</sup> The most common approach to preparing low band gap (LBG) materials is to use the donor-acceptor approach where alternating electron rich and electron poor domains are incorporated into the polymer backbone. This allows for partial charge separation of the excitons and generally results in lower band gaps.<sup>[90]</sup> The greater potential of LBG polymers has led to an increasing interest in these systems, and new LBG polymer:PCBM composites have now overtaken P3HT:PCBM with respect to the maximum achievable power conversion efficiency, seemingly with plenty of room for improvement.<sup>[91-97]</sup> Some of the most promising LBG polymers are shown in Figure 1.9 and corresponding device data are listed in Table 1.1. In recent years the world record PCE report has been held by the few existing OPV producing companies, and currently belongs to Konarka Technologies, inc. who lately reported a PCE of 8.3 % for a small laboratory device (certified by NREL).<sup>[79]</sup>

Among the more promising LBG polymers is the poly[2,6-(4,4-bis-(2-ethylhexyl)-4*H*-cyclopenta-[2,1-*b*;3,4-*b'*]-dithiophene)-*alt*-4,7-(2,1,3-benzothiadiazole)] (PCPDTBT, see Figure 1.9) which has a structurally locked planar cyclopentanedithiophene (CPDB) as the donor unit combined with a benzothiadiazole acceptor unit. This results in a band gap of 1.46 eV.<sup>[93]</sup> Initial reports by Zhu *et al.* showed PCEs up to 3.5% for PCPDTBT/[70]PCBM bulk heterojunction solar cells and with an overall high external quantum efficiency (EQE) in the range of 400-800 nm (above 25%) with a maximum around 700 nm (38%).<sup>[102]</sup> Optimisation of the processing conditions by adding a few volume percent of alkanethiol to the process solution of PCPDTBT:[70]PCBM improved the PCE to 5.5% through altering the heterojunction morphology.<sup>[93]</sup> A remarkably high short circuit current (16.2 mA/cm<sup>2</sup>) was furthermore achieved. A silole analogue to PCPDTBT, where the bridging aliphatic carbon in the CPDT unit has been replaced by Si (PSBTBT, Figure 1.9), has also showed promising results.<sup>[91]</sup> PCEs up to 5.1 % have been achieved for solar cells based on PSBTBT:[70]PCBM blends, and PSBTBT itself has shown hole mobility of  $3 \times 10^{-3}$  cm<sup>2</sup>/(V s) which is 3 times higher than that for PCPDTBT.

Before the companies, who understandably do not willingly reveal the structure of their polymers, took over the lead position with respect to PCE, several claims came right after each other. First Park *et al.* reported a PCE of 6.1% for a bulk heterojunction solar cell based on a blend of the polymer poly[*N*-9''-hepta-decanyl-2,7-carbazole-*alt*-5,5-(4',7'-di-2-thienyl-2',1',3'-benzothiadiazole)] (PCDTBT, Figure 1.9) and [70]PCBM.<sup>[94]</sup> PCDTBT is based on a 4,7-dithienylbenzothiadiazole unit and a soluble carbazole unit that

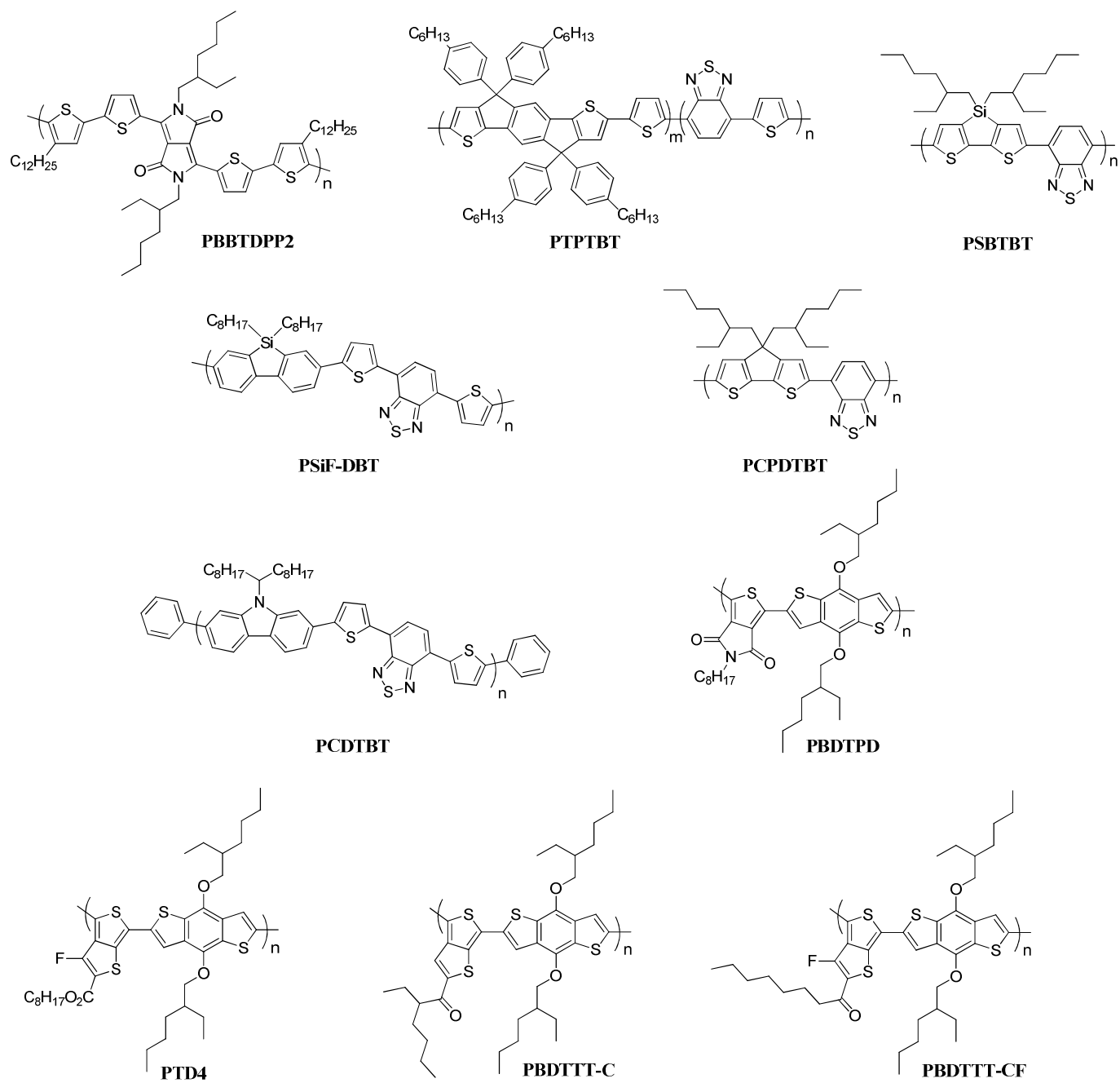


**Figure 1.9:** Chemical structures of some of the promising low band gap polymers for high efficient OPV's .

**Table 1.1:** Photovoltaic performance of some of the best performing polymer materials in blends with PCBM or C<sub>70</sub>-PCBM. Measurements were performed under AM1.5G conditions at 100 mW/cm<sup>2</sup> unless stated otherwise.

Polymer	Acceptor	$E_g^{opt}$ (eV)	$V_{oc}$ (V)	$J_{sc}$ (mA/cm <sup>2</sup> )	FF	$\eta$ (%)	Ref.
PBBTDPP2	C <sub>70</sub> -PCBM	1.4	0.61	11.3	0.58	4.0	[96]
PTPTBT	C <sub>70</sub> -PCBM	1.70	0.80	10.1	0.53	4.3 <sup>b</sup>	[95]
PSBTBT	C <sub>70</sub> -PCBM	1.45	0.68	12.7	0.55	4.7 <sup>b</sup>	[91]
PSiF-DBT	PCBM	1.82	0.9	9.5	0.51	5.4 <sup>c</sup>	[97]
PCPDTBT	C <sub>70</sub> -PCBM	1.46	0.62	16.2	0.55	5.5 <sup>b</sup>	[93]
PCDTBT	C <sub>70</sub> -PCBM	1.88 <sup>a</sup>	0.88	10.6	0.66	6.1	[94]
PBDTPD	PCBM	1.73	11.5	0.85	0.70	6.8	[98]
PTB4	PCBM	1.63	0.74	13.0	0.66	6.1 <sup>d</sup>	[92]
PBDTTT-C	C <sub>70</sub> -PCBM	1.60	0.70	14.7	0.64	6.58 (6.3 <sup>b</sup> )	[99]
PBDTTT-CF	C <sub>70</sub> -PCBM	1.63	0.76	15.2	0.67	7.7	[100]

<sup>a</sup> Retrieved from ref. [101]. <sup>b</sup> Average value. <sup>c</sup> Achieved under AM1.5G conditions at 80 mW/cm<sup>2</sup>. <sup>d</sup> Value after spectral correction.

gives it a optical band gap around 1.88 eV. The high result is thus not a result of a low band gap, but instead a product of the high voltage of the device (0.88 V) which is achieved through a low HOMO level of the polymer. The latter is probably due to the presence of carbazole unit which are known to have low HOMO levels. What is especially interesting with these results is that the authors achieved close to 100% internal quantum efficiency, which show that it is possible to prepare active layers for polymer solar cells where nearly all charge carriers are collected.

Shortly after this publication three consecutive reports on three very similar looking polymers were published in collaboration between the company Solarmer Energy Inc. with the University of Chicago and the University of California, Los Angeles. First the result of 6.1% (after spectral correction) was matched by Liang *et al.* using a low band gap polymer PTB4 (Figure 1.9) and PCBM. PTB4 has a dialkoxy-benzodithiophene as a donor unit and a thieno[3,4-*b*]thiophene ester as an acceptor resulting in an optical band gap of around 1.63 eV.<sup>[92]</sup> Fine tuning of the structure and electronic properties were done by introducing electron-withdrawing fluorine to the thieno[3,4-*b*]thiophene unit, which reduces the HOMO energy level of the polymer.

This was followed by Hou *et al* using a polymer, PBDTTT-C (Figure 1.9), with the same basic structure as Liang *et al.* but with no fluorine and a ketone instead of an ester on the thieno[3,4-*b*]thiophene unit where further fine tuning of the energy levels boosted the efficiency to 6.58%.<sup>[99]</sup>

Finally Chen *et al* showed a major leap, by increasing the efficiency with more than a percent to 7.7% by introducing a fluorine to the ketone substituted thieno[3,4-*b*]thiophene (PBDTTT-CF, Figure 1.9) and changing the chain on the ketone to *n*-heptyl. The large increase in efficiency from PBDTTT-C to PBDTTT-CF is primarily ascribed to an increase in the voltage.

The latest report of a new high performing LBG polymer was published by Piliago *et al*, who also employs a dialkoxy-benzodithiophene as a donor unit, but where the acceptor unit consists of a N-alkylated thienopyrrole-dione (PBDTPD, Figure 1.9).<sup>[98]</sup> This polymer showed a maximum PCE of 6.8%, which is a very good result when considering that the active layer consisted of a blend with PCBM.

In summary, the evolution in PV performance has been increasing rapidly over the last 5 years, and the field of organic photovoltaics has entered a new stage where efforts are mainly focused on development of new polymers. This is opposed to the previous stage, where focus was mainly pointed towards optimization of the P3HT:PCBM system. Nevertheless, further improvements in efficiency are required for large scale commercialization. Aside from the power conversion efficiency, processing and stability are two other important aspects that have to be addressed with equal intensity in order for polymer solar cells to succeed. To combine all three parameters into a useful technology further research in device science and new materials is needed.

## **1.5 Key issues for future OPV success which has been approached in this thesis**

By far the most important issue for organic solar cell success as a source of renewable energy relies on whether mass production of sufficiently stable and efficient OPVs can be achieved. All work performed in this thesis has originated from the wish to approach necessary issues towards such a production by methods like roll-to-roll (R2R) coating. The main focus areas have in this respect been on environmentally friendly processing and improved stability of polymers.

### **1.5.1 Introduction – Roll-to-roll processing of organic solar cells**

Many challenges remain that have to be addressed efficiently before the vision of large scale manufacture and widespread usage of low cost polymer solar cells can be anticipated. Ideally the polymer solar cell should be manufactured in a fast, large area and environmentally friendly process. The methodologies employed in typical laboratory studies do not represent this well. The most commonly employed film

forming technique is spin coating which is incompatible with large areas, large volume and low cost manufacture.

The main focus within the field of organic solar cells is still on small scale spin coated devices. However, attention is increasingly moving towards solving the problems of taking the solar cell out of the lab and into production, although the number of 'participants' is still limited. One of the major hurdles is the cost of the equipment needed as is the cost of running the equipment. Compared to the cost of a simple spin-coater and an evaporator, the cost of R2R- and screen printing machinery is much higher. In addition to this initial hurdle an important factor is the amount of experience of working with larger area solar cells which is very little compared to small scale devices. Even though the principle within the solar cell itself is the same, there are huge differences in preparing a nice film covering a few mm<sup>2</sup> by spin coating, and the preparation of a uniform continuous stripe of 0.5-2 cm wide film on a flexible substrate which in a lab scale R2R process is typically 25-50 m long. As a further challenge evaporation of the back electrode is not suitable for R2R processing, resulting in the need to change the geometry of the cell since printable electrodes in reality is limited to silver

(silver paste) which has a work function that does not allow it to function well in OPVs as the cathode. This results in a so-called inverted geometry which is illustrated in Figure 1.10. In order to facilitate electron transport to the cathode in the inverted geometry, an intermediate layer of ZnO is placed between the active layer and the transparent ITO electrode and the hole conducting PEDOT is applied after the active layer instead of before. This might sound trivial, but the sequence of the layers can be extremely important, as the properties of each layer has an influence on how well the subsequent can be

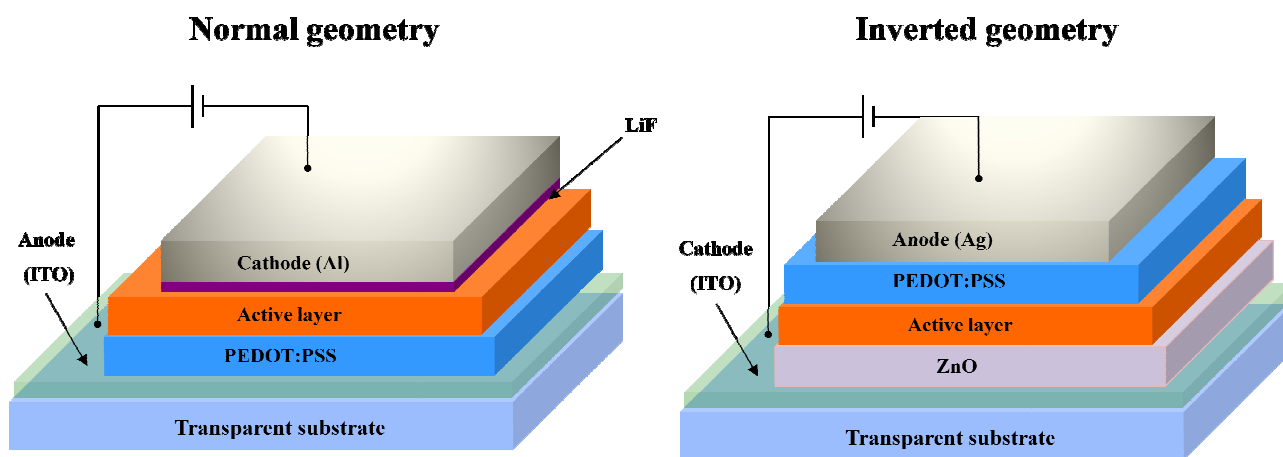


**Figure 1.10** Illustrations of the 'Normal geometry' cell and the 'Inverted geometry' cell. In both cases the buildup of the cell starts with the substrate.



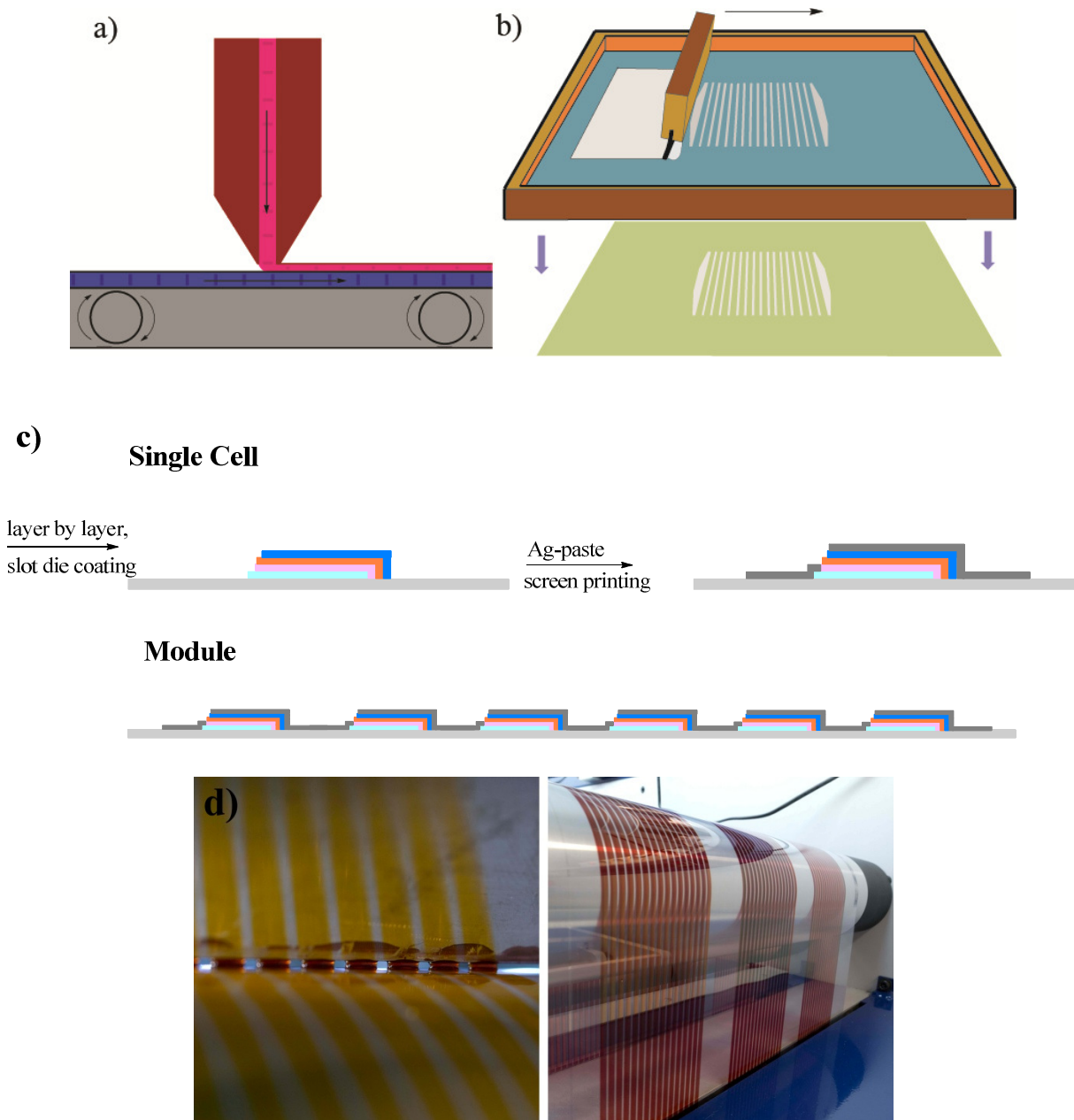


**Figure 1.11** Illustration of the preparation of R2R processing using slot die coating and screen printing. **a)** The principle of slot die coating – here seen from the side. **b)** Principle of screen printing. By pressing the silver paste through the openings in the framed mesh, an imprint of the patterned electrode is generated on top of the substrate. **c)** Illustration of the layered structure of the processed stripes before and after screen printing – here seen along the stripe. Underneath is shown the structure on a series connected module. **d) left:** Picture of slot die coating for a module. **right:** The final stripes for modules.

processed (e.g. how well does the solution wet the surface already processed). In Figure 1.11 is illustrated how R2R processing of large area solar cells is carried out using slot die coating for all layers except silver, which is applied by screen printing. Processing is generally performed using the flexible substrate PET (polyethyleneterphthalate) because of its low cost, but in principle any transparent flexible material can be used. The substrate has been pre-patterned with stripes of the transparent electrode, typically ITO, and the processing is performed as a continuous procedure while transferring the substrate from one roll to another. Each solution processable layer is applied by passing the solution through a slot in the printing head. The slot is placed close to the moving substrate in a manner so the surface tension of the liquid creates a standing 'wall' of solution having the desired width, thus creating the layers as a continuous stripe on the substrate (see Figure 1.11a and d). This is followed by slot die coating of the next layer on top on the former, taking great care that the alignment of the different layer is correct. Finally the silver back electrode is applied by screen printing. Here the silver paste is placed on a framed mesh where all holes but the ones creating the pattern of the back electrode is covered with a filler material. The frame is placed on top of the substrate the silver paste is forced through the patterned area using a squeegee. The paste is pressed through the small holes in the mesh onto the substrate thus creating the patterned electrode on top (see Figure 1.11b). Also here great care must be taken in aligning the substrate and the frame in order to create the final circuit. Generally the whole process is finished off by applying some kind of a barrier layer to increase the stability.

### **1.5.2 Substitution of toxic solvents for more environmentally friendly processing**

A very troublesome aspect in the preparation of OPVs is the use of toxic organic solvents in the film forming process. In a large scale application, where production volumes corresponding to several  $\text{GW}_{\text{peak}}$  are envisaged, this is not a viable approach and alternative solvents will be a requirement. Until now, solvent free or environmentally friendly solvent processing has not been studied to any significant level. An explanation for this can possibly be sought in the delicate interplay between the processing solvent and the performance of the solar cell. In many ways the state-of-the-art polymer solar cell has evolved around aromatic solvents such as chlorobenzene, dichlorobenzene, toluene and xylene. Any change of solvent might adversely affects the nanomorphology of the film and the device performance. The ambition to use more benign solvents will therefore require a redesign of the molecular structures and a re-establishment of the interplay between nanomorphology and processing for the new material-solvent

combination. This calls for new materials that can be processed from some biodegradable solvent – preferably water.

An enormous challenge consequently lies ahead, but the removal of the toxic solvents from the processing procedure will not only be an advantage in the actual production where a lot of safety procedures can be avoided - It is also a must from an environmental aspect if the organic solar cell is to live up to the idea of “green energy”.

### 1.5.3 Increasing the stability of polymers

Long operational life times are crucial for the commercialization of polymer solar cells. Although lifetimes of PV devices has been defined in numerous ways (e.g. as the time needed for a device to reach 50% ( $T_{50}$ ) or 80% ( $T_{80}$ ) of its initial efficiency or as the time it takes the short circuit current to reach half its initial value),<sup>[103]</sup> life times are generally very poor, as polymer and organic solar cells degrade when exposed to illumination and in the dark. Interests in this side of the OPV field has increased in the last couple of years, resulting in numerous publications,<sup>[37,103-110]</sup> as the importance of better understanding and optimization has grown.

The studies span a variety of issues like photodegradation of pure polymers (what mechanisms are the cause of degradation/bleaching of the pure conjugated polymer), degradation of finalized devices under controlled conditions (primarily focusing on examination the influence of temperature, oxygen and water on the different layers in the cell as well as the overall performance) to actual outdoor testing of cells performed under “real life” conditions where the changes in weather conditions exerts stress on the cells with fluctuating temperature and humidity.

An important discovery in the understanding of how polymers degrade was found by Manceau *et al*, who established that for P3HT the main source of photodegradation is caused at the side chains of the polymer. Oxygen promoted generation of radicals is provoked at the  $\alpha$ -carbon next to the thiophene ring, which then through a series of steps leads to oxidation of sulfur in the thiophene ring with consequent destruction of the conjugated backbone (Figure 1.12).<sup>[104,107]</sup> It should be mentioned though that the same authors have also shown that when mixed with PCBM, which acts as a radical scavenger, the photo stability of the active layer blend increases.<sup>[108]</sup>

Similar studies would be very interesting for LBG polymers, as most of the top-performing LBG polymers used in solar cells are very sensitive to water and oxygen, and are as a result too unstable to be used for large area processing when this is carried out in the ambient. As a consequence the P3HT/PCBM system is still ‘the king and queen’ when it comes to large area R2R processed solar cells. In order to be able to

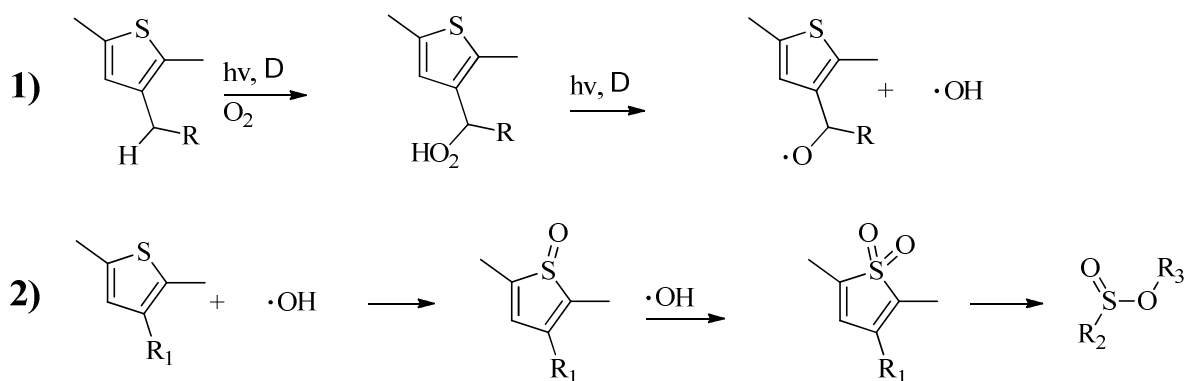


**Figure 1.12:** Two of the key reactions in the suggested mechanism by Manceau *et al* on the destruction of the conjugated backbone of P3HT by photodegradation in the presence of oxygen.

transfer the success of low-band-gap polymers in small scale devices to large area cells, there is a need to develop more stable LBG polymers. These must be able to sustain the, at the present, more ‘rough’ conditions that are the reality in large area processing such as roll-to-roll. A classification of the different properties of a polymer that influences the photochemical stability would therefore be a very useful tool in the preparation of new polymers.

Another very interesting discovery, with respect to the permeability of solar cells, was found by use of time of flight secondary ion mass spectroscopy (TOF-SIMS) and isotopic labeling (<sup>18</sup>O and H<sub>2</sub><sup>18</sup>O).<sup>[37,111,112]</sup> Not only was it shown that the layered structure in a polymer solar cell is permeable to both oxygen and water which can cause reaction with both polymer and the electrodes - also the electrode materials diffuse to through the entire device to the counter electrodes. This means that the solid state of the polymer material is so soft and flexible that the layer structure of the general solar cell cannot be regarded as ‘fixed’, although all layers in a device are considered to be solid.

If these mixing processes are to be avoided, the soft properties of the active layer have to be changed. This challenge has been approached by use of thermocleavable side chains, which has also proven one of the most successful ways of increasing the stability of conjugated polymers.<sup>[105,113-121]</sup> Side chains are necessary for processing of the active layer, as they make it possible to keep the polymer in solution. However, after processing they are of no use as photo absorbers, and they are the main reason for the soft properties of the active layer. By attaching side chains that are removed after processing these properties change, and the active layer is rendered much more rigid, slowing down all diffusion processes and thus increases the stability. From a more practically point of view, the removal of the side chains furthermore changes the solubility and the polymer becomes insoluble. This opens up the possibility to process a

subsequent layer using the same solvent, which is normally not possible as such a practice will lead to destruction of the already processed one.

The use of thermocleavable tertiary ester side chains has proven a successful way of achieving these features. As illustrated for the polymer P3MHOCT in Figure 1.13 the thermocleavage can proceed in two steps when the tertiary ester is attached to a thiophene ring. Initially, around 200 °C, the solubilizing ester substituent will cleave off leaving behind a carboxyl substituted thiophene, which upon further heating to around 300 °C will eliminate CO<sub>2</sub>. Both these stages are insoluble in all solvents and provide improved stability in photovoltaic devices. If the tertiary ester is attached to a benzene ring only cleavage to the carboxylic acid occurs.

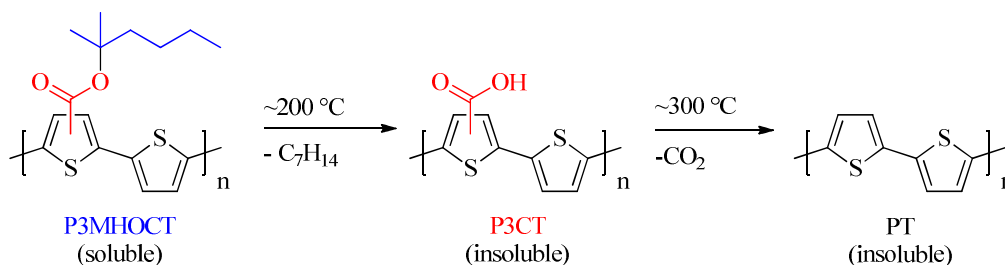


**Figure 1.13** Schematic illustration of the thermocleavage of the polymer P3MHOCT which carries a tertiary ester group attached to thiophene. Cleavage can proceed in two steps consecutive steps with increasing temperature leading to either carboxy-substituted polythiophene (P3CT) or polythiophene (PT), both of which are insoluble.

One major drawback of the use of thermocleavable tertiary ester is that the cleavage temperatures does not comply with processing on flexible substrates like PET as they start deforming at the elevated temperatures (for PET if higher than 140 °C). If the procedure, that stability wise seems very favorable, is to be transferred to flexible substrates it would therefore be necessary to find alternative ways of cleavage or to develop methods to bring down the cleavage temperatures.

## 1.6 Aim and scope of this thesis

The main aim of this project has been to develop a synthetic method of polymer preparation that allow for the substitution of the very toxic solvents that are generally used for the processing of OPVs with more environmentally friendly solvents. The optimal goal was to be able to fabricate a solar cell by performing all processing steps from water.

The secondary aim has been to examine and possibly improve the stability of R2R processed solar cells by the following three focus areas:

- Synthesis of new LBG polymers for examination of their photo-stability in air. As part of a larger study the comparison of similar donor/acceptor combinations in LBG polymers should allow for defining a general rule how to introduce stability to polymers.
- Fabrication of panels with R2R-processed solar cells and performing an outdoor stability study under different climate conditions by setting up the panels in a total of 8 countries selected by their diverse local weather.
- Development of a procedure to lower the temperature of thermocleavage of tertiary esters with the prospect of future use of this method in R2R-processed solar cells.

## 1.7 References

1. Renewable Energy Policy Network for the 21st Century, *Renewables 2010 Global Status Report*, [http://www.ren21.net/Portals/97/documents/GSR/REN21\\_GSR\\_2010\\_full\\_revised%20Sept2010.pdf](http://www.ren21.net/Portals/97/documents/GSR/REN21_GSR_2010_full_revised%20Sept2010.pdf)
2. Becquerel, A. E. Mémoire sur les effets électriques produits sous l'influence des rayons solaires. *Comptes Rendus de l'Académie des sciences* **1839**, 9, 561-567.
3. Becquerel, A. E. Recherches sur les effets de la radiation chimique de la lumière solaire, au moyen des courants électriques *Comptes Rendus de l'Académie des sciences* **1839**, 9, 145-149.
4. Chapin, D. M.; Fuller, C. S.; Pearson, G. L. A New Silicon P-N Junction Photocell for Converting Solar Radiation Into Electrical Power. *J. Appl. Phys.* **1954**, 25 (5), 676-677.
5. Bagnall, D. M.; Boreland, M. Photovoltaic technologies. *Energy Policy* **2008**, 36 (12), 4390-4396.
6. Hanna, M. C.; Nozik, A. J. Solar conversion efficiency of photovoltaic and photoelectrolysis cells with carrier multiplication absorbers. *J. Appl. Phys.* **2006**, 100 (7), 074510.
7. Shockley, W.; Queisser, H. J. Detailed Balance Limit of Efficiency of P-N Junction Solar Cells. *J. Appl. Phys.* **1961**, 32 (3), 510-519.
8. Green, M. A.; Emery, K.; Hishikawa, Y.; Warta, W. Solar cell efficiency tables (version 37). *Prog. Photovolt.* **2011**, 19 (1), 84-92.
9. Peumans, P.; Yakimov, A.; Forrest, S. R. Small molecular weight organic thin-film photodetectors and solar cells. *J. Appl. Phys.* **2003**, 93 (7), 3693-3723.
10. Peumans, P.; Forrest, S. R. Very-high-efficiency double-heterostructure copper phthalocyanine/C-60 photovoltaic cells. *Appl. Phys. Lett.* **2001**, 79 (1), 126-128.
11. Grätzel, M. Photoelectrochemical cells. *Nature* **2001**, 414 (6861), 338-344.
12. Nazeeruddin, M. K.; Kay, A.; Rodicio, I.; Humphry-Baker, R.; Mueller, E.; Liska, P.; Vlachopoulos, N.; Graetzel, M. Conversion of light to electricity by cis-X<sub>2</sub>bis(2,2'-bipyridyl-4,4'-dicarboxylate)ruthenium(II) charge-transfer sensitizers (X = Cl-, Br-, I-, CN-, and SCN-) on nanocrystalline titanium dioxide electrodes. *J. Am. Chem. Soc.* **2002**, 115 (14), 6382-6390.
13. O'Regan, B.; Gratzel, M. A Low-Cost, High-Efficiency Solar-Cell Based on Dye-Sensitized Colloidal TiO<sub>2</sub> Films. *Nature* **1991**, 353 (6346), 737-740.
14. Alstrup, J.; Jørgensen, M.; Medford, A. J.; Krebs, F. C. Ultra Fast and Parsimonious Materials Screening for Polymer Solar Cells Using Differentially Pumped Slot-Die Coating. *ACS Appl. Mater. Interfaces* **2010**, 2 (10), 2819-2827.

15. Blankenburg, L.; Schultheis, K.; Schache, H.; Sensfuss, S.; Schrodner, M. Reel-to-reel wet coating as an efficient up-scaling technique for the production of bulk-heterojunction polymer solar cells. *Sol. Energy Mater. Sol. Cells* **2009**, *93* (4), 476-483.
16. Dennler, G.; Lungenschmied, C.; Neugebauer, H.; Sariciftci, N. S.; Labouret, A. Flexible, conjugated polymer-fullerene-based bulk-heterojunction solar cells: Basics, encapsulation, and integration. *J. Mater. Res.* **2005**, *20* (12), 3224-3233.
17. Krebs, F. C. All solution roll-to-roll processed polymer solar cells free from indium-tin-oxide and vacuum coating steps. *Org. Electron.* **2009**, *10* (5), 761-768.
18. Krebs, F. C.; Jørgensen, M.; Norrman, K.; Hagemann, O.; Alstrup, J.; Nielsen, T. D.; Fyenbo, J.; Larsen, K.; Kristensen, J. A complete process for production of flexible large area polymer solar cells entirely using screen printing-First public demonstration. *Sol. Energy Mater. Sol. Cells* **2009**, *93* (4), 422-441.
19. Krebs, F. C. Polymer solar cell modules prepared using roll-to-roll methods: Knife-over-edge coating, slot-die coating and screen printing. *Sol. Energy Mater. Sol. Cells* **2009**, *93* (4), 465-475.
20. Krebs, F. C. Roll-to-roll fabrication of monolithic large-area polymer solar cells free from indium-tin-oxide. *Sol. Energy Mater. Sol. Cells* **2009**, *93* (9), 1636-1641.
21. Krebs, F. C. Fabrication and processing of polymer solar cells: A review of printing and coating techniques. *Sol. Energy Mater. Sol. Cells* **2009**, *93* (4), 394-412.
22. Krebs, F. C.; Gevorgyan, S. A.; Alstrup, J. A roll-to-roll process to flexible polymer solar cells: model studies, manufacture and operational stability studies. *J. Mater. Chem.* **2009**, *19* (30), 5442-5451.
23. Lungenschmied, C.; Dennler, G.; Neugebauer, H.; Sariciftci, S. N.; Glatthaar, M.; Meyer, T.; Meyer, A. Flexible, long-lived, large-area, organic solar cells. *Sol. Energy Mater. Sol. Cells* **2007**, *91* (5), 379-384.
24. Niggemann, M.; Zimmermann, B.; Haschke, J.; Glatthaar, M.; Gombert, A. Organic solar cell modules for specific applications - From energy autonomous systems to large area photovoltaics. *Thin Solid Films* **2008**, *516* (20), 7181-7187.
25. Tipnis, R.; Bernkopf, J.; Jia, S. J.; Krieg, J.; Li, S.; Storch, M.; Laird, D. Large-area organic photovoltaic module-Fabrication and performance. *Sol. Energy Mater. Sol. Cells* **2009**, *93* (4), 442-446.
26. Zimmermann, B.; Glatthaar, M.; Niggemann, M.; Riede, M. K.; Hinsch, A.; Gombert, A. ITO-free wrap through organic solar cells - A module concept for cost-efficient reel-to-reel production. *Sol. Energy Mater. Sol. Cells* **2007**, *91* (5), 374-378.
27. Pochettino, A. *Acad. Lincei Rend.* **1906**, *15*, 355.
28. Friend, R. H.; Gymer, R. W.; Holmes, A. B.; Burroughes, J. H.; Marks, R. N.; Taliani, C.; Bradley, D. D. C.; Dos Santos, D. A.; Bredas, J. L.; Logdlund, M.; Salaneck, W. R. Electroluminescence in conjugated polymers. *Nature* **1999**, *397* (6715), 121-128.



29. Garnier, F.; Hajlaoui, R.; Yassar, A.; Srivastava, P. All-Polymer Field-Effect Transistor Realized by Printing Techniques. *Science* **1994**, *265* (5179), 1684-1686.
30. Bundgaard, E.; Krebs, F. C. Low band gap polymers for organic photovoltaics. *Sol. Energy Mater. Sol. Cells* **2007**, *91* (11), 954-985.
31. Kippelen, B.; Bredas, J. L. Organic photovoltaics. *Energy & Env. Sci.* **2009**, *2* (3), 251-261.
32. Dennler, G.; Scharber, M. C.; Brabec, C. J. Polymer-Fullerene Bulk-Heterojunction Solar Cells. *Adv. Mater.* **2009**, *21* (13), 1323-1338.
33. Chen, L. M.; Hong, Z. R.; Li, G.; Yang, Y. Recent Progress in Polymer Solar Cells: Manipulation of Polymer: Fullerene Morphology and the Formation of Efficient Inverted Polymer Solar Cells. *Adv. Mater.* **2009**, *21* (14-15), 1434-1449.
34. Günes, S.; Sariciftci, N. S. Hybrid solar cells. *Inorg. Chim. Acta* **2008**, *361* (3), 581-588.
35. Brabec, C. J.; Durrant, J. R. Solution-processed organic solar cells. *MRS Bull.* **2008**, *33* (7), 670-675.
36. Günes, S.; Neugebauer, H.; Sariciftci, N. S. Conjugated polymer-based organic solar cells. *Chem. Rev.* **2007**, *107* (4), 1324-1338.
37. Jørgensen, M.; Norrman, K.; Krebs, F. C. Stability/degradation of polymer solar cells. *Sol. Energy Mater. Sol. Cells* **2008**, *92* (7), 686-714.
38. Kroon, R.; Lenes, M.; Hummelen, J. C.; Blom, P. W. M.; De Boer, B. Small bandgap polymers for organic solar cells (polymer material development in the last 5 years). *Polym. Rev.* **2008**, *48* (3), 531-582.
39. Lloyd, M. T.; Anthony, J. E.; Malliaras, G. G. Photovoltaics from soluble small molecules. *Mater. Today* **2007**, *10* (11), 34-41.
40. Mayer, A. C.; Scully, S. R.; Hardin, B. E.; Rowell, M. W.; McGehee, M. D. Polymer-based solar cells. *Mater. Today* **2007**, *10* (11), 28-33.
41. Rand, B. P.; Genoe, J.; Heremans, P.; Poortmans, J. Solar cells utilizing small molecular weight organic semiconductors. *Prog. Photovolt.* **2007**, *15* (8), 659-676.
42. Thompson, B. C.; Frechet, J. M. J. Organic photovoltaics - Polymer-fullerene composite solar cells. *Angew. Chem. - Int. Ed.* **2008**, *47* (1), 58-77.
43. Winder, C.; Sariciftci, N. S. Low bandgap polymers for photon harvesting in bulk heterojunction solar cells. *J. Mater. Chem.* **2004**, *14* (7), 1077-1086.
44. Helgesen, M.; Søndergaard, R.; Krebs, F. C. Advanced materials and processes for polymer solar cell devices. *J. Mater. Chem.* **2010**, *20* (1), 36-60.
45. Gendron, D.; Leclerc, M. New conjugated polymers for plastic solar cells. *Energy & Env. Sci.* **2011**, *4* (4), 1225-1237.

46. Hecht, D. S.; Hu, L. B.; Irvin, G. Emerging Transparent Electrodes Based on Thin Films of Carbon Nanotubes, Graphene, and Metallic Nanostructures. *Adv. Mater.* **2011**, *23* (13), 1482-1513.
47. Sista, S.; Hong, Z. R.; Chen, L. M.; Yang, Y. Tandem polymer photovoltaic cells-current status, challenges and future outlook. *Energy & Env. Sci.* **2011**, *4* (5), 1606-1620.
48. Boudreault, P. L. T.; Najari, A.; Leclerc, M. Processable Low-Bandgap Polymers for Photovoltaic Applications. *Chem. Mater.* **2011**, *23* (3), 456-469.
49. Facchetti, A. pi-Conjugated Polymers for Organic Electronics and Photovoltaic Cell Applications. *Chem. Mater.* **2011**, *23* (3), 733-758.
50. Xue, J. G. Perspectives on Organic Photovoltaics. *Polym. Rev.* **2010**, *50* (4), 411-419.
51. Hau, S. K.; Yip, H. L.; Jen, A. K. Y. A Review on the Development of the Inverted Polymer Solar Cell Architecture. *Polym. Rev.* **2010**, *50* (4), 474-510.
52. Zhan, X. W.; Zhu, D. B. Conjugated polymers for high-efficiency organic photovoltaics. *Polymer Chemistry* **2010**, *1* (4), 409-419.
53. Siddiki, M. K.; Li, J.; Galipeau, D.; Qiao, Q. Q. A review of polymer multijunction solar cells. *Energy & Env. Sci.* **2010**, *3* (7), 867-883.
54. Chandrasekaran, J.; Nithyaprakash, D.; Ajjan, K. B.; Maruthamuthu, S.; Manoharan, D.; Kumar, S. Hybrid solar cell based on blending of organic and inorganic materials-An overview. *Renewable & Sustainable Energy Reviews* **2011**, *15* (2), 1228-1238.
55. Sonar, P.; Lim, J. P. F.; Chan, K. L. Organic non-fullerene acceptors for organic photovoltaics. *Energy & Env. Sci.* **2011**, *4* (5), 1558-1574.
56. Brabec, C. J.; Gowrisanker, S.; Halls, J. J. M.; Laird, D.; Jia, S. J.; Williams, S. P. Polymer-Fullerene Bulk-Heterojunction Solar Cells. *Adv. Mater.* **2010**, *22* (34), 3839-3856.
57. Arkhipov, V. I.; Bassler, H. Exciton dissociation and charge photogeneration in pristine and doped conjugated polymers. *Physica Status Solidi A-Applied Research* **2004**, *201* (6), 1152-1187.
58. Gregg, B. A.; Hanna, M. C. Comparing organic to inorganic photovoltaic cells: Theory, experiment, and simulation. *J. Appl. Phys.* **2003**, *93* (6), 3605-3614.
59. Halls, J. J. M.; Walsh, C. A.; Greenham, N. C.; Marseglia, E. A.; Friend, R. H.; Moratti, S. C.; Holmes, A. B. Efficient Photodiodes from Interpenetrating Polymer Networks. *Nature* **1995**, *376* (6540), 498-500.
60. Sariciftci, N. S.; Smilowitz, L.; Heeger, A. J.; Wudl, F. Photoinduced Electron-Transfer from A Conducting Polymer to Buckminsterfullerene. *Science* **1992**, *258* (5087), 1474-1476.
61. Sariciftci, N. S.; Braun, D.; Zhang, C.; Srdanov, V. I.; Heeger, A. J.; Stucky, G.; Wudl, F. Semiconducting Polymer-Buckminsterfullerene Heterojunctions - Diodes, Photodiodes, and Photovoltaic Cells. *Appl. Phys. Lett.* **1993**, *62* (6), 585-587.

- 
62. Yu, G.; Heeger, A. J. Charge Separation and Photovoltaic Conversion in Polymer Composites with Internal Donor-Acceptor Heterojunctions. *J. Appl. Phys.* **1995**, *78* (7), 4510-4515.
  63. Granstrom, M.; Petritsch, K.; Arias, A. C.; Lux, A.; Andersson, M. R.; Friend, R. H. Laminated fabrication of polymeric photovoltaic diodes. *Nature* **1998**, *395* (6699), 257-260.
  64. Kietzke, T.; Horhold, H. H.; Neher, D. Efficient polymer solar cells based on M3EH-PPV. *Chem. Mater.* **2005**, *17*, 6532-6537.
  65. Koetse, M. M.; Sweelssen, J.; Hoekerd, K. T.; Schoo, H. F. M.; Veenstra, S. C.; Kroon, J. M.; Yang, X. N.; Loos, J. Efficient polymer : polymer bulk heterojunction solar cells. *Appl. Phys. Lett.* **2006**, *88* (8), 083504.
  66. McNeill, C. R.; Abrusci, A.; Zaumseil, J.; Wilson, R.; McKiernan, M. J.; Burroughes, J. H.; Halls, J. J. M.; Greenham, N. C.; Friend, R. H. Dual electron donor/electron acceptor character of a conjugated polymer in efficient photovoltaic diodes. *Appl. Phys. Lett.* **2007**, *90* (19), 193506.
  67. Allemand, P. M.; Koch, A.; Wudl, F.; Rubin, Y.; Diederich, F.; Alvarez, M. M.; Anz, S. J.; Whetten, R. L. 2 Different Fullerenes Have the Same Cyclic Voltammetry. *J. Am. Chem. Soc.* **1991**, *113* (3), 1050-1051.
  68. Brabec, C. J.; Zerza, G.; Cerullo, G.; De Silvestri, S.; Luzzati, S.; Hummelen, J. C.; Sariciftci, S. Tracing photoinduced electron transfer process in conjugated polymer/fullerene bulk heterojunctions in real time. *Chem. Phys. Lett.* **2001**, *340* (3-4), 232-236.
  69. Wöbkenberg, P. H.; Bradley, D. D. C.; Kronholm, D.; Hummelen, J. C.; de Leeuw, D. M.; Colle, M.; Anthopoulos, T. D. High mobility n-channel organic field-effect transistors based on soluble C-60 and C-70 fullerene derivatives. *Synthetic Metals* **2008**, *158* (11), 468-472.
  70. Rispen, M. T.; Meetsma, A.; Rittberger, R.; Brabec, C. J.; Sariciftci, N. S.; Hummelen, J. C. Influence of the solvent on the crystal structure of PCBM and the efficiency of MDMO-PPV : PCBM 'plastic' solar cells. *Chem. Comm.* **2003**, (17), 2116-2118.
  71. Wienk, M. M.; Kroon, J. M.; Verhees, W. J. H.; Knol, J.; Hummelen, J. C.; van Hal, P. A.; Janssen, R. A. J. Efficient methano[70]fullerene/MDMO-PPV bulk heterojunction photovoltaic cells. *Angew. Chem. - Int. Ed.* **2003**, *42* (29), 3371-3375.
  72. Markov, D. E.; Hummelen, J. C.; Blom, P. W. M.; Sieval, A. B. Dynamics of exciton diffusion in poly(p-phenylene vinylene)/fullerene heterostructures. *Phys. Rev. B* **2005**, *72* (4), 045216.
  73. Scully, S. R.; McGehee, M. D. Effects of optical interference and energy transfer on exciton diffusion length measurements in organic semiconductors. *J. Appl. Phys.* **2006**, *100* (3), 034907.
  74. Tang, C. W. 2-Layer Organic Photovoltaic Cell. *Appl. Phys. Lett.* **1986**, *48* (2), 183-185.
  75. Chamberlain, G. A. Organic Solar-Cells - A Review. *Solar Cells* **1983**, *8* (1), 47-83.

- 
76. Marks, R. N.; Halls, J. J. M.; Bradley, D. D. C.; Friend, R. H.; Holmes, A. B. The Photovoltaic Response in Poly(P-Phenylene Vinylene) Thin-Film Devices. *Journal of Physics-Condensed Matter* **1994**, *6* (7), 1379-1394.
  77. Wohrle, D.; Meissner, D. Organic Solar-Cells. *Adv. Mater.* **1991**, *3* (3), 129-138.
  78. Yu, G.; Gao, J.; Hummelen, J. C.; Wudl, F.; Heeger, A. J. Polymer Photovoltaic Cells - Enhanced Efficiencies Via A Network of Internal Donor-Acceptor Heterojunctions. *Science* **1995**, *270* (5243), 1789-1791.
  79. Konarka Technologies Inc., [www.konarka.com](http://www.konarka.com)
  80. Gadisa, A.; Svensson, M.; Andersson, M. R.; Inganäs, O. Correlation between oxidation potential and open-circuit voltage of composite solar cells based on blends of polythiophenes/fullerene derivative. *Appl. Phys. Lett.* **2004**, *84* (9), 1609-1611.
  81. Mihailitchi, V. D.; Blom, P. W. M.; Hummelen, J. C.; Rispen, M. T. Cathode dependence of the open-circuit voltage of polymer : fullerene bulk heterojunction solar cells. *J. Appl. Phys.* **2003**, *94* (10), 6849-6854.
  82. Ko, C. J.; Lin, Y. K.; Chen, F. C.; Chu, C. W. Modified buffer layers for polymer photovoltaic devices. *Appl. Phys. Lett.* **2007**, *90* (6), 063509.
  83. Li, G.; Shrotriya, V.; Huang, J. S.; Yao, Y.; Moriarty, T.; Emery, K.; Yang, Y. High-efficiency solution processable polymer photovoltaic cells by self-organization of polymer blends. *Nat. Mater.* **2005**, *4* (11), 864-868.
  84. Ma, W. L.; Yang, C. Y.; Gong, X.; Lee, K.; Heeger, A. J. Thermally stable, efficient polymer solar cells with nanoscale control of the interpenetrating network morphology. *Adv. Func. Mater.* **2005**, *15* (10), 1617-1622.
  85. Reyes-Reyes, M.; Kim, K.; Carroll, D. L. High-efficiency photovoltaic devices based on annealed poly(3-hexylthiophene) and 1-(3-methoxycarbonyl)-propyl-1-phenyl-(6,6)C-61 blends. *Appl. Phys. Lett.* **2005**, *87* (8), 083506-3.
  86. Reyes-Reyes, M.; Kim, K.; Dewald, J.; Lopez-Sandoval, R.; Avadhanula, A.; Curran, S.; Carroll, D. L. Meso-structure formation for enhanced organic photovoltaic cells. *Org. Lett.* **2005**, *7* (26), 5749-5752.
  87. Smestad, G. P.; Krebs, F. C.; Lampert, C. M.; Granqvist, C. G.; Chopra, K. L.; Mathew, X.; Takakura, H. Reporting solar cell efficiencies in solar energy materials and solar cells. *Sol. Energy Mater. Sol. Cells* **2008**, *92* (4), 371-373.
  88. Bredas, J. L.; Beljonne, D.; Coropceanu, V.; Cornil, J. Charge-transfer and energy-transfer processes in pi-conjugated oligomers and polymers: A molecular picture. *Chemical Reviews* **2004**, *104* (11), 4971-5003.
  89. Krebs, F. C. *Polymer Photovoltaics: A Practical Approach*; SPIE Press, Bellingham: 2008.

- 
90. van Mullekom, H. A. M.; Vekemans, J. A. J. M.; Havinga, E. E.; Meijer, E. W. Developments in the chemistry and band gap engineering of donor-acceptor substituted conjugated polymers. *Mater. Sci. & Eng., R-Reports* **2001**, *32* (1), 1-40.
  91. Hou, J.; Chen, H.; Zhang, S.; Li, G.; Yang, Y. Synthesis, Characterization, and Photovoltaic Properties of a Low Band Gap Polymer Based on Silole-Containing Polythiophenes and 2,1,3-Benzothiadiazole. *J. Am. Chem. Soc.* **2008**, *130* (48), 16144.
  92. Liang, Y. Y.; Feng, D. Q.; Wu, Y.; Tsai, S. T.; Li, G.; Ray, C.; Yu, L. P. Highly Efficient Solar Cell Polymers Developed via Fine-Tuning of Structural and Electronic Properties. *J. Am. Chem. Soc.* **2009**, *131* (22), 7792-7799.
  93. Peet, J.; Kim, J. Y.; Coates, N. E.; Ma, W. L.; Moses, D.; Heeger, A. J.; Bazan, G. C. Efficiency enhancement in low-bandgap polymer solar cells by processing with alkane dithiols. *Nat. Mater.* **2007**, *6* (7), 497-500.
  94. Park, S. H.; Roy, A.; Beaupre, S.; Cho, S.; Coates, N.; Moon, J. S.; Moses, D.; Leclerc, M.; Lee, K.; Heeger, A. J. Bulk heterojunction solar cells with internal quantum efficiency approaching 100%. *Nature Photonics* **2009**, *3* (5), 297-2U5.
  95. Yu, C. Y.; Chen, C. P.; Chan, S. H.; Hwang, G. W.; Ting, C. Thiophene/Phenylene/Thiophene-Based Low-Bandgap Conjugated Polymers for Efficient Near-Infrared Photovoltaic Applications. *Chem. Mater.* **2009**, *21* (14), 3262-3269.
  96. Wienk, M. M.; Turbiez, M.; Gilot, J.; Janssen, R. A. J. Narrow-bandgap diketo-pyrrolo-pyrrole polymer solar cells: The effect of processing on the performance. *Adv. Mater.* **2008**, *20* (13), 2556-+.
  97. Wang, E. G.; Wang, L.; Lan, L. F.; Luo, C.; Zhuang, W. L.; Peng, J. B.; Cao, Y. High-performance polymer heterojunction solar cells of a polysilafluorene derivative. *Appl. Phys. Lett.* **2008**, *92* (3).
  98. Piliago, C.; Holcombe, T. W.; Douglas, J. D.; Woo, C. H.; Beaujuge, P. M.; Frechet, J. M. J. Synthetic Control of Structural Order in N-Alkylthieno[3,4-c]pyrrole-4,6-dione-Based Polymers for Efficient Solar Cells. *J. Am. Chem. Soc.* **2010**, *132* (22), 7595-7597.
  99. Hou, J. H.; Chen, H. Y.; Zhang, S. Q.; Chen, R. I.; Yang, Y.; Wu, Y.; Li, G. Synthesis of a Low Band Gap Polymer and Its Application in Highly Efficient Polymer Solar Cells. *J. Am. Chem. Soc.* **2009**, *131* (43), 15586.
  100. Chen, H. Y.; Hou, J. H.; Zhang, S. Q.; Liang, Y. Y.; Yang, G. W.; Yang, Y.; Yu, L. P.; Wu, Y.; Li, G. Polymer solar cells with enhanced open-circuit voltage and efficiency. *Nature Photon.* **2009**, *3* (11), 649-653.
  101. Blouin, N.; Michaud, A.; Gendron, D.; Wakim, S.; Blair, E.; Neagu-Plesu, R.; Belletete, M.; Durocher, G.; Tao, Y.; Leclerc, M. Toward a rational design of poly(2,7-carbazole) derivatives for solar cells. *J. Am. Chem. Soc.* **2008**, *130* (2), 732-742.

- 
102. Zhu, Z.; Waller, D.; Gaudiana, R.; Morana, M.; Muhlbacher, D.; Scharber, M.; Brabec, C. Panchromatic conjugated polymers containing alternating donor/acceptor units for photovoltaic applications. *Macromolecules* **2007**, *40* (6), 1981-1986.
  103. Alstrup, J.; Norrman, K.; Jørgensen, M.; Krebs, F. C. Lifetimes of organic photovoltaics: Design and synthesis of single oligomer molecules in order to study chemical degradation mechanisms. *Sol. Energy Mater. Sol. Cells* **2006**, *90* (17), 2777-2792.
  104. Manceau, M.; Rivaton, A.; Gardette, J. L.; Guillerez, S.; Lemaitre, N. The mechanism of photo- and thermooxidation of poly(3-hexylthiophene) (P3HT) reconsidered. *Polymer Degradation and Stability* **2009**, *94* (6), 898-907.
  105. Manceau, M.; Helgesen, M.; Krebs, F. C. Thermo-cleavable polymers: Materials with enhanced photochemical stability. *Polymer Degradation and Stability* **2010**, *95* (12), 2666-2669.
  106. Manceau, M.; Chambon, S.; Rivaton, A.; Gardette, J. L.; Guillerez, S.; Lemaitre, N. Effects of long-term UV-visible light irradiation in the absence of oxygen on P3HT and P3HT:PCBM blend. *Sol. Energy Mater. Sol. Cells* **2010**, *94* (10), 1572-1577.
  107. Manceau, M.; Gaume, J.; Rivaton, A.; Gardette, J. L.; Monier, G.; Bideux, L. Further insights into the photodegradation of poly(3-hexylthiophene) by means of X-ray photoelectron spectroscopy. *Thin Solid Films* **2010**, *518* (23), 7113-7118.
  108. Manceau, M.; Rivaton, A.; Gardette, J. L.; Guillerez, S.; Lemaitre, N. Light-induced degradation of the P3HT-based solar cells active layer. *Sol. Energy Mater. Sol. Cells* **2011**, *95* (5), 1315-1325.
  109. Manceau, M.; Bundgaard, E.; Carle, J. E.; Hagemann, O.; Helgesen, M.; Søndergaard, R.; Jørgensen, M.; Krebs, F. C. Photochemical stability of [small pi]-conjugated polymers for polymer solar cells: a rule of thumb. *J. Mater. Chem.* **2011**, *21* (12), 4132-4141.
  110. Tromholt, T.; Manceau, M.; Helgesen, M.; Carle, J. E.; Krebs, F. C. Degradation of semiconducting polymers by concentrated sunlight. *Sol. Energy Mater. Sol. Cells* **2011**, *95* (5), 1308-1314.
  111. Krebs, F. C.; Norrman, K. Analysis of the failure mechanism for a stable organic photovoltaic during 10000 h of testing. *Prog. Photovolt.* **2007**, *15* (8), 697-712.
  112. Lira-Cantu, M.; Norrman, K.; Andreasen, J. W.; Krebs, F. C. Oxygen release and exchange in niobium oxide MEHPPV hybrid solar cells. *Chem. Mater.* **2006**, *18* (24), 5684-5690.
  113. Bjerring, M.; Nielsen, J. S.; Nielsen, N. C.; Krebs, F. C. Polythiophene by solution processing. *Macromolecules* **2007**, *40* (16), 6012-6013.
  114. Bjerring, M.; Nielsen, J. S.; Siu, A.; Nielsen, N. C.; Krebs, F. C. An explanation for the high stability of polycarboxythiophenes in photovoltaic devices- A solid-state NMR dipolar recoupling study. *Sol. Energy Mater. Sol. Cells* **2008**, *92* (7), 772-784.
  115. Edder, C.; Armstrong, P. B.; Prado, K. B.; Frechet, J. M. J. Benzothiadiazole- and pyrrole-based polymers bearing thermally cleavable solubilizing groups as precursors for low bandgap polymers. *Chem. Comm.* **2006**, (18), 1965-1967.

116. Gevorgyan, S. A.; Krebs, F. C. Bulk heterojunctions based on native polythiophene. *Chem. Mater.* **2008**, *20* (13), 4386-4390.
117. Hagemann, O.; Bjerring, M.; Nielsen, N. C.; Krebs, F. C. All solution processed tandem polymer solar cells based on thermocleavable materials. *Sol. Energy Mater. Sol. Cells* **2008**, *92* (11), 1327-1335.
118. Helgesen, M.; Gevorgyan, S. A.; Krebs, F. C.; Janssen, R. A. J. Substituted 2,1,3-Benzothiadiazole- And Thiophene-Based Polymers for Solar Cells - Introducing a New Thermocleavable Precursor. *Chem. Mater.* **2009**, *21* (19), 4669-4675.
119. Krebs, F. C.; Spanggaard, H. Significant improvement of polymer solar cell stability. *Chem. Mater.* **2005**, *17* (21), 5235-5237.
120. Liu, J. S.; Kadnikova, E. N.; Liu, Y. X.; McGehee, M. D.; Frechet, J. M. J. Polythiophene containing thermally removable solubilizing groups enhances the interface and the performance of polymer-titania hybrid solar cells. *J. Am. Chem. Soc.* **2004**, *126* (31), 9486-9487.
121. Petersen, M. H.; Gevorgyan, S. A.; Krebs, F. C. Thermocleavable Low Band Gap Polymers and Solar Cells Therefrom with Remarkable Stability toward Oxygen. *Macromolecules* **2008**, *41* (23), 8986-8994.

## Chapter 2

# Synthesis of side chains for water processable polymers and fullerene for all water processed solar cells\*

## 2.1 Introduction

One of the major challenges in taking the organic solar cell from the laboratory and into actual production is to find new more environmentally friendly processing solvents to replace the existing toxic and carcinogenic ones like chlorobenzene, dichlorobenzene, chloroform, toluene, xylene, ect.. As pointed out in the introduction chapter, this should preferably be by some biodegradable compound such as simple alcohols or best of all water. In order for this to be possible, the physical properties of especially the active layer components, has to be modified in order to be soluble in such polar solvents. As the backbone of conjugated polymers are generally not very polar, something that is difficult to change, the most straight forward way of doing this is by substituting the normally hydrophobic solubilizing side chains with more hydrophilic chains that can coordinate to the polar solvents. Such polymers already exist. Water soluble analogues to poly(3-hexylthiophene) (P3HT) was first reported in 1987.<sup>[1]</sup> Introduction of sulfonic acid salts at the end of the side chains provided the solubility. Polymers employing the same principle for water solubility using different ions such as sulfonium,<sup>[2,3]</sup> pyridinium<sup>[4]</sup> or ammonium salts<sup>[5,6]</sup> and varying chain lengths have been reported and/or are commercially available (see Figure 2.1). Qiao *et al* have twice reported the use of the water-soluble polythiophene, sodium poly[2-(3-thienyl)-ethoxy-4-butylylsulfonate] (PTEBS) in hybrid solar cells with TiO<sub>2</sub> as the acceptor material.<sup>[7,8]</sup> In both cases the active layer was processed from aqueous solution containing small quantities of dimethylformamide (DMF) or ammonium hydroxide added in order to enhance the dissolution of the polymer. Using an initial device architecture of FTO|PTEBS:TiO<sub>2</sub>|gold (FTO: fluorine doped tin dioxide) they show the importance of barrier layers by increasing the efficiency from 0.04% to 0.17% by introducing a TiO<sub>2</sub> barrier layer between FTO and the active layer. The main effect of this was an increase in the fill factor which was doubled (0.38→0.8), but in both cases the current was quite low (0.12 mA and 0.17 mA). It is worth

\* Some of this work has been published and some patented:

Søndergaard, R.; Helgesen, M.; Jørgensen, M.; Krebs, F. C. *Adv. Energy Mater.* **2011**, *1* (1), 68-71

UK Patent Application No. 1016470.5 "Method of Making Optoelectric Devices

UK Patent Application No. 1016472.1 "Electron Transport Layer

UK Patent Application No. 1016568.9 "Improved ZnO Adhesion"



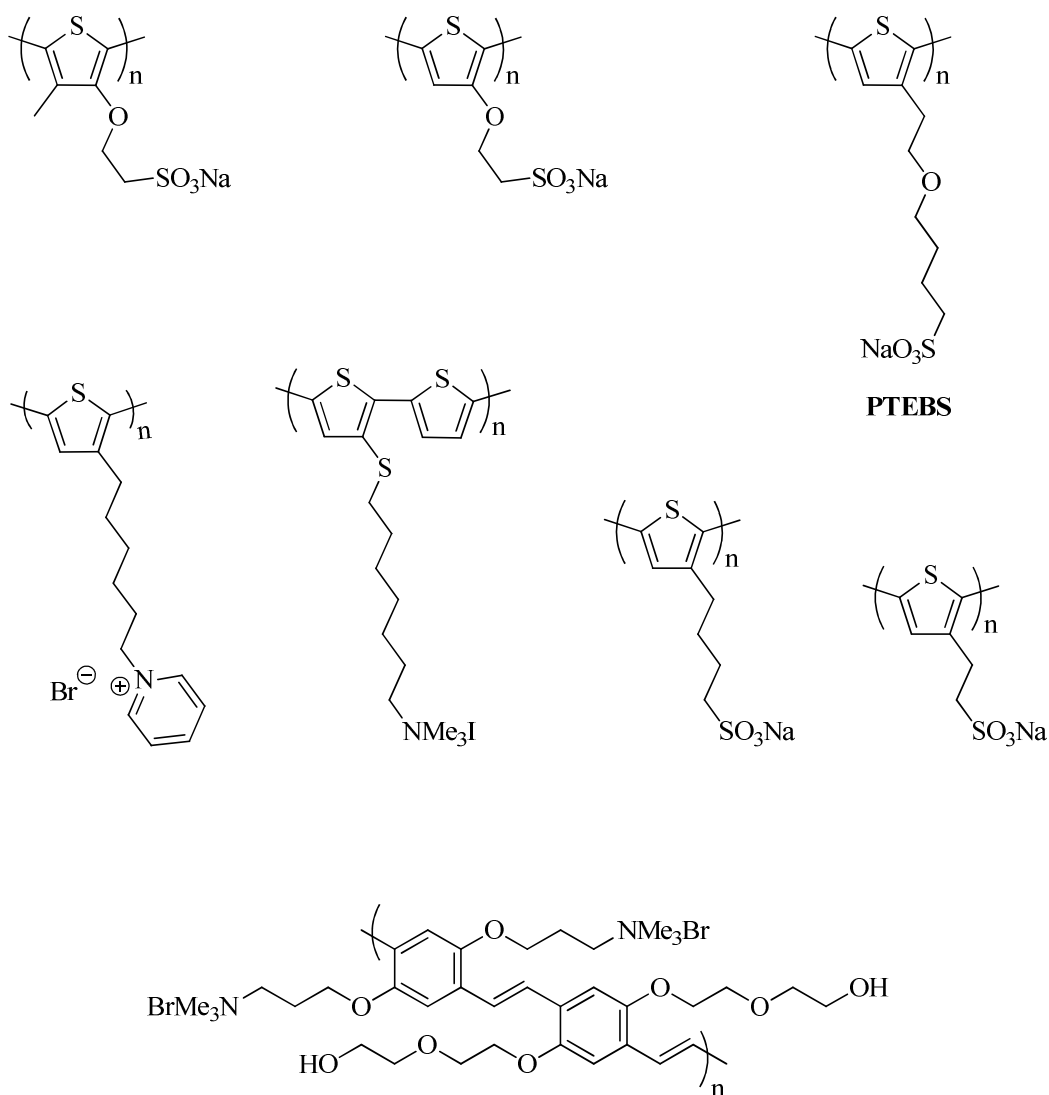


**Figure 2.1:** Overview of some of the existing watersoluble polymers.

mentioning though that the presented  $JV$ -curve is not very nice, and that the very high fill factor of 0.8 might need to be received with some skepticism.

An alternative approach was taken by Rud *et al* who also used PTEBS as polymer but single walled carbon nanotubes (SWNT) as acceptor material (FTO|PTEBS/SWNT|Aluminium).<sup>[9]</sup> Very low current and voltage were reported for this geometry ( $V_{oc}$ : 3 mV,  $I_{sc}$ : 15  $\mu A/cm^2$ ).

A general problem when aiming for processing of multiple layers from aqueous solutions is that the processing of new layers can dissolve/interact with previous ones. One way to circumvent this problem is to use thermocleavable materials in order to switch off the solubility of the polymer after processing by removal of the side chains. Another advantage of thermocleavable materials also is, that by

shedding the side chains the relative density of the chromophores goes up when the side chains evaporates. If an ionic thermocleavable side chain was prepared, this would not be possible because of the non-volatile nature of the ions. Furthermore the presence of such cleaved ionic chains within the active layer could pose potential problems because of the hygroscopic nature of such compounds.

As an alternative to ionic side chains the choice in this work therefore fell on preparing different types of thermocleavable side chains carrying both ethylene glycol moieties, well known for their good coordination to water, as well as free alcohols in order to promote coordination to more polar solvents. Generally all coupling methods used for polymer preparation (Suzuki, Stille, Nigishi, Heck, ect.) lead to the formation of salts during the coupling process, which are afterwards removed by washing with polar solvents. This poses a potential problem in the synthesis of water soluble polymers, as the polymers themselves are soluble in the solvents used to remove the salts. In order to circumvent this and other potential problems associated with workup of polar polymers, it was chosen that the strong hydrophilicity should to be introduced as a final step, thus enabling the use of normal workup procedures for conjugated polymers. In order to do so all free alcohol groups were to be protected by the highly hydrophobic *tert*-butyldimethylsilane (TBDMS) groups which can easily be removed by treatment with *tert*-butylammonium fluoride (TBAF). Because of its amphiphilic character TBAF can be dissolved and thus removed by a variety of different solvents. As shown in Figure 2.2 this approach allows for a multitude of different stages, each with different physical properties, which potentially opens up several applications. In order to keep the structure of the final polymer as simple as possible the ‘main skeleton’ of the previously mentioned thermocleavable polymer, P3MHOCT, was chosen, with the only differences in the

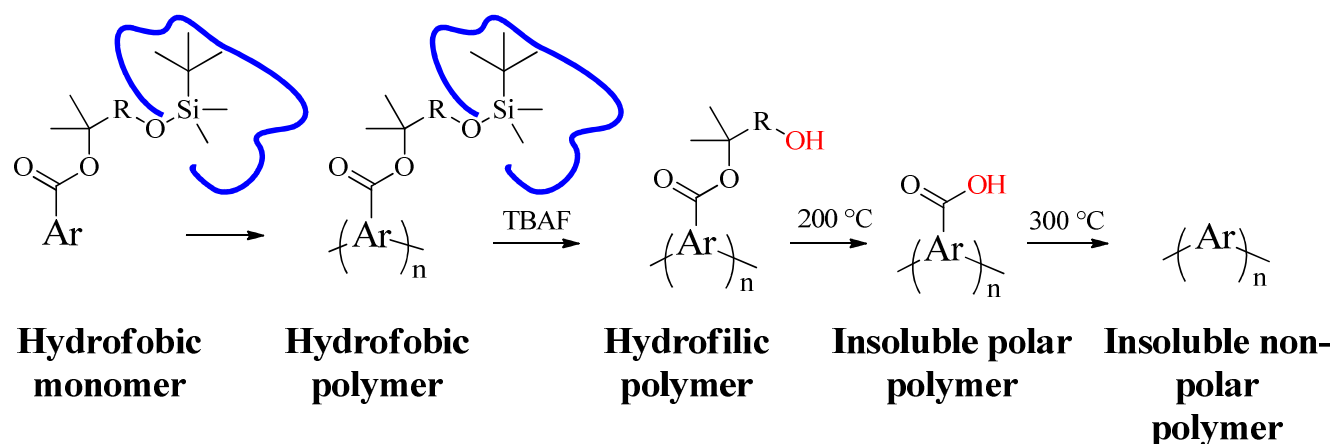


**Figure 2.2** Retro-synthetic approach of how to overcome the potential problems of workup using the highly lipophilic protecting group TBDMS.

prepared polymer being the side chains. This grants the possibility to make a direct comparison of a processed solar cell with those of P3MHOCT, as the polymers after thermocleavage of the side chains should be identical.

## 2.2 Synthesis of polymer side chains with potential for good coordination with polar solvents

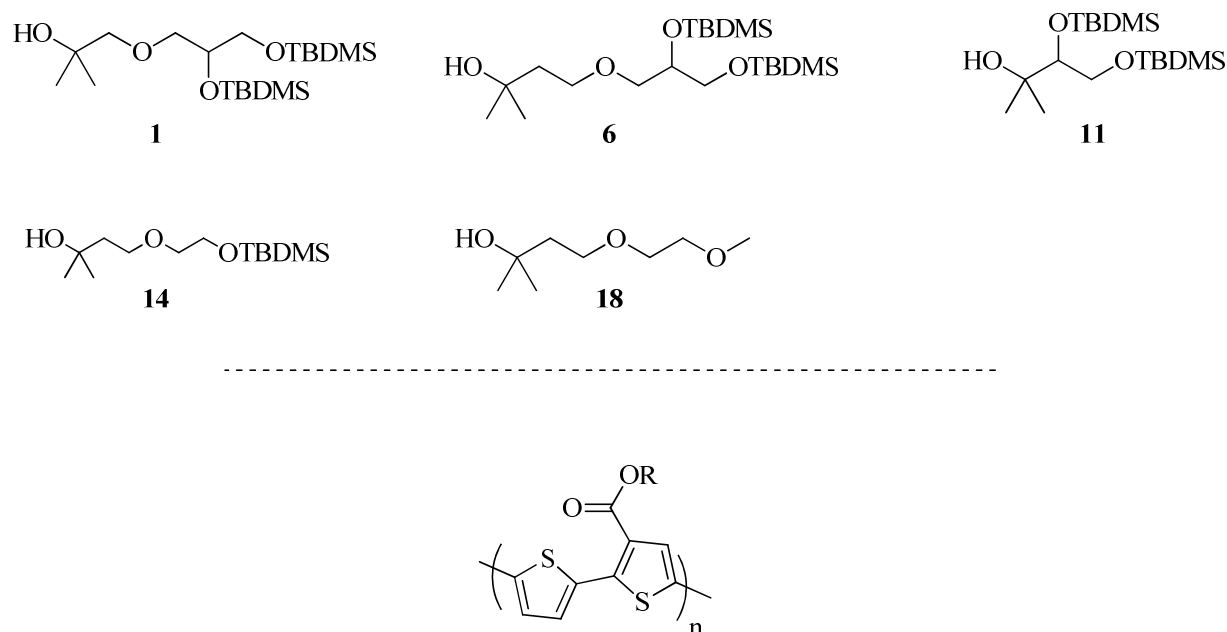


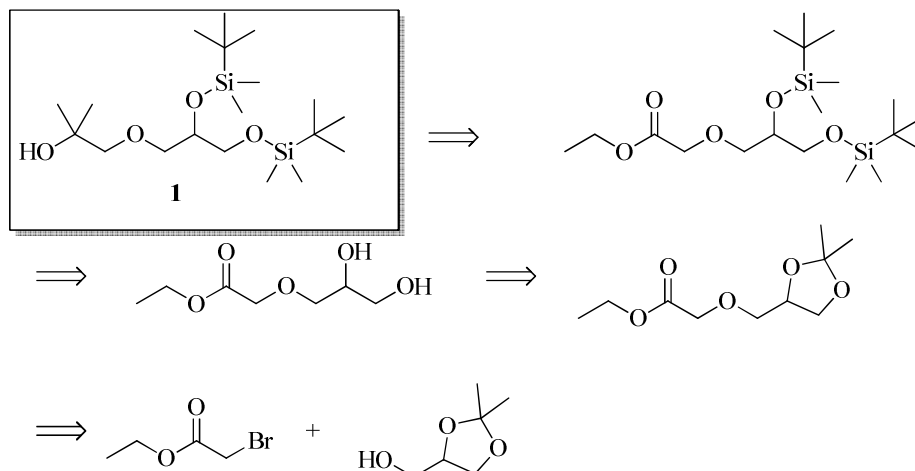
**Figure 2.3** Overview of the tertiary alcohol side chains synthesized and the aimed polymers (R being the different tertiary alcohols)

As illustrated in Figure 2.3, the goal was to prepare different polymers having the same basic structure but with side chains varying in length, bulkiness and number of protected alcohols (potential free alcohols). Such variety allows for comparing which side chains that are the most suitable for aqueous processing of the final polymers.

One of the main challenges in synthesizing water soluble side chains is in fact, that so many of the general techniques and cleaning procedures in organic synthesis rely on the removal of impurities by washing an organic phase with water, and that the compounds themselves can be extracted from water with organic solvents. In the synthesis of such compounds it is therefore often just as important, if not more, to reflect on how to isolate the compound, than on the actual synthesis. It can be incredibly frustrating to know that the right compound is in the ‘soup’, but it is just not possible to separate it from

the rest. Experimental details and synthetic procedures are described in the experimental section (2.6) at the end of this chapter.

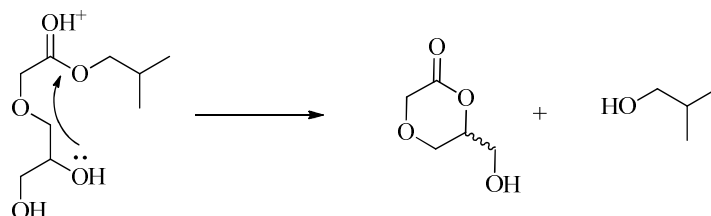
### 2.2.1 Synthesis of 1-(2,3-bis((*tert*-butyldimethylsilyl)oxy)propoxy)-2-methylpropan-2-ol



**Scheme 2.1** Retro-synthetic pathway for the preparation of the tertiary alcohol **1**

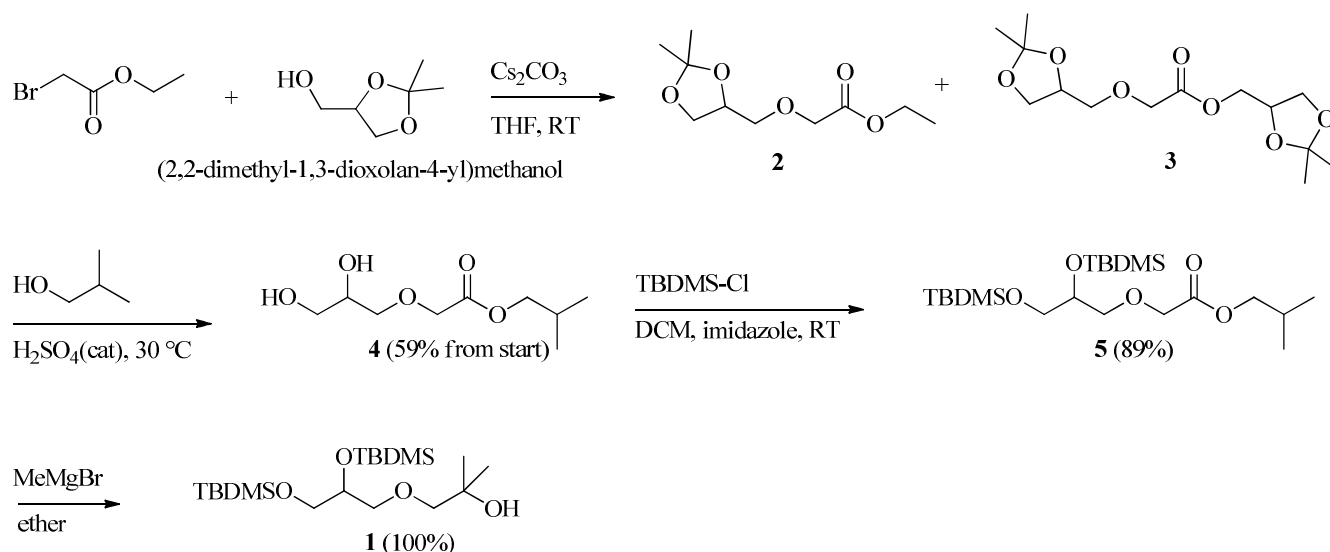
The initial strategy for the preparation of the tertiary alcohol **1** is illustrated in the retro synthesis in Scheme 2.1 and the actual synthetic pathway is outlined in Scheme 2.2. The first reaction between 2-bromoethyl acetate (Br-AcOEt) and 2,2-dimethyl-1,3-dioxolan-4-yl)methanol (solketal) poses several problems because the use of a base is necessary in order to promote nucleophilic attack of the alcohol. A multitude of side reactions can occur such as Claisen condensation and transesterification. Also the base must not be a good nucleophile as it would then react with Br-AcOEt.  $K_2CO_3$  and  $Cs_2CO_3$  were tested at different temperatures, and  $Cs_2CO_3$  at room temperature (RT) showed to be the best choice – probably because of the more soft character of the  $RO-Cs^+$  which promotes nucleophilic attack on the soft C-Br instead of on the harder carbonyl group (according to the HSAB principle). It was not possible to avoid transesterification completely, but by keeping the temperature at RT it was possible to avoid any significant Claisen condensation. The two major products were the desired compound **2** and compound **3**, the latter having undergone transesterification of ethanol with solketal in addition to the desired  $S_N2$ -reaction. These two compounds can be separated by column chromatography, but the procedure is very tedious. Instead it was chosen to proceed to the next reaction without separation in a step where both compound **2** and **3** are transformed into the same compound **4**. By performing the acid catalyzed deprotection of the dioxolanes in *iso*-butanol, deprotection of both compound **2** and **3** occurs and they are

simultaneously transformed into the identical corresponding isobutyl ester **4**. This transesterification step furthermore aided in the workup because of the more hydrophobic properties of *iso*-butanol compared to ethanol. Compound **4** was shown to be extremely sensitive to acidic media as it ring closes even in chloroform (see Figure 2.4).

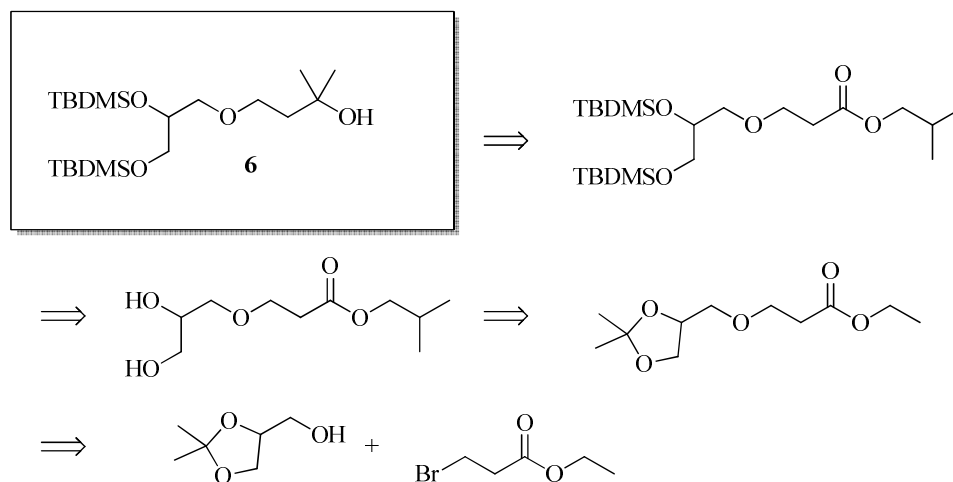


**Figure 2.4** Undesired ring closure reaction of compound **4**

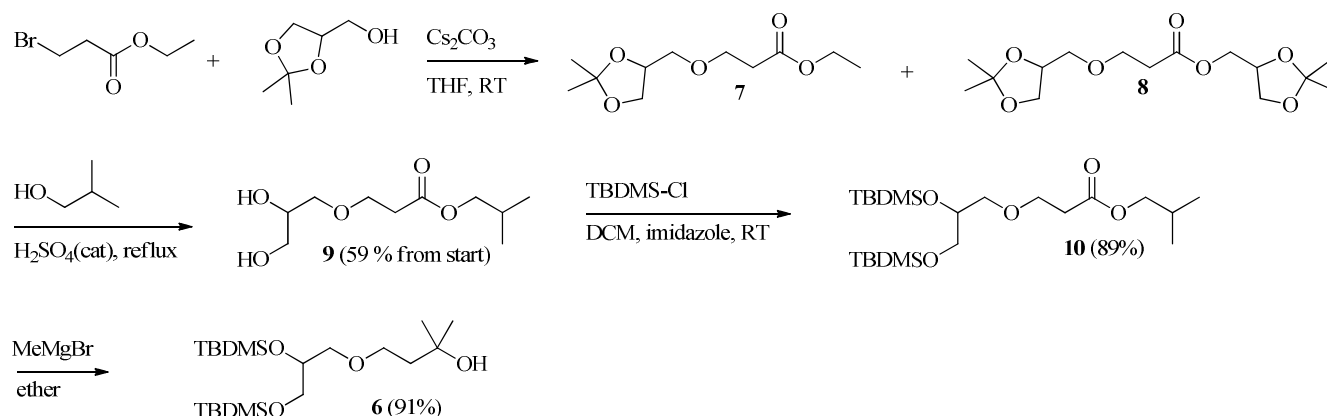
Besides compound **4**, 2-bromoacetic acid isobutyl ester, which is the product of transesterification of unreacted Br-AcOEt, was isolated (19%), showing that the reaction could potentially be further optimized. Double TBDMS protection of the alcohols in compound **4** afforded compound **5** in good yield and subsequent reaction with methyl magnesium bromide afforded the tertiary alcohol **1** quantitatively.



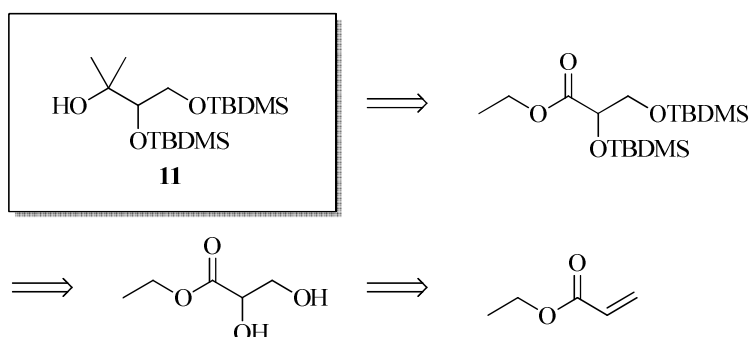
**Scheme 2.2** Synthetic pathway in the preparation of tertiary alcohol **1**

2.2.2 Synthesis of 4-(2,3-bis((*tert*-butyldimethylsilyl)oxy)propoxy)-2-methylbutan-2-olScheme 2.3 Retro-synthetic pathway for the preparation of the tertiary alcohol **6**

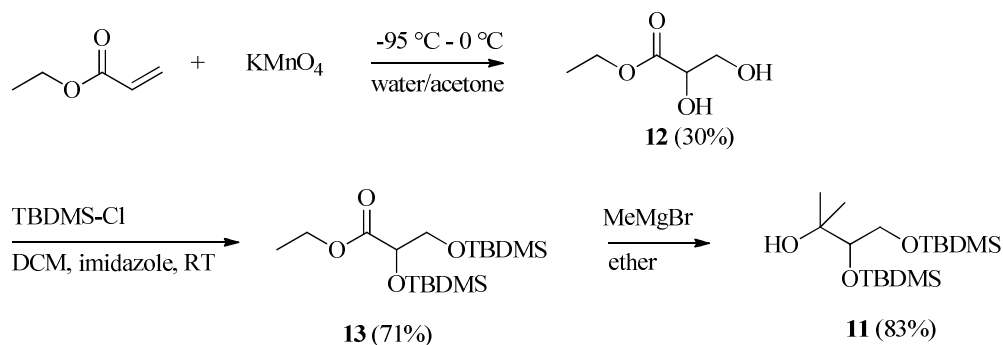
This compound, differing from compound **1** only by having an extra methylene group, was synthesized from 3-bromoethyl propionate and solketal as starting materials using a strategy very similar to the one used for compound **1** as shown in Scheme 2.3. The outline of the synthetic approach is shown in Scheme 2.4. Initial treatment of the starting materials with  $\text{Cs}_2\text{CO}_3$  yielded a mixture of **7** and **8**, which was treated with *iso*-butanol in the presence of catalytic amount of acid in order to deprotect the dioxolanes and simultaneously transform both compounds into the corresponding *iso*-butylester **9** which facilitates workup and separation from the glycerol formed by deprotection of the liberated solketal. Double TBDMS-protection of **9** afforded **10** almost quantitatively and subsequent treatment with methylmagnesium bromide afforded the tertiary alcohol **6**.

Scheme 2.4 Synthetic pathway in the preparation of tertiary alcohol **6**

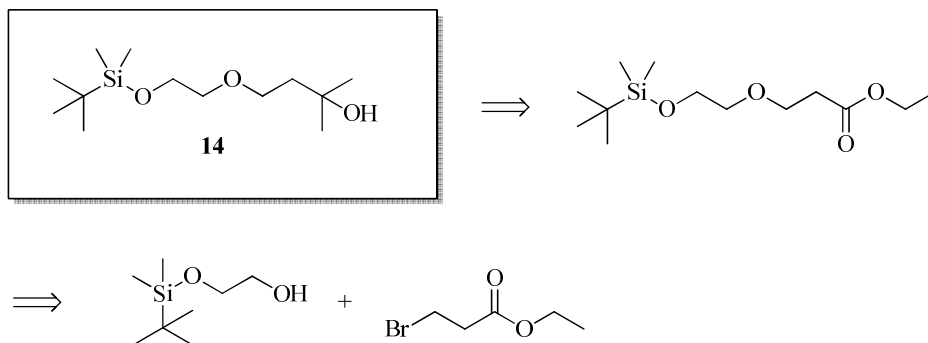
## 2.2.3 Synthesis of 3,4-bis((tert-butyldimethylsilyl)oxy)-2-methylbutan-2-ol

Scheme 2.5 Retro-synthetic pathway for the preparation of the tertiary alcohol **11**

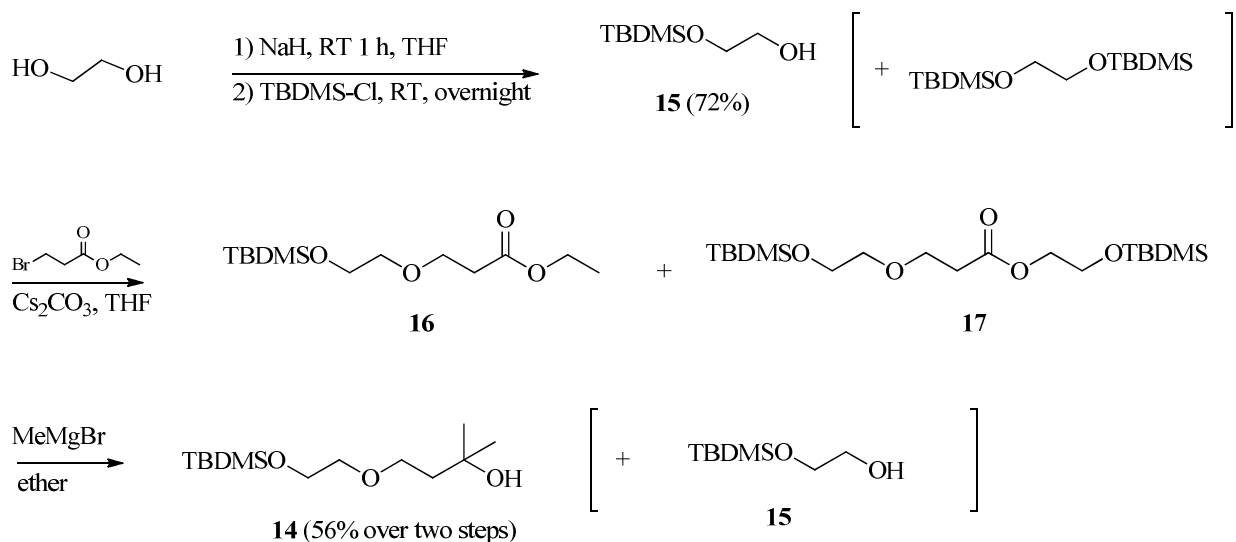
In order to have a shorter side chain compound **11** was synthesized as shown in Scheme 2.6. Initial treatment of ethyl acrylate with  $\text{KMnO}_4$  to produce ethyl glycerate **12** was performed according to the procedure reported by Choi *et al.*<sup>[10]</sup> but differing on two points. The starting temperature was  $-95\text{ }^\circ\text{C}$  instead of  $-78\text{ }^\circ\text{C}$ , and the extracted diol was in this case washed with water in order to remove salts. The yield is somewhat lower than the one reported from Choi *et al.* (50%), which can probably be explained with the washing of the ethyl acetate extract, as the highly polar diol can be removed by water. A second attempt to increase the yield was not performed. The ethyl glycerate was subsequently reacted with TBDMS-Cl to yield the protected compound **13** which upon reaction with methylmagnesium bromide gave the desired tertiary alcohol **11** in good yield.

Scheme 2.6 Synthetic pathway in the preparation of tertiary alcohol **11**

## 2.2.4 Synthesis of 4-(2-((tert-butyldimethylsilyl)oxy)ethoxy)-2-methylbutan-2-ol

Scheme 2.7 Retro-synthetic pathway for the preparation of the tertiary alcohol **14**

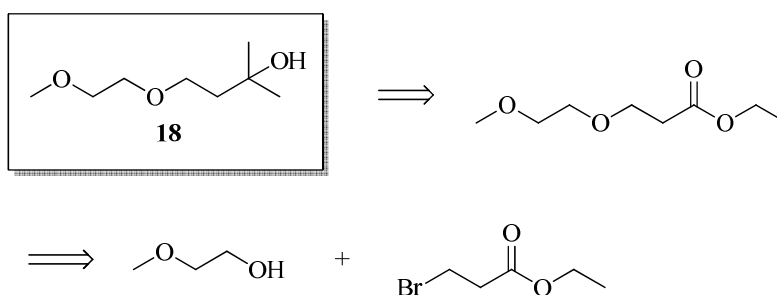
In order to examine the influence of the presence of alcohols in the side chains, a straight analogue with only one potential free alcohol, compound **14**, was prepared as outlined in Scheme 2.7 and Scheme 2.8. Following a slightly modified procedure to the one described by McDougal *et al.*,<sup>[11]</sup> mono-silylation of ethylene glycol anions (pre-prepared by mixing glycerol and sodium hydride) with TBDMS-Cl to give compound **15** was performed in good yield. The original procedure describes workup by flash chromatography but several attempts to recreate the original results failed because of contamination of the di-silylated ethylene glycol. If completely pure compound was to be obtained the yield dropped considerably. The pure compound **15** was instead isolated by microdistillation thus avoiding the disilylated byproduct. The reaction conditions were also changed from equivalent amounts of each

Scheme 2.8 Synthetic pathway in the preparation of tertiary alcohol **14**



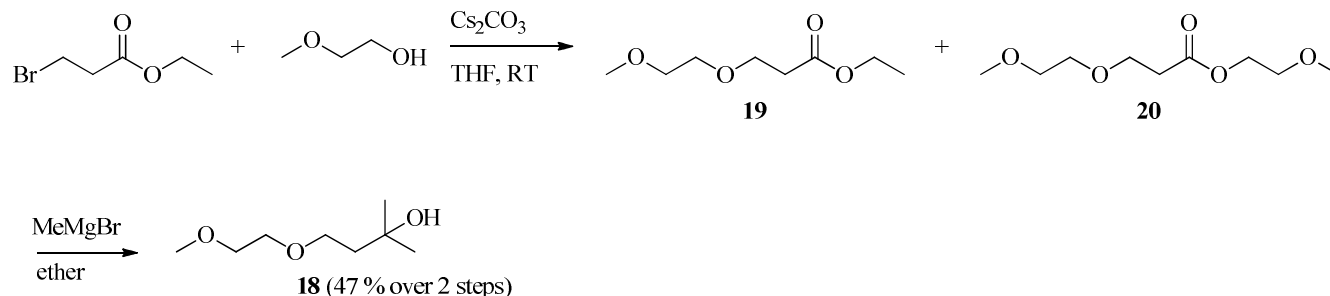
reactant to excess of glycerol anion in order to minimize the amount of formed disilylated product. Compound **15** was subsequently reacted with ethyl 3-bromopropionate using  $\text{Cs}_2\text{CO}_3$  as base and as previously this reaction led to a mixture of two major products **16** and **17**, the desired product and the desired product having undergone transesterification, respectively. The mixture was reacted with methylmagnesium bromide to give the same product as the desired tertiary alcohol **14**. The amount of compound **15** that had been subject to transesterification could be recuperated during workup.

### 2.2.5 Synthesis of 4-(2-methoxyethoxy)-2-methylbutan-2-ol



**Scheme 2.9** Retro-synthetic pathway for the preparation of the tertiary alcohol **18**

Compound **18** was synthesized as an analogue to compound **14**, being methylated at the otherwise free alcohol, in order to be able to compare the differences in solubility with and without a free alcohol group. Reaction of methylethyleneglycol and 3-bromoethylpropionate with  $\text{Cs}_2\text{CO}_3$  in THF yielded mixture of **19** and **20** which were further reacted with methylmagnesium bromide without separation, yielding the desired tertiary alcohol **18**.



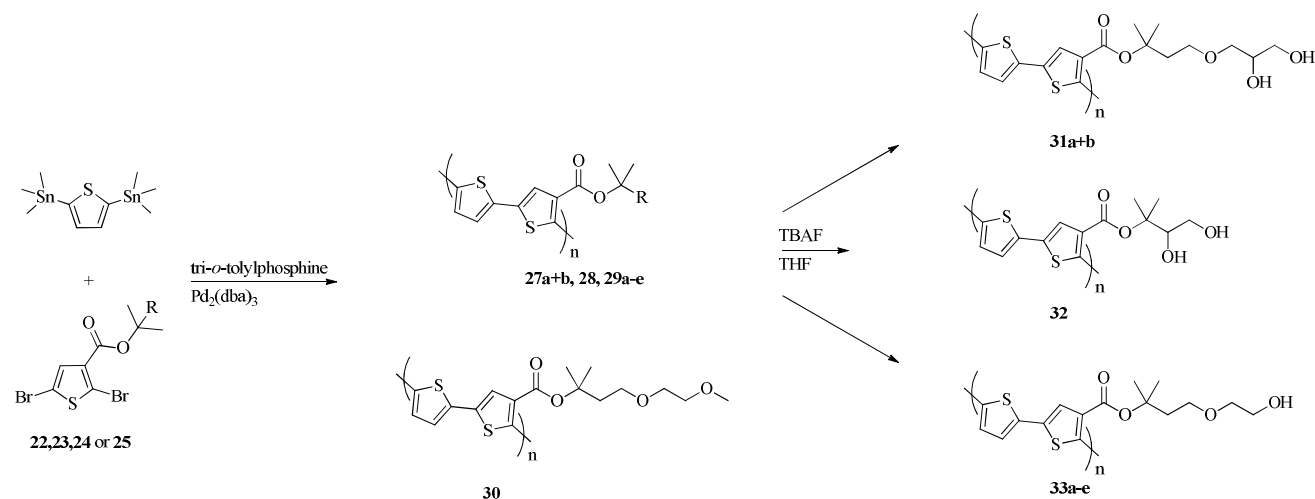
**Scheme 2.10** Synthetic pathway in the preparation of tertiary alcohol **18**



affinity for oxygen, an attempt to perform the coupling between **21** and **14** without scandium was carried out, because purity is of greater importance than high yield. Surprisingly this reaction not only gives products that can easily be purified, but the yield (93%) even largely exceeded the best result from preparation with scandium (57%), where repeated chromatographic workup was necessary. Further test reactions confirm (not described in this thesis) that generally it is not necessary to use scandium when the carboxylic acid is attached to a thiophene compound, whereas it *is* necessary when the acid is attached to a benzene ring. Compound **6**, **11**, **14** and **18** were coupled with compound **21** to give the corresponding tertiary esters in good yield as shown in Scheme 2.11. Compound **1** was never used in the preparation of monomer/polymers, mainly because of its close resemblance to compound **6**.

### 2.3.2 Synthesis of polymers and solubility tests

All polymers were synthesized using Stille cross-coupling between of 2,5-bis(trimethylstannyl)thiophene and the 2,5-dibromothiophene tertiary esters **22-25** as shown in Scheme 2.12 leading to the polymer **27-30**. Subsequent deprotection of the polymer **27-29** by treatment with *tert*-butylammonium fluoride (TBAF) led to the polymers **31-33** which carries free alcohol groups. Interesting enough, all polymers precipitated to some extent from the THF solution and workup could in some cases be performed by filtering the polymer and washing with THF in order to remove the *tert*-butylammonium salts. In cases where the polymers were still partially soluble, precipitation was performed by addition to ethyl acetate (AcOEt), followed by washing of the solid with *iso*-propanol.



**Scheme 2.12** Polymerization by Stille cross-coupling leading to polymer **27-30**. Subsequent deprotection of the TBDMS-groups of **27-29** in 1M *tert*-butylammonium fluoride led to the polymers **31-33**. The notation **a-e** corresponds to different batches of the polymers.

**Table 2.1** Size distribution of the polymers **27-30** and the calculated 'Mw' for the polymers **31-33** assuming complete deprotection from the corresponding TBDMS-protected polymers.

Protected polymers				Hydrophilic polymers
Polymer	Mw	Mn	PD	Calculated 'Mw'
<b>27a</b>	40856	15314	2.67	<b>31a</b> : 25184
<b>27b</b>	38881	14692	2.60	<b>31b</b> : 23966
<b>28</b>	38525	15437	2.50	<b>32</b> : 22748
<b>29a</b>	11435	4327	2.6	<b>33a</b> : 8551
<b>29b</b>	56263	18741	3.0	<b>33b</b> : 42072
<b>29c</b>	24044	10649	2.2	<b>33c</b> : 17979
<b>29d</b>	40347	17245	2.3	<b>33d</b> : 30170
<b>29e</b>	28711	9942	2.88	<b>33e</b> : 21469
<b>30</b>	44206	19543	2.3	

The size distributions of the polymers **27-30** were determined by size exclusion chromatography (SEC) and are shown in Table 2.1. The exact distributions of polymers **31-33** have not been tested, as no appropriate solvents were available for SEC, but are assumed to be the result from complete deprotection of polymers **27-29**. Initial testing of the potential water-solubility of the polymers started with a quite small batch of polymer **33a** which on the very first attempt showed to be soluble in water when added as a suspension in THF directly from the reaction mixture from deprotection of polymer **29a**. Unfortunately the following attempts to reproduce the solubility in water failed when preparing batches with higher molecular weights. The initial solubility in water by **33a** was ascribed to the small molecular size of the polymer, but as attempts to control the size during polymerization proved to be very difficult, the polymer was discarded.

Generally the polymers **33b-e** were insoluble in all pure solvents tested (MeOH, THF, acetone, water, *iso*-propanol, CHCl<sub>3</sub>, dioxane, DMF, ethylene glycol) except for DMSO and DMF or mixtures containing DMSO. Because of its potential as an oxidizing agent, DMSO is generally not considered a suitable solvent for processing of solar cells. The polymer **30** which in many ways should resemble polymer **33** with the only difference being the lacking free alcohol, which is here methylated showed to be completely soluble in THF and DMF, moderately soluble in DMSO and very slightly soluble in ethanol. Attempts to mix THF and other solvents also failed.

Similar disappointing result was achieved with polymer **32** which was only very slightly soluble in THF, soluble in DMF and slightly soluble in DMSO. Fortunately more success was achieved with polymer **31**. Again the polymer was insoluble in most pure solvents except for DMSO and DMF, but was amazingly also soluble in a mixture of equal amounts water and *iso*-propanol when a little THF was present (down to 4% Vol.). The major part of the solubility tests performed is shown in table 2.2.

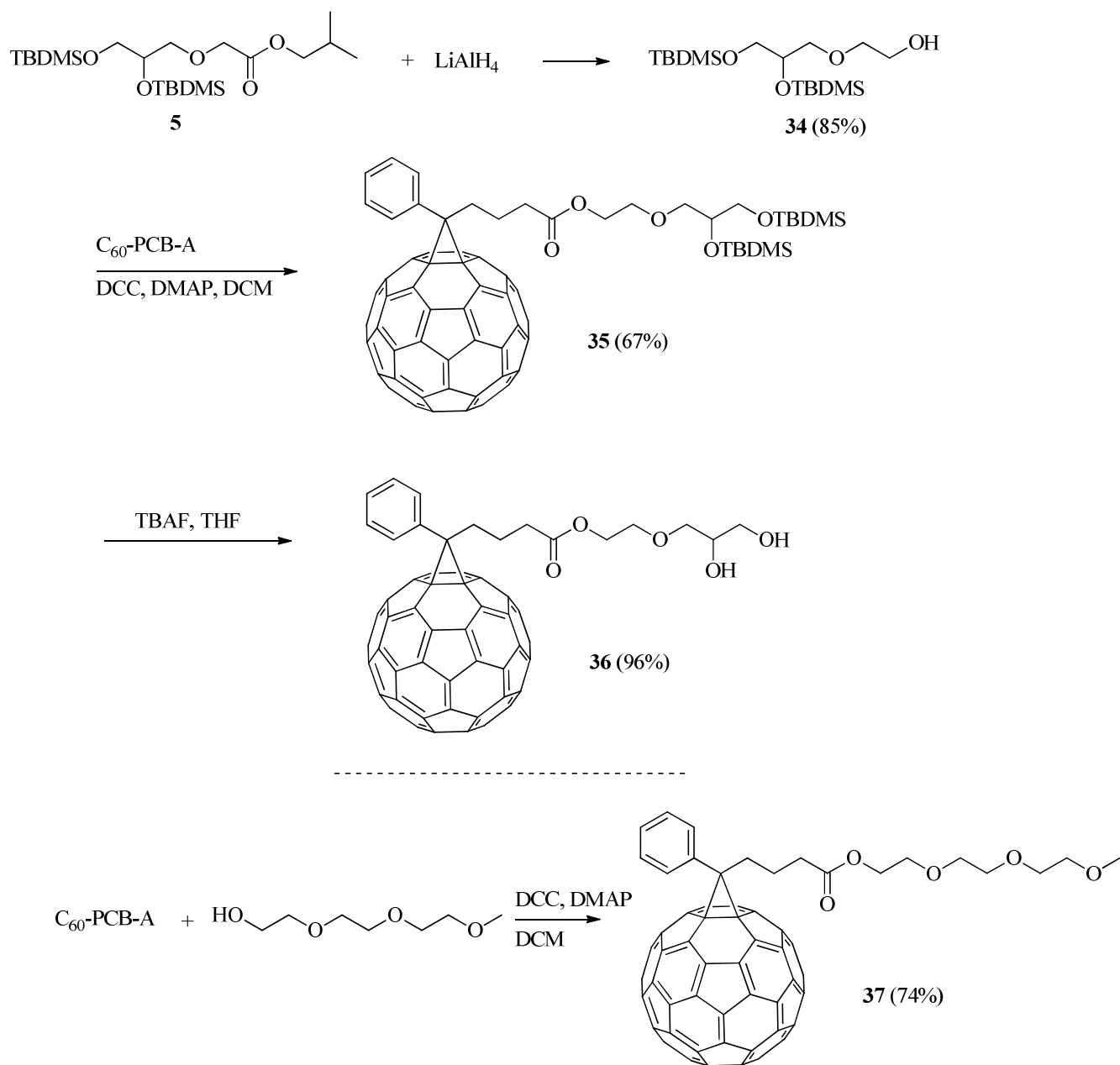
**Table 2.2:** Solubility tests performed on polymer 30-33.

		Polymer				
		30	31	32	33a	33b-e
Solvent	CHCl <sub>3</sub>	S	-	-	-	-
	THF	S	VSS	VSS	-	-
	DMF	S	S	S	nd	S
	DMSO	SS	S	SS	nd	S
	Dioane	-	-	-	nd	-
	Acetone	-	-	-	nd	-
	Ethylene glycol	-	-	-	nd	-
	<i>iso</i> -propanol	-	-	-	nd	-
	ethanol	VSS	-	-	nd	-
	methanol	-	-	-	nd	-
	H <sub>2</sub> O	-	-	-	nd	-
	IP/THF	SS	VSS	-	nd	-
	H <sub>2</sub> O/THF	SS	-	-	S	-
	H <sub>2</sub> O/IP + 4% THF	-	S	-	-	-

**nd:** not determined, **-** : not soluble, **vss:** very slightly soluble, **ss:** slightly soluble, **s:** soluble. **IP:** *iso*-propanol

### 2.3.3 Synthesis of fullerenes for processing of solar cells

In order to prepare a bulk heterojunction solar cell from aqueous solution the acceptor material in the heterojunction as well as the polymer donor need to be processable from such solvents. This is not possible with the commonly used PCBM but it was envisaged that it might be possible using an analogue to PCBM carrying a different ester substituent. Facing the previously mentioned problems of potential



**Scheme 2.13** Synthetic pathways to new fullerenes

removal of already processed layers in an all water based process, a thermocleavable analogue would be preferable. However, after several failed attempts it was instead chosen to prepare a primary analogue to compound **1** as shown in Scheme 2.13, thus enabling the simple coupling with a commercial free acid analogue to PCB, C<sub>60</sub>-PCB-A. Reduction of compound **5** with LiAlH<sub>4</sub> provided the desired alcohol **34**, which was subsequently reacted in a DCC-coupling with PCB-A to give fullerene **35** in acceptable yield as

shown in Scheme 2.13. Unfortunately the deprotected compound **36** was shown to be insoluble in all solvents tested except for DMSO. After dissolving in this solvent water/*iso*-propanol can be added, but as mentioned earlier DMSO is considered as a poor candidate for processing, and compound **36** was discarded as acceptor material.

A new approach was then chosen. As many of the insolubility issues was found to correlate with the presence of free alcohols in the side chains it was instead chosen to use a simple polyether with no free alcohols. Expecting such to be insoluble in water (which allows for subsequent processing) but still containing a good water coordinating side chain, the thought was that the fullerene if mixed with an aqueous solution from a solvent miscible with water, it might be possible to create a micelle or cluster like dispersion that would allow for processing. The inspiration to this was found in a previous work by Deguchi *et al.* who have shown it possible to create monodisperse clusters of C<sub>60</sub> (60 nm) in water through forced precipitation by addition of a THF-solution into water.<sup>[13]</sup>

The fullerene **37** (se Scheme 2.13) containing an ester substituent of triethyleneglycol mono methyl ether to promote coordination to water was therefore prepared from commercial C<sub>60</sub>-PCB-A and triethyleneglycol mono methyl ether by coupling with N,N'-dicyclohexylcarbodiimide (DCC). The purified fullerene was soluble in polar aprotic solvents (DMF, DMSO, and THF).

#### 2.3.4 General discussion of the observed solubilities

The general insoluble behavior of the polymers **31-33** and the fullerene **36**, carrying free alcohol containing side chains, except for in polar aprotic solvents, here especially DMSO and DMF, was a somewhat surprising result. It is just as surprising that as little as 4% THF can make the difference between polymer **31** being completely insoluble in water/*iso*-propanol to make it soluble enough for solar cell preparation. Somehow the amphiphilic properties of the polymer, with a lipophilic backbone and hydrophilic side chains, must be locked in a solid state which can only be separated/dissolved in a very specific environment. The fact that also the fullerene **36** exhibits a general non soluble behavior, except in DMSO, supports this hypothesis. Observing the difference in color of the solutions of the different polymers furthermore suggests that the polymers enter a 'micelle' like or aggregated conformation when the polarity of the solvent reaches a certain state. Where the general color of solutions of P3MHOCT and the polymers **27-30** is bright orange, solutions of the polymers **31-33** are all dark deep red. The same deep red color is observed for polymer **30** when this is dissolved in DMSO, DMF, THF/*iso*-propanol and in THF/water as shown in Figure 2.5.

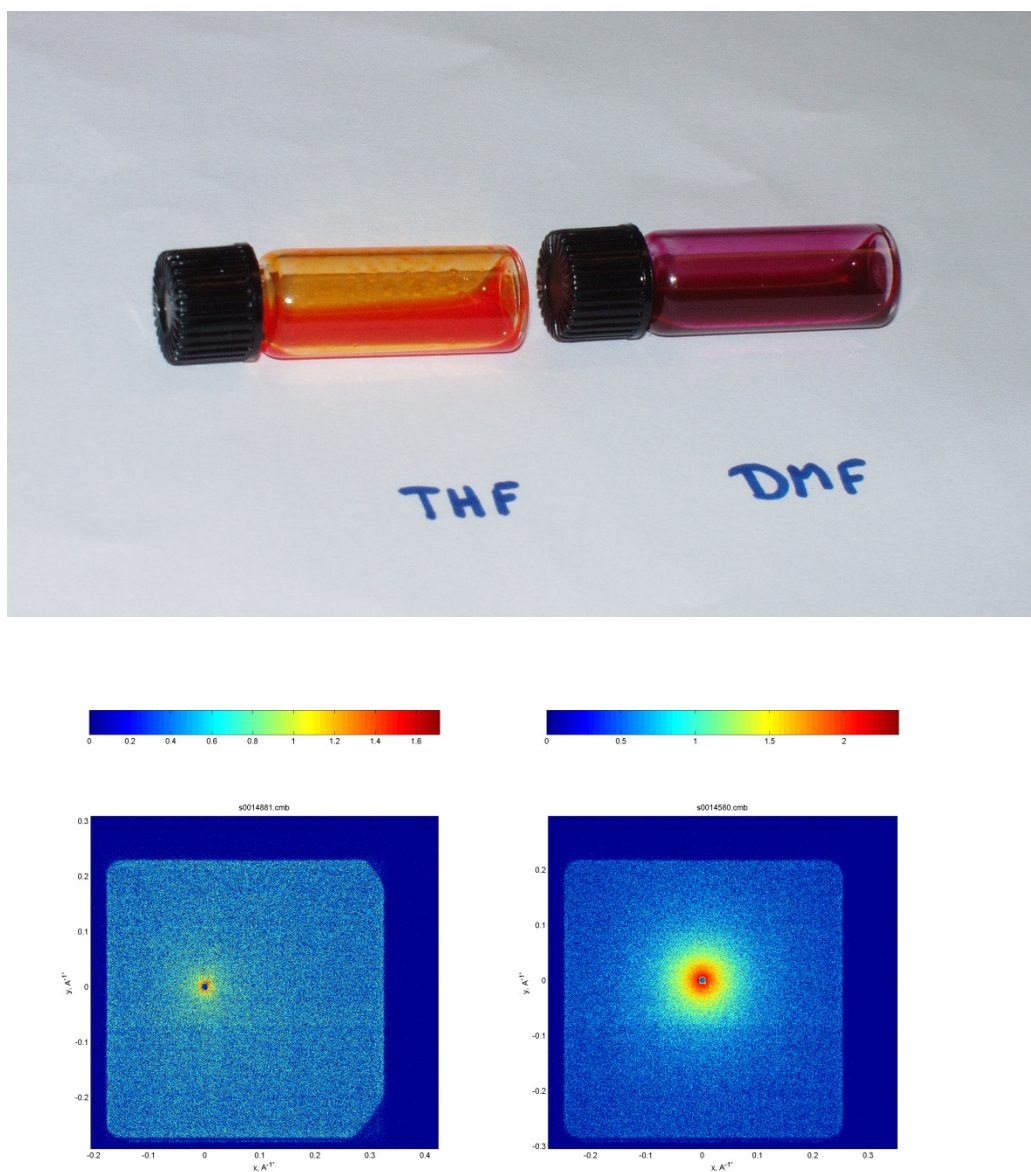


**Figure 2.5:** top: Color difference of polymer **30** in THF and DMF. bottom: Small-angle X-ray scattering of compound **27a** in THF (left) and compound **31a** in water:isopropanol:THF, 47:47:6 (right).

This suggests that more aggregated forms are present in the very polar solutions. In order to examine this hypothesis, small angle X-ray scattering (SAXS) (Figure 2.5) of solutions of polymer **27a** (before removal of the protecting group) in THF and polymer **31a** (free alcohol) in water:isopropanol: THF (47:47:6) were performed. As indicated in Table 2.1 the size of polymer **27a** ( $M_w$ : 40800) is considerably larger than for



polymer **31a** ( $M_w$ : 25000) and if no aggregation is present this should lead to stronger scattering at small angles. In reality the opposite is observed. Whereas almost no scattering is observed for the larger **27a**, clear scattering is found for the smaller polymer **31a**. This implies that the explanation of aggregates in dispersion contrary to solvated molecules is a reasonable suggestion.

## 2.4 Device fabrication of all water processed solar cells

Of the prepared compounds only polymer **31** and fullerene **37** showed potential for preparation of aqueous processed solar cells. Inverted polymer solar cells (substrate | ITO | ZnO | active layer | PEDOT | Ag) were prepared on ITO-substrates. The electron transport layer (ETL) was zinc oxide doped with aluminium obtained as a dispersion of nanoparticles in aqueous solution (see experimental section). The ink can be spin coated or roll-to-roll slot-die coated. An important step is that the initially dry film must be heated for 5-40 minutes at 140 °C to yield charge transporting films. After this treatment the ZnO layer is insoluble and subsequent processing is then possible.

The active layer was prepared by mixing equal amounts of solutions of polymer **31** (15 mg ml<sup>-1</sup> in 47.5% water, 47.5% *iso*-propanol and 5% THF) and the fullerene **37** (15 mg ml<sup>-1</sup> in THF) just prior to spincoating. A thermal treatment (310 °C for approximately 10 s) removed the solubilizing side chains of the polymer leaving an insoluble film. The duration of the thermal treatment is quite critical, as both shorter and longer periods led to a decrease in efficiency of the final devices. This is probably due to either incomplete decarboxylation or some degradation.

The hole transport layer (HTL) was prepared from an aqueous dispersion of PEDOT:PSS diluted with *iso*-propanol that was coated on top of the ZnO/Polymer:Fullerene stack. After heating for 5 min at 140 °C further processing was possible and the device was completed by printing a silver electrode from a paste comprising only silver flakes, water and an aqueous binder. In a final step protection of the electrodes was carried out by encapsulation using a simple food packaging barrier. All preparative steps were carried out in air. Pictures of the printing process and aqueous solutions are shown in figure 2.5. Devices with areas of 0.5 cm<sup>2</sup> gave efficiencies of 0.4-0.7 % with excellent stability during storage and operation under ambient conditions when encapsulated using the simple food packaging barrier. The *J-V* characteristics of a representative of the best performing cells are:  $V_{oc}$ : 0.49 V,  $I_{sc}$ : 2.23 mA, FF: 32% and PCE: 0.70%. In comparison devices prepared with the well-known P3HT:PCBM materials combination showed performances of 1.6-2% when processing the active layer (P3HT:PCBM) from chlorobenzene, while using aqueous processing for all the other layers (ZnO, PEDOT:PSS and silver back electrode). These results are

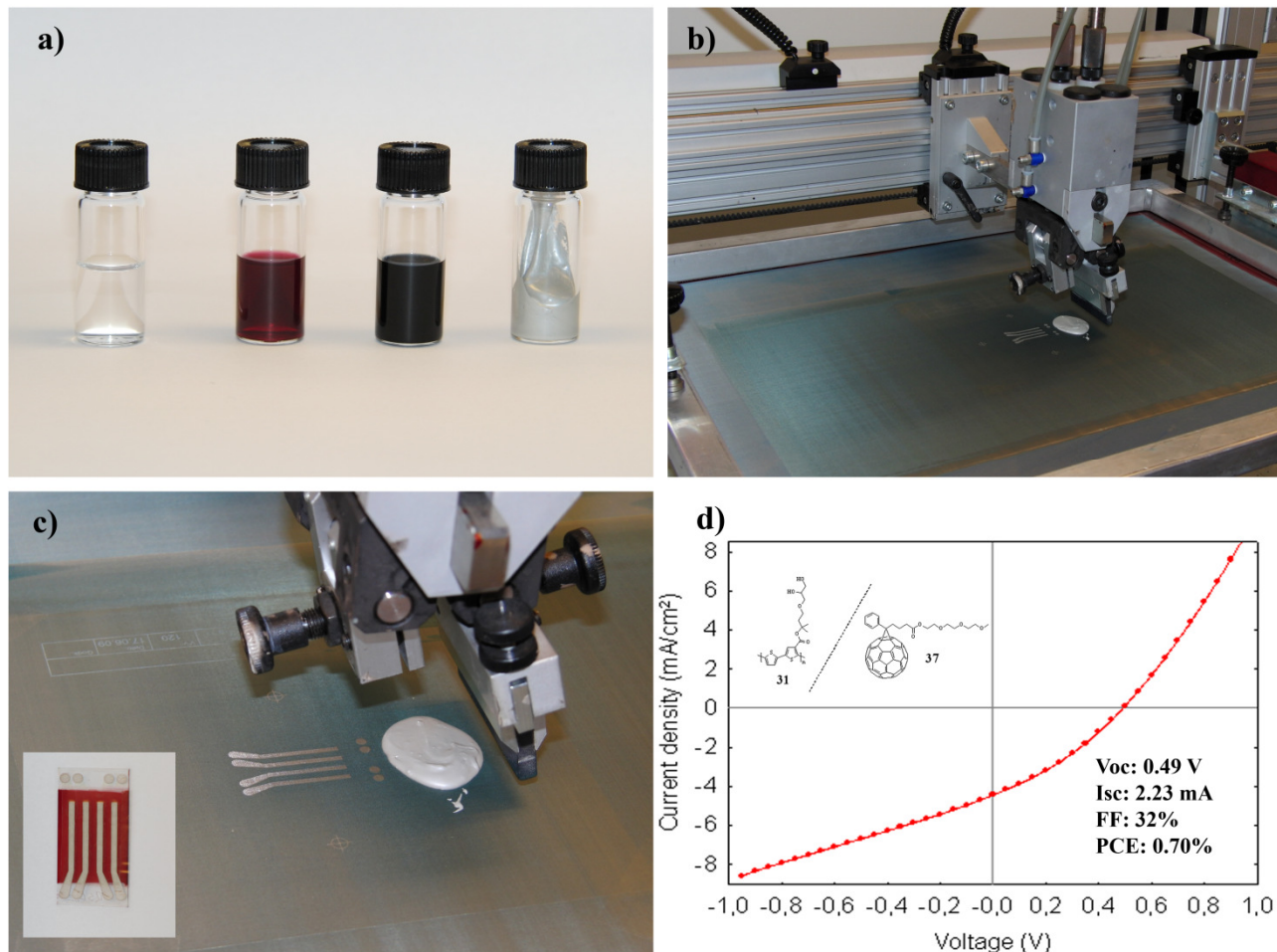


**Fig. 2.6:** **a)** picture of the inks involved in the 'all water based processing'. From left to right: aqueous ZnO-nanoparticles, aqueous solution of polymer **31** (diluted in order to show color), aqueous PEDOT and aqueous silver paste. **b)** Picture of the screen printing machinery. **c)** Close-up of the screen printing process. The silver paste has been applied and is ready to be pushed through the pattern of the mask by swiping of the rubber 'spatula'. Insert shows a picture of the final device after encapsulation. **d)** JV-characteristics of the final device using polymer **31** and fullerene **37**.

admittedly lower than what is commonly reported for P3HT/PCBM devices with evaporated electrodes. It should however be stressed that semi-aqueous processing is a very significant challenge, and these results show convincing feasibility for devices with relatively large active area and also show the potential of the printable aqueous silver as an alternative to evaporation.

## 2.5 Conclusion

Several new polymers carrying specially designed polar side chains have been synthesized with the aim of introducing solubility of conjugated polymers in aqueous media for more environmentally friendly processing. By attaching the side chains as tertiary ester to a thiophene backbone, it is possible to thermocleave the side chains after processing of the active layer making it insoluble. This allows for further processing using the same solvent without damaging the already processed layer. The general design of the side chains, as thermocleavable tertiary esters with polyether backbones and additional free alcohol groups, is not without problems though. Several of seemingly good candidates showed to be soluble in DMSO and DMF only. (Numerous additional attempts of using similar side chains in low-band-gap polymers all failed as the final polymers were insoluble. The syntheses of these are outlined and described in Appendix 1).

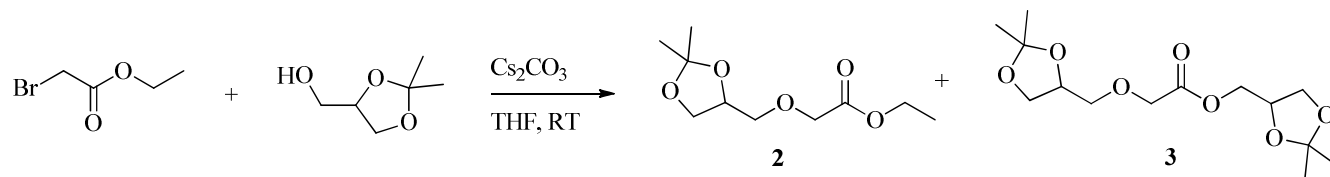
This being said, a polymer was synthesized that is soluble or dispersible in equal amounts of water and *iso*-propanol when as little as 4% THF is present. An analogue to the fullerene PCBM with a more hydrophilic ester side chain was synthesized which when dissolved in THF allowed for mixing with the aqueous polymer solution. Solar cell preparation using aqueous solutions of ZnO, active layer and PEDOT together with a screen printable aqueous silver paste led to the first ever reported solar cells where all layers are processed from aqueous or semi-aqueous solution. Bulk heterojunction solar cells prepared on the basis of these methods exhibited efficiencies up to 0.70% when using water processable polymer and fullerene and up to 2% when processing P3HT/PCBM from chlorobenzene while using aqueous processing for all other layers. Although these are not record breaking values, they are at a level where they must be recognized as important first steps towards more environmentally friendly processing.

## 2.6 Experimental

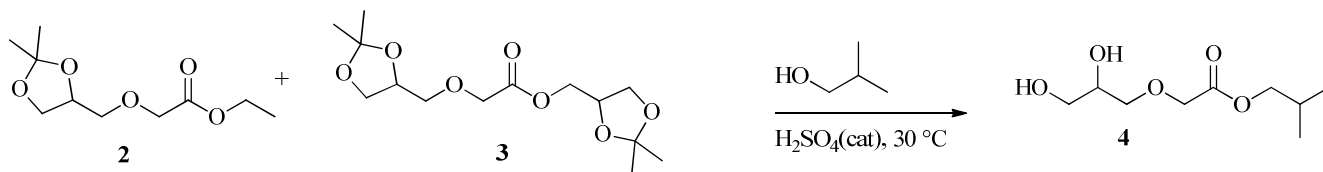
### 2.6.1 Synthesis

**General:** All reagents were purchased from commercial sources and used without further purification unless otherwise noted. Purification by column chromatography was performed by conventional gradient dry column vacuum chromatography<sup>[14]</sup> using Merck Silica Gel 60 (15–40  $\mu\text{m}$ ) (column height 5-7 cm) and suction to drive the mobile phase. Size exclusion chromatography (SEC) was performed in chloroform using either of two preparative Knauer systems employing two gel columns in succession with respectively pore diameters of 100 Å and 1000 Å. The gel columns had dimensions of 25 mm $\varnothing$  x 600 mm.

Combustion analyses (CHN) was performed by Mikro Kemi AB, 750 15 Uppsala, Sweden. High-resolution mass spectroscopy (HR-MS) was performed by the University of Copenhagen, Denmark.

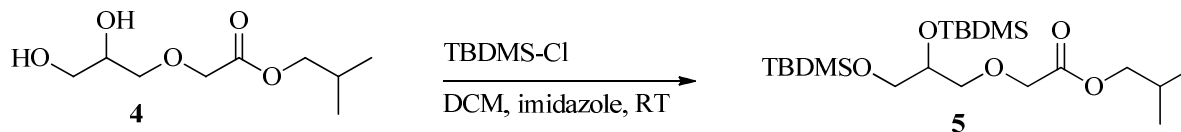


**Mixture of ethyl 2-((2,2-dimethyl-1,3-dioxolan-4-yl)methoxy)acetate (2) and (2,2-dimethyl-1,3-dioxolan-4-yl)methyl 2-((2,2-dimethyl-1,3-dioxolan-4-yl)methoxy)acetate (3):** Ethyl bromoacetate (15 g, 88 mmol), Solketal (13 g, 97 mmol) and Cesium carbonate (57.4 g, 176 mmol) were mixed in THF (40 ml) and stirred at RT for 48 hours. Celite was added to the mixture in order to minimize clogging when filtering through a short column of celite in order to remove solids from the solution. Evaporation of the solvent gave a crude mixture (20.5 g) as a clear colorless oil. This mixture was used without further purification in the following step.

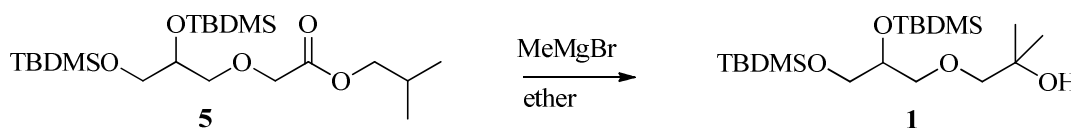


**Isobutyl 2-(2,3-dihydroxypropoxy)acetate (4):** 1/10 of the crude mixture of 2 and 3 (2.05 g, ~8.8 mmol) was dissolved in *iso*-butanol (80 mL) and concentrated sulfuric acid (100  $\mu$ L, 1.88 mmol) was added. The mixture was left at 30  $^{\circ}$ C overnight at reduced pressure (15 mbar) in order to remove evolving acetone and ethanol. Potassium *tert*-butoxide (0.421 g, 3.75 mmol) and then  $\text{NaHCO}_3$  (0.25 g, 3 mmol) was added in order to ensure neutralization of the acid, followed by removal of the solvent at reduced pressure. The remaining oil was dissolved in DCM and was evaporated onto celite followed by gradient column chromatography (10% steps, heptane/AcOEt  $\rightarrow$  AcOEt/THF) to yield the desired pure product (1.07 g, 59%).  $^1\text{H}$  NMR (500 MHz,  $\text{CDCl}_3$ )  $\delta$  4.13 (d,  $J$  = 1.8, 2H), 3.95 (d,  $J$  = 6.7, 2H), 3.91 - 3.84 (m, 1H), 3.75 - 3.60 (m, 4H), 2.83 (s, 2H), 1.95 (m,  $J$  = 6.7, 1H), 0.92 (d,  $J$  = 6.8, 6H).  $^{13}\text{C}$  NMR (126 MHz,  $\text{CDCl}_3$ )  $\delta$  171.50, 73.57, 71.42, 70.57, 68.40, 63.75, 27.81, 19.11.

The procedure furthermore yielded 2-bromoacetic acid isobutyl ester (0.32 g, 19%) originating from transesterification of the 2-bromoethylacetate in the preceding reaction step.



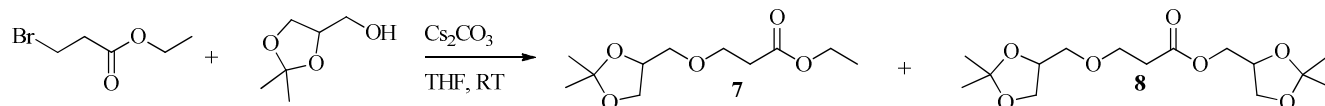
**Isobutyl 2-(2,3-bis((tert-butyldimethylsilyl)oxy)propoxy)acetate (5):** Compound **4** (0.902 g, 4.37 mmol) in DCM (6 ml) was cooled on an ice bath. Imidazole (0.724 g, 10.6 mmol) was added and the mixture was allowed to stir for approximately 10 minutes before adding *tert*-butyldimethylsilyl chloride (1.610 g, 10.68 mmol) in DCM (6 ml). A heavy white precipitate soon formed and the mixture was allowed to stir at room temperature overnight. The mixture was then diluted with DCM (40 ml), followed by washing of the organic phase with water (3 x 20 ml) and brine (20 ml). After drying over  $\text{MgSO}_4$  and evaporation of the solvent, the compound was purified by gradient column chromatography (2% steps, heptane/AcOEt) yielding the pure product as a clear oil (1.69 g, 89%).  $^1\text{H}$  NMR (500 MHz,  $\text{CDCl}_3$ )  $\delta$  4.19 – 4.06 (m, 2H), 3.93 (d,  $J = 6.7$  Hz, 2H), 3.90 – 3.81 (m, 1H), 3.68 – 3.43 (m, 4H), 1.95 (hep,  $J = 6.7$  Hz, 1H), 0.94 (d,  $J = 6.7$  Hz, 6H), 0.91 – 0.87 (m, 18H), 0.09 (s, 6H), 0.05 (s, 6H).  $^{13}\text{C}$  NMR (126 MHz,  $\text{CDCl}_3$ )  $\delta$  170.74, 73.79, 72.87, 70.90, 69.21, 65.06, 27.86, 26.08, 26.00, 19.19, 18.47, 18.31, -4.49, -4.60, -5.24, -5.28.



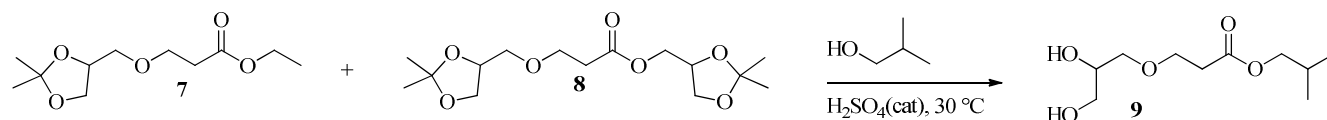
**1-(2,3-bis((tert-butyldimethylsilyl)oxy)propoxy)-2-methylpropan-2-ol (1)**

Compound **5** (1.50 g, 3.45 mmol) in diethyl ether (10 ml) was added drop wise by syringe to a solution of methyl magnesium bromide (3 M in ether, 3.45 ml, 10.35 mmol), and the solution was left stirring overnight. Additional ether (50 ml) was then added followed by quenching with water. A little  $\text{NaHCO}_3(\text{sat})$  was added upon which the solution was neutralized by slowly adding aqueous HCl until bubbles started to form. The mixture was extracted with ether and the combined ethereal phases were washed with water and brine. After drying over  $\text{MgSO}_4$  the solvent was evaporated and the resulting crude oil (1.44 g) was purified by gradient column chromatography (2-3% steps heptane/AcOEt) to yield the desired product as a clear oil (1.35 g, 100%).  $^1\text{H}$  NMR (500 MHz,  $\text{CDCl}_3$ )  $\delta$  3.83 (td,  $J = 10.3, 5.6$  Hz, 1H), 3.66 – 3.45 (m, 4H), 3.29 (s, 2H), 2.29 (s, 1H), 1.24 – 1.16 (m, 6H), 0.97 – 0.83 (m, 18H), 0.08 (s, 6H), 0.05 (s, 6H).  $^{13}\text{C}$  NMR (126

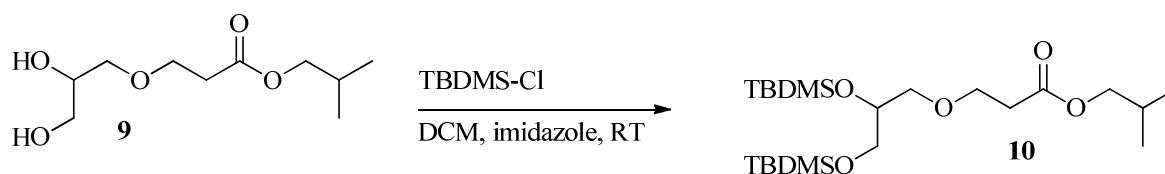
MHz, CDCl<sub>3</sub>) δ 79.12, 72.86, 71.79, 69.43, 64.06, 31.03, 28.17, 25.25, 25.24, 25.09, 24.97, 21.84, 17.51, 17.28, 13.25, -5.40, -5.52, -6.21, -6.26.



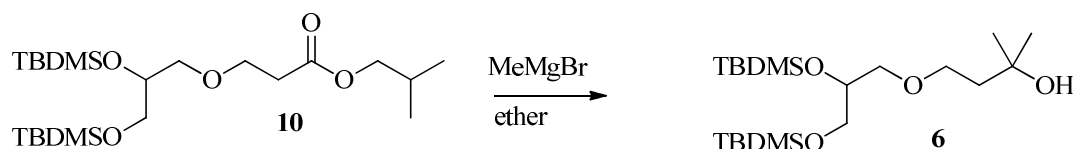
**Ethyl 3-((2,2-dimethyl-1,3-dioxolan-4-yl)methoxy)propanoate (7) and (2,2-dimethyl-1,3-dioxolan-4-yl)methyl 3-((2,2-dimethyl-1,3-dioxolan-4-yl)methoxy)propanoate (8):** A mixture of ethyl 3-bromopropanoate (18.00 g, 97 mmol), solketal (17.25 g, 128 mmol) and Cs<sub>2</sub>CO<sub>3</sub> (63.55 g, 195 mmol) was mixed in THF (40 ml) under argon and left while stirring at RT for 6 days. In order to remove the colloid dispersion of inorganics, the mixture was diluted with DCM, centrifuged and the organic layer was separated by decantation. The inorganic part was extracted with DCM (3 x 150 ml) which was separated by centrifugation/decantation. The collected organic fractions were then passed through a very short silica column in order to remove the last traces of both colloid and dissolved inorganics. Removal of the solvents yielded a crude mixture of 25.3 g. This mixture was used without further purification in the next step.



**Isobutyl 3-(2,3-dihydroxypropoxy)propanoate (9):** The crude mixture of 7 and 8 ('97 mmol') was dissolved in *iso*-butanol (1 L) and 98% sulfuric acid (1.00 ml, 18.8 mmol) was added. The mixture was left at 37 °C for 14 h at reduced pressure (15 mbar) in order to remove evolving acetone and ethanol. Potassium *tert*-butoxide (4.21 g, 37.5 mmol) and then NaHCO<sub>3</sub> (0.25 g, 3 mmol) was then added in order to ensure neutralization of the acid, followed by removal of the solvent at reduced pressure. The resulting clear oil was purified by column chromatography on silica (AcOEt) yielding 5 as a clear oil (12.7 g, 59 %). <sup>1</sup>H NMR (500 MHz, CDCl<sub>3</sub>) δ 3.89 (d, J = 6.7 Hz, 2H), 3.87 - 3.83 (m, 1H), 3.81 - 3.71 (m, 2H), 3.71 - 3.49 (m, 4H), 2.84 - 2.37 (m, 4H), 1.93 (h, J = 6.7 Hz, 1H), 0.92 (d, J = 6.6 Hz, 6H). <sup>13</sup>C NMR (126 MHz, CDCl<sub>3</sub>) δ 172.09, 72.63, 71.00, 70.52, 66.86, 64.00, 35.03, 27.82, 19.16. HR-MS (ESI) *m/z* for M+H (C<sub>10</sub>H<sub>21</sub>O<sub>5</sub>): calc. 221.1389, Found: 221.1391.

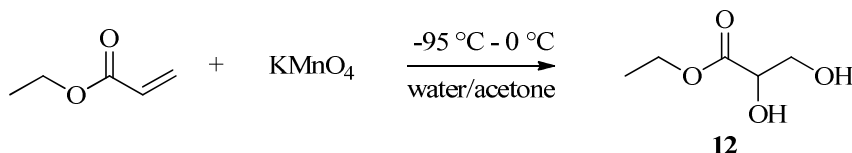


**Isobutyl 3-(2,3-bis((*tert*-butyldimethylsilyl)oxy)propoxy)propanoate (10):** Compound **9** (3.78 g, 17.2 mmol) in DCM (25 ml) was cooled on an ice bath and imidazole (2.35 g, 34.5 mmol) was added. The mixture was allowed to stir for approximately 10 minutes and TBDMS-Cl (5.18 g, 34.4 mmol) in DCM (6 ml) was added leading to a heavy white precipitate. After stirring for ½ hour the ice bath was removed and the mixture was stirred at RT overnight. Heptane (20 ml) was added to the mixture followed by removal of the precipitate by filtration. Column chromatography on silica using heptane/ethyl acetate with gradient steps of 2% yielded the pure product as a clear oil. (6.87 g, 89 %).  $^1\text{H}$  NMR (500 MHz,  $\text{CDCl}_3$ )  $\delta$  3.87 (d,  $J = 6.7$  Hz, 2H), 3.83 – 3.66 (m, 3H), 3.57 – 3.45 (m, 3H), 3.37 (dd,  $J = 9.9, 5.9$  Hz, 1H), 2.58 (t,  $J = 6.6$  Hz, 2H), 1.93 (h,  $J = 6.7$  Hz, 1H), 0.93 (d,  $J = 6.7$  Hz, 6H), 0.88 (2 x s, 18H), 0.05 (2 x s, 12H).  $^{13}\text{C}$  NMR (126 MHz,  $\text{CDCl}_3$ )  $\delta$  171.78, 73.31, 72.84, 70.74, 67.08, 65.26, 35.41, 27.86, 26.10, 26.01, 19.23, 18.49, 18.34, -4.48, -4.53, -5.22, -5.28. HR-MS (ESI)  $m/z$  for  $\text{M}+\text{H}$  ( $\text{C}_{22}\text{H}_{49}\text{O}_5\text{Si}_2$ ): calc. 449.3119, Found: 449.3051.

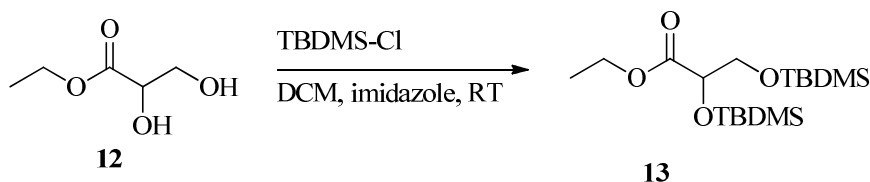


**4-(2,3-bis((*tert*-butyldimethylsilyl)oxy)propoxy)-2-methylbutan-2-ol (6):** Methylmagnesium bromide (3 M, 11.85 ml, 35.6 mmol) was added by syringe to a solution of **10** (5.32 g, 11.85 mmol) in ether (30 ml) under argon resulting in a white precipitate. After stirring for 2½ hours at RT the reaction was quenched with saturated  $\text{NaHCO}_3$  (50 ml) followed by addition of 1 M HCl until  $\text{CO}_2$  evolution was observed. The ethereal phase was separated followed by extraction of the aqueous phase with additional ether (4 x 50 ml). The combined organic fractions were washed with water and brine. After drying over  $\text{MgSO}_4$  the solvent was removed *in vacuo* to yield a crude oil (4.68 g). Purification on silica column using heptane/ $\text{AcOEt}$  (4:1) as eluent yielded the pure product as a clear oil (4.38 g, 91%).  $^1\text{H}$  NMR (500 MHz,  $\text{CDCl}_3$ )  $\delta$  3.68 (dt,  $J = 10.5, 5.2$ , 1H), 3.64 – 3.51 (m, 2H), 3.50 – 3.29 (m, 4H), 3.09 (s, 1H), 1.76 – 1.55 (m, 2H), 1.14 (d,  $J = 1.5$ , 6H), 0.79 (2 x s, 18H), 0.11 – -0.23 (m, 12H).  $^{13}\text{C}$  NMR (126 MHz,  $\text{CDCl}_3$ )  $\delta$  73.25, 72.57, 70.58, 69.26, 64.82, 41.64, 29.74, 29.20, 26.08, 25.99, 18.47, 18.27, -4.45, -4.55, -5.22, -5.27. HR-MS (ESI)

$m/z$  for  $M+H$  ( $C_{20}H_{47}O_4Si_2$ ): Calc.: 407.3013, Found: 407.3007. Microanalysis for  $C_{20}H_{46}O_4Si_2$ : Calc.: C: 59.1, H: 11.4. Found: C: 58.8, H: 11.3.

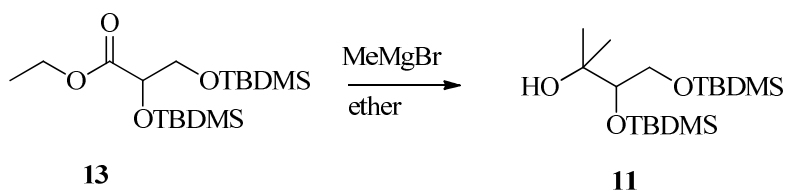


**Ethyl glycerate (12).**<sup>[10]</sup> Potassium permanganate (16 g, 101 mmol) was dissolved in mixture of water (150 ml) and acetone (350 ml) and cooled on  $N_2, liq/MeOH$  (-95 °C). Ethyl acrylate (10 ml, 92 mmol) was slowly added while stirring at -95 °C, after which the mixture was allowed to warm to 0 °C. The inorganic salts were removed by filtration followed by washing with acetone. The combined filtrates were then concentrated by removal of the acetone *in vacuo* (keeping the temperature below 40 °C) and the aqueous phase was then extracted with AcOEt. After washing of the combined organic extracts with water and brine, the solution was dried over  $MgSO_4$ , and the pure compound was isolated as a clear oil (4.03 g, 30%) after removal of the solvent at reduced pressure while keeping the temperature below 40 °C.  $^1H$  NMR (500 MHz,  $CDCl_3$ )  $\delta$  4.31 - 4.20 (m, 3H), 3.85 (ddd,  $J = 15.8, 11.7, 3.6$  Hz, 2H), 3.20 (s, 2H), 1.29 (t,  $J = 7.1$  Hz, 3H).  $^{13}C$  NMR (126 MHz,  $CDCl_3$ )  $\delta$  173.15, 71.83, 64.21, 62.19, 14.23.

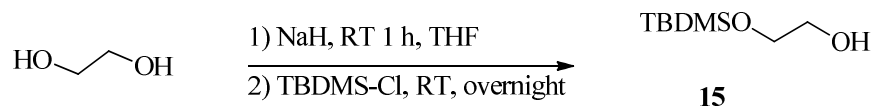


**Ethyl 2,3-bis((*tert*-butyldimethylsilyl)oxy)propanoate (13):** Compound **12** (1.02 g, 7.60 mmol) in DCM (6 ml) was cooled on an ice bath and imidazole (1.061 g, 15.59 mmol) was added. The mixture was allowed to stir for approximately 10 min and TBDMSCl (2.45 g, 16.3 mmol) was added (heavy white precipitate). After stirring for 30 minutes the cooling bath was removed and the mixture was stirred at RT until the next day. Additional DCM (25 ml) was added and the mixture was washed with water (3 x 10 ml) and brine (10 ml). After drying over  $MgSO_4$  the solvent was removed *in vacuo* and the crude oil (2.96 g) was purified by gradient column chromatography (2% steps, heptanes/AcOEt) yielding the pure product as a clear oil (1.97 g, 71%).  $^1H$  NMR (500 MHz,  $CDCl_3$ )  $\delta$  4.25 (m, 1H), 4.22 - 4.09 (m, 2H), 3.78 (m, 2H), 1.28 (t,  $J = 7.1$ , 3H), 0.92 - 0.83 (m, 18H), 0.10 - 0.03 (4 x s, 12H).  $^{13}C$  NMR (126 MHz,  $CDCl_3$ )  $\delta$  172.17, 74.25, 66.17, 60.88, 25.99, 25.88, 18.50, 18.46, 14.36, -4.88, -4.90, -5.24, -5.29.

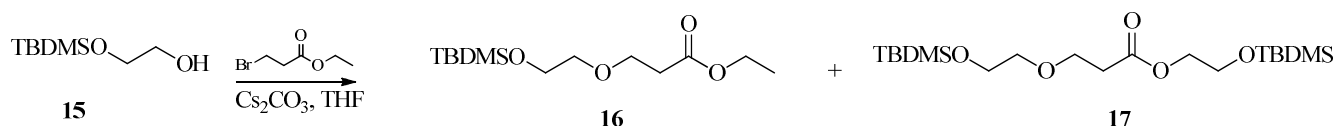




**3,4-bis((*tert*-butyldimethylsilyl)oxy)-2-methylbutan-2-ol (11):** Compound **13** (1.5 g, 4.14 mmol) in diethyl ether (10 ml) was added by syringe to a solution of methyl magnesiumbromide (3 M in ether) (4.14 ml, 12.41 mmol), and the solution was left over night. The mixture was carefully quenched with water after which a little saturated NaHCO<sub>3</sub> solution was added as a buffer and the mixture was neutralized with diluted HCl solution. The mixture was extracted with ether and the combined organic phases were washed with water and brine before drying over MgSO<sub>4</sub>. Removal of the solvent gave the crude product (1.50 g) which was purified by gradient column chromatography (2% steps, heptane/AcOEt) yielding the pure product a an oil (1.20 g, 83%). <sup>1</sup>H NMR (500 MHz, CDCl<sub>3</sub>) δ 3.68 (m, 1H), 3.61 (m, 1H), 3.51 (m, 1H), 1.18 (s, 3H), 1.16 (s, 3H), 0.92 - 0.87 (m, 18H), 0.08 (m, 12H). <sup>13</sup>C NMR (126 MHz, CDCl<sub>3</sub>) δ 77.52, 73.18, 65.45, 26.65, 26.04, 26.01, 24.68, 18.36, 18.19, -3.93, -4.71, -5.40, -5.46.

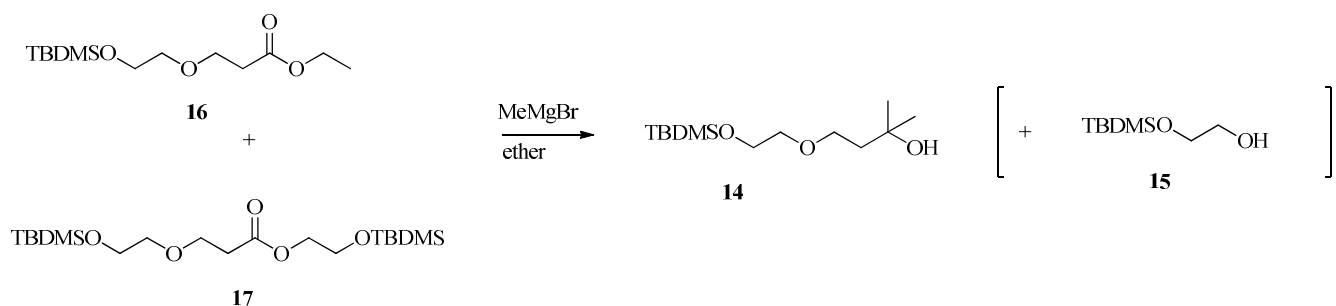


**2-((*tert*-butyldimethylsilyl)oxy)ethanol (15):**<sup>[41]</sup> Ethylene glycol (15.16 ml, 272 mmol) was added at RT to a suspension of sodium hydride 60% (8.08 g, 202 mmol) in THF (200 ml). The mixture was left overnight followed by addition of TBDMSCl (23.81 g, 158 mmol) one portion after which the reaction was left at RT for a few hours. The THF was then evaporated and ether (500 ml) and K<sub>2</sub>CO<sub>3</sub> (1 M, 60 ml) was added. The organic phase was separated and washed with further 1 M K<sub>2</sub>CO<sub>3</sub> (2 x 60 ml) and brine (2 x 60 ml) and was then dried over MgSO<sub>4</sub>. Evaporation of the solvent yielded the crude product (28.7 g) which was distilled on a micro-Claisen fitted with a Vigreux column at reduced pressure (20 mbar, 80-81 °C) to yield the pure product (20.03 g, 72%). <sup>1</sup>H NMR (500 MHz, CDCl<sub>3</sub>) δ 3.74 - 3.68 (m, 2H), 3.67 - 3.61 (m, 2H), 2.05 (t, J = 6.2 Hz, 1H), 0.91 (s, 9H), 0.08 (s, 6H). <sup>13</sup>C NMR (126 MHz, CDCl<sub>3</sub>) δ 64.07, 63.71, 25.90, 18.32, -5.33.



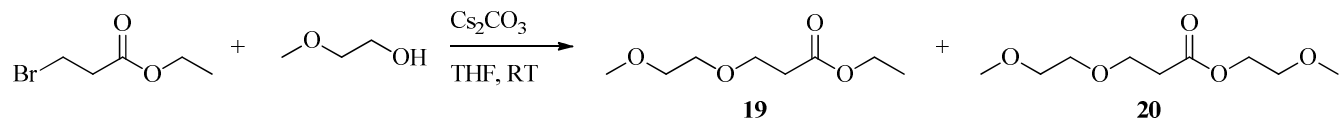
**Ethyl 3-(2-((tert-butyldimethylsilyl)oxy)ethoxy)propanoate and 2-((tert-butyldimethylsilyl)oxy)ethyl 3-(2-((tert-butyldimethylsilyl)oxy)ethoxy)propanoate (**16 + 17**):**

Ethyl 3-bromopropionate (12.02 g, 66.4 mmol), compound **15** (20 g, 113 mmol) and cesium carbonate (54.8 g, 168 mmol) was mixed in dry THF (70 ml) and left stirring under argon at RT for 5 days. DCM (150 ml) was added to the mixture in order to promote precipitation of dissolved salts after which the suspension was centrifuged, the organic phase was separated and the solid was extracted 4 times with DCM. Any remaining inorganics were removed by passing the organic phase through a short silica column which was then eluted with THF. Evaporation of the solvents yielded a crude mixture consisting mainly of **16** and **17**, which was used in the following step without further purification (24.13 g).



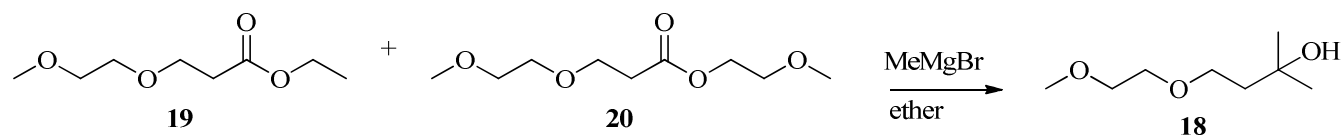
**4-(2-((tert-butyldimethylsilyl)oxy)ethoxy)-2-methylbutan-2-ol (**14**):** The crude mixture of **16** and **17** ('66,4 mmol') was dissolved in diethyl ether (150 ml) and cooled on an ice bath. Methylmagnesium bromide (3 M in ether) (100 ml, 300 mmol) was then added slowly by syringe and the mixture was left over night. The reaction was then quenched by the careful addition of saturated NaHCO<sub>3</sub> (60 ml) followed by the slow addition of 1M HCl until bubbles started to form. The aqueous phase was extracted with ether (4 x 100 ml), and the combined organic phases were dried over MgSO<sub>4</sub> before removal of the solvent *in vacuo*. The crude product (23.7 g) was distilled at reduced pressure (3-4 mbar) removing side products and allowing for collection of regenerated compound **15**. The distillation remanence (10.6 g) was almost completely pure on NMR, but faint shadows of byproduct could be seen on TLC. Final purification was performed using gradient column chromatography (4% steps, heptane/AcOEt) to yield the pure product (9.83 g, 56% over 2 steps). <sup>1</sup>H NMR (500 MHz, CDCl<sub>3</sub>) δ 3.79 – 3.69 (m, 4H), 3.57 – 3.47 (m, 2H), 3.26 (s,

1H), 1.76 (t,  $J = 5.8$  Hz, 2H), 1.24 (s, 6H), 0.89 (s, 9H), 0.06 (s, 6H).  $^{13}\text{C}$  NMR (126 MHz,  $\text{CDCl}_3$ )  $\delta$  72.82, 70.61, 68.99, 62.65, 41.57, 29.48, 26.07, 18.48, -5.18.

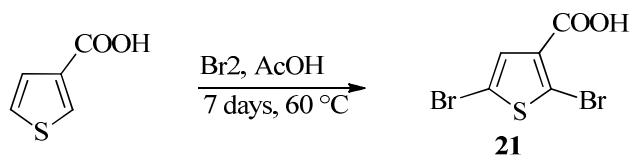


### Ethyl 3-(2-methoxyethoxy)propanoate (19) and 2-methoxyethyl 3-(2-

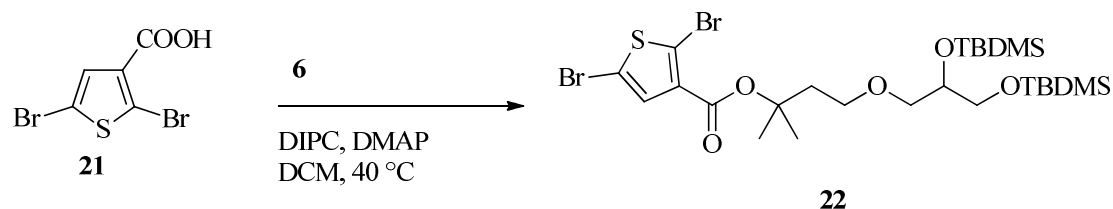
**methoxyethoxy)propanoate(20):** Ethyl 3-propionate (10.0 g, 55.2 mmol) and 2-methoxyethanol (10.90 ml, 138 mmol) was mixed in THF (30 ml) and  $\text{Cs}_2\text{CO}_3$  (54.0 g, 166 mmol) was added and the mixture was stirred under argon for 2 days. DCM was added to the mixture which was centrifuged and the liquid decanted. Extraction of the solid with DCM followed by centrifugation was then performed 3 times. In order to remove dissolved inorganics the combined solution was passed through a short silica column followed by washing with THF. Removal of the solvent yielded a crude oil (10.0 g) that was used without further purification in the subsequent step.



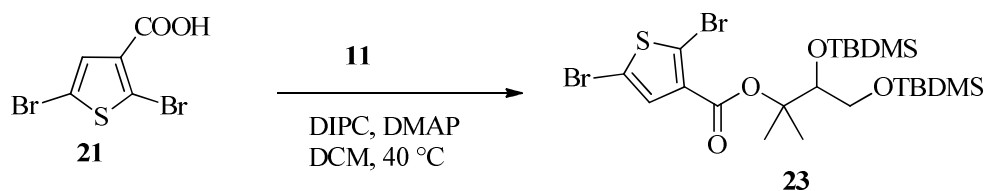
**4-(2-methoxyethoxy)-2-methylbutan-2-ol (18)** The crude mixture of **18** and **19** ('55,2 mmol') was dissolved in diethyl ether (70 ml) and Methylmagnesiumbromide (3 M in ether) (50 ml, 150 mmol) was added slowly leading to a rubbery precipitate. Additional ether (100 ml) was added and the mixture was left while stirring at RT for 2 hours. Careful quenching with ice water (100 ml) was followed by addition of first saturated  $\text{NaHCO}_3$  (40 ml) and then 2M HCl was added slowly until bubbles started to form. The aqueous phase was then reduced to approximately half the volume followed by continuous extraction with ether for 24 hours. After drying the ethereal phase the solvent was removed to give a clear crude oil (8.13 g) which was purified by gradient column chromatography (heptanes/ $\text{AcOEt}$ , 5% steps) to yield the pure product (4.21 g, 47%).  $^1\text{H}$  NMR (500 MHz,  $\text{CDCl}_3$ )  $\delta$  3.72 (t,  $J = 5.6$  Hz, 2H), 3.63 – 3.56 (m,  $J = 4.4, 3.6$  Hz, 2H), 3.55 – 3.49 (m, 2H), 3.36 (s, 3H), 3.21 (s, 1H), 1.77 (t,  $J = 5.6$  Hz, 2H), 1.23 (s, 6H).  $^{13}\text{C}$  NMR (126 MHz,  $\text{CDCl}_3$ )  $\delta$  71.80, 70.41, 70.26, 68.68, 59.03, 41.38, 41.36, 29.41, 29.39.



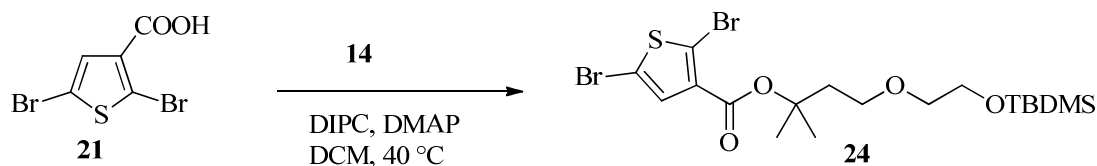
**2,5-dibromothiophene-3-carboxylic acid (21):** Thiophene-3-carboxylic acid (19.5 g, 152 mmol) was dissolved in acetic acid (200 ml) and bromine (170 g, 1.07 mmol, 7 eq.) in acetic acid (240 ml) was added slowly at RT and the mixture was left overnight. The temperature was then raised to 60 °C for 17 hours followed by RT for 3 days. The mixture was poured into ice-water (1000 ml) and the precipitate was filtered and washed extensively first with water, then with aqueous NaHSO<sub>3</sub> (2 M) and finally again with water to yield the pure product as a white solid (42.3 g, 97%). <sup>1</sup>H NMR (500 MHz, DMSO) δ 13.37 (s, 1H), 7.43 (s, 1H). <sup>13</sup>C NMR (126 MHz, DMSO) δ 161.59, 133.10, 132.14, 118.36, 111.13.



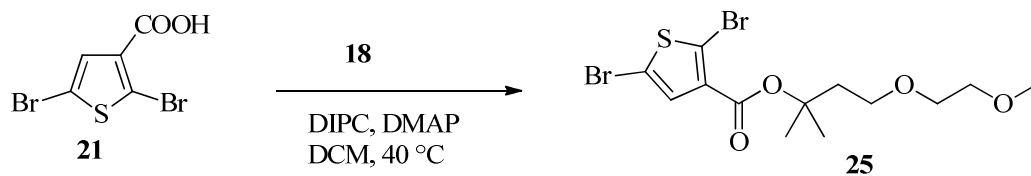
**4-(2,3-bis((*tert*-butyldimethylsilyl)oxy)propoxy)-2-methylbutan-2-yl 2,5-dibromothiophene-3-carboxylate (22):** A mixture of **6** (0.600 g, 1.48 mmol), **21** (0.550 g, 1.92 mmol) and DMAP (0.270 g, 2.21 mmol) in DCM (4 ml) was stirred at RT for ½ hour. *N,N'*-diisopropylcarbodiimide (0.297 ml, 1.92 mmol) was then added, the temperature was raised to 39 °C and the mixture was left stirring for 2 days. Purification on a silica column with gradient eluent (heptanes, increasing with 1% AcOEt steps) yielded the desired product (0.85 g, 86%). <sup>1</sup>H NMR (500 MHz, CDCl<sub>3</sub>) δ 7.27 (s, 1H), 3.80 – 3.74 (m, 1H), 3.63 – 3.49 (m, 4H), 3.40 (ddd, *J* = 15.4, 9.8, 5.1 Hz, 2H), 2.21 – 2.11 (m, 2H), 1.59 (s, 6H), 0.89 – 0.86 (m, 18H), 0.07 – 0.03 (m, 12H). <sup>13</sup>C NMR (126 MHz, CDCl<sub>3</sub>) δ 159.98, 133.41, 132.08, 118.31, 111.15, 83.93, 73.10, 72.85, 67.60, 65.20, 40.46, 26.77, 26.65, 26.10, 26.01, 25.95, 18.50, 18.34, -4.43, -4.51, -5.20, -5.25. HR-MS (ESI) *m/z* for M+Na (C<sub>25</sub>H<sub>46</sub>Br<sub>2</sub>NaO<sub>5</sub>SSi<sub>2</sub>): Calc.: 695.0869, found 695.0836. Microanalysis for C<sub>25</sub>H<sub>46</sub>Br<sub>2</sub>O<sub>5</sub>SSi<sub>2</sub>: Calc.: C: 44.5, H: 6.9. Found: C: 44.5, H: 6.8.



**3,4-bis((*tert*-butyldimethylsilyl)oxy)-2-methylbutan-2-yl 2,5-dibromothiophene-3-carboxylate (23):** Compound **11** (0.600 g, 1.72 mmol), compound **21** (0.645 g, 2.26 mmol) and DMAP (0.315 g, 2.58 mmol) was mixed in DCM (4 ml) at RT for ½ hour. *N,N'*-diisopropylcarbodiimide (0.346 ml, 2.24 mmol) was then added and the temperature raised to 39 °C and the mixture was left stirring under argon for 5 days. Purification was performed by gradient column chromatography (first: heptanes/AcOEt 1% steps; second: hexane/DCM, 2% steps) to yield the desired product as a clear colorless oil (666 mg, 63%). <sup>1</sup>H NMR (500 MHz, CDCl<sub>3</sub>) δ 7.26 (s, 1H), 4.17 (dd, *J* = 5.8, 3.5 Hz, 1H), 3.83 (dd, *J* = 10.6, 3.5 Hz, 1H), 3.57 (dd, *J* = 10.6, 5.9 Hz, 1H), 1.58 (s, 3H), 1.52 (s, 3H), 0.88 (2 x s, 18H), 0.12 (s, 3H), 0.07 – 0.05 (m, 3H), 0.04 (s, 3H), 0.03 (s, 3H). <sup>13</sup>C NMR (126 MHz, CDCl<sub>3</sub>) δ 159.84, 133.28, 132.07, 118.57, 111.11, 86.24, 77.54, 65.42, 26.18, 26.06, 23.98, 22.04, 18.60, 18.31, -3.63, -4.81, -5.24, -5.26.



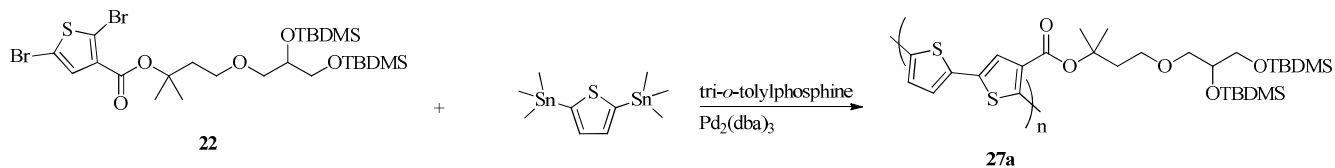
**4-(2-((*tert*-butyldimethylsilyl)oxy)ethoxy)-2-methylbutan-2-yl 2,5-dibromothiophene-3-carboxylate (24):** Compound **14** (1.042 g, 3.77 mmol), compound **21** (1.294 g, 4.53 mmol), DMAP (0.553 g, 4.53 mmol) was mixed in DCM (5ml) under argon for 5 min. *N,N'*-diisopropylcarbodiimide (0.701 ml, 4.53 mmol) was then added, the temperature was raised to 39 °C and the reaction was left at stirring for 2 days. Purification by gradient chromatography on a silica column yielded the pure product as a clear colorless oil (1.862 g, 93%). <sup>1</sup>H NMR (500 MHz, CDCl<sub>3</sub>) δ 7.28 (s, 1H), 3.72 (t, *J* = 5.4 Hz, 2H), 3.62 (t, *J* = 6.7 Hz, 2H), 3.48 (t, *J* = 5.4 Hz, 2H), 2.18 (t, *J* = 6.7 Hz, 2H), 1.59 (s, 6H), 0.89 (s, 9H), 0.05 (s, 6H). <sup>13</sup>C NMR (126 MHz, CDCl<sub>3</sub>) δ 159.85, 133.27, 131.94, 118.15, 110.98, 83.73, 72.40, 67.30, 62.69, 40.22, 26.58, 25.92, 18.36, -5.27.



#### 4-(2-methoxyethoxy)-2-methylbutan-2-yl 2,5-dibromothiophene-3-carboxylate (**25**):

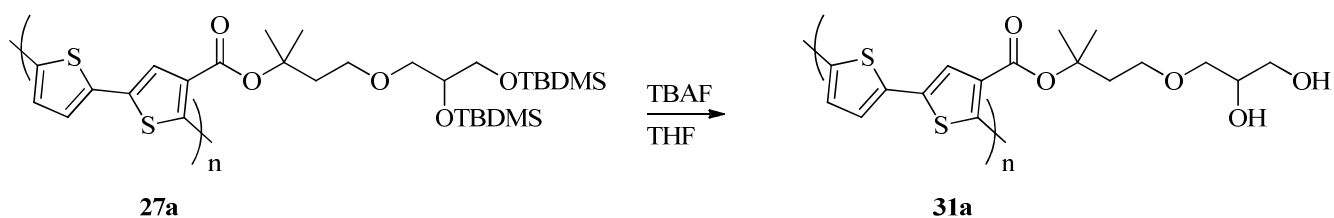
Compound **18** (0.754 g, 4.65 mmol), compound **21** (1.730 g, 6.05 mmol), DMAP (0.866 g, 1.52 mmol) was mixed in DCM (8 ml) at RT for ½ hour under argon. *N,N'*-diisopropylcarbodiimide (0.936 ml, 6.04 mmol) was then added, the temperature was raised to 39 °C and the reaction was left stirring for 4 days.

Purification by gradient column chromatography (heptane/AcOEt, 2% steps) yielded the desired product as a clear oil (1.77 g, 89%). <sup>1</sup>H NMR (500 MHz, CDCl<sub>3</sub>) δ 7.28 (s, 1H), 3.63 (t, *J* = 6.9 Hz, 2H), 3.60 – 3.47 (m, 4H), 3.37 (s, 3H), 2.20 (t, *J* = 6.9 Hz, 2H), 1.59 (s, 6H). <sup>13</sup>C NMR (126 MHz, CDCl<sub>3</sub>) δ 159.98, 133.46, 132.11, 118.28, 111.14, 83.74, 72.13, 70.32, 67.45, 59.21, 40.32, 26.69.



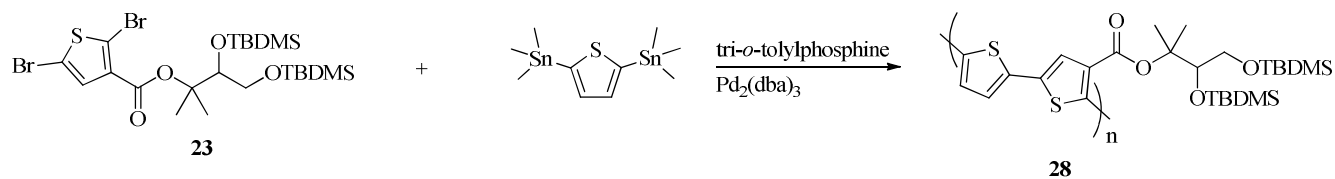
#### Poly(4-(2,3-bis((*tert*-butyldimethylsilyl)oxy)propoxy)-2-methylbutan-2-yl 5,5'-diyl-[2,2'-bithiophene]-4-carboxylate) (**27a**):

Compound **22** (297 mg, 0.440 mmol), 2,5-bis(trimethylstannyl)thiophene (180 mg, 0.440 mmol), tri-*o*-tolyl phosphine (53.6 mg, 0.176 mmol) and Pd<sub>2</sub>(dba)<sub>3</sub> (20.16 mg, 0.022 mmol) were mixed in degassed dry toluene (10 ml). The temperature was raised to 110 °C and the mixture stirred for 2 days. The polymer was precipitated by adding the reaction mixture to methanol, and the solid was purified by soxhlet extraction with methanol (14 h) followed by extraction of the polymer with hexane. After evaporating the solvent, the polymer was redissolved in toluene and precipitated from methanol. (242 mg, 88%). *M<sub>w</sub>*:40856, *M<sub>n</sub>*: 15314, PDI:2.67.



**Poly-( 4-(2,3-dihydroxypropoxy)-2-methylbutan-2-yl 5,5'-diyl-[2,2'-bithiophene]-4-carboxylate)**

**(31a):** Polymer **27a** (202 mg, 0.337 mmol) was dissolved in THF (5 ml) followed by addition of TBAF (1 M in THF) (1.35 ml, 1.35 mmol). The mixture was heated to 35 °C and left standing over night. Methanol (2 ml) was then added and the solution stirred for an additional 24 hours. The deprotected compound was precipitated by drop wise addition to AcOEt, and filtration. The precipitate was washed extensively with *iso*-propanol and then dried in vacuum.



**Poly-( 3,4-bis((*tert*-butyldimethylsilyl)oxy)-2-methylbutan-2-yl 5,5'-diyl-[2,2'-bithiophene]-4-**

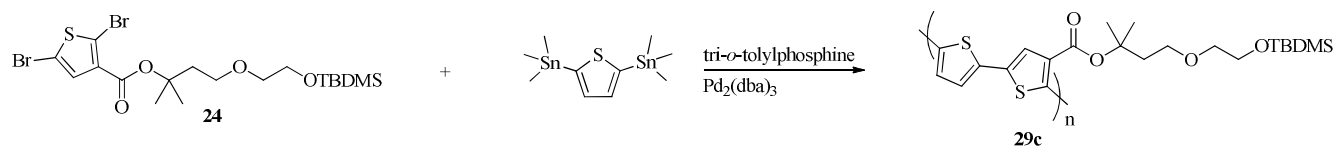
**carboxylate ) (28):** Compound **23** (283.8 mg, 0.460 mmol), 2,5-bis(trimethylstannyl)thiophene (189.2 mg, 0.462 mmol), tri-*o*-Tolyl phosphine (55.5 mg, 0.182 mmol) and Pd<sub>2</sub>(dba)<sub>3</sub> (22.1 mg, 0.024 mmol) was mixed in degassed dry toluene (10 ml). The temperature was raised to 90 °C for 1½ hour and then raised to 110 °C over night. The polymer was precipitated by adding the reaction mixture to MeOH, and the solid was purified by soxhlet extraction with MeOH for 24 h followed by extraction of the polymer with hexane. After removal of the solvent, the polymer was redissolved in toluene and precipitated from methanol. (243 mg, 93%) M<sub>w</sub>: 38525, M<sub>n</sub>: 15437, PDI: 2.50



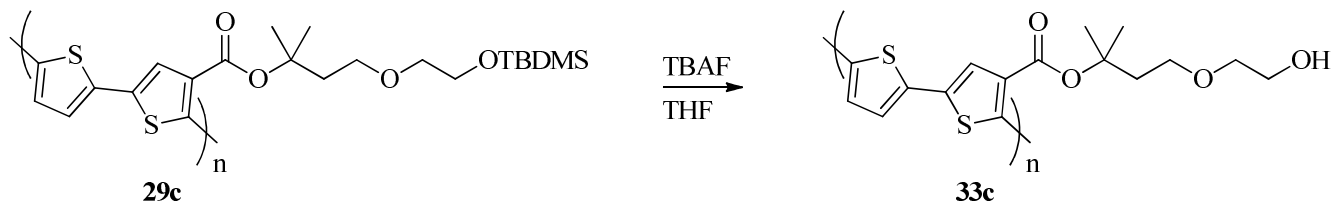
**Poly-(3,4-dihydroxy-2-methylbutan-2-yl 5,5'-diyl-[2,2'-bithiophene]-4-carboxylate) (32):**

Polymer **28** (200,1 mg) was dissolved in THF (5 ml) at RT under argon followed by addition of TBAF (1 M in THF) (1.485 ml, 1.485 mmol). After 10 minutes the solution had turned darker, and MeOH (1 ml) was added.

The mixture was then heated on an oil bath at 40 °C and left standing over night. The now partially precipitated solution was added to AcOEt, and the solid was filtered off and washed extensively with AcOEt, isopropanol and water before drying in vacuum.

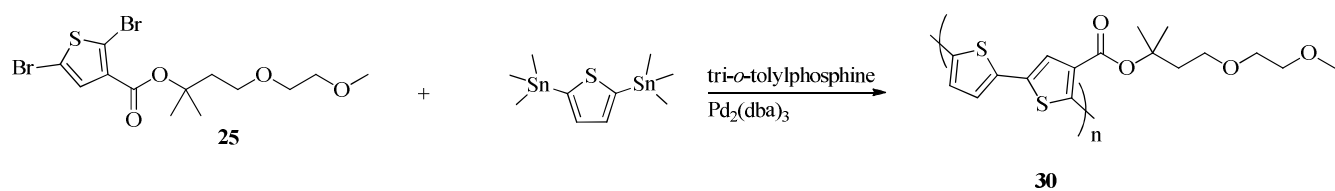


**4-(2-((*tert*-butyldimethylsilyl)oxy)ethoxy)-2-methylbutan-2-yl 5,5'-dimethyl-[2,2'-bithiophene]-4-carboxylate (29c):** 2,5-di(trimethylstannyl)thiophene (233.72 mg, 0.570 mmol) and compound **24** (302.16 mg, 0.570 mmol) was dissolved in dry degassed toluene (10 ml) under argon and tri-*O*-Tolyl phosphine (70.13 mg, 0.230 mmol) and Pd<sub>2</sub>(dba)<sub>3</sub> (26.1 mg, 0.028 mmol) was added. The temperature was raised to reflux for 7 hours after which the temperature was lowered to RT for 2 days. The reaction mixture was precipitated from methanol and the solid was purified by soxhlet extraction with methanol (15 h) followed by extraction of the polymer with hexane. After removal of the solvent, the polymer was redissolved in toluene and precipitated from methanol. (231 mg, 84%), M<sub>w</sub> 24044, M<sub>n</sub> 10649, PDI 2.2



**Poly-(4-(2-hydroxyethoxy)-2-methylbutan-2-yl 5,5'-diyl-[2,2'-bithiophene]-4-carboxylate) (33c):** Polymer **29c** (117 mg) was dissolved in THF (4 ml) and tetrabutylammonium fluoride (1.0 M in THF, 0.728 ml, 0.728 mmol, '3 eq') and the mixture was left overnight at 35 °C. The reaction mixture was precipitated by addition to ethyl acetate and the solid was filtered off and washed thoroughly with *iso*-propanol and dried in vacuum.

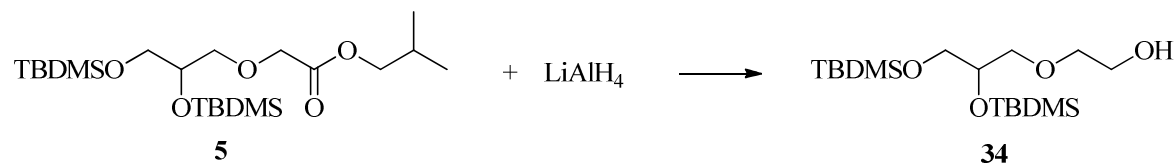




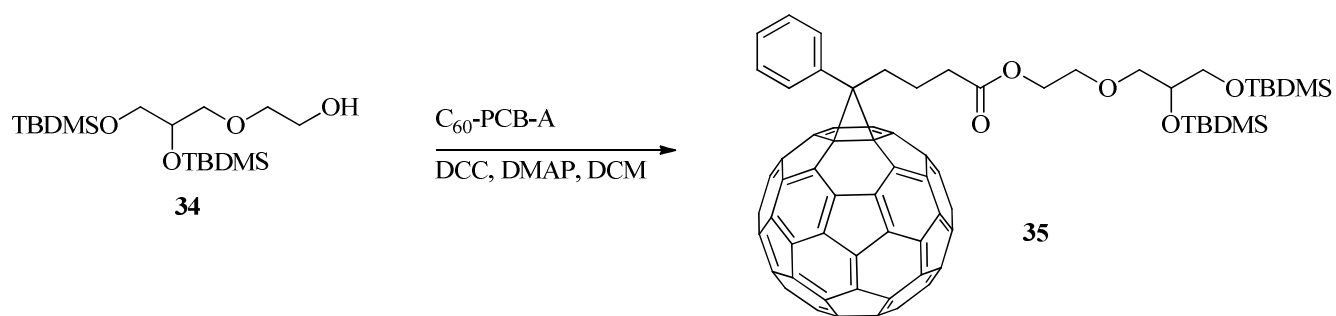
**Poly-(4-(2-methoxyethoxy)-2-methylbutan-2-yl 5,5'-diyl-[2,2'-bithiophene]-4-carboxylate) (30):**

Compound **25** (512 mg, 1.19 mmol), 2,5-bis(trimethylstannyl)thiophene (488 mg, 1.19 mmol), tri-*o*-tolyl phosphine (147 mg, 0.483 mmol) and Pd<sub>2</sub>(dba)<sub>3</sub> (58.3 mg, 0.064 mmol) were mixed in pre-degassed dry toluene (20 ml). The temperature was raised to 110 °C and the reaction was left stirring for 3 days.

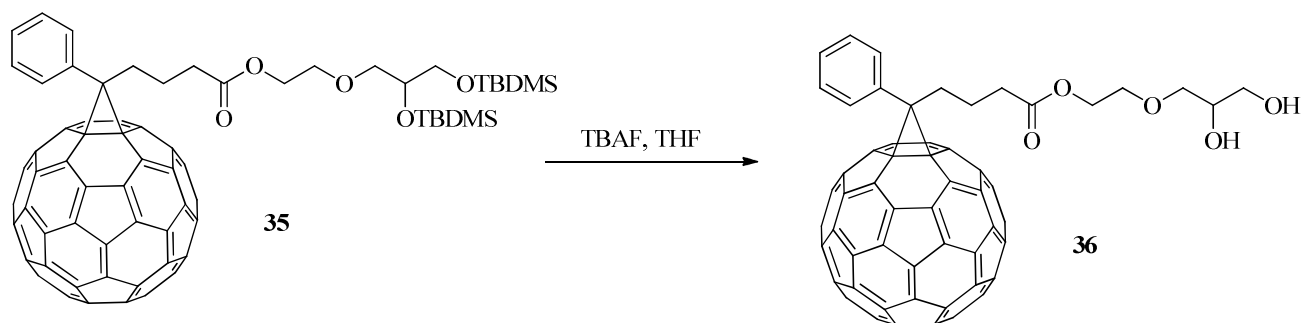
Precipitation of the mixture was performed by addition to methanol, and the formed precipitate was purified by soxhlet extraction with methanol (24 h) and hexane (24 hours) before extracting the polymer with chloroform. The polymer was re-precipitated from a mixture of toluene and chloroform in methanol to give the desired polymer (376 mg). *M<sub>w</sub>*: 44206, *M<sub>n</sub>*: 19543, PDI: 2.3



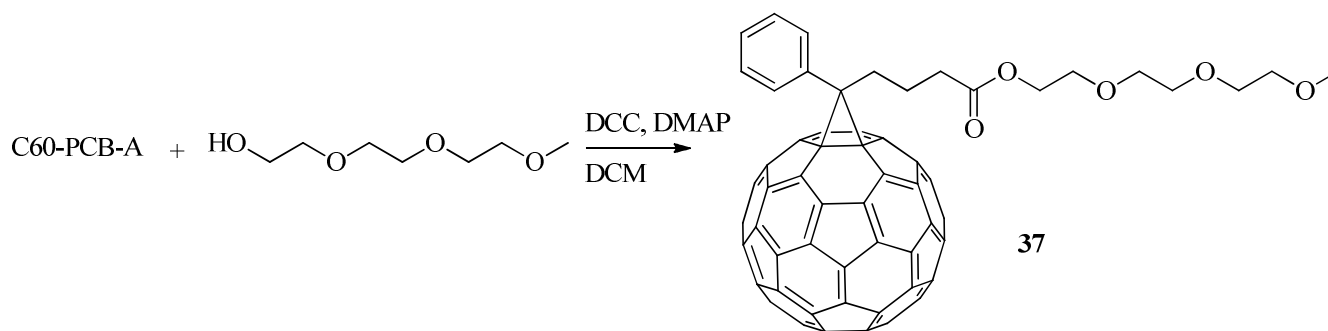
**2-(2,3-bis((tert-butyl)dimethylsilyloxy)propoxy)ethanol (34):** Compound **5** (1.003 g, 2.307 mmol) in dry diethyl ether (6 ml) was added to an ice cooled suspension of LiAlH<sub>4</sub> (0.297 g, 7.83 mmol) in dry diethyl ether (6 ml). After stirring for 5 minutes the temperature was raised to reflux at which the mixture was stirred for 1 hour. The reaction mixture was then very carefully quenched with saturated NaHCO<sub>3</sub> followed by extraction with ether. The collected ethereal phases were washed with brine, dried over MgSO<sub>4</sub> and the solvent was removed to yield the desired product as a colorless clear oil (0.711 g, 85%). <sup>1</sup>H NMR (500 MHz, CDCl<sub>3</sub>) δ 3.88 – 3.77 (m, 1H), 3.75 – 3.68 (m, 2H), 3.61 – 3.46 (m, 6H), 1.79 (s, 1H), 0.89 (2 x s, 18H), 0.11 – 0.01 (m, 12H). <sup>13</sup>C NMR (126 MHz, CDCl<sub>3</sub>) δ 73.12, 72.77, 72.57, 64.99, 61.96, 26.09, 25.99, 18.51, 18.35, -4.43, -4.54, -5.20, -5.25.



**Fullerene 35:** C<sub>60</sub>-PCB-A (104 mg, 0.116 mmol), DMAP (3.81 mg, 0.031 mmol) and compound **34** (65.43 mg, 0.179 mmol) were mixed in DCM and cooled to 0 °C. DCC (29.1 mg, 0.141 mmol) was then added and the mixture was stirred for an additional 10 min at 0 °C after which the temperature was raised to RT and the reaction was monitored by TLC. The mixture was first stirred at RT for 1 day, then at 30 °C for one day and finally an additional day at 30 °C after adding additional DMAP (16 mg, 0.131 mmol) and DCC (24.03 mg, 0.116 mmol). The crude product was purified by gradient column chromatography (First heptane/AcOEt, 1% steps; then heptanes/AcOEt 0.8% steps) to yield the pure product (94.6 mg, 66%). <sup>1</sup>H NMR (500 MHz, CDCl<sub>3</sub>) δ 7.93 (d, *J* = 7.4 Hz, 2H), 7.55 (d, *J* = 7.4 Hz, 2H), 7.47 (d, *J* = 7.4 Hz, 1H), 4.27 – 4.15 (m, 2H), 3.86 – 3.76 (m, 1H), 3.72 – 3.60 (m, 2H), 3.59 – 3.46 (m, 3H), 3.46 – 3.36 (m, 1H), 2.97 – 2.84 (m, 2H), 2.53 (dd, *J* = 9.6, 5.5 Hz, 2H), 2.25 – 2.12 (m, 2H), 0.92 – 0.84 (m, 18H), 0.10 – 0.00 (m, 12H). <sup>13</sup>C NMR (126 MHz, CDCl<sub>3</sub>) δ 173.14, 148.96, 147.95, 145.99, 145.32, 145.28, 145.21, 145.17, 144.92, 144.82, 144.80, 144.64, 144.56, 144.14, 143.90, 143.26, 143.17, 143.12, 143.06, 142.38, 142.31, 142.27, 142.25, 141.13, 140.88, 138.18, 137.70, 136.87, 132.23, 128.57, 128.38, 80.04, 73.46, 72.77, 69.37, 65.05, 63.88, 52.02, 35.05, 34.08, 33.83, 26.08, 26.00, 25.59, 24.81, 22.45, 18.47, 18.32, -4.48, -4.51, -5.22, -5.26



**Fullerene 36:** To a solution of fullerene **35** (94.6 mg, 0.076 mmol) in THF (1 ml) was added TBAF (1.0 M in THF, 0.190 ml, 0.190 mmol), and the mixture was left at RT for approx 4 hours, after which the compound had precipitated on the inside of the reaction vessel. The solid was washed extensively with THF and dried in vacuum (74 mg, 96 %).



**Fullerene 37:** C<sub>60</sub>-PCB-A (97 mg, 0.11 mmol), triethyleneglycol monomethyl ether (72 mg, 0.44 mmol) and DMAP (44 mg, 0.36 mmol) was mixed in DCM (1 ml) followed by cooling on an ice bath.

Dicyclohexylcarbodiimide (108 mg, 0.52 mmol) was then added and the mixture was left stirring at RT for 2 days and at 35 °C for an additional 2 days. Purification on a silica column with gradient eluent (toluene, increasing with 2% AcOEt steps) yielded the desired product (83 mg, 74%).

<sup>1</sup>H NMR (500 MHz, CDCl<sub>3</sub>) δ 7.95 – 7.91 (m, 2H), 7.57 – 7.52 (m, 2H), 7.50 – 7.44 (m, 1H), 4.27 – 4.20 (m, 2H), 3.72 – 3.67 (m, 2H), 3.67 – 3.61 (m, 6H), 3.57 – 3.52 (m, 2H), 3.38 (s, 3H), 2.94 – 2.87 (m, 2H), 2.55 (t, *J* = 7.6 Hz, 2H), 2.24 – 2.13 (m, 2H).

### 2.6.2 Device preparation

**Al doped zinc oxide (ETL):** Zn(OAc)<sub>2</sub>·2H<sub>2</sub>O (20 g), Al(OH)(AOC)<sub>2</sub> (0.3 g) and Zonyl FSO-100 (0.6 g) were mixed in 200 mL of demineralized water. The mixture was stirred for 2 hours and filtered through a 0.45 micron filter to remove insoluble material. The ink was used directly thereafter and could be stored for many months without noticeable change in performance when subsequently used. The ink could be spincoated or roll-to-roll coated. An important step is that the initially dry film must be heated for 5-40 minutes at 140 °C to yield electron transporting films.

**PEDOT:PSS (HTL):** In a typical experiment PEDOT:PSS (Agfa EL-P 5010) was diluted with *iso*-propanol 2:1 (w/w). The ink could be spin coated or slot-die coated. The PEDOT:PSS films were dried at 140 °C for 5 min.

**Metal back electrode:** The metal back electrode comprised silver flake (FS 16 from Johnson Matthey) mixed with an aqueous binder and water. In a typical formulation silver flake (110 g) was mixed well with an aqueous solution of binder. The aqueous solution was prepared by mixing the binder (Viacryl 175W40WAIP from Cytec) (25 g) with water (25 g). The metal paste could be screen printed using a steel mesh (72/36).

## 2.7 References

1. Patil, A. O.; Ikenoue, Y.; Wudl, F.; Heeger, A. J. Water-Soluble Conducting Polymers. *J. Am. Chem. Soc.* **1987**, *109* (6), 1858-1859.
2. Ogawa, M.; Tamanoi, M.; Ohkita, H.; Benten, H.; Ito, S. Fabrication and photovoltaic properties of multilayered thin films designed by layer-by-layer assembly of poly(p-phenylenevinylene)s. *Sol. Energy Mater. Sol. Cells* **2009**, *93* (3), 369-374.
3. Tran-Van, F.; Carrier, M.; Chevrot, C. Sulfonated polythiophene and poly (3,4-ethylenedioxythiophene) derivatives with cations exchange properties. *Synthetic Metals* **2004**, *142* (1-3), 251-258.
4. Rider, D. A.; Worfolk, B. J.; Harris, K. D.; Lalany, A.; Shahbazi, K.; Fleischauer, M. D.; Brett, M. J.; Buriak, J. M. *Adv. Func. Mater.* **2010**, *20*, 2404-2415.
5. Li, H. M.; Li, Y. L.; Zhai, J.; Cui, G. L.; Liu, H. B.; Xiao, S. Q.; Liu, Y.; Lu, F. S.; Jiang, L.; Zhu, D. B. Photocurrent generation in multilayer self-assembly films fabricated from water-soluble poly(phenylene vinylene). *Chemistry-A European Journal* **2003**, *9* (24), 6031-6038.
6. Sgobba, V.; Troeger, A.; Cagnoli, R.; Mateo-Alonso, A.; Prato, M.; Parenti, F.; Mucci, A.; Schenetti, L.; Guldi, D. M. Electrostatic layer-by-layer construction and characterization of photoelectrochemical solar cells based on water soluble polythiophenes and carbon nanotubes. *J. Mater. Chem.* **2009**, *19* (25), 4319-4324.
7. Qiao, Q. Q.; Su, L. Y.; Beck, J.; McLeskey, J. T. Characteristics of water-soluble polythiophene: TiO<sub>2</sub> composite and its application in photovoltaics. *J. Appl. Phys.* **2005**, *98* (9), 094906.
8. Qiao, Q. Q.; Xie, Y.; McLeskey, J. T. Organic/inorganic polymer solar cells using a buffer layer from all-water-solution processing. *J. Phys. Chem., C* **2008**, *112* (26), 9912-9916.
9. Rud, J. A.; Lovell, L. S.; Senn, J. W.; Qiao, Q. Q.; McLeskey, J. T. Water soluble polymer/carbon nanotube bulk heterojunction solar cells. *Journal of Materials Science* **2005**, *40* (6), 1455-1458.
10. Choi, D.; Stables, J. P.; Kohn, H. The anticonvulsant activities of functionalized N-benzyl 2-acetamidoacetamides. The importance of the 2-acetamido substituent. *Bioorganic & Medicinal Chemistry* **1996**, *4* (12), 2105-2114.
11. McDougal, P. G.; Rico, J. G.; Oh, Y. I.; Condon, B. D. A convenient procedure for the monosilylation of symmetric 1,n-diols. *The Journal of Organic Chemistry* **1986**, *51* (17), 3388-3390.
12. Petersen, M. H.; Gevorgyan, S. A.; Krebs, F. C. Thermocleavable Low Band Gap Polymers and Solar Cells Therefrom with Remarkable Stability toward Oxygen. *Macromolecules* **2008**, *41* (23), 8986-8994.
13. Deguchi, S.; Alargova, R. G.; Tsujii, K. Stable dispersions of fullerenes, C-60 and C-70, in water. Preparation and characterization. *Langmuir* **2001**, *17* (19), 6013-6017.

14. Pedersen, D. S.; Rosenbohm, C. Dry column vacuum chromatography. *Synthesis-Stuttgart* **2001**, (16), 2431-2434.

## Chapter 3

### Synthesis of new LBG polymers for analysis of photochemical stability and R2R processed solar cells\*

#### 3.1 Introduction

As mentioned in Chapter 1, the field of polymer solar cell (PSC) has experienced a rapid progress over the last years and many new high performing polymers have been developed and optimized with the introduction of Low-Band-Gap (LBG) polymers. Simultaneously the field has moved from only trying to prepare high efficient cells on a small scale to also include large area fabrications, thus taking the first steps towards manufacture.<sup>[1-4]</sup> Unfortunately most of the high performance polymers from lab scale fabrication are too unstable to be processed in air. This makes the large area processing methods such as roll-to-roll (R2R) coating practically impossible. Processing using R2R coating techniques can be viewed as more ‘rough’ than the laboratory techniques employed during careful optimization of a small scale devices. As a consequence of this, P3HT, which has been a leading material in PSC research for two decades, is still the best choice when it comes to compatibility with large scale processing. Efficiencies in the area of 2-3% have been reported for P3HT,<sup>[3]</sup> while virtually no other polymers have been used in publications of large area solar cells. If the field of PSC’s is to advance further towards actual production, more polymers that can be used in large area PSC’s have to be developed. In such a development it would be practical to have a guideline to what types of donor and acceptor groups, which are susceptible to photodegradation in air. As part of a larger study<sup>[5]</sup> including a multitude of different polymers, the contribution from the work of this thesis was to prepare the monomers corresponding to the highlighted donor and acceptor moieties in Figure 3.1. The benzodithiophens **cBDT** (the two thiophenes are oriented *cis*) and **tBDT** (the two thiophenes are oriented *trans*) were chosen for examination of the effect of having no side chains on the donor moiety of a polymer. The di(thiophene-2-yl)thienoimidazolone (**DTTI**) was

---

\* Some of this work has been published

Manceau, M.; Bundgaard, E.; Carle, J. E.; Hagemann, O.; Helgesen, M.; Søndergaard, R.; Jørgensen, M.; Krebs, F. C.; *J. Mater. Chem.* **2011**, *21* (12), 4132-4141.

Carlé, J. E.; Jørgensen, M.; Manceau, M.; Helgesen, M.; Hagemann, O.; Søndergaard, R.; Krebs F.C. *Sol. Energy Mater. & Sol. Cells* **2011**, *95* (12), 3222-3226

Søndergaard, R.; Manceau, M.; Jørgensen, M.; Krebs, F. C. *Adv. Energy Mater.* **2012**, *2* (4), 415-418

chosen in order to examine the presence of heteroatoms on the donor moiety and the di(thiophene-2-yl)diketo-pyrrolopyrrole (**DTDPP**) was chosen in order to examine the influence on heteroatoms on the acceptor moiety. The non-highlighted moieties correspond to monomers that have not been synthesized as part of this thesis (commercially available or synthesized by others), but have been used in the preparation of the final polymers.

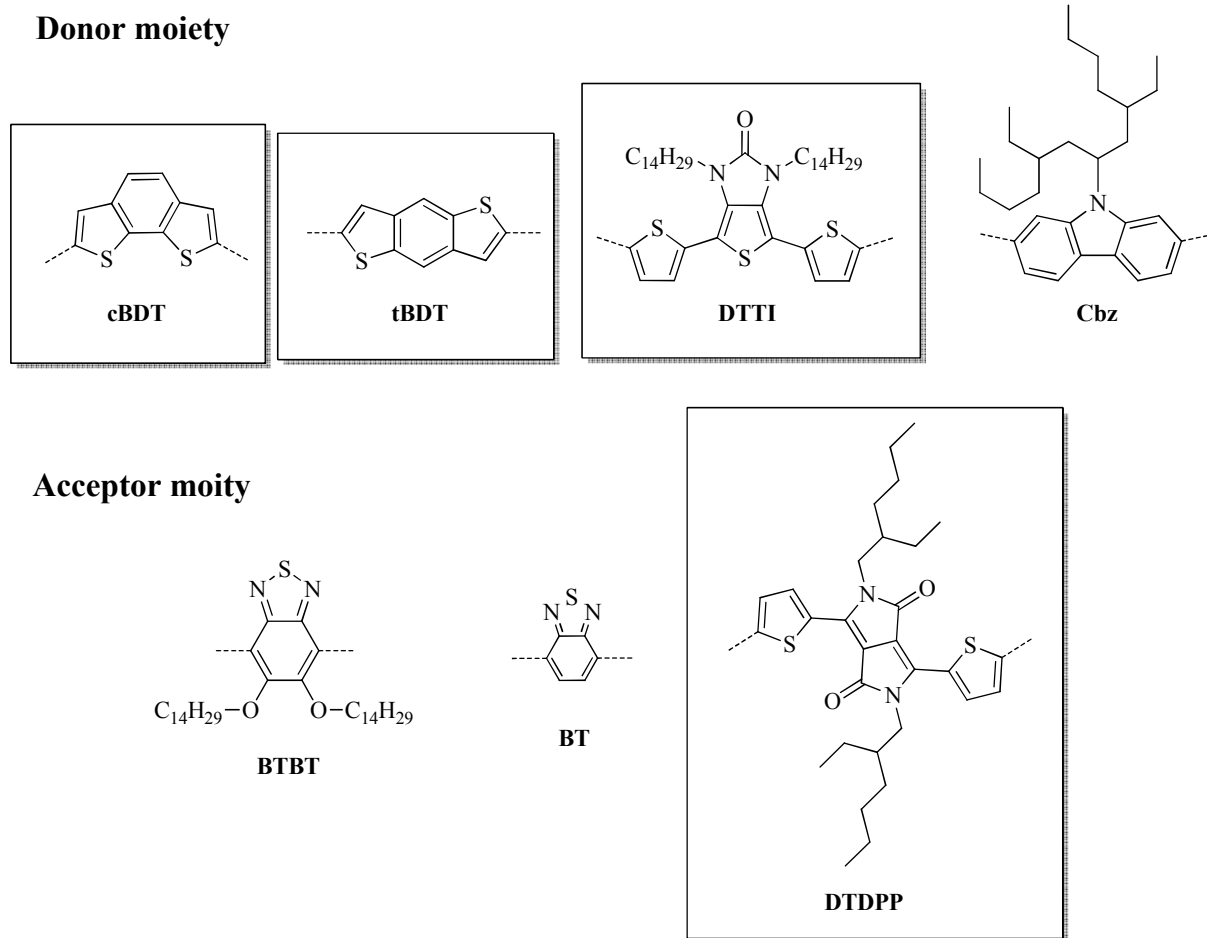


**Figure 3.1** Overview of the different donor and acceptor moieties involved in the polymers synthesized in this study. Monomers corresponding to the highlighted moieties have been prepared in this work, while the remaining have been either commercially available or have been prepared by others. **cBDT**: benzo[1,2-b:6,5-b']dithiophene, **tBDT**: benzo[1,2-b:4,5-b']dithiophene, **DTTI**: 1,3-ditetradecyl-4,6-di(thiophen-2-yl)-1*H*-thieno[3,4-d]imidazol-2(3*H*)-one, **Cbz**: 9-(5,9-diethyltridecan-7-yl)-9*H*-carbazole, **BTBT**: 5,6-bis(tetradecyloxy)benzo[*c*][1,2,5]thiadiazole, **BT**: benzo[*c*][1,2,5]thiadiazole, **DTDPP**: 2,5-bis(2-ethylhexyl)-3,6-di(thiophen-2-yl)pyrrolo[3,4-*c*]pyrrole-1,4(2*H*,5*H*)-dione.

### 3.2 Synthesis of polymers

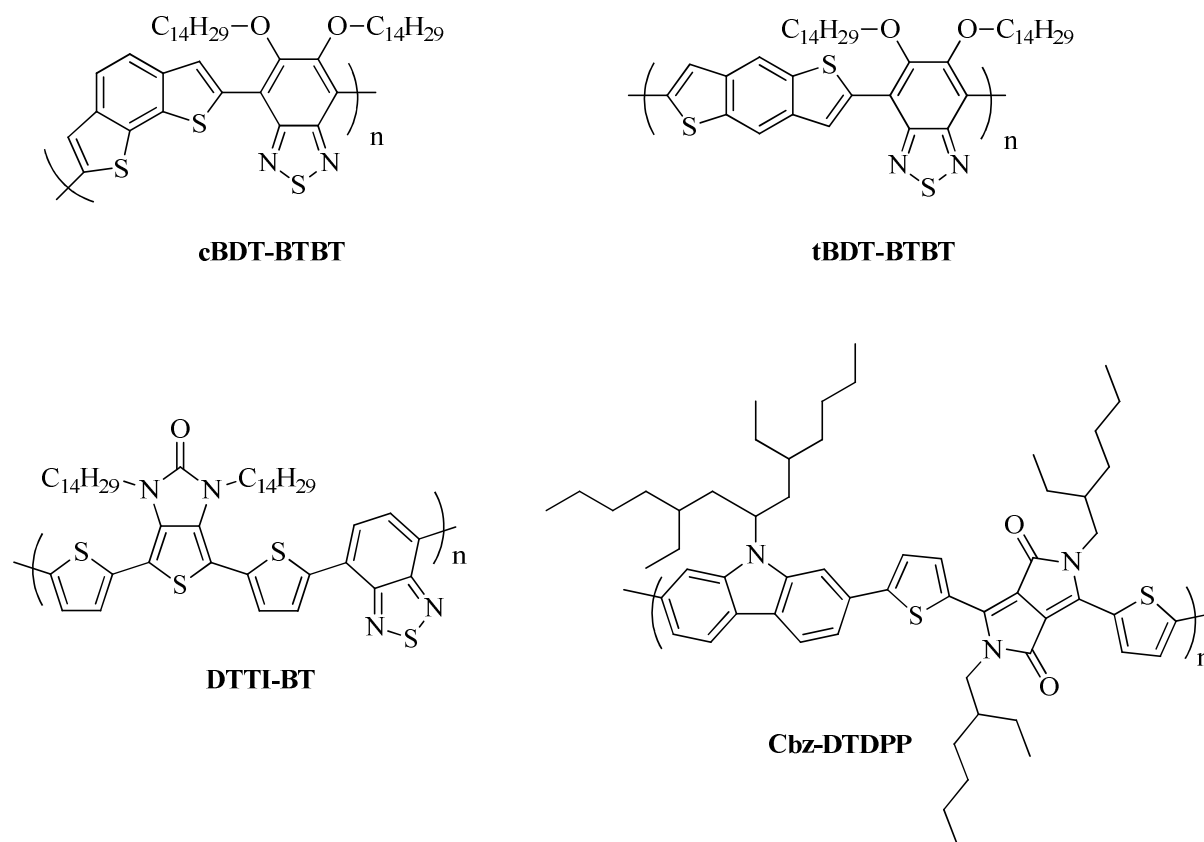


**Figure 3.2** Polymers synthesized for study of their photochemical stability.

The polymers shown in Figure 3.2 were synthesized and their photochemical stability examined. **cBDT-BTBT** and **tBDT-BTBT** were prepared with the aim of examining the influence of attaching the side chains to the acceptor moiety, and in addition to compare if the difference in symmetry of the benzobithiophenes had an influence on stability. **DTTI-BT** and **Cbz-DTDPP** were selected in order to examine the influence of the presence of side-chains attached to nitrogen on polymer stability.

For the polymers **cBDT** and **tBDT** a thorough study of the optimization of R2R coated cells was furthermore performed as well as extensive outdoor stability tests in eight countries which will be discussed in chapter 4.

Synthetic details can be found in the experimental section (3.6) at the end of the chapter.



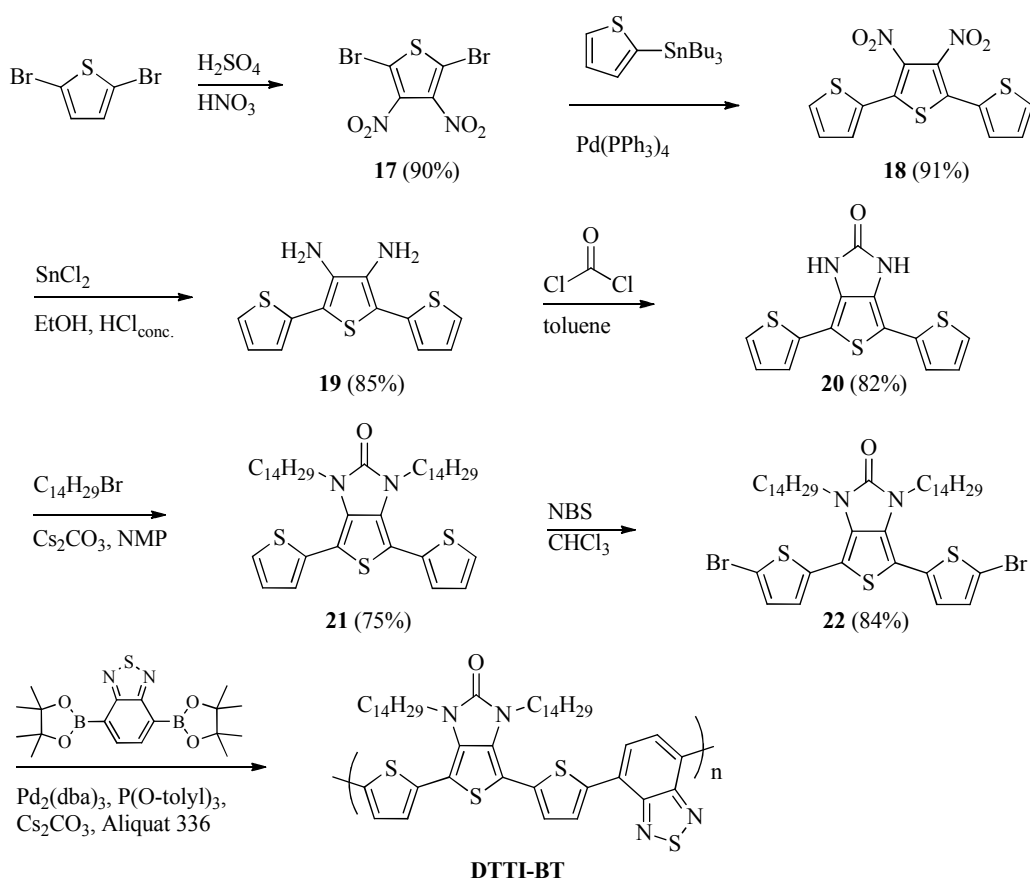




rotavapory system) and the fact that it had been dried in a vacuum oven over night. No attempts were made towards optimizing the synthesis. The subsequent synthesis of compound **13-14** were performed according to the procedure described by Takimya *et al.*<sup>[10]</sup> Selective Sonogashia coupling in the 2 and 5 positions was performed by reaction of compound **12** with ethynyltrimethylsilane to give compound **13**. Care must be taken in this step to keep the temperature down and adding the alkyne slowly (which the authors does not point out) as the reaction is exothermic and formation of the tri-substituted side product by reaction with the bromine occurs if precautions are not taken. Subsequent reaction with first *tert*-BuLi and then sulfur leads to ring closure to the benzobithiophene anion which is neutralized upon treatment with ethanol give compound **14**. Removal of the TMS groups is easily performed with TBAF to give **15** which upon treatment with *n*-BuLi followed by reaction with trimethyltinchloride leads to the desired distannylated benzoedithiophene **16**. **tBDT-BTBT** was finally synthesized by Stille coupling between compounds **11** and **16** ( $M_w$  310000,  $M_n$  80000, PD 3.8).

### 3.2.3 Synthesis of DTTI-BT

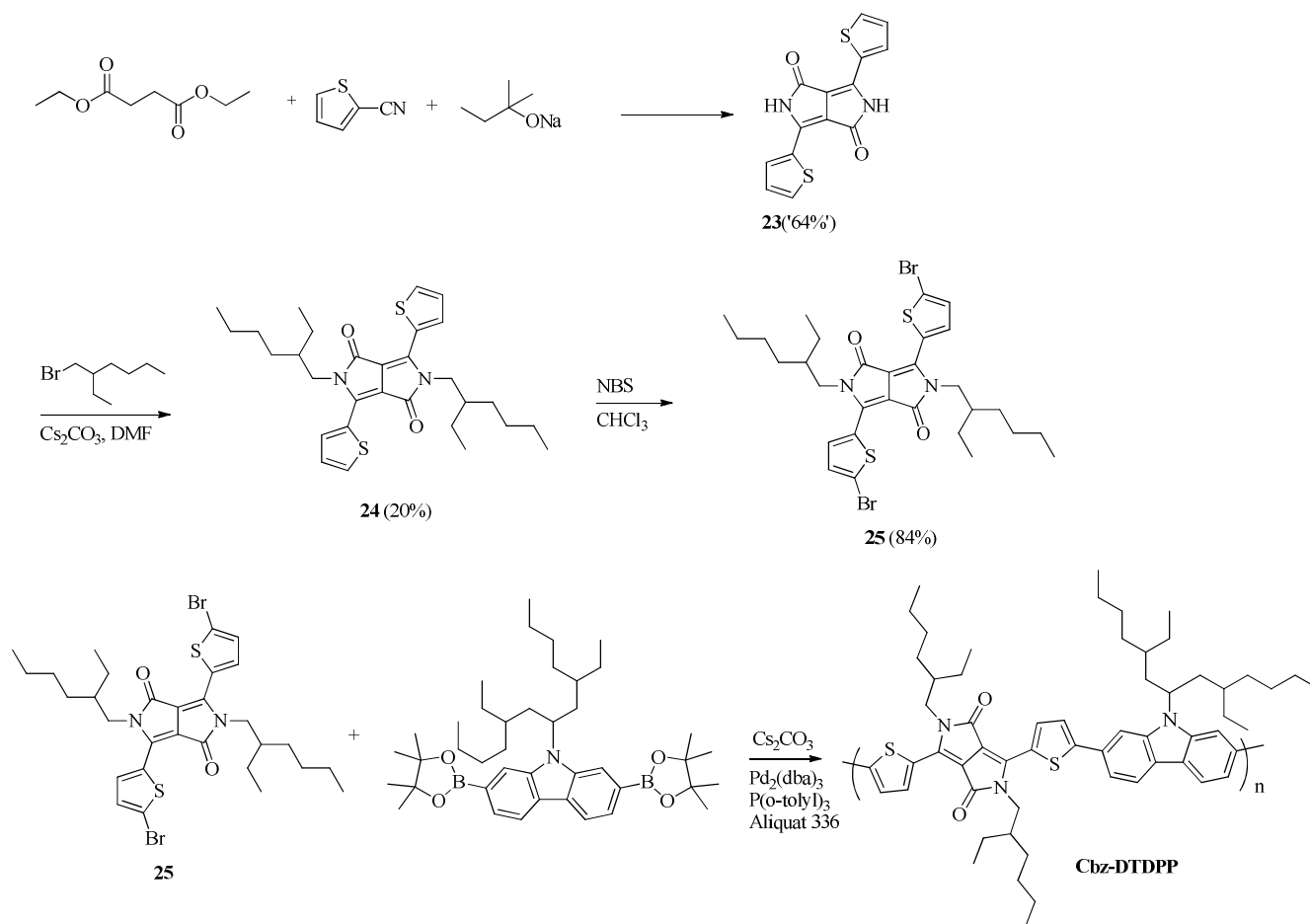
The synthetic route to the polymer **DTTI-BT** is outlined in Scheme 3.3. Nitration of 2,5-dibromothiophene using the procedure published by Wen & Rasmussen<sup>[11]</sup> yielded the desired dinitrated compound in excellent yield. Subsequent Stille coupling with 2-tributyltinthiophene afforded dinitroterthiophene **18** which was reduced to the corresponding diaminoterthiophene **19** with tin(II)chloride in acidic solution. Compound **19** was then reacted with phosgene to yield the thienoimidazolone **20** followed by N,N'-dialkylation, by reaction of **20** with 1-bromotetradecane in N-methyl-2-pyrrolidone (NMP) with cesium carbonate as base, to yield compound **21**. NBS bromination of **21** yielded the final monomer **22** which as a last step was reacted by Suzuki coupling with commercial 2,1,3-Benzothiadiazole-4,7-bis(boronic acid pinacol ester) to yield **DTTI-BT** ( $M_w$  14700,  $M_n$  6000, PDI 2.45).



Scheme 3.3: Synthetic route to DTTI-BT

### 3.2.4 Synthesis of Cbz-DTDP

Using an analogue method to the one published by Morton *et al*<sup>[12]</sup> substituting furan-carbonitrile with thiophene-2-carbonitrile, the latter was reacted with diethyl succinate in the presence of a the sterically hindered base sodium *tert*-pentoxyde which afforded the diketopyrrolopyrrole (DPP) **23**. DPP analogues generally have very low solubilities in all common solvents and impurities trapped within the precipitated solids cannot be easily removed. As the compound is slightly soluble in DMF it could be purified to some degree by passing the DMF solution though a short silica column. An enormous amount of DMF is necessary though, in order to extract the compound from the column, and this procedure was abandoned. The crude product of **23** was instead used in the subsequent reaction without purification. N-alkylation of **23** was performed according to the procedure described by Song *et al*<sup>[13]</sup> with a few modifications (different side chain, Cs<sub>2</sub>CO<sub>3</sub> instead of K<sub>2</sub>CO<sub>3</sub> and prolonged reaction time). Reaction of **23** with 1-bromo-2-ethylhexyl in DMF with Cs<sub>2</sub>CO<sub>3</sub> as base at 55 °C afforded compound **24** in low yield. Others have reported high yields (41-76%)<sup>[14,15]</sup> by performing the reaction at higher temperatures, but attempts to



**Scheme 3.4:** Synthetic route to **Cbz-DTDPP**

duplicate these results did not improve the original yield. It is worth mentioning though that a good yield (72%) with less byproduct was obtained when performing a similar reaction of **23** in N-methyl-2-pyrrolidone (NMP) (instead of DMF) with a differently structured halide (see appendix 1, compound I4). The use of NMP for the preparation of **24** was never attempted, but could be worth trying in future preparation.

Compound **24** was subsequently brominated with NBS in chloroform to give **25** which was coupled with commercial 9-(5,9-diethyltridecan-7-yl)-2,7-bis(4,4,5,5-tetramethyl-1,3,2-dioxaborolan-2-yl)-9H-carbazole to yield **Cbz-DTDPP** ( $M_w$  3150,  $M_n$  1813, PDI 1.7). The relative low molecular size of the polymer was ignored as the main purpose was to examine the photochemical stability, as other have already published the use of the polymer in solar cells.<sup>[16,17]</sup>

### 3.2.4 Optical properties of the polymers

The absorption spectra of the polymers as films on KBr are shown in Figure 3.3. The optical band gaps, defined by the onset of absorption, are quite similar for all the polymers except for **Cbz-DTDPP** which have a somewhat lower bandgap (see Table 3.1).

**Table 3.1**

Molecular weight and optical data for the four polymers

Polymer	Mw (g/mol)	PD	Film		
			$\lambda_{\max}$ (nm)	$\lambda_{\text{onset}}$ (nm)	$E_g$ (eV)
<b>cBDT-BTBT*</b>	170000	2.7	376, 572	661	1.88
<b>tBDT-BTBT*</b>	101000	5.5	376, 607	660	1.88
<b>DTTI-BT</b>	14700	2.45	378, 578	733	1.69
<b>Cbz-DTDPP</b>	3150	1.7	385, 637	800	1.55

\* The molecular weights for polymer **cBDT-BTBT** and **tBDT-BTBT** used for the characterization of the optical properties differ from the ones in the experimental section, as they are from another batch.

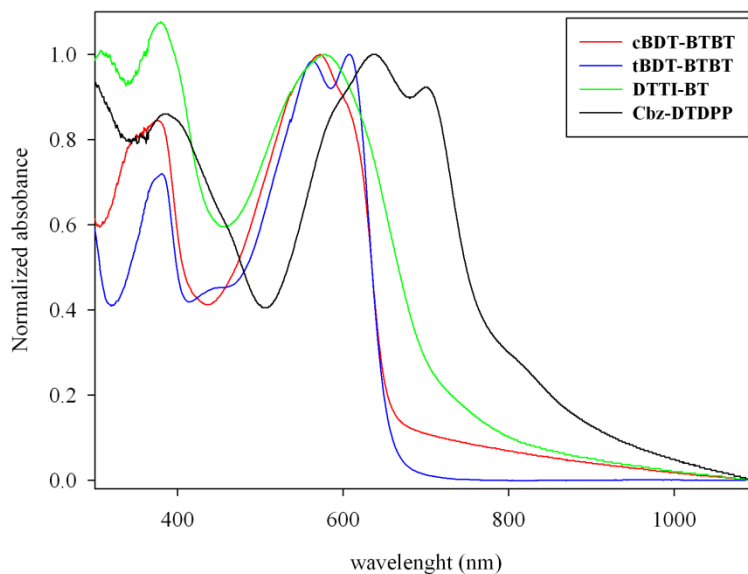


**Figure 3.3:** Thin film UV-absorption spectra of the prepared polymers

### 3.3 Photochemical stability analysis

As mentioned in the introduction of this chapter the polymers **cBDT-BTBT**, **tBDT-BTBT**, **DTTI-BT**, **Cbz-DTDP** were part of a larger comparative study of the influence of different donors and acceptors influence on the photochemical stability of conjugated polymers.<sup>[5]</sup> The polymers were spin coated onto solid KBr and their UV absorption was monitored as a function of exposure time to AM 1.5 conditions (for further details see Manceau *et al* in appendix 2). This work was carried out by Matthieu Manceau, and the overall result can be seen from Figure 3.4.

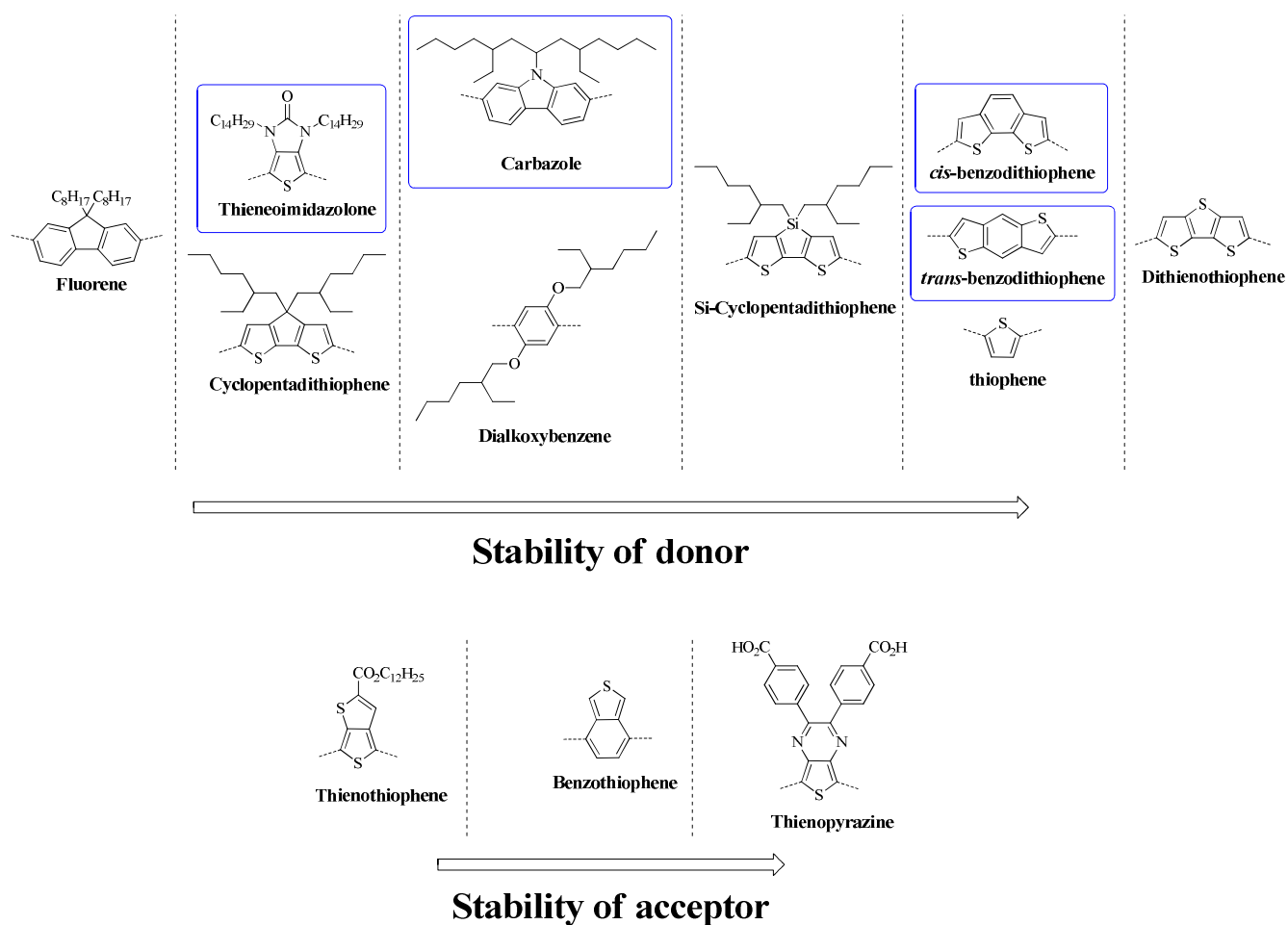


**Figure 3.4:** Results achieved by Manceau *et al* by analyzing the photochemical stability of a large number of polymers. **top:** Donor group stability ranking. **bottom:** Acceptor group stability ranking. Encircled in blue are the groups related to this work. The *cis*-benzodithiophene was not presented in the published work.

The main findings of the study are furthermore summarized below:

1. The use of exocyclic double bonds in the main backbone (MEH-PPV, MDMO-PPV) leads to a poor stability and should be avoided
2. Moieties containing a quaternary site are very unstable (*e.g.* fluorene, cyclopentadithiophene) because of the oxidizability of this site
3. The presence of readily cleavable bonds (such as C – N or C – O) also limits stability
4. Side-chains play a key role in conjugated polymer degradation and their cleavage largely improves stability
5. Aromatic polycyclic units generally exhibit a good photochemical stability.

The polymers **cBDT-BTBT** and **Cbz-DTDPP** were never used in the final publication. **cBDT-BTBT**, because the stability was very comparable with **tBDT-BTBT**. **Cbz-DTDPP**, because in the end only one diketopyrrolopyrrole (DPP) containing polymer was prepared which makes it difficult to draw any comparative conclusions. As the wish was to show general stability trends it was left out.

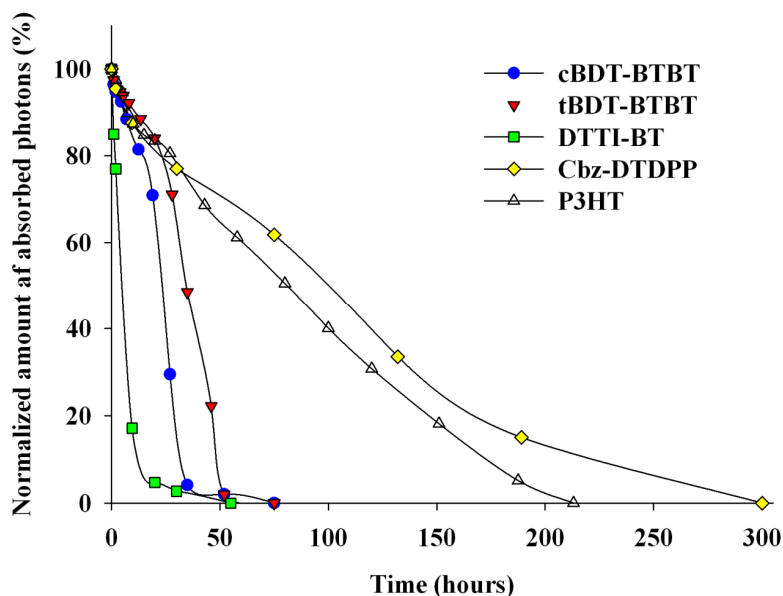


**Figure 3.5** Photoinduced degradation of the polymer and P3HT. Spline curves have been inserted to guide the eye.

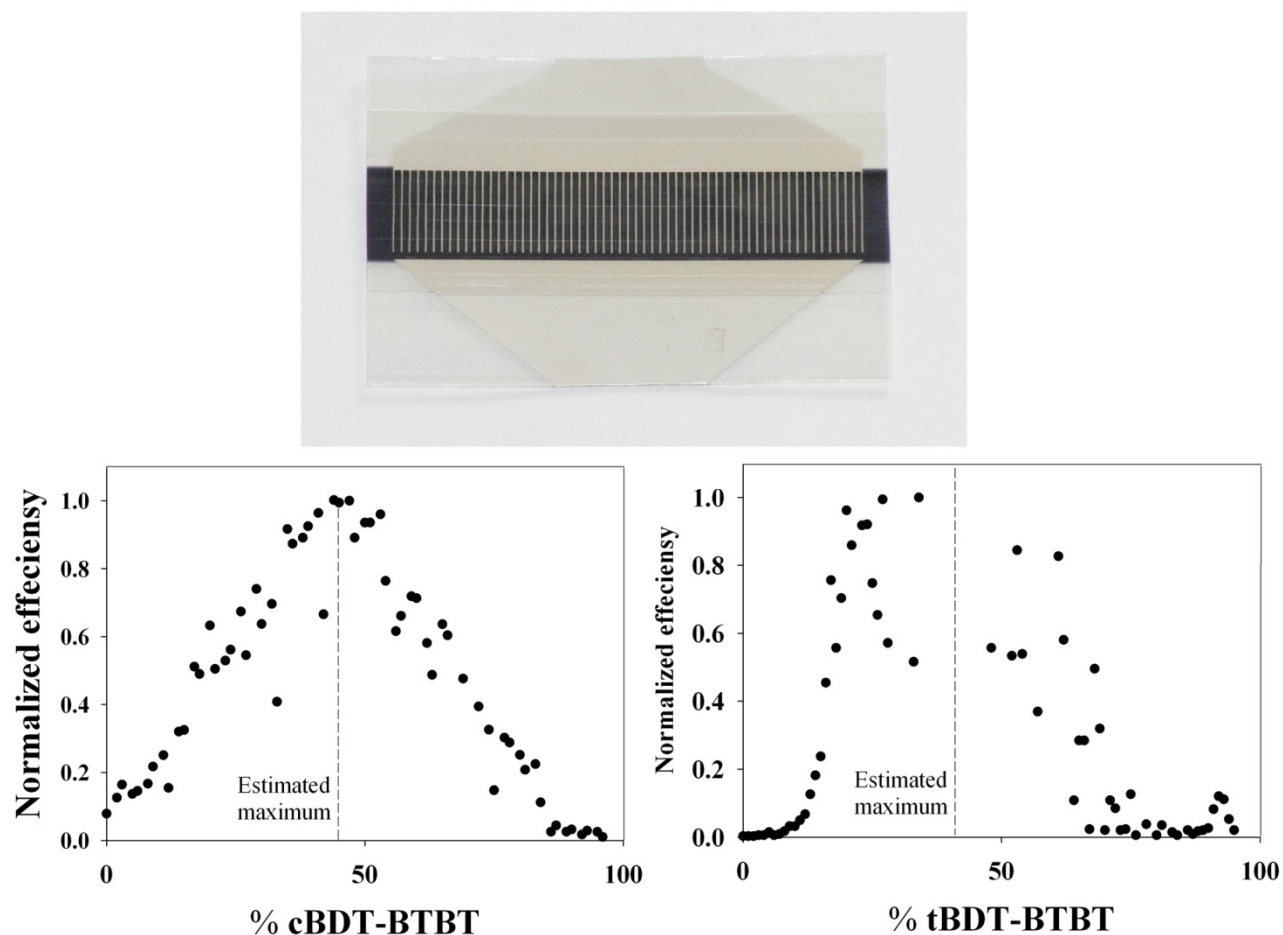


Figure 3.5 shows the photoinduced degradation of synthesized polymers and P3HT, showing a stability ranking **DTTI-BT** < **cBDT-BTBT** < **tBDT-BTBT** < **P3HT** < **Cbz-DTDPP**. **DTTI-BT** was shown to be quite unstable, which is ascribed to the presence of readily cleaved C-N bonds in the thienoimidazolone part of the polymer. **cBDT-BTBT** and **tBDT-BTBT** both show moderately good stabilities (As a comparison a polymer carrying a similar alkoxy-substituted benzothiadiazole acceptor unit and the widely used cyclopentadithiophene donor unit reached bleaching after approximately 7-8 h), but **Cbz-DTDPP** by far shows the highest stability and is even more stable than P3HT. As the carbazole donor in **Cbz-DTDPP** is not a very stability-inducing moiety (see Figure 3.4) the improved stability must be induced by the DPP acceptor. This high stability indicates that it could be worthwhile to look further into the potential use of DPP-containing polymers in R2R-processed solar cells.

### 3.4 Optimization of R2R processing of polymer **cBDT-BTBT** and **tBDT-BTBT**

Because of the relatively good stability of the polymers **cBDT-BTBT** and **tBDT-BTBT**, and because they showed good coating abilities on PET substrates, these were chosen to be examined further for R2R-processing. Using a recently described method where the optimal relative compositions of donor (polymer) and acceptor (PCBM) material in the active layer can be determined very precisely on R2R using a very limited amount of polymer.<sup>[18]</sup> By gradient-appliance of donor, acceptor and solvent using differentially pumped slot-dye-coating, varying either the composition (polymer:PCBM; 0:100 → 100:0, 0.5-1% steps) or the concentration of the active materials in the ink, the use of the R2R procedure allows for much more precise optimization of the active layer buildup than is normally achieved using conventional test of spin-coated devices. Generally only 2-5 different ratio compositions are tested. Here 100-200 ratio compositions can be prepared with roughly the same amount of polymer. As shown in Figure 3.6, the mapping of the relative ratios gives a very precise determination of the optimal blend in the active layer.

The optimizations of solar cells with **cBDT-BTBT** and **tBDT-BTBT** were performed by preparing cells with an inverted structure on PET (PET|ITO|ZnO|active layer|PEDOT|Ag) of a size of 4.2 cm<sup>2</sup>. After optimization, which for **cBDT-BTBT** showed to be a ratio of 45:55 (**cBDT-BTBT** /PCBM) and for **tBDT-BTBT** a ratio of 41:59 (**tBDT-BTBT**:PCBM), cells were prepared under optimized conditions and tested in order to fully characterize the potential of the polymers as active materials in PSC's. A total of 481 solar cells were prepared during the optimization process and an additional 451 cells for the actual



**Figure 3.6:** Graphical representation of the result from differentially pumped slot-dye-coating experiments. **top:** examples of ratio experiments of polymer **cBDT-BTBT** and polymer **tBDT-BTBT** varying the relative composition of the donor and acceptor material.

performance characterization. For the polymer **cBDT-BTBT** the top 100 cells showed average efficiencies of  $1.24 \% \pm 0.13\%$ , open circuit voltage of  $0.68 \text{ V} \pm 0.03 \text{ V}$ , short circuit current of  $5.35 \text{ mA/cm}^2 \pm 0.51 \text{ mA/cm}^2$  and fill factors of  $33.9 \% \pm 1.9\%$ . *JV* characteristics of a representative of the best performing cells using **cBDT-BTBT** was: PCE: 1.72%,  $V_{OC}$ : 0.74 V,  $J_{SC}$ :  $6.40 \text{ mA/cm}^2$ , FF: 36%. These results are comparable to what has previously been achieved in our group using P3HT under similar conditions.

For **tBDT-BTBT** the top 100 cells showed a somewhat inferior result with average efficiencies of  $0.29\% \pm 0.06\%$ , open circuit voltage of  $0.42 \text{ V} \pm 0.06 \text{ V}$ , short circuit current of  $2.33 \text{ mA/cm}^2 \pm 0.29$

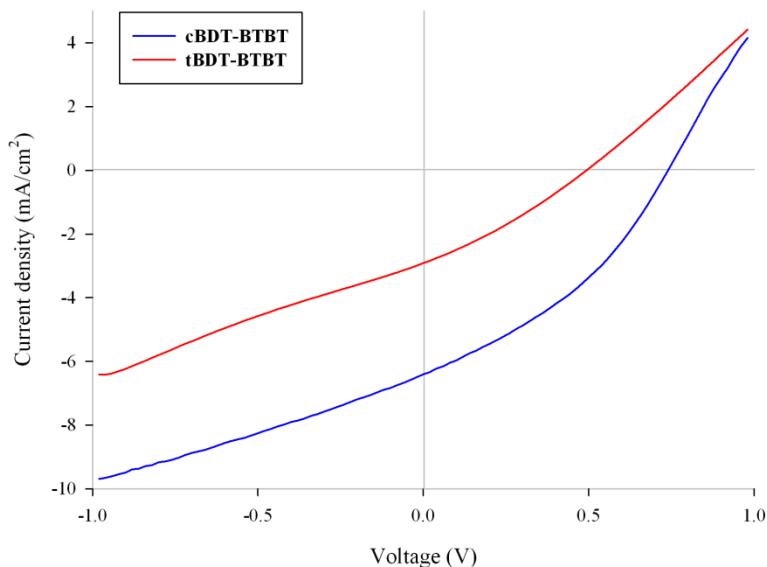


**Figure 3.7:** *JV*-curves of **cBDT-BTBT** and **tBDT-BTBT** from R2R processed cells of 4.2 cm<sup>2</sup>

mA/cm<sup>2</sup> and fill factors of 29.7 %  $\pm$  3.9% and with best *JV* characteristics of: PCE: 0.43%,  $V_{OC}$ : 0.49 V,  $J_{SC}$ : 2.98 mA/cm<sup>2</sup>, FF: 29.8%. Examples of *JV* curves are shown in Figure 3.7.

As an additional examination of the polymers potential small credit card sized modules of both polymers were prepared (16 stripes cells in series with a total active area of 14.5 cm<sup>2</sup>) as illustrated in Figure 3.8. A total of 435 modules of each polymer were prepared, but unfortunately they all suffered from unknown defects. All modules showed a very low initial voltage which could slowly be increased by cycling from negative to positive bias, but in no case were results in efficiencies approaching those of the single cells. In Figure 3.8 is shown the final *JV*-curves of the best performing modules of both polymers. Because of lack of time it was not possible to redo the experiments, but further examination of especially **cBDT-BTBT** is definitely worthwhile for future work.

The polymers **cBDT-BTBT** and **tBDT-BTBT** were furthermore part of a larger outdoor stability study which will be covered in chapter 4.

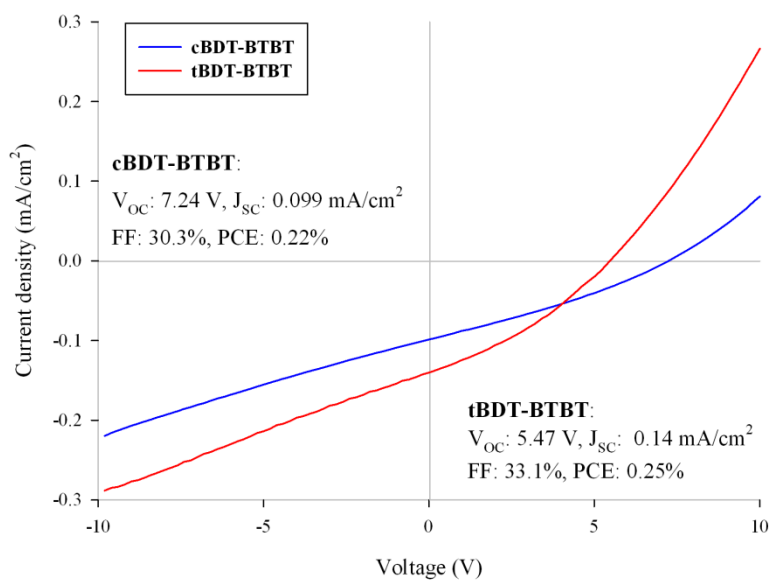
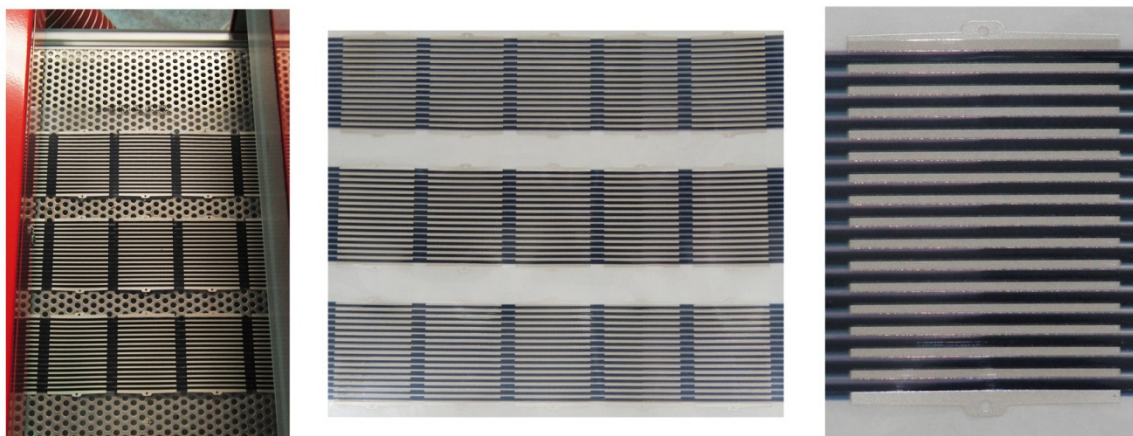
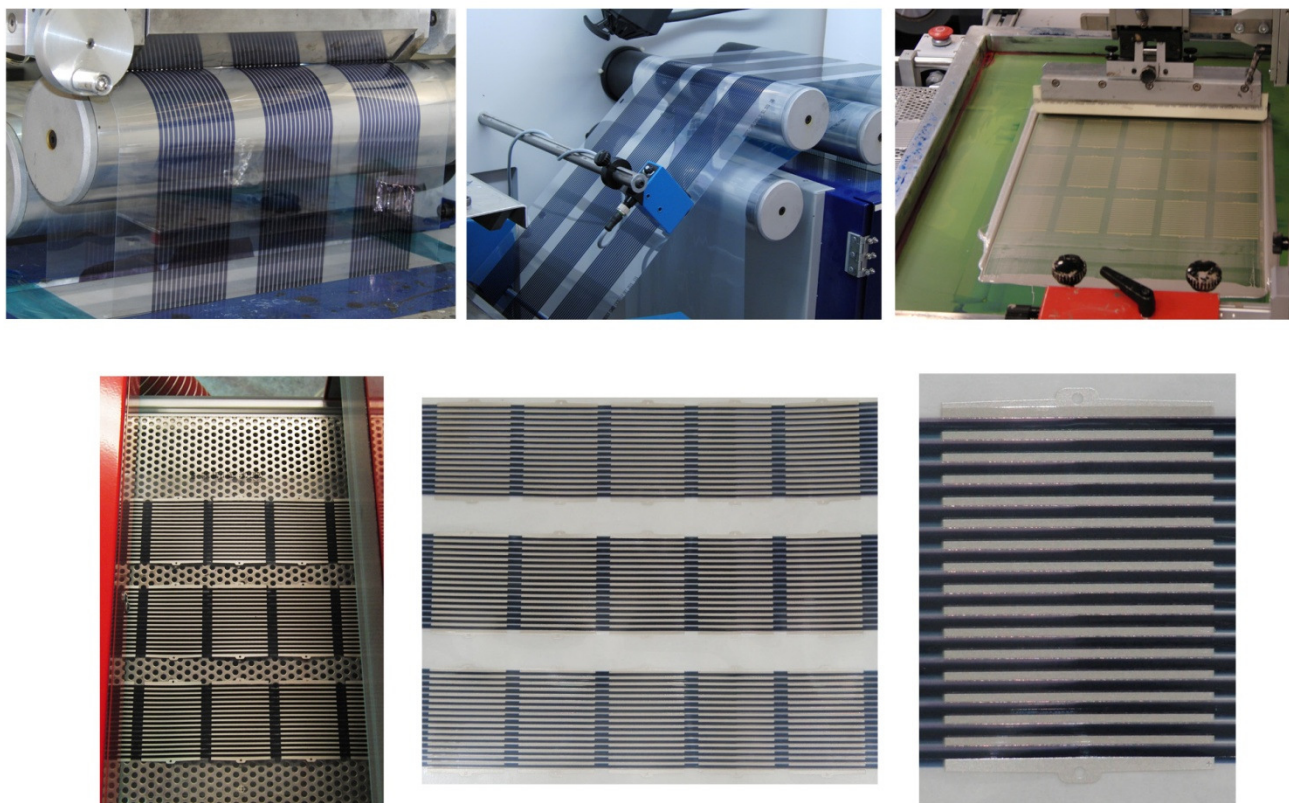


**Figure 3.8 top:** Pictures of the processing of credit card sized modules and of the final modules. **bottom:** *J/V*-curves of the best performing modules prepared with polymer 1 and 2.

### 3.5 Conclusion

Because of the requirement to process polymer solar cells in the ambient, when using large scale production methods like roll-to-roll coating, there is a need for development of new low-band-gap polymers with higher stabilities that can be processed under such conditions.

Four new polymers were therefore synthesized for analysis of their photochemical stabilities, as part of a larger project where a classification of different donors and acceptors has been performed with respect to how susceptible they are to photodegradation. Of the four polymers **DTTI-BT**, containing a N,N'-dialkyl thienoimidazolone donor unit, showed to be the most unstable. This is ascribed to the readily cleaved N-C<sub>alkyl</sub> bond. The polymers **cBDT-BTBT** and **tBDT-BTBT** carrying two different benzobithiophene donors without side chains showed to have acceptable stabilities although still inferior to P3HT. The stabilities are ascribed to the fact that no side chains are attached to the donor unit. The most stable of the four showed to be polymer **Cbz-DTDPP** which have slightly higher photochemical stability than P3HT - this although **Cbz-DTDPP** contains a carbazole donor unit which is moderate in stability. The induced stability must therefore originate from the diketopyrrolopyrrole acceptor moiety, which makes this donor an interesting candidate for future preparation of polymers for large scale production.

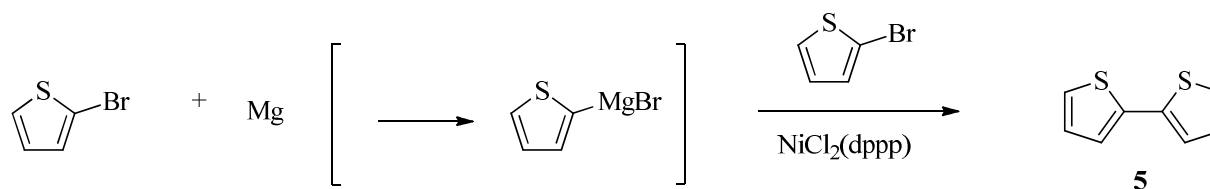
Polymer **cBDT-BTBT** and **tBDT-BTBT** furthermore showed good coating properties on flexible substrates like PET, and a thorough optimization study was performed using gradient appliance of the polymer and PCBM by differentially pumped slot-dye-coating. The optimized ratio was then used in the preparation of cells whose performance were characterized under AM 1.5 conditions. The best results were achieved for polymer **cBDT-BTBT** for which the top 100 cells showed average efficiencies of  $1.24 \% \pm 0.13\%$ , open circuit voltage of  $0.68 \text{ V} \pm 0.03 \text{ V}$ , short circuit current of  $5.35 \text{ mA/cm}^2 \pm 0.51 \text{ mA/cm}^2$  and fill factors of  $33.9 \% \pm 1.9\%$ . Best performing cell showed PCE: 1.72%,  $V_{OC}$ : 0.74 V,  $J_{SC}$ : 6.40  $\text{mA/cm}^2$ , FF: 36%. These are the first results of the use of low-band-gap polymers prepared in a R2R process where the cells show efficiencies approaching those obtainable for P3HT.

Credit card sized modules (435 for each polymer) were furthermore prepared, but none of the prepared modules came near the efficiencies obtained by single cells. The reason for these disappointing results is unknown, and unfortunately time did not allow for redoing the experiment within the time limits of this thesis. Seen in the light of the promising results of the single cells, it should be emphasized that this will probably be worthwhile as future work.

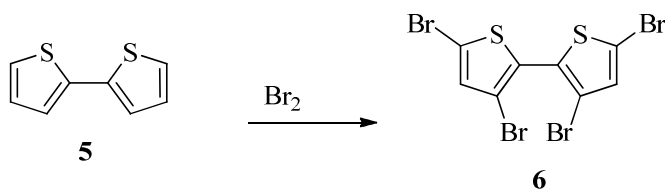
## 3.6 Experimental section

### 3.6.1 Synthesis

**4,7-dibromo-5,6-bis(tetradecyloxy)benzo[c][1,2,5]thiadiazole (11)** was prepared as previously described by Helgesen *et al.*<sup>[8]</sup>

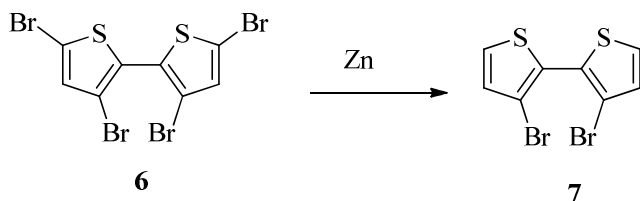


**2,2'-bithiophene(5):** 2-bromothiophene (41 g, 251 mmol) was added to magnesium (10 g, 411 mmol) in diethyl ether (150 ml) over 2 h. The Grignard solution was then added portion wise over 30 min to a solution of 2-bromothiophene (36 g, 221 mmol) in ether diethyl ether (200 ml) with  $\text{NiCl}_2(\text{dppp})$  (0.25 g, 0.461 mmol) as catalyst. The mixture was brought to reflux for 1½ hour after which it was poured into ice water (500 ml) containing a little concentrated HCl (2½ ml). The phases were separated and the aqueous phase was extracted with DCM. After drying of the combined organic phases over  $\text{MgSO}_4$  and evaporation of the solvents a crude dark oil (37.23 g) was isolated that crystallized upon standing. This crude was used in the next step without further purification.

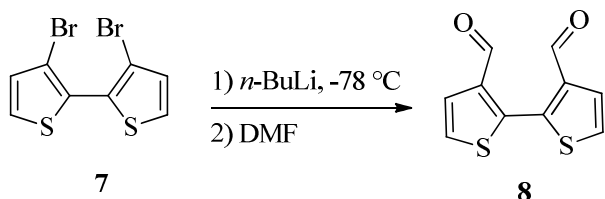


**3,3',5,5'-tetrabromo-2,2'-bithiophene (6):** The crude product of 2,2'-bithiophene ('221 mmol') was dissolved in a mixture of chloroform (400 ml) and acetic acid (150 ml). Bromine (148 g, 928 mmol) was added drop wise over 1 hour, after which the mixture was heated to reflux for a short period (10 min) to drive off excess HBr and  $\text{Br}_2$ . Ice cold 10% NaCl-solution (500 ml) was then added while stirring, and the main part of the aqueous phase was decanted and the chloroform was removed *in vacuo*. Water was added (400 ml) and the solid was filtered off and washed thoroughly with water and a little ethanol. The

solid was triturated in boiling ethanol (1.2 l) and after cooling the light green solid was filtered off and washed with EtOH (2 x 200 ml) giving the desired product (103 g, 97%).  $^1\text{H}$  NMR (500 MHz,  $\text{CDCl}_3$ )  $\delta$  7.05 (s, 2H).  $^{13}\text{C}$  NMR (126 MHz,  $\text{CDCl}_3$ )  $\delta$  133.16, 129.74, 114.98, 112.28.



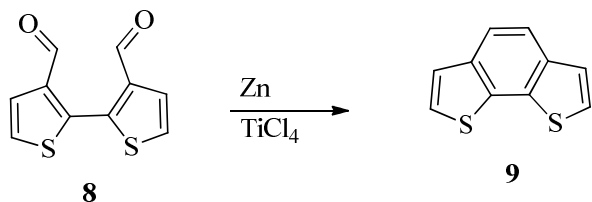
**3,3'-dibromo-2,2'-bithiophene (7):** Zinc dust (25 g, 382 mmol) in a mixture of ethanol (500 ml), acetic acid (120 ml) and water (50 ml) was heated to reflux and 3,3',5,5'-tetrabromo-2,2'-bithiophene (50 g, 104 mmol) was added in small portions over  $\frac{1}{2}$  hour. Reflux was continued for an additional hour, followed by evaporation of the solvents. Water (500 ml) was then added and the mixture was heated to 60 °C for 20 minutes after which the yellow solid was filtered off, and the solid was washed with water and dried in a vacuum oven. The yellow crude (29.94 g) was recrystallized from heptane yielding the desired product (25.3 g, 75%).  $^1\text{H}$  NMR (500 MHz,  $\text{CDCl}_3$ )  $\delta$  7.41 (d,  $J$  = 5.4 Hz, 2H), 7.08 (d,  $J$  = 5.4 Hz, 2H).  $^{13}\text{C}$  NMR (126 MHz,  $\text{CDCl}_3$ )  $\delta$  130.98, 129.08, 127.65, 112.81.



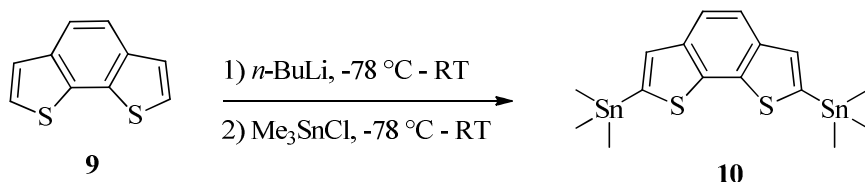
**[2,2'-bithiophene]-3,3'-dicarbaldehyde (8):** In a 1 L threenecked flask  $n\text{-BuLi}$  (98 ml, 157 mmol) in hexanes was cooled to -78 °C and anhydrous THF (600 ml) was added. 3,3'-dibromo-2,2'-bithiophene (17.0 g, 52.5 mmol) in THF (100 ml) was added drop wise over the course of approximately 1½ hours. The mixture was then stirred for an additional 2 hours at -78 °C, followed by addition of  $N,N$ -Dimethylformamide (13 ml, 168 mmol) in one portion after which the reaction mixture allowed to reach RT. Saturated  $\text{NaHCO}_{3(\text{aq})}$  (100 ml) was then added followed by addition of conc. HCl in ice until bubbles started to form. The organic solvent was then evaporated, resulting in the formation of an orange/light brown solid that was filtered off and washed with excess water. After drying the solid in a vacuum oven the crude product (11.9 g) was recrystallized from toluene (~150 ml) to give the pure product (10.0 g, 86 %).

$^1\text{H}$  NMR (500 MHz,  $\text{CDCl}_3$ )  $\delta$  9.90 - 9.82 (m, 1H), 7.64 (d,  $J = 5.4$ , 1H), 7.52 - 7.43 (m, 1H).

$^{13}\text{C}$  NMR (126 MHz,  $\text{CDCl}_3$ )  $\delta$  184.36, 141.34, 140.64, 128.49, 127.47.



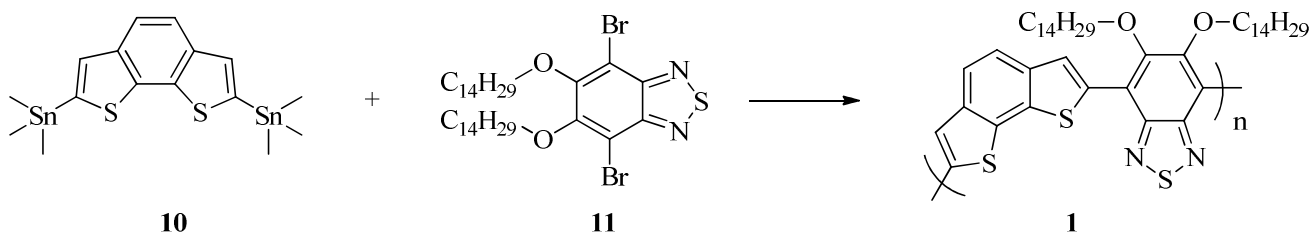
**benzo[1,2-b:6,5-b']dithiophene (9):** Dry THF (800 ml) was cooled on ice/acetone ( $-15\text{ }^\circ\text{C}$ ), followed by the slow addition of titanium tetrachloride (12.1 ml, 110 mmol). Zinc dust (14.4 g, 220 mmol) was then added and the temperature was raised to reflux. [2,2'-bithiophene]-3,3'-dicarbaldehyde (4.07 g, 18.3 mmol) in THF (400 ml) was then added drop wise over the next 4½ hours after which reflux was continued for an additional 1½ hours. The reaction mixture was quenched by the addition of ice (500 g) and saturated  $\text{NaHCO}_3$  (400 ml). After evaporation of the THF *in vacuo* extraction with ether (5x200 ml) was performed on the remainder. The combined organic phases were then washed with brine and dried over  $\text{MgSO}_4$ . After evaporation of the solvent the crude (3.9 g) product was purified by gradient column chromatography (hexane/DCM, 1% steps from 100:0). This yielded the pure product as colorless crystals (2.48 g, 71%).  $^1\text{H}$  NMR (500 MHz,  $\text{CDCl}_3$ )  $\delta$  7.78 (s, 2H), 7.46 - 7.40 (m, 4H),  $^{13}\text{C}$  NMR (126 MHz,  $\text{CDCl}_3$ )  $\delta$  137.29, 133.72, 125.00, 124.39, 120.55.



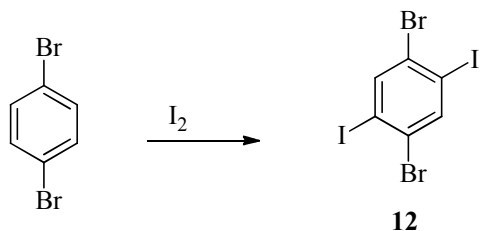
**2,7-bis(trimethylstannyl)benzo[1,2-b:6,5-b']dithiophene (10):** Benzo[1,2-b:6,5-b']dithiophene (0.50 g, 2.63 mmol) was dissolved in dry THF (20 ml) under argon and cooled to  $-78\text{ }^\circ\text{C}$ . Butyllithium (6.75 ml, 1.6 M in hexanes, 10.8 mmol) was then added drop wise causing precipitation to occur. After stirring for 15 min the cooling was removed and the temperature was allowed to reach RT where it was left stirring for ½ hour. The solution was then put back on the cold ( $-78\text{ }^\circ\text{C}$ ), after which chlorotrimethylstannane (3.50 g, 17.6 mmol) was added in one go. The temperature was again allowed to reach RT at which the solution was stirred for an additionally 2 hours. Workup was performed by addition of water followed by extraction with ether. The combined organic phases were washed with water and then brine before drying over  $\text{MgSO}_4$  and evaporation of the solvent. The crude product was purified by quickly passing the compound through a short column of basic  $\text{Al}_2\text{O}_3$ , using toluene with 2%  $\text{NEt}_3$  as eluent. The resulting



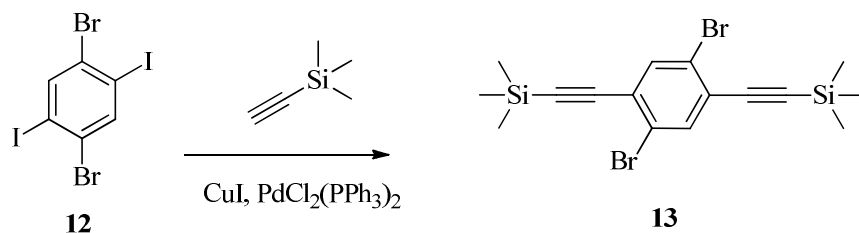
clear oil (1.28 g) was further purified by recrystallization from methanol yielding the pure product as fine white needles (0.92 g, 69%).  $^1\text{H}$  NMR (500 MHz,  $\text{CDCl}_3$ )  $\delta$  7.73 (s, 2H), 7.53 – 7.44 (m, 2H), 0.64 – 0.23 (m, 18H).  $^{13}\text{C}$  NMR (126 MHz,  $\text{CDCl}_3$ )  $\delta$  138.28, 138.13, 138.06, 132.94, 119.66, -6.63, -8.11, -9.60.



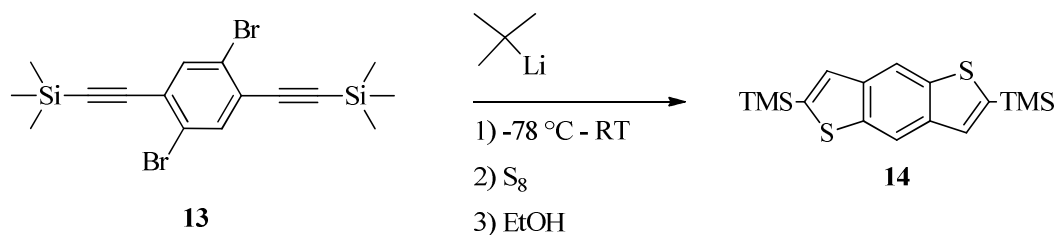
**Polymer 1:** Compound **10** (205.13 mg, 0.398 mmol), Compound **11** (285.96 mg, 0.398 mmol),  $\text{Pd}_2(\text{dba})_3$  (19.4 mg, 0.021 mmol) and tri-*o*-tolyl phosphine (49.2 mg, 0.162 mmol) were mixed in dry, degassed toluene (20 ml) and the temperature was raised to 110 °C. After a few hours the now red-blue solution had turned very thick, and additional toluene (10 ml) was added. The mixture was stirred overnight followed by precipitation of the polymer in methanol and removal of salts and lower molecular weights fractions by soxhlet extractions with methanol, heptanes and chloroform. The polymer was finally collected by dissolving the remaining solid in hot chlorobenzene followed by precipitation in methanol and collection of the solid by filtration (271 mg, 91%).  $M_w$ : 406485,  $M_n$ : 118069, PD: 3.4



**1,4-dibromo-2,5-diiodobenzene (12):** 1,4-dibromobenzene (12 g, 50,9 mmol) and iodine (49.1 g, 193 mmol) in concentrated sulfuric acid (160 ml) was heated to 130 °C for 6 hours while stirring vigorously. The mixture was poured into ice, and the resulting solid was filtrated and washed several times with  $\text{NaHSO}_3$  (2 M), saturated  $\text{NaHCO}_3$  and water. After drying in vacuum the solid was recrystallized from toluene to give the desired compound as white needle like crystals (9.19 g, 37%).  $^1\text{H}$  NMR (500 MHz,  $\text{CDCl}_3$ )  $\delta$  8.04 (s, 2H).  $^{13}\text{C}$  NMR (126 MHz,  $\text{CDCl}_3$ )  $\delta$  142.47, 129.36, 101.46.

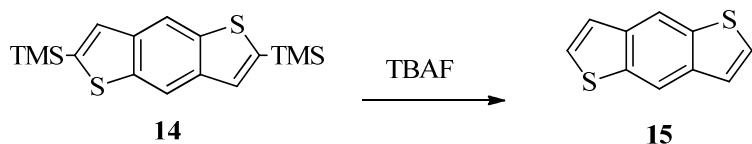


**((2,5-dibromo-1,4-phenylene)bis(ethyne-2,1-diyl))bis(trimethylsilane) (13):** A mixture of benzene (240 ml) and di-*iso*-propylamine (130 ml) were degassed with argon for ½ hour. 20 ml were extracted and 1,4-dibromo-2,5-diiodobenzene (24.22, 49.7 mmol), copper(I) iodide (0.88, 4.6.2 mmol) and PdCl<sub>2</sub>(PPh<sub>3</sub>)<sub>2</sub> (1.57 g, 2.24 mmol) were added. A solution of ethynyltrimethylsilane (14.1 ml 102 mmol) in the previously extracted 20 ml solvent was added drop wise over a period of 15 minutes, while cooling on an ice bath, keeping the temperature below 20 °C. The mixture was then stirred for an additional hour at RT after which water (400 ml) was added and the phases were separated. The aqueous phase was extracted with ether (2 x 200 ml) and the collected organic phases were washed with water (2 x 100 ml) and brine (100 ml). Evaporation of the solvent after drying over MgSO<sub>4</sub> gave a white/brown solid (23.6 g) which was purified by column chromatography (hexane) yielding the desired compound (19.43 g, 91 %). <sup>1</sup>H NMR (500 MHz, CDCl<sub>3</sub>) δ 7.67 (s, 2H), 0.27 (s, 18H). <sup>13</sup>C NMR (126 MHz, CDCl<sub>3</sub>) δ 136.42, 126.44, 123.70, 103.07, 101.36, -0.33.

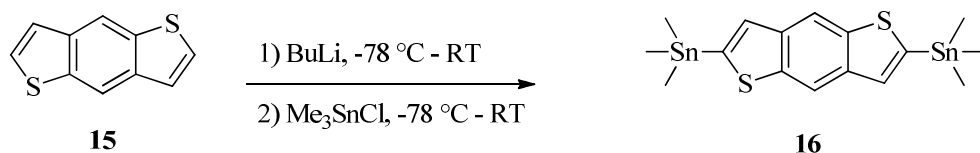


**2,6-bis(trimethylsilyl)benzo[1,2-b:4,5-b']dithiophene (14):** Compound **13** (4.0 g, 9.34 mmol) was dissolved in ether (150 ml) and cooled to -78 °C. *tert*-butyllithium in pentane (1.7 M, 22 ml, 37.4 mmol) was added (solution turns yellow) and the mixture was stirred for 15 minutes after which the temperature gradually raised to RT. Sulfur (601 mg, 18.7 mmol) was then added in one portion and stirring was continued for 15 minutes followed by addition of ethanol (300 ml) and stirring for an additional hour. Water (150 ml) was then added and the organic solvents were removed *in vacuo*. The formed precipitate was filtered off and washed with excess water and methanol MeOH (4 x 25 ml) and dried in a vacuum oven. The crude product (1.89 g) was purified by column chromatography (heptane

with 2-3% AcOEt) yielding the desired product (1.81 g, 65%).  $^1\text{H}$  NMR (500 MHz,  $\text{CDCl}_3$ )  $\delta$  8.27 (s, 2H), 7.46 (s, 3H), 0.39 (s, 18H).  $^{13}\text{C}$  NMR (126 MHz,  $\text{CDCl}_3$ )  $\delta$  143.83, 140.84, 139.30, 130.00, 116.18, -0.24.

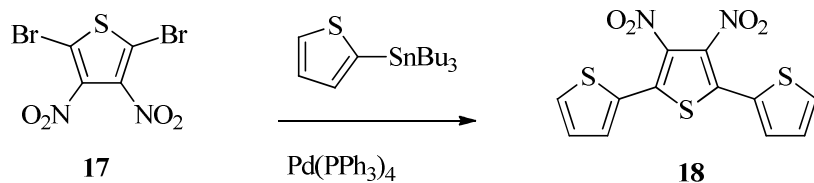


**benzo[1,2-b:4,5-b']dithiophene (15):** To a solution of **9** (0.800 g, 2.391 mmol) in THF (30 ml) was added a solution of TBAF in THF (1 M, 5.26 ml, 5.26 mmol). The mixture was allowed to stir at RT for 3 hours. The solution was added to water (100 ml) after which the THF was evaporated and the end the precipitate was filtered off and washed with excess water and a mixture of water/MeOH (1:1). Purification by gradient column chromatography (heptanes/AcOEt, 2% steps) yielded the pure product (416 mg, 91%).  $^1\text{H}$  NMR (500 MHz,  $\text{CDCl}_3$ )  $\delta$  8.32 (s, 1H), 7.47 (d,  $J = 5.5$  Hz, 1H), 7.37 (d,  $J = 5.5$  Hz, 1H).  $^{13}\text{C}$  NMR (126 MHz,  $\text{CDCl}_3$ )  $\delta$  137.66, 137.29, 127.18, 123.07, 116.99.

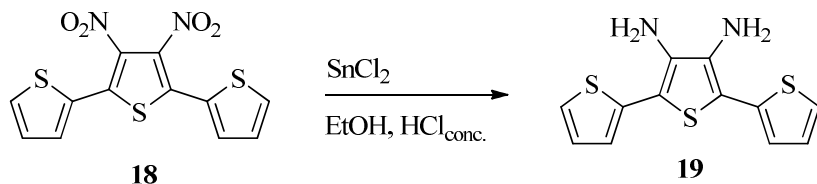


**2,6-bis(trimethylstannyl)benzo[1,2-b:4,5-b']dithiophene (16):** Compound **10** (0.410 g, 2.155 mmol) in THF (20 ml) was cooled to  $-78$   $^\circ\text{C}$ . *n*-BuLi (1.6 M in hexanes, 5.39 ml, 8.62 mmol) was then added after which the solution was allowed to reach room temperature. This was followed by re-cooling the mixture to  $-78$   $^\circ\text{C}$  after which trimethyltin chloride (2.62 g, 13.15 mmol) was added and the mixture was allowed to reach room temperature at which the mixture was stirred for an additional two hours. Workup was performed by addition of water followed by extraction with ether. The combined organic phases were washed with water and then brine before drying over  $\text{MgSO}_4$  and evaporation of the solvent. The crude product was purified by quickly passing the compound through a short column of basic  $\text{Al}_2\text{O}_3$ , using toluene with 2%  $\text{NEt}_3$  as eluent. The crude product (0.976 g) was further purified by recrystallization from methanol yielding the pure product as fine white needles (0.715 g, 64%).  $^1\text{H}$  NMR (500 MHz,  $\text{CDCl}_3$ )  $\delta$  8.27 (s, 1H), 7.49 – 7.32 (m, 1H), 0.58 – 0.25 (m, 1H).  $^{13}\text{C}$  NMR (126 MHz,  $\text{CDCl}_3$ )  $\delta$  141.91, 141.52, 138.77, 131.21, 131.09, 130.98, 115.23, -6.75, -6.82, -8.21, -8.23, -9.65, -9.71.

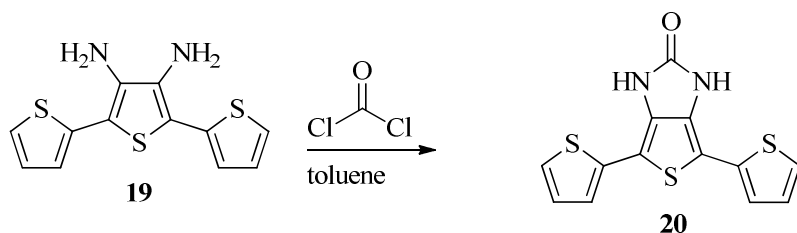




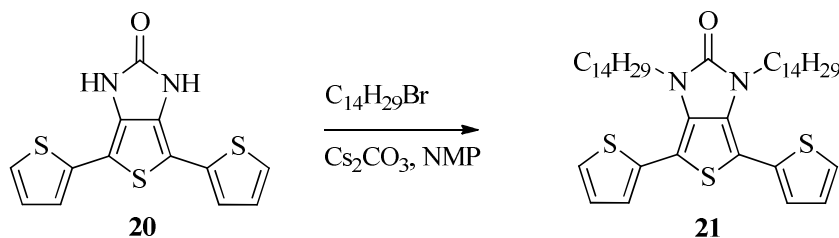
**3',4'-dinitro-2,2':5',2''-terthiophene (18):** 2-tributyltinthiophene (58.8 g, 158 mmol), 2,5-dibromo-3,4-dinitrothiophene (25.5 g, 77 mmol) and tetrakis (0.9 g, 0.779 mmol) was dissolved in toluene (200 ml) and heated at reflux for 2½ hours. The heat was turned off and the mixture was allowed to cool to RT. The formed precipitate was filtered off and was washed with petrol ether (200 ml) which yielded the product as gold like flakes (19.31 g). The liquid phase was reduced in vacuum and the slurry was treated with petrol ether and filtrated to yield another 4.38 g of pure product (23.7 g, 91%). <sup>1</sup>H-NMR (CDCl<sub>3</sub>): δ = 7.62 (dd, *J* = 5.2 Hz, *J* = 1.1 Hz, 2H), 7.55 (dd, *J* = 3.6 Hz, *J* = 1.1 Hz, 2H), 7.18 (dd, *J* = 5.2 Hz, *J* = 3.6 Hz, 2H). <sup>13</sup>C-NMR (CDCl<sub>3</sub>): δ = 133.9, 131.3, 131.1, 128.4, 128.0.



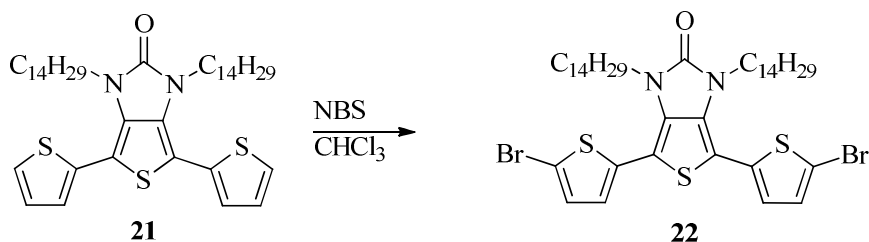
**3',4'-diamino-[2,2';5',2'']terthiophene (19):** A mixture of 3',4'-dinitro-[2,2';5',2'']terthiophene (23.0 g, 68.0 mmol) and Sn(II)Cl<sub>2</sub> (100 g, 527 mmol) in ethanol (250 ml) and THF (150 ml) was stirred while adding hydrochloric acid (37%, 100 ml) drop wise. The mixture was allowed to stand at RT overnight. The solvents were removed *in vacuo*. Ice (3-400 g) was added and the resulting slurry was basified by addition of potassium hydroxide pellets and 25% potassium hydroxide. The mixture was transferred to a continuous extraction apparatus and continuous extraction was performed with ether over night. Gradient column chromatography (heptane/CHCl<sub>3</sub> start 50:50, then 5% steps followed by CHCl<sub>3</sub>/THF, 1% steps) yielded the desired diaminotertthiophene as a 'gold flaky' solid (16.1 g, 85%). <sup>1</sup>H NMR (500 MHz, CDCl<sub>3</sub>) δ 7.27 (dd, *J* = 5.0, 1.3 Hz, 2H), 7.12 – 7.06 (m, 4H), 3.69 (s, 4H). <sup>13</sup>C NMR (126 MHz, CDCl<sub>3</sub>) δ 136.10, 133.74, 127.88, 124.13, 124.06, 110.30.



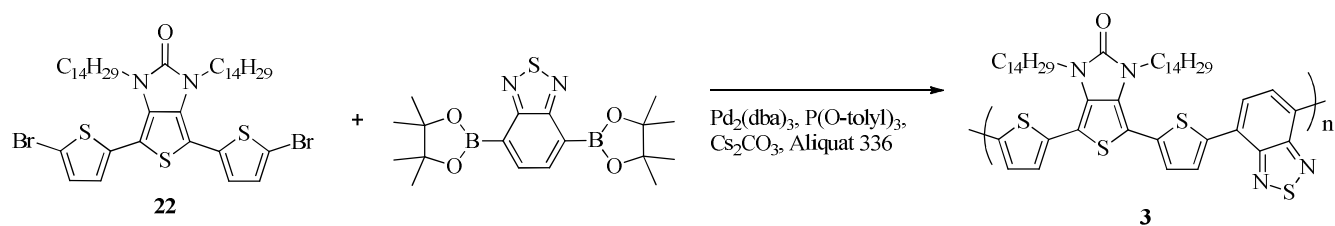
**4,6-di(thiophen-2-yl)-1H-thieno[3,4-d]imidazol-2(3H)-one (20):** Compound **19** (3.0 g, 10.78 mmol) and triethylamine (4.7 ml, 33.4 mmol) was dissolved in toluene (60 ml) and cooled on an ice bath. Phosgene (20% in toluene) (6.3 ml, 12.10 mmol) in additional toluene (30.0 ml) was then added dropwise over 20 minutes while stirring (immediate precipitation - green). The reaction was then stirred at RT overnight. MeOH was added (400 ml) and the precipitate filtered off (2.12 g). Evaporation of the solvents from the toluene/MeOH filtrate and treatment of the resulting solid with water (200 ml) and drying in vacuum yielded a crude (1.13 g) which after purification by gradient column chromatography (heptane/AcOEt, 5% steps) resulted in additional pure compound (0.57 g), thus giving a total yield of 2.69 g (82%).  $^1\text{H}$  NMR (500 MHz, DMSO)  $\delta$  11.09 (s, 2H), 7.48 (dd,  $J$  = 5.1, 0.7 Hz, 2H), 7.39 (dd,  $J$  = 3.6, 0.7 Hz, 2H), 7.17 – 7.06 (m, 2H).  $^{13}\text{C}$  NMR (126 MHz, DMSO)  $\delta$  160.21, 133.91, 128.51, 127.79, 124.44, 123.98, 103.32.



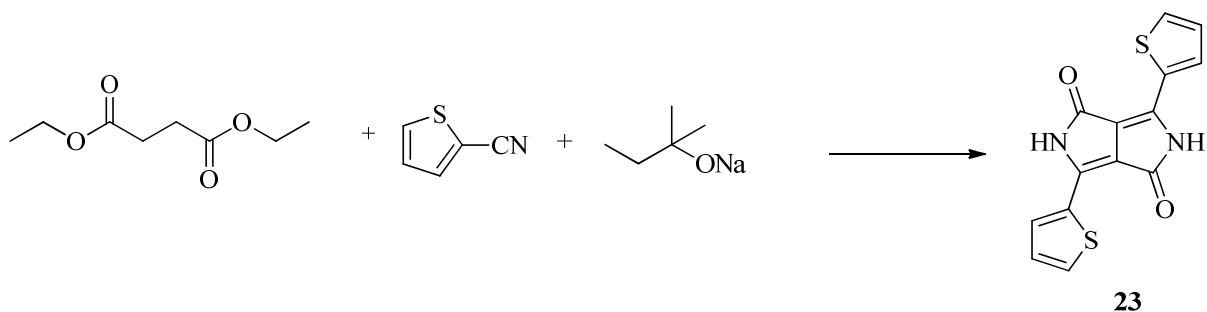
**1,3-ditetradecyl-4,6-di(thiophen-2-yl)-1H-thieno[3,4-d]imidazol-2(3H)-one (21):** Compound **20** (1.0 g, 3.29 mmol), 1-bromotetradecane (2.37 g, 8.54 mmol) and cesium carbonate (3.2 g, 9.9 mmol) in N-methyl-2-pyrrolidinone (11 ml) was heated to 120 °C for 3 hours. Water was added and the mixture extracted with ether. The collected organic phases were washed extensively with water followed by wash with brine and drying over  $\text{MgSO}_4$ . Evaporation of the solvent yielded a crude (2.84 g) which was purified by gradient column chromatography (heptanes/DCM, 6% steps) yielding the pure product (1.71 g, 75%).  $^1\text{H}$  NMR (500 MHz,  $\text{CDCl}_3$ )  $\delta$  7.37 (dd,  $J$  = 5.2, 1.2, 2H), 7.13 (dd,  $J$  = 3.5, 1.2, 2H), 7.08 (dd,  $J$  = 5.2, 3.5, 2H), 3.78 (t,  $J$  = 7.5, 4H), 1.38 - 1.03 (m, 48H), 0.87 (t,  $J$  = 7.0, 6H).  $^{13}\text{C}$  NMR (126 MHz,  $\text{CDCl}_3$ )  $\delta$  158.65, 132.47, 128.77, 128.68, 127.49, 127.11, 104.95, 42.25, 32.08, 29.86, 29.83, 29.82, 29.78, 29.67, 29.52, 29.21, 29.09, 26.46, 22.85, 14.28.



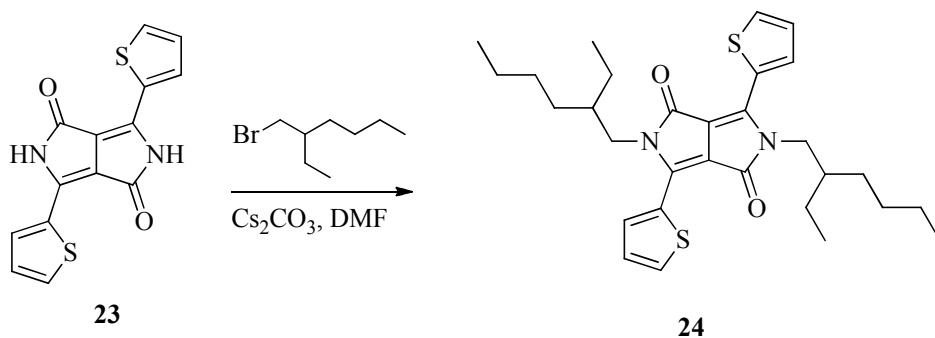
**4,6-bis(5-bromothiophen-2-yl)-1,3-ditetradecyl-1H-thieno[3,4-d]imidazol-2(3H)-one (22):** To a solution of **21** (1.42 g, 2.04 mmol) in  $\text{CHCl}_3$  (50 ml) was added NBS (1.80 g, 10.11 mmol) in small portions (200 mg at a time) over a period of 18 hours while simultaneously monitoring the reaction by TLC. The reaction mixture was then washed with water and brine and then dried over  $\text{MgSO}_4$ . Removal of the solvent in vacuo yielded a crude (1.9 g) which upon purification by gradient column chromatography (heptanes/DCM) yielding the pure product (1.46 g, 84%).  $^1\text{H}$  NMR (500 MHz,  $\text{CDCl}_3$ )  $\delta$  7.04 (d,  $J = 3.8$  Hz, 2H), 6.88 (d,  $J = 3.8$  Hz, 2H), 3.80 – 3.72 (m, 4H), 1.41 – 1.32 (m, 4H), 1.33 – 1.06 (m, 44H), 0.88 (t,  $J = 7.0$  Hz, 6H).  $^{13}\text{C}$  NMR (126 MHz,  $\text{CDCl}_3$ )  $\delta$  158.42, 133.82, 130.42, 129.19, 129.03, 113.53, 104.23, 42.30, 32.08, 29.86, 29.84, 29.82, 29.80, 29.69, 29.55, 29.52, 29.22, 29.11, 26.48, 22.85, 14.27.



**Polymer 3:** (171.7 mg, 0.201 mmol), 2,1,3-Benzothiadiazole-4,7-bis(boronic acid pinacol ester) (82.2 mg, 0.201 mmol),  $\text{Cs}_2\text{CO}_3$  (654 mg, 2.01 mmol),  $\text{Pd}_2(\text{dba})_3$  (11.5 mg, 0.013 mmol), tri-*o*-tolylphosphine (25 mg, 0.082 mmol) and a drop of Aliquat 336 is mixed in dry, degassed toluene (8 ml) and degassed Water (0.75 ml). The temperature was then raised to 90 °C and the mixture was stirred for 24 hours. Precipitation of the polymer was performed by drop wise addition of the mixture to methanol (120 ml), and the polymer was subsequently purified by soxhlet extraction with MeOH (24 h) and hexane (24 h) followed by extraction with chloroform, evaporation of the solvent and reprecipitation from toluene solution to methanol.  $M_w$  14700,  $M_n$  6000, PDI 2.45.

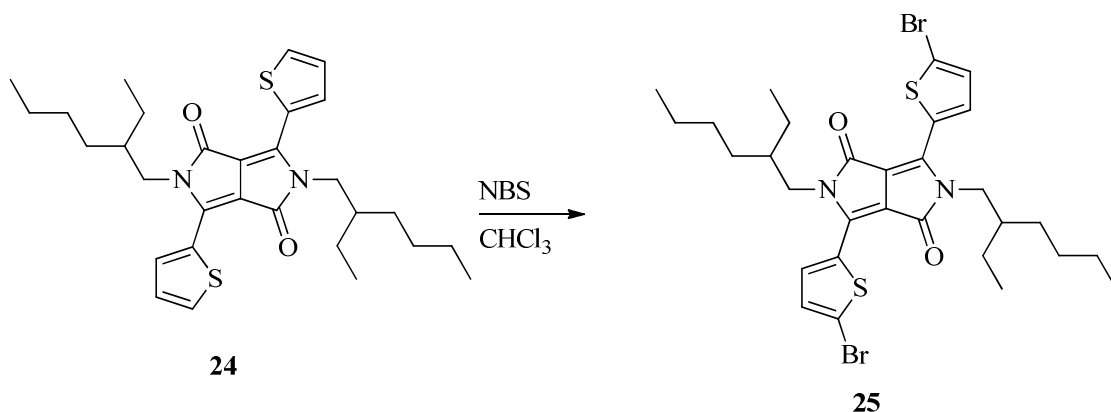


**3,6-di(thiophen-2-yl)pyrrolo[3,4-c]pyrrole-1,4(2H,5H)-dione (23):** A mixture of Diethyl succinate (7.18 ml, 42.4 mmol) and 2-thiophenecarbonitrile (7.98 ml, 85 mmol) in 2-methyl-2-butanol (30 ml) was added drop wise over a period of 1½ h to a boiling mixture of sodium *tert*-pentoxide (17.20 g, 148 mmol) in 2-methyl-2-butanol (125 ml) under argon. The mixture was then allowed to reflux for an additional ½ hour, after which it was added slowly to an ice cooled mixture of methanol (500 ml) and concentrated HCl (21 ml). The purple precipitate was filtered off and washed with water and methanol before drying in vacuum (8.2 g, '64%'). <sup>1</sup>H NMR (500 MHz, DMSO) δ 11.23 (s, 2H), 8.21 (d, *J* = 3.1 Hz, 1H), 7.95 (d, *J* = 4.6 Hz, 1H), 7.30 (dd, *J* = 4.9, 3.8 Hz, 1H). The compound was used in subsequent steps without further purification.



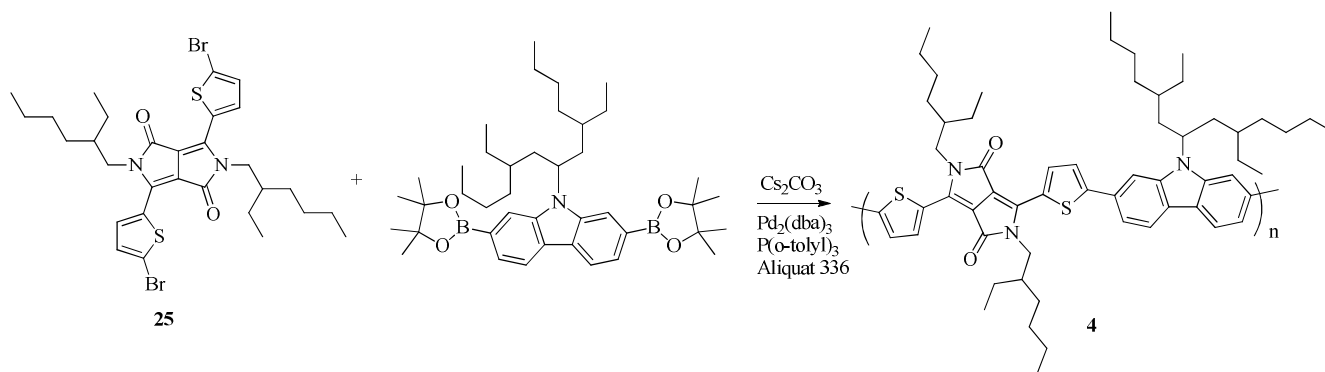
**2,5-bis(2-ethylhexyl)-3,6-di(thiophen-2-yl)pyrrolo[3,4-c]pyrrole-1,4(2H,5H)-dione (24):** **23** (1.00 g, 3.33 mmol), cesium carbonate (10.85 g, 33.3 mmol) and 2-ethylhexyl bromide (1.278 ml, 6.83 mmol) in DMF (30 ml) was stirred under argon at 55 °C for two days. An additional equivalent of 2-ethylhexyl bromide (0.623 ml, 3.33 mmol) was then added and the mixture left for another 24 hours. Purification of the crude product by gradient column chromatography (heptane:AcOEt. 2% step until 6%, then 1 %) yielded the desired product (341 mg, 20%). <sup>1</sup>H NMR (500 MHz, CDCl<sub>3</sub>) δ 8.88 (dd, *J* = 3.9, 1.1 Hz, 2H), 7.62 (dd, *J* = 5.0, 1.1 Hz, 2H), 7.30 – 7.23 (m, 2H), 4.12 – 3.92 (m, 4H), 1.92 – 1.78 (m, 2H), 1.38 – 1.19 (m, 16H), 0.93 – 0.76 (m, 12H). <sup>13</sup>C NMR (126 MHz, CDCl<sub>3</sub>) δ 161.90, 140.57, 135.39, 130.64, 129.98, 128.55, 108.09, 46.00, 39.22, 30.37, 30.35, 28.50, 23.69, 23.19, 14.14, 10.62.





**3,6-bis(5-bromothiophen-2-yl)-2,5-bis(2-ethylhexyl)pyrrolo[3,4-c]pyrrole-1,4(2H,5H)-dione (25):**

**24** (300 mg, 0.572 mmol) was dissolved in  $\text{CHCl}_3$  and NBS N-Bromosuccinimide (208 mg, 1.17 mmol) was added in the dark and the mixture was left stirring at RT overnight. The organic phase was washed with water and brine, followed by drying over  $\text{MgSO}_4$  and evaporation of the solvent. The crude product was triturated with hot methanol and the desired product (328 mg, 84%) was isolated by filtration of the cooled solution and drying in vacuum.  $^1\text{H NMR}$  (400 MHz,  $\text{CDCl}_3$ )  $\delta$  8.64 (d,  $J = 4.2$  Hz, 2H), 7.22 (d,  $J = 4.2$  Hz, 2H), 4.04 – 3.80 (m, 4H), 1.90 – 1.76 (m, 2H), 1.39 – 1.21 (m, 16H), 0.95 – 0.79 (m, 12H).



**Polymer 4:** Compound **24** (104.89 mg, 0.154 mmol), 9-(5,9-diethyltridecan-7-yl)-2,7-bis(4,4,5,5-tetramethyl-1,3,2-dioxaborolan-2-yl)-9H-carbazole (101 mg, 0.154 mmol),  $\text{Pd}_2(\text{dba})_3$  (8.5 mg, 9.28  $\mu\text{mol}$ ) was mixed with dry, degassed toluene (5 ml) for approximately 30 minutes. Degassed water (0.5 ml),  $\text{Cs}_2\text{CO}_3$  (501 mg, 1.54 mmol) and a drop of Aliquat 336 was added and the mixture was heated to 90  $^\circ\text{C}$  and stirring was continued for 4 days resulting a blue reaction mixture. This was poured into methanol and the solid was Soxhlet extracted with methanol (24 h), hexane (24 h) and was finally collected by extraction with chloroform (95 mg,  $M_w$  3150,  $M_n$  1813, PDI 1.7).

### 3.6.2 Device preparation and testing

*Slot-Die Coating Head, Pumping, and Mixing.* A standard slot-die coating head with a working width of 250 mm and a dead volume of 50 mL in the feed manifold was employed for coating of the zinc oxide layer and the PEDOT:PSS layer. The ZnO layer was applied by use of a piston pump (Knauer) with a pumping capacity of up to 50 mL min<sup>-1</sup> in steps of 10  $\mu$ L. The PEDOT:PSS was applied using a static pressure tank for feeding the ink. The custom-made mini slot-die coating head had a single slot 13 mm wide, 40 mm long and 0.05 mm thick giving a dead volume of 26  $\mu$ L. The single slot coating head was fed by 1/16 in. tubing with an internal diameter of 0.1 mm and a length of 800 mm giving a nominal dead volume of 6.2  $\mu$ L. The two pumps (Knauer) had a maximum pumping capacity of 10 mL min<sup>-1</sup> in steps of 1  $\mu$ L. The exit from each pump was fed into a mixing-T (UP-U428, Upchurch) with a nominal dead volume of 2.8  $\mu$ L. The total dead volume from the mixing-T through the wire and the mini slot-die coating head to the substrate was approximately 35  $\mu$ L. The nominal volume required for one solar cell repeat with a wet thickness of 9.6  $\mu$ m is 10.3  $\mu$ L.

*Coating and Printing of the Layers.* The zinc oxide layer was coated on all stripes simultaneously using the standard slot-die coating head. The web speed was 2 m min<sup>-1</sup> and the ink was supplied to the coating head at a rate of 2 mL min<sup>-1</sup> giving a wet layer thickness 4.8  $\mu$ m. The dried ZnO layer was cured for 10 min at 140 °C. The active layer was then coated in single stripes as described above. The PEDOT:PSS was applied using the standard slot-die coating head while coating only the 6 of the stripes where experiments were made. In principle all 16 stripes could be employed but it was found most practical to have some spacing between experiments and thus a practical choice of 6 experiments per roll width was made. Finally a silver back electrode was applied onto the substrate as grid structure with a 20% area coverage using screen printing.

*Device Testing:* The conditions of the characterization under simulated sunlight were KHS 575 using a solar simulator from Steuernagel Lichttechnik operating at 1000 Wm<sup>-2</sup>, AM1.5G. The spectrum of the solar simulator was checked using an optical spectrum analyzer made for measuring irradiance, and its intensity was calibrated bolometrically using a precision spectral pyranometer from Eppley Laboratories. During measurements, the incident light intensity was monitored continuously using a CM4 high-temperature pyranometer from Kipp & Zonen.

### 3.7 Reference list

1. Krebs, F. C. Fabrication and processing of polymer solar cells: A review of printing and coating techniques. *Sol. Energy Mater. Sol. Cells* **2009**, *93* (4), 394-412.
2. Krebs, F. C.; Nielsen, T. D.; Fyenbo, J.; Wadstrom, M.; Pedersen, M. S. Manufacture, integration and demonstration of polymer solar cells in a lamp for the "Lighting Africa" initiative. *Energy & Env. Sci.* **2010**, *3* (5), 512-525.
3. Krebs, F. C.; Fyenbo, J.; Jorgensen, M. Product integration of compact roll-to-roll processed polymer solar cell modules: methods and manufacture using flexographic printing, slot-die coating and rotary screen printing. *J. Mater. Chem.* **2010**, *20* (41), 8994-9001.
4. Krebs, F. C.; Tromholt, T.; Jorgensen, M. Upscaling of polymer solar cell fabrication using full roll-to-roll processing. *Nanoscale* **2010**, *2* (6), 873-886.
5. Manceau, M.; Bundgaard, E.; Carle, J. E.; Hagemann, O.; Helgesen, M.; Søndergaard, R.; Jørgensen, M.; Krebs, F. C. Photochemical stability of [small pi]-conjugated polymers for polymer solar cells: a rule of thumb. *J. Mater. Chem.* **2011**, *21* (12), 4132-4141.
6. Usta, H.; Lu, G.; Facchetti, A.; Marks, T. J. Dithienosilole- and dibenzosilole-thiophene copolymers as semiconductors for organic thin-film transistors. *J. Am. Chem. Soc.* **2006**, *128* (28), 9034-9035.
7. Yoshida, S.; Fujii, M.; Aso, Y.; Otsubo, T.; Ogura, F. Novel Electron-Acceptors Bearing A Heteroquinonoid System .4. Syntheses, Properties, and Charge-Transfer Complexes of 2,7-Bis(Dicyanomethylene)-2,7-Dihydrobenzo[2,1-B-3,4-B']Dithiophene, 2,7-Bis(Dicyanomethylene)-2,7-Dihydrobenzo[1,2-B-4,3-B']Dithiophene, and 2,6-Bis(Dicyanomethylene)-2,6-Dihydrobenzo[1,2-B-4,5-B']Dithiophene. *J. Org. Chem.* **1994**, *59* (11), 3077-3081.
8. Helgesen, M.; Gevorgyan, S. A.; Krebs, F. C.; Janssen, R. A. J. Substituted 2,1,3-Benzothiadiazole- And Thiophene-Based Polymers for Solar Cells - Introducing a New Thermocleavable Precursor. *Chem. Mater.* **2009**, *21* (19), 4669-4675.
9. Hart, H.; Harada, K.; Du, C. J. F. Synthetically Useful Aryl Aryl Bond Formation Via Grignard Generation and Trapping of Arynes - A One-Step Synthesis of Para-Terphenyl and Unsymmetric Biaryls. *J. Org. Chem.* **1985**, *50* (17), 3104-3110.
10. Takimiya, K.; Konda, Y.; Ebata, H.; Niihara, N.; Otsubo, T. Facile synthesis, structure, and properties of benzo[1,2-b : 4,5-b ' ]dichalcogenophenes. *J. Org. Chem.* **2005**, *70* (25), 10569-10571.
11. Wen, L.; Rasmussen, S. C. Synthesis and structural characterization of 2,5-dihalo-3,4-dinitrothiophenes. *Journal of Chemical Crystallography* **2007**, *37* (6), 387-398.

12. Morton, C. J. H.; Gilmour, R.; Smith, D. M.; Lightfoot, P.; Slawin, A. M. Z.; MacLean, E. J. Synthetic studies related to diketopyrrolopyrrole (DPP) pigments. Part 1: The search for alkenyl-DPPs. Unsaturated nitriles in standard DPP syntheses: a novel cyclopenta[c]pyrrolone chromophore. *Tetrahedron* **2002**, *58* (27), 5547-5565.
13. Song, B.; Wang, Z. Q.; Chen, S. L.; Zhang, X.; Fu, Y.; Smet, M.; Dehaen, W. The introduction of pi-pi stacking moieties for fabricating stable micellar structure: Formation and dynamics of disklike micelles. *Angew. Chem. - Int. Ed.* **2005**, *44* (30), 4731-4735.
14. Hou, J. H.; Park, M. H.; Zhang, S. Q.; Yao, Y.; Chen, L. M.; Li, J. H.; Yang, Y. Bandgap and molecular energy level control. of conjugated polymer photovoltaic materials based on benzo[1,2-b : 4,5-b']dithiophene. *Macromolecules* **2008**, *41* (16), 6012-6018.
15. Tamayo, A. B.; Tantiwivat, M.; Walker, B.; Nguyen, T. Q. Design, synthesis, and self-assembly of oligothiophene derivatives with a diketopyrrolopyrrole core. *J. Phys. Chem., C* **2008**, *112* (39), 15543-15552.
16. Zhou, E. J.; Yamakawa, S. P.; Tajima, K.; Yang, C. H.; Hashimoto, K. Synthesis and Photovoltaic Properties of Diketopyrrolopyrrole-Based Donor-Acceptor Copolymers. *Chem. Mater.* **2009**, *21* (17), 4055-4061.
17. Zhou, E. J.; Wei, Q. S.; Yamakawa, S.; Zhang, Y.; Tajima, K.; Yang, C. H.; Hashimoto, K. Diketopyrrolopyrrole-Based Semiconducting Polymer for Photovoltaic Device with Photocurrent Response Wavelengths up to 1.1  $\mu$  m. *Macromolecules* **2010**, *43* (2), 821-826.
18. Alstrup, J.; Jorgensen, M.; Medford, A. J.; Krebs, F. C. Ultra Fast and Parsimonious Materials Screening for Polymer Solar Cells Using Differentially Pumped Slot-Die Coating. *ACS Appl. Mater. Interfaces* **2010**, *2* (10), 2819-2827.

## Chapter 4

**The use of polyurethane as encapsulation method for organic solar cells – an outdoor field study on the influence of local climate on device stability.\***



\* This work has been published:

Søndergaard, R.; Makris, T.; Lianos, P.; Manor, A.; Katz, E. A.; Gong, W.; Tuladhar, S. M.; Nelson, J.; Sommerling, P.; Veenstra, S. C.; Rivaton, A.; Dupuis, A.; Teran-Escobar, G.; Lira-Cantu, M.; Sabkota, S. B.; Zimmermann, B.; Würfel, U.; Krebs, F. C., *Sol. Energy Mater. Sol. Cells* **2012**, 99, 292-300

## 4.1 Introduction

In Denmark a PhD-student must be subjected to an environmental change in order to gain new contacts and experience alternative approaches than the ones at their own institutions. This is generally carried out as a stay at a foreign institution working with subjects somehow related to the ones the PhD-student is working with. The external stay generally has a duration of 4-6 months.

Because of my family situation (working wife and two small children) this was not an option for me, and it was therefore decided that the external stay should be carried out as a series of visits with shorter duration doing an outdoor stability study of organic solar cells involving numerous international groups.

Because organic solar cell in recent years have reached levels that allow for outdoor stability testing,<sup>[1-4]</sup> a need for development and testing of new encapsulation methods has emerged. One of the first real outdoor studies was performed by Katz *et al* in the Negev desert on organic solar cells on glass,<sup>[2]</sup> sealed by using glass fiber reinforced thermosetting epoxy (preg) by the procedure described by Krebs.<sup>[5]</sup> They found that the efficiency of P3HT/PCBM-cells dropped to approximately 10% after 32 days of outdoor exposure. An alternative approach was used by Hauch *et al*, who used a transparent barrier film (WVTR rate of 0.03 g/(m<sup>2</sup> day) at 38 °C/100% rh) to encapsulate flexible P3HT:PCBM modules on PET.<sup>[1]</sup> They experienced full retention and even a slight increase in efficiency after 14 months of outdoor rooftop exposure, mainly due to an increase in the fill factor by 11%. The reported current was more or less identical to the initial, whereas a slight drop in the voltage was observed. This amazing result should probably be received with some skepticism though, as improvements to the module clearly happen after outdoor exposure. This is best illustrated by the final improved fill factor and by the fact that the authors show that the power density increases to approximately 140% of the initial value within a few days. It would have been more appropriate to have measured the *IV*-characteristics after the increase in power density, and then compare with the final characteristics, which would still show a really good stability. In a recent inter-laboratory study by Gevorgyan *et al*, flexible modules of P3HT:PCBM on PET were encapsulated by a barrier film from Amcor Flexibles and studied at different outdoor locations.<sup>[4]</sup> Average efficiencies of approximately 40% of original were observed after approximately 1000 h (~42 days) of outdoor exposure. As a final example, Medford *et al* prepared large panels of P3HT/PCBM flexible modules in series, testing different encapsulation methods for outside conditions. The one that showed the best preservation properties involved pre-lamination of the freshly prepared cells with a ~100 μm thick PET gas barrier layer from Amcor Flexibles with a ~50 μm pressure-sensitive acrylic adhesive. These were further laminated between a 4 mm tempered glass window and black Tetlar foil using two

sheets of 0.5 mm thick ethylene vinyl acetate (EVA) which was heated to 150 °C for 30 minutes causing the EVA to liquefy. The panel having an active area of 9180 cm<sup>2</sup> showed 54% of the original efficiency after 6 months outdoor exposure. Also Krebs have performed 'hot lamination' in the encapsulation of indium-tin-oxide free cells using EVA, but no outdoor test were performed.<sup>[6]</sup>

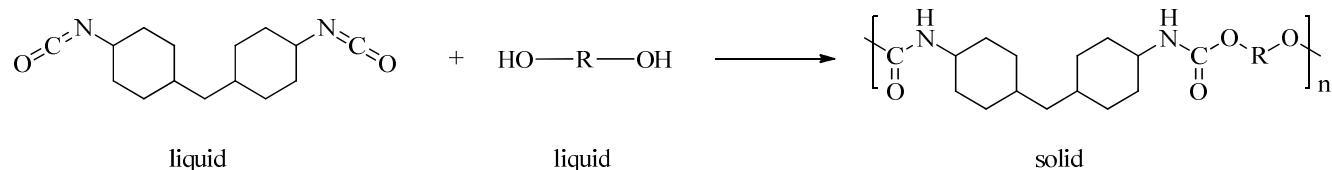
In this study the aim has been to evaluate the use of polyurethane as encapsulation method. As local weather conditions (amount of rain/snow, amount of sun, humidity, ambient temperature, temperature fluctuations, salt content in the air, ect.) can differ considerably depending on the location (country, mountains, the sea...) it was of great interest to perform the study in several countries differing in the parameters that could potentially have an influence on organic solar cell stability. Previously performed inter-laboratory-studies and round robins,<sup>[4,7]</sup> which are important and useful methods to reach consensus of solar cells properties and establishing standard procedures for the characterization of such, have shown not to be without problems. In those studies cells were shipped to different locations to be characterized, but two major weaknesses were related to this approach. First of all different people approach an assignment in different ways, and even if detailed procedures are outlined for what to do, researchers tend to have their own opinion on what is 'the right way' of doing things. As a consequence some procedures are at times left out 'because they are *not* necessary' while others were added 'because they *are* necessary'. The outcome is that although everybody is seemingly doing the same thing in fact they are not, and the significance of such deviations can be difficult to analyze.

Just as important different laboratories tend to have different equipment (reference cells, artificial suns ect.) which makes it difficult to compare results afterwards.

Ideally such studies should be performed by a single person to ensure that everything is done as similar as possible, using the same measuring equipment to rule out deviations. This study has been an attempt to do just that. Besides Risø-DTU (Roskilde, Denmark, by a fjord), the institution and locations that have been involved in the study was: University of Patras (Patras, Greece, by the Mediterranean Sea), Ben-Gurion University of the Negev (Sede Boker, Israel, inland in the Negev desert), Imperial College London (London, southern United Kingdom, inland), Energy Research Centre of the Netherlands (ECN, Petten, The Netherlands, by the North Sea), Clermont Université - Université Blaise Pascal (Clermont-Ferrand, France, inland in the mountainous Massif Central), Fraunhofer Institute for Solar Energy Systems ISE (Freiburg, southern Germany, inland), Centre d'Investigació en Nanociència i Nanotecnologia (CIN2, Barcelona, Spain, by the Mediterranean Sea)

## 4.2 Preparation of the solar panels

The general idea behind the study was to use polyurethane to encapsulate polymer solar cells, thus shielding them from water and oxygen, which can diffuse freely within the cells causing them to degrade if no measures are taken.<sup>[8-10]</sup> Polyurethanes are generally prepared by reaction of an di-isocyanate and a polyol, which slowly polymerizes upon mixing to form a solid (See Scheme 4.1).



**Scheme 4.1** Polymerization of a di-isocyanate compound and a polyol. The di-isocyanate used in this study was 4,4'-methylenedicyclohexylisocyanate (above) and an unknown polyol.

A commercial product (Translux A 260 Polyol and Translux A 260 Isocyanate from Axson technologies) which are mixed in a 50:50 volume ratio was used in this work for the preparations of polyurethane. Because of the viscous, but still liquid properties of the blend just after mixing it is possible to embed a solar cell within the liquid before it polymerizes.

### 4.2.1 Type of cells used

The polymer solar modules and cells used in the study consisted of four types of geometries (see Figure 4.1) and four types of active material inks. All were prepared with an inverted geometry on ITO patterned PET substrates (PET|ITO|ZnO|active layer|PEDOT|Ag) using R2R slot die coating for all layer except for the silver which was screen printed using UV-curable silver paste.<sup>[11]</sup>

Each panel contained ten modules/single cells. Module **1-3** were P3HT:PCBM modules consisting of 16 cells in series with an active area of 35.5 cm<sup>2</sup> differing only in the geometry of the silver back electrode used. For module **1** a simple busbar was used, just connecting the ITO of one cell with the PEDOT of the next to make the series connection, but leaving the main part of the PEDOT uncovered. In module **2** the connecting busbar was supplied with a silver grid, in order to facilitate charge collection, and finally in module **3** the silver fully covered the part of the PEDOT that was over the active area.

Module **4** had the same geometry as module **1** but was prepared using the commercial ink PV2000 from Plextronics. All modules were prepared during a workshop in relation with the ISOS3 conference held at Risø in October 2010.



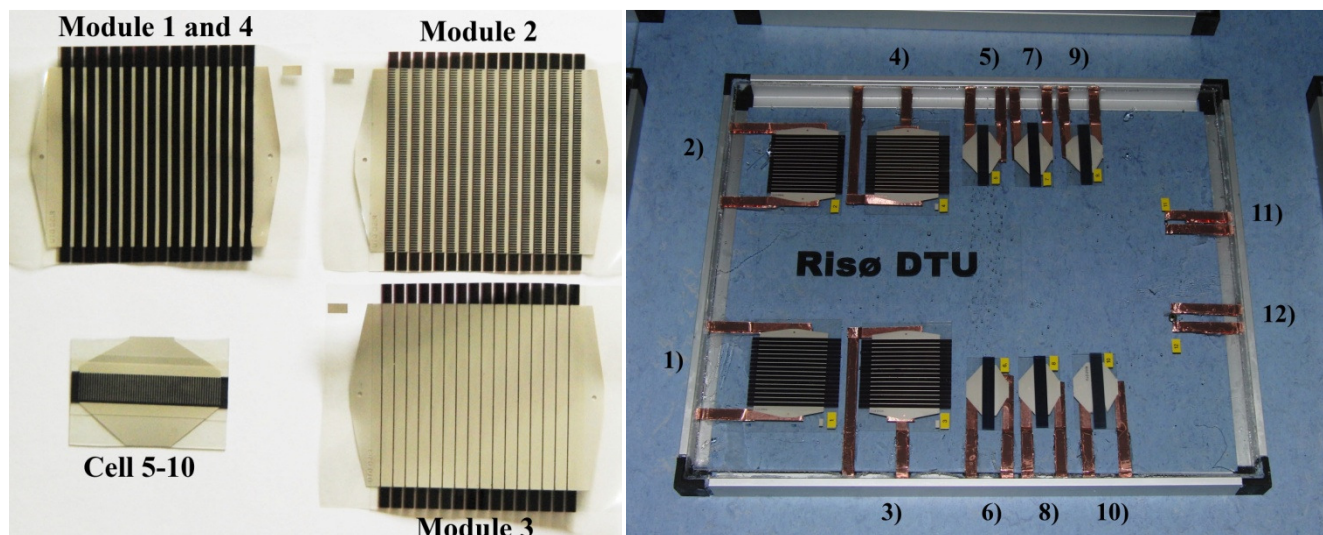


**Figure 4.1** Type of geometries used and their placement in the final panels: Modules (35.5 cm<sup>2</sup>) with just a simple busbar (module 1 and 4) connecting each cell in series in the module, a busbar with a grid (module 2), a full silver back electrode (module 3) and single cells (4.2 cm<sup>2</sup>) with a silver grid (cell 5-10).

The cells 5-10 were all single cells with an active area of 4.2 cm<sup>2</sup> and a grid patterned silver back electrode. The single cells involved the optimized cells of polymer **cBDT-BTBT** and **tBDT-BTBT** previously described in chapter 3 (see Figure 4.2). In cells 5-8 the polymer employed was polymer **cBDT-BTBT** and in cell 9 and 10 polymer **tBDT-BTBT** was used. The single cells were prepared just before assembling the panels in November 2010.

From a total of 723 modules/cells the best of each type were selected for the preparation of nine panels each containing modules/cells 1-10 as well as two reference silicon photodiodes, cell 11 (BPW21 from Centronic, without UV filter) and cell 12 (BPW 34B from Osram, with UV-filter). Assuming a linear relation between light intensity and the corresponding current of cell 11 and 12 allows for the use of these as references for the light intensity.

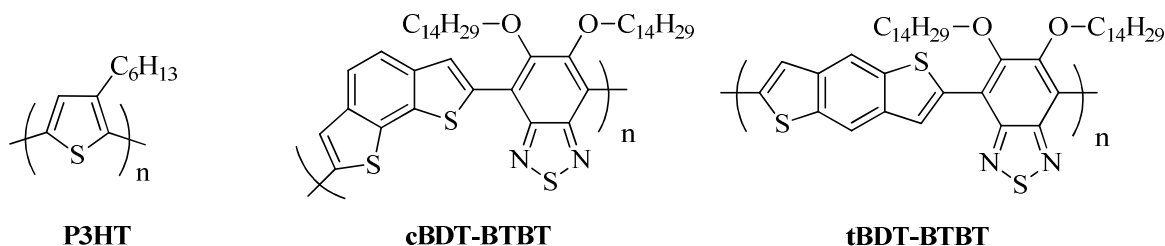


**Figure 4.2:** Chemical structures of the polymers used in the modules. The chemical composition of the Plextronics ink is not known

### 4.2.2 Assembly of the solar panels

The panels were fabricated in a way so the final product consisted of the modules/cells embedded in polyurethane between a tempered glass front plate and a polycarbonate backside. The connection to the exterior from the embedded circuitries was made by use of copper tape. Figure 4.3 illustrates the step wise procedure: 1) the cleaned tempered glass plate was covered with a layer of freshly prepared and degassed 50:50 mixture (mixed and subjected to reduced pressure,  $\sim 20$  mbar, for 5 minutes) of the before mentioned commercially di-isocyanate and polyol compounds. The modules/cells **1-12** were placed in the viscous but still liquid mixture with the front side down making sure that no air was trapped underneath and that the electrodes were not covered. The isocyanate/polyol mixture was then left over night to fully

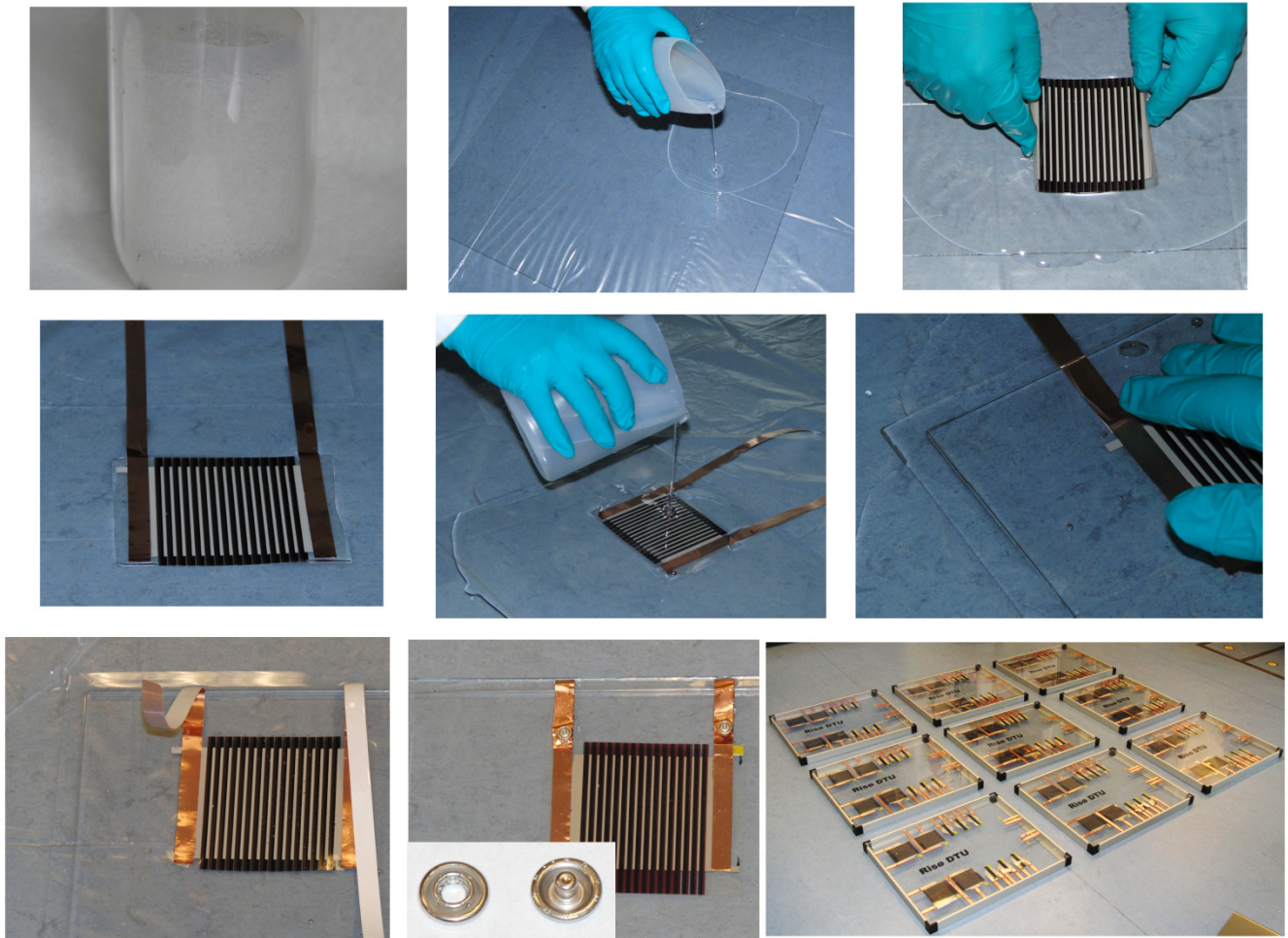
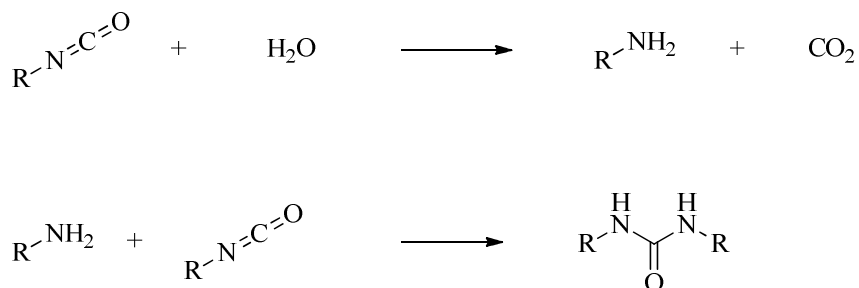


**Figure 4.3:** Illustration of the different steps in the fabrication process of the panels

polymerize to polyurethane. 2) the electrodes of each module/cell was then connected to the exterior of the panel edge by use of copper tape followed by covering the whole with another layer of 50:50 mixture of isocyanate and polyol upon which a polycarbonate plate was placed, again making sure that air is not trapped in the viscous liquid underneath the polycarbonate plate. Once more the panels were left over night to ensure full polymerization to polyurethane. 3) To every electrode was then attached the 'male' part of a simple snap button (used in clothes, allows for easy connection to the electrodes) before gluing the copper tape onto the polycarbonate plate with epoxy glue.

Finally an aluminum frame was mounted to give the finished panel. Of nine prepared panels eight were tested outside. In the fabrication process it should be stressed that fresh batches of the two components for the polyurethane must be used in order to get a good solid encapsulation. The reason for this is that the isocyanates reacts with water upon exposure to air under formation of carbon dioxide and a primary amine which can react with yet an isocyanate group under formation of a urea compound as shown in Scheme 4.2.



**Scheme 4.2** The side reactions caused of isocyanates with water

If the di-isocyanate component has reacted with water to some degree termination of the polymerization will occur each time an isocyanate-urea compound is involved and there will be an excess of the polyol. Figure 4.4 shows an example where this was the case which resulted in delamination and development of bubbles within the incompletely polymerized polyurethane when the panel was exposed to higher temperatures during measurements.



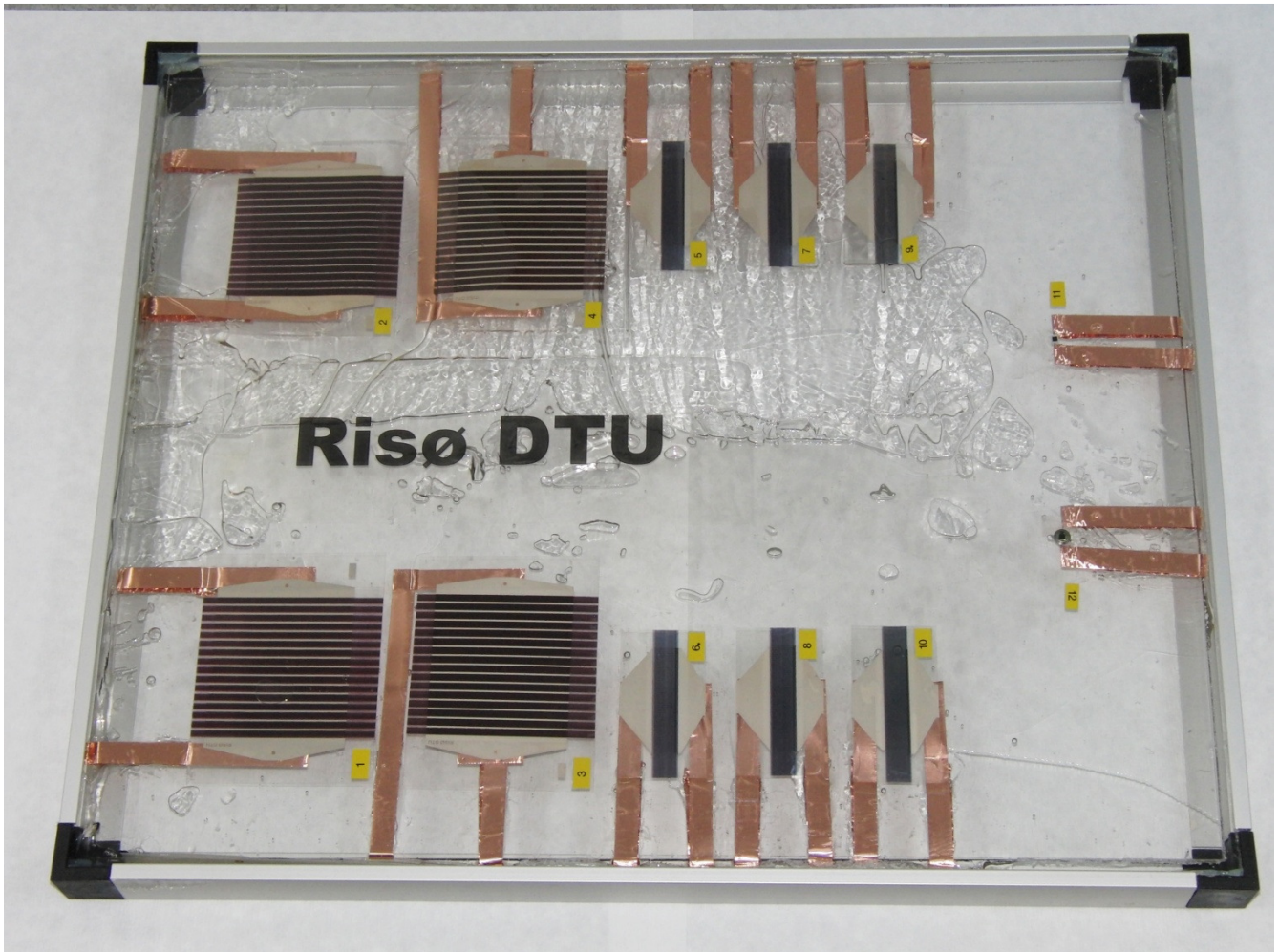


**Figure 4.4:** Picture of a delaminated panel as a result of incomplete polymerization to polyurethane.

### 4.3 Measuring and installing the panels

Two types of measurements were performed in this study: 1) Full *IV*-curves using a Keithley 2400 sourcemeter and a Kip & Zonen CM4 high temperature pyranometer for calibration/measurement of the light intensity. 2) Simple measurement of the  $V_{OC}$  and the  $I_{SC}$  using an Alcron AC-9074 multimeter.

*IV*-measurements of each panel were performed

$t_0$ : at Risø DTU before shipping the panels to the location using a simulated sunlight.

$t_0'$ : at the location before mounting the panel, in order to ensure that nothing had happened during transportation. Depending on the available equipment and weather conditions this was performed indoor under simulated sunlight or/and outside under the real sun.

$t_x'$ : at the location after approximately 4½ months of outdoor exposure. The measurement served to test if something had happened to the cells during shipment before the final measurement at Risø. Again depending on the available equipment and the weather these measurements were performed indoor under simulated light or outside under the real sun.

$t_x$ : at Risø after receiving the panels from the location.

$V_{OC}$  and  $I_{SC}$  measurements: During the 4½ month exposure time, measurements were performed directly on the mounted panels by representatives of the collaborative institutions on each location on days with constant light intensity using identical multimeters which was supplied by Risø DTU. By performing the measurements under constant light intensity, it is possible to use the build-in silicon photodiodes **11** and **12** as references for the light intensity, which allowed for a crude monitoring of the cell conditions during the whole study.

The panels were installed during the month of December 2010 and the beginning of January 2011. Travelling between the different locations a minimum of two full workdays were spent at each institution, in order to have time to solve eventual problems. Each site had been informed of the dimensions of the panels, which had been shipped with a small stock of hinges, screws and other bits and pieces for attaching the panels under different conditions. Despite this, ingenuity and alternative thinking was often needed in order to find needed solutions. Examples of this are illustrated in Figure 4.5 for the installation and measurements in Barcelona. As the panel was too big to enter the normal setup of their artificial sun, a trip to the local hardware store to buy supplies was necessary in order to build a wooden frame for the sun simulator. As for the frame for the actual attachment of the panel in Barcelona, this was a simple rack normally used for paper towels, which was then attached on the outside of building facade railing.



**Figure 4.5 left:** The construction of a wooded frame in a Barcelona created enough space for the panel to be measured under their sun simulator. **right:** the panel in Barcelona attached to a simple rack for paper towels.

When mounting the panels practical considerations such as sufficiently solid support onto which to attach the panel as well as administrative permissions had to be taken into account. This led to diversity in inclinations of the panels as well as the orientations. As a result of this the panels were mounted with inclination angles from 30-55° and facing compass directions of 130-210°. The panel at Risø was an exception as it was mounted on a solar tracker ensuring a perpendicular orientation towards the sun for maximum exposure.

#### 4.4 Results and discussion

Following the period of approximately 4½ months outdoor exposure, where the monitoring had been performed by local representatives at each location, the whole trip was done again (late April to mid May 2011) in order to re-measure and uninstall the panels for shipment back to Denmark. Because attention had to be taken towards having local personnel present at the different institutions, the travelling order of destinations was not the same on the two trips, which resulted in slight deviations in the exposure time at the different locations. An overview of exposure time and placement of the different panels is given in Table 4.1.

**Table 4.1** Overview of locations and outdoor placements of the individual panels.

Location	Panel elevation from horizontal	Compass direction the panel faced	Placement of the panel	Total days of outdoor exposure
Sede Boker, Israel	55°	180°	In the open attached to a pipe	144
Patras, Greece	45°	149°	In the open on a rooftop wall	150
Clermont-Ferrand, France	43°	180°	In the open on a rooftop on a preinstalled rack	140
Barcelona, Spain	47°	130°	On a railing on a building façade.	138
Freiburg, Germany	48°	210°	On a scaffold mounted to a building facade	139
Petten, Holland	30°	170°	In the open on a rooftop on a preinstalled rack.	105
London, UK	43°	172°	In the open onto a rail on a rooftop wall	128
Roskilde, Denmark			In the open on a Solar tracker	135

#### 4.4.1 Outdoor $V_{OC}$ and $I_{SC}$ measurements

The results from the continuous outdoor measurements of  $I_{SC}$  and  $V_{OC}$  are illustrated in Figure 4.6-4.8. Figure 4.6 shows the average normalized relative  $I_{SC}$  of the modules/cells **1-10** (relative to the current of cell **11** except for in London and Freiburg where the currents of cell **12** was used instead because of malfunctioning of cell **11**) for each of the panels over time. Figure 4.7 and Figure 4.8 respectfully show the more detailed evolutions in relative normalized currents and normalized voltages for each type of modules/cells. It should be emphasized that the overall increase in ambient temperatures at all locations during the study has not been taken into account, and that the results especially toward the end of the study probably would have showed lower currents if measured at the original temperatures.

The outdoor  $V_{OC}$  and  $I_{SC}$  measurements generally showed quite similar tendencies of slow decrease in  $I_{SC}$  while  $V_{OC}$  was relatively stable, and no remarkable differences were found between the different architectures or different materials used. This result is somewhat surprising as photodegradation is normally considered a major contributor to the degradation of organic solar cells.

Although the average trends are similar for all locations, the deviations seem to be larger on locations situated by the sea, and a larger number of the cells in these panels actually stopped working during the study. This appeared to originate from contacting problems both externally and internally in the panels.

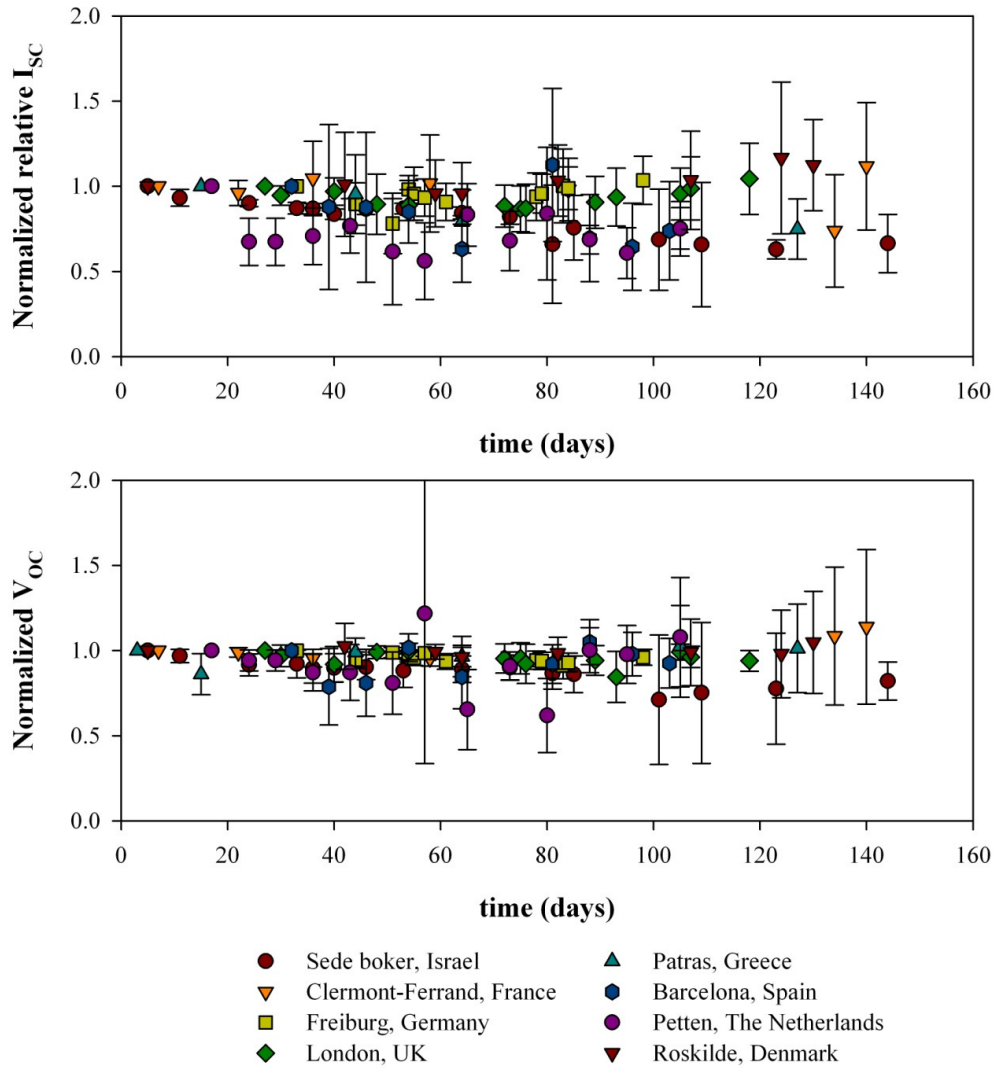


**Figure 4.6** Outdoor  $I_{SC}$  and  $V_{OC}$  measurements of the panels during the periods of outdoor exposure. **top:** Average normalized relative  $I_{SC}$  for the modules/cells 1-10 (relative to  $I_{SC}$  of the reference cell 11) for all panels. **bottom:** Average normalized  $V_{OC}$  for the modules/cells 1-10 for all panels.



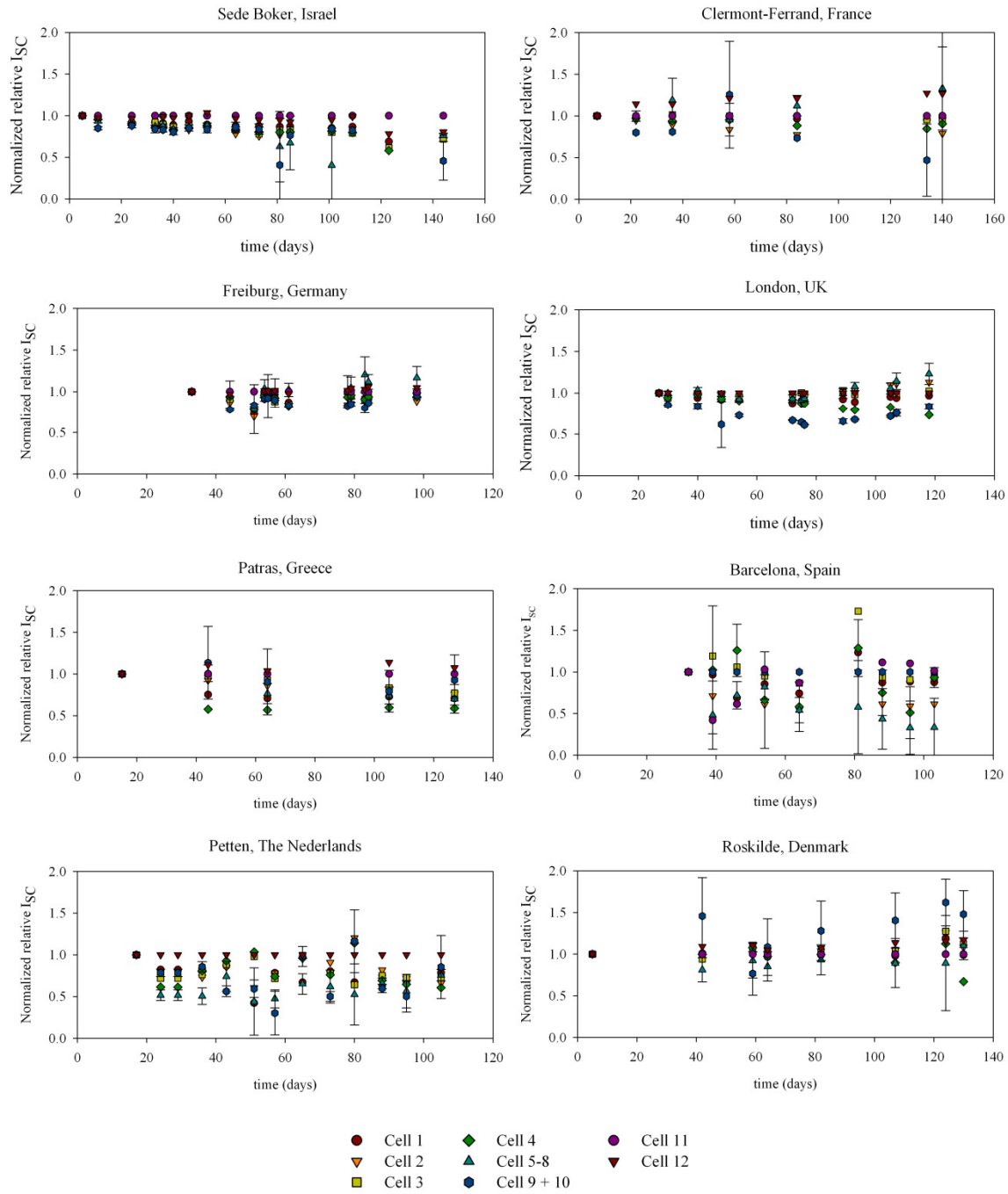


**Figure 4.7** Normalized relative  $I_{sc}$  [relative to  $I_{sc}$  of the silicon photodiode Ref **11** included in each panel) measured in the different countries. In the UK and the Nederland the Ref **11** failed and the relative  $I_{sc}$  was in these cases calculated relative to  $I_{sc}$  of Ref **12**. The top four results are from locations situated ‘inland’ while the bottom four are situated by or near the sea.

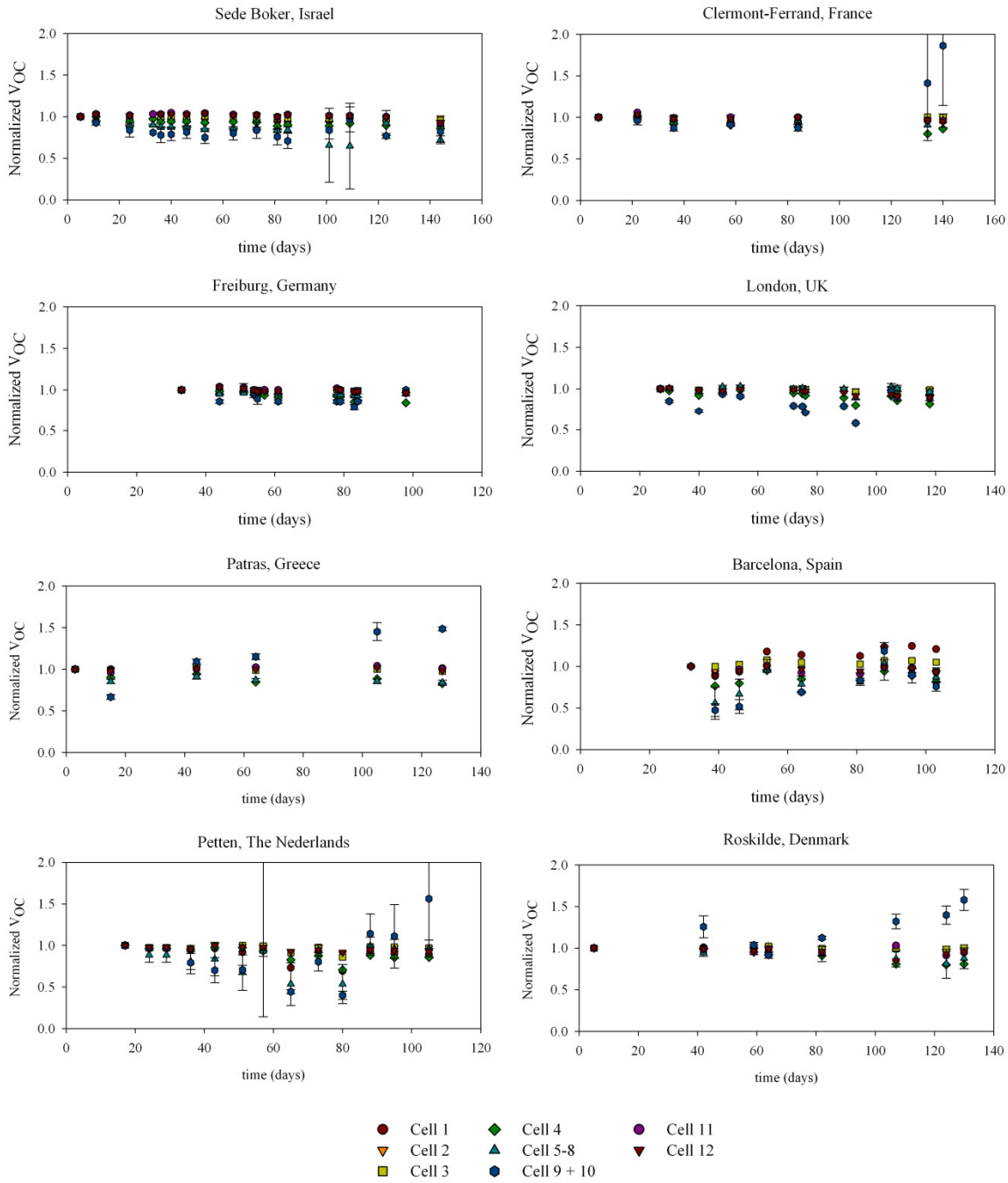


**Figure 4.8** Normalized  $V_{OC}$  measured in each country. The top four results are from locations situated ‘inland’ while the bottom four are situated by or near the sea.

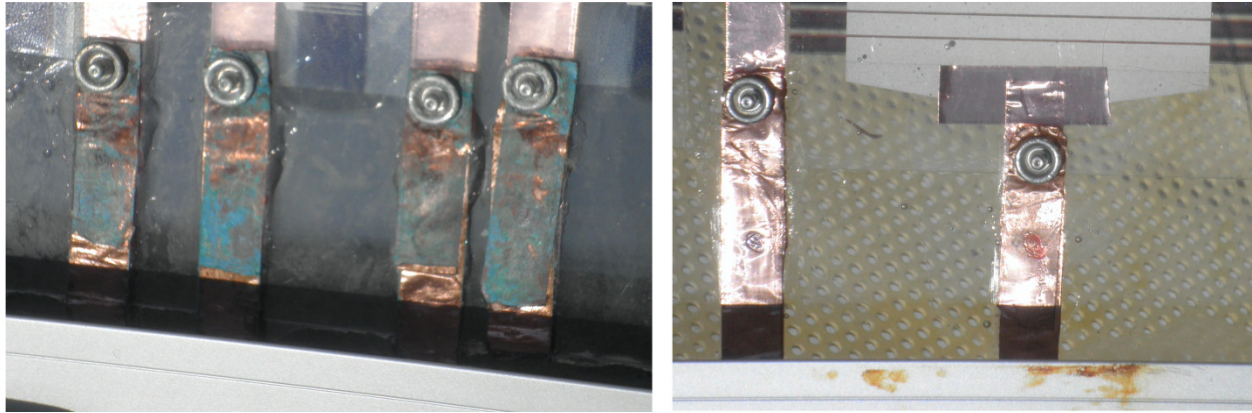


**Figure 4.9** Corrosion of the external part of the electrodes in Petten (the Netherlands) (**left**) compared to the non-corroded electrodes on the panel from Clermont-Ferrand (France) (**right**).

Especially in the Netherlands by the North Sea which has a higher salt concentration than the other locations, external corrosion of the copper electrodes appeared as illustrated in Figure 4.9.

In all panels problems were encountered to some degree with the internal contact between the copper tape and the printed silver electrodes which had a tendency to detach - probably caused by the temperature fluctuations which are unavoidable in outdoor testing. This contact could in almost all cases be momentarily repaired though, by appliance of pressure on the polycarbonate backside of the panel, allowing for measurements to be performed. Although it was thus possible to perform measurements it is strongly recommended that alternative connection to the exterior is used in future projects.

#### 4.4.2 Overall performance after outdoor exposure

Comparison of  $IV$ -curves at  $t_0/t_0'$  and  $t_x/t_x'$  showed in no cases significant deviations indicating that no damage had happened to the panels during shipments between the destinations. Figure 4.10 shows the changes in  $IV$ -characteristics of the different types of cells used in the study ( $t_0-t_x$ ).

For the P3HT modules **1-3**, module **2** and module **3** shows the largest decreases in efficiency, primarily because of a larger drop in FF and for module **2** also in current. The FF for **2** and **3** were originally better ( $t_0$ ) than for module **1** and **4**, but the relative gain in FF by appliance of grid or full silver structured back electrodes becomes less pronounced on a long-term basis.

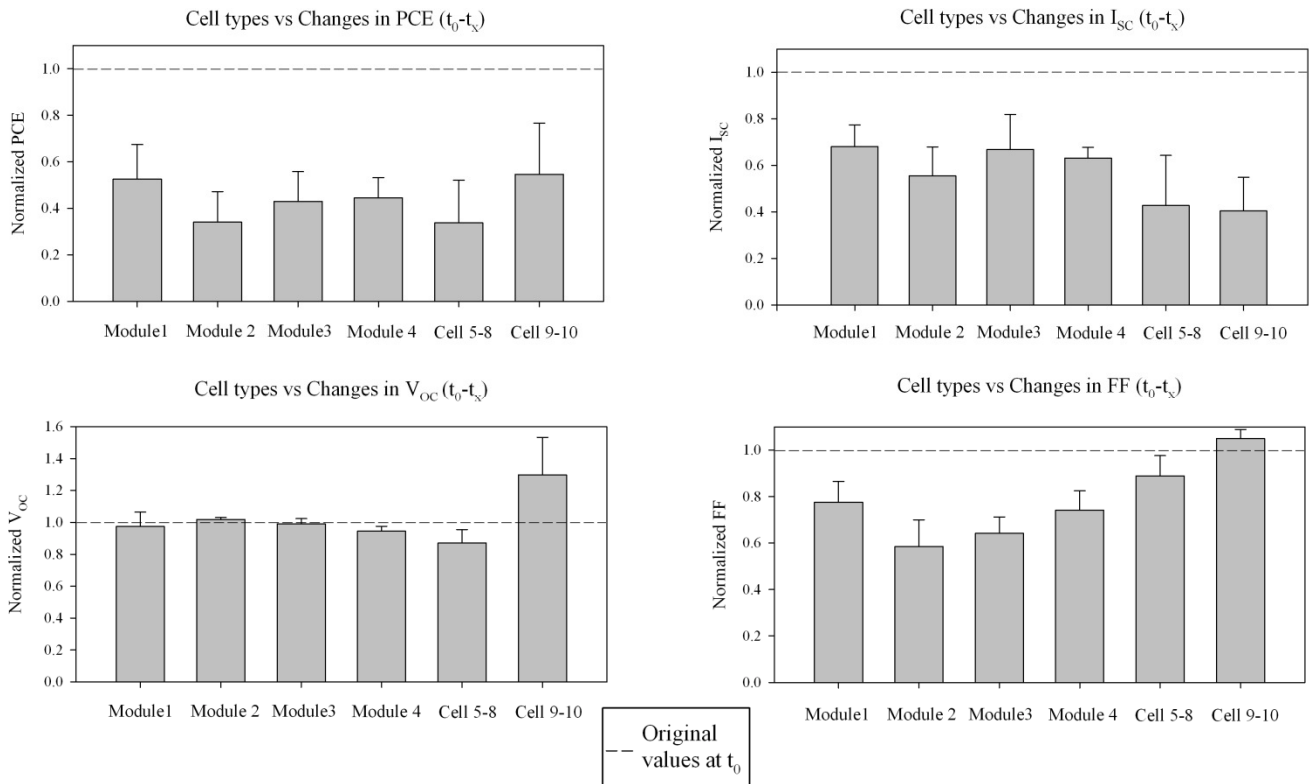


**Figure 4.10** Normalized IV-data at  $t_x$  (approximately 4½ months) showing the changes for the different types of cells used in the study.

The commercial polymer PV2000 used in module **4** showed to have similar stability as the P3HT module **1** having the same structure. Generally all modules show excellent preservation of the voltages and no extreme deviations are observed for the current.

For the single cells the polymer **tBDT-BTBT** ( cells **9-10**) is seemingly more stable than polymer **cBDT-BTBT** (cells **5-8**), but the difference is mainly due to an increase in voltage to a level *higher* than before outdoor exposure and must therefore be looked at with suspicion. The currents of the single cells are all reduced more than the modules, which is probably a sign of higher photodegradation of the active material. This correlates well with the previous finding on the photo-stability of the two polymers compared to P3HT, described in chapter 3.

Looking at the average *IV*-characteristic after outdoor exposure for the specific panels placed at the different locations, shown in Figure 4.11, all panels have roughly experienced the same drop in efficiencies, when taking the exposure time into consideration. Although the most southern and more sunny locations seems to be slightly lower than the northern ones, the tendency is not pronounced, which

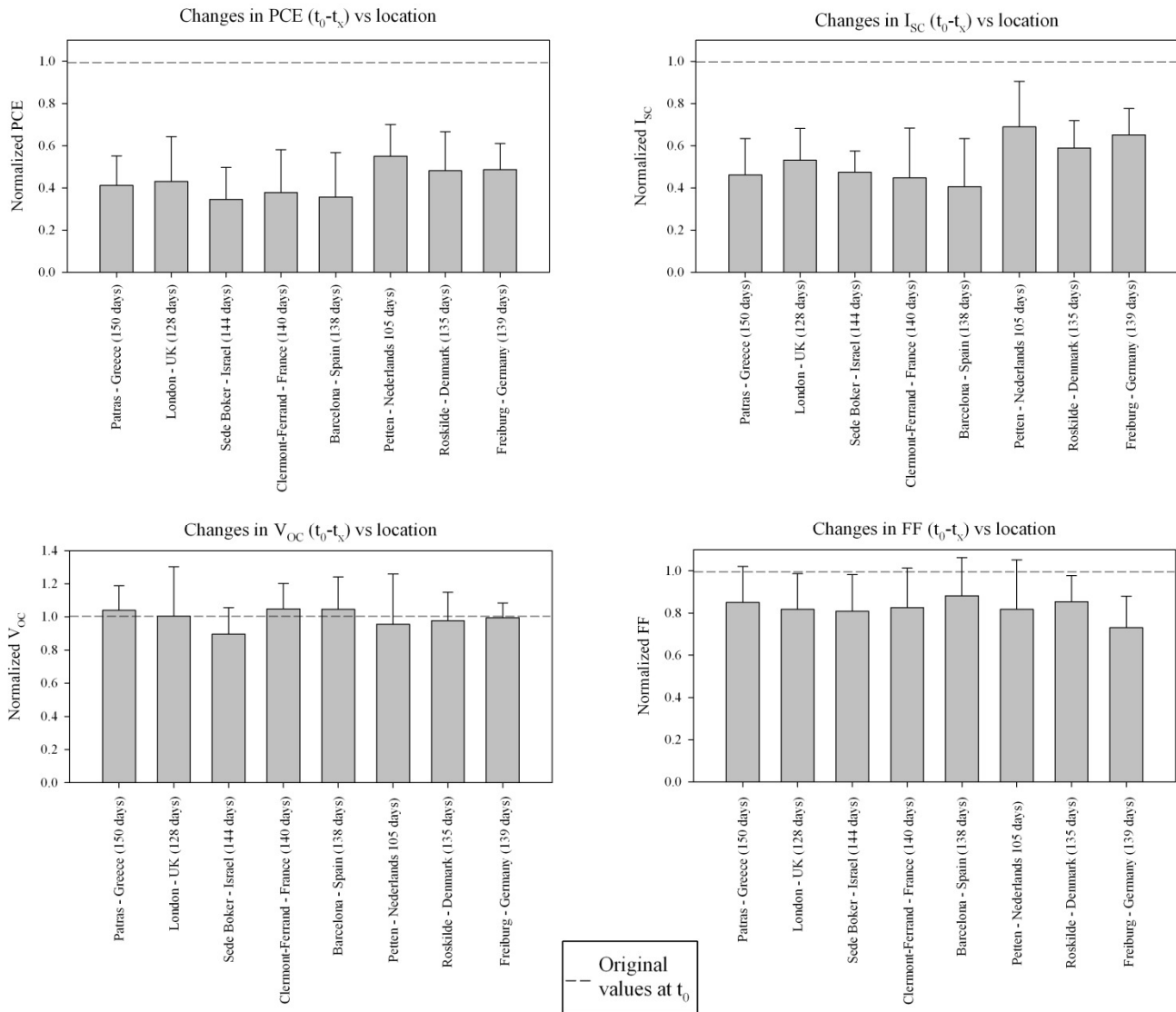


**Figure 4.11** Normalized IV-data at  $t_x$  showing the changes at the different locations used in the study. The outdoor exposure time in days is noted in parenthesis.

indicates that other factors than photodegradation must play an important role in the degradation of the cells. This is best illustrated comparing the panel mounted in the often cloudy and rainy London (128 days of outdoor exposure, average PCE at  $t_x$  around 42% or original) and the panel mounted in the almost always sunny Negev desert (Sede Boker, 144 days of outdoor exposure, average PCE at  $t_x$  around 35% of original). Taking the general weather conditions, the shorter outdoor exposure time and the generally shorter days in London during the period of exposure (hours of daylight: London ( $t_0 \sim 8$  h,  $t_x \sim 14$  h), Israel ( $t_0 \sim 10$  h,  $t_x \sim 13$  h)) the difference would be expected to be much more pronounced if

photodegradation was the only degradation mechanism. It is difficult to say what other mechanisms are contributing to the degradation as they could originate from numerous changes. Potential explanations include morphology or chemical composition changes at the interfaces in the layered solar cell structure by slow detachment or 'mixing' of the individual layers at the interfaces, changes in the homogeneity of the active layer, changes in the conducting properties of for example zinc oxide. Further examination of the individual layers need to be performed in order to determine this. Such work is outside the scope of this thesis and must remain for future studies.

To evaluate the usefulness of polyurethane as encapsulation method of organic solar cells, comparison can be made with the previously mentioned results by Gevorgyan *et al*,<sup>[4]</sup> where P3HT modules similar to module 3 were tested outside after encapsulation with barrier foil on both back and front. Where the average PCE using barrier foil was reduced to approximately 40% after 1000 h (~42 days) of outdoor exposure, the embedding of the cells in polyurethane has prolonged this period to 4½ months, which must be considered a significant improvement.

#### **4.4.3 Evaluation of the panel design**

Besides the already mentioned contact problem between the silver electrodes of the polyurethane embedded modules/cells and the copper tape leading to the exterior, a major problem in the design was delamination at the polyurethane/glass interface caused by the different expansion coefficients of the materials when exposed to temperature fluctuations. The design originally consisted of using polycarbonate on both front and back side of the panels but due to the UV cutoff by polycarbonate this idea had to be discarded as the zinc oxide layer needs photo-doping with UV light in order to maintain good conductivity.<sup>[12]</sup> The choice of using a tempered glass plate as the front of the panel solved this problem, but the use of three different materials (glass, polyurethane and polycarbonate) caused the mentioned problems of delamination. Probably the use of two glass plates can solve the problem, but for future use of polyurethane as encapsulation, more tests needs to be performed beforehand in order to avoid this.

## 4.5 Conclusion

A total of nine panels each containing 10 polymer solar modules/cells were fabricated using polyurethane as encapsulation sandwiched between a tempered glass plate and polycarbonate plate. Four different cell geometries and four different active materials were used in the study. Eight of the panels were installed outside at locations in eight different countries chosen for their diversity in weather conditions in order to fully test the usefulness of the encapsulation method. In order to limit deviations caused by human factors and equipment a single person was responsible for the preparation, measurement (before and after outdoor expose), and installation of the panels at the test locations, using the same equipment for all measurements and calibrations. Further monitoring was carried out by local representatives who measured  $I_{sc}$  and  $V_{oc}$  on days with constant light intensity allowing following the development of the cells during the experiment by comparison with two reference silicon photodiodes also mounted on the panel. These measurements showed a general trend of slow decrease in the current while the voltage remained more or less constant.

Examination of the *IV*-characteristics of P3HT modules with different silver back electrodes before and after outdoor exposure, showed that although an initial improvement of the fill factor can be obtained by using a grid structure or a full covering of the active area compared to a simple busbar, this improvement becomes much less pronounced after outdoor exposure. In the comparison of the overall performances of the panels, it was found that although slightly lower final efficiencies were found for the panels which had been exposed at the most southern (more sunny) locations, the panes had roughly experienced the same amount degradation, indicating that photodegradation is not the only source of degradation of the cells. Compared to previously published results the use of polyurethane as encapsulation method has proven to significantly reduce the degradation and average efficiencies around 40% of the original was observed after 4½ months outdoor exposure.

On a more personal level the external stay proved to be an enormous success and a great experience, as it has allowed me to meet and work with a large number of central people within the organic solar cell community.

## 4.6 References

1. Hauch, J. A.; Schilinsky, P.; Choulis, S. A.; Childers, R.; Biele, M.; Brabec, C. J. Flexible organic P3HT : PCBM bulk-heterojunction modules with more than 1 year outdoor lifetime. *Sol. Energy Mater. Sol. Cells* **2008**, *92* (7), 727-731.
2. Katz, E. A.; Gevorgyan, S.; Orynbayev, M. S.; Krebs, F. C. Out-door testing and long-term stability of plastic solar cells. *European Physical Journal-Applied Physics* **2006**, *36* (3), 307-311.
3. Medford, A. J.; Lilliedal, M. R.; Jorgensen, M.; Aaro, D.; Pakalski, H.; Fyenbo, J.; Krebs, F. C. Grid-connected polymer solar panels: initial considerations of cost, lifetime, and practicality. *Optics Express* **2010**, *18* (19), A272-A285.
4. Gevorgyan, S. A.; Medford, A. J.; Bundgaard, E.; Sapkota, S. B.; Schleiermacher, H. F.; Zimmermann, B.; Wurfel, U.; Chafiq, A.; Lira-Cantu, M.; Swonke, T.; Wagner, M.; Brabec, C. J.; Haillant, O. O.; Voroshazi, E.; Aernouts, T.; Steim, R.; Hauch, J. A.; Elschner, A.; Pannone, M.; Xiao, M.; Langzettel, A.; Laird, D.; Lloyd, M. T.; Rath, T.; Maier, E.; Trimmel, G.; Hermenau, M.; Menke, T.; Leo, K.; Rosch, R.; Seeland, M.; Hoppe, H.; Nagle, T. J.; Burke, K. B.; Fell, C. J.; Vak, D.; Singh, T. B.; Watkins, S. E.; Galagan, Y.; Manor, A.; Katz, E. A.; Kim, T.; Kim, K.; Sommeling, P. M.; Verhees, W. J. H.; Veenstra, S. C.; Riede, M.; Christoforo, M. G.; Currier, T.; Shrotriya, V.; Schwartz, G.; Krebs, F. C. An inter-laboratory stability study of roll-to-roll coated flexible polymer solar modules. *Sol. Energy Mater. Sol. Cells* **2011**, *95* (5), 1398-1416.
5. Krebs, F. C. Encapsulation of polymer photovoltaic prototypes. *Sol. Energy Mater. Sol. Cells* **2006**, *90* (20), 3633-3643.
6. Krebs, F. C. Roll-to-roll fabrication of monolithic large-area polymer solar cells free from indium-tin-oxide. *Sol. Energy Mater. Sol. Cells* **2009**, *93* (9), 1636-1641.
7. Krebs, F. C.; Gevorgyan, S. A.; Gholamkhash, B.; Holdcroft, S.; Schlenker, C.; Thompson, M. E.; Thompson, B. C.; Olson, D.; Ginley, D. S.; Shaheen, S. E.; Alshareef, H. N.; Murphy, J. W.; Youngblood, W. J.; Heston, N. C.; Reynolds, J. R.; Jia, S. J.; Laird, D.; Tuladhar, S. M.; Dane, J. G. A.; Atienzar, P.; Nelson, J.; Kroon, J. M.; Wienk, M. M.; Janssen, R. A. J.; Tvingstedt, K.; Zhang, F. L.; Andersson, M.; Inganas, O.; Lira-Cantu, M.; de Bettignies, R.; Guillerez, S.; Aernouts, T.; Cheyns, D.; Lutsen, L.; Zimmermann, B.; Wurfel, U.; Niggemann, M.; Schleiermacher, H. F.; Liska, P.; Gratzel, M.; Lianos, P.; Katz, E. A.; Lohwasser, W.; Jannon, B. A round robin study of flexible large-area roll-to-roll processed polymer solar cell modules. *Sol. Energy Mater. Sol. Cells* **2009**, *93* (11), 1968-1977.
8. Krebs, F. C.; Norrman, K. Analysis of the failure mechanism for a stable organic photovoltaic during 10000 h of testing. *Prog. Photovolt.* **2007**, *15* (8), 697-712.
9. Lira-Cantu, M.; Norrman, K.; Andreasen, J. W.; Krebs, F. C. Oxygen release and exchange in niobium oxide MEHPPV hybrid solar cells. *Chem. Mater.* **2006**, *18* (24), 5684-5690.
10. Jørgensen, M.; Norrman, K.; Krebs, F. C. Stability/degradation of polymer solar cells. *Sol. Energy Mater. Sol. Cells* **2008**, *92* (7), 686-714.
11. Krebs, F. C.; Tromholt, T.; Jørgensen, M. Upscaling of polymer solar cell fabrication using full roll-to-roll processing. *Nanoscale* **2010**, *2* (6), 873-886.



12. Lilliedal, M. R.; Medford, A. J.; Madsen, M. V.; Norrman, K.; Krebs, F. C. The effect of post-processing treatments on inflection points in current-voltage curves of roll-to-roll processed polymer photovoltaics. *Sol. Energy Mater. Sol. Cells* **2010**, *94* (12), 2018-2031.

## Chapter 5

### Acid catalyzed thermocleavage of thiophene polymers with ester side chains\*

#### 5.1 Introduction

One of the major challenges, within the field of polymer solar cells, has shown to be stabilization of the active layer of the cells. As mentioned in previous chapters the use of thermocleavable materials has in recent years proved to be a reliable source of introducing higher photo-stability to the active layer.<sup>[1-10]</sup> Side chains are essential with respect to solubilizing the polymer thus allowing for solution processing of the active layer, but they also make the layer soft, and allows for diffusion of oxygen and water to occur easily. By using thermocleavable side chains it is possible to remove these by subsequent heating after processing of the active layer. The film then becomes much harder and less susceptible to the reactions that lead to photo degradation. The key problem in the process is that quite high temperatures (up to 300 °C) are needed in order to perform the thermocleavage reactions. These therefore have to be performed on substrates that can sustain such temperatures, and is in reality limited to glass. In order for this procedure to be of any real interest for large scale production, thermocleavage must be performed on cheap flexible substrates such as PET. This limits the maximum temperature employed to around 140 °C in order to avoid deformation of the substrate, and changes in the reaction conditions are therefore required.

---

\* Some of this work has been published:

Søndergaard, R.; Norrman, K.; Krebs, F.C. Low temperature side chain cleavage and decarboxylation of polythiophene esters by acid catalysis. *J. Polym. Sci. A Polym. Chem.* 2012, 50 (6), 1127-1132.

## 5.2 Thermocleavage of P3MHOCT in the presence of strong acid

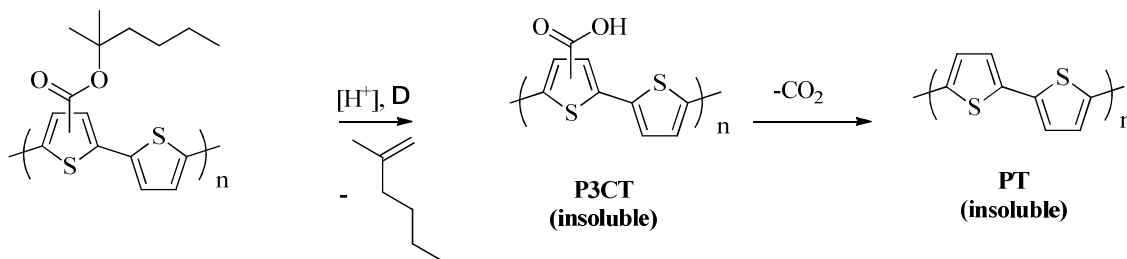
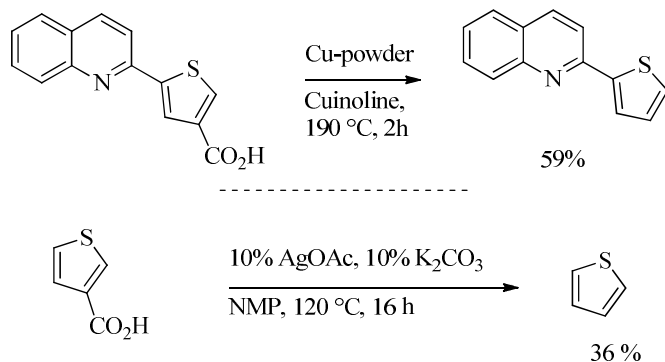


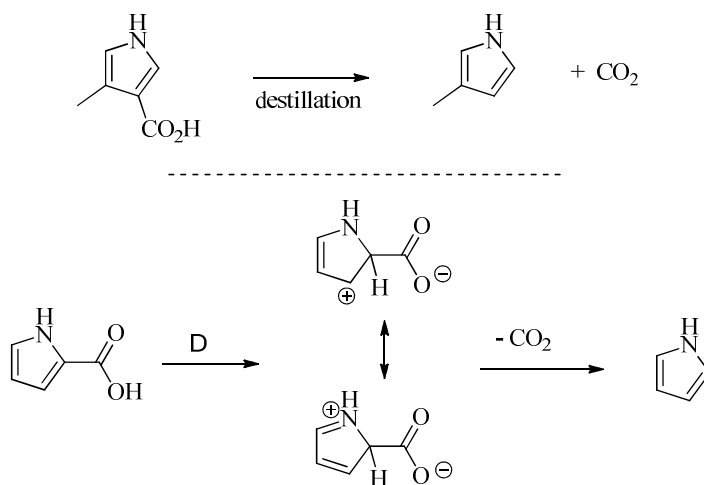
**Figure 5.1** Acid catalyzed side chain cleavage and decarboxylation of the polymer P3MHOCT.

In the thermocleavage of tertiary thiophene esters it is the decarboxylation step that requires the highest temperature, and from a processing standpoint/view thus the most critical. Lowering of the decarboxylation of 3-carboxythiophenes has previously been performed using copper<sup>[11]</sup> or silver catalyst<sup>[12]</sup> (see Scheme 5.1) but the use of metal catalysts does not comply with solar cell fabrication as the reaction has to be performed during the processing step and metals are impossible to remove and are prone to create shorts in a prepared film.

It was instead thought that an alternative approach using volatile, strong organic acids might be possible. Because of the volatile nature of the acids it should be possible to remove the acid, thus making the process compatible with solar cell processing.



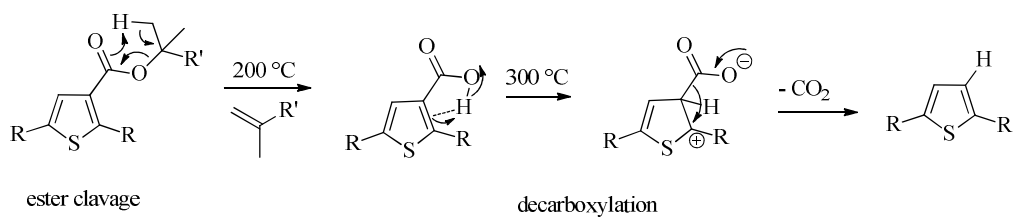
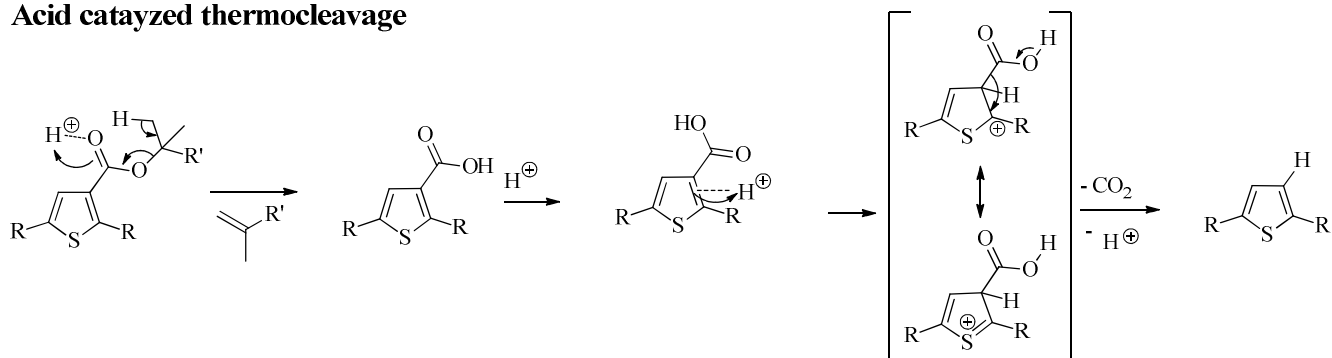
**Scheme 5.1** Examples of previous reports of lowering of decarboxylation of 3-carboxythiophenes



**Scheme 5.2: Top** Example of decarboxylation of a 3-carboxypyrrrole.<sup>[13]</sup> **Bottom:** mechanism suggested for the decarboxylation of pyrrole-2-carboxylic acid.<sup>[14]</sup>

It has long been known that the analogous reaction of decarboxylation of pyrrole carboxylic acids to pyrroles can also be performed by simple heating as shown in Scheme 5.2 for 3-carboxy-4-methylpyrrole,<sup>[13]</sup> and more interestingly it has been shown that the decarboxylation of pyrrole-2-carboxylic acid to proceed via *ipso*-displacement of CO<sub>2</sub> by hydrogen.<sup>[14]</sup> The general ease of decarboxylation of carboxy-pyrroles thus seems to originate from resonance stabilization of the formed carbocation formed by protonization of the aromatic ring.

To my knowledge no mechanism has been determined for the decarboxylation of 3-carboxythiophenes, but taking the many similarities between pyrrole and thiophene into consideration it is reasonable to expect that the mechanism is the same for thiophene acids and that such a reaction would be catalyzed by strong acids. In addition to this it is commonly known that esters are prone to cleavage when exposed to acid and the presence of acid thus might lower the cleavage temperature of both side chain elimination and decarboxylation. The assumed reaction mechanisms without and with catalytic acid is shown in Figure 5.2.

**No acid****Acid catalyzed thermocleavage**

**Figure 5.2:** Suggested mechanisms for the ester cleavage and subsequent decarboxylation reaction with and without acid catalysis.

### 5.2.1 Examination of the cleavage temperatures of the tertiary ester moiety in the polymer P3MHOCT in the presence of catalytic amounts of different strong acids

In order to examine whether the cleavage temperatures by acid catalysis could be lowered enough to be of interest for further examination, a series of TGA-MS experiments were performed on blends of the tertiary polymer P3MHOCT with varying catalytic amounts of different strong acids. The experiments were performed by mixing stock solutions of the polymer and the acid in different ratio followed by evaporation of the solvent in air with subsequent TGA-MS experiment. All experiments started at 50 °C with an increase in temperature by 10 °C/min while monitoring specific masses with the MS-unit. As all the added acids evaporate to some extent during the experiment, TGA data are only reliable for the pure P3MHOCT, which is shown in Figure 5.3a along with MS-data. In order to simplify the illustration of the comparative studies a single representative mass ( $m/z$  55, C<sub>4</sub>H<sup>+</sup>) for the thermocleavage of the ester

moiety is illustrated as well as the mass of  $\text{CO}_2$  ( $m/z$  44) for the monitoring of the decarboxylation process. An example of a full MS-experiment is shown for P3MHOCT in figure 5.3b. The TGA-MS data show a good correlation between the observed losses in weight from the TGA-data and the simultaneous raise in

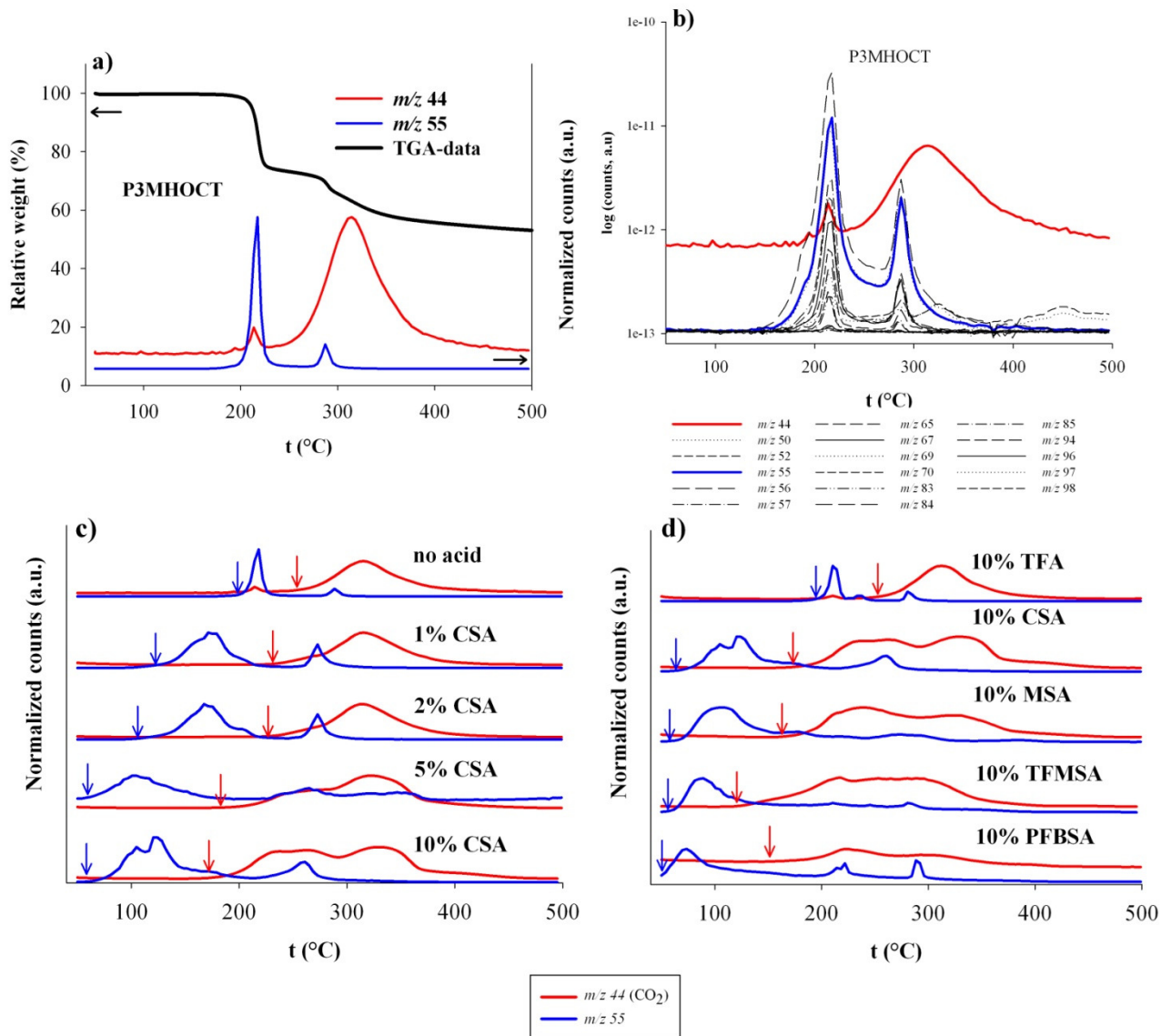


**Figure 5.3:** TGA-MS data for acid catalyzed cleavage of P3MHOCT. The mass  $m/z$  55 is representative for the cleavage of the ester bond under formation of P3CT, and the mass  $m/z$  44 show the evolution of  $\text{CO}_2$  from the decarboxylation of P3CT to PT. The onset-temperatures of both reactions are in all cases marked with arrows. **a)** TGA and characteristic fragmentation ions of P3MHOCT without addition of acid. **b)** An example of a complete MS-experiment where a range of masses are monitored – here for P3MHOCT without added acid. **c)** P3MHOCT with different amounts of catalytic CSA. **d)** P3MHOCT with addition of 10 mol% of different strong acids. **CSA:** Camphor sulphononic acid, **TFA:** Trifluoroacetic acid, **MSA:** methanesulphonic acid, **TFMSA:** trifluoromethanesulphonic acid, **PFBSA:** Perfluorobutanesulphonic acid.

intensity of the characteristic masses in the MS-experiment. Although the TGA-data cannot be used as a clear marker for the thermocleavage reaction when acid has been added, it is possible to monitor the characteristic mass fragmentations in the MS-experiment and in this way observe the acid catalyzed cleavage temperatures. A range of different acids were tested: Trifluoroacetic acid (TFA), Camphor sulphonic acid (CSA), methanesulphonic acid (MSA), trifluoromethanesulphonic acid TFMSA and perfluorobutanesulphonic acid (PFBSA). Selected experiments are shown in Figure 5.3c-d. The reactions were found to be very dependent on both the acid strength and the catalytic amount of acid added (the noted percentage of added acid is the relative mol% compared to the theoretical presence of ester groups in the polymer employed). Figure 5.3c clearly shows that especially the cleavage of the ester group is easily catalyzed by even small amounts of CSA, whereas the decarboxylation requires larger amounts in order to effectively catalyze the reaction. The importance of the acid strength is furthermore illustrated in Figure 5.3d where a lowering of the cleavage temperatures for both ester and acid is observed with increasing acid strength. Where TFA hardly has any effect at all, CO<sub>2</sub>-evolution commences at as low temperatures as 110-120 °C for the much stronger acid TFMSA. In most cases an increase in the *m/z* 55 is observed at around the same temperature where CO<sub>2</sub>-evolution starts. This is ascribed to the fact that the hardening of the polymer bulk lowers the permeability towards gasses, and it is thus reasonable to expect that not all the side chains 'escape' the bulk after the initial side chain cleavage. When CO<sub>2</sub> evolution starts, CO<sub>2</sub> acts like a carrier gas and pulls some of the remaining side chains to the surface. Such retention of gasses would also explain why CO<sub>2</sub> in several cases is liberated over a rather large temperature span. The obtained results furthermore suggest that the decarboxylation of 3-thiophene could not be prepared. When using PFBSA all films had an even quality without any precipitation. After coating the PET-foil was led through an oven at 140 °C for 5 minutes and the resulting films were subsequently analyzed by XPS. Each experiment was performed twice giving a total of 16 films. The XPS-results are shown in Figure 5.4. By comparing the chemical composition of P3MHOCT, the side chain cleaved P3CT and the completely cleaved PT it is possible to evaluate the degree of cleavage. The data shows that the addition of 1 mol% acid was not enough to fully cleave the side chains, but that this could be achieved when adding 5-10 mol% of TFMSA or 3-5 mol% of PFBSA. In the case of 10% TFMSA precipitation had occurred to such an extent that no useful XPS-data could be obtained from the inhomogeneous film. In none of the experiments was cleavage to PT observed. This is probably due to the fact that the temperature employed is only slightly above the starting temperature for CO<sub>2</sub> cleavage and that the heating time is relatively short. The XPS data furthermore showed that only some of the acid was removed in the process, which

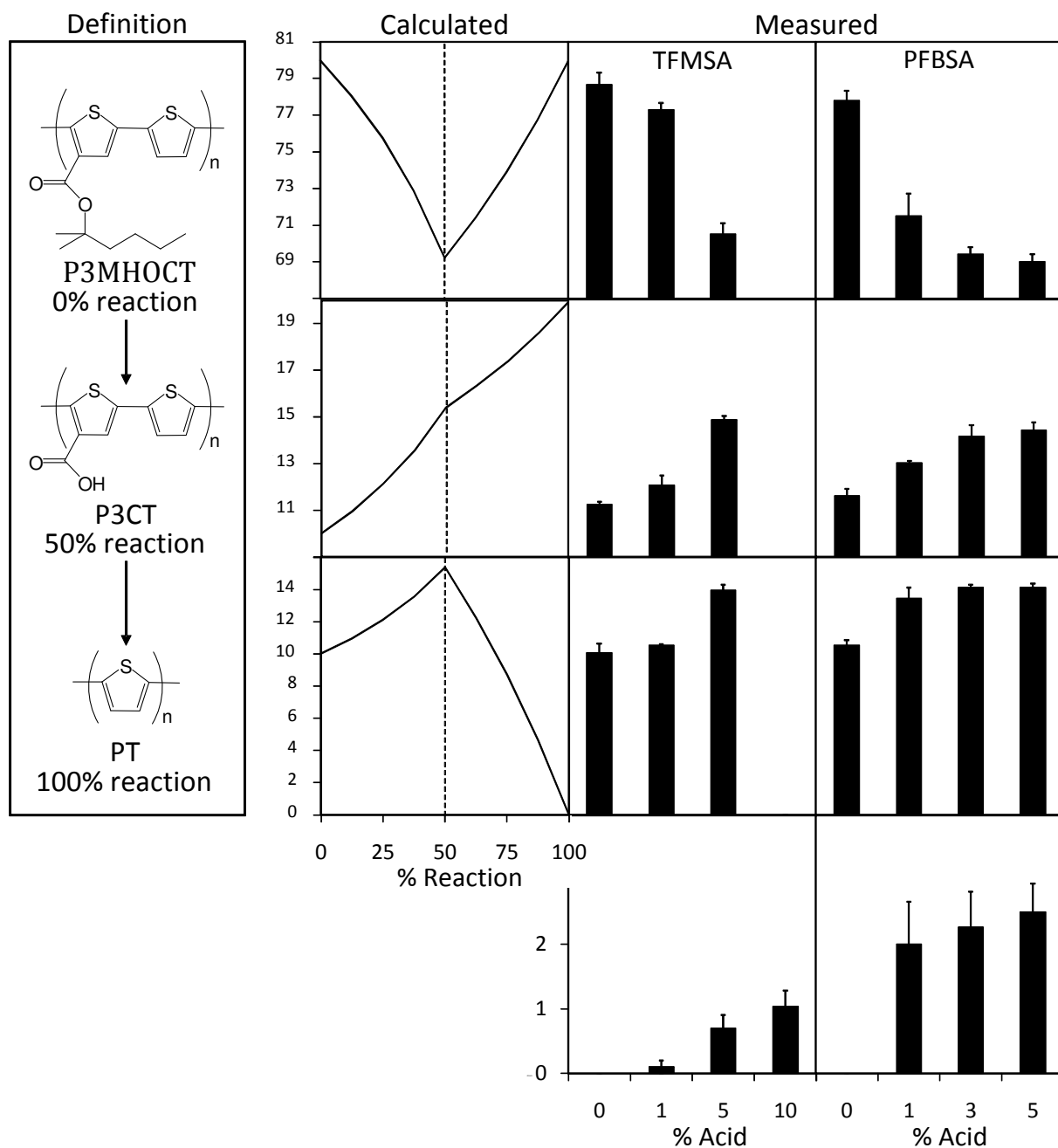


**Figure 5.4** XPS results of the analysis of films on PET prepared using P3MHOCT and various catalytic amounts of acids TFMSA and PSBSA for thermocleavage at 140 °C. The curves on the left shows graphical representation of the relative calculated atom% distribution of carbon, sulfur and oxygen during a reaction where 0% reaction is P3MHOCT, 50% reaction is P3CT and 100 % reaction is PT. To the right of these are shown the actual atom% measured by XPS for all 16 experiments. As a measure of how much acid is still left in the film, the atom% of fluorine found in the respective films is shown in the bottom row.

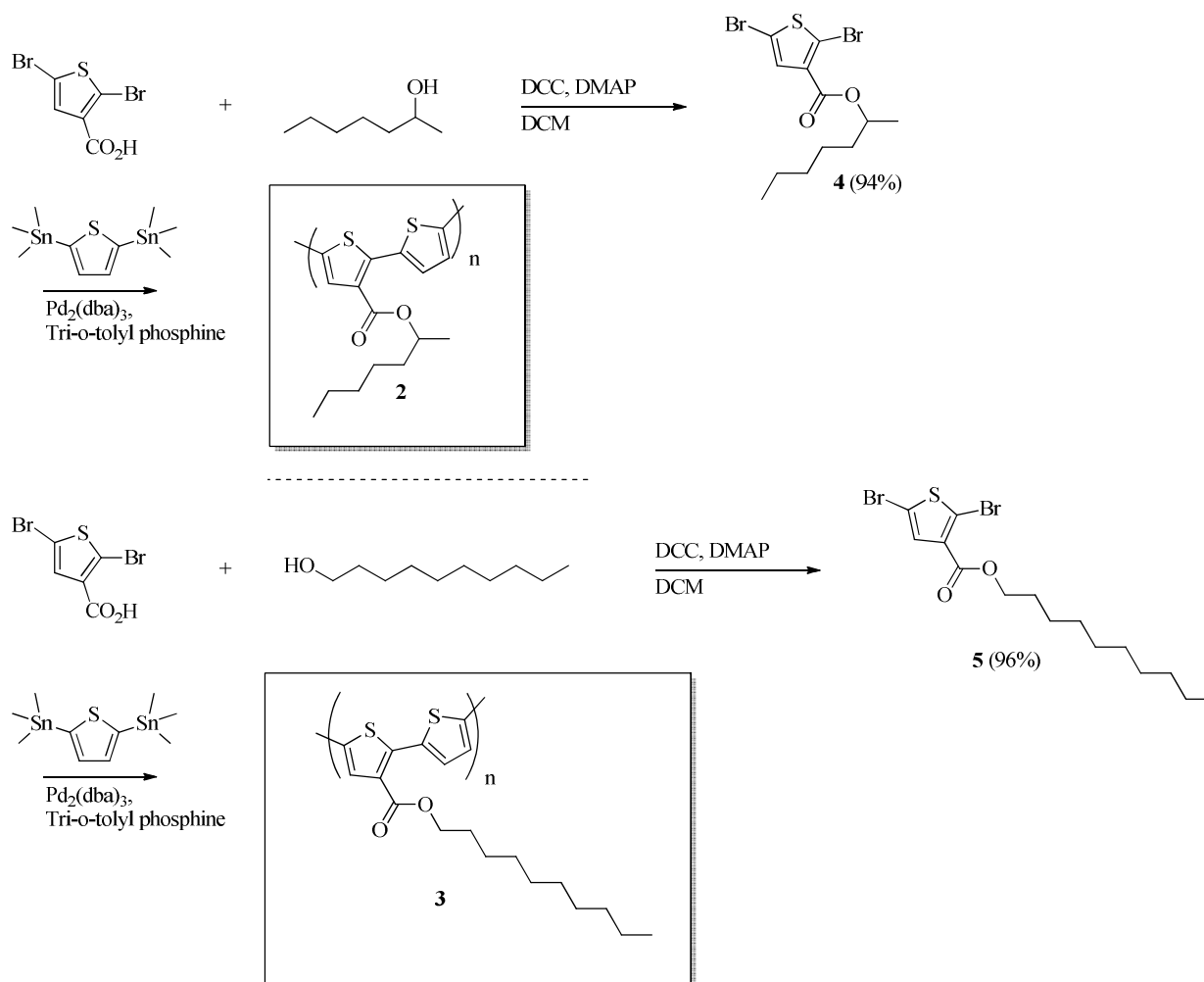


could be related to the previously mentioned hardening of the active layer which reduces the permeability.

Further studies using longer cleavage times will have to determine whether it is possible to cleave the polymers further to the PT stage and in the same step remove more of the acid. Unfortunately it was not possible to perform these within the time limit of this thesis.

### 5.3 Examination of the influence of catalytic amounts of strong acid on the thermocleavage of polymers carrying secondary and primary ester side groups.

#### 5.3.1 Synthesis of secondary and primary ester analogues to P3MHOCT



**Scheme 5.2** Synthesis of polymers with secondary ester groups (polymer 2) and primary ester groups (polymer 3)

Thermocleavage of polymers carrying secondary or primary ester side chains have not previously been reported for solar cells, probably because of the very high temperatures necessary for the reactions to occur. In order to examine whether it was possible to extend acid catalyzed cleavage to these two types of side chains, two analogues to P3MHOCT were synthesized as shown in Scheme 5.2. DCC coupling of 2,5-dibromothiophene-3-carboxylic acid with the either 2-heptanol or 1-dacanol in both cases yielded the corresponding ester in excellent yield, and subsequent Stille coupling with 2,5-bis(trimethylstannyl)thiophene yielded the desired polymers carrying secondary (polymer **2**) or primary (polymer **3**) side chains. The experimental details of the polymers are given in the experimental section 5.5.

### 5.3.2 Examination of the cleavage temperatures for thiophene polymers with secondary and primary side chains

The TGA-MS experiment previously described for P3MHOCT was performed on polymer **2** and **3**. When comparing the MS-data of the thermocleavage of the three polymers as shown in Figure 5.5, the shift from a tertiary ester to a secondary raises the cleavage temperature of the side chain slightly (50-120 °C), but the decarboxylation reaction remains the same as expected. When going to a primary ester, the cleavage of the side chain happens at higher temperature (150-170 °C) than where decarboxylation of the free acid

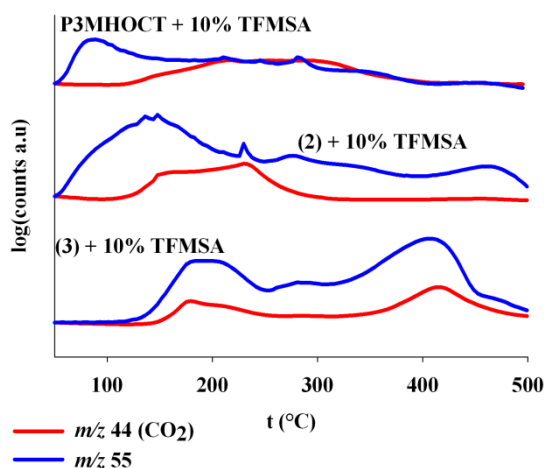


**Figure 5.5** Comparative illustrations of the TGA-MS data of P3MHOCT, polymer **2** and polymer **3** in the presence of 10 mol% TFMSA

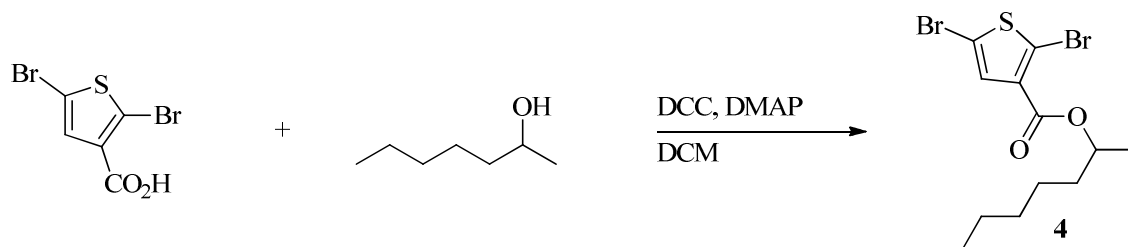
would commence and hence the CO<sub>2</sub>-evolution is observed immediately after/simultaneous with the signal from the side chain. As secondary and primary esters are generally much easier to prepare, and thus cheaper to produce, these are very interesting results as they indicate the possible use of such side chains in thermocleavable polymers for organic solar cells. Especially the results for polymer **3** are noticeable as the experiment shows that the polymer is stable in the acidic solution below 100 °C. This is interesting as it opens up for the possibility of preparation of an acidic ink which could potentially be stored at RT. The cleavage temperature is a little too high though in order to be used on PET.

## 5.4 Conclusion

In summary the influence of strong acids on the thermocleavage temperature of thiophene polymer P3MHOCT carrying tertiary side chains has been examined by means of TGA-MS and XPS. By monitoring of characteristic fragments in MS a considerable lowering of the cleavage temperatures of both side chains (200-220 °C → RT to 50 °C) and the subsequent decarboxylation (250-300 °C → 120-150°C) is observed when using sufficiently strong acids like trifluoromethanesulfonic acid. XPS data of roll-to-roll (R2R) processed films of P3MHOCT and catalytic amounts of strong acid on PET showed that heating of the processed film to 140 °C for 5 minutes is sufficient to achieve cleavage to the insoluble acid stage but no indication of decarboxylation was observed. Unfortunately XPS-data indicate that only some of the acid was removed in the drying/heating process. Prolonged drying times might change this, but further investigations of this are necessary before any final conclusions can be made.

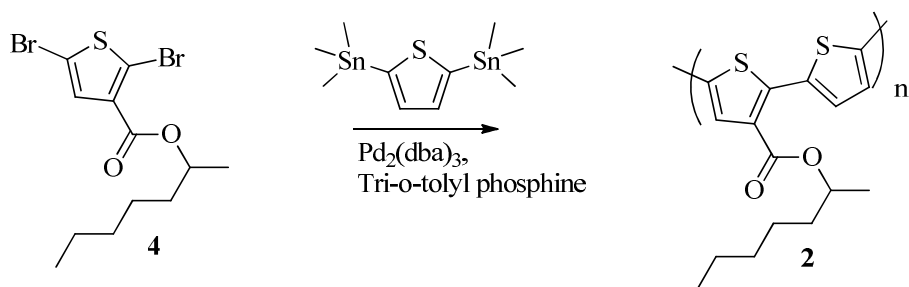
Finally TGA-MS experiments with polymers carrying secondary (**2**) and primary (**3**) ester side chains showed a lowering of the ester cleavage to 65-120 °C and 140-170 °C respectively, and the temperature for decarboxylation as expected was either the same as for P3MHOCT or in the case of the primary ester the same as the side chain cleavage temperature. The fact that the cleavage temperature of secondary and primary thiophene esters can be lowered so much makes these compounds potential cheaper candidates for thermocleavable polymers in organic solar cells. Overall several issues still need to be resolved, such as complete removal of the used acid, in order for this procedure to be applicable in solar cell preparation on flexible substrates like PET, but a promising first step towards lowering thermocleavage temperatures to acceptable levels has been achieved.

## 5.5 Experimental section

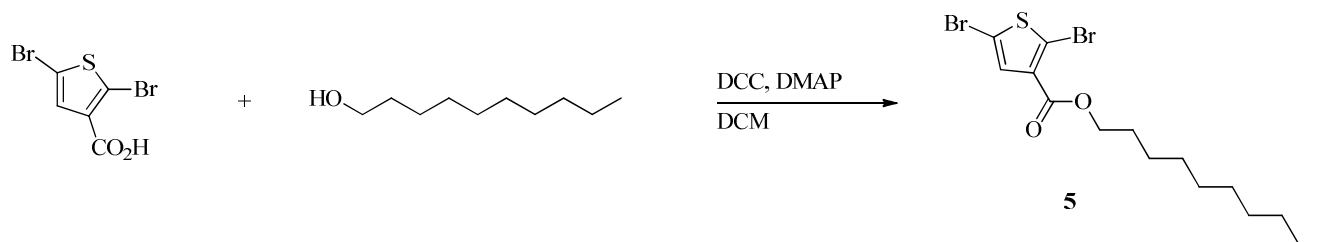


**Heptan-2-yl 2,5-dibromothiophene-3-carboxylate (4):** 2,5-dibromothiophene-3-carboxylic acid (3.0 g, 10.5 mmol), DMAP (0.130 g, 1.06 mmol) and heptan-2-ol (1.644 ml, 11.6 mmol) in DCM (10 ml) was cooled to 0 °C on an ice bath. DCC (2.38 g, 11.5 mmol) was hereafter added in small portions over 5 minutes, left stirring while cooling for an additional 10 minutes and then left stirring at RT for an additional 2½ hours. The mixture was filtrated and the solid was washed thoroughly with DCM. The filtrate was then washed with aqueous HCl (0.5 M, 2 x 25 ml), NaHCO<sub>3</sub> (2 x 25 ml) and brine (25 ml) followed by drying over MgSO<sub>4</sub>. Evaporation of the solvent yielded a crude (4.77 g) which upon gradient column chromatography (heptane/AcOEt, 1% steps) yielded the desired compound a clear colorless oil (3.9 g, 94 %).

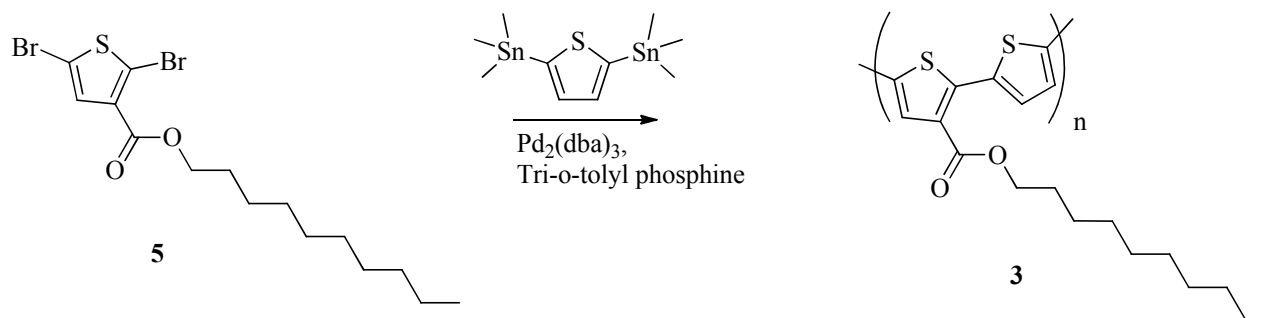
<sup>1</sup>H NMR (500 MHz, CDCl<sub>3</sub>) δ 7.33 (s, 1H), 5.09 (hex, *J* = 6.4 Hz, 1H), 1.78 – 1.55 (m, 2H), 1.43 – 1.26 (m, 9H), 0.89 (t, *J* = 6.9 Hz, 3H). <sup>13</sup>C NMR (126 MHz, CDCl<sub>3</sub>) δ 160.64, 132.52, 131.91, 118.91, 111.35, 72.70, 36.04, 31.78, 25.21, 22.68, 20.15, 14.15.



**Polymer 2:** Monomer **4** (504 mg, 1.31 mmol), 2,5-bis(trimethylstannyl)thiophene (538 mg, 1.31 mmol), tri-*o*-tolyl phosphine (160 mg, 0.525 mmol), Pd<sub>2</sub>(dba)<sub>3</sub> (60.1 mg, 0.066 mmol) was mixed in degassed toluene (20 ml) under argon. The temperature was raised to 110 °C and the mixture was left while stirring for 20 hours. The polymer was precipitated by addition of the reaction mixture to methanol, and the solid was purified by soxhlet extraction with methanol for 24 hours, followed by soxhlet with hexane for 6 hours. The polymer was extracted with chloroform at re-precipitated from toluene in methanol after removal of the chloroform. Mw 32269, Mn 11179, PDI 2.9



**Decyl 2,5-dibromothiophene-3-carboxylate (5):** 2,5-dibromothiophene-3-carboxylic acid (2.0 g, 6.99 mmol), DMAP (0.085 g, 0.70 mmol) and decan-1-ol (2.482 ml, 14.0 mmol) mixed in DCM (7 ml) under argon was cooled on an ice bath. DCC (1.587 g, 7.69 mmol) was added and the mixture was allowed to stir for 10 min after which the ice bath was removed and stirring was continued for an additional 2 hours at RT. The solid in the mixture was filtered off and washed thoroughly with DCM. After removing the solvent the crude was purified by gradient column chromatography (heptane/AcOEt, 2% steps) yielding the pure product (2.87 g, 96 %). <sup>1</sup>H NMR (500 MHz, CDCl<sub>3</sub>) δ 7.34 (s, 1H), 4.27 (t, *J* = 6.7 Hz, 2H), 1.79 – 1.64 (m, 2H), 1.48 – 1.14 (m, 16H), 0.88 (t, *J* = 7.0 Hz, 3H). <sup>13</sup>C NMR (126 MHz, CDCl<sub>3</sub>) δ 161.06, 132.23, 131.91, 119.08, 111.45, 65.63, 32.04, 29.67, 29.64, 29.44, 29.36, 28.72, 26.15, 22.82, 14.25.



**Polymer 3:** Monomer 5 (0.502 g, 1.18 mmol), 2,5-bis(trimethylstannyl)thiophene (0.482 g, 1.18 mmol), tri-*o*-tolyl phosphine (0.148g, 0.486 mmol) and Pd<sub>2</sub>(dba)<sub>3</sub> (0.055 g, 0.060 mmol) were mixed in dry degassed toluene (20 ml) and the temperature was raised to 110 °C. The mixture was left stirring for 18 hours after which the mixture was precipitated by addition into methanol. The solid was purified by soxhlet extraction with methanol (1 day) and hexane (1 day) followed by extraction of the polymer with chloroform. After removing the solvent the polymer was re-dissolved in toluene and precipitated in methanol. Mw 16974, Mn 6911, PDI 2.4

**TGA-MS:**

General procedure: Stock solutions containing the respective polymers (40 mg/ml, chloroform) and the respective acids (1 mol%, 2 mol%, 5 mol% and 10 mol% in chloroform (for PFBSA chloroform/methanol 200:1) – the concentrations were calculated from the theoretical abundance of ester groups in the polymers) were mixed in a TGA platinum pan (100  $\mu$ L), and the solvent was allowed to evaporate in air. The TGA experiment was then started at 50 °C with a subsequent increase of 10 °C/min during the experiment. MS-data for selected masses were simultaneously collected allowing for monitoring of the thermocleavage reaction.

## 5.6 References

1. Bjerring, M.; Nielsen, J. S.; Nielsen, N. C.; Krebs, F. C. Polythiophene by solution processing. *Macromolecules* **2007**, *40* (16), 6012-6013.
2. Bjerring, M.; Nielsen, J. S.; Siu, A.; Nielsen, N. C.; Krebs, F. C. An explanation for the high stability of polycarboxythiophenes in photovoltaic devices- A solid-state NMR dipolar recoupling study. *Sol. Energy Mater. Sol. Cells* **2008**, *92* (7), 772-784.
3. Edder, C.; Armstrong, P. B.; Prado, K. B.; Frechet, J. M. J. Benzothiadiazole- and pyrrole-based polymers bearing thermally cleavable solubilizing groups as precursors for low bandgap polymers. *Chem. Comm.* **2006**, (18), 1965-1967.
4. Gevorgyan, S. A.; Krebs, F. C. Bulk heterojunctions based on native polythiophene. *Chem. Mater.* **2008**, *20* (13), 4386-4390.
5. Hagemann, O.; Bjerring, M.; Nielsen, N. C.; Krebs, F. C. All solution processed tandem polymer solar cells based on thermocleavable materials. *Sol. Energy Mater. Sol. Cells* **2008**, *92* (11), 1327-1335.
6. Helgesen, M.; Gevorgyan, S. A.; Krebs, F. C.; Janssen, R. A. J. Substituted 2,1,3-Benzothiadiazole- And Thiophene-Based Polymers for Solar Cells - Introducing a New Thermocleavable Precursor. *Chem. Mater.* **2009**, *21* (19), 4669-4675.
7. Krebs, F. C.; Spanggaard, H. Significant improvement of polymer solar cell stability. *Chem. Mater.* **2005**, *17* (21), 5235-5237.
8. Liu, J. S.; Kadnikova, E. N.; Liu, Y. X.; McGehee, M. D.; Frechet, J. M. J. Polythiophene containing thermally removable solubilizing groups enhances the interface and the performance of polymer-titania hybrid solar cells. *J. Am. Chem. Soc.* **2004**, *126* (31), 9486-9487.
9. Manceau, M.; Helgesen, M.; Krebs, F. C. Thermo-cleavable polymers: Materials with enhanced photochemical stability. *Polymer Degradation and Stability* **2010**, *95* (12), 2666-2669.
10. Petersen, M. H.; Gevorgyan, S. A.; Krebs, F. C. Thermocleavable Low Band Gap Polymers and Solar Cells Therefrom with Remarkable Stability toward Oxygen. *Macromolecules* **2008**, *41* (23), 8986-8994.
11. Zemtsova, M. N.; Lipkin, A. E.; Zimichev, A. V. Nitration of 2-(2-quinolyl)thiophene and 5-(2-quinolyl)-2,2'-dithiophene. *Chemistry of Heterocyclic Compounds* **1974**, *10* (10), 1153-1155.
12. Goossen, L. J.; Linder, C.; Rodriguez, N.; Lange, P. P.; Fromm, A. Silver-catalysed protodecarboxylation of carboxylic acids. *Chem. Comm.* **2009**, (46), 7173-7175.
13. Lancaster, R. E.; Vanderwerf, C. A. An Improved Synthesis of 3-Methylpyrrole. *J. Org. Chem.* **1958**, *23* (8), 1208-1209.
14. Dunn, G. E.; Lee, G. K. J. Kinetics and Mechanism of Decarboxylation of Pyrrole-2-Carboxylic Acid in Aqueous Solution. *Canadian Journal of Chemistry* **1971**, *49* (7), 1032-1035.

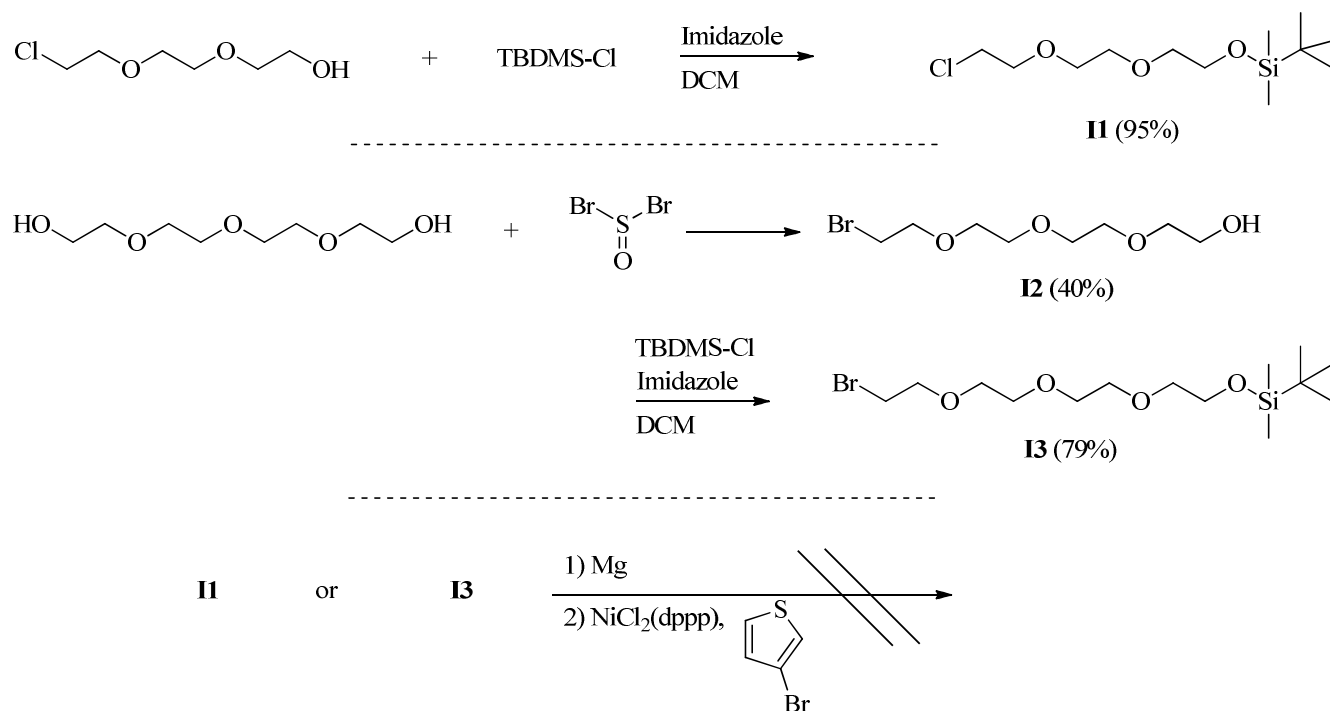
## Appendix 1

### Non successful synthesis

Below is a series of syntheses, involving the use of potential polar side chains, which after one or more successful synthetic steps did not lead to the desired products, or where the products proved to be useless.

#### Attempts to prepare alkyl substituted thiophene monomers with polar side chains

As an attempt to prepare alkyl substituted thiophene monomers with water coordinating abilities compound **I1** was prepared by TBDMS protection of commercial 2-(2-(2-chloroethoxy)ethoxy)ethanol. Unfortunately subsequent attempts to perform Kumada coupling with 3-bromothiophene all failed. As it was envisaged that the problem originated in problems of producing the Grignard compound from the chloride, it was instead decided to prepare a similar bromocompound by first brominating tetraethylene glycol with thionylbromide to give **I2** followed by TBDMS protection to **I3**, but also the reaction of **I3** with 3-bromothiophene failed. The reaction was then abandoned.

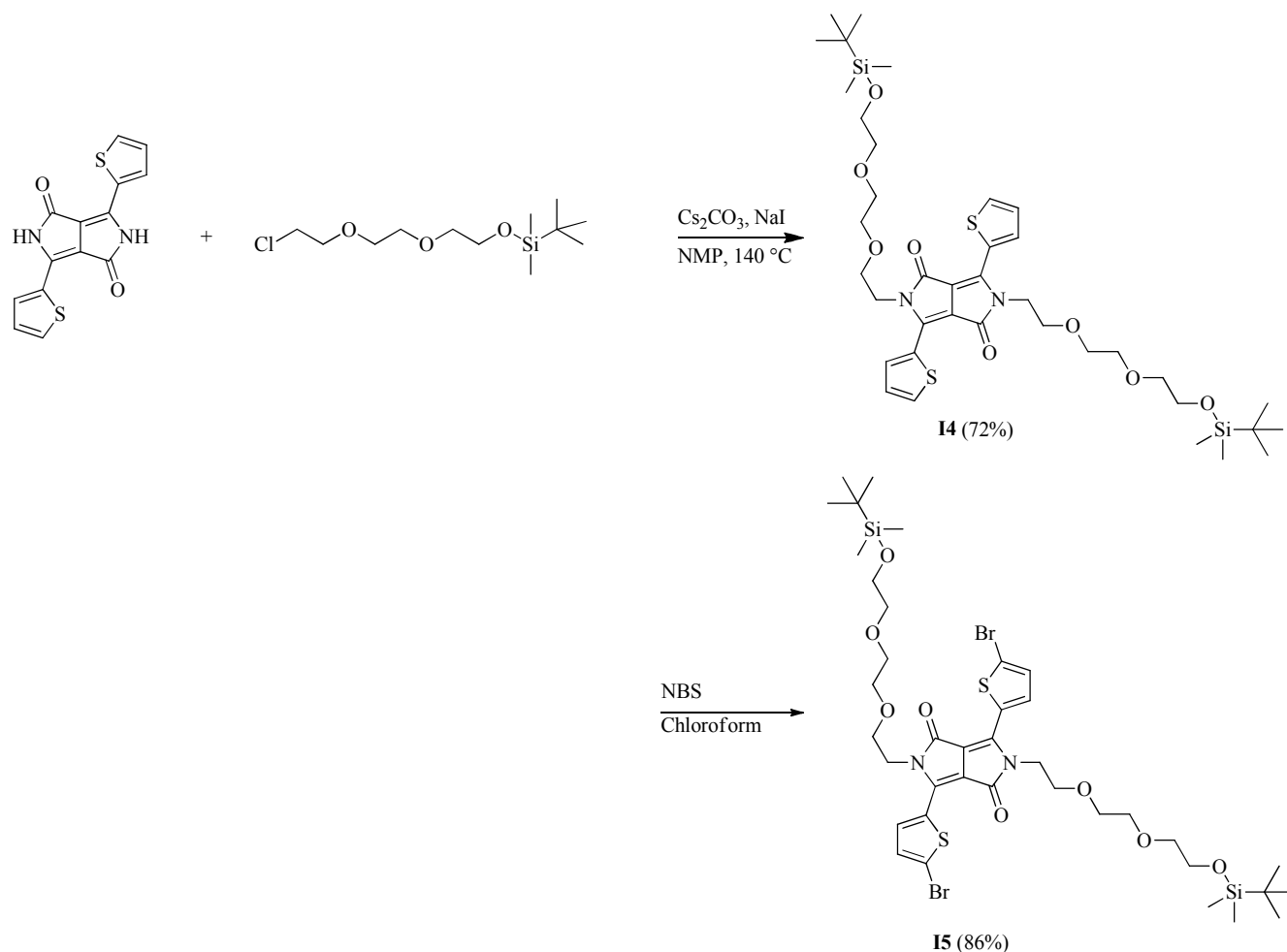


Scheme I1.1



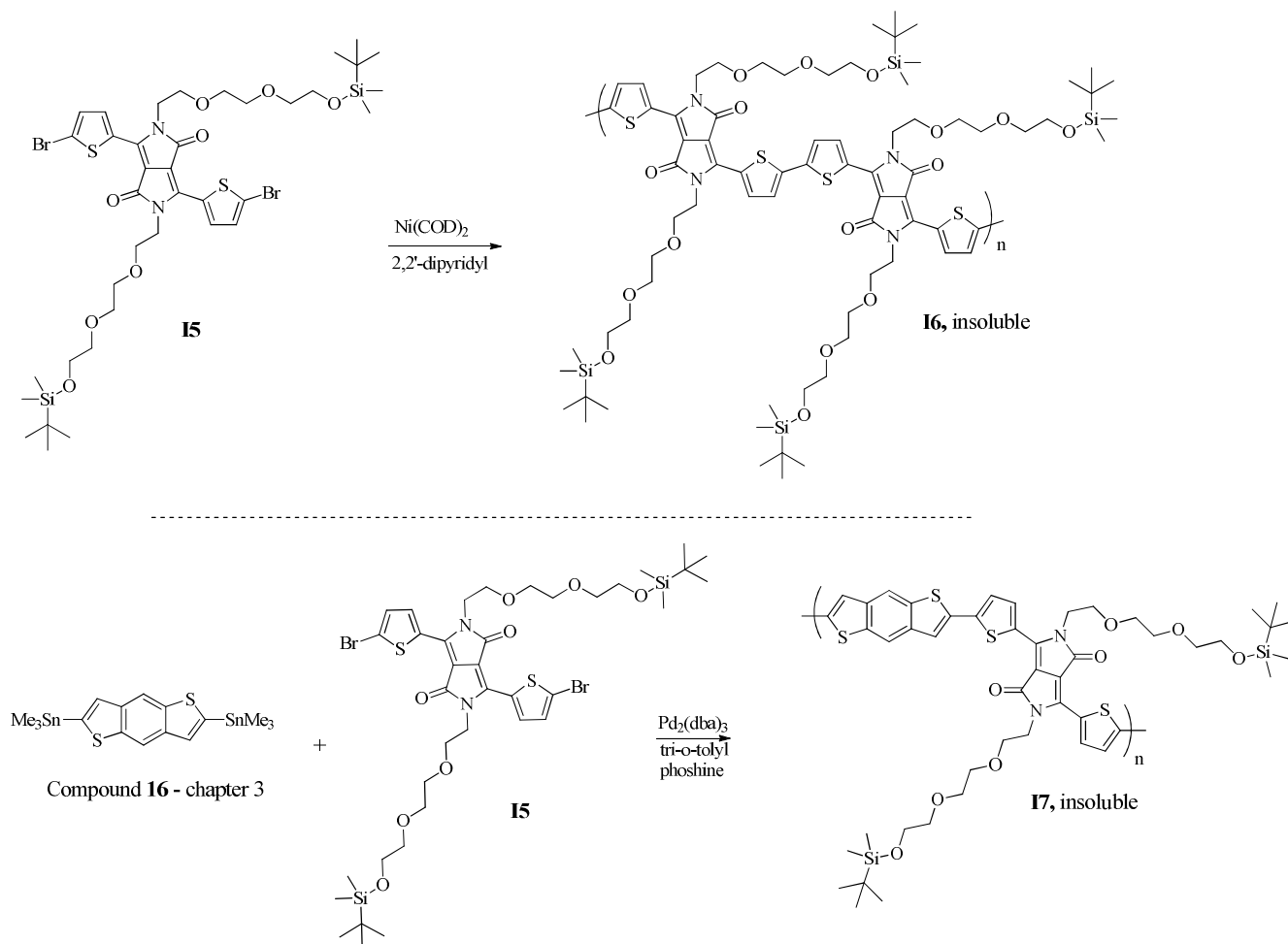
**Polymerizations involving a DPP-monomer containing potential polar side chains:**

In order to examine if the type of potential polar side chains described in chapter 2 could also be used in LBG polymers, an analogue (**15**) to the diketopyrrolopyrrole-monomer described in chapter 3 (**DTDPP**) in was prepared by initial reaction of 3,6-di(thiophen-2-yl)pyrrolo[3,4-c]pyrrole-1,4(2*H*,5*H*)-dione with compound **11** in NMP using CsCO<sub>3</sub> as base (See Scheme I1.2). The reaction proceeds in very high yield compared to the analogue preparation of compound **24** in chapter 3. Subsequent NBS bromination also proceeded in good yield.



Scheme I1.2

Unfortunately all subsequent polymerization reactions using this monomer using Yamamoto and Stille couplings led to insoluble polymers as indicated in scheme I1.3.



Scheme I1.3

## Experimental:

**12-chloro-2,2,3,3-tetramethyl-4,7,10-trioxa-3-siladodecane (11):** Commercial 2-(2-(2-chloroethoxy)ethoxy)ethanol (14.11 g, 80 mmol) in DCM (30 ml) was cooled on an ice bath 1*H*-imidazole (5.53 g, 80 mmol) was added and the solution was stirred for 10 min. TBDMS-Cl (12.5 g, 80 mmol) was then added and the solution was stirred at 0 °C for 1½ hour followed by 24 hours at RT. A little heptane was added to promote precipitation of salts and the solution was filtered and the precipitate washed thoroughly with DCM. Evaporation of the solvent gave a crude (25.2 g) which upon gradient column

chromatography (heptane/AcOEt, 2% step until 20%, then 20%) yielded the pure product (21.6 g 95%).  $^1\text{H}$  NMR (500 MHz,  $\text{CDCl}_3$ )  $\delta$  3.79 – 3.74 (m, 4H), 3.67 (s, 4H), 3.63 (t,  $J$  = 6.0 Hz, 1H), 3.57 (t,  $J$  = 5.4 Hz, 2H), 0.89 (s, 9H), 0.07 (s, 6H).  $^{13}\text{C}$  NMR (126 MHz,  $\text{CDCl}_3$ )  $\delta$  72.90, 71.54, 70.90, 62.89, 42.84, 26.08, 18.52, -5.12.

**2-(2-(2-(2-bromoethoxy)ethoxy)ethoxy)ethanol (I2):** To a stirred solution of tetraethylene glycol (25 g, 129 mmol) in anhydrous DCM (1000 ml) at 0 °C, thionyl bromide (5 ml, 64.7 mmol) was added drop wise. The solution was allowed to reach RT and was left overnight. Water was then added, followed by saturated  $\text{NaCO}_3$  until effervescence ceased. The phases were partitioned, and the aqueous phase extracted with DCM (2\* 300 ml). The combined organic extracts were washed with water (2\*300 ml) and brine (200 ml) and dried over  $\text{MgSO}_4$ . Evaporation of the solvents yielded a crude (8.05 g) which upon purification by gradient column chromatography (heptane/DCM 25% steps followed by DCM/THF 2.5% steps) yielded the pure product (6.58 g, 40%).  $^1\text{H}$  NMR (500 MHz,  $\text{CDCl}_3$ )  $\delta$  3.81 (t,  $J$  = 6.3 Hz, 2H), 3.77 – 3.70 (m, 2H), 3.71 – 3.65 (m, 8H), 3.64 – 3.59 (m, 2H), 3.48 (t,  $J$  = 6.3 Hz, 2H).  $^{13}\text{C}$  NMR (126 MHz,  $\text{CDCl}_3$ )  $\delta$  72.61, 71.38, 70.85, 70.71, 70.67, 70.53, 61.94, 30.38.

**15-bromo-2,2,3,3-tetramethyl-4,7,10,13-tetraoxa-3-silapentadecane (I3):**

Compound **I2** (4.28 g, 16.65 mmol) and TBDMS-Cl (2.38 g, 15.79 mmol) in DCM (12 ml) was cooled on an ice bath and imidazole (1.09 g, 16.1 mmol) was added. The solution was stirred at 0 °C for 2h and 20 min after which a little heptane was added and the solution filtered. The filtrate was washed thoroughly with DCM/hep, after which the solvents were evaporated and the crude (6.32 g) was purified by gradient column chromatography (heptane/AcOEt 1% steps until 16%, then 2% steps) to give the desired product (4.91 g, 79 %).  $^1\text{H}$  NMR (500 MHz,  $\text{CDCl}_3$ )  $\delta$  3.81 (t,  $J$  = 6.4 Hz, 2H), 3.76 (t,  $J$  = 5.4 Hz, 2H), 3.72 – 3.61 (m, 8H), 3.56 (t,  $J$  = 5.4 Hz, 2H), 3.47 (t,  $J$  = 6.4 Hz, 2H), 0.91 – 0.84 (m, 9H), 0.10 – 0.01 (m, 6H).  $^{13}\text{C}$  NMR (126 MHz,  $\text{CDCl}_3$ )  $\delta$  72.83, 71.37, 70.89, 70.77, 70.72, 62.86, 30.40, 26.07, 18.51, -5.12.

**2,5-bis(2,2,3,3-tetramethyl-4,7,10-trioxa-3-siladodecan-12-yl)-3,6-di(thiophen-2-yl)pyrrolo[3,4-c]pyrrole-1,4(2H,5H)-dione (I4):** 3,6-di(thiophen-2-yl)pyrrolo[3,4-c]pyrrole-1,4(2H,5H)-dione (2,28 g, 7.58 mmol), compound **I1** (6.00 g, 21.2 mmol), sodium iodide (3.41 g, 22.7 mmol) and cesium carbonate (7.40 g, 22.7 mmol) in N-Methyl-2-pyrrolidinone (30 ml) was heated to 140 °C for 3 hours. Water (200 ml) was added and the mixture extracted with ether. The organic phases were washed extensively with water to remove NMP followed by wash with,  $\text{NaHCO}_3$  and brine. After drying over  $\text{MgSO}_4$  the solvent was removed and the resulting crude (6.83 g) was purified twice by gradient column chromatography (1: heptane/AcOEt, 5% steps, 2: heptane/AcOEt, 4 %) to yield the pure product (4.30 g, 72%).  $^1\text{H}$  NMR (500 MHz,  $\text{CDCl}_3$ )  $\delta$  8.75 (dd,  $J$  = 3.9, 1.1, 2H), 7.63 (dd,  $J$  = 5.0, 1.1, 2H), 7.27 - 7.24 (m, 2H), 4.27 (t,  $J$  = 6.4, 4H), 3.79 (t,  $J$  = 6.4, 4H), 3.72 (t,  $J$  = 5.4, 4H), 3.65 - 3.57 (m, 9H), 3.50 (t,  $J$  = 5.4, 4H), 0.87 (s, 18H), 0.04 (s, 12H).  $^{13}\text{C}$  NMR (126 MHz,  $\text{CDCl}_3$ )  $\delta$  161.69, 140.56, 134.88, 130.95, 129.84, 128.59, 108.06, 72.87, 70.91, 70.80, 69.10, 62.87, 42.01, 26.09, 18.51, -5.10.

**3,6-bis(5-bromothiophen-2-yl)-2,5-bis(2,2,3,3-tetramethyl-4,7,10-trioxa-3-siladodecan-12-yl)pyrrolo[3,4-c]pyrrole-1,4(2H,5H)-dione (I5):**

To an ice cooled solution of **I4** (2.15 g, 2.70 mmol) in chloroform (50 ml) was added NBS (1.07 g, 6.01 mmol) was added in small portions over 5 hours while monitoring the reaction by TLC. Saturated  $\text{NaHCO}_3$  (50 ml) was added, and the organic phase was washed with water (2 x 50 ml) and brine. After drying over  $\text{MgSO}_4$  the solvent was evaporated and the crude (2.74 g) was purified by gradient column chromatography (1: hep/AcOEt, 4% fractions, 2: [DCM/heptane 1:4]:AcOEt, 2% steps). To give the desired compound (2.21 g, 86%).  $^1\text{H}$  NMR (500 MHz,  $\text{CDCl}_3$ )  $\delta$  8.49 (d,  $J$  = 4.2, 2H), 7.20 (d,  $J$  = 4.2, 2H), 4.17 (t,  $J$  = 6.0, 4H), 3.78 (t,  $J$  = 6.0, 4H), 3.72 (t,  $J$  = 5.4, 4H), 3.64 - 3.57 (m, 8H), 3.50 (t,  $J$  = 5.4, 4H), 0.88 (s, 18H), 0.04

(s, 12H).  $^{13}\text{C}$  NMR (126 MHz,  $\text{CDCl}_3$ )  $\delta$  161.45, 139.65, 134.97, 131.54, 131.28, 119.51, 108.16, 72.90, 70.99, 70.80, 69.12, 62.89, 42.40, 26.09, 18.51, -5.09.

**Polymer I6:**

$\text{Ni}(\text{COD})_2$  (192 mg, 0.698 mmol) and 2,2'-bipyridyl (109 mg, 0.698 mmol) was mixed in dry degassed toluene (30 ml). The mixture was heated to 80 °C followed by addition of **I5** (221 mg, 0.233 mmol). The mixture was left while stirring for 48 hours. Subsequent attempt to dissolve the polymer after purification by soxhlet extraction failed.

**Polymer I7**

Compound **16** (chapter 3) (80 mg, 0.156 mmol), compound **I5** (141.1 mg, 0.148 mmol),  $\text{Pd}_2(\text{dba})_3$  (10 mg, 11  $\mu\text{mol}$ ) and tri-*o*-tolyl phosphine (27 mg, 0.089 mmol) was mixed in dry degassed toluene (12 ml). The temperature was raised to 110 °C and the mixture left while stirring for two days. It proved impossible to dissolve the polymer after purification by soxhlet extraction.

## Appendix 2

### Publication list:

#### Published articles:

##### A2.1:

Helgesen, M.; Søndergaard, R.; Krebs, F. C. Advanced materials and processes for polymer solar cell devices. *J. Mater. Chem.* **2010**, *20* (1), 36-60.

##### A2.2:

Søndergaard, R.; Helgesen, M.; Jørgensen, M.; Krebs, F. C. Fabrication of Polymer Solar Cells Using Aqueous Processing for All Layers Including the Metal Back Electrode. *Adv. Energy Mater.* **2011**, *1* (1), 68-71.

##### A2.3

Krebs, F. C.; Søndergaard, R.; Jørgensen, M. Printed metal back electrodes for R2R fabricated polymer solar cells studied using the LBIC technique. *Sol. Energy Mater. Sol. Cells* **2011**, *95* (5), 1348-1353.

##### A2.4

Manceau, M.; Bundgaard, E.; Carle, J. E.; Hagemann, O.; Helgesen, M.; Søndergaard, R.; Jørgensen, M.; Krebs, F. C. Photochemical stability of  $\pi$ -conjugated polymers for polymer solar cells: a rule of thumb. *J. Mater. Chem.* **2011**, *21* (12), 4132-4141.

##### A2.5

Carlé, J. E.; Jørgensen, M.; Manceau, M.; Helgesen, M.; Hagemann, O.; Søndergaard, R.; Krebs F.C. *Sol. Energy Mater. & Sol. Cells* **2011**, *95* (12), 3222-3226

##### A2.6

Søndergaard, R.; Krebs, F. C. The Challenge of Synthesizing Oligomers for Molecular Wires. *Polymers* **2011**, *3* (1), 545-557.

##### A2.7

Søndergaard, R.; Strobel, S.; Bundgaard, E.; Norrman, K.; Hansen, A. G.; Albert, E.; Csaba, G.; Lugli, P.; Tornow, M.; Krebs, F. C. Conjugated 12 nm long oligomers as molecular wires in nanoelectronics. *J. Mater. Chem.* **2009**, *19* (23), 3899-3908.

(The experimental work of this publication was performed before the start of this thesis, but the writing of the article has been performed during the three year period as a PhD student)

**A2.8**

Søndergaard, R.; Manceau, M.; Jørgensen, M.; Krebs, F. C. New Low-Band-Gap Materials with Good Stabilities and Efficiencies Comparable with P3HT in R2R Coated Solar Cells. *Adv. Energy Mater.* **2012**, *2* (4), 415-418.

**A2.9**

Søndergaard, R.; Makris, T.; Lianos, P.; Manor, A.; Katz, E. A.; Gong, W.; Tuladhar, S. M.; Nelson, J.; Sommerling, P.; Veenstra, S. C.; Rivaton, A.; Dupuis, A.; Teran-Escobar, G.; Lira-Cantu, M.; Sabkota, S. B.; Zimmermann, B.; Würfel, U.; Krebs, F. C. The use of Polyurethane as Encapsulating Method for Polymer Solar Cells – an Inter Laboratory Study on Outdoor Stability in 8 Countries. *Sol. Energy Mater. Sol. Cells* **2012**, *99*,292-300.

**A2.10**

Søndergaard, R.; Norrman, K.; Krebs, F.C. Low temperature side chain cleavage and decarboxylation of polythiophene esters by acid catalysis. *J. Polym. Sci. A Polym. Chem.* 2012, *50* (6), 1127-1132.

**Book Chapters:**

**A2.11**

“Polymer Solar Cells: Materials, Design, Processing”

Gevorgyan, S. A.; Søndergaard, R.; Krebs, F. C.; Introduction, DEStech Publications, Inc 2010; pp 1-12

**A2.12**

“Polymer Solar Cells: Materials, Design, Processing”

Søndergaard, R.; Gevorgyan, S. A.; Krebs, F. C. Materials and processing. DEStech Publications, Inc.: 2010; pp 13-66.

**Patents**

Three patents has furthermore been filed during the thesis, but as they are still in the filing process they cannot be enclosed as appendix. The three patents all have four inventors Frederik C. Krebs, Roar Søndergaard, Kion Norrman and Mikkel Jørgensen with equal share in the inventions.

UK Patent Application No. 1016470.5 "Method of Making Optoelectric Devices"

UK Patent Application No. 1016472.1 "Electron Transport Layer"

UK Patent Application No. 1016568.9 "Improved ZnO Adhesion"

# Advanced materials and processes for polymer solar cell devices

Martin Helgesen, Roar Søndergaard and Frederik C. Krebs\*

Received 3rd July 2009, Accepted 22nd August 2009

First published as an Advance Article on the web 14th October 2009

DOI: 10.1039/b913168j

The rapidly expanding field of polymer and organic solar cells is reviewed in the context of materials, processes and devices that significantly deviate from the standard approach which involves rigid glass substrates, indium-tin-oxide electrodes, spincoated layers of conjugated polymer/fullerene mixtures and evaporated metal electrodes in a flat multilayer geometry. It is likely that significant advances can be found by pursuing many of these novel ideas further and the purpose of this review is to highlight these reports and hopefully spark new interest in materials and methods that may be performing less than the current state-of-the-art in their present form but that may have the potential to outperform these pending a larger investment in effort.

## Introduction

Encouraging progress has been made over the last few years in the field of photovoltaics using organic materials. Conventional solar cells are built from inorganic materials such as silicon. While the efficiency of such conventional solar cells is high, very expensive materials and energy consuming processing techniques are required. The main reason for the extensive interest in organic semiconducting materials is their potential for the realization of a low cost, easily processed and flexible renewable energy source. Conjugated polymers are an especially attractive alternative to the traditional silicon photovoltaics because they are strong absorbers of visible light and can be deposited onto flexible substrates over large areas using wet-processing techniques such as roll-to-roll coating or printing. Many reviews,<sup>1–26</sup> special issues,<sup>27–33</sup> and books<sup>34–38</sup> on the topic of polymer solar cells have been published during the past 5 years and the definitions are quite broad spanning all polymer solar cells,

polymer–fullerene solar cells, small molecule and hybrid solar cells. Polymer–fullerene solar cells based on composites of an electron-donating conjugated polymer and an electron-accepting fullerene has proven to be the most successful of them so far and is advancing rapidly towards commercial viability. Although the performance of polymer solar cells has increased steadily with power conversion efficiencies (PCEs) exceeding 6%, further improvements in efficiency are required for large scale commercialization. Aside from the power conversion efficiency, processing and stability are two other important aspects that have to be addressed with equal intensity for the success of polymer and organic solar cells. To combine all three parameters into a useful technology further research in device science and new materials is needed.

## Aim of this review

We seek to identify novel ideas in the form of materials, methods and device concepts that can potentially house the possibility to go beyond the current state-of-the-art. Armed with the identity of the potential candidates we further suggest how research might be directed towards real progress in terms of better

*Risø National Laboratory for Sustainable Energy, Technical University of Denmark, Frederiksborgvej 399, DK-4000 Roskilde, Denmark. E-mail: frkr@risoe.dtu.dk*



Martin Helgesen

*Martin Helgesen received his Master of Science in Chemistry from The University of Copenhagen in 2006. The same year he began his PhD under the mentorship of Frederik Christian Krebs at Risø National Laboratory for Sustainable Energy, Technical University of Denmark. His research interests are in developing thermocleavable low band gap polymers and their thin films for organic photovoltaics.*



Roar Søndergaard

*Roar Søndergaard received his M.Sc. in 2005 from the Department of Chemistry at the University of Copenhagen. After working as a research assistant first at The University of Copenhagen and later at Risø DTU National Laboratory for Sustainable Energy he is currently pursuing his PhD at Risø DTU. His research interests include synthesis of conjugated polymers and synthesis of polymers that allow for different processing methods when preparing organic photovoltaics.*

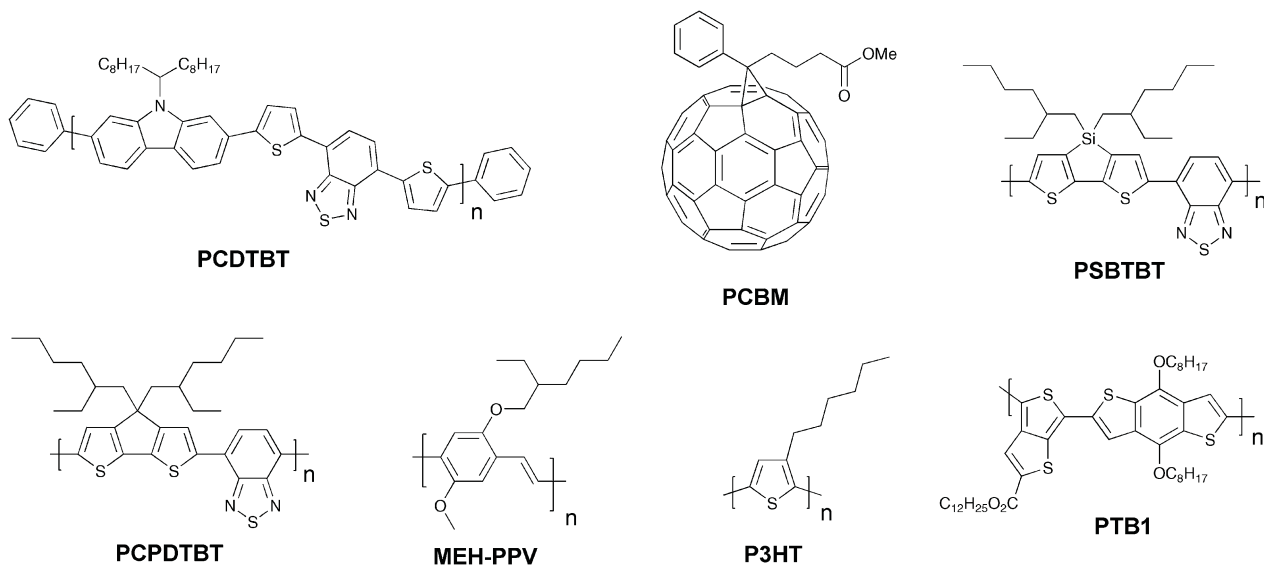


Fig. 1 Donor and acceptor materials used in polymer solar cells.

performance, higher operational stability, facile processing and easier, faster and lower cost production.

## Materials

### State-of-the-art

Since the first report of photoinduced charge transfer from a conjugated polymer to a buckminsterfullerene (C<sub>60</sub>) in 1992 by Sariciftci *et al.*,<sup>39</sup> the field of polymer–fullerene solar cells has been through a dynamic development. In 1995 Yu *et al.* demonstrated a successful method to dissociate excitons and produce free charge carriers in organic semiconductors.<sup>40</sup> For the photoactive layer the authors used a blend of 2-methoxy-5-(2-ethylhexyloxy)-polyphenylenevinylene (MEH-PPV) as the electron donor and the soluble fullerene derivative [6,6]-phenyl C<sub>61</sub> butyric acid methyl ester (PCBM) as the electron acceptor (Fig. 1).

The solar cell based on a MEH-PPV:PCBM composite or a so called bulk heterojunction (BHJ) showed an estimated efficiency of nearly 1% which was a major breakthrough for organic

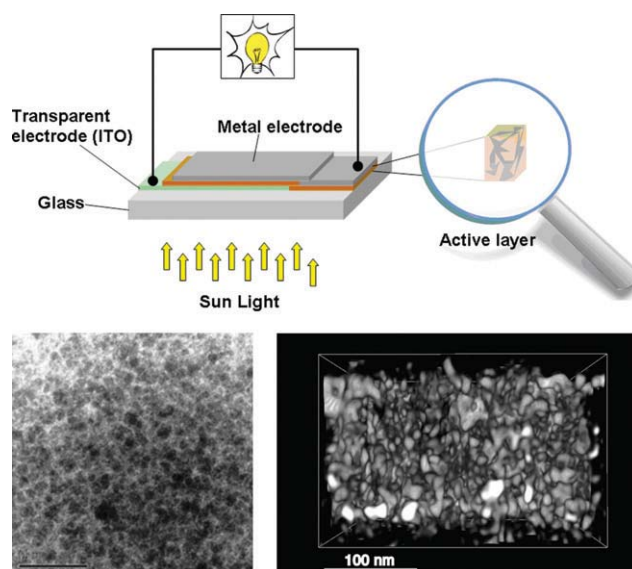


Fig. 2 A schematic illustration of a bulk heterojunction device showing electrical contacts (**top**) and a TEM image of a phase separated blend (**bottom left**). Reprinted with permission from ref. 44. © 2007 John Wiley & Sons, Ltd.) and a reconstructed tomographic 3D-image (**bottom right**). Reprinted with permission from ref. 45. © 2009 American Chemical Society).



Frederik C. Krebs

*Frederik Christian Krebs received his PhD from the Technical University of Denmark in year 2000 and has since then worked in the field of polymer solar cells at Risø National Laboratory for Sustainable Energy. The areas of research include new materials with low band gap and novel processing capability, large area processing and manufacture of polymer solar cells, stability and lifetime testing, degradation mechanism studies, outside testing and demonstration.*

photovoltaics. When organic semiconductors absorb sunlight they mainly create excitons (electron–hole pairs) that are bound at room temperature. The exciton has to reach the donor–acceptor interface within its lifetime to transfer a free electron to the acceptor material and create a photovoltaic effect. Since the exciton diffusion range is limited, typically ~3–10 nm in most organic semiconductors,<sup>41–43</sup> which is much smaller than the necessary film thickness for effective optical absorption (50–250 nm), the key to an efficient solar cell requires that the excitons are generated in a nanoscale interpenetrating bicontinuous network of donor and acceptor materials within the entire



photoactive layer. A schematic illustration of a bulk heterojunction is shown in Fig. 2.

From a materials point of view the state-of-the-art in the field of organic photovoltaics is currently represented by bulk heterojunction solar cells based on poly(3-hexylthiophene) (P3HT) and the fullerenes [60]PCBM (Fig. 1) and [70]PCBM where efficiencies in the 4–5% range have been reported.<sup>46–50</sup> It should be noted that the reproducibility and average efficiencies are significantly lower than these “hero” devices which is caused by the sensitivity to the fabrication process. In addition the field has seen some inconsistent reports of unrealistically high efficiencies<sup>51–54</sup> and this has led to the introduction of editorial procedures to avoid and/or eliminate fraud reports.<sup>54</sup> To improve efficiencies further towards 10% new materials are needed because the P3HT:PCBM system is approaching optimal device performance. The main disadvantage of P3HT is the poor matching of its absorption spectrum with the solar emission spectrum. The band gap of P3HT is around 1.9 eV, limiting the absorbance to wavelengths below 650 nm. Since the photon flux reaching the surface of the earth from the sun has a maximum of approximately 1.8 eV (700 nm) P3HT is only able to harvest up to 22.4% of the available solar photons.<sup>6,20,54</sup> Therefore, by decreasing the band gap of the active material it is possible to harvest a larger amount of the solar photons and thereby increase the power conversion efficiency. One of the most common techniques used to synthesise low band gap polymers is the donor–acceptor approach where alternating electron-rich and electron-poor units are incorporated in the polymer backbone. This causes a partial charge separation along the polymer backbone which generally gives the polymer a lower band gap.<sup>55</sup> New low band gap polymer:PCBM composites have already shown device efficiencies close to and even exceeding that of P3HT:PCBM with plenty of room for improvement.<sup>56–58</sup> One of the most efficient low band gap polymers to date is poly[2,6-(4,4-bis-(2-ethylhexyl)-4*H*-cyclopenta[2,1-*b*;3,4-*b'*]-dithiophene)-*alt*-4,7-(2,1,3-benzothiadiazole)] (PCPDTBT) (Fig. 1) which is based on a benzothiadiazole unit (acceptor) and a 4,4-bis(2-ethylhexyl)-4*H*-cyclopenta[2,1-*b*;3,4-*b'*]dithiophene unit (donor) that gives it an optical band gap around 1.46 eV. Zhu *et al.* have reported power conversion efficiencies up to 3.5% for bulk heterojunction solar cells based on PCPDTBT and [70]PCBM

with a maximum EQE of 38% around 700 nm and over 25% in the wavelength range between 400 and 800 nm.<sup>59</sup> Moreover it was demonstrated that by incorporating a few volume per cent of alkanedithiols in the solution used to process the films of PCPDTBT and [70]PCBM, the power-conversion efficiency could be increased to 5.5% through altering the bulk heterojunction morphology.<sup>58</sup> This is one of the highest reported efficiencies for a low band gap polymer to date and there is still room for improvement according to the electrooptical properties of the polymer.<sup>60–62</sup> Recently a power conversion efficiency of 6.1% was reported for a bulk heterojunction solar cell based on a blend of the polymer poly[*N*-9''-hepta-decanyl-2,7-carbazole-*alt*-5,5-(4',7'-di-2-thienyl-2',1',3'-benzothiadiazole)] (PCDTBT) and [70]PCBM.<sup>63</sup> The PCDTBT:[70]PCBM solar cells demonstrate the best performance of any single junction polymer solar cell studied to date. PCDTBT (Fig. 1) is based on a 4,7-dithienyl-benzothiadiazole unit and a soluble carbazole unit that gives it an optical band gap around 1.88 eV.

### Polymer–polymer solar cells for potentially higher performance

It is remarkable how little effort that has been put into making novel materials that deliberately solves the problems that limit the performance, stability and processing of the existing materials into devices. From this point of view the field has been highly successful and have managed to optimize the few known materials to their best level of performance by investing most of the effort into device optimisation using mainly physical techniques. It is noteworthy that the state-of-the-art solar cell has not evolved much since 1995 from a materials point of view and still comprise a polymer such as P3HT and a fullerene such as PCBM. However, it should be mentioned that significant progress has been made in developing novel materials, of both donor and fullerene acceptors, with optimal energy levels to improve the PCE.<sup>57,64–66</sup>

Photovoltaic devices based on a blend of two conjugated polymers as the photoactive layer was first reported back in the 1990s,<sup>67,68</sup> and as with polymer–fullerene solar cells, polymer–polymer solar cells are also based on a donor–acceptor pair. The first realizations of polymer–polymer solar cells were prepared from blends of MEH-PPV and poly(2,5,2',5'-tetrahexyloxy-7,8'-dicyano-di-*p*-phenylenevinylene) (CN-PPV) (Fig. 3). MEH-PPV

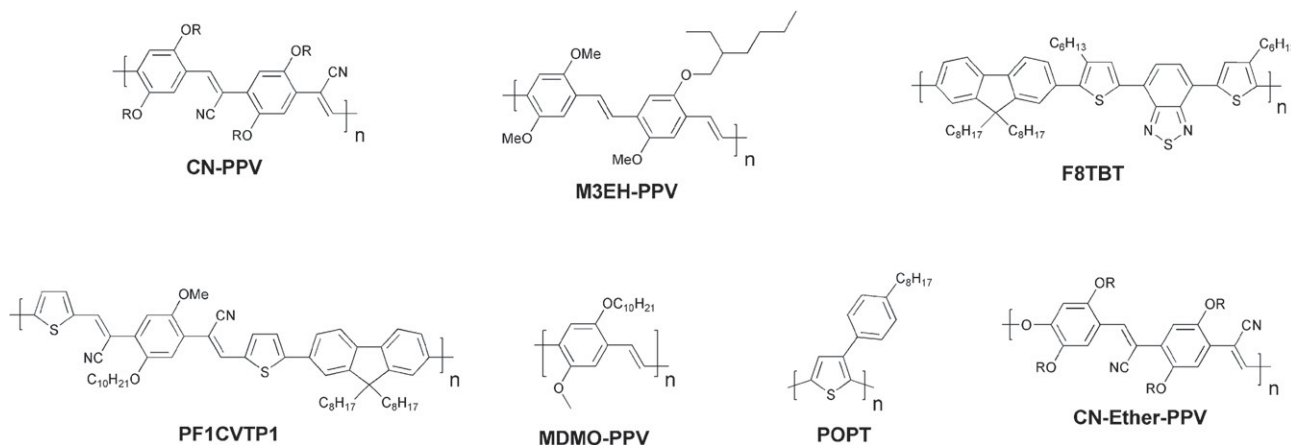


Fig. 3 Donor and acceptor materials used in polymer–polymer solar cells.

was acting as the donor and CN-PPV as the acceptor polymer. Since this initial report of polymer–polymer solar cells, they have not attracted as much attention as the polymer–fullerene solar cells. Despite their moderate performance (up to ~1.8% PCE)<sup>69</sup> photovoltaic devices based on polymer–polymer composites should potentially have several advantages to offer. While polymer:PCBM devices have shown efficiencies exceeding 6% it is predominantly the polymer that absorbs light since PCBM has a very weak overlap with the solar emission spectrum. Although [70]PCBM absorb more light and thus solves this problem to a limited degree, from a scientific point of view,<sup>70</sup> a blend of two conjugated polymers could exhibit a high optical absorption coefficient and enable absorption of solar light over a wider spectral range. Furthermore, it is relatively uncomplicated to tune the donor–acceptor energy levels when using polymers as electron acceptors because of greater flexibility in the design of the materials. Polymer–polymer solar cells have a high potential but there is a big challenge in designing conducting n-type polymers with acceptor properties up to a level that can compete with fullerenes. A problem is that polymer blends have a tendency to phase separate into domains with dimensions of several micrometres and thus is not within the exciton diffusion range. Therefore the challenge for these systems is to find a combination where the two polymers have the right morphology for efficient phase separation into an interpenetrating network that allows for efficient charge carrier generation and transport. McNeill *et al.* have reported one of the best performing polymer–polymer solar cells to date with a PCE of 1.8%.<sup>69</sup> The authors used a blend of P3HT as the donor component and poly[(9,9-dioctylfluorene)-2,7-diyl-*alt*-[4,7-bis(3-hexylthien-5-yl)-2,1,3-benzothiadiazole]-2,2-diyl] (F8TBT) as the n-type polymer (Fig. 3). The efficiency is somewhat lower than the state-of-the-art polymer–fullerene solar cell by a factor of 3–4 but higher efficiencies should be reachable if spectral overlap of the two polymers could be reduced, resulting in a wider spectral coverage. High efficiencies have also been reported for the polymer–polymer composites based on POPT:CN-PPV, MDMO-PPV:PF1CVTP1 and M3EH-PPV:CN-Ether-PPV (Fig. 3).<sup>71–73</sup>

### Thermocleavable materials for higher level processing and stability

Historically conjugated polymer materials were prepared *via* a precursor route whereby a thermal treatment was used to

remove the solubilising groups and upon their elimination the conjugated and insoluble polymer formed. The best known examples are the synthetic routes leading to native polyphenylenevinylene (PPV) and polyacetylene (PA) as exemplified by the Wessling route<sup>74–77</sup> and the Durham route<sup>78–80</sup> as shown in Fig. 4.

Initially the potential of the precursor route was not realised and it was dismissed in the middle of the 1990s<sup>77</sup> when soluble PPVs were made *via* the Wessling route. New methods appeared that avoided some of the problems of the early Wessling method that involved an ionic precursor polymer. This was then quickly replaced by the Gilch<sup>81,82</sup> and sulfinyl polymerisation types<sup>83–85</sup> which are similarly precursor routes to PPV but they do not involve ionic precursors. In addition transition metal catalyzed cross couplings entered the scene and were employed in polymerisations of prototypical materials such as P3HT using the Rieke<sup>86,87</sup> or the McCullough<sup>88</sup> route. Today, virtually all of the known transition metal catalyzed organic chemical reactions have been employed for the polymerisation of conjugated materials (Stille, Heck, Suzuki *etc.*). The development was at that point in time (1995–2005) driven by the desire to be able to engineer new materials and generate new chemical structures. The development did thus not pay attention to the needs for the polymer photovoltaic technology but only focussed on the materials development and employed a standard polymer solar cell scheme for materials evaluation (*i.e.* glass, ITO, PEDOT, evaporated metal back electrodes). Especially the transition metal catalyzed methods do sometimes introduce an often neglected problem of residual catalyst in the form of metallic nanoparticles in the polymer products. While it is easy to miss the presence of sub percent quantities of metallic nanoparticles (*e.g.* palladium) in a conjugated polymer product the consequences when applied in an electroactive device may be severe.<sup>89</sup> Methods to detect and remove the transition metal impurities have however been developed.<sup>90–92</sup> As the field of polymer solar cells have developed more focus has recently been placed on materials properties and purity. The interplay between the device film preparation methodology and the device performance became broadly known in 2005<sup>47,48</sup> and it was found that the device performance ultimately hinges on parameters such as the solvents used for film processing, the nature of the materials (molecular weight, polydispersity), the method of film formation (coating/printing technique, drying time) and treatments of the device film post formation (thermal annealing, solvent annealing). The route to a high performing device from a particular

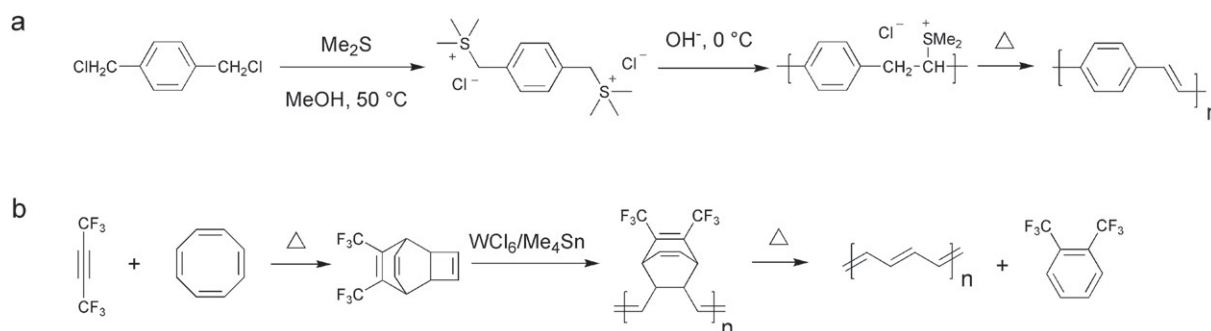


Fig. 4 The Wessling (a) and the Durham (b) route to respectively PPV and PA.

material thus follows a hair fine path where any deviation may lead to poor performance.

### Thermocleavable materials (solution-processable precursors)

One route, taking the above mentioned issues into consideration, could be exploring the many possibilities in employing a conjugated material that is either reached through a precursor route or through a route where sidechains are removed *post* film formation. One can view these materials as bringing an extra dimension into the optimisation scheme where the device film in addition to thermal annealing and solvent annealing can be altered chemically. Both precursor and thermocleavable sidechain routes follow chemical reactions whereby a part of the material that constitutes the formed film is removed (sometimes up to 50% or more of the film weight or volume). The possibilities that thermocleavable materials have to offer warrant exploitation and certainly house the potential for bringing polymer solar cells to a more advanced level through materials design. To make polymer materials solution-processable, the introduction of solubilising groups is required. This is normally achieved by attaching solubilising side chains such as alkyl groups onto the conjugated polymer backbone. However, typical nonconjugated solubilising groups reduce the density of chromophores in the polymer and do not contribute to light harvesting and charge transport. Furthermore, the side chains make the material soft and allow for both morphological changes and diffusion of small molecules and constituents.<sup>93–96</sup> The softness provided by alkyl groups is related to the instability of polymer solar cells, and more rigid systems have proven to give devices with a better stability.<sup>93</sup> From this point of view, it is of some interest to prepare polymer solar cells *via* solution processing where it is possible to remove the solubilising side chains after the active layer has been deposited.

The application of thermocleavable materials fulfils this requirement. With thermocleavable materials you exploit the

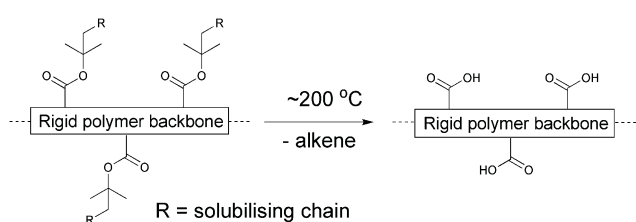


**Fig. 5** Thermocleavable ester groups attached to the polymer backbone. After a thermal treatment around 200 °C the solubilising groups are eliminated.

instability of a bond in the molecule. The labile bond functions as the linker between the solubilising group and the active material. The most recent developments are the thermocleavable ester groups and the dithiocarbamate precursor route. With regard to the thermocleavable ester groups the solubilising group is typically a branched alkyl chain attached to the active conjugated polymer backbone through an ester bond (Fig. 5). When heated this bond breaks, eliminating a volatile alkene and leaving the polymer component insoluble. The thermal treatment can be viewed as a way of performing an *in situ* chemical reaction thereby allowing for the alteration of both physical and chemical properties such as solubility, hardness, hydrogen bonding, polarity, density and ionicity after the final device film has been prepared. In terms of stability and operational lifetime polymer solar cells generally perform poorly. It was however demonstrated that heterojunction devices based on poly-3-(2-methylhexan-2-yl)-oxy-carbonylbithiophene (P3MHOCT) and C<sub>60</sub> can provide very stable behaviour after thermal elimination of the solubilising groups.<sup>93</sup> The device film is prepared with standard solution processing methods followed by a thermal treatment around 200 °C (Fig. 6) where P3MHOCT eliminates the solubilising group as 2-methylhexene.

After the thermal treatment P3MHOCT is converted to the more rigid and insoluble poly-3-carboxydithiophene (P3CT) which significantly improves the stability of the solar cell. The improved stability of this system has been linked to the rigid nature, cross-linking through a hydrogen-bonded network (Fig. 7) and a partially oxidized state.<sup>97</sup>

Furthermore, in the case of carboxylic esters attached to thiophenes, the processing offer removal of the esters at lower temperatures and the acid groups at higher temperatures allowing for multistep processing.<sup>98</sup> Thermogravimetric data for P3MHOCT in the temperature range 25–475 °C shows two distinct weight loss mechanisms. The first weight loss at ~200 °C accounts for the ester cleavage and the second weight loss at ~300 °C is decarboxylation (Fig. 8). During the annealing, it is possible to visually see the color change of the sample from red to orange (conversion from P3MHOCT to P3CT) and then from orange to purple-red (conversion from P3CT to PT) (Fig. 9a). The UV-vis absorption spectra of P3MHOCT and [60]PCBM or [70]PCBM mixtures are shown in Fig. 9b. It shows a significant change of the absorption coefficient at different temperatures. In addition a small red shift of the peaks (at 500 nm) can be seen when the samples were heated up to 310 °C.

This finding offers a route to native polythiophene (PT) by solution processing which has not been possible before. A plot of the power conversion efficiency, for P3MHOCT:PCBM devices, compared to the annealing temperature shows some interesting

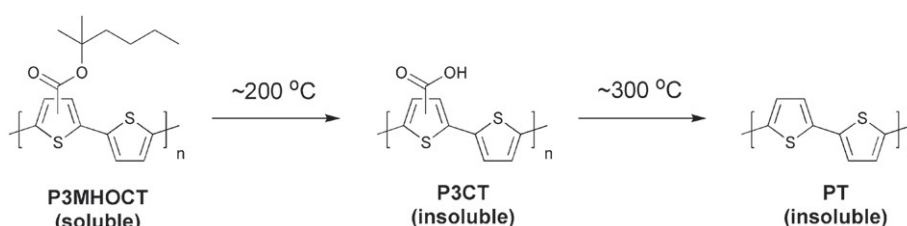


**Fig. 6** Preparation of PT *via* a thermolytic reaction.

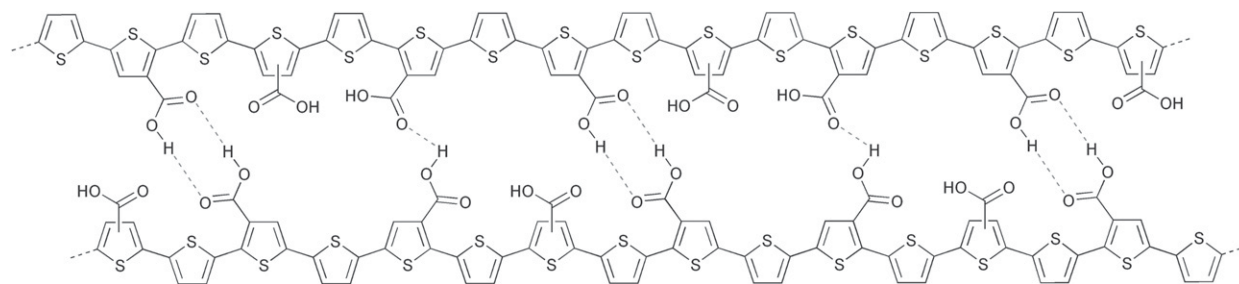


Fig. 7 Proposed cross-linked structure of P3CT through a hydrogen-bonded network.

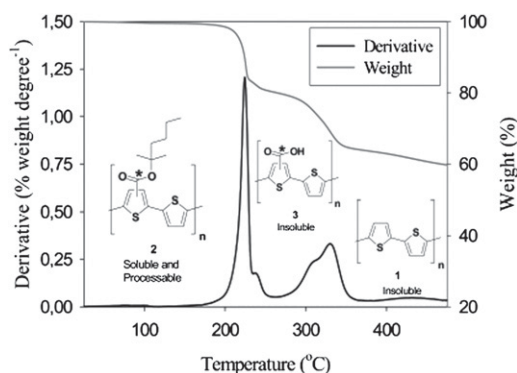


Fig. 8 Thermogravimetric data for P3MHOCT in the temperature range 25–475 °C. Reprinted with permission from ref. 98. © 2007 American Chemical Society.

results.<sup>99</sup> The power conversion efficiency of the bulk heterojunctions at room temperature was in the range 0.7–0.9% and was found to decrease as the device film was annealed at temperatures below the cleavage temperature ( $\sim 200$  °C) of P3MHOCT to P3CT. After the transformation to P3CT a broad minimum is reached with power conversion efficiencies in the range 0.1–0.4%. When reaching the temperatures of the second transformation ( $\sim 300$  °C) from P3CT to PT, a dramatic increase in power conversion efficiency was observed. Up to 0.6% in the case of [60]PCBM and as high as 1.5% in the case of [70]PCBM as shown in Fig. 9c. Clearly the morphology is changing with the chemical transformations and this is part of the explanation to the variable power conversion efficiency of this system. Another part of the explanation is the change in energy levels as the electron withdrawing carboxylic acid groups are removed from the conjugated polythiophene backbone. The use of thermocleavable conjugated polymer materials in polymer solar cells has been relatively limited due to the low performance observed when preparing devices from them. The preparation of efficient devices from native polythiophene *via* a thermocleavable route should be seen as the first breakthrough in the use of thermocleavable materials for polymer solar cells.<sup>98,99</sup> The parameter space is enormous and the added complexity of thermocleavable materials (both their synthesis and processing into devices) combined with perhaps a poor starting point have resulted in a small investment in them in terms of research effort. The fact that efficiencies approaching 2% can be reached shows that it is not impossible to prepare efficient polymer solar cell devices from thermocleavable materials and it is interesting to speculate

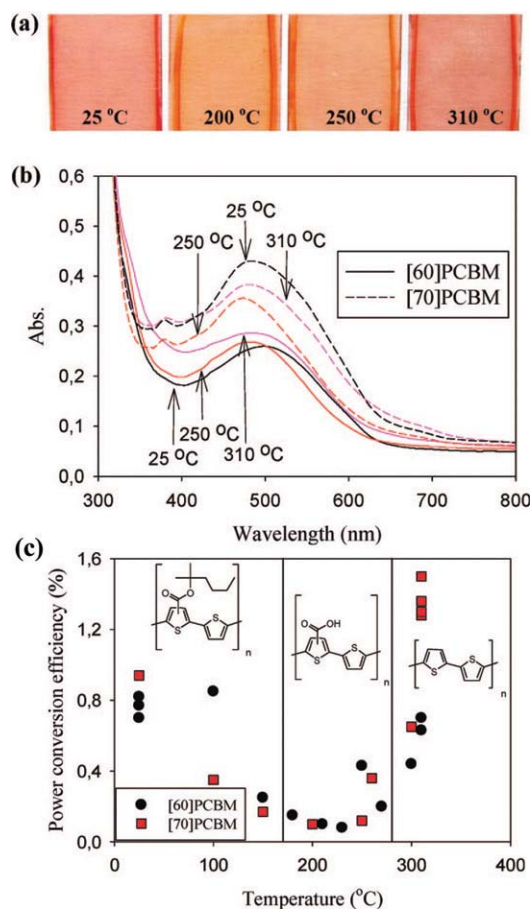
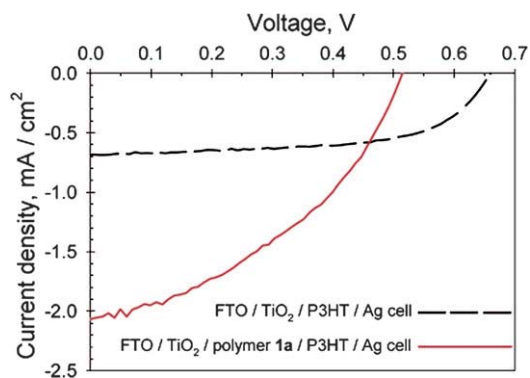


Fig. 9 (a) A photograph showing the appearance of films based on P3MHOCT:[70]PCBM when heated to different temperatures. (b) UV-vis spectra of films based on P3MHOCT and [60]PCBM or [70]PCBM mixtures spincoated on glass slides and annealed at three different temperatures (25, 250, and 310 °C). (c) Efficiency *versus* annealing temperature for bulk heterojunctions based on P3MHOCT and [60]PCBM/[70]PCBM. Reprinted with permission from ref. 99. © 2008 American Chemical Society.

how far thermocleavable materials could have been pushed pending the same investment of research effort that has gone into materials such as MEH-PPV or P3HT.

The use of cleavable P3MHOCT in thin film devices was first introduced by Liu *et al.*<sup>100</sup> The idea, besides improving the chromophore density, was to enable the interaction at the interface between the polymer and TiO<sub>2</sub> in a (FTO/TiO<sub>2</sub>/P3CT/





**Fig. 10**  $J$ - $V$  curves of a FTO/TiO<sub>2</sub>/P3CT/P3HT/Ag cell (solid line) and a FTO/TiO<sub>2</sub>/P3HT/Ag cell (dashed line) under 39 mW/cm<sup>2</sup> 514 nm illumination. Reprinted with permission from ref. 100. © 2004 American Chemical Society.

P3HT/Ag) photovoltaic cell (FTO = fluorine doped tin oxide). The device showed a 3-fold improvement in photocurrent compared to a reference cell without P3CT (Fig. 10). Under illumination the FTO/TiO<sub>2</sub>/P3CT/P3HT/Ag cell had an external quantum efficiency (EQE) of 12.6% and a power conversion efficiency of 1.10%, while the reference cell (FTO/TiO<sub>2</sub>/P3HT/Ag) had an EQE of 4.2% and a power conversion efficiency of 0.69%. The improvement in photocurrent/performance upon introduction of the P3CT layer may be related to several factors. Cleaving the solubilising groups results in higher chromophore density and the chelation of -COOH groups in P3CT to the TiO<sub>2</sub> may enhance the interfacial charge-transfer efficiency.

Other thermocleavable materials exploited as semiconductors are the dithiocarbamate precursors. Poly-(2,5-thienylene vinylene) (PTV) has been synthesised *via* the dithiocarbamate precursor route which exploits the lability of the linking thiocarbamate bond in the molecule (Fig. 11).<sup>101–105</sup> The solution-processable non-conjugated precursor polymer is cleavable around 160 °C leaving a rigid conjugated polymer (PTV). Bulk-heterojunction solar cells based on blends of the precursor PTV and PCBM have demonstrated power conversion efficiencies of up to 0.76% after the thermal treatment.<sup>102</sup>

In terms of stability PTV is like PPV,<sup>106</sup> sensitive to oxygen due to the vinylene groups that are susceptible to photo-oxidation resulting in a short lifetime of the devices. The chemical

degradation is initiated by the formation of singlet oxygen by energy transfer from the photoexcited polymer to ground state oxygen molecules.<sup>107</sup> The singlet oxygen can then react with the vinylene groups through a 2 + 2 cycloaddition reaction forming an intermediate dioxetane (Fig. 11) while other reactions are also possible. Finally the dioxetane can break down resulting in chain scission. As mentioned above more rigid systems generally give devices with a better stability and therefore improved stability of PTV devices prepared with the dithiocarbamate precursor route may be expected. The use of thermocleavable materials offers several advantages in the context of polymer solar cells. Most importantly the side chains that constitute a significant proportion of the final film are eliminated and ideally the final film comprises only the active component. Since bulk heterojunctions of polymer and PCBM are not directly compatible with the high temperatures acquired for elimination one aim is to achieve as low a temperature of elimination as possible. This has been investigated by Petersen *et al.* for thermocleavable esters of low band gap monomers and polymers based on diphenyldithienylthienopyrazine (Table 1).<sup>108</sup> The temperature of elimination of a series of different ester groups was studied with thermogravimetric analysis (Fig. 12a).

It showed that the thermal treatment is limited to simple secondary and tertiary esters where the alcohol is saturated in order to ensure that the alkene that is eliminated is removed efficiently without undesired side reactions.

As expected the tertiary esters eliminated at the lowest temperatures (200–250 °C) and even lower cleavage temperatures should be possible. The UV-vis absorption spectra of polymer **4** in thin film are shown in Fig. 12b. Upon thermocleavage of the film by heating it at 250 °C for 1 min the absorption spectrum shows a less intense absorption and a smaller band gap (1.2 eV) compared to the uncleaved film (1.3 eV). The lower absorption intensity can be explained by the associated change in film thickness and dielectric constant which may lead to changes in the reflection phenomena.<sup>108</sup> In addition, the intensity of absorption quite often decreases as the band gap is lowered. In contrast to P3MHOCT where the ester resides on a thiophene ring, decarboxylation does not take place ahead of decomposition for the diphenyldithienylthienopyrazines. Table 1 also shows photovoltaic parameters of polymers **1–4** before and after thermocleavage. A general observation is that the devices perform significantly worse after thermocleavage as indicated by

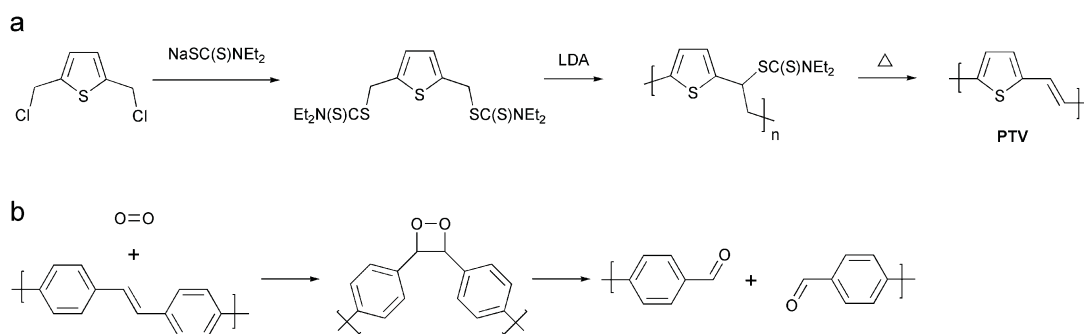


**Fig. 11** (a) Preparation of PTV *via* the dithiocarbamate precursor route (b) Reaction of the vinylene bond in a PPV polymer with singlet oxygen. Singlet oxygen adds to the vinylene bond forming an intermediate dioxetane followed by chain scission. The aldehyde products shown can react further with oxygen.

**Table 1** Photovoltaic parameters of polymers 1–4

**1-4**

R=

- 1) 2-heptyl
- 2) 5-nonyl
- 3) 2-methyl-3-hexyl
- 4) 2-methyl-2-hexyl

Polymer	$J_{sc}$ (mA/cm <sup>2</sup> )	$V_{oc}$ (V)	FF	PCE (%)	Cleaving temp. (°C)	Solubility in DCB
<b>1</b>	1.52	0.14	0.25	0.05	Uncleaved	Easy to dissolve
	0.41	0.16	0.26	0.017	310	
<b>2</b>	2.1	0.4	0.29	0.25	Uncleaved	Hard to dissolve
	0.36	0.14	0.27	0.013	310	
<b>3</b>	2.55	0.41	0.29	0.3	Uncleaved	Easy to dissolve
	0.24	0.08	0.26	0.005	310	
<b>4</b>	2.4	0.46	0.36	0.4	Uncleaved	Easy to dissolve
	1.94	0.4	0.33	0.25	230	

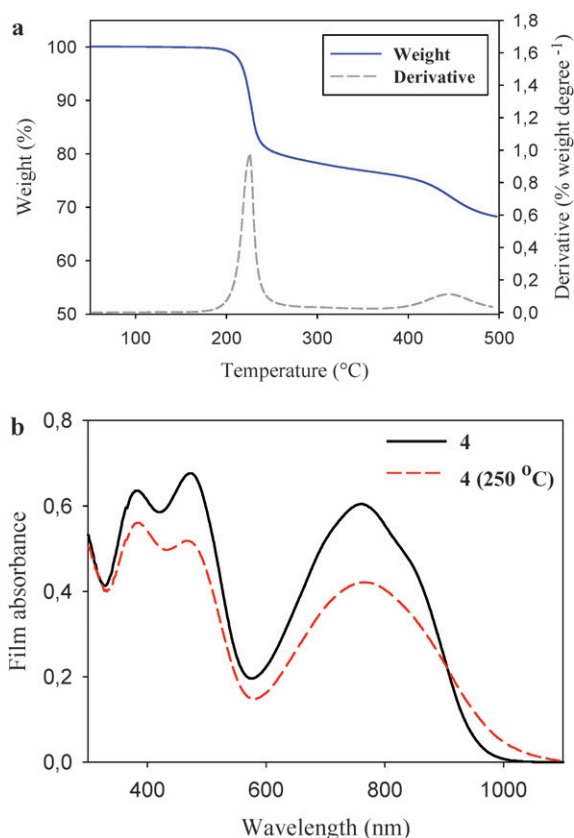


**Fig. 12** (a) Thermogravimetric data for polymer **4** (see Table 1) in the temperature range 50–500 °C. (b) UV-vis absorption spectra of polymer **4** in thin film before and after thermocleavage. Reprinted with permission from ref. 108. © 2008 American Chemical Society.

a decrease in voltage and current. Polymers **1–3** require high cleaving temperatures (310 °C) which could be the reason for the drastic drop in performance compared to **4** that only shows a minor drop in performance. To compare with earlier reported

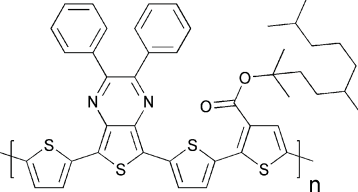
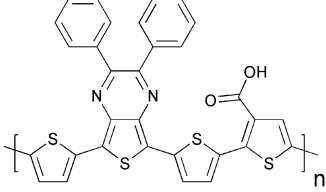
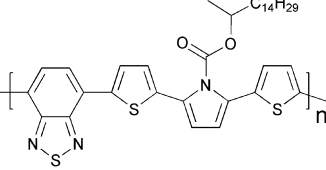
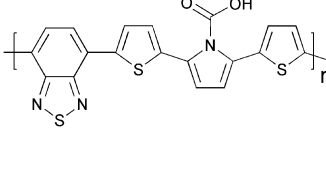
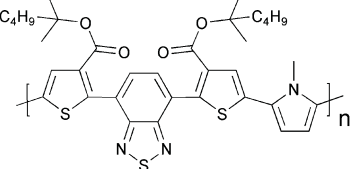
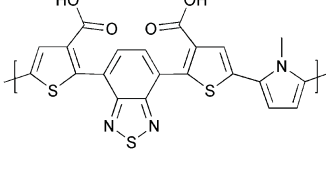
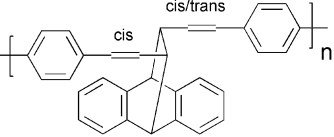
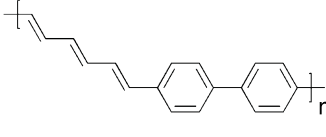
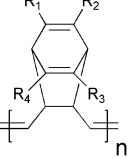
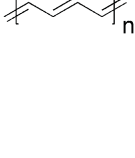
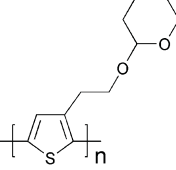
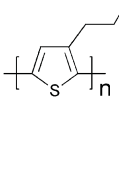
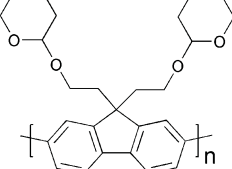
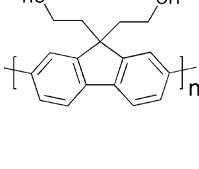
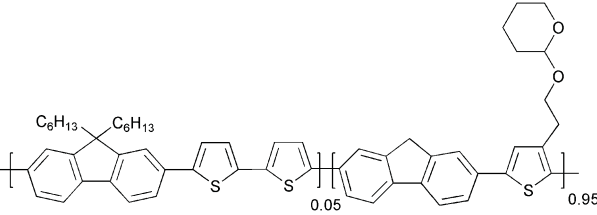
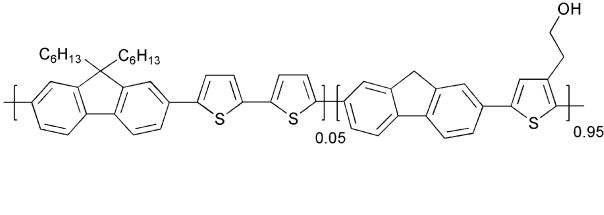
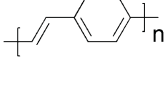
photovoltaic parameters for P3MHOCT the performance dropped around 10-fold when cleaved to P3CT and then improved 15-fold when cleaved further to PT (Fig. 9). In addition to the thermocleavable materials described above other examples have been described in the literature. These are summarized in Table 2.

### Cross-linking

Several investigations of the most widely used bulk heterojunction of P3HT/PCBM with a special focus on thermal stability have shown a drastic drop in performance due to morphological changes where large aggregations of PCBM appear in the films upon prolonged thermal treatment.<sup>117–121</sup> One way of approaching this problem has been by design of cross-linkable molecules/polymers (see Table 3) that can ‘lock’ the morphology and thus hinder the extensive phase separation. Zhu *et al.* and Drees *et al.* both succeeded in suppressing the aggregation by synthesising fullerene derivatives containing a glycidyl functionality (PCBG).<sup>122,123</sup> Bulk heterojunctions of P3HT/PCBG cross-linked by Lewis acid catalysis showed enhanced morphological stability upon thermal annealing. Nevertheless, the efficiencies of the cells dropped considerably compared to the corresponding non-cross-linked P3HT/PCBM system. Zhu *et al.* also reports some initial attempts of using cross-linkable polymers with either epoxy- or furoyl containing side chains, that are cross-linked by use of a photoacid. The films are reported to be insoluble in THF, but no devices were prepared.

A more successful approach in preparing cross-linkable polymers have recently been reported by Myanishi *et al.*<sup>124</sup> They have prepared a cross-linkable P3HT-analogue, poly(3-(5-hexenyl)thiophene) (P3HNT), where the hexyl group on thiophene is substituted with a 5-hexenyl. The polymer was prepared by polymerisation of 2,5-dibromo-3-(6-bromo-hexenyl) (regioregularity above 97% plus  $M_n$  and  $M_w/M_n$  values of 32 000 and 1.30 respectively) followed by conversion of the 6-bromohexyl into the corresponding iodide. Finally basic elimination affords the desired compound (Fig. 13).

**Table 2** Thermocleavable materials

Precursor	Polymer	Reference
		109
		110
		110
		111
		112
		113
		114
		115
		116

The cross-linking process was performed by prolonged heating of the spincoated films at 150 °C. Films prepared in this way showed enhanced insolubility in chloroform, and cross-linked bulk heterojunction films (P3HNT/PCBM) showed a suppressed deterioration of PCE after annealing for 10 h (3.03% before annealing → 1.74% after annealing) compared to a corresponding P3HT/PCBM device (3.11% before annealing → 1.00% after annealing).

It should be mentioned that several attempts of cross-linking conjugated polymers have been reported in the context of organic light emitting diodes (OLEDs) with various degrees of success.<sup>125–131</sup> Even though some of the polymers used in the OLED cross-linking experiments are different to those employed in solar cells, the methods of cross-linking the polymers could be relevant in the context of polymer photovoltaics.

## Processing

The performance of polymer solar cells is intimately linked to the processing conditions during device preparation and when taking this further than the successful laboratory devices it is evident that the successful large scale preparation of polymer solar cells implies control over the interplay between process and device performance. The solutions to this puzzle for a chosen materials combination will have to be sought through the device geometry and the processing/fabrication method. Thermocleavable materials as an example have much to offer in the context of processing multilayered polymer solar cells industrially. When processing multilayer structures sequentially the processing of subsequent layers must ideally not affect the underlying layers and this is particularly important when using solution processing. The common way of solving this has been to use orthogonal solvents for adjacent layers. In the extreme case water is used as the solvent for the first layer and an organic solvent is used for the next layer. This has been the traditional way of making polymer solar cells based on a glass-ITO substrate where poly(3,4-ethylenedioxythiophene):poly(styrenesulfonate) (PEDOT:PSS) is spincoated onto the ITO from an aqueous dispersion followed by spincoating of the active layer from an organic solvent and completion of the device through evaporation of a metal back electrode. It is fortuitous that the standard laboratory polymer solar cell has only needed these two solution processed layers for several reasons. Firstly, the surface energy of a solid PEDOT:PSS film is higher than the surface tension of active materials in typical organic solvents making wetting easy. Secondly, additional layers would be faced with the problem of finding an additional solvent orthogonal to the two previously deposited layers. These two problems may seem trivial but they are at the heart of what has limited the early emergence of a low cost industrial and large scale process. The fact that the technology has evolved around fixed ingredients (*i.e.* glass, ITO, PEDOT:PSS, metal electrode) and fixed methods of application (*i.e.* spincoating, metal evaporation) implies that development has been slow towards alternative approaches such as ITO free and inverted device geometries that enables the use of printed electrodes. One way to obtain orthogonality between the processing conditions for subsequent layers is by transformation of the last processed layer into an insoluble film thus enabling free choice of processing conditions for the subsequent layers. This has been achieved unintentionally in the case of oxide layers such

**Table 3** Structural representation of different molecules used in cross-linking processes in polymer photovoltaics and OLEDs

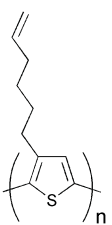
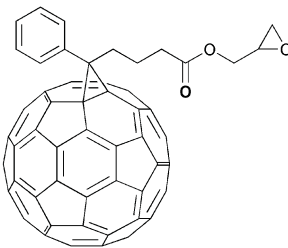
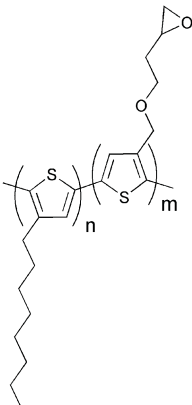
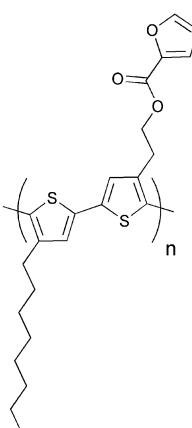
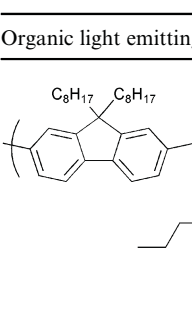
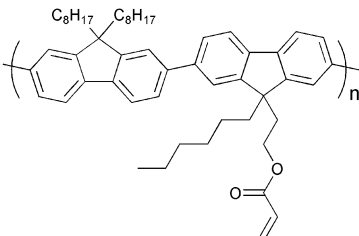
Polymer photovoltaics	Ref.
	124
	122,123
	123
	123
	123
Organic light emitting diodes	Ref.
	128



Table 3 (Contd.)

Organic light emitting diodes

Ref.

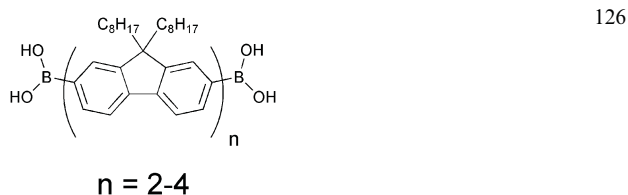
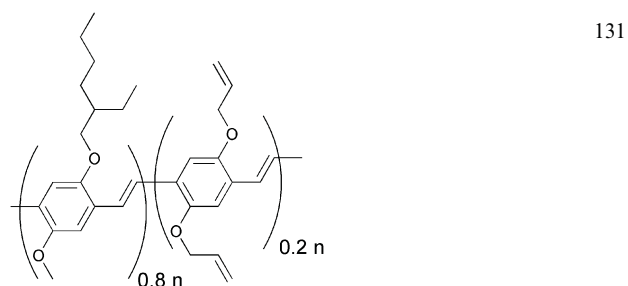
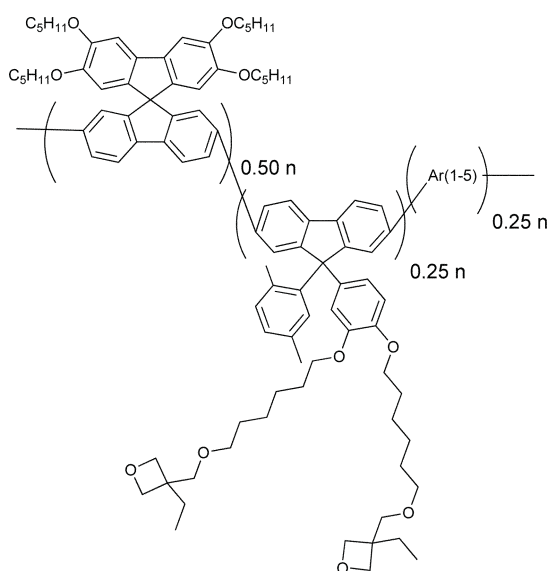
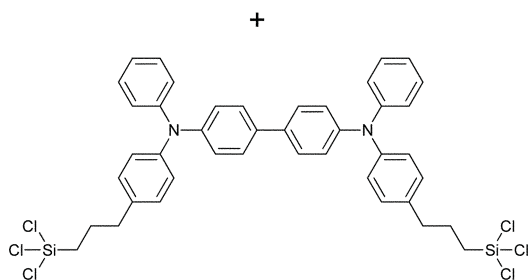
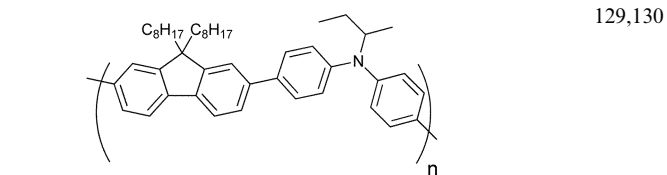
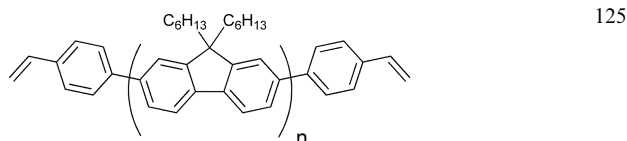


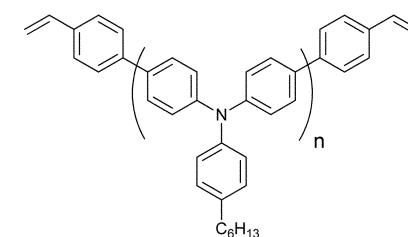
Table 3 (Contd.)

Organic light emitting diodes

Ref.



and



Blends (90:10 - 40:60)

as zinc oxide and titanium dioxide employed in hybrid solar cells and can be achieved intentionally with thermocleavable materials where insolubility arises upon thermocleavage as detailed above. Deliberate use of thermocleavable materials has been shown in one development of a process for industrially processed polymer solar cells.<sup>132-135</sup>

### Hybrid solar cells

Hybrid solar cells (HSC) have a heterojunction consisting of both organic and inorganic materials, thus trying to combine the advantages of each of these. Polymers generally have high hole mobility but a low electron mobility, and this intrinsic carrier mobility imbalance in the polymer is overcome by incorporation of an n-type inorganic material to act as the electron acceptor and a pathway for electron transport. The efficiency of the heterojunction is limited by the exciton diffusion length as excitons formed at positions further away from an interface than the exciton diffusion length have a lower probability of efficient charge separation and harvesting. Efficient charge separation can only occur at the p-n interface and ideally the heterojunction should be constructed in a manner such that the excitons are generated in the vicinity of the interface. At the same time the constructed heterojunction should ensure a direct or percolating pathway of the charge carriers to the relevant electrodes in order to effectively transport and collect the charges. The semiconducting properties in HSC of several different inorganic materials have been examined with promising results, *i.e.*  $TiO_2$ ,<sup>136-145</sup>  $ZnO$ ,<sup>146-158</sup>  $CdSe$ ,<sup>159-164</sup>  $CdS$ ,<sup>165,166</sup>  $PbS$ ,<sup>167</sup>  $PbSe$ ,<sup>168</sup>  $SnO_2$ ,<sup>169</sup> and  $Si$ ,<sup>170,171</sup> as presented in Table 4. In recent years research has largely focused on the use of  $TiO_2$ ,  $ZnO$  and  $Si$ , mainly because of the environmental harmfulness and toxicity of many of the others. The choice of polymer used in HSCs has usually been P3HT or different PPV polymers as they have shown good hole conducting properties.

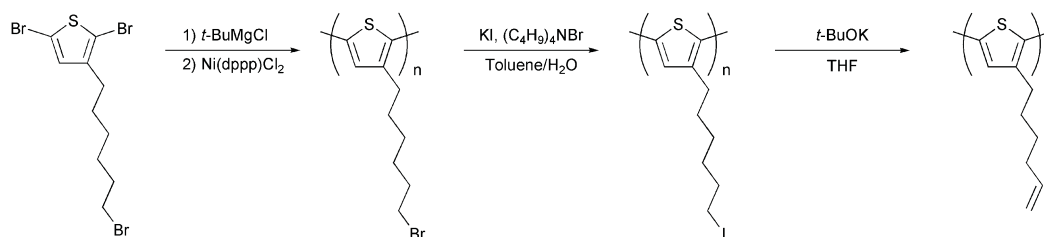


Fig. 13 Polymerisation and side chain conversion reactions for the synthesis of P3HNT.

Various approaches in HSC design have been explored and they generally fall into 4 architectural categories:

- (1) planar bilayer;
- (2) nanoparticle/polymer blends;
- (3) *in situ* generation of the n-type inorganic in the polymer;
- (4) nanostructured: infiltrating rigid nanoporous or nanorod structures with a polymer.

The schematic representation of these is shown in Fig. 14.

Covering a planar layer of inorganic semiconductor with a polymer film is the most direct approach to a hybrid solar cell, but the design has limited application as the active layer of polymer has to be very thin in order to make use of all the excitons. The simplicity of the architecture though renders it very applicable for routine evaluation of the properties of new polymers and measurement of exciton diffusion lengths.

When using nanoparticle/polymer blends the active layer is normally prepared by spincoating a solution containing dissolved polymer and suspended nanoparticles, thus enabling deposition of both semiconductors in a single step. The procedure should in principle ensure intimate mixing of the acceptor and donor, but great care must be taken in tuning the surface chemistry of the nanoparticles in order to prevent these from aggregating and at the same time ensuring a good interface for charge transfer.<sup>172</sup> Nanoparticle aggregation is believed to be one of the limiting factors of the efficiency in nanoparticle/polymer devices.<sup>173</sup>

Examples of this include the use of tetrapod, hyperbranched and nanorod CdSe nanoparticles in combination with conjugated polymers where efficiencies are approaching 3%.<sup>159–164</sup> Essential for the good performance is to replace the nanoparticle surface ligands with a volatile molecule (for example replacement of tri-*n*-octylphosphine oxide with pyridine), allowing for evaporation of the surface ligands during film processing. This again allows for better contact between the polymer and the nanocrystals and between the individual nanoparticles.

In one example Beek *et al.* have achieved a PCE of 1.6% and avoid the problem of surface ligands by using crystalline ZnO nanoparticles, which are soluble in organic solvents and therefore can be mixed directly with the polymer.<sup>146,147</sup>

An alternative approach to individual nanoparticles was introduced by van Hal *et al.* that prepared a continuous interpenetrating network of TiO<sub>x</sub> created *in situ* within the conjugated polymer film after spincoating a mixture of MDMO-PPV and a precursor for TiO<sub>x</sub> (Ti(OC<sub>3</sub>H<sub>7</sub>)<sub>4</sub>).<sup>174</sup> Subsequent exposure of the cast film to moisture from the air led to the formation of a TiO<sub>x</sub> network. The photoluminescence (PL) of the MDMO-PPV:TiO<sub>x</sub> heterojunction was significantly quenched compared to a pristine MDMO-PPV film (PL is reduced by a factor 19 with

a 50% w/w content of TiO<sub>x</sub>) indicating an efficient charge separation of photoinduced excitons. These experiments were later confirmed by Slooff *et al.* where additional experiments were performed with poly(3-octyl thiophene) (P3OT) as the polymer.<sup>175</sup> Scanning electron microscopy (SEM) images taken after removal of the polymers by UV–ozone treatment revealed TiO<sub>x</sub> phases with sizes on the order 100–200 nm for P3OT blends and 20–30 nm for MDMO-PPV blends. The difference is assumed to be caused by the tendency of P3OT to aggregate more easily as compared to MDMO-PPV (Fig. 15).

Despite the good interpenetrating network of TiO<sub>x</sub>, photovoltaic devices showed rather low power conversion efficiencies which is ascribed to the fact that the inorganic phase is essentially amorphous.<sup>147</sup> Crystallisation of TiO<sub>x</sub> into the anatase phase of TiO<sub>2</sub> would require high temperatures (>350 °C).<sup>176</sup>

A similar approach was taken by Beek *et al.* using MDMO-PPV and diethylzinc as a ZnO precursor.<sup>147</sup> ZnO is known to crystallise at much lower temperatures than TiO<sub>2</sub>, and heating to 110 °C under nitrogen at 40% relative humidity promoted crystallisation. The final device gave a PCE of 1.1%. Moet *et al.* later reported partial degradation of the polymer during processing of MDMO-PPV and diethylzinc and that P3HT (no vinyl groups) show better stability and higher performance (PCE 1.4%).<sup>150</sup>

The last architectural approach involves the filling of a pre-created inorganic nanostructure (vertical structured nanopores or vertically oriented nanorods/nanopillars) with a polymer (examples are given in Fig. 16). The aim is to create a structure where the separation of the phases is in the order where complete exciton harvesting and charge collection is possible and where the straight pore/channel network provides the most direct pathway for the charges to the anode and cathode. Several techniques<sup>137,139,170,177–181</sup> have been developed in order to create controlled structures pursuing the alleged optimal conditions. Among the published results on solar cells Olson *et al.* reported the fabrication and characterisation of heterojunctions consisting of P3HT and a mesoporous structure of ZnO nanofibers.<sup>152</sup> The nanofibers were grown hydrothermally on a glass/ITO substrate which was subsequently filled with P3HT by spincoating and annealed to ensure intercalation into the voids between the nanofibers. The final device showed a 3.5 times increase in PCE (to 0.53%) compared to the corresponding bilayer device of P3HT on planar ZnO.

Kuo *et al.* recently showed good results for ordered heterojunctions with vertically aligned TiO<sub>2</sub> nanorods and P3HT.<sup>139</sup> The vertical TiO<sub>2</sub> nanorods were prepared by spincoating a TiO<sub>2</sub> precursor into the pores of an aluminium anodic oxide (AAO) template pregrown on an ITO/glass substrate. After sintering, the AAO template was removed by dissolving it in aqueous

**Table 4** Materials and performance parameters for a range of selected polymer–inorganic solar cells. All measurements are performed in the vicinity of AM 1.5 conditions (90–100 mW/cm<sup>2</sup>) unless stated otherwise<sup>a</sup>.

Inorganic semiconductor	Polymer	Architectural category	V <sub>oc</sub> (V)	J <sub>sc</sub> (mA/cm <sup>2</sup> )	FF	η(%)	Comments	Ref.
<b>CdSe</b>	OC1C10-PPV	Tetra-pod NP	0.76	9.1	0.44	2.8	V <sub>oc</sub> and J <sub>sc</sub> were extracted from a figure	162
	P3HT	Nanorod P	0.62	8.79	0.50	2.6		163
	APFO-3 <sup>b</sup>	Nanorod P	0.95	7.23	0.38	2.6		164
	P3HT	Hyperbranched P	~0.6	~7.0	—	2.2		159
	OC1C10-PPV	Tetra-pod NP	0.65	7.3	0.35	1.8		161
	P3HT	Nanorod P	0.7	5.7	0.4	1.7		160
<b>CdS</b>	P3HT	Surf. mod. NP	0.54	4.84	0.45	1.18	Surf. mod. with a polyacetylene containing quaternary pyridinium salts	165
	MEH-PPV	Multiarmed nanorod P	0.85	2.96	0.47	1.17		166
	P3HT	NP	0.35	1.08	0.37	0.14		168
<b>PbS</b>	MEH-PPV	NP	1	0.13	0.28	0.7	AM 1.5 conditions but at low power (5 mW/cm <sup>2</sup> )	167
<b>SnO<sub>2</sub></b> <b>ZnO</b>	MDMO-PPV	Surf. mod. nanoporous NP layer	0.65	0.32	0.42	0.085	Surf. mod. with C <sub>60</sub> C(COOH) <sub>2</sub> Surf. mod. with N719	169
	P3HT/PCBM	Vertical nanorod array	0.58	10.4	0.65	3.9		154
	P3HT/PCBM	Vertical nanorod array	0.57	9.6	0.50	2.7		153
	P3HT/PCBM	Vertical nanorod array	0.475	10	0.43	2.03		151
	P3HT/PCBM	Surf. mod. vertical nanorod array	0.57	8.89	0.41	2.0		155
	MDMO-PPV	NP	0.81	2.4	0.59	1.6		146
	P3HT	<i>In situ</i> prepared	0.83	3.3	0.50	1.4		150
	MDMO-PPV	<i>In situ</i> prepared	1.14	2.0	0.42	1.1		147
	P3HT	Vertical nanorod array	0.44	2.17	0.56	0.53		152
	P3HT	Surf. mod. vertical nanorod array	0.46	2.45	0.46	0.52		149
<b>Si</b>	APFO-3 <sup>b</sup>	NP	0.51	3.1	0.36	0.45	Diethylzinc as ZnO-precursor Diethylzinc as ZnO-precursor Surf. mod. with mercurochrome	156
	P3HT/PCBM	Vertical nanowires	0.43	11.6	0.39	1.93		170
	P3HT	NP	0.75	3.3	0.46	1.15		171
	P3HT	Surf. mod. nanorod P	0.78	4.33	0.65	2.20		141
<b>TiO<sub>2</sub></b>	P3HT	Surf. mod. nanorod P	0.75	3.49	0.65	1.70	Surf. mod. with N3-dye Surf. mod. with anthracene-9-carboxylic acid	140
	P3HT	Nanorod P	0.64	2.73	0.56	0.98		142
	P3HT	Nanorod P	0.52	2.97	0.54	0.83		144
<b>ZnO + TiO<sub>2</sub></b>	MEH-PPV	Bilayer	1	1.8	0.37	0.67	Surf. mod. with N719-dye Surf. mod. with N3-dye Surf. mod. with black dye	136
	P3HT/PMMA	Nanorod P	0.53	2.57	0.48	0.65		143
	P3HT	Vertical nanorod array	0.32	3.89	0.41	0.51		139
	P3HT	Surf. mod. nanofiber mat	0.57	1.27	0.40	0.29		145
	P3HT	Surf. mod. nanoporous NP layer	0.64	1.11	0.34	0.24		138
	MEH-PPV	Vertical array of hexagonal pores	0.79	0.56	0.47	0.21		137
	P3HT	Surf. mod. bilayer	0.46	0.67	0.48	0.15		138
	P3HT	Vertical ZnO nanorod array + TiO <sub>2</sub> nanorod P	0.49	2.67	0.45	0.59		148

<sup>a</sup> Abbreviations: **NP**: nanoparticle; **P**: particle; **Surf. mod.**: surface modified. <sup>b</sup> APFO-3: poly(2,7-(9,9-dioctylfluorene)-alt-5,5-(4',7'-di-2-thienyl-2',1',3'-benzothiadiazole)).

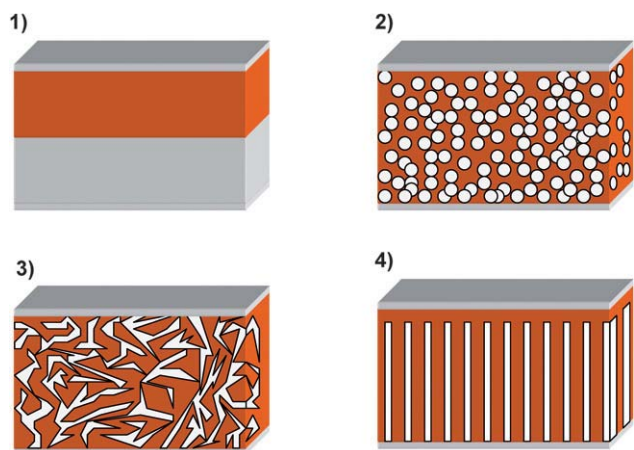


**Fig. 14** The different geometries of hybrid solar cells: (1) Planar bilayer—the polymer added onto a flat inorganic surface; (2) nanoparticle/polymer blends—a mixture of the polymer and suspended inorganic particles is applied; (3) *in situ* generation of the inorganic within the polymer—a mixture of the polymer and a soluble precursor to the inorganic is applied and solidification of the inorganic is then performed after film preparation; (4) nanostructured—a rigid nanoporous or nanorod structure of inorganic is filled with the polymer.

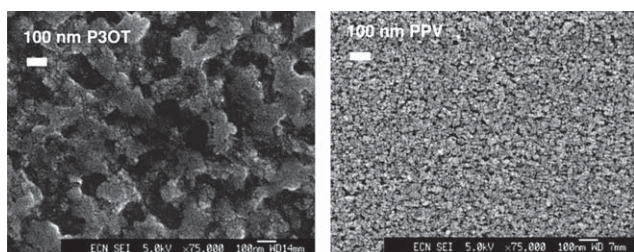


**Fig. 15** SEM of the  $\text{TiO}_x$  phase after removal of the polymer by UV-ozone treatment for 10 min. Left: from a P3OT: $\text{TiO}_x$  (12 vol%  $\text{TiO}_x$ ) blend. Right: from a MDMO-PPV: $\text{TiO}_x$  (14 vol%  $\text{TiO}_x$ ) blend. Reprinted with permission from ref. 175. © 2003 Elsevier B.V.

NaOH. The nanorods are approximately 200 nm long and with a diameter 30–60 nm. The resulting solar cell after spincoating of P3HT and annealing showed to be 4.3 times more efficient (PCE of 0.51%) than planar  $\text{TiO}_2$ :P3HT.

As can be seen from Table 4, several of the reports with the highest efficiencies are reported for P3HT/PCBM blends and an inorganic semiconductor. The inorganic material here functions as an extra electron carrier. Takanezawa *et al.* showed that incorporation of the P3HT/PCBM bulk heterojunction into a vertical ZnO nanorod array led to an increase in PCE from 1.8% for a normal P3HT/PCBM heterojunction on top of a seed layer of ZnO to a PCE of 3.9% when growing the seed layer to nanorods with a length of 300 nm before spincoating the P3HT/PCBM solution.<sup>153,154</sup> As seen in Fig. 17 the ZnO rods can act as an extra electron carrier at the p–n interface with P3HT but can also operate as an intermediate between PCBM and ITO.

Another tendency in Table 4 that leads to relatively high efficiencies is the use of the surface modified inorganics, typically with a dye that can assist in charge separation and prevents back recombination. (For all results involving surface modification presented in Table 4 the concentration of the interfacial

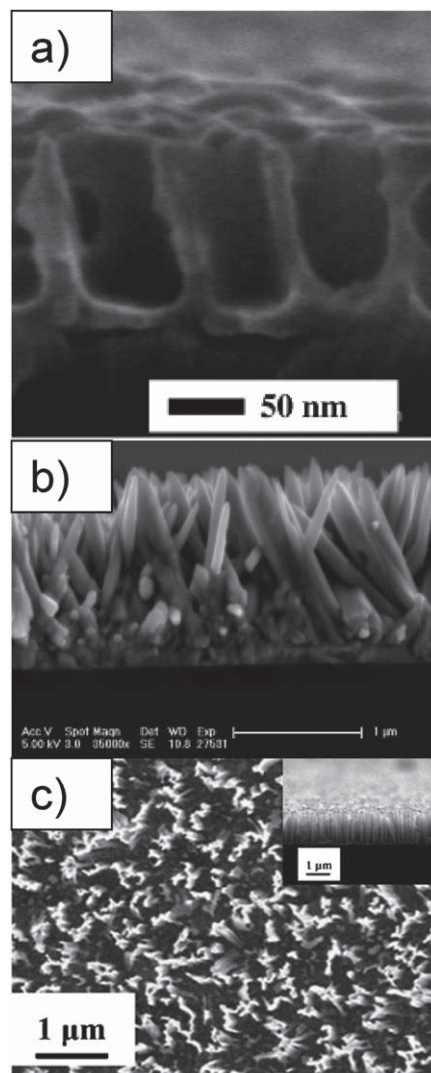


**Fig. 16** SEM images of (a) cross sectional view of embossed  $\text{TiO}_2$  structures on FTO substrate after calcinations. Reprinted with permission from ref. 178. © 2005 American Chemical Society. (b) ZnO nanorods grown on dense ZnO backing layer on ITO substrate (cross section). Reprinted with permission from ref. 181. © 2006 American Chemical Society. (c) Top view of Si-nanowires on silicon wafer prepared by wet etching, with an insert of the cross sectional view. Reprinted with permission from ref. 170. © 2008 Elsevier B.V.

molecules is so small that they only have a minimal or negligible contribution to the light absorption, and the polymer is thus the main contributor to absorption.) Lin *et al.* have recently demonstrated that surface modification by ligand exchange of the surface ligands of freshly prepared nanorods (~20–30 nm in length and 4–5 nm in diameter) with different dyes led to improved performances compared to ‘normal’ ligand exchange with pyridine, a near doubling of the PCE (from 1.12% to 2.20%) was observed in a HSC with P3HT.<sup>141</sup> The authors ascribe the large increase in PCE to be partially an effect of enhanced charge separation but mainly to be attributed to a strong suppression of back transfer and recombination of carriers at the interfaces. In Fig. 18 the energy diagram of  $\text{TiO}_2$ , the dye ligands, and P3HT are shown. All the dyes showed improved performance when



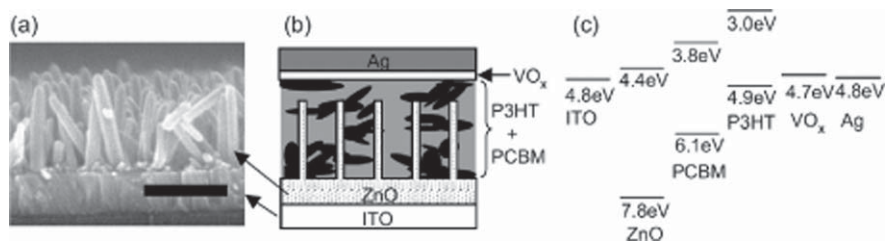


**Fig. 17** (a) FE-SEM cross-section image of the ZnO nanorod arrays (scale bar: 300 nm), (b) schematic structure of a ZnO/organic hybrid device with a  $\text{VO}_x$  buffer layer, and (c) energy diagram of the ITO/ZnO/PCBM:P3HT/ $\text{VO}_x$ /Ag device. Reprinted with permission from 154. © 2008 American Institute of Physics.

used as surface modifiers in the order  $\text{N3}$  (2.20%) >  $\text{CuPc}$  (1.80%) >  $\text{ACA}$  (1.67%).

The results for the P3HT/PCBM:n-inorganic and the use of surface modified inorganics show that ‘tuning’ the charge separation and back recombination by adding a third component might be a promising path for future research. The third component is typically added at the interface between the inorganic semiconductor and the polymer *vis-à-vis* the well known dye sensitized solar cells where it serves the purpose of facilitating charge injection from the polymer to the semiconductor while preventing back recombination.

### Tandem cells

So far the power conversion efficiency of single bulk heterojunction solar cells has reached 6% while higher power conversion efficiencies are possible from a theoretical point of view. One drawback of single junction polymer devices is their narrow absorption window compared to the solar cells based on inorganic semiconductors. A possible approach to efficiently harvest light at both short and long wavelengths is by stacking different band gap materials/devices on top of each other. This can be done by placing the cells in series giving devices known as tandem cells.<sup>1,13,14</sup> By stacking different band gap materials on top of each other the tandem cell should be

able to exceed the maximum theoretical efficiency of a single junction solar cell because it increases the absorption of solar light and allows exploiting the photon energy more efficiently. When two cells (in a two terminal tandem cell) are connected in series the open-circuit voltage ( $V_{oc}$ ) is the sum of the  $V_{oc}$ 's of the subcells,  $V_{oc1} + V_{oc2} + V_{oc3...} = V_{oc(tandem)}$ .

Fig. 19 illustrates a typical organic tandem cell architecture comprised of two distinct active layers stacked on top of each other. Both of them are based on a donor–acceptor composition and the use of materials with different band gaps enables absorption of solar light over a wider spectral range. Typically a material with a wide band gap is used for the first cell and a low band gap material is used for the second cell. In order to prevent charge build-up within the cells a transparent intermediate layer is positioned between the two active layers. The intermediate layer ensures recombination of the electrons created in the first cell with the holes created in the second cell. In addition, it can act as a protective layer to support the bottom cell during deposition of the top active layer. This can generally be accomplished with a thin inorganic layer. Several methods have been employed in the fabrication of tandem cells depending on the materials used for the active and the intermediate layer. The mode of preparation can be divided in three categories: all vacuum processing by evaporation of low molecular weight

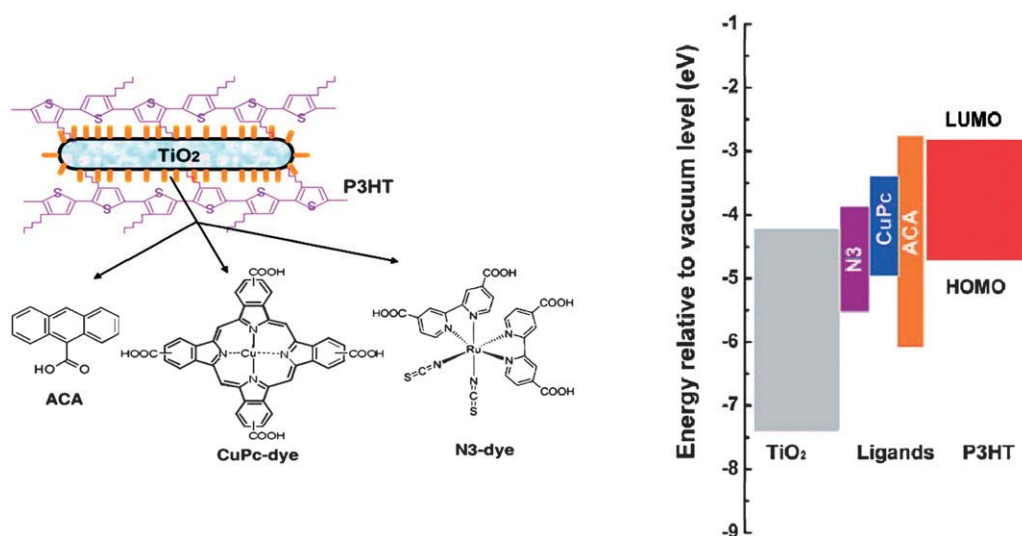


**Fig. 18** Left: Schematic representations of P3HT/ $\text{TiO}_2$  nanorod hybrid after interface modification and chemical structures of different interfacial molecules of ACA,  $\text{CuPc}$ -dye, and  $\text{N3}$ -dye molecules respectively. Right: The corresponding energy levels of the various materials. Reprinted with permission from ref. 141. © 2009 American Chemical Society.

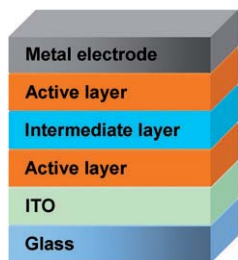


Fig. 19 Typical device setup for an organic tandem cell.

molecules, a combination of vacuum and solution processing and all solution processing. Due to the complexity of multilayer solution processing caused by interlayer mixing, the early reports of organic tandem cells are based on the vacuum deposition of small molecules and they certainly show increased  $V_{oc}$  and efficiencies.<sup>182–186</sup> Also a combination of vacuum and solution processing is a fine approach where the solution processed underlying layer is not disturbed during subsequent vacuum processing.<sup>187–190</sup> However, from an industrial point of view, all solution processing without the use of vacuum where each layer is processed from solution (including the metal electrode) is the most appealing because techniques like ink-jet printing, screen printing and roll-to-roll coating are less time and energy consuming and enable large scale organic solar cell production. Gilot *et al.* were the first to demonstrate a polymer tandem cell with each layer processed from solution (the metal electrode was evaporated).<sup>191</sup>

The technique relies on the choice of solvent for the different layers. They have to be complementary in the sense that the next solvent in the process is not affecting the material in the underlying layer. Fig. 20 illustrates the device setup realized by Gilot *et al.* The challenging step is the spincoating of the intermediate layer where the authors used a layer of zinc oxide nanoparticles spincoated from acetone prior to a layer of pH neutral PEDOT. The ZnO/PEDOT recombination layer was not affecting the underlying active layer of MDMO-PPV:PCBM and was also acting as a protective layer to support the bottom cell during deposition of the second active layer consisting of a P3HT:PCBM bulk heterojunction. The solution processed tandem cell has led to an efficiency of 6.5% for a polymer solar cell with an evaporated metal back electrode.<sup>192</sup> It was demonstrated by Kim *et al.* with a bulk heterojunction composite of PCPDTBT (Fig. 1) and PCBM for the bottom cell and a layer of

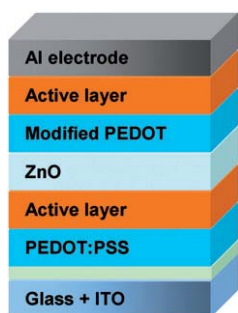


Fig. 20 Device setup for the tandem solar cell realized by Gilot *et al.*

P3HT:[70]PCBM for the top cell. For the intermediate layer the authors used a layer of  $TiO_x$  spincoated from a  $TiO_x$  precursor solution (sol–gel chemistry)<sup>193</sup> prior to a layer of PEDOT. The  $TiO_x$  precursor hydrolyses to  $TiO_x$  during 1 hour in air (Fig. 21) and the final  $TiO_x$  layer offers high mechanical stability to the tandem cell. The final polymer tandem cell showed an improvement of 38% in performance *versus* the best single cell.

An all solution processed tandem polymer solar cell based on thermocleavable materials has been reported by Hagemann *et al.*<sup>109</sup> The authors used solution-processable precursors that allow for conversion to an insoluble state by a thermal treatment. A bulk heterojunction composite of P3MHOCT and ZnO was used for the bottom cell and a blend of poly-[(3'-(2,5,9-trimethyldecan-2-yl)-oxy-carbonyl)-[2,2';5',2'']terthiophene-1,5''-diyl]-co-(2,3-diphenylthieno[3,4-b]pyrazine-5,7-diyl)] (P3TMDCTTP) and ZnO was used for the top cell (Fig. 22). Straight after each film preparation a short thermal treatment eliminated the solubilising group converting P3MHOCT to P3CT and P3TMDCTTP to P3CTTP. To separate the bottom cell from the top cell an intermediate layer of PEDOT:PSS and ZnO were used. The final tandem cell performed relatively poorly but did not involve the use of fullerenes and efficiently solved the problems associated with solubility during application of subsequent layers. In addition a solution processed metal electrode was employed. An obvious advantage of thermocleavable materials is that they offer new levels of processing after film forming. Due to the insoluble nature of the active materials after the thermal treatment there is no limit in the choice of solvents when processing the subsequent layers in the tandem cell and more research into this field appears worthwhile.

Recently a novel concept was introduced whereby the tandem solar cell is realized in a reflective geometry where the reflected light of one cell is directed towards the second one.<sup>194–197</sup>

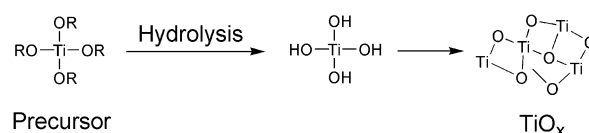


Fig. 21 Preparation of the  $TiO_x$  layer.

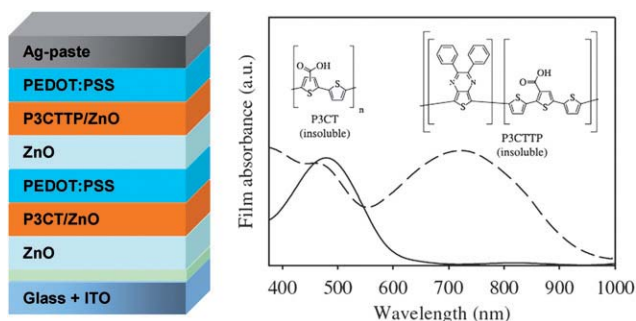
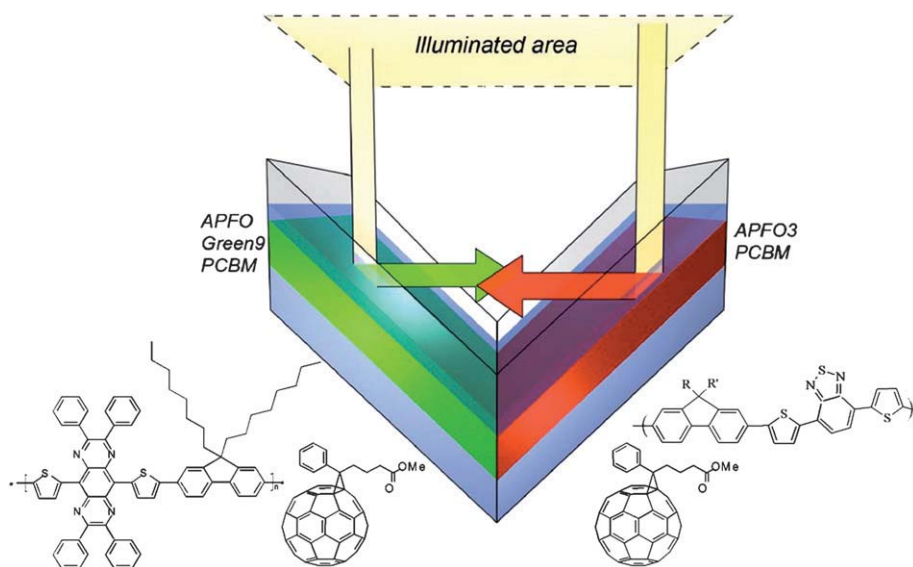


Fig. 22 Tandem solar cell based on thermocleavable materials realized by Hagemann *et al.* The active layer film absorption spectra are also shown with P3CT/ZnO plotted with a solid line and P3CTTP/ZnO plotted with a broken line. Reprinted with permission from ref. 109. © 2008 Elsevier B.V.



**Fig. 23** Folded tandem cell realized by Tvingstedt *et al.* Sketch of the folded tandem cell and the chemical structures of the exploited alternating polyfluorenes APFO3, APFO Green-9, and the acceptor molecule PCBM. Reprinted with permission from ref. 196. © 2007 American Institute of Physics.

Tvingstedt *et al.* demonstrated that by folding two planar cells with different band gap materials toward each other, spectral broadening and light trapping are combined to give an improvement of PCE from 2% up to 3.7% upon folding from 0° to 70° (Fig. 23).<sup>196</sup> A bulk heterojunction composite of APFO3 and PCBM was used for one cell and APFO-Green9:PCBM for the second cell. The advantage of the folded tandem device is that it avoids complex multilayer solution processing and other problems related to multijunction stacking

### Control of the nanomorphology

The nanoscale morphology is an important factor in the construction of functional organic bulk-heterojunction solar cells as it is of interest to be capable of controlling the dimension of the domains in the nanostructure such that all domain boundaries are within the exciton diffusion range in the photoactive layer. Han *et al.* have demonstrated a novel procedure to create morphologically controlled nano/microscale patterns of  $\pi$ -conjugated polymers.<sup>114</sup> An acidic mixture of polyfluorene or polythiophene bearing solubilising thermocleavable tetrahydropyranyl (THP) groups, and poly(methyl methacrylate)

(PMMA) is used for the active layer. After spincoating on substrates phase separation is induced by the chemical dissimilarity of the two polymers giving rise to a nano/microscale morphology. After an acid catalyzed thermal treatment where the THP groups are eliminated the insoluble conjugated polymer remains (Fig. 24). Subsequently, PMMA is removed by treating the films with a chlorobenzene/hexane solution leaving a dot matrix of the conjugated polymer (Fig. 25).

This method, where a template is used to control the nanostructure of conjugated polymers, has been exploited by Andreasen *et al.* in a solar cell context.<sup>198</sup> Instead of PMMA, copper nanoparticles with an average diameter of 32 nm were used as the template to nanostructure a conjugated polymer based on P3MHOCT. Mixtures of P3MHOCT and the copper nanoparticles are processed into thin films followed by a thermal treatment whereby the solubilising side chains of the polymer were eliminated, leaving an insoluble film of conjugated P3CT with included copper nanoparticles. The copper nanoparticles could then be removed by treating the films with a THF solution of phenylazodiethylthioformamide (copper-specific solubilising agent<sup>90,91</sup>) leaving voids in place of the copper nanoparticles (Fig. 26). Finally the voids in the dried nanoporous films were

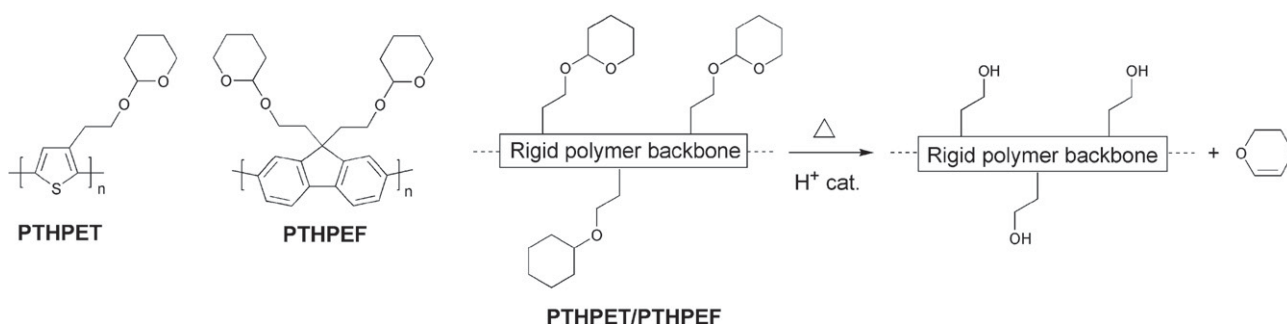


**Fig. 24** Thermocleavable polymers PTHPET and PTHPEF and acid-catalyzed elimination of dihydropyran from the polymer backbone.

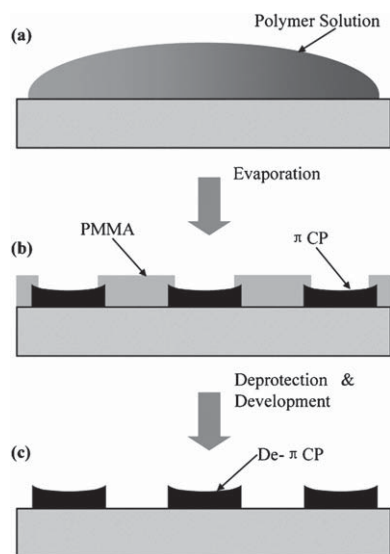


**Fig. 25** Schematic illustration of the formation of a well-ordered micro and nanometre-sized  $\pi$ -conjugated polymer features (PTHPET or PTHPEF) by (a) solution casting, (b) self-organization, and (c) catalytic reaction and development. Reprinted with permission from ref. 114. © 2007 WILEY-VCH.

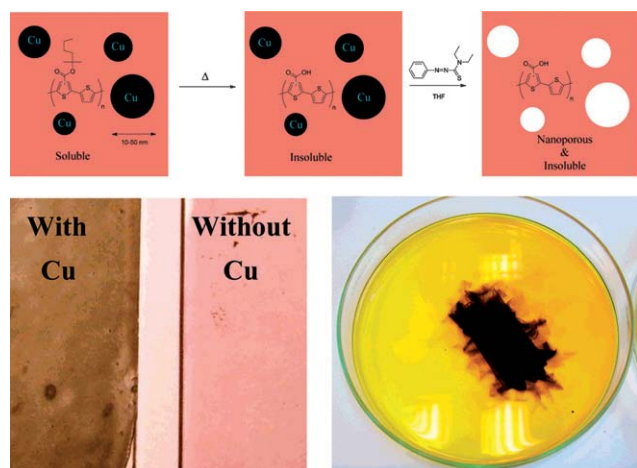


**Fig. 26** Reaction scheme for the process (above) and pictures of the films before and after removal of the copper nanoparticles. The film loaded with copper nanoparticles has a black appearance whereas the film where the copper nanoparticles have been removed had a red color (lower left). The dissolution step is also shown where a device slide (50 mm  $\times$  25 mm) is covered with a THF solution of azothioformamide. The dark color is due to the formation of the copper complex of azothioformamide (lower right). Reprinted with permission from ref. 198. © 2007 American Chemical Society.

filled with PCBM by doctorblading forming a donor–acceptor bulk heterojunction.

However, the nanostructures had little influence on the photovoltaic effect. The best device (active area of 3 cm<sup>2</sup>) had an open-circuit voltage of 0.43 V, a short-circuit current of 0.19 mA cm<sup>-2</sup>, a fill factor of 27.4%, and a power conversion efficiency of 0.02% (0.1–0.4% for P3CT:[60]PCBM). These data are much lower than the state-of-the-art and is ascribed to the low porosity of the films (<20%) and the large size of the PCBM domains. The

ideal size of the PCBM domains should be of the order of 5–10 nm, and the porosity should be closer to 50% or more. This method may find importance in the modification of nanoscale morphologies for polymer solar cell devices if it could be advanced for incorporation of larger amounts of well-distributed smaller nanoparticles (5–10 nm) into the conjugated polymer film.

Laser-induced thermal patterning is another technique to control the morphology of conjugated polymers. Gordon *et al.* have developed a method for direct thermal patterning of a thermocleavable  $\pi$ -conjugated polymer film containing a near-infrared (NIR) sensitive dye.<sup>199</sup> The NIR dye (Fig. 27) is incorporated directly into the polymer film by spincoating a NIR dye/polymer blend on a substrate.

When the film is exposed to NIR light pulses from an 830 nm laser beam the dye absorbs the irradiation and converts the NIR photons into heat by internal conversion. The polymer (PTHPET) does not absorb the NIR light. The heat produced by the dye induces thermocleavage of the THP groups. Subsequently, the NIR dye is removed by rinsing the films with methanol followed by THF leaving patterned  $\pi$ -conjugated polymer (Fig. 28). The patterned  $\pi$ -conjugated polymer shows a significant reduction in the quantum yield, compared to a pure

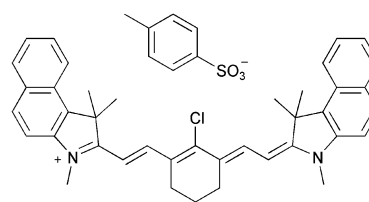


**Fig. 27** NIR dye used by Gordon *et al.*<sup>199</sup>

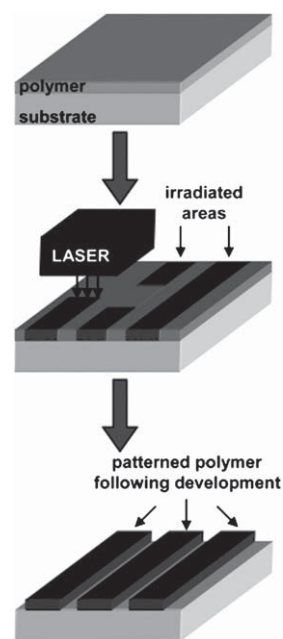


**Fig. 28** Schematic diagram for the direct thermal patterning of a  $\pi$ -conjugated polymer using a NIR laser realized by Gordon *et al.* Reprinted with permission from ref. 199. © 2007 American Chemical Society.



PTHPET film, which is ascribed to either the presence of residual NIR dye remaining in the film after rinsing or/and coplanarisation and chain aggregation after thermocleavage of the THP groups.

To overcome this problem novel strategies have been developed where the NIR dye is not incorporated into the film. Gordon *et al.* have described a bilayer approach,<sup>115</sup> wherein a NIR dye is contained in a film of poly(2-hydroxyethylmethacrylate) [p(HEMA)] spincoated onto a thermocleavable  $\pi$ -conjugated polymer film of poly(9,9-dihexylfluorene-*alt*-2-(2-thiophen-3-ethoxy)tetrahydro-pyran)-*co*-(9,9-dihexylfluorene-*alt*-bithiophene) (PFT-TT) (Fig. 29).

After exposure of the bilayer film to 830 nm NIR laser irradiation the p(HEMA)/NIR dye layer is removed by rinsing with methanol. Subsequent treatment of the remaining film with a THF/hexane solution removes non-cleaved PFT-TT (unexposed p(HEMA)/NIR dye regions) leaving a patterned  $\pi$ -conjugated polymer (Fig. 30). Using this bilayer film architecture the active conjugated polymer layer can be heated by exposure to NIR irradiation while minimizing deleterious mixing of the polymer with the NIR dye. Compared to the monolayer approach described above the  $\pi$ -conjugated polymer retains its

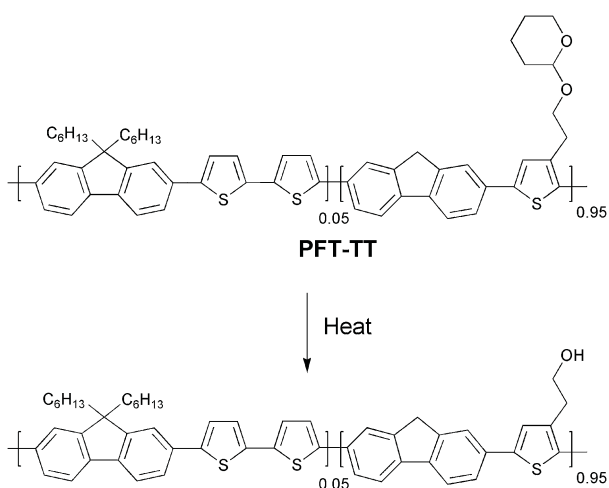


Fig. 29 PFT-TT with thermocleavable THP groups.

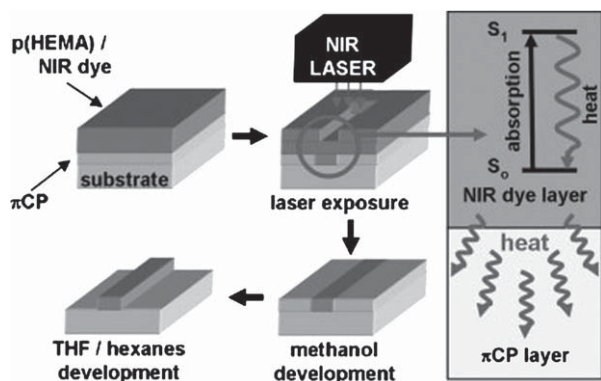


Fig. 30 Bilayer approach to laser induced direct thermal patterning of a  $\pi$ -conjugated polymer realized by Gordon *et al.* Reprinted with permission from ref. 115. © 2008 WILEY-VCH.

photoluminescent properties showing quantum yields as high as 86% of the pristine polymer. The method is capable of imaging large surface areas, up to 1 m<sup>2</sup>, at relatively high throughput and with micrometre size resolution (typically 5–10  $\mu$ m), and thus could be valuable in the context of processing of thermocleavable polymers for solar cells.

### ITO-freedom and advanced device concepts

The most commonly used transparent electrode in organic photovoltaics is based on indium-tin-oxide (ITO) which has the disadvantage of being rather expensive due to the scarcity of indium which is the main material in ITO by weight. In addition, the expanding market for optoelectronic devices could create a demand so high that securing a steady supply of indium might be problematic in the near future. This generates the need of new transparent semiconducting materials with good conductivity to minimize ohmic losses or new techniques/designs of devices. There has been relatively few reports on polymer solar cells that do not employ indium.<sup>200–208</sup> Of these, three are directly relevant to industrial manufacturing processes.<sup>200,201,208</sup> The wrap through concept is well known from 1<sup>st</sup> generation photovoltaics<sup>209</sup> and has later been demonstrated to work well for polymer solar cells,<sup>208</sup> and some of the ITO free polymer solar cell module concepts have been demonstrated to work in a full roll-to-roll process.<sup>200,201</sup> For the latter though, the performance was significantly lower than what could be obtained using ITO based flexible substrates in a similar roll-to-roll process as shown in Fig. 31.

An alternative approach to avoid the use of indium has been introduced by Niggemann *et al.*,<sup>210</sup> who report the fabrication of a novel architecture in organic photovoltaic devices without the use of transparent electrodes and with extremely high voltages. Built on substrates of transparent lamellar nanostructured polymer, devices consisting of series of interconnected elementary cells (up to 1390 cells/mm) are prepared (Fig. 32). Anodes and cathodes are deposited on the vertical walls of the lamellas by thermal evaporation of titanium or MoO<sub>3</sub> respectively from inclined incident angles, such that anode and cathode pairs of adjacent elementary cells are interconnected at the tip of the nanolamellae. The photoactive composite (P3HT/PCBM - 3:2) is then spincoated in the final process step.

In order to suppress interconnection of adjacent cell elements by the photoactive composite, a dielectric layer of lithium fluoride was furthermore deposited at an angle on the tip of the lamellae prior to spincoating. Under AM1.5 illumination, a 17.4 mm  $\times$  7.9 mm photovoltaic nanomodule prepared in this way generated an open circuit voltage of 880 V and a short circuit current of  $2 \times 10^{-8}$  A. The solar power conversion efficiency is stated to be 0.008% when considering a fill factor of 25%. The concept of *wrap through* was first introduced in 1993 by Gee *et al.*<sup>209</sup> for silicon based solar cells and have now been implemented in polymer based photovoltaics by Zimmermann *et al.*<sup>208</sup> in order to avoid the use of transparent electrodes. The general idea behind wrap trough is to have both electrodes on the back side of the device, one having a traditional layered contact with the light absorber, and the other being connected to the absorber through a series of holes/channels, leading through the device, that have been filled with a highly conducting material. The holes

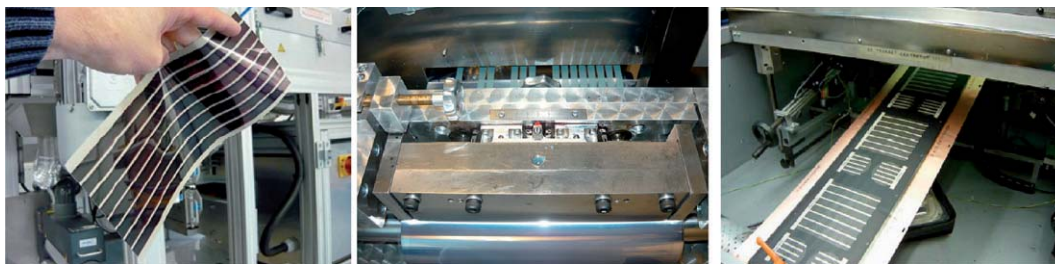


Fig. 31 Roll-to-roll coated polymer solar cells using an ITO based process (left) and ITO-free processes (middle and right).

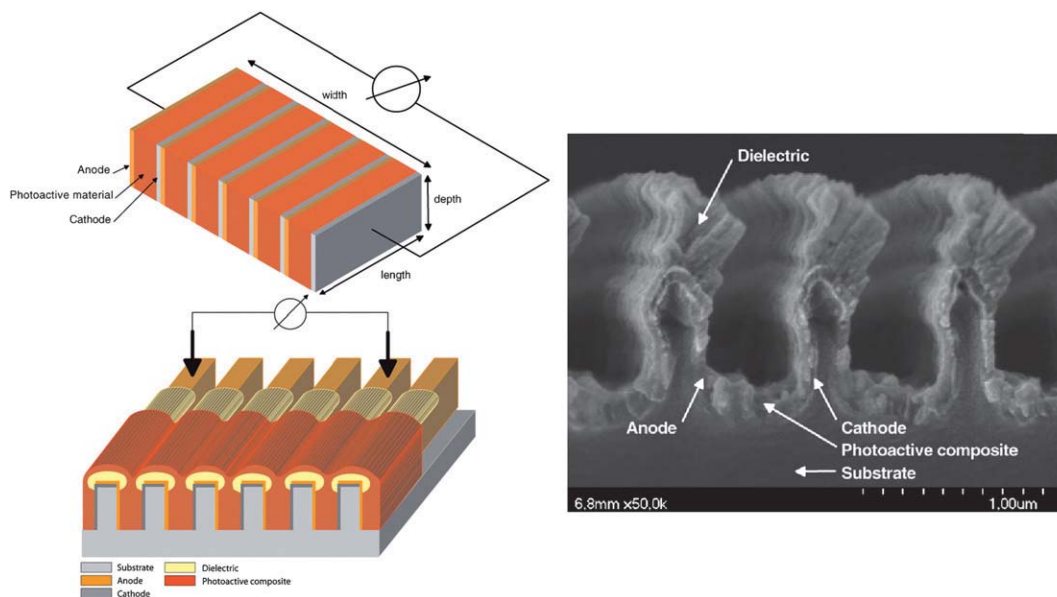


Fig. 32 High voltage devices. **Upper left:** Basic sketch of a series interconnected photovoltaic nanomodule. An elementary cell is represented by the photoactive volume sandwiched between an anode and a cathode. **Lower left:** Schematic drawing of the series interconnected photovoltaic nanomodule. Anodes and cathodes are deposited on the walls of the nanolamellae by evaporation from an inclined incident angle. The series interconnection of adjacent elementary cells is carried out by overlapping the electrodes at the tips of the lamellae. In order to suppress charge carrier recombination, the tips of the nanolamellae are coated with a dielectric layer. The electrical contact is provided *via* two contact tips positioned onto the metallised nanolamellae. **Right:** SEM cross-section of a photovoltaic nanomodule. The tips of the lamellae are coated with lithium fluoride by thermal evaporation under inclined incident angles. Reprinted with permission from ref. 210. © 2008 Wiley-VCH Verlag GmbH & Co. KGaA, Weinheim.

are placed in a pattern throughout the device that ensures good efficiency. The organic solar cell by Zimmermann *et al.* is built on a thin plastic substrate with inverted layer sequence, *i.e.* starting with the metallic electron contact. Then the active absorber layer is applied, followed by the PEDOT:PSS layer as shown in Fig. 33.

The holes/channels through the device are now created by perforation of the device with a hot needle followed by a second layer of PEDOT:PSS forming the wrap through contact. As the last step a metal (Au) back contact was evaporated thermally. Power conversion efficiencies of up to 2% were reached for parallel wrap through and 1.1% was reached for serial circuitry using simulated solar irradiation ( $1000 \text{ W/m}^2$ ).

## Summary and outlook

From a materials point of view, the state-of-the-art in the field of organic photovoltaics has for long been represented by bulk heterojunction solar cells based on P3HT and a fullerene. Power conversion efficiencies in the 4–5% range have been reported for

P3HT:PCBM devices,<sup>46–50</sup> but reproducibility has been difficult and average efficiencies are significantly lower than the highest reported. P3HT can only absorb light up to 650 nm, and this limited absorption of the available solar photons (up to 22.4%) has in recent years led several research teams to focus on preparation of low band gap polymers in order to be able to exploit a larger part of the solar spectrum. Recently new low band gap polymer:PCBM composites have shown device efficiencies close to and even exceeding that of P3HT:PCBM with plenty of room for improvement.<sup>56–58,192</sup>

Another trail deviating from the traditional P3HT:PCBM blends is the use of two different polymers to act as donor and acceptor in a polymer:polymer heterojunction. Although very little effort has been put into this area moderately good results have been achieved (~1.8%).<sup>69</sup> The advantages of a heterojunction consisting only of absorbing materials, allowing for absorption over a wider spectral range, together with the relative ease of tuning the donor–acceptor energy levels make the polymer:polymer solar cell a potential player in future research. Two major challenges will be the design of good n-type polymers and

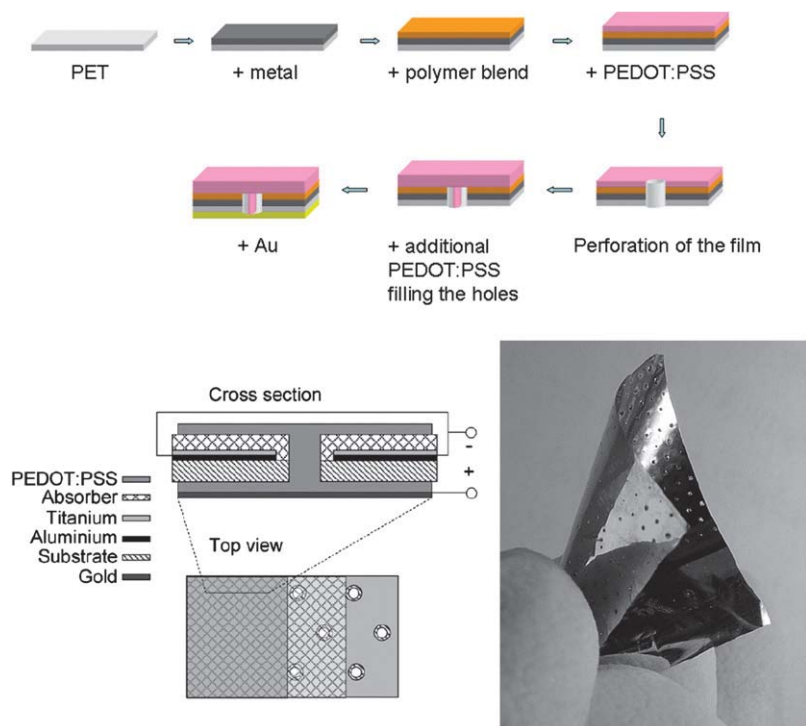


**Fig. 33** Wrap through cells. **Top and lower left:** Schematic representation of the inverted layer sequence starting with the metallic contact on the plastic substrate followed by the active polymer blend and PEDOT:PSS. After perforation of the film a second layer of PEDOT:PSS is applied forming the wrap through contact and a gold back electrode is applied to finish the circuitry. **Right:** Picture of a wrap through device. The two bottom representations are reprinted with permission from ref. 211. © 2007 Elsevier B. V.

dealing with the tendency for phase separation of the polymers into larger domains instead of into a fine interpenetrating network that allows for efficient charge separation and transport.

The use of precursor or thermocleavable sidechain routes also results in a higher concentration of the photoactive participant. Heat treatment of the device film results in chemical reactions whereby removal of part of the material (sometimes up to 50% or more by weight) that constitutes the original film is achieved. Thus formed conjugated polymers have no solubilising side-chains and are insoluble in all solvents which induce stability towards degradation and furthermore allows for preparation of multilayer devices by all solution processing.<sup>109</sup> Light cleavage using a near-infrared (NIR) dye that is either incorporated in the polymer film or employed as a separate layer on top of the polymer is a sophisticated form of dealing with thermocleavable materials which allows for patterning as thermocleavage only occurs in areas exposed to NIR light.<sup>114,115,199</sup> The non-exposed areas which are still soluble can subsequently be removed.

Multilayer devices (tandem cells) allow for use of several types of polymer that each absorb light at different regions of the solar spectrum and hence render the exploitation of the incoming light more effective. The main challenge when preparing all solution processed multilayer devices is to find a way to add a new layer without destroying the underlying layer. Besides the method of rendering the polymer insoluble this can be done by careful tuning of the solvents used for each layer so that the top layer is always insoluble in the solvent used next. PCEs of up to 6.5% have been reported by the latter method.<sup>192</sup> An alternative approach to the already mentioned is to use a reflective geometry

where the reflected light from one cell is directed towards another and *vice versa*. This again allows for the use of supplementary polymers that each absorbs light at different wavelengths.

With respect to methods trying to induce stability to the device the use of materials that can be cross-linked after film preparation and consequently a 'locking' of the morphology, should be mentioned. Limited research has been carried out within this area that has the potential of solving the problem of phase separation/aggregation that is observed for P3HT:PCBM devices upon thermal treatment. Finding ways to prepare highly cross-linked films would also make the process useful for multilayer devices.

Fabrication of hybrid solar cells is an area that has received quite a lot of attention with respect to device architecture trying to optimize charge separation and collection. Designs where the inorganic part of the heterojunction is represented as nanoparticles, are generated *in situ*, or as nanorod or -pore structures have been investigated and recently several reports of combining the traditional P3HT:PCBM setup with an inorganic into a 3-component heterojunction has been successful in improving the efficiencies compared with the corresponding P3HT:PCPM devices without the inorganic. Similar tendencies have been reported for heterojunctions of surface modified inorganics with different dyes, where the concentration of the dye is so small that its contribution to absorption is minimal to negligible. Instead the dye aids in charge separation and suppresses back recombination. The latter two examples are good indicators that combining techniques and thinking differently can lead to improvement.



The latest reports are dealing with the fact that indium, which is a major component in the most commonly used transparent electrodes (ITO), is a scarce and expensive element in a world market with a growing demand because of the development within optoelectronics. In order to approach this problem new device designs have been developed to function without ITO. High voltage devices yielding open circuit voltages up to 880 V,<sup>210</sup> introduction of the *wrap through* concept implemented for polymer based solar cells on thin flexible plastic substrates,<sup>208</sup> and some of the ITO free polymer solar cell module concepts have even been demonstrated to work in a full roll-to-roll process.<sup>200,201</sup> These new concepts still need optimization, but they are approaching relevant issues for industrial manufacturing processes.<sup>134,212</sup>

It is our opinion that, if the field of polymer solar cells is to advance to a degree where it finally succeeds in leaving the lab to go into actual production and enjoy widespread use, it will be necessary to deviate, in much larger extent than seen so far, from the tendency to just accept the flaws of the 'main road' in stead of trying to deal with them. Besides development of new device designs, new materials have to be developed. Tuning of donor-acceptor energy levels in polymer:polymer heterojunctions, in hybrid solar cells or a combination of both, attempts to minimize the amount of non-absorbing or -conducting material from the heterojunction as well as stabilising the same by use of thermocleavable materials are some of the paths where we see a large potential.

There is furthermore a need for more approaches to implement the laboratory small scale fabrication of devices into actual large scale production, in order to gain familiarity with the inevitable problems and challenges that are related to this. This will place demands on the materials properties such that they match relevant processes. This area is relatively new.

## Conclusion

Materials, processes and devices that deviate significantly from the standard approach, of rigid glass substrates, indium-tin-oxide electrodes, spincoated layers of conjugated polymer/fullerene mixtures and evaporated metal electrodes in a flat multilayer geometry, that is generally used in the preparation of polymer and organic solar cells, have been presented in this review. Advanced materials such as thermocleavable polymers, for higher level processing and stability, in combination with advanced device concepts like tandem cells and ITO free roll-to-roll coating. All have the potential to go beyond the current state-of-the-art towards real progress in terms of better performance, higher operational stability, facile processing and easier, faster and lower cost production.

## Acknowledgements

This work was supported by the Danish Strategic Research Council (DSF 2104-05-0052 and 2104-07-0022).

## References

- 1 T. Ameri, G. Dennler, C. Lungenschmied and C. J. Brabec, *Energy Environ. Sci.*, 2009, **2**, 347–363.
- 2 J. Bouclé, P. Ravirajan and J. Nelson, *J. Mater. Chem.*, 2007, **17**, 3141–3153.
- 3 C. J. Brabec, N. S. Sariciftci and J. C. Hummelen, *Adv. Funct. Mater.*, 2001, **11**, 15–26.
- 4 C. J. Brabec, J. A. Hauch, P. Schilinsky and C. Waldauf, *MRS Bull.*, 2005, **30**, 50–52.
- 5 C. J. Brabec and J. R. Durrant, *MRS Bull.*, 2008, **33**, 670–675.
- 6 E. Bundgaard and F. C. Krebs, *Sol. Energy Mater. Sol. Cells*, 2007, **91**, 954–985.
- 7 L. M. Chen, Z. R. Hong, G. Li and Y. Yang, *Adv. Mater.*, 2009, **21**, 1434–1449.
- 8 K. M. Coakley and M. D. McGehee, *Chem. Mater.*, 2004, **16**, 4533–4542.
- 9 K. M. Coakley, Y. X. Liu, C. Goh and M. D. McGehee, *MRS Bull.*, 2005, **30**, 37–40.
- 10 G. Dennler, M. C. Scharber and C. J. Brabec, *Adv. Mater.*, 2009, **21**, 1323–1338.
- 11 S. Günes, H. Neugebauer and N. S. Sariciftci, *Chem. Rev.*, 2007, **107**, 1324–1338.
- 12 S. Günes and N. S. Sariciftci, *Inorg. Chim. Acta*, 2008, **361**, 581–588.
- 13 A. Hadipour, B. De Boer and P. W. M. Blom, *Org. Electron.*, 2008, **9**, 617–624.
- 14 A. Hadipour, B. De Boer and P. W. M. Blom, *Adv. Funct. Mater.*, 2008, **18**, 169–181.
- 15 H. Hoppe and N. S. Sariciftci, *J. Mater. Res.*, 2004, **19**, 1924–1945.
- 16 R. A. J. Janssen, J. C. Hummelen and N. S. Sariciftci, *MRS Bull.*, 2005, **30**, 33–36.
- 17 M. Jørgensen, K. Norrman and F. C. Krebs, *Sol. Energy Mater. Sol. Cells*, 2008, **92**, 686–714.
- 18 B. Kippelen and J. L. Bredas, *Energy Environ. Sci.*, 2009, **2**, 251–261.
- 19 F. C. Krebs, *Refocus*, 2005, **6**, 38–39.
- 20 R. Kroon, M. Lenes, J. C. Hummelen, P. W. M. Blom and B. De Boer, *Polym. Rev.*, 2008, **48**, 531–582.
- 21 M. T. Lloyd, J. E. Anthony and G. G. Malliaras, *Mater. Today*, 2007, **10**, 34–41.
- 22 A. C. Mayer, S. R. Scully, B. E. Hardin, M. W. Rowell and M. D. McGehee, *Mater. Today*, 2007, **10**, 28–33.
- 23 B. P. Rand, J. Genoe, P. Heremans and J. Poortmans, *Prog. Photovolt.: Res. Appl.*, 2007, **15**, 659–676.
- 24 H. Spanggaard and F. C. Krebs, *Sol. Energy Mater. Sol. Cells*, 2004, **83**, 125–146.
- 25 B. C. Thompson and J. M. J. Frechet, *Angew. Chem., Int. Ed.*, 2008, **47**, 58–77.
- 26 C. Winder and N. S. Sariciftci, *J. Mater. Chem.*, 2004, **14**, 1077–1086.
- 27 J. Wood (Ed.), *Mater. Today*, 2007, **10**, pp. 1–50.
- 28 S. E. Shaheen, D. S. Ginley, and G. E. Jabbour (Guest Eds.), *MRS Bull.*, 2005, **30**, pp. 10–52.
- 29 J. Poortmans (Guest Ed.), *Prog. Photovolt.*, 2007, **15**, pp. 657–754.
- 30 F. C. Krebs (Guest Ed.), *Sol. Energy Mater.*, 2004, **83**, pp. 125–321.
- 31 F. C. Krebs (Guest Ed.), *Sol. Energy Mater.*, 2007, **91**, pp. 953–1036.
- 32 F. C. Krebs (Guest Ed.), *Sol. Energy Mater.*, 2008, **92**, pp. 685–820.
- 33 F. C. Krebs (Guest Ed.), *Sol. Energy Mater.*, 2009, **93**, pp. 393–538.
- 34 *Organic Photovoltaics: Concepts and Realization*, ed. Brabec, C. J., Dyakonov, V., and Parisi, J., Springer, New York, 2003.
- 35 *Organic Photovoltaics: Mechanisms, Materials and Devices*, ed. Sun, S. S. and Sariciftci, N. S., CRC Press, Taylor & Francis Group, Florida, USA, 2005.
- 36 *Nanostructured Materials for Solar Energy Conversion*, ed. Soga, T., Elsevier, UK, 2006.
- 37 *Polymer Photovoltaics: A Practical Approach*, ed. Krebs, F. C., SPIE Press, Bellingham, 2008.
- 38 *Organic Photovoltaics: Materials, Device Physics and Manufacturing Technologies*, ed. Brabec, C. J., Scherf, U., and Dyakonov, V., Wiley-VCH, Weinheim, 2008.
- 39 N. S. Sariciftci, L. Smilowitz, A. J. Heeger and F. Wudl, *Science*, 1992, **258**, 1474–1476.
- 40 G. Yu, J. Gao, J. C. Hummelen, F. Wudl and A. J. Heeger, *Science*, 1995, **270**, 1789–1791.
- 41 Shawn R. Scully and Michael D. McGehee, *J. Appl. Phys.*, 2006, **100**, 034907.
- 42 D. E. Markov, J. C. Hummelen, P. W. M. Blom and A. B. Sieval, *Phys. Rev. B: Condens. Matter Mater. Phys.*, 2005, **72**, 045216.
- 43 P. Peumans, A. Yakimov and S. R. Forrest, *J. Appl. Phys.*, 2003, **93**, 3693–3723.
- 44 O. Douheret, A. Swinnen, S. Bertho, I. Haeldermans, J. D'Haen, M. D'Olieslaeger, D. Vanderzande and J. V. Manca, *Prog. Photovolt.: Res. Appl.*, 2007, **15**, 713–726.

- 45 B. V. Andersson, A. Herland, S. Masich and O. Inganas, *Nano Lett.*, 2009, **9**, 853–855.
- 46 C. J. Ko, Y. K. Lin, F. C. Chen and C. W. Chu, *Appl. Phys. Lett.*, 2007, **90**, 063509.
- 47 G. Li, V. Shrotriya, J. S. Huang, Y. Yao, T. Moriarty, K. Emery and Y. Yang, *Nat. Mater.*, 2005, **4**, 864–868.
- 48 W. L. Ma, C. Y. Yang, X. Gong, K. Lee and A. J. Heeger, *Adv. Funct. Mater.*, 2005, **15**, 1617–1622.
- 49 M. Reyes-Reyes, K. Kim and D. L. Carroll, *Appl. Phys. Lett.*, 2005, **87**, 083506–3.
- 50 M. Reyes-Reyes, K. Kim, J. Dewald, R. Lopez-Sandoval, A. Avadhanula, S. Curran and D. L. Carroll, *Org. Lett.*, 2005, **7**, 5749–5752.
- 51 G. Dennler, *Mater. Today*, 2007, **10**, 56.
- 52 J. Gilot, M. M. Wienk and R. A. J. Janssen, *Nat. Mater.*, 2007, **6**, 704.
- 53 M. K. Riede, T. Mueller, B. Maennig, K. Leo, K. O. Sylvester-Hvid, B. Zimmermann, M. Niggemann and A. Gombert, *Appl. Phys. Lett.*, 2008, **92**, 076101.
- 54 G. P. Smestad, F. C. Krebs, C. M. Lampert, C. G. Granqvist, K. L. Chopra, X. Mathew and H. Takakura, *Sol. Energy Mater. Sol. Cells*, 2008, **92**, 371–373.
- 55 H. A. M. van Müllekom, J. A. J. M. Vekemans, E. E. Havinga and E. W. Meijer, *Mater. Sci. Eng., R*, 2001, **32**, 1–40.
- 56 J. H. Hou, H. Y. Chen, S. Q. Zhang, G. Li and Y. Yang, *J. Am. Chem. Soc.*, 2008, **130**, 16144.
- 57 Y. Y. Liang, D. Q. Feng, Y. Wu, S. T. Tsai, G. Li, C. Ray and L. P. Yu, *J. Am. Chem. Soc.*, 2009, **131**, 7792–7799.
- 58 J. Peet, J. Y. Kim, N. E. Coates, W. L. Ma, D. Moses, A. J. Heeger and G. C. Bazan, *Nat. Mater.*, 2007, **6**, 497–500.
- 59 Z. Zhu, D. Waller, R. Gaudiana, M. Morana, D. Muhlbacher, M. Scharber and C. Brabec, *Macromolecules*, 2007, **40**, 1981–1986.
- 60 S. R. Forrest, *MRS Bull.*, 2005, **30**, 28–32.
- 61 L. J. A. Koster, V. D. Mihailetschi and P. W. M. Blom, *Appl. Phys. Lett.*, 2006, **88**, 093511.
- 62 M. C. Scharber, D. Wuhlbacher, M. Koppe, P. Denk, C. Waldauf, A. J. Heeger and C. L. Brabec, *Adv. Mater.*, 2006, **18**, 789.
- 63 S. H. Park, A. Roy, S. Beaupre, S. Cho, N. Coates, J. S. Moon, D. Moses, M. Leclerc, K. Lee and A. J. Heeger, *Nat. Photonics*, 2009, **3**, 297–302.
- 64 N. Blouin, A. Michaud, D. Gendron, S. Wakim, E. Blair, R. Neagu-Plesu, M. Belletete, G. Durocher, Y. Tao and M. Leclerc, *J. Am. Chem. Soc.*, 2008, **130**, 732–742.
- 65 J. H. Hou, M. H. Park, S. Q. Zhang, Y. Yao, L. M. Chen, J. H. Li and Y. Yang, *Macromolecules*, 2008, **41**, 6012–6018.
- 66 F. B. Kooistra, J. Knol, F. Kastenberg, L. M. Popescu, W. J. H. Verhees, J. M. Kroon and J. C. Hummelen, *Org. Lett.*, 2007, **9**, 551–554.
- 67 J. J. M. Halls, C. A. Walsh, N. C. Greenham, E. A. Marseglia, R. H. Friend, S. C. Moratti and A. B. Holmes, *Nature*, 1995, **376**, 498–500.
- 68 G. Yu and A. J. Heeger, *J. Appl. Phys.*, 1995, **78**, 4510–4515.
- 69 C. R. McNeill, A. Abrusci, J. Zaumseil, R. Wilson, M. J. McKiernan, J. H. Burroughes, J. J. M. Halls, N. C. Greenham and R. H. Friend, *Appl. Phys. Lett.*, 2007, **90**, 193506.
- 70 M. M. Wienk, J. M. Kroon, W. J. H. Verhees, J. Knol, J. C. Hummelen, P. A. van Hal and R. A. J. Janssen, *Angew. Chem., Int. Ed.*, 2003, **42**, 3371–3375.
- 71 M. Granstrom, K. Petritsch, A. C. Arias, A. Lux, M. R. Andersson and R. H. Friend, *Nature*, 1998, **395**, 257–260.
- 72 T. Kietzke, H. H. Horhold and D. Neher, *Chem. Mater.*, 2005, **17**, 6532–6537.
- 73 M. M. Koetse, J. Sweelssen, K. T. Hoekerd, H. F. M. Schoo, S. C. Veenstra, J. M. Kroon, X. N. Yang and J. Loos, *Appl. Phys. Lett.*, 2006, **88**, 083504.
- 74 R. A. Wessling, *J. Pol. Sci. - Pol. Symp.*, 1985, 55–66.
- 75 D. R. Gagnon, J. D. Capistran, F. E. Karasz, R. W. Lenz and S. Antoun, *Polymer*, 1987, **28**, 567–573.
- 76 R. W. Lenz, C. C. Han, J. Stengersmith and F. E. Karasz, *J. Polym. Sci., Part A: Polym. Chem.*, 1988, **26**, 3241–3249.
- 77 R. O. Garay, B. Mayer, F. E. Karasz and R. W. Lenz, *J. Polym. Sci., Part A: Polym. Chem.*, 1995, **33**, 525–531.
- 78 W. J. Feast and J. N. Winter, *J. Chem. Soc., Chem. Commun.*, 1985, 202–203.
- 79 D. C. Bott, C. S. Brown, C. K. Chai, N. S. Walker, W. J. Feast, P. J. S. Foot, P. D. Calvert, N. C. Billingham and R. H. Friend, *Synth. Met.*, 1986, **14**, 245–269.
- 80 A. Furlani, C. Napoletano, M. V. Russo and W. J. Feast, *Polym. Bull.*, 1986, **16**.
- 81 H. G. Gilch and W. L. Wheelwri, *J. Polym. Sci., Part A-1*, 1966, **4**, 1337–1347.
- 82 H. Spreitzer, H. Becker, E. Kluge, W. Kreuder, H. Schenk, R. Demandt and H. Schoo, *Adv. Mater.*, 1998, **10**, 1340–1343.
- 83 F. Louwet, D. Vanderzande, J. Gelan and J. Mullens, *Macromolecules*, 1995, **28**, 1330–1331.
- 84 F. Louwet, D. Vanderzande and J. Gelan, *Synth. Met.*, 1995, **69**, 509–510.
- 85 F. Louwet, D. Vanderzande and J. Gelan, *Synth. Met.*, 1992, **52**, 125–130.
- 86 T. A. Chen and R. D. Rieke, *J. Am. Chem. Soc.*, 1992, **114**, 10087–10088.
- 87 T. A. Chen, X. M. Wu and R. D. Rieke, *J. Am. Chem. Soc.*, 1995, **117**, 2313–244.
- 88 R. D. McCullough, R. D. Lowe, M. Jayaraman and D. L. Anderson, *J. Org. Chem.*, 1993, **58**, 904–912.
- 89 F. C. Krebs, R. B. Nyberg and M. Jørgensen, *Chem. Mater.*, 2004, **16**, 1313–1318.
- 90 K. T. Nielsen, K. Bechgaard and F. C. Krebs, *Macromolecules*, 2005, **38**, 658–659.
- 91 K. T. Nielsen, K. Bechgaard and F. C. Krebs, *Synthesis*, 2006, 1639–1644.
- 92 K. T. Nielsen, P. Harris, K. Bechgaard and F. C. Krebs, *Acta Crystallogr.*, 2007, **B-63**, 151–156.
- 93 F. C. Krebs and H. Spanggaard, *Chem. Mater.*, 2005, **17**, 5235–5237.
- 94 F. C. Krebs and K. Norrman, *Progr. Photovolt.: Res. Appl.*, 2007, **15**, 697–712.
- 95 K. Norrman, J. Alstrup, M. Jørgensen, M. Lira-Cantu, N. B. Larsen and F. C. Krebs, *Organic Photovoltaics VII*, 2006, **6334**, U100–U111.
- 96 K. Norrman and F. C. Krebs, *Sol. Energy Mater.*, 23-1-2006, **90**, 213–227.
- 97 M. Bjerring, J. S. Nielsen, A. Siu, N. C. Nielsen and F. C. Krebs, *Sol. Energy Mater. Sol. Cells*, 2008, **92**, 772–784.
- 98 M. Bjerring, J. S. Nielsen, N. C. Nielsen and F. C. Krebs, *Macromolecules*, 2007, **40**, 6012–6013.
- 99 S. A. Gevorgyan and F. C. Krebs, *Chem. Mater.*, 2008, **20**, 4386–4390.
- 100 J. S. Liu, E. N. Kadnikova, Y. X. Liu, M. D. McGehee and J. M. J. Frechet, *J. Am. Chem. Soc.*, 2004, **126**, 9486–9487.
- 101 F. Banishoeib, P. Adriaenssens, S. Berson, S. Guillerez, O. Douheret, J. Manca, S. Fourier, T. J. Cleij, L. Lutsen and D. Vanderzande, *Sol. Energy Mater. Sol. Cells*, 2007, **91**, 1026–1034.
- 102 F. Banishoeib, A. Henckens, S. Fourier, G. Vanhooyland, M. Breselge, J. Manca, T. J. Cleij, L. Lutsen, D. Vanderzande, L. H. Nguyen, H. Neugebauer and N. S. Sariciftci, *Thin Solid Films*, 2008, **516**, 3978–3988.
- 103 C. Girotto, D. Cheynts, T. Aernouts, F. Banishoeib, L. Lutsen, T. J. Cleij, D. Vanderzande, J. Genoe, J. Poortman and P. Heremans, *Org. Electron.*, 2008, **9**, 740–746.
- 104 A. Henckens, K. Colladet, S. Fourier, T. J. Cleij, L. Lutsen, J. Gelan and D. Vanderzande, *Macromolecules*, 2005, **38**, 19–26.
- 105 L. H. Nguyen, S. Gunes, H. Neugebauer, N. S. Sariciftci, F. Banishoeib, A. Henckens, T. Cleij, L. Lutsen and D. Vanderzande, *Sol. Energy Mater. Sol. Cells*, 2006, **90**, 2815–2828.
- 106 F. Padinger, T. Fromherz, P. Denk, C. J. Brabec, J. Zettner, T. Hierl and N. S. Sariciftci, *Synth. Met.*, 2001, **121**, 1605–1606.
- 107 R. D. Scurlock, B. J. Wang, P. R. Ogilby, J. R. Sheats and R. L. Clough, *J. Am. Chem. Soc.*, 1995, **117**, 10194–10202.
- 108 M. H. Petersen, S. A. Gevorgyan and F. C. Krebs, *Macromolecules*, 2008, **41**, 8986–8994.
- 109 O. Hagemann, M. Bjerring, N. C. Nielsen and F. C. Krebs, *Sol. Energy Mater. Sol. Cells*, 2008, **92**, 1327–1335.
- 110 C. Edder, P. B. Armstrong, K. B. Prado and J. M. J. Frechet, *Chem. Commun.*, 2006, 1965–1967.
- 111 G. A. Power, P. Hodge and N. B. McKeown, *Chem. Commun.*, 1996, 655–656.
- 112 J. H. Edwards, W. J. Feast and D. C. Bott, *Polymer*, 1984, **25**, 395–398.
- 113 J. F. Yu and S. Holdcroft, *Macromolecules*, 2000, **33**, 5073–5079.

- 114 X. Han, X. W. Chen and S. Holdcroft, *Adv. Mater.*, 2007, **19**, 1697–1702.
- 115 T. J. Gordon, G. Vamvounis and S. Holdcroft, *Adv. Mater.*, 2008, **20**, 2486–2490.
- 116 J. H. Burroughes, D. D. C. Bradley, A. R. Brown, R. N. Marks, K. Mackay, R. H. Friend, P. L. Burns and A. B. Holmes, *Nature*, 1990, **347**, 539–541.
- 117 S. Bertho, I. Haelderms, A. Swinnen, W. Moons, T. Martens, L. Lutsen, D. Vanderzande, J. Manca, A. Senes and A. Bonfiglio, *Sol. Energy Mater. Sol. Cells*, 2007, **91**, 385–389.
- 118 S. Bertho, G. Janssen, T. J. Cleij, B. Conings, W. Moons, A. Gadisa, J. D'Haen, E. Goovaerts, L. Lutsen, J. Manca and D. Vanderzande, *Sol. Energy Mater. Sol. Cells*, 2008, **92**, 753–760.
- 119 K. Sivula, C. K. Luscombe, B. C. Thompson and J. M. J. Frechet, *J. Am. Chem. Soc.*, 2006, **128**, 13988–13989.
- 120 K. Sivula, Z. T. Ball, N. Watanabe and J. M. J. Frechet, *Adv. Mater.*, 2006, **18**, 206.
- 121 C. H. Woo, B. C. Thompson, B. J. Kim, M. F. Toney and M. J. Frechet, *J. Am. Chem. Soc.*, 2008, **130**, 16324–16329.
- 122 M. Drees, H. Hoppe, C. Winder, H. Neugebauer, N. S. Sariciftci, W. Schwinger, F. Schaffler, C. Topf, M. C. Scharber, Z. G. Zhu and R. Gaudiana, *J. Mater. Chem.*, 2005, **15**, 5158–5163.
- 123 Z. Zhu, S. Hadjikyriacou, D. Waller and R. Gaudiana, *J. Macromol. Sci., Part A: Pure Appl. Chem.*, 2004, **41**, 1467–1487.
- 124 S. Miyaniishi, K. Tajima and K. Hashimoto, *Macromolecules*, 2009, **42**, 1610–1618.
- 125 L. D. Bozano, K. R. Carter, V. Y. Lee, R. D. Miller, R. DiPietro and J. C. Scott, *J. Appl. Phys.*, 2003, **94**, 3061–3068.
- 126 Y. N. Li, J. F. Ding, M. Day, Y. Tao, J. P. Lu and M. D'orio, *Chem. Mater.*, 2003, **15**, 4936–4943.
- 127 C. D. Müller, A. Falcou, N. Reckefuss, M. Rojahn, V. Wiederhorn, P. Rudati, H. Frohne, O. Nuyken, H. Becker and K. Meerholz, *Nature*, 2003, **421**, 829–833.
- 128 G. L. Wu, C. H. Yang, B. H. Fan, B. Zhang, X. M. Chen and Y. F. Li, *J. Appl. Polym. Sci.*, 2006, **100**, 2336–2342.
- 129 H. Yan, P. Lee, N. R. Armstrong, A. Graham, G. A. Evmenenko, P. Dutta and T. J. Marks, *J. Am. Chem. Soc.*, 2005, **127**, 3172–3183.
- 130 H. Yan, M. H. Yoon, A. Facchetti and T. J. Marks, *Appl. Phys. Lett.*, 2005, **87**, 183501–1.
- 131 C. H. Yang, J. H. Hou, B. Zhang, S. Q. Zhang, C. He, H. Fang, Y. Q. Ding, J. P. Ye and Y. F. Li, *Macromol. Chem. Phys.*, 2005, **206**, 1311–1318.
- 132 M. Jørgensen, O. Hagemann, J. Alstrup and F. C. Krebs, *Sol. Energy Mater. Sol. Cells*, 2009, **93**, 413–421.
- 133 F. C. Krebs and M. Jørgensen, WO, 2007118850, 2007.
- 134 F. C. Krebs, M. Jørgensen, K. Norrman, O. Hagemann, J. Alstrup, T. D. Nielsen, J. Fyenbo, K. Larsen and J. Kristensen, *Sol. Energy Mater. Sol. Cells*, 2009, **93**, 422–441.
- 135 F. C. Krebs, *Sol. Energy Mater. Sol. Cells*, 2009, **93**, 465–475.
- 136 E. Itoh, Y. Takamizawa and K. Miyairi, *Jpn. J. Appl. Phys.*, 2008, **47**, 509–512.
- 137 S. S. Kim, J. Jo, C. Chun, J. C. Hong and D. Y. Kim, *J. Photochem. Photobiol., A*, 2007, **188**, 364–370.
- 138 N. Kudo, S. Honda, Y. Shimazaki, H. Ohkita, S. Ito and H. Benten, *Appl. Phys. Lett.*, 2007, **90**, 183513.
- 139 C. Y. Kuo, W. C. Tang, C. Gau, T. F. Guo and D. Z. Jeng, *Appl. Phys. Lett.*, 2008, **93**, 033307.
- 140 Y. Y. Lin, T. H. Chu, C. W. Chen and W. F. Su, *Appl. Phys. Lett.*, 2008, **92**, 053312.
- 141 Y. Y. Lin, T. H. Chu, S. S. Li, C. H. Chuang, C. H. Chang, W. F. Su, C. P. Chang, M. W. Chu and C. W. Chen, *J. Am. Chem. Soc.*, 2009, **131**, 3644–3649.
- 142 M. C. Wu, C. H. Chang, H. H. Lo, Y. S. Lin, Y. Y. Lin, W. C. Yen, W. F. Su, Y. F. Chen and C. W. Chen, *J. Mater. Chem.*, 2008, **18**, 4097–4102.
- 143 Ming-Chung Wu, Hsueh-Chung Liao, Hsi-Hsing Lo, Sharon Chen, Yun-Yue Lin, Wei-Che Yen, Tsung-Wei Zeng, Chun-Wei Chen, Yang-Fang Chen and Wei-Fang Su, *Sol. Energy Mater. Sol. Cells*, 2009, **93**, 961–965.
- 144 Tsung-Wei Zeng, Hsi-Hsing Lo, Chia-Hao Chang, Yun-Yue Lin, Chun-Wei Chen and Wei-Fang Su, *Sol. Energy Mater. Sol. Cells*, 2009, **93**, 952–957.
- 145 R. Zhu, C. Y. Jiang, X. Z. Liu, B. Liu, A. Kumar and S. Ramakrishna, *Appl. Phys. Lett.*, 2008, **93**, 013102.
- 146 W. J. E. Beek, M. M. Wienk and R. A. J. Janssen, *Adv. Mater.*, 2004, **16**, 1009–1013.
- 147 W. J. E. Beek, L. H. Slooff, M. M. Wienk, J. M. Kroon and R. A. J. Janssen, *Adv. Funct. Mater.*, 2005, **15**, 1703–1707.
- 148 Y. Y. Lin, C. W. Chen, T. H. Chu, W. F. Su, C. C. Lin, C. H. Ku, J. J. Wu and C. H. Chen, *J. Mater. Chem.*, 2007, **17**, 4571–4576.
- 149 Y. Y. Lin, Y. Y. Lee, L. W. Chang, J. J. Wu and C. W. Chen, *Appl. Phys. Lett.*, 2009, **94**, 063308.
- 150 D. J. D. Moet, L. J. A. Koster, B. De Boer and P. W. M. Blom, *Chem. Mater.*, 2007, **19**, 5856–5861.
- 151 D. C. Olson, J. Pirus, R. T. Collins, S. E. Shaheen and D. S. Ginley, *Thin Solid Films*, 2006, **496**, 26–29.
- 152 D. C. Olson, S. E. Shaheen, R. T. Collins and D. S. Ginley, *J. Phys. Chem. C*, 2007, **111**, 16670–16678.
- 153 K. Takanezawa, K. Hirota, Q. S. Wei, K. Tajima and K. Hashimoto, *J. Phys. Chem. C*, 2007, **111**, 7218–7223.
- 154 K. Takanezawa, K. Tajima and K. Hashimoto, *Appl. Phys. Lett.*, 2008, **93**, 063308.
- 155 R. Thitima, C. Patcharee, S. Takashi and Y. Susumu, *Solid-State Electron.*, 2009, **53**, 176–180.
- 156 H. M. P. Wong, P. Wang, A. Abruci, M. Svensson, M. R. Andersson and N. C. Greenham, *J. Phys. Chem. C*, 2007, **111**, 5244–5249.
- 157 F. C. Krebs, *Sol. Energy Mater. Sol. Cells*, 2008, **92**, 715–726.
- 158 F. C. Krebs, Y. Thomann, R. Thomann and J. W. Andreasen, *Nanotechnology*, 2008, **19**, 424013.
- 159 I. Gur, N. A. Fromer, C. P. Chen, A. G. Kanaras and A. P. Alivisatos, *Nano Lett.*, 2007, **7**, 409–414.
- 160 W. U. Huynh, J. J. Dittmer and A. P. Alivisatos, *Science*, 2002, **295**, 2425–2427.
- 161 B. Q. Sun, E. Marx and N. C. Greenham, *Nano Lett.*, 2003, **3**, 961–963.
- 162 B. Q. Sun, H. J. Snaith, A. S. Dhoot, S. Westenhoff and N. C. Greenham, *J. Appl. Phys.*, 2005, **97**, 014914.
- 163 B. Q. Sun and N. C. Greenham, *Phys. Chem. Chem. Phys.*, 2006, **8**, 3557–3560.
- 164 P. Wang, A. Abruci, H. M. P. Wong, M. Svensson, M. R. Andersson and N. C. Greenham, *Nano Lett.*, 2006, **6**, 1789–1793.
- 165 W. Lee, S. Shin, S. H. Han and B. W. Cho, *Appl. Phys. Lett.*, 2008, **92**, 193307.
- 166 L. Wang, Y. S. Liu, X. Jiang, D. H. Qin and Y. Cao, *J. Phys. Chem. C*, 2007, **111**, 9538–9542.
- 167 A. A. R. Watt, D. Blake, J. H. Warner, E. A. Thomsen, E. L. Tavenner, H. Rubinsztein-Dunlop and P. Meredith, *J. Phys. D: Appl. Phys.*, 2005, **38**, 2006–2012.
- 168 D. H. Cui, J. Xu, T. Zhu, G. Paradee, S. Ashok and M. Gerhold, *Appl. Phys. Lett.*, 2006, **88**, 183111.
- 169 N. Kudo, Y. Shimazaki, H. Ohkita, M. Ohoka and S. Ito, *Sol. Energy Mater. Sol. Cells*, 2007, **91**, 1243–1247.
- 170 J. S. Huang, C. Y. Hsiao, S. J. Syu, J. J. Chao and C. F. Lin, *Sol. Energy Mater. Sol. Cells*, 2009, **93**, 621–624.
- 171 C. Y. Liu, Z. C. Holman and U. R. Kortshagen, *Nano Lett.*, 2009, **9**, 449–452.
- 172 N. C. Greenham, X. G. Peng and A. P. Alivisatos, *Phys. Rev. B: Condens. Matter Mater. Phys.*, 1996, **54**, 17628–17637.
- 173 B. R. Saunders and M. L. Turner, *Adv. Colloid Interface Sci.*, 2008, **138**, 1–23.
- 174 P. A. van Hal, M. M. Wienk, J. M. Kroon, W. J. H. Verhees, L. H. Slooff, W. J. H. van Gennip, P. Jonkheijm and R. A. J. Janssen, *Adv. Mater.*, 2003, **15**, 118.
- 175 L. H. Slooff, M. M. Wienk and J. M. Kroon, *Thin Solid Films*, 2004, **451–452**, 634–638.
- 176 M. Okuya, K. Nakade and S. Kaneko, *Sol. Energy Mater. Sol. Cells*, 2002, **70**, 425–435.
- 177 K. M. Coakley and M. D. McGehee, *Appl. Phys. Lett.*, 2003, **83**, 3380–3382.
- 178 C. Goh, K. M. Coakley and M. D. McGehee, *Nano Lett.*, 2005, **5**, 1545–1549.
- 179 V. Gowrishankar, N. Miller, M. D. McGehee, M. J. Misner, D. Y. Ryu, T. P. Russell, E. Drockenmuller and C. J. Hawker, *Thin Solid Films*, 2006, **513**, 289–294.
- 180 G. K. Mor, O. K. Varghese, M. Paulose, K. Shankar and C. A. Grimes, *Sol. Energy Mater. Sol. Cells*, 2006, **90**, 2011–2075.
- 181 P. Ravirajan, A. M. Peiro, M. K. Nazeeruddin, M. Graetzel, D. D. C. Bradley, J. R. Durrant and J. Nelson, *J. Phys. Chem. B*, 2006, **110**, 7635–7639.



- 182 D. Cheyns, H. Gommans, M. Odijk, J. Poortmans and P. Heremans, *Sol. Energy Mater. Sol. Cells*, 2007, **91**, 399–404.
- 183 B. P. Rand, P. Peumans and S. R. Forrest, *J. Appl. Phys.*, 2004, **96**, 7519–7526.
- 184 J. Xue, S. Uchida, B. P. Rand and S. R. Forrest, *Appl. Phys. Lett.*, 2004, **84**, 3013–3015.
- 185 J. Xue, S. Uchida, B. P. Rand and S. R. Forrest, *Appl. Phys. Lett.*, 2004, **85**, 5757–5759.
- 186 A. Yakimov and S. R. Forrest, *Appl. Phys. Lett.*, 2002, **80**, 1667.
- 187 A. Colsmann, J. Junge, C. Kayser and U. Lemmer, *Appl. Phys. Lett.*, 2006, **89**, 203506.
- 188 G. Dennler, H. J. Prall, R. Koeppe, M. Egginger, R. Autengruber and N. S. Sariciftci, *Appl. Phys. Lett.*, 2006, **89**, 073502.
- 189 A. Hadipour, B. De Boer, J. Wildeman, F. B. Kooistra, J. C. Hummelen, M. G. R. Turbiez, M. M. Wienk, R. A. J. Janssen and P. W. M. Blom, *Adv. Funct. Mater.*, 2006, **16**, 1897–1903.
- 190 H. J. Prall, R. Koeppe, R. Autengruber, M. Egginger, D. Dennler, and N. S. Sariciftci, *From Evaporation to Solution Processed Organic Tandem Solar Cells*, Gombert, Andreas, Strasbourg, France, 21–4–2006.
- 191 J. Gilot, M. M. Wienk and R. A. J. Janssen, *Appl. Phys. Lett.*, 2007, **90**, 143512–143513.
- 192 J. Y. Kim, K. Lee, N. E. Coates, D. Moses, T. Q. Nguyen, M. Dante and A. J. Heeger, *Science*, 2007, **317**, 222–225.
- 193 J. Y. Kim, S. H. Kim, H. H. Lee, K. Lee, W. L. Ma, X. Gong and A. J. Heeger, *Adv. Mater.*, 2006, **18**, 572–576.
- 194 V. Andersson, K. Tvingstedt and O. Inganas, *J. Appl. Phys.*, 2008, **103**, 094520.
- 195 S. B. Rim, S. Zhao, S. R. Scully, M. D. McGehee and P. Peumans, *Appl. Phys. Lett.*, 2007, **91**, 243501.
- 196 K. Tvingstedt, V. Andersson, F. Zhang and O. Inganas, *Appl. Phys. Lett.*, 2007, **91**, 123514–3.
- 197 Y. H. Zhou, F. L. Zhang, K. Tvingstedt, W. J. Tian and O. Inganas, *Appl. Phys. Lett.*, 2008, **93**, 033302.
- 198 J. W. Andreasen, M. Jørgensen and F. C. Krebs, *Macromolecules*, 2007, **40**, 7758–7762.
- 199 T. J. Gordon, J. F. Yu, C. Yang and S. Holdcroft, *Chem. Mater.*, 2007, **19**, 2155–2161.
- 200 F. C. Krebs, *Org. Electron.*, 2009, **10**, 761–768.
- 201 F. C. Krebs, *Sol. Energy Mater.*, 2009, **93**, 1636–1641.
- 202 T. Aernouts, P. Vanlaeke, W. Geens, J. Poortmans, P. Heremans, S. Borghs, R. Mertens, R. Andriessen and L. Leenders, *Thin Solid Films*, 2004, **451–452**, 22–25.
- 203 A. Gadisa, K. Tvingstedt, S. Admassie, L. Lindell, X. Crispin, M. R. Andersson, W. R. Salaneck and O. Inganas, *Synth. Met.*, 2006, **156**, 1102–1107.
- 204 J. Y. Lee, S. T. Connor, Y. Cui and P. Peumans, *Nano Lett.*, 2008, **8**, 689–692.
- 205 M. Strange, D. Plackett, M. Kaasgaard and F. C. Krebs, *Sol. Energy Mater. Sol. Cells*, 2008, **92**, 805–813.
- 206 K. Tvingstedt and O. Inganas, *Adv. Mater.*, 2007, **19**, 2893–2897.
- 207 B. Winther-Jensen and F. C. Krebs, *Sol. Energy Mater. Sol. Cells*, 2006, **90**, 123–132.
- 208 B. Zimmermann, M. Glatthaar, M. Niggemann, M. K. Riede, A. Hinsch and A. Gombert, *Sol. Energy Mater. Sol. Cells*, 2007, **91**, 374–378.
- 209 J. M. Gee, W. K. Schubert, and P. A. Basore, *Photovoltaic Specialists Conference, Conference Record of the Twenty Third IEEE*, 1993, 265–270.
- 210 M. Niggemann, W. Graf and A. Gombert, *Adv. Mater.*, 2008, **20**, 4055.
- 211 M. Niggemann, B. Zimmermann, J. Haschke, M. Glatthaar and A. Gombert, *Thin Solid Films*, 2008, **516**, 7181–7187.
- 212 F. C. Krebs, S. A. Gevorgyan and J. Astrup, *J. Mater. Chem.*, 2009, **19**, 5442–5451.

# Fabrication of Polymer Solar Cells Using Aqueous Processing for All Layers Including the Metal Back Electrode

Roar Søndergaard, Martin Helgesen, Mikkel Jørgensen, and Frederik C. Krebs\*

Utilization of sunlight as an energy source is one of the least exploited carbon-neutral methods available today. The potential is enormous, with a wide range of possible applications such as large scale energy production, small standalone energy production units in remote areas situated 'off the power grid' or tiny power production units aimed at recharging small electronic equipment that we surround ourselves with.

Over recent years polymer and organic solar cells have been perfected at the laboratory level and the performance now approaches many of the inorganic thin film solar cells. It has been argued that the ~8% power conversion efficiency recently reported for polymer solar cells might challenge polycrystalline silicon when projecting the steady increase in polymer solar cell performance a few years into the future. Many challenges remain that have to be addressed efficiently before the vision of large scale manufacture and widespread usage of low cost polymer solar cells can be anticipated. Ideally the polymer solar cell should be manufactured in a fast, large-area, environmentally friendly process. The methodologies employed in typical laboratory studies do not represent this well. The most commonly employed film forming technique is spin-coating which is incompatible with large areas, large volume, and low cost. Another troublesome aspect is the use of toxic organic solvents in the film-forming process. In the large-scale application where production volumes corresponding to several  $\text{GW}_{\text{peak}}$  are envisaged this is not a viable approach and alternative solvents will be a requirement. Until now, solvent-free or environmentally friendly solvent processing have not been studied to any significant level. An explanation for this can possibly be sought in the delicate interplay between the processing solvent and the performance of the solar cell. In many ways the state-of-the-art polymer solar cell has evolved around aromatic solvents such as chlorobenzene, dichlorobenzene, toluene, and xylene. Any change of solvent adversely affects the nanomorphology of the film and the device performance. The ambition to use more benign solvents would require a redesign of the molecular structures and a re-establishment of the interplay between nanomorphology and processing for the new material-solvent

combination. Most of the top-performing polymer solar cells are furthermore very sensitive to water and oxygen which lead to the requirement that all processes have to be performed in a protected atmosphere that, while possible, makes everything much more complex. Finally, the state-of-the-art polymer solar cell employs evaporated metal electrodes such as aluminium as the back electrode – a process that does not at all correlate well with high throughput production because of the high vacuum required for the deposition. The general processing steps of laboratory solar cells are shown in **Figure 1**.

We present an alternative environmentally friendly process that is also outlined in **Figure 1** where all the processing steps are aqueous and vacuum deposition of metal electrodes has been replaced by printing of an aqueous metal ink. The geometry of the device is of the "inverted" type with a zinc oxide electron transport layer (ETL) on an ITO coated glass substrate.

On top of this is a spin-coated active layer comprising a new developed water soluble polymer and a phenyl- $\text{C}_{61}$ -butyric acid methylester (PCBM) type acceptor, which will be discussed later. This is then followed by a hole transport layer (HTL) of polyethylenedioxythiophene: poly(styrene sulfonate) (PEDOT:PSS) and finally a printed counter electrode is applied in the form of a silver ink.

Water soluble analogues to poly(3-hexylthiophene) (P3HT), which is probably the most abundantly used polymer used in solar cells until now, was first reported in the mid 1980s.<sup>[1]</sup> Introduction of sulfonic acid salts at the end of the side chains provided the solubility, and polymers employing the same principle for water solubility using different ions such as sulfonium,<sup>[2,3]</sup> pyridinium<sup>[4]</sup> or ammonium salts<sup>[5,6]</sup> and varying chain lengths have been reported and/or are commercially available.

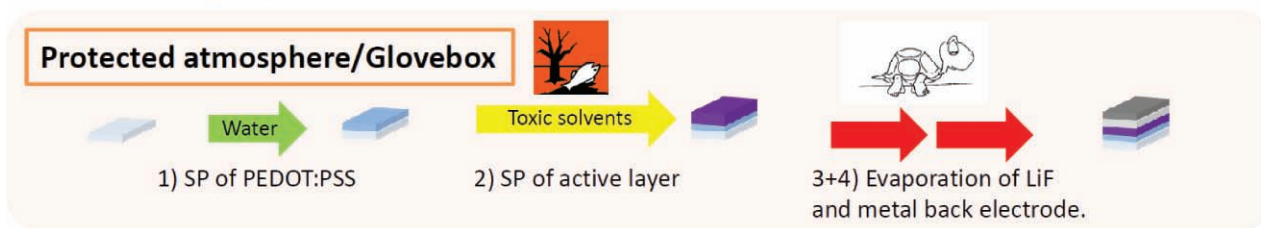
Unfortunately these polymers are not compatible with processing of multilayer films from the same processing solvent (i.e. water) since each new layer can dissolve/interact with previous ones. One way to circumvent this problem is to use thermo-cleavable materials in order to switch off the solubility of the polymer after film processing by removal of side chains. This led us to develop a new thiophene based polymer incorporating this concept shown in **Scheme 1**. The use of tertiary esters as thermo-cleavable side chains on polymers for solubility switching is a well known process, which, when the tertiary ester is attached to a thiophene unit, can proceed in two steps with increasing temperature by initial removal of the tertiary substituent followed by decarboxylation.<sup>[7,8]</sup> Both products are insoluble, but have different electronic properties of which the final decarboxylated product has been found to perform best in solar cells.<sup>[8]</sup> Besides the obvious processing

R. Søndergaard, M. Helgesen, M. Jørgensen, Prof. F. C. Krebs  
Solar Energy Programme  
Risø National Laboratory  
Technical University of Denmark – DTU  
Building 124, P.O. Box 49, DK-4000 Roskilde, Denmark  
E-mail: frkr@risoe.dtu.dk

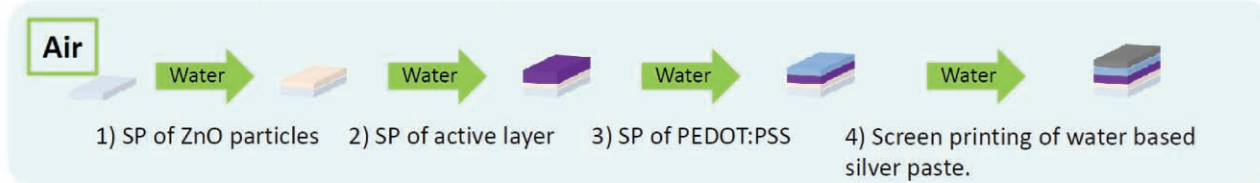
DOI: 10.1002/aenm.201000007



### Processing steps of a 'Normal' structure solar cell:



### Processing steps of all-water-processable solar cell with 'Inverted' structure:



SP: Solution processing

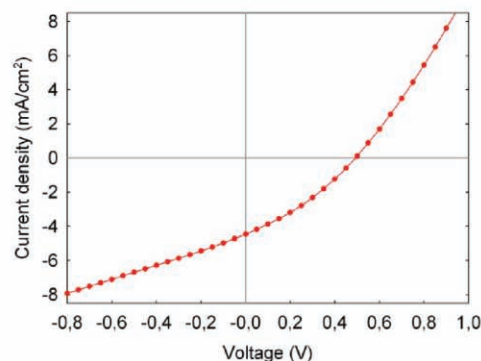
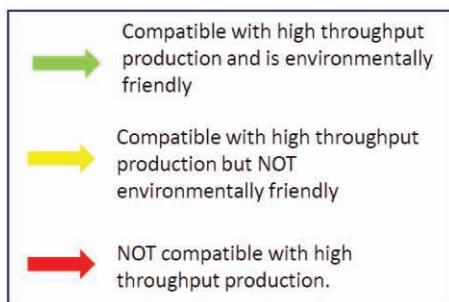
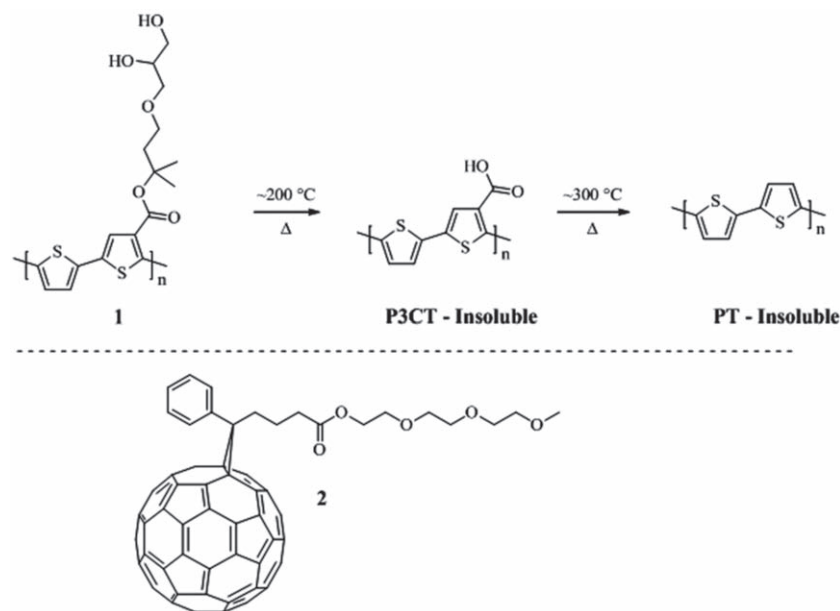


**Figure 1.** Comparison of the potential for high throughput production using the standard laboratory buildup of a solar cell, which involves both the use of toxic solvents and the slow metal deposition by evaporation (top) and the all-water-processable method where all steps are processed from aqueous solution, which makes it compatible with high throughput processing like roll-to-roll-coating. Furthermore the use of water based solutions guarantees a minimal impact on the environment (middle). The environmental compatibility of the processing steps is shown (lower left) along with an IV-curve for a device prepared using the aqueous processing of all layers described here (lower right).

advantages of solubility switching, removal of the side chains from the bulk of the active layer furthermore means removal of non-absorbing material, and several studies show enhanced stability of the active layer towards general degradation.<sup>[9–11]</sup> A tertiary ester side chain containing polyether units as well as free alcohol groups was synthesized in order to promote solubility towards aqueous media and simultaneously allowing for evaporative removal of the cleaved side chains from the active layer after cleavage – a feat that would not have been possible if ionic containing side chains had been used.

A tertiary alcohol with two additional tert-butyldimethylsilyl (TBDMS) protected alcohols was prepared and coupled with 2,5-dibromothiophene-3-carboxylic acid to give the corresponding tertiary ester. This was then reacted with 2,5-bis(trimethylstannyl)thiophene in a Stille coupling afforded the initial polymer which, because of the TBDMS-protected alcohols, could undergo normal workup procedures. Removal of the TBDMS-groups was performed with TBAF in THF/

MeOH solution yielding the final polymer **1**. The polymer showed to be soluble only in DMF and DMSO when using pure solvents, and was also soluble in a mixture of equal amounts water and isopropanol when a little THF was present (down to 4 vol%). In addition to the thermocleavable polymer a new acceptor material had to be prepared, as the generally used PCBM-acceptor is too insoluble to be processed when water is present. After several failed attempts to prepare a thermocleavable fullerene that could be rendered insoluble by the same processes as the polymer, a different approach was chosen. Previous work by Deguchi *et al.* have shown it possible to create monodisperse clusters of C<sub>60</sub> (60 nm) in water through forced precipitation by addition of a THF-solution into water.<sup>[12]</sup> The thought was that a PCBM-analogue, that was not soluble in water, which would allow for subsequent processing, but still containing coordination properties towards aqueous media, might behave in a similar way if mixed with an aqueous solution from THF. The fullerene **2** (see **Scheme 1**) containing an



**Scheme 1.** Top: Chemical structure of polymer 1 and the reaction products forming during the thermocleavage process as the temperature rises. Initially poly-3-carboxydithiophene (P3CT) is formed followed by decarboxylation into polythiophene (PT) at higher temperatures. Both compounds are insoluble but have different electronic properties. Bottom: Chemical structure of the modified PCBM-analogue used for aqueous processing.

ester substituent of triethyleneglycol mono methyl ether to promote coordination to water was therefore prepared from commercial C<sub>60</sub>-PCBA and triethyleneglycol mono methyl ether by coupling with dicyclohexylcarbodiimide. The purified fullerene was soluble in polar aprotic solvents dimethylformamide, dimethylsulfoxide and tetrahydrofuran (DMF, DMSO, and THF).

Inverted structure polymer solar cells (substrate | ITO | ZnO | active layer | PEDOT | Ag, (ITO: indium tin oxide)) were prepared on ITO-substrates. The electron transport layer (ETL) was zinc oxide doped with aluminium obtained from aqueous solution (see Supporting Information). The advantage of the aqueous ink formulation is that the inflection point that ZnO based devices exhibit as a consequence of photodoping is alleviated. The ink could be spin coated or roll-to-roll slot-die coated. An important step is that the initially dry film must be heated for 5–40 min at 140 °C to yield electron-transporting films. After this treatment the ZnO layer is insoluble and subsequent processing is then possible.

The active layer was prepared by mixing equal amounts of solutions of polymer 1 (15 mg ml<sup>-1</sup> in 47.5% water, 47.5% isopropanol and 5% THF) and the fullerene 2 (15 mg ml<sup>-1</sup> in THF) just prior to spin-coating. A thermal treatment (310 °C for approximately 10 s) removed the solubilizing side chains of the polymer leaving an insoluble film. The duration of the thermal treatment is quite critical, as both shorter and longer periods led to a decrease in efficiency of the final devices. This is probably due to either incomplete decarboxylation or some degradation. The hole transport layer (HTL), comprising an aqueous dispersion of PEDOT:PSS diluted with isopropanol, was coated on top of the ZnO/polymer:fullerene stack. After heating

for 5 min at 140 °C further processing was possible and the device was completed by printing a silver electrode from a paste comprising only silver flakes, water and an aqueous binder. The final printing step is finalized in 2 min and is finished off by protection of the electrodes by encapsulation using a simple food packaging barrier. All preparative steps were carried out in air. Pictures of the printing process and aqueous solutions are shown in Figure 2. Devices with areas of 0.5 cm<sup>2</sup> gave efficiencies of 0.4–0.7% with excellent stability during storage and operation under ambient conditions when encapsulated using the simple food packaging barrier. The *J*-*V* characteristics of a representative solar cell are: open-circuit voltage *V*<sub>oc</sub>: 0.49 V, short-circuit current *I*<sub>sc</sub>: 4.46 mA cm<sup>-2</sup>, fill factor FF: 32%, and power conversion efficiency PCE: 0.70%. In comparison devices prepared with the well known P3HT:PCBM materials combination showed performances of 1.6–2% when processing the active layer (P3HT:PCBM) from chlorobenzene while using aqueous processing for all the other layers (ZnO, PEDOT:PSS and silver back electrode). These results are

admittedly lower than what is commonly reported for P3HT/PCBM devices with evaporated electrodes. We would however like to stress that aqueous processing is a very significant challenge and our results show convincing feasibility for devices with relatively large active area and also show the potential of the printable aqueous silver as an alternative to evaporation.

In summary we have successfully developed four new methods which allow for aqueous processing of all layers in polymer based solar cells and solves the problem of the inflection point in ZnO. Bulk heterojunction solar cells prepared on the basis of these methods exhibited efficiencies up to 0.70% when using specially prepared water processable polymer and fullerene and up to 2% when processing P3HT/PCBM from chlorobenzene while using aqueous processing for all other layers. This result must be considered an essential first step on the way to an environmentally friendly large scale production of polymer solar cells using only printing techniques and water as the processing solvent.

## Experimental Section

Experimental details on the synthesis of the polymer 1 and of the modified PCBM-analogue, fullerene 2, can be found in the Supporting Information.

**Device Fabrication:** ITO-substrates were first cleaned in isopropanol and water for 10 min respectively using an ultrasonic bath. The ZnO precursor solution was then applied by spin-coating at 1000 rpm and after drying this was followed by heating for at least 5 min at 140 °C to convert to ZnO. The active layer was prepared by mixing a solution of polymer 1 (15 mg/ml) in a mixture of water/isopropanol/THF (47.5:47.5:5) and the fullerene 2 (15 mg/ml) in THF just prior to spin coating at 400 rpm after drying the ITO:ZnO:active layer the substrate was heated on a hotplate at



**Figure 2.** Top: picture of the inks involved in the ‘all water based processing’. From left to right: aqueous ZnO precursor solution, aqueous solution of polymer **1** (diluted in order to show color), aqueous PEDOT:PSS with isopropanol and aqueous silver paste. Middle: Picture of the screen printing machinery. Bottom: Close-up of the screen printing process. The silver paste has been applied and is ready to be pushed through the pattern of the mask by sweeping the squeegee across the steel mesh screen. Insert shows a picture of the final device after encapsulation.

310 °C for approximately 10 s in order to perform the thermocleavage of the side chains to yield native polythiophene. (For P3HT/PCBM devices (1.2:1) a 44 mg/ml solution in chlorobenzene was spin coated at 800 rpm,

followed by annealing at 140 °C for 2 min). This was followed by application of PEDOT:PSS (Agfa EL-P 5010) diluted with isopropanol 2:1 (w/w) by spin-coating at 1000 rpm for 15 s and then drying on a hotplate at 140 °C for 5 min. The device was finished by screen printing of a silverpaste prepared from silver flakes (FS 16 from Johnson Matthey) mixed with an aqueous binder (Viacryl 175W40WAIP from Cytec) and water, followed by heat treatment at 140 °C for 2 min.

**Device Testing:** The conditions of the characterization under simulated sunlight were KHS 575 using a solar simulator from Steuernagel Lichttechnik operating at 1000 Wm<sup>-2</sup>, AM1.5G. The spectrum of the solar simulator was checked using an optical spectrum analyzer made for measuring irradiance, and its intensity was calibrated bolometrically using a precision spectral pyranometer from Eppley Laboratories. During measurements, the incident light intensity was monitored continuously using a CM4 high-temperature pyranometer from Kipp & Zonen.

## Supporting Information

Supporting Information is available from the Wiley Online Library or from the author.

## Acknowledgements

This work was supported by the Danish Strategic Research Council (2104-07-0022), EUDP (j. nr. 64009-0050) and PV-ERA-NET (project acronym POLYSTAR).

Received: October 22, 2010

Revised: November 29, 2010

Published online: December 10, 2010

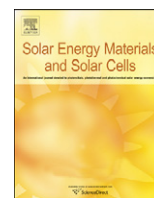
- [1] A. O. Patil, Y. Ikenoue, F. Wudl, A. J. Heeger, *J. Am. Chem. Soc.* **1987**, *109*, 1858.
- [2] M. Ogawa, M. Tamanoi, H. Ohkita, H. Benten, S. Ito, *Sol. Energy Mater. & Sol. Cells* **2009**, *93*, 369.
- [3] F. Tran-Van, M. Carrier, C. Chevrot, *Synth. Met.* **2004**, *142*, 251.
- [4] D. A. Rider, B. J. Worfolk, K. D. Harris, A. Lalany, K. Shahbazi, M. D. Fleischauer, M. J. Brett, J. M. Buriak, *Adv. Funct. Mater.* **2010**, *20*, 2404.
- [5] H. M. Li, Y. L. Li, J. Zhai, G. L. Cui, H. B. Liu, S. Q. Xiao, Y. Liu, F. S. Lu, L. Jiang, D. B. Zhu, *Chem. Eur. J.* **2003**, *9*, 6031.
- [6] V. Sgobba, A. Troeger, R. Cagnoli, A. Mateo-Alonso, M. Prato, F. Parenti, A. Mucci, L. Schenetti, D. M. Guldi, *J. Mater. Chem.* **2009**, *19*, 4319.
- [7] M. Bjerring, J. S. Nielsen, N. C. Nielsen, F. C. Krebs, *Macromol.* **2007**, *40*, 6012.
- [8] S. A. Gevorgyan, F. C. Krebs, *Chem. Mater.* **2008**, *20*, 4386.
- [9] M. Bjerring, J. S. Nielsen, A. Siu, N. C. Nielsen, F. C. Krebs, *Sol. Energy Mater. & Sol. Cells* **2008**, *92*, 772.
- [10] F. C. Krebs, H. Spanggaard, *Chem. Mater.* **2005**, *17*, 5235.
- [11] M. H. Petersen, S. A. Gevorgyan, F. C. Krebs, *Macromol.* **2008**, *41*, 8986.
- [12] S. Deguchi, R. G. Alargova, K. Tsujii, *Langmuir* **2001**, *17*, 6013.



ELSEVIER

Contents lists available at ScienceDirect

# Solar Energy Materials & Solar Cells

journal homepage: [www.elsevier.com/locate/solmat](http://www.elsevier.com/locate/solmat)

## Printed metal back electrodes for R2R fabricated polymer solar cells studied using the LBIC technique

Frederik C. Krebs, Roar Søndergaard, Mikkel Jørgensen\*

Risø National Laboratory for Sustainable Energy, Technical University of Denmark, Frederiksborgvej 399, DK-4000 Roskilde, Denmark

### ARTICLE INFO

#### Article history:

Received 3 September 2010

Received in revised form

5 November 2010

Accepted 11 November 2010

Available online 30 November 2010

#### Keywords:

Polymer solar cells

Roll-to-roll coating

Light beam induced current (LBIC)

Modules

Printed metal electrodes

Aqueous processing

### ABSTRACT

The performance of printable metal back electrodes for polymer solar cells were investigated using light beam induced current (LBIC) mapping of the final solar cell device after preparation to identify the causes of poor performance. Three different types of silver based printable metal inks were employed. Organic solvent based, UV-curable and water based silver inks were tested. Both grid electrodes and full electrodes were employed and it was shown via the grid electrode that the organic solvent based ink adversely affects the device performance under the printed metal whereas both the UV-curable and the water based inks were neutral to improving device performance. Complete roll-to-roll (R2R) processed modules were also tested and some limitations of the LBIC technique was identified for serially connected modules.

© 2010 Elsevier B.V. All rights reserved.

## 1. Introduction

Standard laboratory polymer solar cells [1–4] are almost exclusively prepared by spin coating a polymer/acceptor blend active layer on top of a transparent electrode (usually ITO/PEDOT) followed by vacuum deposition of a metal back electrode. This technique has been perfected to a level where efficiencies of up to above 8% have been achieved for very small active areas [5]. This procedure is however not amenable to large scale production of polymer solar cells using roll-to-roll (R2R) technology [6–11] that is required for demonstration and application of the technology [12–16]. Here we focus on the alternative printed metal back electrode that can be applied in the R2R process using flat bed or rotary screen printing technology, thus avoiding a slow/cumbersome vacuum step in the manufacturing process. Screen printing of metal electrodes is used industrially in high volume to produce consumer electronics and hence a range of metal based screen printing inks are available. These inks are usually silver based with micro or nanosized metal particles in an organic binder fluid. We have previously reported a study on the comparison of ten different commercial silver inks used to prepare P3HT based R2R coated polymer solar cells [9]. The resulting solar cells varied considerably in efficiency and stability and showed that application of a printed metal back electrode, while technically suitable in the R2R process, requires optimization both in the choice of ink type, but also in electrode geometry. Traditional electrical characterization of solar cells by performing an IV scan and extracting the

open circuit voltage ( $V_{oc}$ ), short circuit current ( $I_{sc}$ ), fill factor and power conversion efficiency (PCE,  $\eta$ ) is useful for determining the overall parameters of solar cells. Here this type of measurement is complemented with light beam induced current (LBIC) mapping of the devices to gain further insight into how the different types of silver inks and their patterning in the back electrode affects the solar cell performance. The LBIC technique is used both to map out the “good/bad” parts of the solar cell with respect to the electrodes and active layer and also to find defects. The LBIC technique has previously been applied to solar cells [17,18] and to organic solar cells in a limited number of cases [19–21].

In this paper we have employed the LBIC technique to investigate three different silver based inks as printed back electrode in polymer solar cells with the so called inverted geometry (substrate/ITO/ZnO/active layer/PEDOT/silver). One of them is a commercial type with organic binders and solvents that is cured in an oven at 140 °C. The formulation of two other types is also described. One is water based and one is a UV-curable silver ink. They are cured by heating at 140 °C or using UV-light at ambient temperature.

## 2. Experimental

### 2.1. General procedure to formulate screen printable silver and metal inks

The formulation of a screen printable metal ink follows the general idea that a fine metal powder is dispersed in a solvent and a binder. The particle size for the metal is preferably in the range of

\* Corresponding author. Tel.: +45 4677 4717; fax: +45 4677 4791.  
E-mail address: [mijq@risoe.dtu.dk](mailto:mijq@risoe.dtu.dk) (M. Jørgensen).



200 nm to 2  $\mu\text{m}$ . Larger particles can be employed but the mesh size of the printing screen has to be larger. The principle is that when the solvent is removed the dry film presents mainly the metal particles that are glued together by the binder. In the context of polymer solar cells the nature of the binder and the solvents can critically influence the performance of the final device and therefore it is an advantage to be able to adjust the nature of the binder and solvents (i.e. polarity, surface tension). Since most active materials for OPV are soluble in organic solvents it is an advantage to formulate the printable silver inks without solvents (UV-curable) or with a polar solvent (water, alcohol etc.). Below we give two examples and employ them later. The metal particles in this case were commercially available silver flakes from Johnson Matthey (FS 16) but in principle any metal powder, nanoparticles or flake can be used. We have successfully employed this procedure for making screen printable inks based on chromium, molybdenum, vanadium, titanium, zinc and gold.

## 2.2. UV-curable ink

110 g of silver flake (FS 16 from Johnson Matthey) was placed in a glass container with a large opening. 30 g of UV-curable binder (Ebecryl 15 from Cytec) was added and the mixture is stirred manually using a glass rod. Initially the mixture presents a semi-dry appearance with the metal flake covering droplets of the binder. After mixing for 10 min the mixture presents a thick and smooth printable paste that can be used directly or stored in the dark in the refrigerator. The ink can be screen printed and depending on the thickness and the initiator cured using a dose of about  $1000 \text{ mJ cm}^{-2}$  corresponding to a curing time of 1–2 min. For less reflective metal powders the radiation dose has to be significantly higher as the penetration depth of the UV-light depends on the UV-transmission of the cured binder and the reflectivity of the metal particles. There is for a given metal particle type and binder a maximum thickness that can be cured using UV. The typical wet thickness of the inks prepared here was 8–10  $\mu\text{m}$ .

## 2.3. Water based silver ink

110 g of silver flake (FS 16 from Johnson Matthey) was mixed well with an aqueous solution of binder following the mixing procedure described above (Section 2.2). The aqueous solution of the binder was prepared by mixing 25 g of the binder (Viacryl 175W40WAIP from Cytec) with 25 g of water. The ink could be dried at  $140^\circ\text{C}$  for 2–5 min after printing.

## 2.4. Screen printing of the silver inks

The screen-printer was a sheet fed or a R2R machine [9,22,23]. Both employed a similar printer type (AT701 from Alraun Technik). The masks were prepared using 110 mesh polyester screens for the heat curable ink (PV410, Dupont) and the UV-curable ink and a 72/32 steel mesh for the water based silver ink. The mesh was mounted at a tension of, respectively, 25 and 35 N. The squeegee speed was  $550 \text{ mm s}^{-1}$ . The inks were cured as described in Sections 2.2 and 2.3.

## 2.5. Solar cell preparation

Solar cell preparation was carried out using an inverted geometry (substrate/ITO/ZnO/Active layer/PEDOT/Silver) as described in the literature [7] on two types of substrates: glass and PET. Briefly: the inks were the same for both spin coating and slot-die coating and were as follows: the ZnO ink comprised methoxyethoxyacetic acid (MEA) stabilized nanoparticles (3–5 nm) in acetone ( $45 \text{ mg mL}^{-1}$ ), P3HT (Sepiolid P200 from BASF,  $22 \text{ mg mL}^{-1}$ ) and

PCBM (from Solenne BV,  $18.5 \text{ mg mL}^{-1}$ ) in chlorobenzene and PEDOT:PSS (Agfa EL-P 5010 diluted 10:5 w/w with isopropanol to a viscosity of  $270 \text{ mPa s}$ ). The preparation on glass substrates employed spin coating of the ZnO ( $1000 \text{ rpm}$ ), P3HT:PCBM ( $800 \text{ rpm}$ ) and PEDOT:PSS ( $500 \text{ rpm}$ ) layer and screen printing of the silver layer using one of the above silver inks. Those devices had a nominal active area of  $3 \text{ cm}^2$ . The preparation of devices using R2R techniques on PET employed slot-die coating of the ZnO ( $2 \text{ m min}^{-1}$ ), P3HT:PCBM ( $1.6 \text{ m min}^{-1}$ ) and PEDOT:PSS ( $0.3 \text{ m min}^{-1}$ ) layers and screen printing of the silver layer using one of the above silver inks as reported earlier [7]. All layers were dried at  $140^\circ\text{C}$  during R2R processing. The oven length was 1 m. The R2R processed devices comprised both single cells and complete modules and had a nominal active area of, respectively,  $4.2$  and  $35.5 \text{ cm}^2$ . The thickness of the ZnO layer was 15 nm, the thickness of the active layer was 200 nm and the thickness of the PEDOT:PSS layer was 15  $\mu\text{m}$  for spincoated devices and 25 nm, 250 nm and 25  $\mu\text{m}$  for the R2R coated devices.

## 2.6. Light beam induced current (LBIC) mapping

The LBIC experiments were carried out using a custom made setup with 410 nm laser diode (5 mW output power,  $100 \mu\text{m}$  spot size  $\approx 65 \text{ W/cm}^2$ , ThorLabs) mounted on a computer controlled XY-stage and focused to a spot size of  $< 100 \mu\text{m}$ . The short circuit current from the device under study was measured using a computer controlled source measure unit (SMU, a Keithley 2400 instrument). A custom written computer program was used to scan the solar cell devices in a raster pattern in  $200 \mu\text{m}$  steps in the X and the Y directions, logging the coordinates and measured current. The results were then converted to yellow/blue colored bitmaps in 255 different hues with another custom written program. Bright yellow represents the highest absolute current extracted while blue represents the lowest current. Current profiles along selected directions were taken from these maps to visualize the relative differences in different regions. A positive bias current was applied in one case with a module consisting of sixteen serially connected cells. Non-illuminated cells may behave as blocking diodes reducing the current from an illuminated cell. The positive bias then forces the diode behavior to be open.

## 3. Results and discussion

### 3.1. Effects of three types of silver ink

Three P3HT based solar cells with were prepared with three different types of silver ink: heat curable (PV410 from Dupont), UV curable and a water based heat curable silver ink were investigated with the LBIC technique and the results are shown in Fig. 1.

In all three cases current was extracted from areas covered by both the ITO and the PEDOT pattern. The most striking result was obtained for the heat cured organic solvent based silver electrode where current extraction almost falls to zero under the printed silver. For the two other types of silver electrode, current extraction occurred under the full area. The heat cured organic solvent based silver thus dramatically impedes the solar cell function. A plausible explanation could be that solvents in this particular silver ink mixes in and partly dissolves the active layer and thereby destroy the morphology of the bulk hetero junction before heat curing is completed. This effect is not seen with the UV curable ink and the water based ink. On the contrary, with the UV cured silver electrode it is clear that the region of the solar cell above the silver contributes more to the current than the surrounding area that is only connected to the PEDOT:PSS electrode. The water based

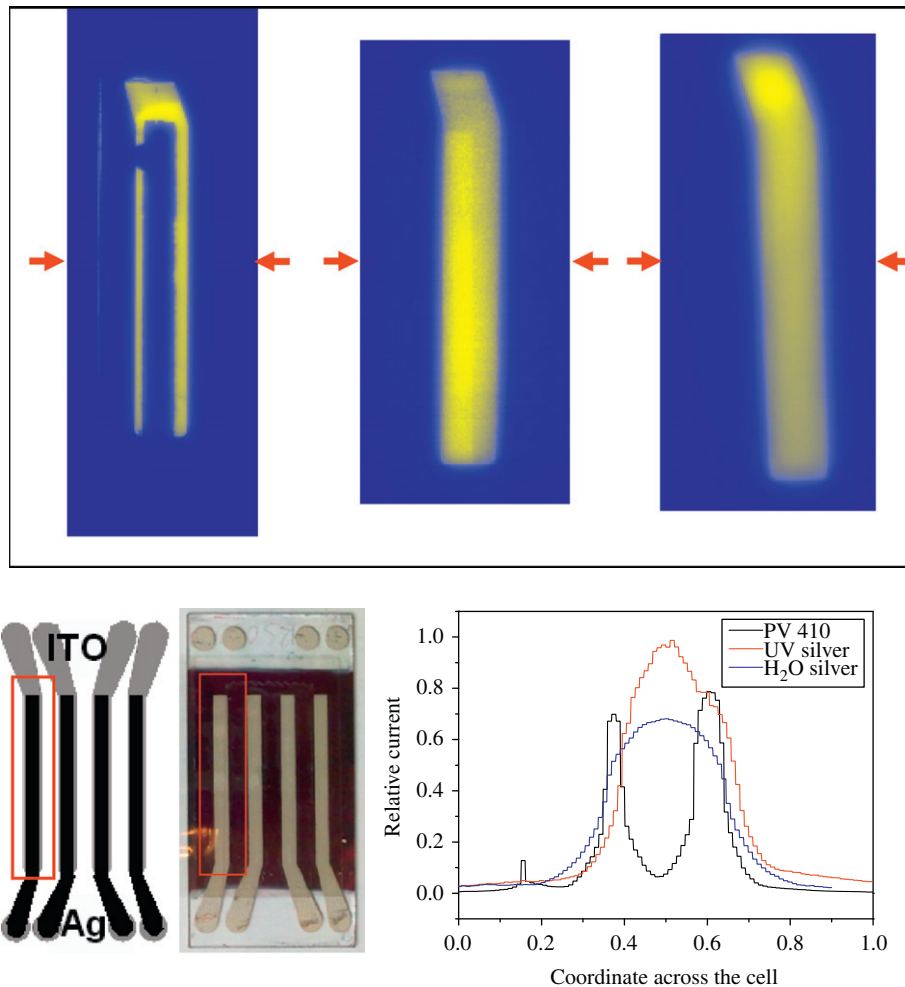


**Fig. 1.** Top: LBIC of the leftmost cell in each device. The silvered area can be recognized for the PV410 silver (left) and the UV-cured silver (middle), but not for the H<sub>2</sub>O silver (right). Current extraction is seen in most of the ITO covered area which extends in a diagonal direction to the upper left above the silvered area. Bottom: outline of the cell with the ITO pads in gray overlaid with the silver pattern in black (left). An image of one device (middle). The area of interest is represented by the red box. Current profiles across the cells were obtained as indicated by the red arrows (right). (For interpretation of the references to color in this figure legend, the reader is referred to the web version of this article.)

silver electrode is intermediary with current extraction over the whole region.

### 3.2. Effect of the pattern of the silver back electrode

The pronounced effects of the type of silver electrode and the discovery of efficient carrier extraction outside the silvered area prompted us to investigate how patterning of the silver electrode would influence the LBIC experiment. Roughly square devices partially covered with striped silver electrodes were fabricated again with the three different types of silver (PV410, UV-cured and H<sub>2</sub>O-silver). As shown below the striped pattern of the electrodes is clearly reproduced in the LBIC experiment (Fig. 2). As with the simple silver electrodes shown above the PV410 type silver clearly reduced current extraction directly above the silver, while in the case of the UV-cured and the water silver improved current extraction in these regions were observed. The detrimental effect of the PV410 does not extend beyond the electrode area making it possible to obtain functional devices. Visual inspection of devices with grid electrodes, that have been cleaved at the PEDOT/active layer interface, clearly show that the PV410 ink alters the absorption directly beneath the silver. This effect is much less pronounced with the UV and water based silver. The metal inks will also damage

the PEDOT layer to some extent which is alleviated by using a thicker layer.

### 3.3. Roll-to-roll coated devices

The LBIC characterization technique was extended to roll-to-roll (R2R) coated devices. Single striped cells were prepared as described elsewhere consisting of the following layers: PET/ITO/ZnO/P3HT-PCBM/PEDOT/silver. The silver back electrode was either a simple filled rectangle covering most of the cell or a striped pattern connected to one side with a bus bar as shown in Fig. 3.

Only the UV-cured type of silver was used for the R2R coated devices. The results are similar to those obtained for the devices prepared on glass substrates. The stripe pattern generated in the R2R coating process is clearly reproduced in the LBIC images. With the simple rectangular silver electrode current extraction is efficient over most of the cell and there is a large contrast to areas without silver. The cell having the silver grid electrode is also well reproduced in the LBIC image with slightly less current directly above the grid lines. Defects and thickness variations due to the R2R coating technique are most easily seen in the LBIC image for the cell with the fully covering silver electrode. There are small dark spot

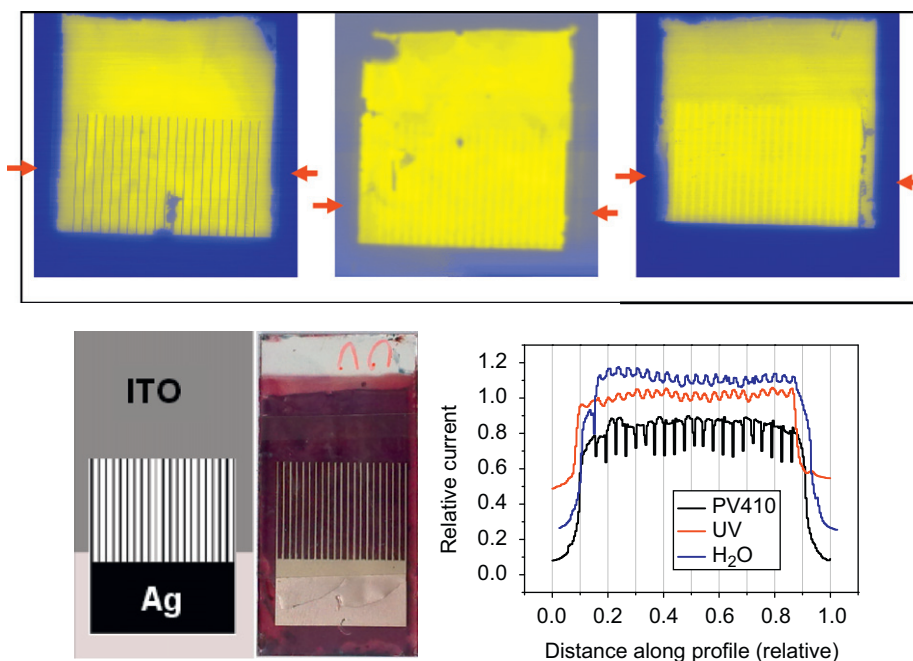


**Fig. 2.** Top: LBIC experiments with different striped silver electrodes; PV410 silver (left), UV silver (middle), H<sub>2</sub>O silver (right). Bottom: outline of the cell with the rectangular ITO area shaded gray overlaid with the striped silver electrode pattern and a rectangular silver bus shaded black (left) and an image of one of the devices seen from the silver electrode side (middle). Profiles (indicated by red arrows) were taken across the striped pattern in each LBIC map to show the relative current change (right). The profiles have been displaced along the current-axis to show the pattern more clearly. Notice also that while the current drops significantly above the PV410 silver a slight increase is visible for the UV- and H<sub>2</sub>O-silver. (For interpretation of the references to color in this figure legend, the reader is referred to the web version of this article.)

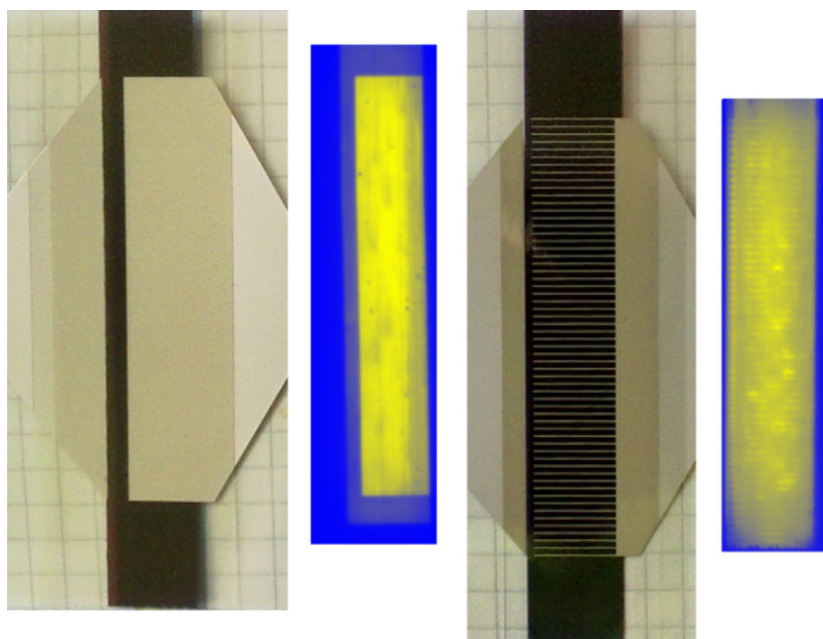


**Fig. 3.** Single cell R2R coated devices. Left: solid rectangular silver electrode. Right: grid silver electrode.

like features that may originate from point defects. This type of defects could arise from either minute bubbles in one of the coating solutions or point defects in a lower layer that inhibits coating (dewetting). This type of defect is limited to a very small area of the cell and does not catastrophically impede the overall functioning of the cell e.g. by short circuiting but may result in partial shunting and cause a lower fill factor. Weak darker lines and areas that are seen to run along the R2R stripe pattern may be due to thickness variations inherent in this type of coating process.

A single module with sixteen serially connected cells was also investigated by LBIC (Fig. 4). Initial studies using zero bias voltage indicated very uneven current production with most of the individual sixteen cells not contributing significantly. It was realized that the cells that were not illuminated could act as blocking diodes. Initial attempts to overcome this using a white light bias proved unsuccessful due to the geometry of the setup. Instead different bias voltages were applied and an optimum at +1 V was found.

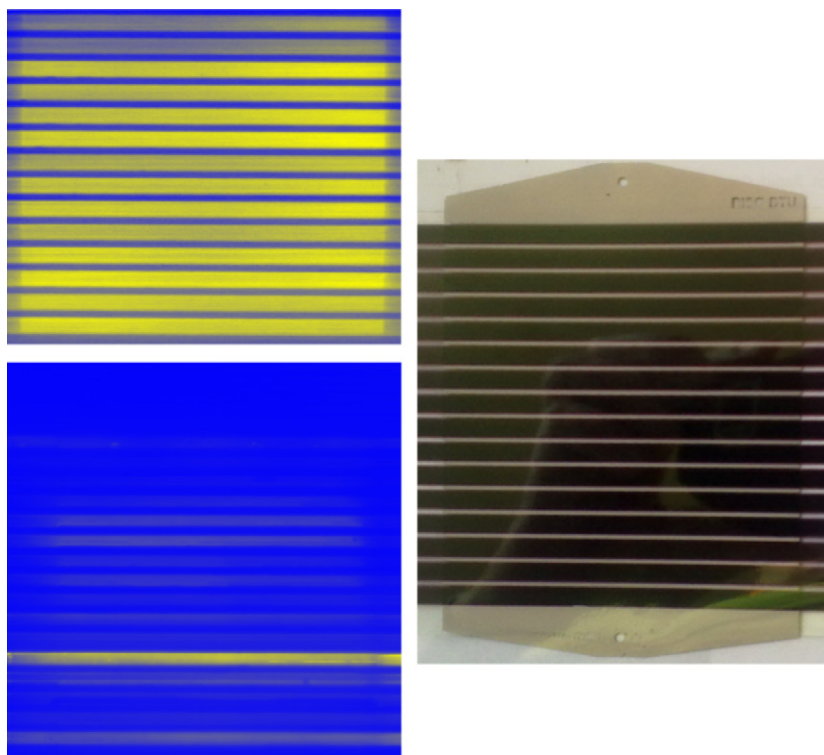


**Fig. 4.** R2R coated module. In the LBIC images (left) a functioning module is shown on top with a rather uniform current extraction and below a failed module with only one fully functional stripe. To the right is shown a picture of a module from the front with serially connected solar cells as dark stripes and the printed silver back electrodes.

The back electrode was again a screen printed fully covering rectangular silver electrode printed with UV curable silver ink. Due to the much larger area the data collection took much longer time and it was found necessary to use a positive bias voltage (+1 V) to overcome the blocking behavior of some of the non-illuminated cells. Current extraction is observed for all stripes measured. An even current is measured along the stripe through the cells showing that the coating process was uniform and that the conductivity of both the silver and the ITO electrodes is so high as not to cause significant losses in efficiency. An LBIC image of a defect module device is also included in Fig. 4 to illustrate how the LBIC technique can be used to identify the failed areas of the device.

#### 4. Conclusion

The LBIC technique gives additional valuable information about the functioning of organic solar cells through mapping. In the present context the difference between three different silver inks for silk screen printing of the back electrode was clearly shown by the LBIC images. The contrast between the current generation under the silver electrode and adjoining ITO covered areas was markedly different. In the case of the heat cured ink (PV410) a large drop in current above the silvered area was observed, while a slight increase was seen for the UV cured ink and the water formulated ink. The PV410 ink had already been tested in a previous study using standard IV characterization where it also gave rise to less efficient solar cell devices. The silver electrode is the last printed layer of the device and the LBIC result suggest that the heat cured ink in contrast to the other silver inks somehow destroy the ordering of the underlying layers. This effect could be due to small molecule solvents present in the PV410 ink that partially dissolve and destroy the morphology of the active layer. An important observation is that this detrimental effect is limited to the area immediately under the silver. This was tested using grid type

electrodes where the drop in current generation is seen to be limited to the area in direct contact with the grid while adjacent areas were unaffected. It is therefore possible to use the heat cured ink if the loss of current generation from the silver covered areas is acceptable. Grid type electrodes are also attractive since less ink is used with corresponding savings on the relatively costly silver metal. The LBIC technique can be useful in determining the necessary area and geometry of the grid silver electrode for optimum performance. LBIC images of R2R coated devices presented other important information. These types of devices showed some variation in current generation that can be ascribed to both point and line defects, but also to the thickness variation that is to some extent inherent in the R2R coating technique. Taking the much larger active area prepared by R2R coating into consideration the evenness of the measured LBIC images of these devices attests to the ability to reliably coating polymer solar cells.

#### Acknowledgements

This work was supported by the Danish Strategic Research Council (DSF 2104-05-0052 and 2104-07-0022), EUDP (j. nr. 64009-0050) and PV ERA-NET transnational POLYMOL project PolyStaR.

#### References

- [1] M. Helgesen, R. Søndergaard, F.C. Krebs, Advanced materials and processes for polymer solar cell devices, *J. Mater. Chem.* 20 (2010) 36–60.
- [2] G. Dennler, M.C. Scharber, C.J. Brabec, Polymer-fullerene bulk-heterojunction solar cells, *Adv. Mater.* 21 (2009) 1323–1338.
- [3] I. Gonzalez-Valls, M. Lira-Cantu, Vertically-aligned nanostructures of ZnO for excitonic solar cells: a review, *Energy Environ. Sci.* 2 (2009) 19–34.
- [4] T.D. Nielsen, C. Cruickshank, S. Foged, J. Thorsen, F.C. Krebs, Business, market and intellectual property analysis of polymer solar cells, *Sol. Energy Mater. Sol. Cells* 94 (2010) 1553–1571.
- [5] <www.solarmer.com>.



- [6] F.C. Krebs, Fabrication and processing of polymer solar cells. A review of printing and coating techniques, *Sol. Energy Mater. Sol. Cells* 93 (2009) 394–412.
- [7] F.C. Krebs, S.A. Gevorgyan, J. Alstrup, A roll-to-roll process to flexible polymer solar cells: model studies, manufacture and operational stability studies, *J. Mater. Chem.* 19 (2009) 5442–5451.
- [8] F.C. Krebs, All solution roll-to-roll processed polymer solar cells free from indium-tin-oxide and vacuum coating steps, *Org. Electron.* 10 (2009) 761–768.
- [9] F.C. Krebs, T. Tromholt, M. Jørgensen, Upscaling of polymer solar cell fabrication using full roll-to-roll processing, *Nanoscale* 2 (2010) 878–886.
- [10] F.C. Krebs, Polymer solar cell modules prepared using roll-to-roll methods: knife-over-edge coating, slot-die coating and screen printing, *Sol. Energy Mater. Sol. Cells* 93 (2009) 465–475.
- [11] F.C. Krebs, K. Norrman, Using light induced thermocleavage in a roll-to-roll process for polymer solar cells, *ACS Appl. Mater. Interfaces* 2 (2010) 877–887.
- [12] F.C. Krebs, M. Jørgensen, K. Norrman, O. Hagemann, J. Alstrup, T.D. Nielsen, J. Fyenbo, K. Larsen, J. Kristensen, A complete process for production of flexible large area polymer solar cells entirely using screen printing—first public demonstration, *Sol. Energy Mater. Sol. Cells* 93 (2009) 422–441.
- [13] F.C. Krebs, S.A. Gevorgyan, B. Gholamkhash, S. Holdcroft, C. Schlenker, M.E. Thompson, B.C. Thompson, D. Olson, D.S. Ginley, S.E. Shaheen, H.N. Alshareef, J.W. Murphy, W.J. Youngblood, N.C. Heston, J.R. Reynolds, S. Jia, D. Laird, S.M. Tuladhar, J.G.A. Dane, P. Atienzar, J. Nelson, J.M. Kroon, M.M. Wienk, R.A.J. Janssen, K. Tvingstedt, F. Zhang, M. Andersson, O. Inganäs, M. Lira-Cantu, R. de Bettignies, S. Guillerez, T. Aernouts, D. Cheyns, L. Lutsen, B. Zimmermann, U. Würfel, M. Niggemann, H.-F. Schlieiermacher, P. Liska, M. Grätzel, P. Lianos, E.A. Katz, W. Lohwasser, B. Jannon, A round robin study of flexible large-area roll-to-roll processed polymer solar cell modules, *Sol. Energy Mater. Sol. Cells* 93 (2009) 1968–1977.
- [14] F.C. Krebs, T.D. Nielsen, J. Fyenbo, M. Wadstrøm, M.S. Pedersen, Manufacture, integration and demonstration of polymer solar cells in a lamp for the “Lighting Africa” initiative, *Energy Environ. Sci.* 3 (2010) 512–525.
- [15] A.J. Medford, M.R. Lilliedal, M. Jørgensen, D. Aarø, H. Pakalski, J. Fyenbo, F.C. Krebs, Grid-connected polymer solar panels: initial considerations of cost, lifetime, and practicality, *Opt. Express* 18 (S3) (2010) A272–A285.
- [16] F.C. Krebs, J. Fyenbo, M. Jørgensen, Product integration of compact roll-to-roll processed polymer solar cell modules: methods and manufacture using flexographic printing, slot-die coating and rotary screen printing, *J. Mater. Chem.* 20 (2010) 8994–9001.
- [17] B. Moralejo, M.A. González, J. Jiménez, V. Parra, O. Martínez, J. Gutiérrez, O. Charro, LBIC and Reflectance Mapping of Multicrystalline Si Solar Cells, *J. Electron. Mater.* 39 (2010) 663–670.
- [18] N.M. Thantsha, E.Q.B. Macabebe, F.J. Vorster, E.E. van Dyk, Opto electronic analysis of silicon solar cells by LBIC investigations and current-voltage characterization, *Physica B* 404 (2009) 4445–4448.
- [19] P.M. Sirimanne, T. Jeranko, P. Bogdanoff, S. Fiechter, H. Tributsch, On the photo-degradation of dye sensitized solid-state TiO<sub>2</sub> |dye| CuI cells, *Semicond. Sci. Technol.* 18 (2003) 708–712.
- [20] S. Cataldo, S. Fabiano, F. Ferrante, F. Previti, S. Patané, B. Pignataro, Organoboron polymers for photovoltaic bulk heterojunctions, *Macromol. Rapid Commun.* 31 (2010) 1281–1286.
- [21] T.A. Bull, L.S.C. Pingree, S.A. Jenekhe, D.S. Ginger, C.K. Luscombe, The role of mesoscopic PCBM crystallites in solvent vapor annealed copolymer solar cells, *ACS Nano* 3 (2009) 627–636.
- [22] F.C. Krebs, J. Alstrup, H. Spanggaard, K. Larsen, E. Kold, Production of large-area polymer solar cells by industrial silk screen printing, lifetime considerations and lamination with polyethyleneterephthalate, *Sol. Energy Mater. Sol. Cells* 83 (2004) 293–300.
- [23] F.C. Krebs, H. Spanggaard, T. Kjær, M. Biancardo, J. Alstrup, Large area plastic solar cell modules, *Mater. Sci. Eng. B* 138 (2007) 106–111.

Cite this: *J. Mater. Chem.*, 2011, **21**, 4132

www.rsc.org/materials

PAPER

## Photochemical stability of $\pi$ -conjugated polymers for polymer solar cells: a rule of thumb†

Matthieu Manceau, Eva Bundgaard, Jon E. Carlé, Ole Hagemann, Martin Helgesen, Roar Søndergaard, Mikkel Jørgensen and Frederik C. Krebs\*

Received 15th September 2010, Accepted 16th December 2010

DOI: 10.1039/c0jm03105d

A comparative photochemical stability study of a wide range of  $\pi$ -conjugated polymers relevant to polymer solar cells is presented. The behavior of each material has been investigated under simulated sunlight (1 sun, 1000 W m<sup>-2</sup>, AM 1.5G) and ambient atmosphere. Degradation was monitored during ageing combining UV-visible and infrared spectroscopies. From the comparison of the collected data, the influence of the polymer chemical structure on its stability has been discussed. General rules relative to the polymer structure–stability relationship are proposed.

### Introduction

Polymer-based solar cells (PSCs) have the potential to become one of the future's renewable and environmentally friendly energy sources. Combining several attractive properties—flexibility, low manufacturing costs, low capital investment in equipment, a low thermal budget and the use of only abundant elements in the active layer—they open up a variety of new market opportunities and applications and have thus been under intense research focus during the last decade.<sup>1–6</sup> This development has led to a significantly improved device power conversion efficiency, that now exceeds 8%.<sup>7</sup> To reach this, many classes of new polymers have been designed, synthesized, characterized and incorporated into photovoltaic devices.<sup>1,2,8–11</sup> Consequently, a very broad range of material families have already been investigated in order to create polymers with good solubility, small band-gap, strong absorbance, appropriate HOMO and LUMO energy levels and high charge carrier mobilities.

However efficient and promising these materials are, their practical use in large-scale PSC production can only be successful if they also provide a good processability, a sufficient photochemical stability and device stability.<sup>12,13</sup> So far, this last point has received limited attention and the literature is still scarce. As a result, the relationship between the polymer chemical structure and the expected device efficiency is rather well explored, the chemical structure–photochemical stability relationship, however, remains largely unknown.

From a simplified chemical point of view, polymers for organic solar cells can be described as the combination of a rigid  $\pi$ -conjugated backbone regularly substituted by side-chain groups ensuring their solution processability. Previously published papers already identified the critical role of the side-chain in the polymer degradation processes.<sup>14–16</sup> A large difference in terms of the stability between MDMO–PPV and P3HT—two of the most studied polymers in the field—was also reported, P3HT being much more stable whatever the ageing conditions.<sup>17</sup> However, to our knowledge, no detailed studies have yet been dedicated to the influence of the backbone nature on the polymer stability.

In this work, we present a photochemical stability study in air on 24 different polymers (34 including the thermo-cleaved derivatives) relevant to PSCs. Samples were selected to cover a very broad range of polymer types (purely donor, donor/acceptor, thermo-cleavable, *etc.*) and chemical structures. Many of the moieties commonly used in the PSCs field are thus included in this paper. As all the experiments were conducted under the same conditions, comparison of the collected data was possible and the influence of different points is discussed (donor and acceptor group nature, side-chain type). This screening finally allowed for the description of general rules for the  $\pi$ -conjugated polymer photochemical stability.

### Experimental

#### Samples preparation

Synthetic procedures and characterization data for the materials have either been described in detail elsewhere<sup>18–24</sup> or are given in the ESI†. Molecular weights and optical band-gaps of the samples are collected in Table S1, ESI† (where available, power conversion efficiencies have been added).

Pure polymer samples were spin-coated on KBr plates from chlorobenzene solutions. The polymer concentration in the

Riso National Laboratory for Sustainable Energy, Technical University of Denmark, P.O. Box 49, DK-4000 Roskilde, Denmark. E-mail: frkr@riso.dtu.dk; Fax: +45 46 77 47 91; Tel: +45 46 77 47 99

† Electronic supplementary information (ESI) available: Characterization data of the polymers, list of abbreviations, thermal cleavage conditions and IR spectra recorded along ageing. See DOI: 10.1039/c0jm03105d

spin-coating solutions were adjusted to get a maximum peak absorbance of about 0.8 for each material.

Thermal cleavage was performed in the inert atmosphere of a glove box and the reaction progress was checked by IR spectroscopy. The heating step was kept as short as possible to avoid undesirable thermal degradation reactions. For cleavage temperatures and durations, see Table S2, ESI†.

### Ageing and characterization

Samples were illuminated under 1 sun and ambient air with monitoring of the relative humidity (but no control) using a standard solar simulator from Steuernagel Lichttechnik (KHS 575, AM 1.5G, 1000 W m<sup>-2</sup>, 85 °C, 30 ± 10% RH). The samples were removed periodically and UV-visible absorbance and IR spectra were recorded to monitor the degradation. UV-visible absorbance spectra were recorded from 200 to 1100 nm using a UV-1700 spectrometer from Shimadzu. IR spectroscopy was conducted with a Spectrum One from PerkinElmer operating in transmission mode (4 cm<sup>-1</sup> resolution, 32 scans summation).

### Stability evaluation

To quantitatively compare all the materials, the total amount of absorbed photons ( $N_{\text{Tot}}^t$ ) was monitored *versus* ageing time over the range  $\lambda_1 - \lambda_2$  by summation over the polymer absorption peaks (Table S1, ESI†). This value was calculated according to the following equation:

$$N_{\text{Tot}}^t = \sum_{\lambda_1}^{\lambda_2} N_0(\lambda) \times (1 - 10^{-A'(\lambda)})$$

where  $A'(\lambda)$  is the absorbance at a given wavelength ( $\lambda$ ) and time ( $t$ ), and  $N_0(\lambda)$  is the incident photon flux.  $A'(\lambda)$  was directly extracted from the UV-visible absorbance spectra of the sample at the corresponding ageing time ( $t$ ). The ASTM G173 standard was used as a reference for the incident photon flux.<sup>25</sup>

At the end of the degradation, the quantity of absorbed photons systematically reached a constant value ( $N_{\text{Tot}}^\infty$ ) after which no absorbance evolution followed. This value was always above zero due to the absorption, reflection and scattering of the KBr substrate. Finally, the normalized number of photons absorbed by the polymer was calculated by:

$$N_{\text{Photons}}^t = \frac{N_{\text{Tot}}^t - N_{\text{Tot}}^\infty}{N_{\text{Tot}}^0 - N_{\text{Tot}}^\infty}$$

For a great majority of the experiments,  $N_{\text{Photons}}^t$  exhibited a linear decay. In that case, the experimental data were then fitted with a straight curve. Quantitative comparisons of the respective stability of different samples were then established using the slopes of these curves. In some cases a logarithmic time scale was used for the sake of clarity.

### Naming of compounds

Different abbreviations can often be found in the literature for the same material due to the very complex IUPAC names that these materials generally present. We have employed the most commonly employed abbreviations for these materials and also

provide a list of the studied chemical units along with their full IUPAC names and the abbreviations in the ESI†.

## Results and discussion

### Pure donor polymers

During the last decade, two polymer families have played a major role in the development of PSCs: polyphenylenevinylene derivatives and polythiophene. For example, polymers such as poly(2-methoxy-5-(2'-ethylhexyloxy)-1,4-phenylenevinylene) (MEH-PPV), poly(2-methoxy-5-(3',7'-dimethyloctyloxy)-1,4-phenylenevinylene) (MDMO-PPV) and poly(3-hexylthiophene) (P3HT) have been widely studied as they used to give the best device performances. A few reports on the photochemical stability of these materials have been published.<sup>14-17</sup> Some of these studies revealed that polyphenylenevinylene derivatives are extremely unstable under photo-oxidative conditions.<sup>14</sup> This behavior has been attributed both to the presence of the vinylene bond and of the alkoxy substituents. Conversely, P3HT has been shown to be much more stable.<sup>17</sup>

In this first part of the study, we compare the photochemical behavior in air of two donor conjugated polymers: MEH-PPV and poly(2,2'-(2,5-bis(2-hexyldecyloxy)-1,4-phenylene)-dithiophene) (JC1) (Fig. 1).

Both materials are comprised of a dialkoxybenzene unit alternating either with a vinylene bond (MEH-PPV) or a bithiophene group (JC1). P3HT data were also added and used as a benchmark. From the results presented in Fig. 1, it is very clear that JC1 is much more stable than MEH-PPV. This result confirms that the exocyclic double bond has a very strong detrimental effect on the MEH-PPV stability. This very low stability is due to the fact that vinylene bonds can be easily saturated by the radicals formed after side-chain cleavage.<sup>14</sup> Owing to its aromaticity, thiophene is much more difficult to saturate. Replacing the vinylene unit by a bithiophene thus greatly enhances the whole polymer stability.

Very interestingly, JC1 is observed to be as stable as P3HT which could be surprising as alkoxy side-chains are well-known for their poor stability. It should, however, be recalled that P3HT instability has been ascribed to the *hexyl* side-chains. The presence of two unsubstituted thiophene rings in JC1 then probably balances the presence of the alkoxy substituents on the *phenyl* ring and explains our finding.

### Donor-acceptor copolymers, backbone composition effect

Presently, strong efforts are directed towards the synthesis of materials absorbing at longer wavelengths (*i.e.* with lower band-gaps) that can harvest a larger fraction of the solar spectrum. The most common strategy to control the band-gap is to alternate the electron-rich (donor) and electron-poor (acceptor) groups in the main chain of the polymer.<sup>8,26-28</sup> An Internal Charge Transfer (ICT) from the donor to the acceptor occurs and a reduction of the band-gap is achieved. In this part of the study, attention will be focused on these so-called donor/acceptor polymers.

**Influence of the donor group.** Five series of polymers were aged to investigate the influence of the donor group on the stability of

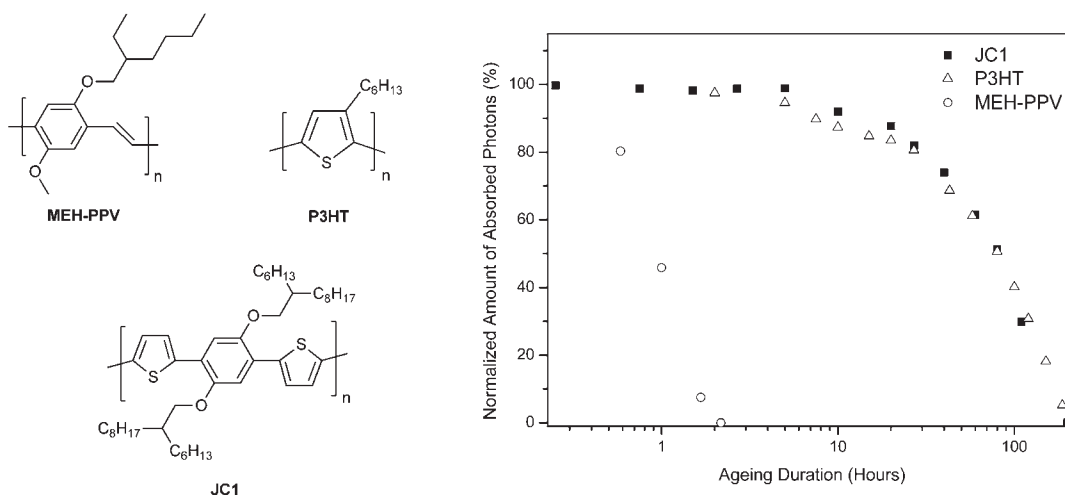


**Fig. 1** (Left) Chemical structure of the investigated samples, (right) evolution of the normalized amount of absorbed photons during photochemical ageing. Note how MEH-PPV degrades very quickly.

the polymer. For a given series of compounds, the only difference between the samples was the nature of the donor moiety.

**Dithienylthienopyrazine series.** Materials belonging to this first class are copolymers based on dithienylthienopyrazine bearing thermo-cleavable tertiary esters on the pyrazine ring, alternating with different donor groups: fluorene, carbon-bridged cyclopentadithiophene (CPDT), silicon-bridged cyclopentadithiophene (Si-CPDT) and thiophene (Fig. 2).

Fig. 3 presents the evolution of the normalized amount of absorbed photons *versus* ageing time for each polymer. As clearly observed, the stability ranking from the lowest to the highest is as follows: fluorene-CPDT-Si-CPDT-thiophene. It is also worth noting that an identical ranking is obtained with the cleaved materials but on a very different timescale (Fig. 3). This second point will be discussed in detail later. Different comments can be made based on this ranking. First of all, the two least stable polymers contain a quaternary carbon atom in their backbone. As this type of site can be readily oxidized,<sup>29,30</sup> this can explain the poor stability of these two polymers that are completely bleached after less than 100 hours. Secondly, it can be noticed

that the substitution of this quaternary carbon atom by a silicon atom results in a significant improvement in the stability. One could imagine that this increase originates from a lowering of the HOMO level when carbon is replaced by silicon, as a deeper HOMO enhances the oxidative stability.<sup>31</sup> However, *Scharber et al.* and *Chen et al.* previously showed that the nature of the bridging atom (C or Si) had almost no influence on the HOMO and LUMO levels of the polymer.<sup>32,33</sup> This implies that the observed stability improvement cannot result from a lower HOMO level. But, it could be explained by the presence of the silicon atom which is known to be less easily oxidized than the carbon. Finally, using unsubstituted thiophene as a donor group highly improves the photochemical stability. More than 600 hours of irradiation are necessary to achieve full degradation. It is likely that this increase comes from the absence of both the quaternary site and side-chain in this donor moiety.

In parallel, the behavior of the non-cleaved samples was monitored by IR spectroscopy all along the ageing process (see Fig. S1, ESI†). Interestingly, very similar modifications are observed for the different polymers albeit on different timescales. Indeed, one can systematically notice: (i) a decrease in the intensity of the signals coming from the alkyl side-chains (3000–2850  $\text{cm}^{-1}$ ); (ii) the development of a broad signal in the carbonyl range (1800–1600  $\text{cm}^{-1}$ ) and (iii) the appearance of signals characteristic for sulfinic esters (1115 and 620  $\text{cm}^{-1}$ ). As reported in the case of P3HT, the observation of these latter bands indicates that the final degradation stages of the thiophene rings are reached.<sup>15</sup> Their appearance is then a good indicator of how advanced the sample degradation is. Here we noticed that such signals appeared very quickly for the fluorene and CPDT-based compounds (about 20 hours). On the contrary, they were only detected after 200 hours for the thiophene.

As for cleaved materials, the behavior was very similar to the pristine polymers, but changes in the IR spectrum were much slower after cleavage. This is in good agreement with our previously published results.<sup>34</sup>

**Dithienylbenzothiadiazole (Series 1).** To check the consistency of the previous results, three of the four previous donor

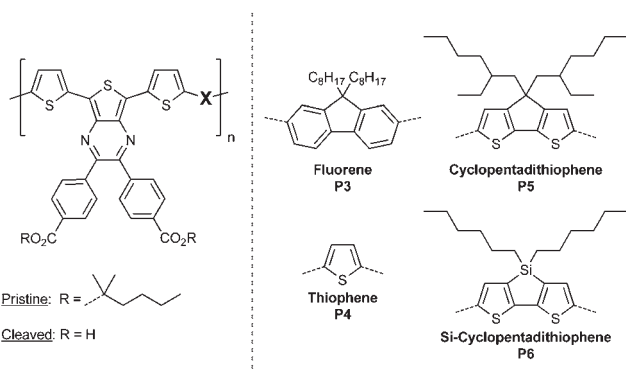


**Fig. 2** Chemical structure of the materials in the series of materials using a thermo-cleavable dithienylthienopyrazine (shown left). The X in the polymer backbone designates one of four donor groups shown to the right of the broken line.

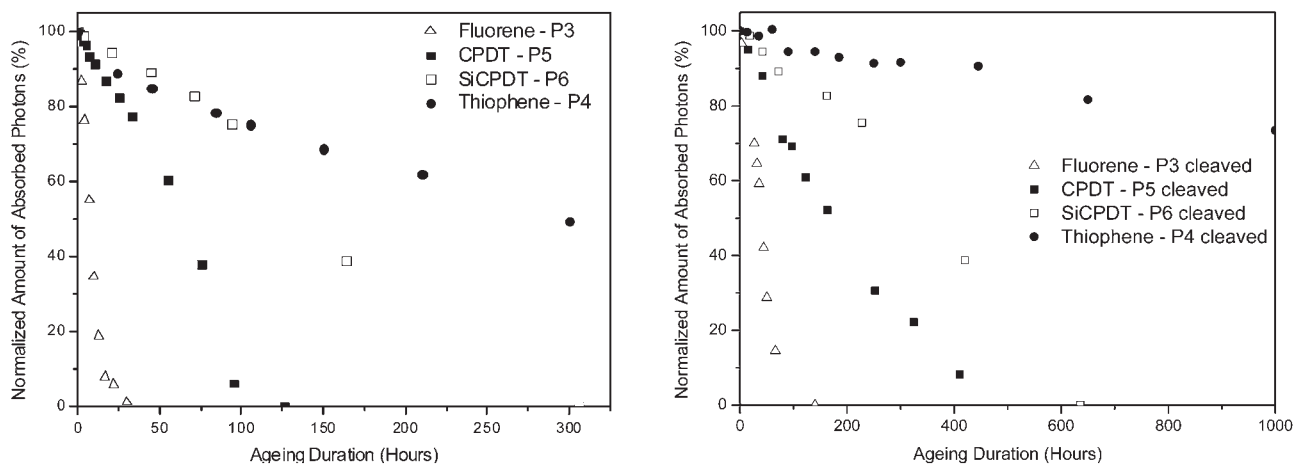


Fig. 3 Evolution of the normalized amount of absorbed photons during photochemical ageing. (Left) Pristine polymers, (right) cleaved polymers.

groups—thiophene, CPDT and Si-CPDT—were investigated in a second set of experiments. Here, samples were based on an electron-deficient benzothiadiazole group with two flanking thiophene rings substituted by a cleavable ester moiety (Fig. 4). From Fig. 4, it is obvious that the stability ranking remains identical to the one reported in the previous section.

This means that even though different parameters can influence the stability of a polymer (e.g. molecular weight, regiorregularity, purity) the chemical nature remains the most important one.

*Dithienylbenzothiadiazole (Series 2).* In a third step, three new electron-rich moieties were introduced—dialkoxybenzene, carbazole, thienimidazolone—and compared to thiophene and CPDT. These donor moieties were copolymerized with a central benzothiadiazole flanked by two unsubstituted thiophene rings (Fig. 5). Here again, the evolution of the amount of absorbed photons has been recorded all along ageing and results are shown in Fig. 5. IR data are also provided in the ESI (Fig. S2†).

The thienimidazolone-based sample appeared to be as unstable as the one based on CPDT. This is related to the presence of the imide group that is photochemically unstable.<sup>35</sup> As evidenced by *Arnaud et al.*, irradiation of this unit causes the homolysis of the C–N bonds which leads to the degradation of the whole unit through oxidation of the formed radicals. This is confirmed here, as the IR bands characteristic for the imide group (1725 and 1560  $\text{cm}^{-1}$ ) disappeared after only a few hours of irradiation. As the donor unit is quickly degraded, the ICT is prevented and a rapid absorbance loss takes place.

Attention should also be drawn to the fact that the polymers containing the carbazole and dialkoxybenzene groups were more stable than polymers containing the CPDT moiety. However, they all degrade relatively quickly as complete photo-bleaching was achieved after less than 100 hours. A rapid decrease in the IR bands coming from carbazole moieties (e.g. 1600  $\text{cm}^{-1}$ ) was evidenced confirming the limited stability of this moiety. This can be ascribed to various phenomena. First, it is due to the presence of the  $\text{C}_{\text{sp}^3}\text{--N}$  bond that can be easily cleaved as previously reported.<sup>36</sup> A carbazolyl radical is generated, that can further

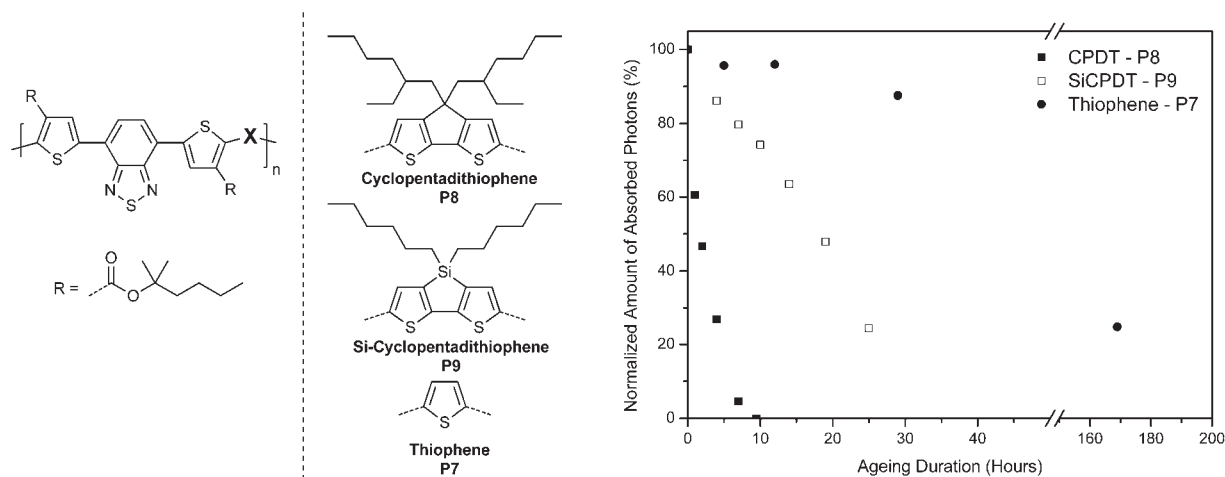
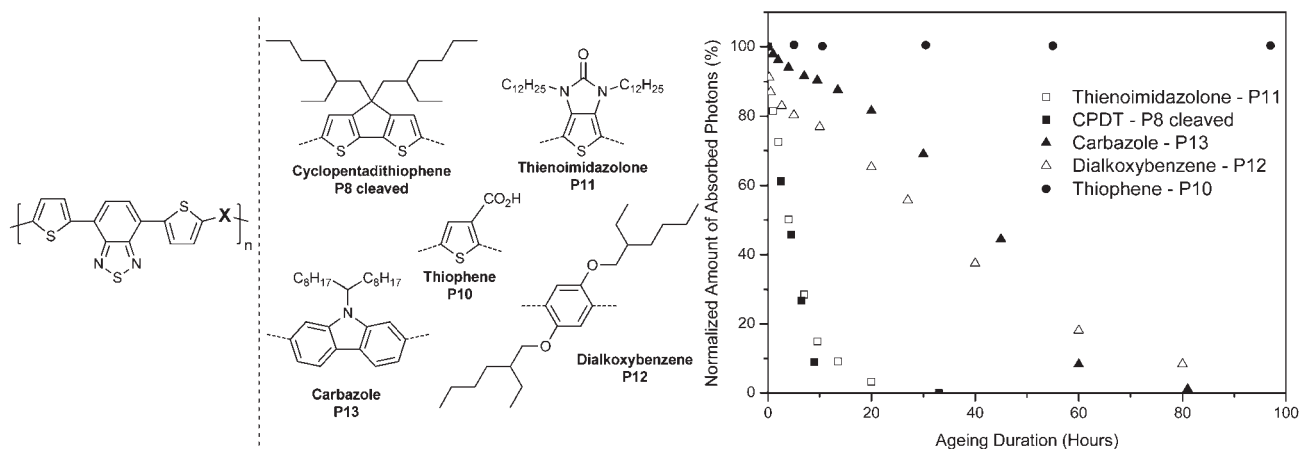


Fig. 4 Chemical structures of the investigated polymer samples (left). The X denotes one of the three donor units shown to the right of the broken line (middle). The evolution of the normalized amount of absorbed photons during photochemical ageing of all materials is shown in the plot (right).





**Fig. 5** Chemical structure of the investigated polymer samples (left). The X denotes one of the five donor units shown to the right of the broken line (middle). The evolution of the normalized amount of absorbed photons during photochemical ageing of all materials is shown in the plot (right).

react with oxygen. This ends up in the degradation of the carbazole group, and thus in the interruption of the  $\pi$ -conjugated system. The C–N bond cleavage was confirmed by the IR monitoring, as signals characteristic for alkyl side-chains ( $\nu_{\text{C-H}} \approx 3000$  to  $2850 \text{ cm}^{-1}$ ) and  $\text{C}_{\text{sp}^3}\text{-N}$  bonds ( $\nu_{\text{C-N}} \approx 1330 \text{ cm}^{-1}$ ) quickly vanished. Pfister and Williams also suggested that irradiation of the carbazole group leads to the formation of quinonic oxidized structures after reaction with the superoxide anion  $\text{O}_2^{\cdot-}$ .<sup>37</sup> This second pathway can also contribute to the photodegradation of the sample.

The dialkoxybenzene-based polymer appeared to be approximately as stable as the carbazole-based sample. This finding can seem rather surprising as alkoxy side-chains are usually known for their very negative impact on the polymer stability. The C–O bond is indeed readily cleavable under irradiation<sup>38</sup> and as expected, the intensity of the IR bands coming from the side-chains ( $\nu_{\text{C-H}} \approx 3000$  to  $2850 \text{ cm}^{-1}$  and  $\nu_{\text{C-O}} 1385 \text{ cm}^{-1}$ ) gradually

decreases all along ageing. However, the breaking of this bond does not affect the conjugated backbone of the polymer directly as it is the case for C–N homolysis in the carbazole moiety. This could explain why the dialkoxybenzene unit gives a photochemical stability comparable to that of the carbazole.

Finally, and as one could have expected, the thiophene-based polymer was once again shown to be the most stable among the investigated materials although it was substituted by a carboxylic acid. This is due to the simultaneous absence of breakable bonds (C–O, C–N), of the quaternary carbon and of cleavable side-chain.

*Dithienylbenzothiadiazole (Series 3)*. This fourth class is similar to the previous one except that the benzothiadiazole unit bears two solubilizing alkoxy side-chains (Fig. 6). Three donor units have been studied—CPDT, Si-CPDT, carbazole—and the results are presented in Fig. 6. First, it is further confirmed that

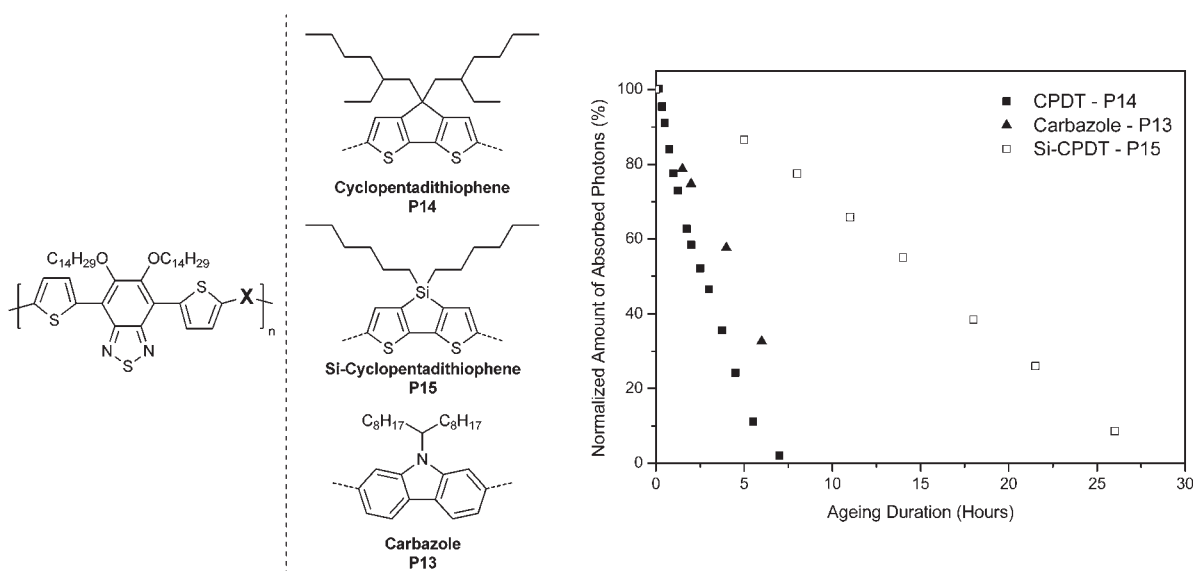


**Fig. 6** Chemical structure of the investigated polymer samples (left). The X denotes one of the three donor units shown to the right of the broken line (middle). The evolution of the normalized amount of absorbed photons during photochemical ageing of all materials is shown in the plot (right).

the use of Si-CPDT provides a greater stability than CPDT. This finding is consistent with the previously discussed data.

Secondly, we observe that carbazole is less stable than Si-CPDT. As deduced from these results, the stability ranking from the lowest to the highest for this series of compounds is: CPDT–Carbazole–Si-CPDT.

**Benzothiadiazole series.** So far the unsubstituted thiophene ring has been shown to be the most stable moiety especially because this moiety is side-chain free. So, in a last series of experiments, different unsubstituted aromatic donor groups were investigated: thiophene, benzodithiophene and dithienothiophene. Samples were based on a benzothiadiazole unit bearing solubilizing alkoxy side-chains without flanking thiophenes (Fig. 7).

As observed in Fig. 7, the change of the thiophene by a benzodithiophene results approximately in a twofold stability increase. One can also easily notice that the dithienothiophene derivative provides by far the highest stability. Obviously, the use of unsubstituted polycyclic aromatic units is thus beneficial in terms of the photochemical stability.

In summary, a combination of all the results collected so far enables the formulation of a global stability ranking for the investigated donor groups as shown in Fig. 8. One can conclude that the presence of a quaternary carbon atom or an easily cleavable bond leads to a rather low stability. Conversely, donor units that provide the highest stability are those without any side-chain.

**Influence of the acceptor group.** In a similar fashion, the influence of the acceptor group on the photochemical stability of conjugated polymers was investigated.

**Dithienocyclopentadithiophene series.** To begin, we studied benzothiadiazole (BTD) and thienopyrazine (TPz) units. As illustrated in Fig. 9, samples were based on a dithienocyclopentadithiophene electron-rich group. In order to minimize the effects of the side-chain, we chose to study a TPz unit substituted by the carboxylic acid (*i.e.* thermo-cleaved).

From Fig. 9, it is very clear that the sample containing the TPz unit is significantly more stable. This effect cannot be explained by the presence of side-chains or by a difference in the samples HOMO position. *Blouin et al.* reported that the substitution of a BTD unit by a TPz should theoretically lead to an increase in the polymer HOMO energy level.<sup>39</sup> This was confirmed experimentally by *Bijleveld et al.* and should engender a lower oxidative stability of the TPz-based compound.<sup>40</sup> The superior stability of the sample based on the TPz moiety must then come from a greater intrinsic photochemical stability of this unit.

**Si-bridged cyclopentadithiophene series.** A second set of polymers was then studied. This one was based on the Si-CPDT unit associated either with a benzothiadiazole (BTD) unit or an ester-substituted thienothiophene (Fig. 10). This latter has recently given very good results in terms of efficiencies.<sup>10,11</sup>

According to the results presented in Fig. 10, the BTD-based polymer appears to be much more stable than the thienothiophene. However, it should be emphasized that, whereas the BTD group is not substituted, the thienothiophene unit bears a primary ester side-chain. It is thus very likely that the rather fast degradation originates from this group as IR monitoring of the degradation shows a decrease in the signals pertaining to this ester moiety (*e.g.*  $\nu_{C-O} \approx 1350 \text{ cm}^{-1}$ , see Fig. S3, ESI†). In addition, signals characteristic for the degradation of the sulfur-containing rings appeared quickly (around 1115 and 620  $\text{cm}^{-1}$ ). As previously stated, the observation of such signals implies an opening of the ring and thus an advanced degradation level. The presence of this side-chain is, however, required to adjust the position of the energy levels.<sup>10</sup> It should be added that very good performance has also been obtained using the thienothiophene group substituted by a ketone.<sup>11</sup> Ketones are well-known to be highly unstable under irradiation as they readily evolve through Norrish reactions.<sup>41</sup> It can be anticipated that the photochemical stability of the whole sample will be rather limited.

As for the previous section dedicated to the donor group, the different data were combined to establish the stability ranking given in Fig. 11. Here again the most stable moieties are the ones without side-chains or readily cleavable bonds.

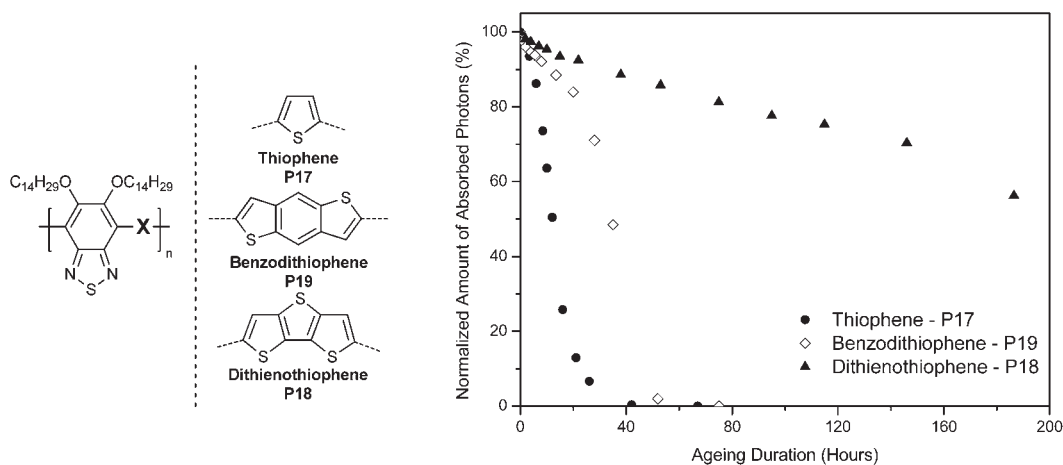


**Fig. 7** Chemical structure of the investigated polymer samples (left). The X denotes one of the three donor units shown to the right of the broken line (middle). The evolution of the normalized amount of absorbed photons during photochemical ageing of all materials is shown in the plot (right).

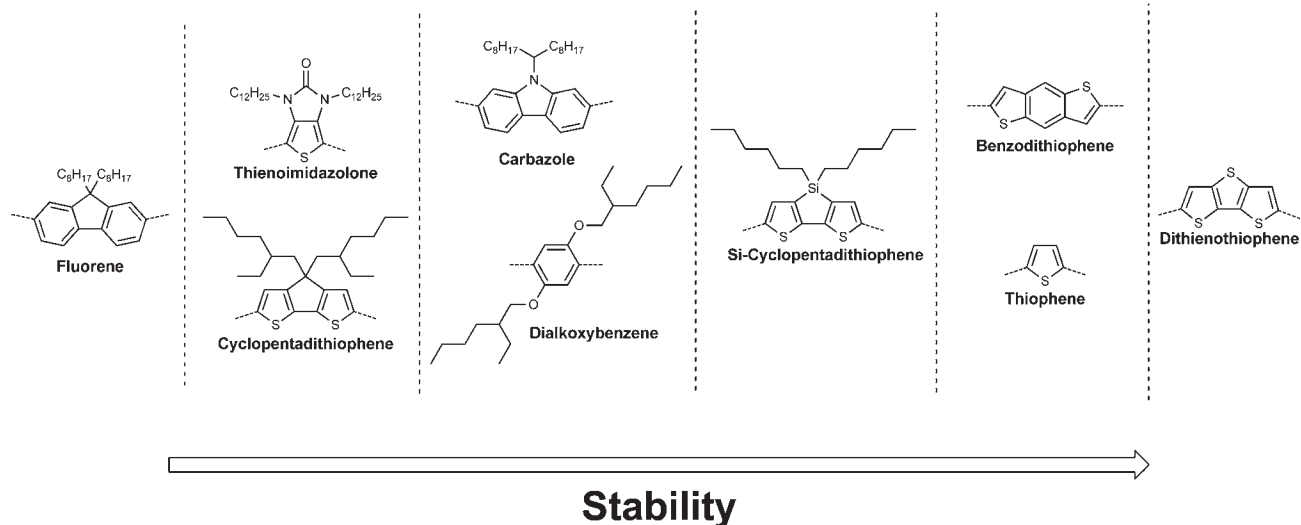


Fig. 8 Donor group stability ranking.

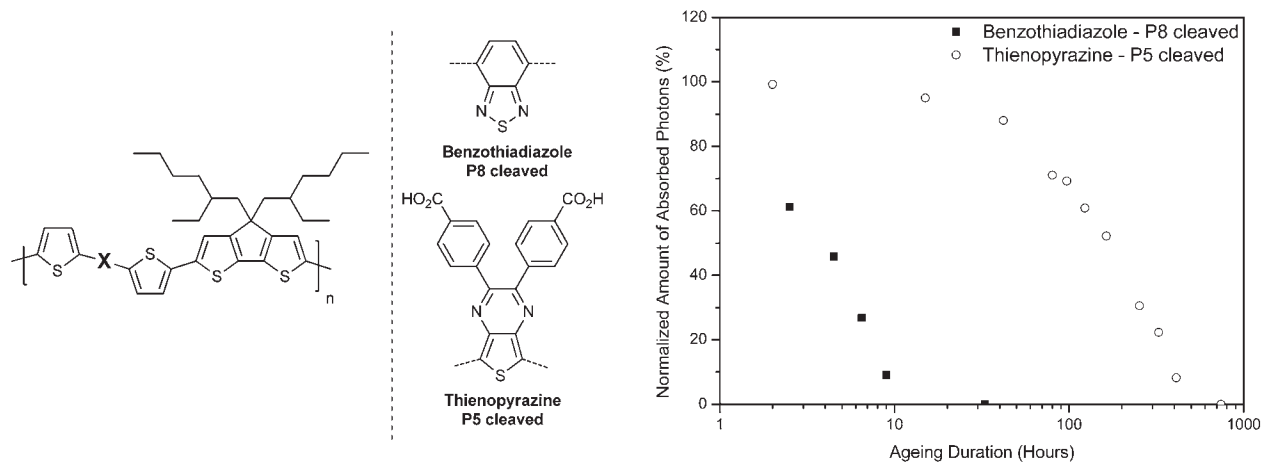


Fig. 9 Chemical structure of the investigated polymer samples (left). The X denotes one of the two acceptor units shown to the right of the broken line (middle). The evolution of the normalized amount of absorbed photons during photochemical ageing of all materials is shown in the plot (right).

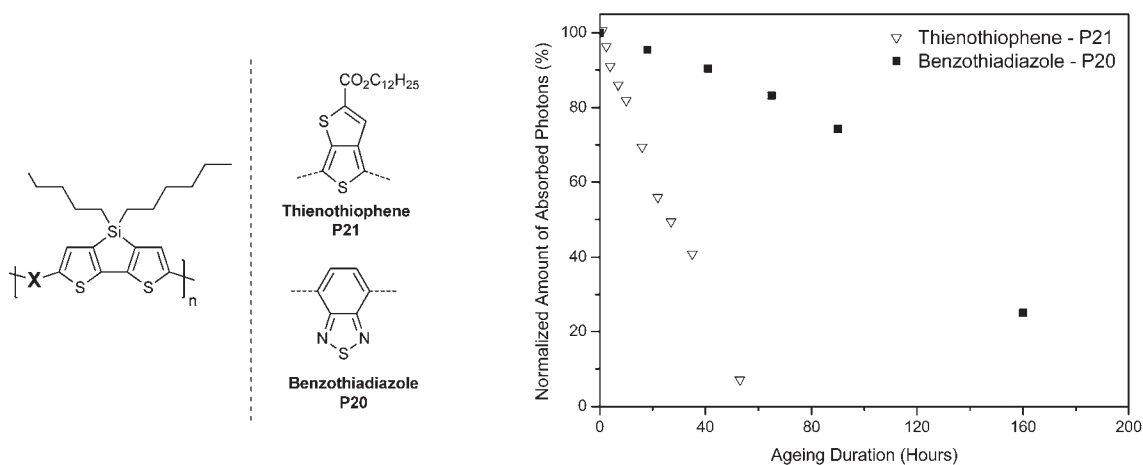


Fig. 10 Chemical structure of the investigated polymer samples (left). The X denotes one of the two acceptor units shown to the right of the broken line (middle). The evolution of the normalized amount of absorbed photons during photochemical ageing of all materials is shown in the plot (right).



### Side-chain effect

**Influence of the nature of side-chains.** The presence of side-chains is necessary to ensure a sufficient solubility of the sample and thus allows the solution-processability of the PSCs active layer. However, side-chains can also be used to tune other properties of the materials such as the positions of the HOMO and LUMO levels or the packing of the macromolecular chains.<sup>10</sup>

To begin, we studied different alternating polymers based on a dithienocyclopentadithiophene unit associated with a benzothiadiazole group. This latter was either unsubstituted or substituted with one of the following side-chains: ether or ester (Fig. 12). As in the previous experiments, the total number of absorbed photons was recorded all along ageing and the results are presented on Fig. 12.

According to these results, the stability ranking from the lowest to the highest is as follows: CO<sub>2</sub>R < OR < H. As expected, the unsubstituted BTD demonstrates the highest stability among the three samples although the durability difference with the other samples is surprisingly low. On the contrary, ester and alkoxy substituents gave a lower stability, the latter being slightly more stable.

**Thermo-cleavable polymers.** As described in previously published papers<sup>14–16</sup> and also shown before in this study, side-chains have a negative influence on the polymer photochemical stability. In addition, in a previous paper we showed that side-chain thermal cleavage systematically lead to a strong increase in the sample photochemical stability.<sup>34</sup> Here, the study was extended to various new thermo-cleavable polymers, and a total of 8 different samples were investigated.

Whatever the sample nature, thermo-cleavage systematically led to an increase in the stability as exemplified on Fig. 3. In every case, the amount of absorbed photons exhibited a quasi-linear decay and the experimental data were thus fitted with a straight curve. The stability improvement provided by thermal cleavage was then estimated quantitatively for each sample by comparing the slope of the curves before and after side-chain cleavage. These results are reported in the ESI (Table S2<sup>†</sup>). Depending on

the backbone chemical structure, it was noticed that thermo-cleaved samples are approximately between 2 and 20 times more stable than corresponding pristine materials. This set of results further confirms the higher potential stability offered by thermo-cleaved conjugated polymers. Among the investigated materials, the beneficial effect of thermal cleavage surprisingly appeared to be more pronounced for those which are the most stable before cleavage. This is of course a very interesting and fortunate result.

It should finally be mentioned that some of the thermo-cleaved polymers exhibited a very high photochemical stability. For example, 1000 hours irradiation of the polymer based on a thienopyrazine unit and three thiophene rings only lead to a 20% decrease in the amount of absorbed photons.

### Summary

As clearly demonstrated in the present work, slight changes in the material's chemical structure can result in huge variations in the photochemical stability. Indeed, polymer durability was shown to cover a very broad range of values, from very few hours (*e.g.* MEH-PPV) to several thousands of hours (*e.g.* thermo-cleaved samples). Several crucial parameters influencing the stability have been identified through this study and the main findings have been summarized in the following basic rules.

1. The use of exocyclic double bonds in the main backbone (MEH-PPV, MDMO-PPV) leads to a poor stability and should be avoided,

2. Moieties containing a quaternary site are very unstable (*e.g.* fluorene, cyclopentadithiophene) because of the oxidizability of this site,

3. The presence of readily cleavable bonds (such as C–N or C–O) also limits stability,

4. Side-chains play a key role in conjugated polymer degradation and their cleavage largely improves stability,

5. Aromatic polycyclic units generally exhibit a good photochemical stability.

Indirectly, it was also shown that the position of the HOMO level for the polymers is not a sufficient criterion to conclude on the photochemical stability.

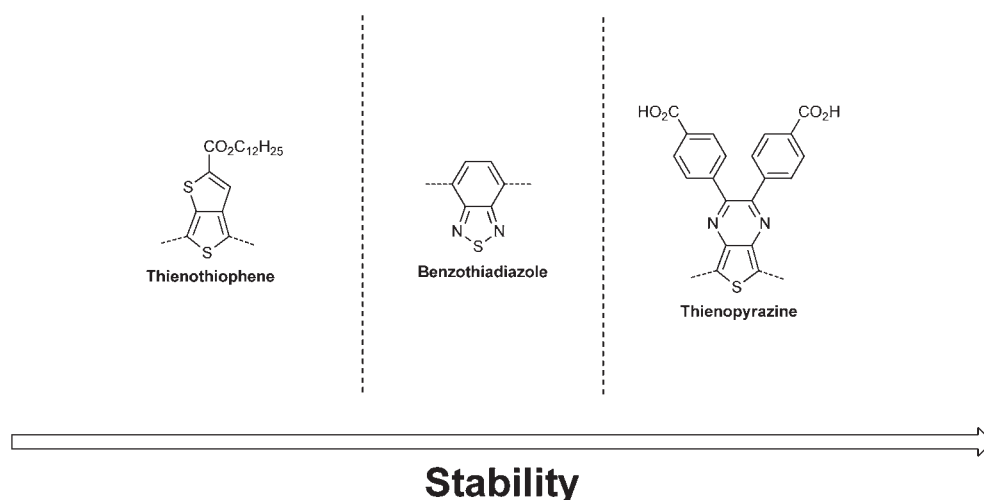
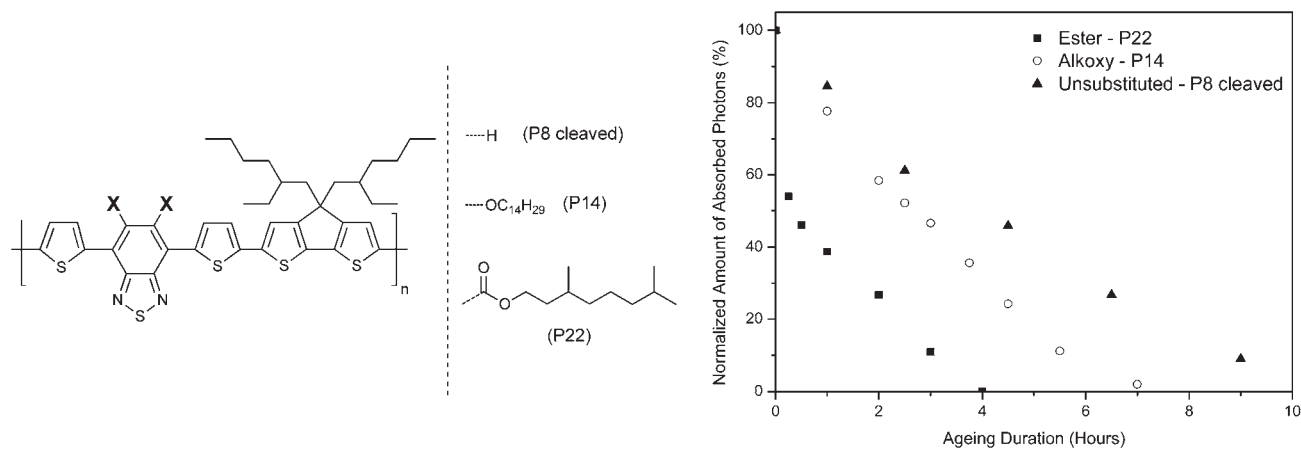
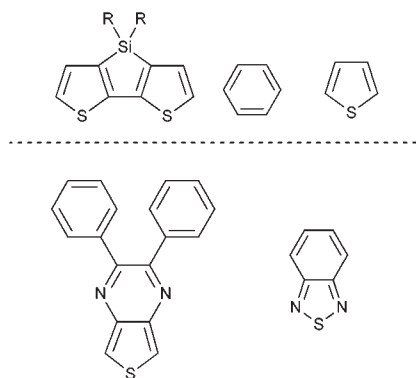


Fig. 11 Acceptor group stability ranking.



**Fig. 12** Chemical structure of the investigated polymer samples (left). The X denotes one of the three substituents shown to the right of the broken line (middle). The evolution of the normalized amount of absorbed photons during photochemical ageing of all materials is shown in the plot (right).



**Fig. 13** Most stable donor (top) and acceptor units (bottom) identified within this study.

Fig. 13 provides a list of the most stable donor and acceptor building blocks we identified. Assembly of these units into larger aromatic ones is also expected to lead to stable blocks as evidenced by the behavior of the dithienothiophene group. Finally, for the side-chains, a good rule of thumb is to keep their amount as low as possible whatever their chemical nature.

## Conclusions

In conclusion, we have mapped the photochemical stability in air for a wide range of  $\pi$ -conjugated polymers relevant to PSCs. By comparing the data collected for more than 25 different samples, various points critical for the polymer stability have been identified. This enabled us to rationalize how variations in the chemical structure of  $\pi$ -conjugated polymers impact the photochemical stability. Our results thus provide a better description of the structure–stability relationship, as well as important insight that will prove useful to anyone in the process of designing new materials for PSCs. We are of course fully aware that the photochemical stability is only one aspect of the complex PSC stability problem and that stable but inefficient polymers are rather useless. However, we believe that this study can provide meaningful help if one's aim is to synthesize new good candidates for PSCs that unite efficiency and stability.

## References

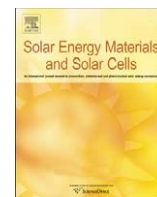
- 1 S. Beaupré, P.-L. T. Boudreault and M. Leclerc, *Adv. Mater.*, 2010, **22**, E6–E27.
- 2 M. Helgesen, R. Søndergaard and F. C. Krebs, *J. Mater. Chem.*, 2010, **20**, 36–50.
- 3 T. D. Nielsen, C. Cruickshank, S. Foged, J. Thorsen and F. C. Krebs, *Sol. Energy Mater. Sol. Cells*, 2010, **94**, 1553–1571.
- 4 F. C. Krebs, T. D. Nielsen, J. Fyenbo, M. Wadstrøm and M. S. Pedersen, *Energy Environ. Sci.*, 2010, **3**, 512–525.
- 5 F. C. Krebs, J. Fyenbo and M. Jørgensen, *J. Mater. Chem.*, 2010, **20**, 8994–9001.
- 6 F. C. Krebs, T. Tromholt and M. Jørgensen, *Nanoscale*, 2010, **2**, 873–886.
- 7 Konarka <http://www.konarka.com/>, accessed on 19/01/2011.
- 8 E. Bundgaard and F. C. Krebs, *Sol. Energy Mater. Sol. Cells*, 2007, **91**, 954–985.
- 9 X. Zhan and D. Zhu, *Polym. Chem.*, 2010, **1**, 410–419.
- 10 Y. Liang and L. Yu, *Acc. Chem. Res.*, 2010, **43**, 1227–1236.
- 11 H.-Y. Chen, J. Hou, S. Zhang, Y. Liang, G. Yang, Y. Yang, L. Yu, Y. Wu and G. Li, *Nat. Photonics*, 2009, **3**, 649–653.
- 12 F. C. Krebs, *Sol. Energy Mater. Sol. Cells*, 2009, **93**, 394–412.
- 13 M. Jørgensen, K. Norrman and F. C. Krebs, *Sol. Energy Mater. Sol. Cells*, 2008, **92**, 686–714.
- 14 S. Chambon, A. Rivaton, J.-L. Gardette, M. Firon and L. Lutsen, *J. Polym. Sci., Part A: Polym. Chem.*, 2007, **45**, 317–331.
- 15 M. Manceau, A. Rivaton, J.-L. Gardette, S. Guillerez and N. Lemaitre, *Polym. Degrad. Stab.*, 2009, **94**, 898–907.
- 16 H. Hintz, H.-J. Egelhaaf, H. Peisert and T. Chassé, *Polym. Degrad. Stab.*, 2010, **95**, 818–825.
- 17 M. Manceau, S. Chambon, A. Rivaton, J.-L. Gardette, S. Guillerez and N. Lemaitre, *Sol. Energy Mater. Sol. Cells*, 2010, **94**, 1572–1577.
- 18 F. C. Krebs, J. E. Carlé, N. Cruys-Bagger, M. Andersen, M. R. Lilledal, M. A. Hammond and S. Hvidt, *Sol. Energy Mater. Sol. Cells*, 2005, **86**, 499–516.
- 19 J. E. Carlé, J. W. Andreasen, M. Jørgensen and F. C. Krebs, *Sol. Energy Mater. Sol. Cells*, 2010, **94**, 774–780.
- 20 M. Helgesen and F. C. Krebs, *Macromolecules*, 2010, **43**, 1253–1260.
- 21 M. Helgesen, S. A. Gevorgyan, F. C. Krebs and R. A. J. Janssen, *Chem. Mater.*, 2009, **21**, 4669–4675.
- 22 M. Helgesen, F. C. Krebs, M. Bjerring and N. C. Nielsen, *Chem. Mater.*, 2010, **22**, 5617–5624.
- 23 E. Bundgaard, O. Hagemann, M. Manceau, M. Jørgensen and F. C. Krebs, *Macromolecules*, 2010, **43**, 8115–8120.
- 24 J. Liu, E. N. Kadnikova, Y. Liu, M. D. McGehee and J. M. J. Fréchet, *J. Am. Chem. Soc.*, 2004, **126**, 9486–9487.
- 25 NREL's AM1.5 Standard Dataset: <http://rredc.nrel.gov/solar/spectra/am1.5/>, accessed on 15/09/2010.
- 26 E. E. Havinga, W. Hoeve and H. Wynberg, *Polym. Bull.*, 1992, **29**, 119–126.
- 27 E. E. Havinga, W. Hoeve and H. Wynberg, *Synth. Met.*, 1993, **55**, 299–306.

- 28 P. M. Beaujuge, C. M. Amb and J. R. Reynolds, *Acc. Chem. Res.*, 2010, **43**, 1396–1407.
- 29 L. J. Lindgren, X. Wang, O. Inganäs and M. R. Andersson, *Synth. Met.*, 2005, **154**, 97–100.
- 30 A. Rivaton, B. Mailhot, J. Soulestin, H. Varghese and J.-L. Gardette, *Eur. Polym. J.*, 2002, **38**, 1349–1363.
- 31 D. M. de Leeuw, M. M. J. Simenon, A. R. Brown and R. E. F. Einerhand, *Synth. Met.*, 1997, **87**, 53–59.
- 32 M. C. Scharber, M. Koppe, J. Gao, F. Cordella, M. A. Loi, P. Denk, M. Morana, H.-J. Egelhaaf, K. Forberich, G. Dennler, R. Gaudiana, D. Waller, Z. Zhu, X. Shi and C. J. Brabec, *Adv. Mater.*, 2009, **21**, 1–4.
- 33 C.-H. Chen, C.-H. Hsieh, M. Dubosc, Y.-J. Cheng and C.-S. Hsu, *Macromolecules*, 2010, **43**, 697–708.
- 34 M. Manceau, M. Helgesen and F. C. Krebs, *Polym. Degrad. Stab.*, 2010, **95**, 2666–2669.
- 35 R. Arnaud, E. Fanton and J.-L. Gardette, *Polym. Degrad. Stab.*, 1994, **45**, 361–369.
- 36 A. Rivaton, B. Mailhot, G. Derderian, P. O. Bussiere and J.-L. Gardette, *Macromolecules*, 2003, **36**, 5815–5824.
- 37 G. Pfister and D. J. Williams, *J. Chem. Phys.*, 1974, **61**, 2416–2426.
- 38 S. Chambon, A. Rivaton, J.-L. Gardette and M. Firon, *Sol. Energy Mater. Sol. Cells*, 2008, **92**, 785–792.
- 39 N. Blouin, A. Michaud, D. Gendron, S. Wakim, E. Blair, R. Neagu-Plesu, M. Belletête, G. Durocher, Y. Tao and M. Leclerc, *J. Am. Chem. Soc.*, 2008, **130**, 732–742.
- 40 J. C. Bijleveld, M. Shahid, J. Gilot, M. M. Wienk and R. A. J. Janssen, *Adv. Funct. Mater.*, 2009, **19**, 3262–3270.
- 41 C. H. Bamford and R. G. W. Norrish, *J. Chem. Soc.*, 1935, 1504; R. G. W. Norrish and C. H. Bamford, *Nature*, 1936, **138**, 1016; R. G. W. Norrish and C. H. Bamford, *Nature*, 1937, **140**, 195; R. G. W. Norrish, *Trans. Faraday Soc.*, 1937, **33**, 1521.



Contents lists available at ScienceDirect

## Solar Energy Materials &amp; Solar Cells

journal homepage: [www.elsevier.com/locate/solmat](http://www.elsevier.com/locate/solmat)

## Fused thiophene/quinoxaline low band gap polymers for photovoltaic's with increased photochemical stability

Jon E. Carlé\*, Mikkel Jørgensen, Matthieu Manceau, Martin Helgesen, Ole Hagemann, Roar Søndergaard, Frederik C. Krebs

Risø National Laboratory for Sustainable Energy, Technical University of Denmark, Frederiksborgvej 399, DK-4000 Roskilde, Denmark

## ARTICLE INFO

## Article history:

Received 8 February 2011

Received in revised form

6 July 2011

Accepted 14 July 2011

## Keywords:

Polymer photovoltaic

Low band gap

Quinoxaline

Fused thiophene

Photochemical stability

## ABSTRACT

We investigate a family of low band-gap polymers based on the common acceptor moiety 2,3-bis-(3-octyloxyphenyl)quinoxaline (Q) combined with thiophene (T) or the fused thiophene systems: benzo[2,1-b:3,4-b']-dithiophene (BDT) or dithieno[3,2-b,2',3'-d]-thiophene (DTT). The photochemical stability of the three polymers was examined and compared to P3HT. They were found to be substantially more robust than P3HT with a ranking of DTTQ > BDTQ > TQ1 ≫ P3HT, indicating that the fused ring systems of DTT and BDT impart a large degree of photochemical stability than thiophene. Furthermore devices with normal and inverted geometry were prepared and tested in air. The normal geometry devices showed the highest efficiencies compared to the inverted, in particular owing to a higher  $V_{oc}$ , with TQ1 being the most efficient with a power conversion efficiency (PCE) of 1.5% ( $1000 \text{ W m}^{-2}$ , AM1.5 G). For the inverted devices TQ1 and DTTQ showed the best PCEs of 0.9%.

© 2011 Elsevier B.V. All rights reserved.

## 1. Introduction

Much of the present research effort within the field of polymer photovoltaic's is directed towards increasing the power conversion efficiency (PCE) now in the range of 8% or higher [1]. A common trend is the development of the so-called low band-gap materials with alternating donor-acceptor motifs. Polymers of this type display additional optical absorption bands due to charge-transfer transitions at longer wavelengths [2]. The result is typically a better match with the solar spectrum, harvesting of more photons and the ability to offer higher current densities. Just as important, but somewhat less explored is the stability of the photovoltaic devices. Most of the high performance devices presented in the literature are prepared and studied under inert atmosphere conditions. The combination of high efficiency and good stability in the same device/materials are essential for the transfer to practical use and large scale production by roll-to-roll manufacture [3]. The stability of polymer photovoltaics depends on a complex interplay between many factors such as the photochemical reactivity of the polymer and on the physical/chemical stability of electrodes [4,5]. Enhanced stability has been observed for photovoltaic devices with the so-called "inverted" geometry [3,6] (see Fig. 1) with the front ITO electrode as the electron collector and the back metal electrode as the hole

collector. In the inverted geometry, the metal back electrode can be screen printed using a silver paste in contrast to the evaporated aluminum electrode used in the "normal" geometry device. The enhanced stability of these inverted devices is in part due to the lower reactivity of the silver electrode towards oxygen. Another attraction of the inverted geometry is the applicability in the fabrication of roll-to-roll coated devices [7–10].

In the present work, we investigate a family of low band-gap polymers based on the common acceptor moiety 2,3-bis-(3-octyloxyphenyl)quinoxaline (Q) combined with thiophene (T) or fused thiophene systems: benzo[2,1-b:3,4-b']-dithiophene (BDT) or dithieno[3,2-b,2',3'-d]-thiophene (DTT) as shown in Scheme 1. The simplest polymer in this series (TQ1) has already been investigated by Wang et al. [11] who obtained devices with efficiencies up to 6.0% with TQ1 in combination with [70] PCBM and 4.9% in combination with [60] PCBM. The synthesis and characterization of the polymers are presented together with photovoltaic devices in both the normal and inverted type geometry. Recently a fast method for assessing the photochemical stability of conjugated polymers was established by Manceau et al. and used in our group to rank the stability of more than 20 polymers used in OPV [12]. We have used this method to rank the stability of this series of polymers against standard P3HT. Part of the inspiration for this series of polymers also came from an OPV study by Bundgaard et al. [13] who investigated the low band-gap polymer formed from the DTT donor moiety and a dialkoxy-benzothiadiazole acceptor. They demonstrated power conversion efficiencies of 0.6% on  $96 \text{ cm}^2$  roll-to-roll coated modules and also

\* Corresponding author.

E-mail address: [jegc@risoe.dtu.dk](mailto:jegc@risoe.dtu.dk) (J.E. Carlé).

showed that this polymer had a superior photochemical stability compared to P3HT. Similarly the BDT donor has been copolymerized with a pyrrolo[3,4-c]pyrrole-1,4-dione acceptor by Hou et al. [14] to create a low band-gap polymer achieving a reported photovoltaic efficiency of 4.5% together with [70] PCBM.

## 2. Experimental

### 2.1. Synthesis

The monomers 5,8-dibromo-2,3-bis(3-(octyloxy)phenyl)quinoxaline [11], 2,5-bis(trimethylstannyl)-thiophene [15], ditrimethyltin dithieno[3,2-*b*:2',3'-*d*]thiophene[13] and benzo[2,1-*b*:3,4-*b'*]-dithiophene (BDT) were prepared according to literature.

#### 2.1.1. Synthesis of 2,7-bis(trimethylstannyl)benzo[12-*b*:6,5-*b'*]dithiophene.

BDT (0.50 g, 2.63 mmol) was dissolved in dry THF (20 ml) under argon and cooled to  $-78^{\circ}\text{C}$ . *n*-Butyllithium (6.75 ml, 1.6 M in hexanes, 10.8 mmol) was then added dropwise causing precipitation to occur. After stirring for 15 min at  $-78^{\circ}\text{C}$ , it was allowed to reach

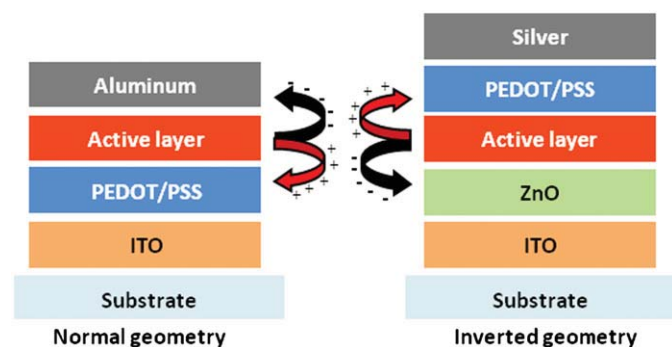


**Fig. 1.** Schematic representation of OPV devices with: (a) normal geometry where the electrons are collected at the back electrode (normally evaporated aluminum) and (b) inverted geometry where the electrons are collected at the front electrode (ITO).

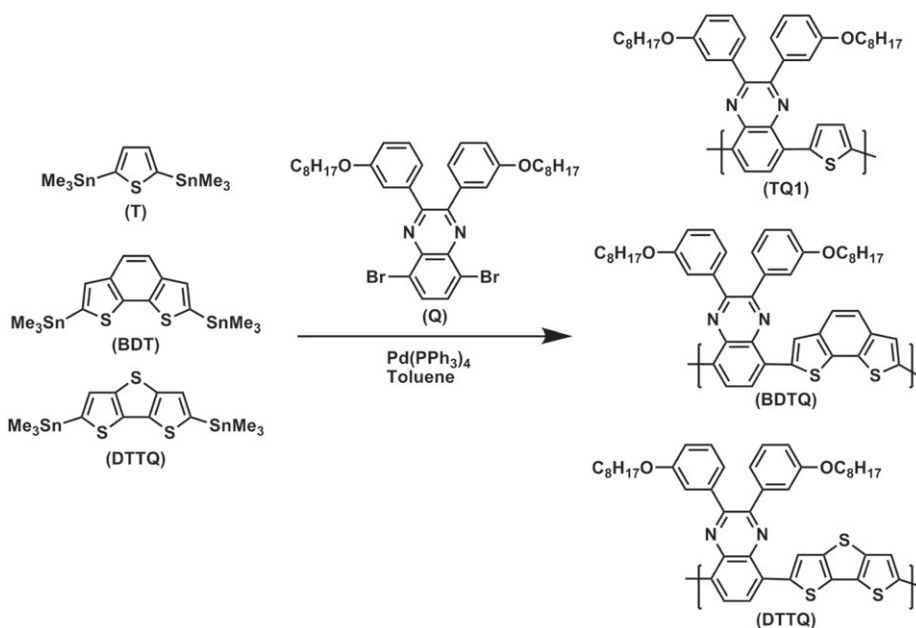
room temperature (RT) where it was left stirring for  $\frac{1}{2}$  h. The solution was then cooled back to  $-78^{\circ}\text{C}$ , after which chlorotrimethylstannane (3.50 g, 17.6 mmol) was added in one portion. The temperature was again allowed to reach RT at which the solution was stirred for an additional 2 h. Workup was performed by the addition of water followed by extraction with diethyl ether. The combined organic phases were washed with water and brine before drying over  $\text{MgSO}_4$  and evaporation of the solvent. The crude product was purified by quickly passing the compound through a column of basic  $\text{Al}_2\text{O}_3$ , using toluene with 2%  $\text{NEt}_3$  as eluent. The resulting product was further purified by recrystallization from methanol yielding the pure product as fine white needles (0.92 g, 69%).  $^1\text{H}$  NMR (500 MHz,  $\text{CDCl}_3$ )  $\delta$  7.73 (s, 2 H), 7.49 (s, 2 H), 0.64–0.23 (s, 18 H).  $^{13}\text{C}$  NMR (126 MHz,  $\text{CDCl}_3$ )  $\delta$  138.28, 138.13, 138.06, 132.94, 119.66,  $-8.11$ .

#### 2.1.2. General procedure for Stille cross coupling polymerization

One equivalent of the Q monomer and the appropriate donor monomer (T, BDT or DTT) were dissolved in degassed toluene of 0.04 M solution. Tri-*o*-tolylphosphine (0.1 mol%) and tris-(dibenzylidene acetone) dipalladium(0) (0.02 mol%) were added and the solution was brought to reflux where it was stirred for at least 24 h under nitrogen atmosphere. The polymer was precipitated to about 10 times the volumes of methanol. The suspension was filtered to give the polymer, which was purified by Soxhlet extraction, first with methanol, then with hexane and finally with chloroform or chlorobenzene. The polymer was then precipitated by slowly adding into 10 times the volume of methanol. The suspension was filtered and dried in vacuum oven to give the purified polymer.

#### 2.1.3. Synthesis of poly[2,3-bis(3-(octyloxy)phenyl)quinoxaline-5,8-diyl-*alt*-thiophene-2,5-diyl] (TQ1)

2,3-bis(3-(octyloxy)phenyl)quinoxaline (Q) (403.8 mg, 0.580 mmol), thiophene (T) (238.0 mg, 0.580 mmol), tri-*o*-tolylphosphine (10.0 mg, 0.033 mmol) and tris(dibenzylideneacetone)dipalladium(0) (6.0 mg, 6.55  $\mu\text{mol}$ ), yield: (324 mg, 90%).



**Scheme 1.** Polymerization of the three polymers through a Stille cross coupling polymerization. 2,3-Bis(3-(octyloxy)phenyl)quinoxaline (Q) is the acceptor moiety, which is coupled with a donor moiety, being either thiophene (T), benzo[2,1-*b*:3,4-*b'*]dithiophen (BDT) or dithieno[3,2-*b*:2',3'-*d*]thiophene (DTT), to give the polymers TQ1, BDTQ and DTTQ, respectively.



#### 2.1.4. Synthesis of poly[2,3-bis-(3-octyloxyphenyl)quinoxaline-benzo[2,1-b:3,4-b']dithiophen (BDTQ)

2,3-Bis(3-(octyloxy)phenyl)quinoxaline(Q) (193.3 mg, 0.373 mmol), benzo[2,1-b:3,4-b']dithiophen (BDT) (260.0 mg, 0.373 mmol), tri-*o*-tolylphosphine (9.1 mg, 0.030 mmol) and tris(dibenzylideneacetone)-dipalladium(0) (6.84 mg, 7.46  $\mu\text{mol}$ ). yield: (168 mg, 62%).

#### 2.1.5. Synthesis of poly[2,3-bis-(3-octyloxyphenyl)quinoxaline-dithieno[3,2-b:2',3'-d]thiophene (DTTQ)

2,3-Bis(3-(octyloxy)phenyl)quinoxaline Q (270.0 mg, 0.388 mmol), dithieno[3,2-b:2',3'-d]thiophene (DDT) (203.0 mg, 0.388 mmol), tri-*o*-tolylphosphine (9.4 mg, 0.031 mmol) and tris(dibenzylideneacetone)-dipalladium(0) (7.10 mg, 7.75  $\mu\text{mol}$ ), yield: (90 mg, 32%).

### 2.2. Photochemical stability

Pure polymer samples—TQ1, BDTQ, DTTQ and P3HT—were spin-coated under air on glass slides from chlorobenzene solutions. The solution concentrations and spinning speeds were adjusted to get a maximum peak absorbance of about 0.2 for each material. P3HT was bought as Sepiolid P200 from BASF.

Samples were aged under 1 sun and ambient air using a standard solar simulator from Steuernagel Lichttechnik (KHS 575, AM 1.5 G, 1000 W m<sup>-2</sup>, 85 °C). To monitor the degradation progress, samples were removed periodically and UV-visible spectrum was recorded from 200 to 1100 nm using a UV-1700 spectrometer (Shimadzu). The total amount of absorbed photons was monitored versus ageing time over the whole absorption range for each sample using the ASTM G173 standard as a reference for the incident photon flux [12,16]. This allowed for a fair quantitative comparison of the material's respective stability.

### 2.3. Device preparation

All preparations and measurements of the devices were carried out in air. The active layer was, for both the normal and the inverted geometry, spin coated from a filtered chlorobenzene solution consisting of the polymer and [60] PCBM (1:3), with a concentration of 50 mg/mL. The glass substrates coated with ITO had an active area of 0.5 cm<sup>2</sup>.

#### 2.3.1. Normal geometry devices

The prefabricated glass substrates coated with a patterned ITO were first ultrasonically cleaned with water and 2-propanol. A filtered aqueous solution of poly(3,4-ethylenedioxythiophene):poly(styrenesulfonate) (PEDOT:PSS) (from Sigma-Aldrich), was spin coated on top of the ITO, and dried at 150 °C for 1 min. The substrates were further heated at 150 °C for 5 min before the active layer was spin coated upon the PEDOT:PSS layer. The aluminum electrode was applied by thermal evaporation at a pressure below 10<sup>-6</sup> mBar. The system was brought to atmospheric pressure and the devices were analyzed immediately after in air.

#### 2.3.2. Inverted geometry devices

The glass substrates coated with ITO were cleaned in the same way as described above. Zinc oxide nanoparticles prepared according to [17] were spin coated from ethanol upon the ITO at 1000 rpm and the devices were annealed at 140 °C for 5 min. The active layer was then spin coated onto the devices followed by spin coating of a PEDOT/PSS (Agfa EL-P 5010) layer at 1000 rpm. The devices were then annealed at 110 °C for 5 min. The silver back electrode consisting of silver paste prepared from silver flakes (FS 16 from Johnson Matthey) was screen printed on the back and dried at 140 °C for 2 min.

### 2.4. Device testing

The inverted geometry devices were analyzed under simulated sunlight using a sun simulator from Steuernagel Lichttechnik operating at 1000 W m<sup>-2</sup>, AM1.5 G. The devices were masked before analyzing to ensure that only the active layer was illuminated. The normal geometry devices were analyzed using a LED lamp with 18 different wavelength diodes as described earlier [18].

## 3. Results and discussion

### 3.1. Characterization of the polymers

The polymers were characterized by size exclusion chromatography (SEC) with chloroform as the solvent, using polystyrene as a standard (see Table 1). The DTTQ polymer was not soluble in chloroform, and it was therefore not possible to determine the molecular weight of this polymer. TQ1 showed a relatively high molecular weight ( $M_n$ ) of 21 kDa, while BDTQ had a  $M_n$  of 8 kDa with a large PD of 5. The lower  $M_n$  of BDTQ is probably due to its lower solubility compared to TQ1.

Absorption spectra of each polymer were acquired both in chlorobenzene solution and on thin films spin coated on glass substrates from a chlorobenzene solution (see Table 1 and Fig. 2A and B). The spectra of all the three polymers have similar features with a  $\pi \rightarrow \pi^*$  transition at ca. 360 nm and charge transfer transitions in the 500–700 nm range. With fused donor systems in DTTQ and BDTQ the CT band splits up into two. The CT band of DTTQ is significantly red shifted by approximately 75 nm relative to BDTQ in the solution spectra. This shift is remarkable since the only chemical difference between the two polymers is the sulfur/ethylene fragment of the central ring of the fused donor. The result is that the band gap values for TQ1 and BDTQ are quite similar at ca. 1.8 eV corresponding to a cut-off wavelength at about 700 nm while DTTQ has a band gap value of 1.59 eV (800 nm), in the film spectra. The extinction coefficients for the polymers with the fused ring systems are appreciably higher than that of TQ1 in accordance with their extended coplanar conjugated structure.

### 3.2. Stability

The photochemical stability of the three polymers was evaluated under air. The normalized amount of absorbed photons is

**Table 1**  
Molecular weight and optical data for the three polymers.

Polymer	$M_n$ (kDa)	PDI	Solution (chlorobenzene)		Film	
			$\lambda_{\text{max}}$ (nm) ( $\epsilon$ )	Band gap (eV)	$\lambda_{\text{max}}$ (nm)	Band gap (eV)
TQ1	21	2.9	356 (16,200), 599 (14,800)	1.82	364, 625	1.76
BDTQ	8	5	364 (27,900), 560 (22,900)	1.83	377, 574	1.81
DTTQ	<sup>a</sup>	<sup>a</sup>	363 (22,900), 623 (18,500)	1.60	400, 638	1.59

<sup>a</sup> Could not be determined by SEC.

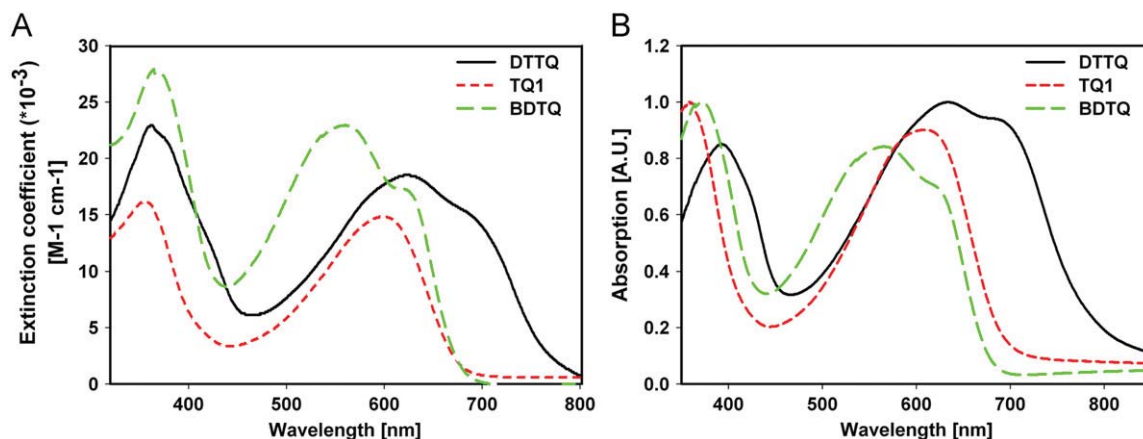


Fig. 2. UV-vis absorption spectra of the three polymers—DTTQ (black solid line), TQ1 (red short dash line) and BDTQ (green long dash line). (A) In chlorobenzene solution and (B) as thin film (for interpretation of the references to color in this figure legend, the reader is referred to the web version of this article).

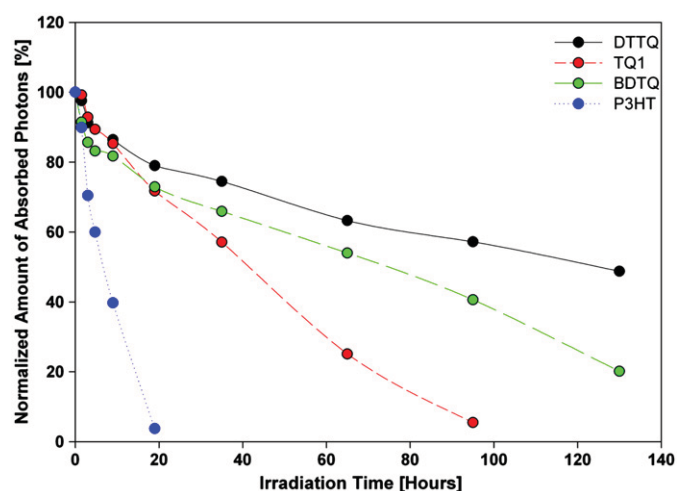


Fig. 3. Evolution of the normalized amount of absorbed photons during photochemical ageing of DTTQ (black solid line), TQ1 (red short dash line), BDTQ (green long dash line) and P3HT (blue dotted line) (for interpretation of the references to color in this figure legend, the reader is referred to the web version of this article).

plotted versus irradiation time for the different materials (see Fig. 3). P3HT data has been added as a benchmark. From these results, one can first notice that the three quinoxaline-based copolymers are more stable than P3HT, although they bear alkoxy groups. This can be explained by the absence of substituents on the donor moiety of these compounds. The implication of side-chains in conjugated polymer degradation has indeed been clearly demonstrated and P3HT instability for instance has been ascribed to the presence of *hexyl* groups [12,19,20]. The presence of an unsubstituted unit in the three quinoxaline-based samples lowers the “side-chains content” and hence overbalances the presence of the alkoxy substituents.

Considering only the quinoxaline derivatives, it is clear that the thiophene-based one is the least stable. The replacement of the thiophene by a benzodithiophene unit leads to a 50% increase in stability. Durability is further increased when a dithienothiophene block is used as electron donor. From the lowest to the highest, the stability ranking is as follows: TQ1 < BDTQ < DTTQ. These findings are fully consistent with some recent observations and confirm that unsubstituted aromatic polycyclic units exhibit good photochemical stability [12].

### 3.3. Photovoltaic devices

Photovoltaic devices, with both normal and inverted geometry, were prepared from each of the three polymers blended with [60] PCBM in the ratio 1:3. Fig. 4 shows the I–V curves for representative devices, which were carried out under AM1.5G conditions. In Table 2 the photovoltaic properties, short-circuit current density ( $J_{sc}$ ), open-circuit voltage ( $V_{oc}$ ), the fill-factor (FF) and the power-conversion efficiency (PCE), for the devices, are listed.

TQ1 in normal geometry devices showed the highest efficiency (1.5%) of all the different devices. 1.5% is much lower than the 4.9% reported by Wang et al. [11]. The lower efficiency is due to the lower  $J_{sc}$  and FF, while the  $V_{oc}$  is in the range of the reported. DTTQ gives device efficiency of 1.1% with a relative high  $J_{sc}$  of 4.7 mA/cm<sup>2</sup> but with a lower  $V_{oc}$  and FF compared to TQ1 based devices. Devices based on BDTQ shows the lowest efficiency of 0.5%. This is owed to a low  $J_{sc}$ , while the  $V_{oc}$  is respectable. This is in contrast to DTTQ, which shows a relative low  $V_{oc}$  but a high  $J_{sc}$ .

Common for the inverted devices are that they show lower efficiency than the normal geometry devices, in particular due to a decrease in the  $V_{oc}$ . Among the inverted devices TQ1 and DTTQ showed the highest efficiency (0.9%) followed by BDTQ (0.3%). Devices based on DTTQ show almost the same photovoltaic properties for normal and inverted geometry.

## 4. Conclusion

A series of three polymers based acceptor 2,3-bis-(3-octyloxyphenyl)-quinoxaline (Q) and a donor moiety consisting of either thiophene (T), benzo[2,1-b;3,4-b']dithiophene (BDT) or dithieno[3,2-b;2',3'-d]thiophene (DTT) have been prepared. The photochemical stability of the three new polymers was evaluated from the normalized absorption as a function of irradiation time and compared with that of the well-known P3HT polymer. They were found to be substantially more robust than P3HT with a ranking of DTTQ > BDTQ > TQ1 > P3HT, indicating that the fused ring systems of DTT and BDT impart more stability than thiophene. The absorption spectra showed that substituting thiophene in TQ1 with one of the fused donor systems, DDTQ and BDTQ, resulted in splitting and broadening of the CT band. The band gap of TQ1 and BDTQ are similar, around 1.8 eV, while the band gap of DTTQ is quite lower, 1.59 eV, in the film spectra. Furthermore photovoltaic device with both normal and inverted geometry has been prepared and tested in air. The normal geometry devices showed higher efficiencies

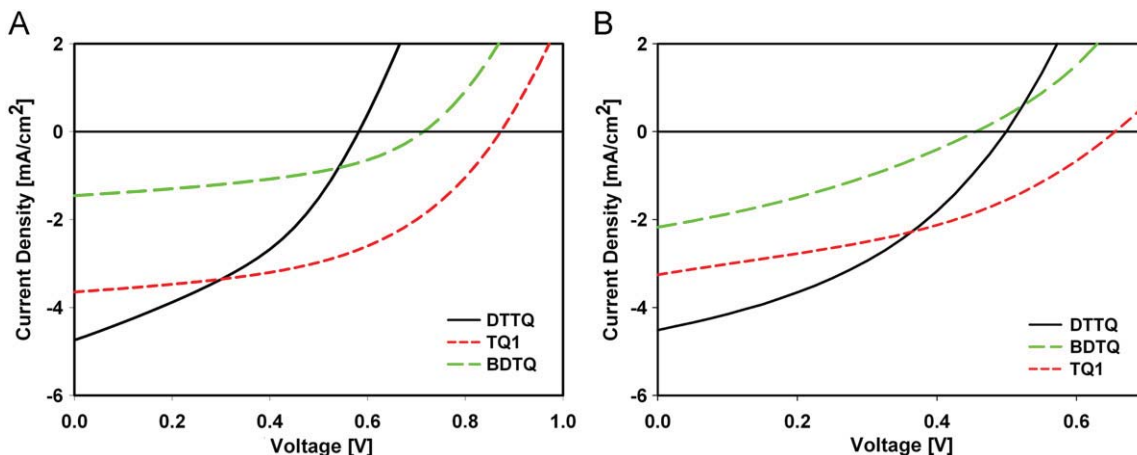


**Fig. 4.**  $J$ - $V$  curves of the best devices. (A)  $J$ - $V$  curves obtained from device with normal geometry and (B)  $J$ - $V$  curves obtained from devices with inverted geometry. DTTQ (black solid line), TQ1 (red short dash line) and BDTQ (green long dash line) (for interpretation of the references to color in this figure legend, the reader is referred to the web version of this article).

**Table 2**

Photovoltaic parameters for normal and inverted devices.

Polymer	Device geometry	Polymer/PCBM	$J_{sc}$ (mA/cm <sup>2</sup> )	$V_{oc}$ (V)	FF (%)	PCE (%)
TQ1 <sup>a</sup>	Normal	1:3	3.6	0.87	49	1.5
TQ1 <sup>b</sup>	Inverted	1:3	3.2	0.66	40	0.9
BDTQ <sup>a</sup>	Normal	1:3	1.5	0.71	44	0.5
BDTQ <sup>b</sup>	Inverted	1:3	2.2	0.46	32	0.3
DTTQ <sup>a</sup>	Normal	1:3	4.7	0.58	39	1.1
DTTQ <sup>b</sup>	Inverted	1:3	4.5	0.50	39	0.9

<sup>a</sup> Measured at 74 mW/cm<sup>2</sup>.

<sup>b</sup> Measured at 100 mW/cm<sup>2</sup>.

compared to the inverted, owned in particular to higher  $V_{oc}$ , with TQ1 (1.5%) as the most efficient. Within the inverted devices TQ1 and DTTQ showed the best efficiency with 0.9%.

## Acknowledgments

This work was supported by the Danish Strategic Research Council (DSF 2104-07-0022).

## References

- [1] <[http://konarka.com/index.php/site/pressreleasedetail/konarkas\\_power\\_plastic\\_a\\_chieves\\_world\\_record\\_83\\_efficiency\\_certification\\_fr](http://konarka.com/index.php/site/pressreleasedetail/konarkas_power_plastic_a_chieves_world_record_83_efficiency_certification_fr)>, 2011 (accessed 01.25.11).
- [2] E. Bundgaard, F.C. Krebs, Low band gap polymers for organic photovoltaics, *Sol. Energy Mater. Sol. C* 91 (2007) 954–985.
- [3] F.C. Krebs, Air stable polymer photovoltaics based on a process free from vacuum steps and fullerenes, *Sol. Energy Mater. Sol. C* 92 (2008) 715–726.
- [4] M. Jørgensen, K. Norrman, F.C. Krebs, Stability/degradation of polymer solar cells, *Sol. Energy Mater. Sol. C* 92 (2008) 686–714.
- [5] F.C. Krebs, H. Spanggaard, T. Kjaer, M. Biancardo, J. Alstrup, Large area plastic solar cell modules, *Mater. Sci. Eng. B* 138 (2007) 106–111.
- [6] S.K. Hau, H.L. Yip, N.S. Baek, J.Y. Zou, K.O. Malley, A.K.Y. Jen, Air-stable inverted flexible polymer solar cells using zinc oxide nanoparticles as an electron selective layer, *Appl. Phys. Lett.* 92 (2008).
- [7] F.C. Krebs, J. Fyenbo, M. Jørgensen, Product integration of compact roll-to-roll processed polymer solar cell modules: methods and manufacture using flexographic printing, slot-die coating and rotary screen printing, *J. Mater. Chem.* 20 (2010) 8994–9001.
- [8] F.C. Krebs, S.A. Gevorgyan, J. Alstrup, A roll-to-roll process to flexible polymer solar cells: model studies, manufacture and operational stability studies, *J. Mater. Chem.* 19 (2009) 5442–5451.
- [9] F.C. Krebs, Polymer solar cell modules prepared using roll-to-roll methods: knife-over-edge coating, slot-die coating and screen printing, *Sol. Energy Mater. Sol. C* 93 (2009) 465–475.
- [10] K. Norrman, M.V. Madsen, S.A. Gevorgyan, F.C. Krebs, Degradation patterns in water and oxygen of an inverted polymer solar cell, *J. Am. Chem. Soc.* 132 (2010) 16883–16892.
- [11] E. Wang, L. Hou, Z. Wang, S. Hellström, F. Zhang, O. Inganäs, M.R. Andersson, An easily synthesized blue polymer for high-performance polymer solar cells, *Adv. Mater.* 22 (2010) 5240–5244.
- [12] M. Manceau, E. Bundgaard, J.E. Carlé, O. Hagemann, M. Helgesen, R. Søndergaard, M. Jørgensen, F.C. Krebs, Photochemical stability of pi-conjugated polymers for polymer solar cells: a rule of thumb, *J. Mater. Chem.* 21 (2011) 4132–4141.
- [13] E. Bundgaard, O. Hagemann, M. Manceau, M. Jørgensen, F.C. Krebs, Low band gap polymers for roll-to-roll coated polymer solar cells, *Macromolecules* 43 (2010) 8115–8120.
- [14] L.J. Huo, J.H. Hou, H.Y. Chen, S.Q. Zhang, Y. Jiang, T.L. Chen, Y. Yang, Bandgap and molecular level control of the low-bandgap polymers based on 3,6-dithiophen-2-yl-2,5-dihydropyrrolo[3,4-c]pyrrole-1,4-dione toward highly efficient polymer solar cells, *Macromolecules* 42 (2009) 6564–6571.
- [15] M. Helgesen, S.A. Gevorgyan, F.C. Krebs, R.A.J. Janssen, Substituted 2,1,3-benzothiadiazole- and thiophene-based polymers for solar cells—introducing a new thermocleavable precursor, *Chem. Mater.* 21 (2009) 4669–4675.
- [16] <<http://rredc.nrel.gov/solar/spectra/am1.5/>>, 2011 (accessed 01.25.11).
- [17] W.J.E. Beek, M.M. Wienk, M. Kemerink, X. Yang, R.A.J. Janssen, Hybrid zinc oxide conjugated polymer bulk heterojunction solar cells, *J. Phys. Chem. B* 109 (2005) 9505–9516.
- [18] F.C. Krebs, K.O. Sylvester-Hvid, M. Jørgensen, A self calibrating LED based solar test platform, *Prog. Photovolt.: Res. Appl.* 19 (2011) 97–112.
- [19] M. Manceau, A. Rivaton, J.L. Gardette, S. Guillerez, N. Lemaitre, The mechanism of photo- and thermooxidation of poly(3-hexylthiophene) (P3HT) reconsidered, *Polym. Degrad. Stabil.* 94 (2009) 898–907.
- [20] H. Hintz, H.J. Egelhaaf, H. Peisert, T. Chasse, Photo-oxidation and ozonization of poly(3-hexylthiophene) thin films as studied by UV/Vis and photoelectron spectroscopy, *Polym. Degrad. Stabil.* 95 (2010) 818–825.



*Article*

## The Challenge of Synthesizing Oligomers for Molecular Wires

**Roar Søndergaard and Frederik C. Krebs \***

Risø National Laboratory for Sustainable Energy, Technical University of Denmark, Frederiksborgvej 399, DK-4000 Roskilde, Denmark; E-Mail: rosq@risoe.dtu.dk

\* Author to whom correspondence should be addressed; E-Mail: frkr@risoe.dtu.dk;  
Tel.: +45-4677-4799; Fax: +45-4677-4791.

*Received: 17 January 2011; in revised form: 6 February 2011 / Accepted: 23 February 2011 /  
Published: 28 February 2011*

---

**Abstract:** Controlling the size of the oligomer and introducing functional groups at the ends of the oligomer that allow it to react with separate electrodes are critical issues when preparing materials for molecular wires. We demonstrate a general synthetic approach to oligophenylenevinylene (OPV) derivative molecules with a molecular length up to 9–10 nm which allow for the introduction of aromatic thioacetate functionality in fully conjugated oligomer systems. Oligomers containing 3–15 phenyl units were synthesized by step wise Horner-Wadsworth-Emmons (HWE) reactions of a bifunctional OPV-monomer, which demonstrated good control of the size of the OPVs. Workup after each reaction step ensures a high purity of the final products. End group functionalization was introduced as a last step.

**Keywords:** molecular wire; oligomer; oligophenylenevinylene; aromatic thioacetate

---

### 1. Introduction

In recent years, many efforts have been made in order to produce molecular wires, with the prospect of creating nanoelectronics and of better understanding what happens at the molecular level in conductive processes [1–16]. Most of these previous studies have focused on preparation and examination of relatively small molecules (<3–4 nm), but such molecules have limited applications because of their relatively small size. Others have prepared really large molecules from a solid support by step wise elongation, but as very few chemical reactions proceed in quantitative yield the use of a

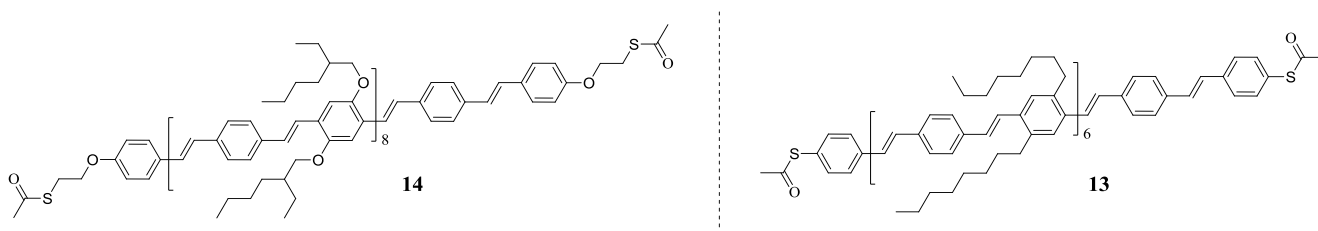
solid support is a problematic pathway for achieving a narrow size distribution, as workup between the steps is not possible. As an illustration, a reaction running at 90% yield (which is normally considered a good yield for a reaction) over 10 steps potentially only contains  $0.9^{10} = 35\%$  of the right compound.

Three of the major challenges in the preparation of large monodisperse wires are: First, complete control of the size of the oligomer in order to obtain a pure monodisperse size distribution. In order to obtain this, one must either operate with chemical reactions that proceed in quantitative yields with no byproducts, or a purification step must be included after each step. Unfortunately none of the known quantitative reactions such as 'Click'-reactions or 'Living Polymerization' reactions such as atom transfer radical polymerization (ATRP) or Anionic Polymerization leads to the conjugated system needed in a molecular wire, leaving workup as the only option for obtaining monodispersity. Second, choosing a design of the side chains that will make it possible to both prepare and later dissolve the oligomer. The side chains are essential for keeping the molecules in solution, and thus enabling chemical reactions. It should be emphasized that large molecules generally always requires high dilution which in some cases can render otherwise standard reactions impossible. Third, the introduction of functional groups at the ends of the wire that allows for connecting the molecules to a circuit. Depending on the desired functionality, one has to carefully consider whether this group should be introduced from the start, which requires that the functionality can sustain the reaction conditions of the oligomerization, or whether the introduction should instead be performed as a last step, associated with the potential difficulties in performing chemistry on very large molecules. Due to the excellent binding of sulfur to gold, thiol linkers in conjugation with gold have been used almost exclusively in previous reports, but there should in principle be many other possible substrate materials such as semiconducting oxides (*i.e.*, TiO<sub>2</sub>, ZnO) where carboxylic acids, alcohols and phenols have a high affinity.

We have previously reported the synthetic approach of up to 12 nm long oligophenylenevinylene (OPV) derivatives (19 phenyls) using step wise Horner-Wadsworth-Emmons (HWE) condensation [16]. Others have reported the synthesis of OPV's of varying size (4–11 phenyls) using the HWE condensation—both unidirectional [17–23] and bidirectional [24,25]—but none as large as these. Final group functionalities were introduced as a last step and successful attachment of thioacetate functionalized oligomers to separate gold electrodes over a 9 nm nanogap was achieved. The thioacetate moiety was introduced to short non-conjugated linkers attached to each end of the molecule (compound **14** in Figure 1). One of the reasons for introducing the gold attaching thioacetate functionality on a non-conjugated linker was the wish to prepare very long wires. The use of ethylhexyloxy (EHO) side chains had previously been shown to provide excellent results, as the solubility was largely improved compared to other side chains [17], but this choice of side chain rendered the only known procedure of introduction of an aromatic thioacetate as a last step impossible, as it involves the cleavage of aromatic *tert*-butyl thio ethers (Ar–S–C(CH<sub>3</sub>)<sub>3</sub>) using BBr<sub>3</sub> as a deprotecting reagent [26], *i.e.*, a procedure which will cleave the ether bond of the EHO side chains. Other options for thiol precursors that could potentially be inserted as an initial step, such as thiol itself (–SH) or methyl protected thiol (–SMe), were discarded: the former because of the tendency of thiols to dimerize under formation of a –S–S– bond and the latter because tests showed a much lower reactivity with gold than the thioacetate. Here we report the synthesis of large OPV's up to ~10 nm

(15 benzene rings) that allow for introduction of an aromatic thioacetate functionalization with the potential to create a fully conjugated wire if attached to separate electrodes (Figure 1).

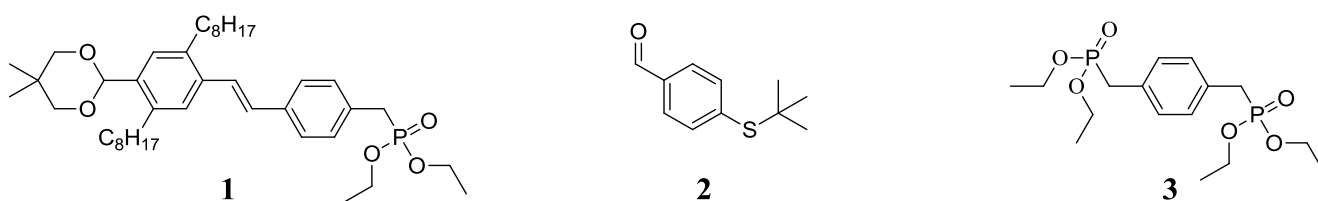
**Figure 1. left:** Chemical structure of previously reported oligomer **14** containing an aliphatic thioacetate functionality which allows for attachment between two separate gold electrodes, allowing it to function as a molecular wire [16]. As the thioacetate functionality is not in direct contact with the conjugate oligomer, the transport of electrons between the oligomer and the gold electrodes of electrons has to happen through tunneling. **right:** A newly synthesized oligomer **13** containing an aromatic thioacetate functionality which has the potential to create a fully conjugated organic system between two gold electrodes by creation of a Ar-S-Au bond.

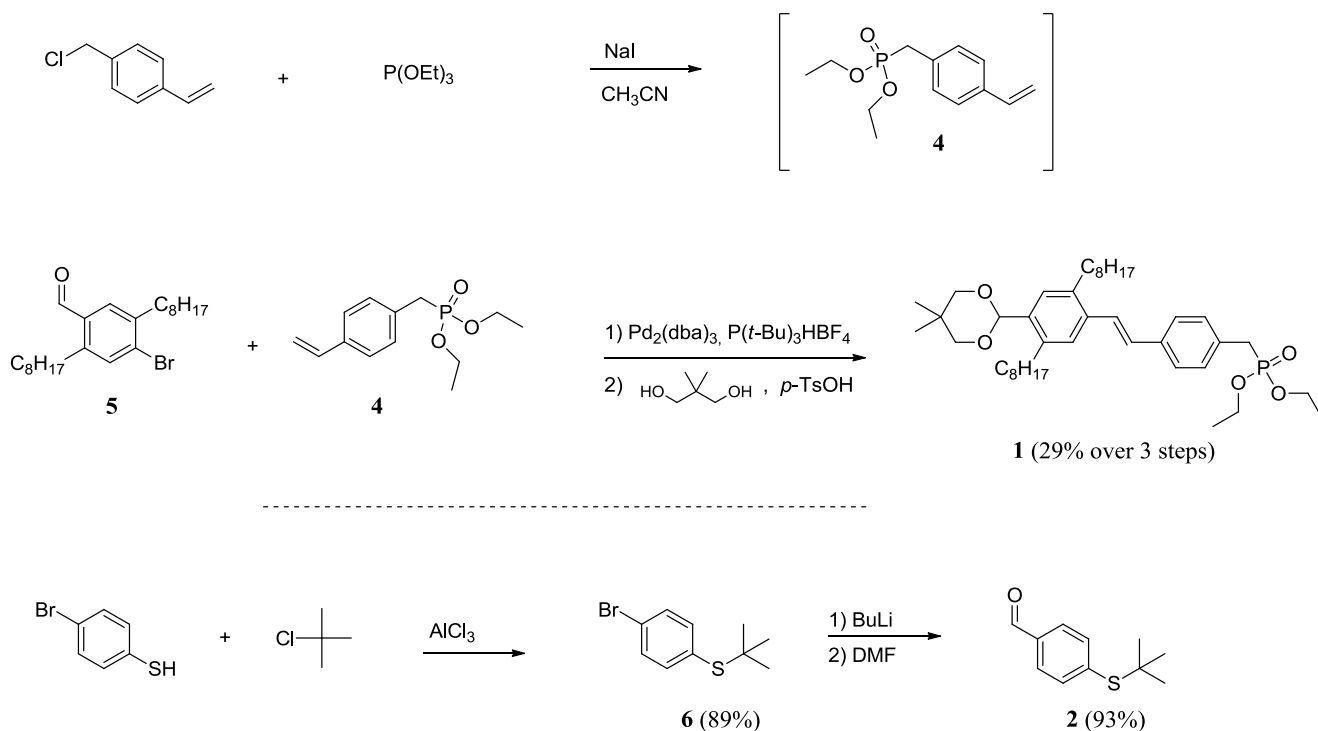


## 2. Results and Discussion

The oligomers were prepared by sequential HWE condensations using three building blocks as shown in Figure 2. The main building block, compound **1**, is a modification of the one used for the previously reported oligomer in Figure 1, in which the EHO side chains have been replaced with *n*-octyl. The prediction was that this would lead to a decrease in solubility compared to the original oligomers, but that it would simultaneously allow for the transformation of aromatic *tert*-butyl thio ethers into the corresponding thioacetate, by use of  $\text{BBR}_3$  in the presence of acetyl chloride, without cleavage of the side chains. The synthesis of compound **1** and **2** is outlined in Scheme 1. Initial reaction of 4-(chloromethyl)styrene with triethyl phosphite yielded compound **4**, which is very unstable and has to be stored in the freezer if not used immediately. This was then reacted in a Heck coupling with 4-bromo-2,5-dioctylbenzaldehyde (**5**), which was synthesized as previously described [27], followed by protection of the aldehyde. The instability of compound **4** is reflected in the Heck-reaction, where up to 51% of the bromo starting compound was recollected, which is probably due to polymerization of the vinyl-groups of compound **4**.

**Figure 2.** Chemical structure of the three building blocks used for in the preparation of the oligomers.

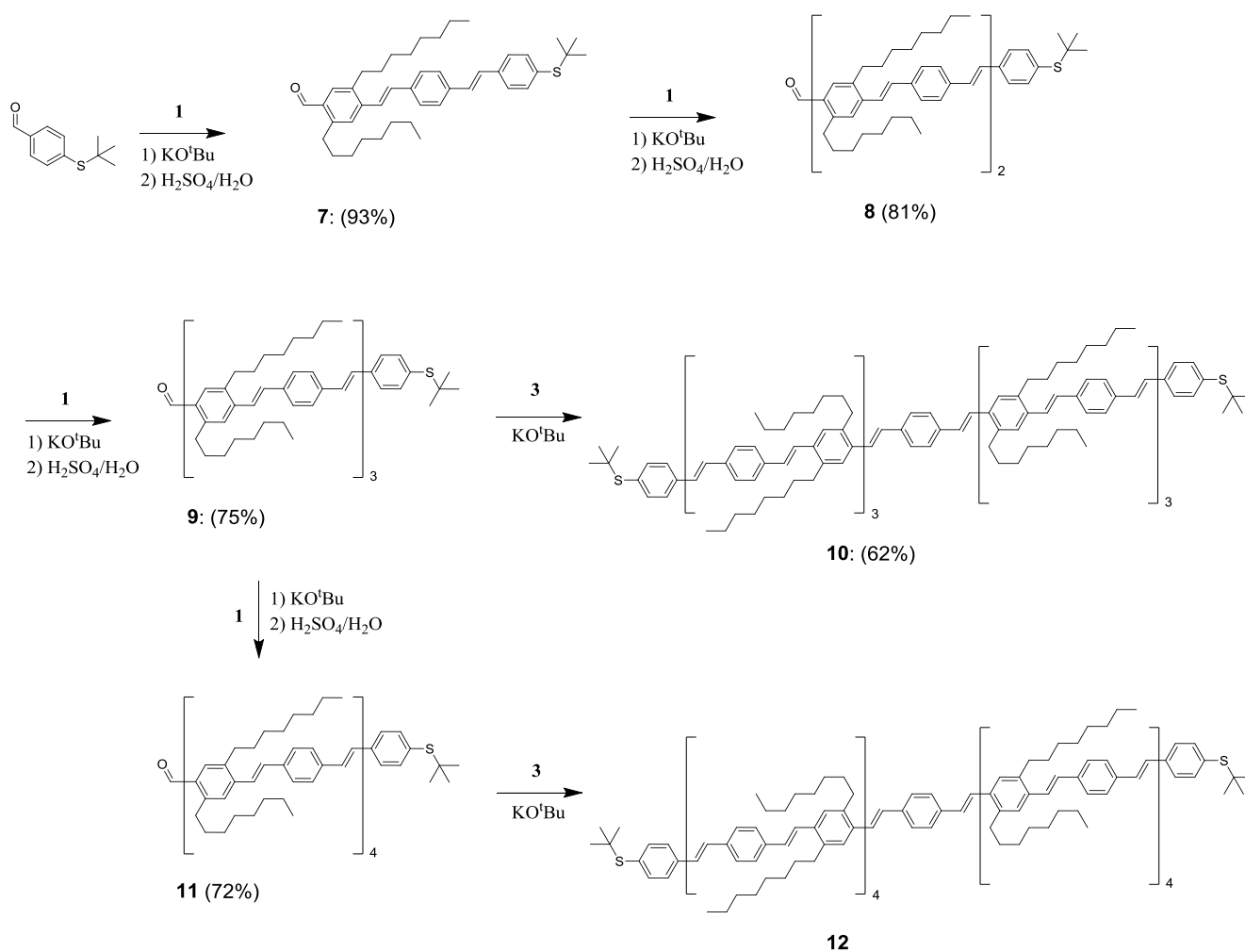


**Scheme 1.** Synthetic route to Compound **1** and **2**.

Compound **2**, which carries the initial end-group functionality, was prepared in good yield over two steps by first reacting 4-bromothiophenol and *tert*-butyl chloride in the presence of  $\text{AlCl}_3$  to give compound **6** followed by the conversion of the bromide into an aldehyde group by reaction first with *n*-butyl lithium and then DMF. Compound **3** was prepared as previously described [16].

After coupling compound **1** and **2** in order to functionalize the oligomer, step wise elongation using HWE condensation was then performed, resulting in oligomer ‘arms’ (compound **7**, **8**, **9** and **11**) carrying two different end groups as shown in Scheme 2. The largest of these were then coupled with diphosphonate ester **3**, providing a symmetric polymer with a doubling of the length of the molecule in one reaction (Scheme 2). Workup was performed after each step, using gradient silica chromatography and forced precipitation after each step, and the purity was controlled by NMR and size exclusion chromatography (SEC, see supporting information). Compared to previous results using this method of purification, the method seemed somewhat less efficient. This is ascribed to two main properties: higher hydrophobicity and lower solubility of the materials. Due to the more hydrophobic character of the oligomers, separation by gradient column chromatography was shown to be less efficient as the gradient could not be varied to the same extent as for the previous reported oligomers. Furthermore, because of the lower solubility, great care had to be taken in order to prevent precipitation of the larger bifunctional oligomers on the column. The larger symmetric oligomer **10** proved too insoluble for column chromatography, and the largest oligomer **12** was practically insoluble in all solvents. These results really show the difference in solubility for an oligomer carrying EHO side chains compared to *n*-octyl. Where no problems were encountered in the chromatographic workup of even the largest oligomer (19 phenyls) carrying the EHO, the replacement with *n*-octyl led to highly reduced solubility at 15 phenyl groups and to insolubility in all ordinary solvents at 19 phenyls.

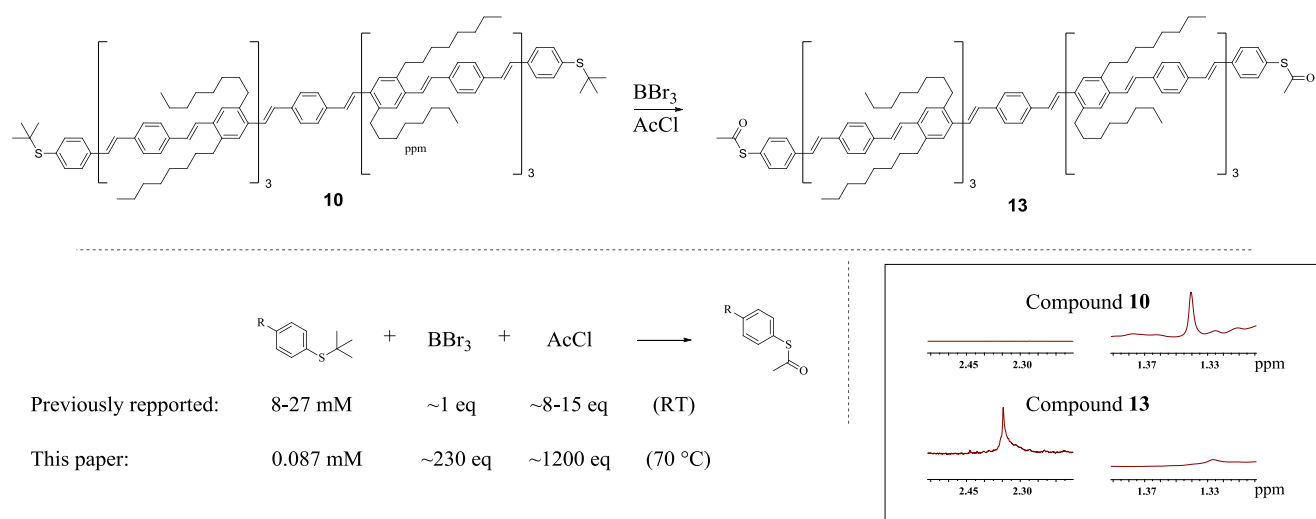
**Scheme 2.** Reaction steps in the preparation of the oligomers. The synthesis of the “arms” of the molecule starts with the introduction of the termination group followed by growth of the arm and final doubling of the size of the molecule by attaching two “arms” to a core molecule, which in this work is a simple benzene ring.



This reduced solubility also played a key role in the preparation of the corresponding aromatic thioacetate of oligomer **10**. Due to the heavily reduced solubility, it was impossible to carry out the transformation under the conditions reported for this reaction (see Scheme 3). Dilution of a magnitude of 100–300 times compared to the original description was necessary and a large excess of BBr<sub>3</sub> (~230 times more) and AcOEt (~80–150 times more) compared to the original report was required in order to obtain the thioacetate. Many experiments were necessary in order to find these relationships, and the final procedure involved running the reaction in deuterated dichlorobenzene with several additions of BBr<sub>3</sub> and AcCl in order to follow the reaction by NMR to find the conditions required. These findings are additional proof that reaction conditions, when performed on very large molecules, can sometimes deviate enormously from standard conditions. A final yield of ‘107%’ in the last reaction is ascribed to the difficulty of weighing a very small amount of compound, and is probably due to a change in air humidity or a small amount of residual solvent (C<sub>6</sub>H<sub>4</sub>Cl<sub>2</sub>).

All attempts to do further chemistry on compound **12** proved impossible because of the lack of solubility.

**Scheme 3. top:** Thioacetate functionalization of oligomer with 15 phenyls. **Bottom left:** Schematic representation of the reaction conditions previously reported for the conversion of aromatic *tert*-butyl thioether into the corresponding aromatic thioacetates (Ref. [26]) compared to the reaction conditions required for the transformation of oligomer **10**. This demonstrates that reaction conditions on very large molecules cannot always be directly transferred from standard reactions. **Bottom right:** <sup>1</sup>H-NMR of compound **10** and **13** in C<sub>6</sub>D<sub>4</sub>Cl<sub>2</sub> showing disappearance of the singlet signal (~1.33 ppm) from the *tert*-butyl thioether of compound **10** and formation of the singlet signal (2.35 ppm) from the CH<sub>3</sub>-group in the formed aromatic thioacetate **13**.



Comparing the synthetic pathway and the resulting properties of the two oligomers in Figure 1 clearly demonstrate the importance of careful consideration when choosing which side chains to use. Although similar in structure, the oligomers have very different solubilities, and they also have different restrictions to what chemistry can be performed in order to carry out end group functionalization. Where the ethylhexyloxy containing OPVs are so soluble that column chromatography can be performed even with very large molecules (19 phenyls), the *n*-octyl containing OPVs start showing problems of precipitation on the column even in the preparation of the ‘arms’ of (up to 9 phenyls). On the other hand, the latter can sustain chemical conditions that would destroy the former, making it possible to produce an aromatic thioacetate functionalized oligomer.

### 3. Experimental Section

#### 3.1. General

All solvents used were HPLC grade. Purification by column chromatography was performed by conventional gradient dry column vacuum chromatography [28] or ‘flash’ column chromatography using Merck Silica Gel 60 (15–40 μm) (column height 5–7 cm) and suction to drive the mobile phase.

Size exclusion chromatography (SEC) was performed in chloroform using either of two preparative Knauer systems employing two gel columns in succession with respective pore diameters of 10<sup>4</sup> Å and 10<sup>6</sup> Å. The gel columns had dimensions of 25 mmØ × 600 mm.

### 3.2. Synthesis

***p*-xylylene-bis-phosphonic acid tetraethyl ester (3):** was prepared as previously described [16].

**4-bromo-2,5-dioctylbenzaldehyde (5):** was synthesized according to a previously described procedure [27].

**Diethyl 4-vinylbenzylphosphonate (4):** 4-(chloromethyl)styrene (115.3 g, 680 mmol) and sodium iodide (102 g, 680 mmol) in acetonitrile (600 mL) under argon was heated to around boiling after which triethyl phosphite (143 mL, 817 mmol) was added in small portions in a manner such that the solution was boiling the whole time. After addition, the mixture was left at reflux for an additional 0.5 h, after which a mixture of ice and water (500 mL) was added, followed by extraction with ether (4 × 100 mL). After removal of the solvent *in vacuo* the resulting oil was redissolved in ether (400 mL) and washed with water (4 × 60 mL) and brine (60 mL). The organic phase was then dried over MgSO<sub>4</sub>, followed by evaporation of the solvent. The resulting crude oil (190 g) was distilled at oil pump pressure (134.5 g). The product is unstable and must be kept in a freezer. The product was used in the next step without further purification.

**(E)-diethyl 4-(4-(5,5-dimethyl-1,3-dioxan-2-yl)-2,5-dioctylstyryl)benzylphosphonate (1):** Compound 4 and 4-bromo-2,5-dioctylbenzaldehyde (42.6 g, 104 mmol) in triethylamine (40 mL) was purged with argon for 5 min. Pd<sub>2</sub>(dba)<sub>3</sub> (180 mg, 0.197 mmol) and P(*t*-Bu)<sub>3</sub>HBF<sub>4</sub> (260 mg, 0.896 mmol) was added and the reaction mixture was heated to reflux (turns dark) and left for 17 h. The solvent was then removed from the now greenish mixture, followed by dilution in ether (300 mL). The organic phase was washed with aqueous HCl (2 M, 2 × 125 mL), water (2 × 125 mL) and brine (200 mL). After drying over MgSO<sub>4</sub>, the solvent was removed *in vacuo* and the crude product was purified by gradient silica column chromatography (heptane/AcOEt, 10% steps). This separation yielded the Bromo-starting compound (21.63 g, 51%) and the initial aldehyde (22.6 g, 37%). This aldehyde was then transformed into the corresponding acetal by reaction with 2,2-dimethylpropane-1,3-diol (4.2 g, 40.3 mmol) in toluene (150 mL) under reflux for 1 hour using a Dean-Stark. The cooled mixture was washed with saturated Na<sub>2</sub>CO<sub>3</sub> (50 mL), water (2 × 50 mL) and brine (50 mL). After drying over MgSO<sub>4</sub>, removal of the solvent *in vacuo* yielded the desired protected acetal (26.0 g, 29% over 3 steps from 4-(chloromethyl)styrene).

<sup>1</sup>H NMR (500 MHz, CDCl<sub>3</sub>) δ 7.52–6.86 (m, 8H), 5.56–5.45 (m, 1H), 4.12–3.91 (m, 4H), 3.85–3.57 (m, 4H), 3.25–3.06 (m, 2H), 2.78–2.57 (m, 4H), 1.73–1.51 (m, 4H), 1.44–1.20 (m, 29H), 0.91–0.84 (m, 6H), 0.81 (s, 3H). <sup>13</sup>C NMR (126 MHz, CDCl<sub>3</sub>) δ 138.61, 138.20, 136.67, 136.64, 136.15, 135.25, 130.97, 130.89, 130.23, 130.17, 129.41, 129.40, 129.17, 128.36, 127.48, 126.80, 126.78, 126.45, 126.44, 125.43, 100.07, 78.06, 62.33, 62.27, 34.30, 33.38, 33.20, 32.35, 32.06, 32.03, 31.85, 31.52, 30.36, 29.93, 29.87, 29.63, 29.58, 29.42, 23.41, 22.83, 22.80, 22.06, 21.48, 16.55, 16.51, 14.26, 14.24.

**(4-bromophenyl)tert-butylthioether (6):** A mixture of 4-bromothiophenol (10.0 g, 52.9 mmol) in *tert*-butyl chloride (25 mL, 52.9 mmol) was placed under argon, after which aluminum trichloride

(0.35 g, 2.62 mmol) was added in portions followed by heating until HCl-gas started to form (the gas was neutralized by leading it through a NaOH solution). The reaction was followed by TLC until no more starting compound was present. During the reaction, additional aluminum trichloride (0.35 g, 2.62 mmol) was added portion wise in order to keep the reaction running. After reaction end, water (50 mL) was added and the mixture was extracted with pentane (3 × 40 mL). The collected organic phases were washed with water (3 × 25 mL) and brine (25 mL). After drying over MgSO<sub>4</sub>, the solvent was removed *in vacuo* and the resulting slightly yellowish oil (crude 12.45 g) was micro-distilled to obtain the pure product as a clear oil (11.5 g, 89%). <sup>1</sup>H NMR (500 MHz, CDCl<sub>3</sub>) δ 7.50–7.33 (m, 4H), 1.28 (s, 9H). <sup>13</sup>C NMR (126 MHz, CDCl<sub>3</sub>) δ 139.05, 132.02, 131.79, 123.59, 46.26, 31.03.

**4-(*tert*-butylthio)benzaldehyde (2):** (4-bromophenyl)(*tert*-butyl)sulfane (10.5 g, 42.8 mmol) was added drop wise to a solution of n-BuLi (28 mL, 44.8 mmol) in anhydrous THF (45 mL) cooled to –40 °C causing precipitation to occur. The temperature was then lowered to –78 °C for 20 min after which anhydrous DMF (9 mL, 116 mmol) was added. Cooling was removed and the mixture was allowed to reach RT where it was stirred for an additional 0.5 h. Water was added and the mixture was extracted with hexane. The combined organic phases were washed with water and brine before drying over MgSO<sub>4</sub> and removal of the solvent. The slightly yellow crude oil (8.37 g) was purified by kugelrohr distillation (approx 120 °C) to yield a clear oil (8.12 g, 93%). <sup>1</sup>H NMR (500 MHz, CDCl<sub>3</sub>) δ 10.03 (s, 1H), 7.83 (d, J = 8.1 Hz, 2H), 7.68 (d, J = 8.1 Hz, 2H), 1.34 (s, 9H). <sup>13</sup>C NMR (126 MHz, CDCl<sub>3</sub>) δ 191.65, 141.35, 137.00, 135.89, 129.42, 47.16, 31.15.

**4-((*E*)-4-((*E*)-4-(*tert*-butylthio)styryl)styryl)-2,5-dioctylbenzaldehyde (7):** Compound **1** (5.37 g, 8.03 mmol) and compound **2** (1.80 g, 9.26 mmol) in THF (80 mL) were cooled on an acetone/dry ice bath after which potassium *tert*-butoxide (2.50 g, 22.3 mmol) was added followed by removal from the cold and stirring at RT for 1 hour. The reaction mixture was then recooled followed by addition of THF (100 mL) and a premixed blend of H<sub>2</sub>SO<sub>4</sub>:H<sub>2</sub>O (100 mL, 9:1) in THF (100 mL). The reaction was then allowed to reach RT followed by heating to 40 °C for 1 hour. The mixture was then extracted with ether (4 × 100 mL), which was washed with water (3 × 100 mL), saturated NaHCO<sub>3</sub> (100 mL) and brine (100 mL). Evaporation of the solvent after drying over MgSO<sub>4</sub> yielded a crude (5.60 g) which was purified by flash chromatography (heptane:CHCl<sub>3</sub>, 1:1) yielding the pure compound (4.67 g, 93%) <sup>1</sup>H NMR (500 MHz, CDCl<sub>3</sub>) δ 10.25 (s, 1H), 7.67–7.03 (m, 14H), 3.07–2.97 (m, 4H), 2.83–2.73 (m, 4H), 1.73–1.44 (m, 4H), 1.44–1.13 (m, 29H), 0.88 (m, 6H). <sup>13</sup>C NMR (126 MHz, CDCl<sub>3</sub>) δ 191.91, 143.60, 141.32, 138.92, 137.90, 137.75, 137.27, 136.85, 132.72, 132.68, 132.37, 132.21, 129.17, 128.38, 127.98, 127.37, 127.20, 126.63, 125.33, 46.41, 33.05, 32.78, 32.46, 32.03, 31.14, 31.12, 29.81, 29.68, 29.61, 29.57, 29.42, 29.40, 29.17, 22.84, 22.81, 14.26.

**4-((*E*)-4-((*E*)-4-((*E*)-4-((*E*)-4-(*tert*-butylthio)styryl)styryl)-2,5-dioctylstyryl)styryl)-2,5-dioctylbenzaldehyde (8):** Compound **7** (4.6 g, 7.38 mmol) and compound **1** (5.81 g, 8.69 mmol) in dry THF (100 mL) under argon were cooled on acetone/dry ice. Potassium *tert*-butoxide (2.54 g, 22.6 mmol) was added and the reaction was removed from the cold (turned dark red) and was left stirring while being monitored by TLC for approximately 1 hour. THF was then added and the mixture cooled on acetone/dry ice followed by slow addition of a premixed solution of H<sub>2</sub>SO<sub>4</sub>:H<sub>2</sub>O (60 mL,



9/1) in THF (60 mL). The mixture was allowed to reach RT followed by heating to 40 °C for 0.5–1 hour while monitoring by TLC. The mixture was extracted with ether, and the collected organic phases were washed with water, saturated NaHCO<sub>3</sub> and brine. Drying over MgSO<sub>4</sub> followed by removal of the solvent *in vacuo* yielded a dark yellow crude (9.49 g) which was purified by flash chromatography (CHCl<sub>3</sub>:heptane, 60:40) yielding the pure compound as a yellow solid (6.26 g, 81%). <sup>1</sup>H NMR (500 MHz, CDCl<sub>3</sub>) δ 10.24 (s, 1H), 7.74–6.94 (m, 24H), 3.08–2.97 (m, 2H), 2.85–2.70 (m, 6H), 1.74–1.57 (m, 8H), 1.47–1.21 (m, 49H), 0.87 (m, 12H). <sup>13</sup>C NMR (126 MHz, CDCl<sub>3</sub>) δ 191.92, 143.61, 141.40, 138.90, 138.85, 138.08, 137.90, 137.65, 136.53, 136.50, 135.28, 135.09, 132.69, 132.31, 132.18, 129.38, 129.14, 128.96, 127.96, 127.89, 127.37, 127.14, 127.09, 127.03, 126.89, 126.59, 126.24, 125.10, 46.39, 33.47, 33.07, 32.79, 32.47, 32.08, 32.04, 31.63, 31.15, 29.83, 29.69, 29.64, 29.62, 29.58, 29.47, 29.43, 29.40, 29.17, 22.84, 22.82, 14.28, 14.26.

**4-((E)-4-((E)-4-((E)-4-((E)-4-((E)-4-((E)-4-(tert-butylthio)styryl)styryl)-2,5-dioctylstyryl)styryl)-2,5-dioctylstyryl)styryl)-2,5-dioctylbenzaldehyde (9):** Compound **8** (5.54 g, 5.27 mmol) and compound **3** (4.11 g, 6.14 mmol) in dry THF (160 mL) under argon were cooled until precipitation started. Potassium *tert*-butoxide (1.85 g, 16.5 mmol) was added and the reaction was left stirring at RT while being monitored by TLC for approximately 1 hour. A premixed solution of H<sub>2</sub>SO<sub>4</sub>:H<sub>2</sub>O (100 mL, 9/1) in THF (200 mL) was added (which caused precipitation) followed by heating to 40 °C for 0.5–1 hour while monitoring by TLC. The mixture was extracted with ether, and the collected organic phases were washed with water, saturated NaHCO<sub>3</sub> and brine. Drying over MgSO<sub>4</sub> followed by removal of the solvent *in vacuo* yielded a crude, which showed the presence of approximately 10% acetal. After a coarse workup by flash chromatography, the mixture was redissolved in THF (200 mL), premixed solution of H<sub>2</sub>SO<sub>4</sub>:H<sub>2</sub>O (50 mL, 9/1) in THF (100 mL) was added and the mixture stirred at 40 °C for 1 hour. After workup (extraction with ether, wash with water, saturated NaHCO<sub>3</sub>, brine and drying over MgSO<sub>4</sub>) the crude product was purified by gradient flash chromatography (CHCl<sub>3</sub>:heptane, 40:60–60:40) yielding the desired compound (5.87 g, 75%). <sup>1</sup>H NMR (500 MHz, CDCl<sub>3</sub>) δ 10.27 (s, 1H), 7.74–6.98 (m, 34H), 3.07–2.96 (m, 2H), 2.78 (t, J = 6.5 Hz, 10H), 1.74–1.57 (m, 12H), 1.49–1.20 (m, 69H), 0.89 (m, 18H). <sup>13</sup>C NMR (126 MHz, CDCl<sub>3</sub>) δ 191.92, 143.61, 141.40, 138.89, 138.85, 138.82, 138.79, 138.10, 137.90, 137.68, 137.34, 136.49, 135.34, 135.23, 135.13, 135.03, 132.69, 132.32, 132.17, 129.40, 129.24, 129.16, 129.05, 128.92, 127.96, 127.86, 127.37, 127.14, 127.08, 127.03, 126.87, 126.59, 126.29, 126.07, 126.00, 125.09, 46.38, 33.48, 33.07, 32.79, 32.48, 32.08, 32.04, 31.63, 31.15, 29.84, 29.69, 29.65, 29.62, 29.58, 29.47, 29.43, 29.40, 22.84, 22.82, 14.28, 14.27.

**1,4-bis((E)-4-((E)-4-((E)-4-((E)-4-((E)-4-((E)-4-(tert-butylthio)styryl)styryl)-2,5-dioctylstyryl)styryl)-2,5-dioctylstyryl)styryl)-2,5-dioctylstyryl)benzene (10):** Compound **9** (300 mg, 0.203 mmol) and compound **3** (35.2 mg, 0.093 mmol) in THF (60 mL) were heated to 50 °C, after which potassium *tert*-butoxide (100 mg, 0.891 mmol) was added. Stirring was continued for approximately 0.5 h after which the heat was removed and stirring was continued for an additional 0.5 h. The volume of the mixture was then reduced to approximately half, and the resulting mixture was filtered and the solid washed with THF and dried in vacuum (175 mg, 62%).

<sup>1</sup>H NMR (500 MHz, CDCl<sub>3</sub>) δ 7.66–6.94 (m, 76H), 2.87–2.70 (m, 24H), 1.71–1.61 (m, 24H), 1.49–1.22 (m, 138H), 0.94–0.82 (m, 36H). <sup>13</sup>C NMR (126 MHz, CDCl<sub>3</sub>) δ 138.83, 138.81, 137.94,

137.90, 137.69, 137.34, 135.25, 135.21, 135.15, 132.19, 129.44, 129.16, 129.07, 127.85, 127.15, 127.03, 126.95, 126.86, 126.60, 126.33, 126.08, 46.39, 33.49, 32.09, 31.64, 31.16, 29.86, 29.66, 29.48, 22.85, 14.29.

**4-((E)-4-((E)-4-((E)-4-((E)-4-((E)-4-((E)-4-((E)-4-((E)-4-((E)-4-(tert-butylthio)styryl)styryl)-2,5-dioctylstyryl)styryl)-2,5-dioctylstyryl)styryl)-2,5-dioctylstyryl)styryl)-2,5-dioctylbenzaldehyde (11):** Compound **9** (1.50 g, 1.01 mmol) and compound **1** (0.79 g, 1.18 mmol) were dissolved in THF (120 mL) under argon, after which potassium *tert*-butoxide (0.346 g, 3.08 mmol) was added and the mixture was left at RT for 1 hour while monitoring by TLC. Deprotection of the acetal was performed by treatment with a cold mixture of H<sub>2</sub>SO<sub>4</sub>:H<sub>2</sub>O (50 mL, 9:1) in THF (100 mL) for 1 hour at 40 °C, followed by extraction with ether, washing of the organic phase with water, saturated NaHCO<sub>3</sub> and brine. Evaporation of the solvent after drying over MgSO<sub>4</sub> gave a crude that still showed the presence of unhydrolyzed acetal on NMR. The crude was therefore redissolved in THF (100 mL) and re-treated with a cold mixture of H<sub>2</sub>SO<sub>4</sub>:H<sub>2</sub>O (50 mL, 9:1) in THF (100 mL). After extraction, washing and drying, the crude was purified by flash chromatography using pure CHCl<sub>3</sub> as eluent as attempts to use a gradient of CHCl<sub>3</sub>:heptane caused precipitation on the column. (Yield: 1.40 g, 72%). <sup>1</sup>H NMR (500 MHz, CDCl<sub>3</sub>) δ 10.24 (s, 1H), 7.71–6.96 (m, 44H), 3.06–2.98 (m, 2H), 2.82–2.74 (m, 14H), 1.74–1.55 (m, 16H), 1.48–1.19 (m, 89H), 0.96–0.82 (m, 24H).

**1,4-bis((E)-4-((E)-4-((E)-4-((E)-4-((E)-4-((E)-4-((E)-4-((E)-4-((E)-4-(tert-butylthio)styryl)styryl)-2,5-dioctylstyryl)styryl)-2,5-dioctylstyryl)styryl)-2,5-dioctylstyryl)styryl)-2,5-dioctylstyryl)benzene (12):** Compound **11** (31.3 mg, 0.016 mmol) and compound **3** (3.04 mg, 8.04 μmol) were dissolved in dry THF (40 mL) and heated to 50 °C. Potassium *tert*-butoxide (9.0 mg, 0.080 mmol) was then added causing a slight color shift and precipitation. The mixture was stirred overnight. Filtering of the solid and washing with THF resulted in an insoluble solid (21.4 mg).

**1,4-bis((E)-4-((E)-4-((E)-4-((E)-4-((E)-4-((E)-4-((E)-4-((E)-4-((E)-4-(acetylthio)styryl)styryl)-2,5-dioctylstyryl)styryl)-2,5-dioctylstyryl)styryl)-2,5-dioctylstyryl)styryl)-2,5-dioctylstyryl)benzene 13:** Compound **10** (1.05 mg, 0.346 μmol) in CD<sub>4</sub>Cl<sub>2</sub> (2.0 mL) under argon was heated to 70 °C after which a total amount of tribromoborane (80 μL, 0.080 mmol) and acetyl chloride (30 μL, 0.422 mmol) was added in small portions over the next 24 hours while continuously monitoring by NMR. The reaction mixture was then diluted with C<sub>6</sub>H<sub>4</sub>Cl<sub>2</sub> (20 mL) and the solvent and excess BBr<sub>3</sub> and AcCl was removed in high vacuum. After removal, the crude was redissolved in C<sub>6</sub>H<sub>4</sub>Cl<sub>2</sub> (20 mL) and filtrated before the solvent was removed once more to obtain the final product (1.11 mg, '107%').

<sup>1</sup>H NMR (500 MHz, C<sub>6</sub>D<sub>4</sub>Cl<sub>2</sub>) δ 7.96–6.57 (m, 76H), 2.93 (s, 24H), 2.35 (s, 6H), 1.88–1.63 (m, 24H), 1.57–1.16 (m, 120H), 0.93 (t, *J* = 7.0 Hz, 36H).

#### 4. Conclusions

A chemical approach to prepare large alkyl substituted phenylene vinylene oligomers up to ~10 nm (15 phenyls), which can be end group functionalized with aromatic thioacetates as a final step, was shown. The introduction of a thioacetate onto the conjugated backbone of the oligomer makes this a

potential candidate for the preparation of a fully conjugated OPV molecular wire attached directly to two separate gold electrodes. The oligomers were prepared by step wise HWE condensation, using the three building blocks shown in Figure 2, to create bifunctional ‘arms’ that were then reacted with a symmetrical core, creating a symmetrical oligomer and at the same time doubling the size. The thioacetate functionality was introduced as a last step by cleavage of aromatic tertbutylthio ethers, situated at the end of the symmetrical oligomer, with a large excess of  $\text{BBr}_3$  in the presence of large excess of acetyl chloride. These reaction conditions differ largely with those previously reported in the respect that high dilution of the oligomer and a large excess of the other reactants was necessary—conditions that are ascribed to the very low solubility of the larger oligomers which makes this otherwise standard reaction very difficult.

The generally low solubility of the oligomers made workup more tedious when compared with previously reported oligomers with more or less identical structures except for the side chains. Where the present oligomers carry *n*-octyl side chains in order to be resilient to the final aromatic functionalization (treatment with  $\text{BBr}_3$ ), the previously reported oligomers carried ethylhexyloxy chains, which are very comparable in size with the *n*-octyl but involve an ether functionality, which makes treatment with  $\text{BBr}_3$ , and thus the aromatic thioacetalization, impossible. These examples demonstrate that one has to carefully select which side chains to choose when preparing larger oligomers.

## Acknowledgements

This work was supported by EU STREP project no. 026714 with the acronym VERSATILE.

## Reference

1. Ashwell, G.J.; Tyrrell, W.D.; Urasinska, B.; Wang, C.S.; Bryce, M.R. Organic rectifying junctions from an electron-accepting molecular wire and an electron-donating phthalocyanine. *Chem. Comm.* **2006**, doi: 10.1039/B600617E.
2. Ashwell, G.J.; Urasinska, B.; Wang, C.S.; Bryce, M.R.; Grace, I.; Lambert, C.J. Single-molecule electrical studies on a 7 nm long molecular wire. *Chem. Comm.* **2006**, doi: 10.1039/B613347A.
3. Choi, S.H.; Kim, B.; Frisbie, C.D. Electrical resistance of long conjugated molecular wires. *Science* **2008**, *320*, 1482-1486.
4. Choi, S.H.; Frisbie, C.D. Enhanced hopping conductivity in low band gap donor-acceptor molecular wires up to 20 nm in length. *J. Am. Chem. Soc.* **2010**, *132*, 16191-16201.
5. Danilov, A.; Kubatkin, S.; Kafanov, S.; Hedegard, P.; Stuhr-Hansen, N.; Moth-Poulsen, K.; Bjørnholm, T. Electronic transport in single molecule junctions: Control of the molecule-electrode coupling through intramolecular tunneling barriers. *Nano Lett.* **2008**, *8*, 1-5.
6. Huang, W.; Masuda, G.; Maeda, S.; Tanaka, H.; Ogawa, T. Molecular junctions composed of oligothiophene dithiol-bridged gold nanoparticles exhibiting photoresponsive properties. *Chem. Eur. J.* **2006**, *12*, 607-619.
7. Kubatkin, S.; Danilov, A.; Hjort, M.; Cornil, J.; Bredas, J.L.; Stuhr-Hansen, N.; Hedegard, P.; Bjørnholm, T. Single-electron transistor of a single organic molecule with access to several redox states. *Nature* **2003**, *425*, 698-701.

8. Li, Z.H.; Pobelov, I.; Han, B.; Wandlowski, T.; Blaszczyk, A.; Mayor, M. Conductance of redox-active single molecular junctions: An electrochemical approach. *Nanotechnology* **2007**, *18*, 044018.
9. Liang, T.T.; Naitoh, Y.; Horikawa, M.; Ishida, T.; Mizutani, W. Fabrication of steady junctions consisting of alpha,omega-bis(thioacetate) oligo(p-phenylene vinylene)s in nanogap electrodes. *J. Am. Chem. Soc.* **2006**, *128*, 13720-13726.
10. Liang, Y.Y.; Wang, H.B.; Yuan, S.W.; Lee, Y.G.; Yu, L.P. Conjugated block copolymers and co-oligomers: From supramolecular assembly to molecular electronics. *J. Mater. Chem.* **2007**, *17*, 2183-2194.
11. Moth-Poulsen, K.; Bjørnholm, T. Molecular electronics with single molecules in solid-state devices. *Nat. Nanotechnol.* **2009**, *4*, 551-556.
12. Osorio, E.A.; O'Neill, K.; Wegewijs, M.; Stuhr-Hansen, N.; Paaske, J.; Bjørnholm, T.; van der Zant, H.S.J. Electronic excitations of a single molecule contacted in a three-terminal configuration. *Nano Lett.* **2007**, *7*, 3336-3342.
13. Seferos, D.S.; Blum, A.S.; Kushmerick, J.G.; Bazan, G.C. Single-molecule charge-transport measurements that reveal technique-dependent perturbations. *J. Am. Chem. Soc.* **2006**, *128*, 11260-11267.
14. van der Zant, H.S.J.; Kervennic, Y.V.; Poot, M.; O'Neill, K.; de Groot, Z.; Thijssen, J.M.; Heersche, H.B.; Stuhr-Hansen, N.; Bjørnholm, T.; Vanmaekelbergh, D.; van Walree, C.A.; Jenneskens, L.W. Molecular three-terminal devices: Fabrication and measurements. *Faraday Discuss.* **2006**, *131*, 347-356.
15. Wang, C.S.; Batsanov, A.S.; Bryce, M.R. Nanoscale aryleneethynylene oligomers incorporating fluorenone units as electron-dopable molecular wires. *Faraday Discuss.* **2006**, *131*, 221-234.
16. Søndergaard, R.; Strobel, S.; Bundgaard, E.; Norrman, K.; Hansen, A.G.; Albert, E.; Csaba, G.; Lugli, P.; Tornow, M.; Krebs, F.C. Conjugated 12 nm long oligomers as molecular wires in nanoelectronics. *J. Mater. Chem.* **2009**, *19*, 3899-3908.
17. Alstrup, J.; Norrman, K.; Jørgensen, M.; Krebs, F.C. Lifetimes of organic photovoltaics: Design and synthesis of single oligomer molecules in order to study chemical degradation mechanisms. *Sol. Energy Mater. Sol. Cells* **2006**, *90*, 2777-2792.
18. Hagemann, O.; Jørgensen, M.; Krebs, F.C. Synthesis of an all-in-one molecule (for organic solar cells). *J. Org. Chem.* **2006**, *71*, 5546-5559.
19. Jørgensen, M.; Krebs, F.C. Stepwise and directional synthesis of end-functionalized single-oligomer OPVs and their application in organic solar cells. *J. Org. Chem.* **2004**, *69*, 6688-6696.
20. Jørgensen, M.; Krebs, F.C. Stepwise unidirectional synthesis of oligo phenylene vinylenes with a series of monomers. Use in plastic solar cells. *J. Org. Chem.* **2005**, *70*, 6004-6017.
21. Peeters, E.; van Hal, P.A.; Knol, J.; Brabec, C.J.; Sariciftci, N.S.; Hummelen, J.C.; Janssen, R.A.J. Synthesis, photophysical properties, and photovoltaic devices of oligo(p-phenylene vinylene)-fullerene dyads. *J. Phys. Chem. B* **2000**, *104*, 10174-10190.
22. Sugiono, E.; Metzroth, T.; Detert, H. Practical synthesis of vinyl-substituted p-phenylenevinylene oligomers and their triethoxysilyl derivatives. *Adv. Synth. Catal.* **2001**, *343*, 351-359.

23. Wong, M.S.; Li, Z.H. Multifunctional properties of monodisperse end-functionalized oligophenylenevinylenes. *Pure Appl. Chem.* **2004**, *76*, 1409-1419.
24. Detert, H.; Sadovski, O. Triarylaminines connected via phenylenevinylene segments. *Synth. Met.* **2003**, *138*, 185-188.
25. Giacalone, F.; Segura, J.L.; Martin, N.; Ramey, J.; Guldi, D.M. Probing molecular wires: Synthesis, structural, and electronic study of donor-acceptor assemblies exhibiting long-range electron transfer. *Chem. Eur. J.* **2005**, *11*, 4819-4834.
26. Stuhr-Hansen, N.; Christensen, J.B.; Harrit, N.; Bjørnholm, T. Novel synthesis of protected thiol end-capped stilbenes and oligo(phenylenevinylene)s (OPVs). *J. Org. Chem.* **2003**, *68*, 1275-1282.
27. Krebs, F.C.; Jørgensen, M. High carrier mobility in a series of new semiconducting PPV-type polymers. *Macromolecules* **2003**, *36*, 4374-4384.
28. Pedersen, D.S.; Rosenbohm, C. Dry column vacuum chromatography. *Synthesis-Stuttgart* **2001**, doi: 10.1055/s-2001-18722.

© 2011 by the authors; licensee MDPI, Basel, Switzerland. This article is an open access article distributed under the terms and conditions of the Creative Commons Attribution license (<http://creativecommons.org/licenses/by/3.0/>).

# Conjugated 12 nm long oligomers as molecular wires in nanoelectronics†

Roar Søndergaard,<sup>a</sup> Sebastian Strobel,<sup>b</sup> Eva Bundgaard,<sup>a</sup> Kion Norrman,<sup>a</sup> Allan G. Hansen,<sup>c</sup> Edgar Albert,<sup>d</sup> Gyorgy Csaba,<sup>d</sup> Paolo Lugli,<sup>d</sup> Marc Tornow<sup>c</sup> and Frederik C. Krebs<sup>\*a</sup>

Received 24th December 2008, Accepted 31st March 2009

First published as an Advance Article on the web 28th April 2009

DOI: 10.1039/b823158c

We demonstrate a generic synthetic approach to oligophenylenevinylene (OPV) derivative molecules with a molecular length of up to 12 nm and a relatively free choice of end group that can attach to different electrodes such as metallic gold or potentially transition metal oxide semiconductors. OPVs containing 3–19 phenyl units were synthesised by step wise HWE-reactions of a bifunctional OPV-monomer which allowed for complete control of the sizes of the OPVs. Workup and analysis (<sup>1</sup>H- and <sup>13</sup>C-NMR, mass spectrometry and size exclusion chromatography) of each step ensured a high purity of the final products. Final end group functionalities of the OPVs were introduced either as the first step (alcohol) or the last step (thioacetate). We further demonstrate a fabrication method for well defined nanogap electrode devices based on silicon-on-insulator technology, featuring a gap distance of down to 9 nm. Assembling the OPV derivatives onto these devices enabled preliminary investigations of their low-temperature transport properties, revealing a pronounced non-linear current–voltage characteristic at 4.2 K. We studied the electronic states of the molecule by Density Functional Theory (DFT) in order to show the effect of the ligands and of the gold contacts. By using the results of the DFT calculations in a non-equilibrium Green's function model, the current–voltage characteristics of OPVs have been analyzed, showing a good qualitative agreement with the experimental data.

## Introduction

In nanoelectronic devices are based on nanostructures that are generally governed by quantum mechanical processes. In recent years a variety of experiments have shown that single molecules can function as electronic devices capable of providing, *e.g.*, switching and rectification.<sup>1,2</sup> The accumulated experience in the field of molecular electronics has underlined the challenge and need for making functional conjugated molecules sufficiently large<sup>3</sup> and the contacts to the external circuit sufficiently small to make ends meet. While it is possible to create sufficiently small gaps between electrodes by a variety of techniques,<sup>4,5</sup> solutions to fabricating nanogap devices of predetermined spacing which can be integrated into standard silicon technology have been rarely reported. It is equally difficult to prepare reasonably pure monodisperse molecules with a length approaching even a few nanometres. Conjugated and electronically active molecules have a typical size of the order of 1 nm and the smallest structures that can be prepared reproducibly from bulk materials by semiconductor processing are currently of the order of 10 nm. The

simplest electronic component is a two terminal device and we thus envisage that at least two electrical connections must be made to the molecule, *i.e.*, one at each end of the molecule. The large discrepancy between the shortest distance at which we can place two electrically isolated electrodes and the size of the molecules that we are able to prepare can be used to summarize two of the largest challenges in molecular electronics that are: contacting the exterior circuitry to the molecular device, and, miniaturization of the external contacts such that they reach the same scale as the molecules (a few nanometres). There are both advantages and disadvantages when comparing organic oligomers (or single organic molecules) in electronic devices to traditional, inorganic semiconductors. The most obvious advantage is the size of molecules that may represent the ultimate miniaturization that can be achieved.<sup>6</sup> One disadvantage is that there is currently no specific method for making contact between the one particular molecular component and an external circuit. Further, while it is possible to make large molecules in the form of the well known polymers which are disperse with respect to their size (molecular weight), it is anticipated that for a molecule to be useful in a nanoelectronic circuit a good degree of control over the size of the molecule and its terminal binding groups is required. At the same time, there is the definite need for a good degree of control over the gap between the electrodes and for the compatibility with standard silicon process technology.

In the literature molecular junctions<sup>7</sup> based on the following oligomers are described: oligothiophenes,<sup>8,9</sup> blockoligomers based on PV/thiophene and thiophene/thiazole,<sup>10</sup> violegen<sup>11</sup> and arylene-ethylene with fluorine incorporated in the backbone.<sup>12,13</sup>

Furthermore, several experimental investigations have been reported in the literature regarding transport measurements on relatively short OPV derivatives, which include studies of the

<sup>a</sup>Riso National Laboratory for Sustainable Energy, Technical University of Denmark, Frederiksborgvej 399, DK-4000 Roskilde, Denmark. E-mail: frederik.krebs@risoe.dk

<sup>b</sup>Walter Schottky Institut, Technische Universität München, Am Coulombwall 3, 85748 Garching, Germany

<sup>c</sup>Institut für Halbleitertechnik, Technische Universität Braunschweig, Hans-Sommer-Straße 66, 38106 Braunschweig, Germany

<sup>d</sup>Institute for Nanoelectronics, Technische Universität München, 80333 Munich, Germany

† Electronic supplementary information (ESI) available: Synthesis procedures, control of purity by size exclusion chromatography, attachment experiments, XPS analysis and control experiments. See DOI: 10.1039/b823158c

dependence on substitutional side groups and terminal linkers to the electrodes,<sup>14,15</sup> which lead to the observation of, *e.g.*, single electron transport phenomena in single OPVs.<sup>16–19</sup> An obvious method for increasing the number of possibilities available to the experimenter would be devising a generic synthetic route to significantly longer conjugated molecules with flexibility in the choice of end groups. The larger size would make the molecules more compatible with the nanogaps that can be prepared with ease currently ( $\geq 10$  nm). In terms of connecting the molecules to a circuit, thiol linkers in conjunction with gold metal have been used almost exclusively due to the excellent binding of thiols to gold. There should in principle be many other possible substrate materials such as semiconductor oxides (*i.e.*, TiO<sub>2</sub>, ZnO) where carboxylic acids, alcohols and phenols have a high affinity. A desirable requirement to the synthetic procedure is therefore flexibility in the available end groups.

Most approaches followed in the literature employ thiol end groups and short oligomers of phenylenevinylene with 3 or 5 benzene rings. In one case the chemical nature of the linker was correlated to the transport properties for distyrylbenzenes<sup>14</sup> and it was found that conjugation all the way to the linker gives the best transport. The use of oligomers of poly(phenylene vinylene) (PPV) has many advantages including relatively easy synthetic routes and a moderate stability of the molecules in the absence of oxygen. PPVs have been studied in the context of organic photovoltaics,<sup>20–24</sup> organic transistors,<sup>25</sup> and electroluminescent devices.<sup>26</sup> Oligomers of PPV have served as models for polymers and have provided specific information about fundamental properties such as solubility, absorption, emission, conjugation length and carrier transport. It has been found that the electrical and optical properties of OPVs are comparable to the properties of PPVs.<sup>27,28</sup> Oligomers of PV have previously been prepared in numerous ways and with various lengths of the final products. Among these can be mentioned several variants of stepwise

Horner–Wadsworth–Emmons (HWE) condensations both unidirectional<sup>29–34</sup> and bidirectional<sup>35,36</sup> (the length of the OPVs vary from 4 to 11 phenyls), bidirectional stepwise Wittig reaction<sup>37</sup> (9 phenyls), unidirectional sequential Heck and HWE reactions<sup>38,39</sup> (12–14 phenyls), unidirectional stepwise Suzuki coupling<sup>40</sup> (14 phenyls) and unidirectional stepwise Siegrist condensation followed by a McMurry reaction as the finishing step<sup>41</sup> (16 phenyls). With respect to the aim of using OPVs as molecular wires the HWE, Siegrist and the Wittig reactions have the advantage of avoiding possible contamination with catalytic metal nanoparticles.<sup>42–45</sup>

Here we report the synthesis of large oligomers of PV with the possibility for a molecular length of up to 12 nm (19 phenyls) and different termination groups. We further demonstrate how a well defined nanogap as small as 9 nm can be fabricated using standard silicon process technology. We functionalize the nanogap device with a particular,  $\sim 12$  nm long OPV species and demonstrate the applicability of the oligomers as components in electronic devices between two electrodes by performing first electrical transport measurements. Our modeling based on density functional theory coupled to a non-equilibrium Green function approach provides an adequate interpretation of the molecular transport processes.

## Results and discussion

### Synthesis

The oligomers (Fig. 1) were prepared by sequential Horner–Wadsworth–Emmons (HWE) condensations which resulted in phenylenevinylene oligomers with different end groups (Fig. 2). These were then coupled in a final HWE condensation to a diphosphonate ester giving a symmetric oligomer with a doubling of the length of the molecule (Fig. 2). This approach has been used previously to prepare a PV oligomer with

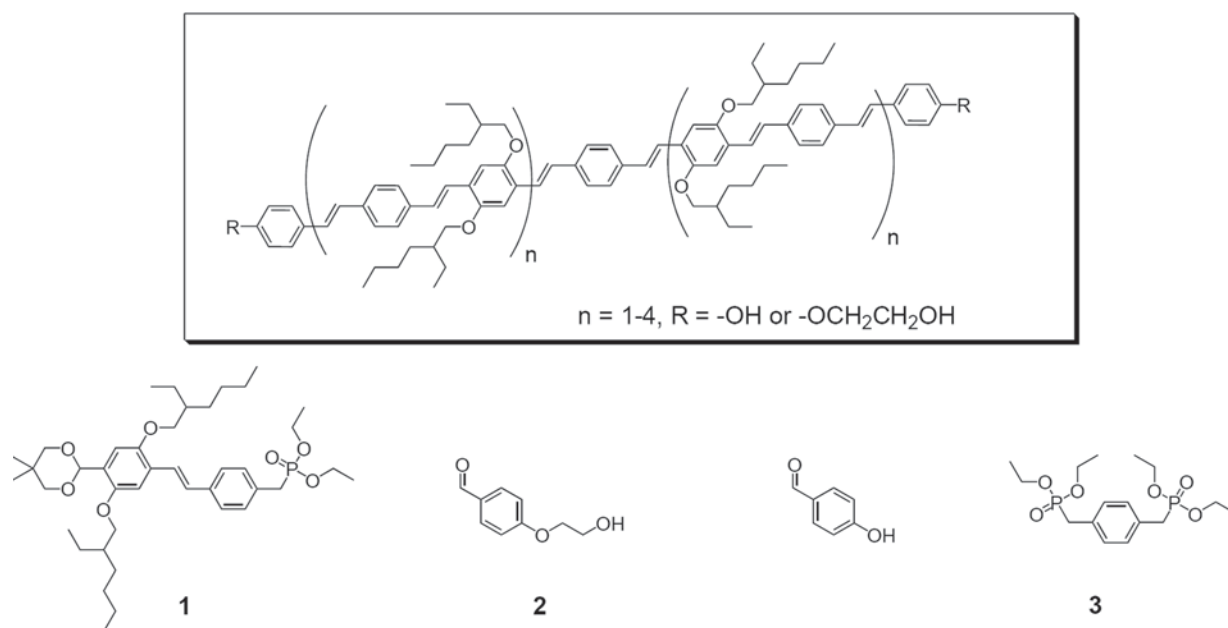


**Fig. 1** The synthesized oligomers based on phenylene vinylene with two different end groups (R) are shown above starting from four simple starting materials shown below.  $n = 1-4$  for  $R = -OCH_2CH_2OH$  (are converted to  $R = -OCH_2CH_2SAc$  in the final step) or  $R = -OH$ .

11 benzene rings.<sup>29–31</sup> The limitation in the previous work was the solubilizing side groups that were either propyl or propoxy groups which limited the solubility of the product when a length of 11 benzene rings was reached. This was later solved by Alstrup *et al.* where ethylhexyloxy sidechains were employed giving a much better solubility.<sup>46</sup> The ethylhexyloxy substituted monomer from that study was employed here. In the synthetic approach of the PPV oligomers aimed for attachment to gold surfaces, several issues had to be taken into account. Due to the high affinity of gold for sulfur, it would be highly advantageous in the attachment process to gold surfaces if the termination

group of the OPV has a sulfur containing functionality, i.e. –SH, –SMe or –SAc as demonstrated in the literature.<sup>28,47</sup>

The –SH group was, however, discarded due to its undesirable ability to dimerize forming a –S–S– bond. A test compound with thioacetate functionality (R–SAc) was prepared (see ESI†) to compare the ability of this group to attach to gold with the commercially available methyl-*p*-tolyl sulfide (R–SMe). Based on these results oligomers with thioacetate functionality were prepared. As the thioacetate functionality is not stable under the reaction conditions required for the build-up of the oligomers (strong base, strong acid), the thioacetate had to be introduced at

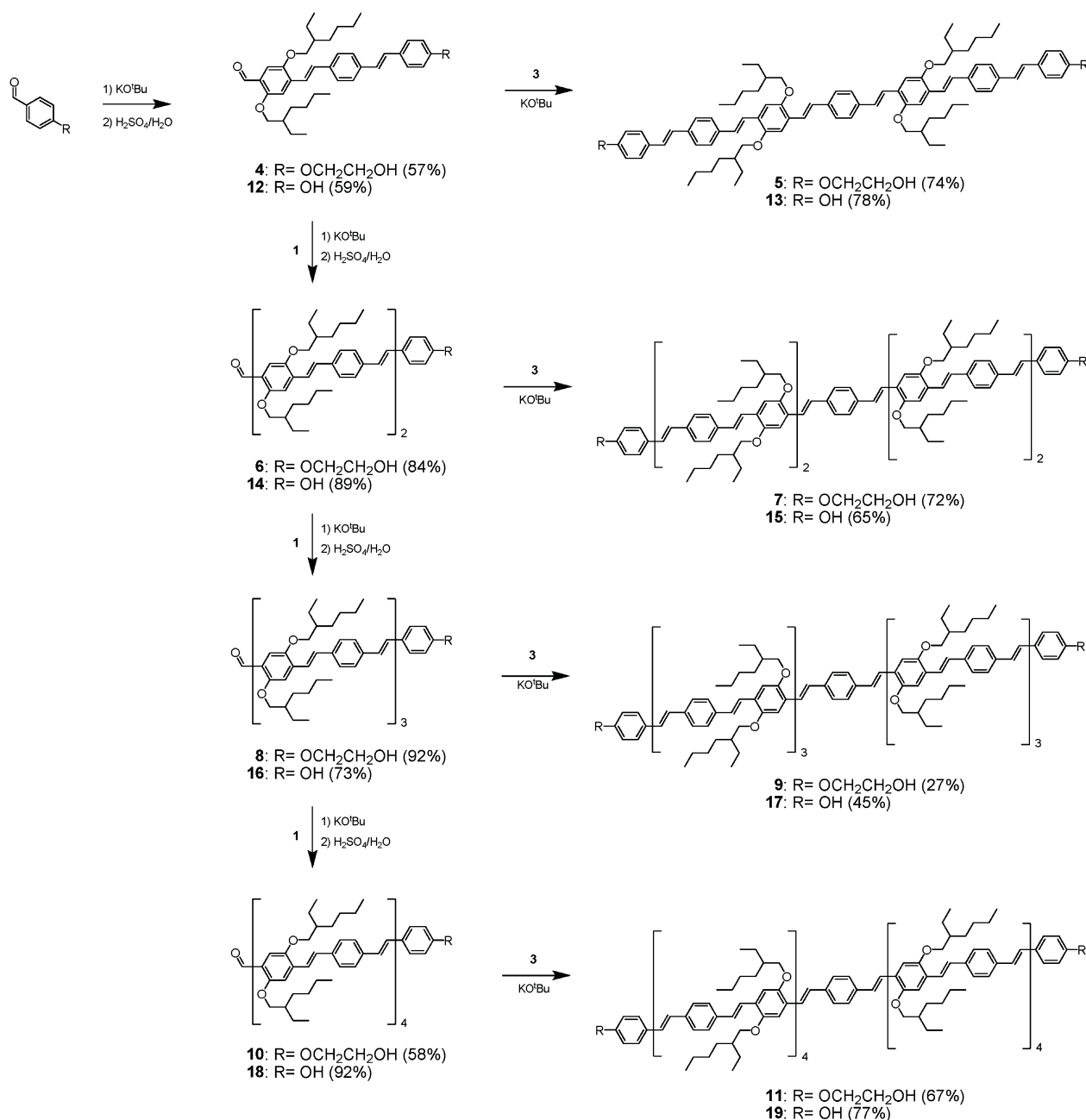


**Fig. 2** Strategy for the synthesis of the oligomers showed in Fig. 1. The synthesis of the “arms” of the molecule starts with the introduction of the termination group followed by growth of the arm and final doubling of the size of the molecule by attaching two “arms” to a core molecule which in this work is a simple benzene ring.



the final step. This imposes great demands to the solubility of the OPVs as it should be emphasized that chemistry performed on large molecules often requires high dilutions which can make otherwise standard reactions impossible.

The idea of preparing an aromatic thioacetate (Ar-SAc), which would provide a fully conjugated molecular 'wire' if attached to separate electrodes at each end of the molecule, was discarded. The only known procedure to introduce an aromatic thioacetate functionality as a last step is by employing *tert*-butyl thio ethers (Ar-S-C(CH<sub>3</sub>)<sub>3</sub>) using BF<sub>3</sub> as a deprotecting reagent.<sup>47</sup> The use of BF<sub>3</sub> could also result in cleavage of the alkoxy side chains which would lead to unnecessary complications.

It was instead chosen to use an alcohol precursor and to perform the final thioacetate introduction *via* a triflate by reaction with a thioacetate salt. For this last step (S<sub>N</sub>2 reaction) to be possible, the alcohol has to be aliphatic. In a first attempt we employed a benzylic alcohol, in order to have the thioacetate functionality as close to the conjugated system as possible. However, during deprotection of the acetal, incomplete hydrolysis took place which could not be improved by longer reaction times or additional acid. This is ascribed to the positive polarization formed near the acetal by resonance of the benzylic alcohol (when protonated), giving it benzylic cation properties.

To avoid this problem a 2-phenoxyethanol precursor to the thioacetate was used instead. The deprotection of the aldehyde has previously been carried out using concentrated HCl in THF under reflux conditions.<sup>29–31</sup> This procedure, however, results in the formation of 4-chlorobutanol as a byproduct through S<sub>N</sub>2 reaction of Cl<sup>-</sup> with protonated THF. The oligomers described in the literature were solids and removal of 4-chlorobutanol which is a liquid easily took place during filtration and washing of the product with ethanol. However, the smaller oligomers prepared in this work were oils and purification from the 4-chlorobutanol was not as simple. The deprotection was therefore carried out using a mixture of H<sub>2</sub>SO<sub>4</sub>/H<sub>2</sub>O followed by addition of water to push the equilibrium completely towards the alcohol/aldehyde. Extraction with ether and neutralization gave the oligomer after evaporation. The ethanolic termination group (Ar-OCH<sub>2</sub>CH<sub>2</sub>OH) was transformed into the thioacetate *via* a triflate as shown in Fig. 3. Synthesis of the triflate was carried out with various bases and the best result was achieved with 2,4,6-collidine. The triflate was then reacted in a straightforward S<sub>N</sub>2 reaction to give the thioacetate.

Workup of all compounds 4–11 to pure compounds could be performed using standard chromatographic methods using silica

gel. This is possible because of the alcohol functionality in the 2-hydroxyethoxy end group that causes good retention to the silica column material allowing good separation with chloroform/THF as eluent. The purity of the end products was verified by size exclusion chromatography (SEC) (see ESI†).

The oligomers of PPV aimed at attachment to transition metal oxide semiconductors such as ZnO surfaces were prepared with phenol terminal groups introduced in the first step followed by the general procedure. Though it is possible to obtain relatively good purity of compounds 12–19 by using the same procedures as for the 2-hydroxyethoxy compounds, purification by SEC was necessary to obtain pure samples (all yields for compounds 12–19 in Fig. 2 are for 'pure by TLC'). This is largely ascribed to the fact that all reaction steps involving use of base is in fact performed with large anionic reactants (the phenolic end groups will be the first to deprotonise). Longer reaction times and excess base are expected from this, allowing for side reactions to compete with the otherwise very fast HWE reaction.

### UV-vis spectroscopy

The oligomers were characterized by UV-vis (Fig. 4). In previous studies<sup>39</sup> it was found that λ<sub>max</sub> increases with an increase in *n* until a maximal red shift of 32 nm whereafter no additional shift of λ<sub>max</sub> is observed with further increase in *n*. An equivalent tendency is observed in Fig. 4 where λ<sub>max</sub> increases with an increase in *n*. However, a maximum λ<sub>max</sub> has not been reached and a further increase in *n* would eventually result in a λ<sub>max</sub> closer to λ<sub>max</sub> of MEHPPV. From the absorption spectra the band gap of the oligomers are derived and these are summarized in Table 1. The band gap of the oligomers is decreasing with an increase in *n*. Compared to MEH-PPV the band gap of the oligomers are as expected larger. In addition MEH-PPV bears two ethylhexyloxy groups on every phenylene ring whereas the oligomers prepared here bear two ethylhexyloxy groups on every second phenylene ring.

### Attachment to surfaces

The relative affinity (*i.e.* relative grafting efficiency) of different species towards gold can be determined in various ways. Furthermore, some work described in the literature include the use of acid or base (HCl(aq) or NH<sub>4</sub>OH(aq)) in the grafting solution to accelerate binding (for thioacetates).<sup>48</sup> These phenomena are described in the ESI† and involves selected illustrative compounds, *e.g.* methyl-*p*-tolyl sulfide, S-2-(*p*-tolyl)oxyethyl

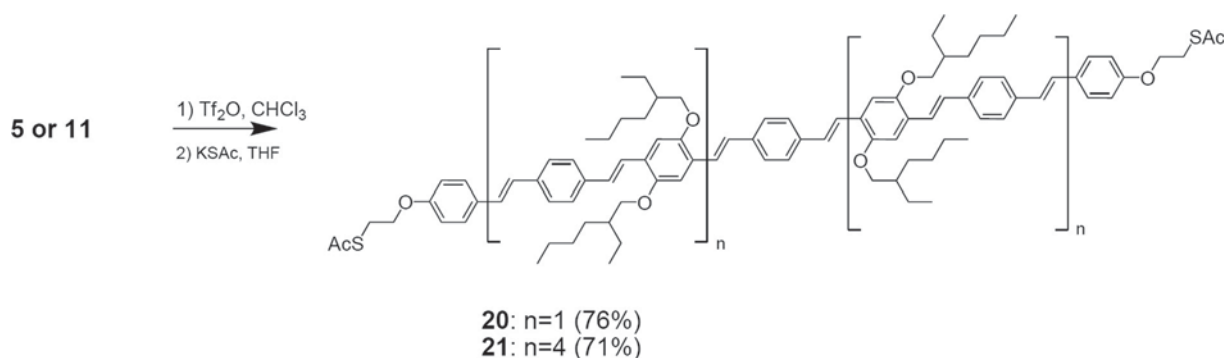


Fig. 3 Conversion of the desired oligomer molecule to a protected thiol end group.

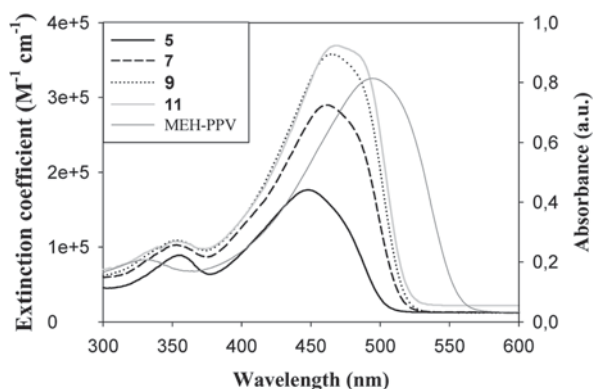


Fig. 4 Absorption spectra of MEH-PPV, **5**, **7**, **9** and **11** in  $\text{CHCl}_3$ .

Table 1 Optical band gap of **5**, **7**, **9**, **11** and MEH-PPV

Compound	$\lambda_{\text{max}}/\text{nm}$	Optical band gap/eV
<b>5</b>	448	2.46
<b>7</b>	461	2.42
<b>9</b>	465	2.40
<b>11</b>	469	2.39
MEH-PPV	495	2.22

ethanethioate, compound **20**, and compound **21**. Attempts to show grafting of the phenolic compounds to ZnO were unfortunately inconclusive.

### X-ray photoelectron spectroscopy (XPS)

In order to confirm that the thioacetates indeed are chemically bonded to the gold substrate *via* the sulfur and not just lying freely on the substrate as thioacetates or disulfides a XPS sulfur 2p study was carried out based on the work by Castner *et al.*<sup>49</sup> Fig. 5 shows XPS  $\text{S}_{2\text{p}}$  spectra for compound **20**, compound **21**, and a reference sample consisting of a freshly prepared gold substrate. In Fig. 5a the compounds were applied on the substrate by adding a few drops of a solution of the compound and letting the solvent (THF) evaporate thus leaving the compounds unbound to the substrate as thioacetates. In Fig. 5b the compounds were grafted to the surface according to the procedure described in the ESI,<sup>†</sup> which ensures that a chemical bond between the gold substrate and the sulfur atom in the compound is formed. The  $\text{S}_{2\text{p}}$  electron binding energy is determined by the molecular surroundings and mainly on what sulfur is bounded to directly, *i.e.* S–H, S–S, S–COCH<sub>3</sub>, and S–Au each have slightly different  $\text{S}_{2\text{p}}$  binding energies. Typical  $\text{S}_{2\text{p}_{3/2}}$  (hereafter called  $\text{S}_{2\text{p}}$ ) binding energies for unbound alkane thiols and dialkyl disulfides are between 163 and 164 eV.<sup>49</sup> Self assembly of these compounds on a gold substrate results in a peak at 161.9 eV, which is believed to be caused by the formation of a S–Au bond. The binding energies of the unbound thioacetates (compounds **20** and **21**) can be extracted from Fig. 5a which provides a binding energy of 163.2 eV for both compounds (it was not possible to detect a possible difference). The peaks in Fig. 5a were curve fitted (not shown) with no constraints. As expected the best fit was based on a doublet that

gave a 2 : 1 area ratio, a splitting of 1.2 eV, and a FWHM value of 1.13 eV. The peaks at 161.4 eV in Fig. 5b confirm that the grafting procedure resulted in a chemical bond between the gold substrate and the sulfur in compounds **20** and **21**. The S–Au binding energy obtained in this work is 0.5 eV lower compared to the literature value of 161.9 eV for alkane thiols.<sup>49</sup> Since compounds **20** and **21** each have an ethylene group between the sulfur and the rest of the molecule (R–CH<sub>2</sub>CH<sub>2</sub>–S–Au) one would intuitively have expected to measure a value that corresponds to an alkane thiol (*i.e.* 161.9 eV). The binding energy scales were referenced by setting the  $\text{Au}_{4\text{f}_{7/2}}$  binding energy to 84.0 eV. As a double check heptane thiol was grafted to a gold substrate under equivalent conditions, which resulted in a  $\text{S}_{2\text{p}}$  binding energy of 161.9 eV (inset in Fig. 5a) in perfect agreement with the literature value.<sup>49</sup> It is evident from Fig. 5b that peaks are present other than the bound thiols at 161.4 eV. Compounds **20** and **21** have thioacetate groups in each molecular end. Based on the results in Fig. 5 it is not possible to conclude whether both thioacetate groups from the same molecule have reacted with the gold substrate. Attempts to curve fit (not shown) the peaks in Fig. 5b with the intention to quantify the contribution from

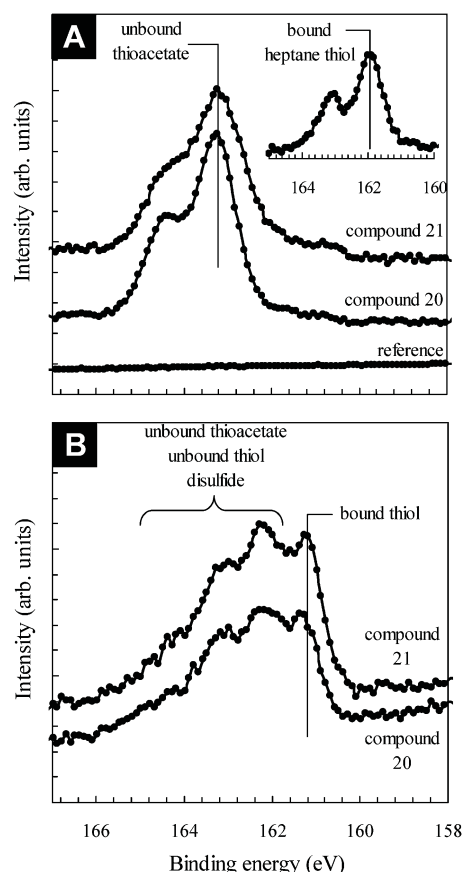


Fig. 5 XPS  $\text{S}_{2\text{p}}$  spectra for compound **20** and compound **21** applied onto a gold substrate by (A) adding a few drops of the compound from a solution and letting the solvent evaporate thus leaving the compound unbound to the substrate, and (B) by a grafting process that results in a chemical bond between the gold substrate and the sulfur atom in the compound. (A) The reference sample is a freshly prepared gold substrate, and the inset is the XPS  $\text{S}_{2\text{p}}$  spectrum for bound heptane thiol.

unbound thioacetate, unbound thiol, and possible disulfide failed. It was found that at least three (more likely four) sets of doublets are needed in order to adequately fit the data in Fig. 5b. However, due to the many variables several different fitting parameters provided adequate fitting results, so it was not possible to unambiguously quantify the contribution from other sulfur species. In summary, the  $S_{2p}$  binding energies for the bound thiols (S–Au) that originate from compounds **20** and **21** were both found to be 161.4 eV, which are easily distinguishable from the unbound thioacetates that both were measured to 163.2 eV. It was not possible to distinguish the contribution from unbound sulfur in the possible forms of thioacetate, unbound thiol, and possible disulfide. The XPS observations are however in good agreement with our model of a monolayer (see ellipsometric data in the ESI†) where the thiol in one end of the molecule is bound to gold and the thiol in the other end is not. Since we observe both bound and unbound thiol this is in good accordance. The complication that has arisen through the possibility of many different unbound sulfur species (thioacetate, thiol and disulfide) did not allow for a quantification of the bound/unbound sulfur ratio (ideally this ratio should equal one).

#### Nanogap device fabrication and characterization

To characterize the electronic transport properties of our synthesized OPV derivatives and verify their suitability as long molecular wires we self-assembled them on the electrodes of vertical nanogap electrode devices (VNDs). VNDs have been reported in different architectures, and using various substrate materials.<sup>50–55</sup> The preparation of Silicon-on-Insulator (SOI) based VNDs used in this study follows mainly our previously reported fabrication route<sup>56</sup> which we substantially extended here towards smaller gaps, to match the length of the molecular wires under study.

Briefly, a SOI material layer structure featuring a 20 nm thick buried oxide layer is patterned using a combination of dry plasma and selective wet etching steps in such a way, that a few nanometre wide trench is exposed at the side wall of a pillar-like SOI structure. After deposition of a metal thin film (3 nm Ti/25–30 nm Au) from an angular direction (65° with respect to the surface normal) two electrodes are formed which are separated by a few nanometres distance, precisely tailored by the chosen process parameters and metal thickness. Note that the lateral width of the electrodes is of macroscopic dimension ( $\sim 5 \mu\text{m}$ ), as determined by standard optical lithography and a metal “lift-off” procedure. Fig. 6 shows a schematic image of such prepared SOI-VND, together with a cross-sectional transmission electron microscopy (TEM) image of a sample which was identically processed as the one used for the transport measurements reported below.

#### Nanogap device functionalization and transport measurements

The fabricated nanogap devices were functionalized with OPV molecules using a combined from-solution assembly and subsequent annealing procedure (data in ESI†).

For low-temperature electronic transport measurements<sup>57</sup> the samples were mounted into ceramic chip carriers, Au wire bonded and inserted into a shielded measurement rod. The rod

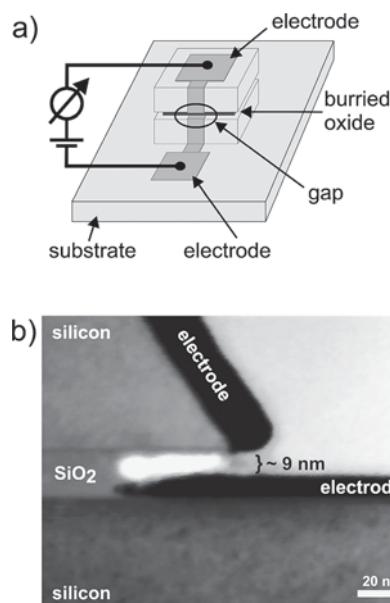


**Fig. 6** (a) Schematic of an SOI vertical nanogap device (VND), electrically contacted for conductance measurements. The metal thin film disconnects at the position of the recess-etched, buried  $\text{SiO}_2$  layer thereby forming the two electrodes in the denoted “gap” region. (b) Scanning transmission electron microscope (STEM) cross sectional image of a complete nanogap device with estimated gap separation 9 nm, taken after focused ion beam (FIB) milling sample preparation. The evaporated metal layer is visible as dark regions (“electrodes”). Note the apparent difference in metal layer thickness resulting from an evaporation direction rotated by  $\sim 65^\circ$  with respect to the surface normal. The FIB/STEM analysis was performed at the application labs of Zeiss SMT AG, Oberkochen, Germany.

was subsequently inserted into a  $\text{He}^4$  dewar vessel and thermally equilibrated. Fig. 7 displays a typical current–voltage ( $I$ – $V$ ) characteristic of a device that had been identically processed as the one displayed in Fig. 6 b), taken at liquid helium temperatures (4.2 K). Compared to the un-functionalised device whose data are included in Fig. 7 for reference, the electrical properties changed significantly after coating, clearly indicating the impact of molecular electronic conduction: while the reference

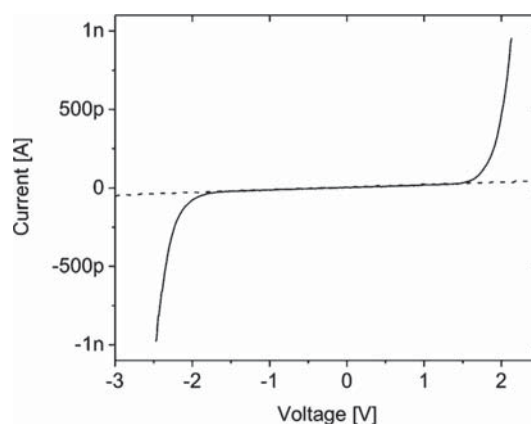


**Fig. 7**  $I$ – $V$  characteristics of a nanogap device after electrode functionalization with OPV derivatives, measured at 4.2 K (full line), compared to the data of the same sample before functionalization (dashed).

measurement showed a leakage current corresponding to  $\sim 60$  G $\Omega$  up to  $\pm 3$  V, only, a pronounced non-linear I–V characteristic emerged after functionalization, featuring a strong, exponential-like increase in current above approx. 1.3 V for positive bias, and below approx.  $-1.5$  V for negative bias. During measurements the upper electrode was connected to the positive and the lower electrode to the negative relative potential of the voltage source, respectively (*cf.* Fig. 6 a)). We observed qualitatively similar behaviour on 14 individual devices out of 22 functional junctions, all functionalized using the same procedure and showing an onset of increasing conductance varying within the range 1.0–2.0 V, and asymmetrically shifted towards more negative bias voltage. Four devices stayed highly insulating which may be assigned to small device-to-device variations in the electrodes separation, leading to the situation where the gap may just have not been bridged. Other four devices showed unstable and irreproducible I–V characteristics which possibly originated from gap contaminations or electrode failure by electric discharge. To unambiguously assign the measured characteristics to the functionalization with OPV<sup>58</sup> we performed two kinds of additional reference measurements (see ESI†): (1) After having taken the I–V displayed in Fig. 7 we removed all organic surface adsorbates, *i.e.*, including the OPV molecules, by treating the sample with oxygen plasma (Technics Plasma barrel etcher,  $2 \times 60$  s, 75 W). The subsequently measured I–V characteristic showed the same insulating behaviour as before functionalization. (2) A similar, completely independently processed sample having Pt electrodes was treated with the same functionalization procedure however using solvent without any dissolved OPV molecules. The recorded I–V trace exhibited an isolation resistance of  $\sim 100$  G $\Omega$  up to  $\pm 3$  V, while neighbouring devices on the same chip functionalised with OPV showed qualitatively the same non-linear I–V as observed in Fig. 7.

### Theoretical investigation of charge transport in OPVs

For the interpretation of the measured I–V characteristics we have relied on a numerical tool that allows one to calculate the current across molecules connected to metallic electrodes starting from the electronic states of the complete systems. This type of approach is well known in the literature<sup>59–62</sup> where quantum-chemistry methods such as density functional theory (DFT) have

been employed. DFT methods have reached a high level of maturity and are accredited with good predictive power for the determination of formation energies and molecular geometries. DFT methods have in addition been extended beyond their original purpose to treat non-equilibrium transport processes through single molecules (or a small collection of molecules). Unlike in standard quantum chemistry, open boundary conditions should be implemented. The usual choice is a Green-functional formulation. A representative example of molecular conduction codes is TRANSIESTA, built around the successful SIESTA code, which uses norm-conserving, localized pseudo-potentials as a LCAO basis.<sup>63</sup> TRANSIESTA uses a self-consistent loop to calculate the shift of energy levels due to the current.<sup>64</sup> It couples the density functional (DFT) calculation of the electronic states to the non-equilibrium Green's function approach (NEGF), in order to enable the computation of the current between two contacts in a manner consistent with the open boundaries and non-equilibrium conditions that naturally arise in coherent transport problems.<sup>65</sup> A three-dimensional Poisson solver provides an internal field that is self-consistent with the charge distribution. This additional self-consistent loop increases computational demand significantly and makes it less attractive for larger molecules. Indeed, it has been possible to calculate the current characteristics only for short OPVs.

Fig. 8 shows the electron density of the HOMO (left) and LUMO (right) orbital of an isolated oligomer corresponding to compound **20** calculated with SIESTA. It is clear that the molecular conjugation extends up to the two terminal oxygen atoms but that it does not extend through the aliphatic CH<sub>2</sub> groups (as expected). From an electrical point of view, such groups constitute an electrostatic barrier that confines the electrons in the central conjugated part of the OPV. The calculated HOMO–LUMO gap is around 1.95 eV. It is hard to extract a trend for the dependency of the gap from the molecule length.

It should be noticed that the molecules do lose their planarity even in the equilibrium configuration. Such loss of the original symmetry is affecting the shape of the molecular orbitals and the HOMO–LUMO gap.

In order to perform electrical measurements, the molecule has to be attached to metallic electrodes. In Fig. 9 we show the HOMO and LUMO orbitals for the complete systems, namely the thiol analogue of compound **20** with two Au electrodes.

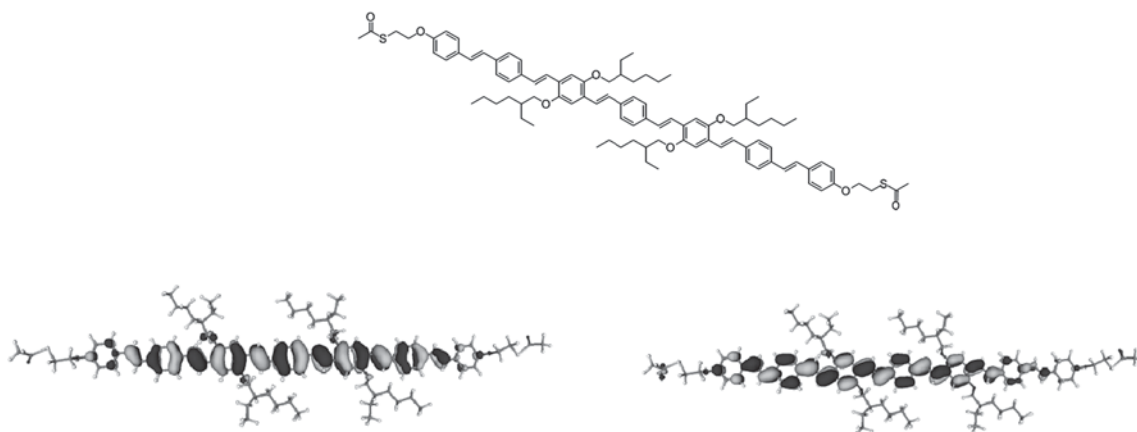


Fig. 8 Structure (above), HOMO (left) and LUMO (right) orbitals of compound **20**.



Clearly, the presence of the gold electrodes does not modify significantly the molecular orbitals. The HOMO–LUMO gap is slightly increased to 2.04 eV, with the LUMO level about 0.15 eV above the gold Fermi level.

The full calculation of the current characteristic for compound **20** is computationally too demanding. We have therefore simplified the molecules, eliminating the side branches and restricting the conjugated portion to five benzene rings. The gap of such a molecule (when isolated) is 2.18 eV, relatively close to one of the longer OPVs. We expect therefore that the current calculated for the simplified molecule is representative also for the measured OPVs. The calculated current voltage characteristics are displayed in Fig. 10, together with the LUMO orbitals. A clear threshold is found at a bias of around 1.5 V, followed by a steep increase of the current. Such behaviour is typical for

conjugated molecules. At low voltages, the Fermi contacts of the right and left electrodes coincide energetically with the HOMO–LUMO gap of the molecule.

Thus a current (that is an electron flux from the grounded electrode towards the positively biased one) is only possible *via* electron tunnelling across the gap. Since such a process has a low probability, the corresponding current is negligible. The threshold corresponds to the bias at which the LUMO (or the HOMO) level becomes aligned with one of the Fermi levels, thus giving the possibility for the electron to go across such a resonance state, with a much lower overall resistance. At higher voltages, two competing effects occur. On the one hand, more and more resonances become available to the contact electrons as the bias moves the Fermi level of the opposite contacts apart, leading to a sharp increase in the current. On the other hand, the

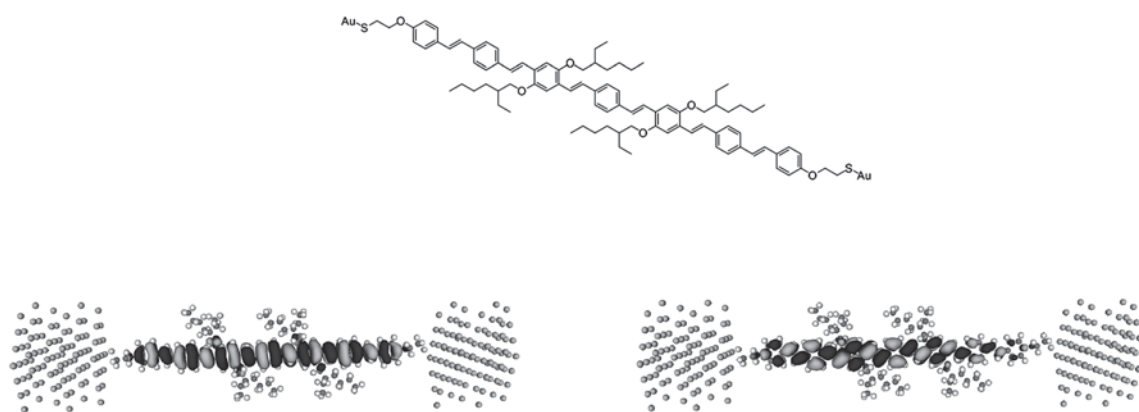


**Fig. 9** Structure (above), HOMO (left) and LUMO (right) orbitals of compound **20** attached to Au electrodes.

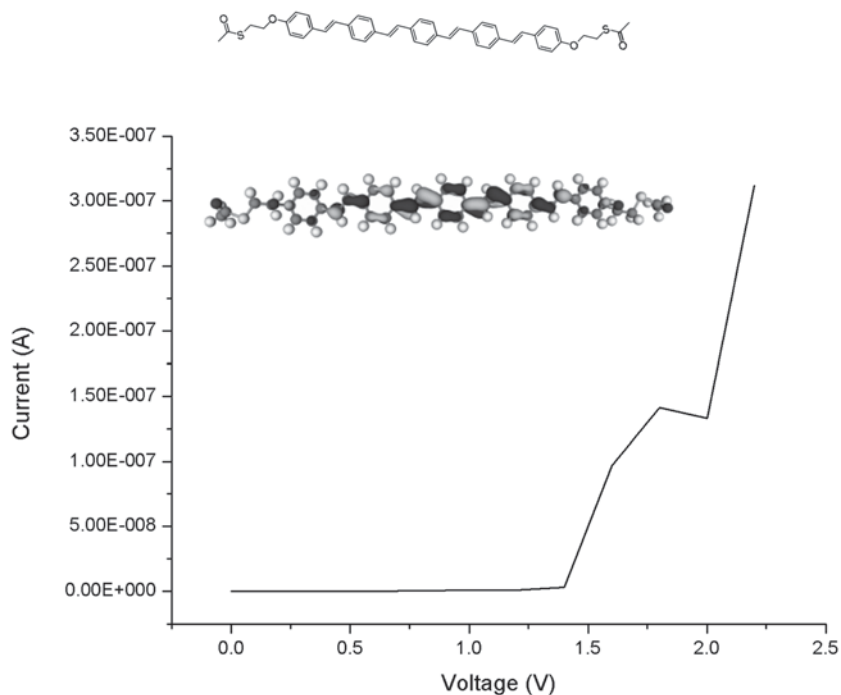


**Fig. 10** Structure and LUMO orbital for a simplified molecule (shown as an inset) and the calculated voltage characteristics showing a clear onset in charge transport at around 1.5 V bias.

strong electric field is responsible for a broadening of the resonant states, which implies a reduction of the transmission probability and in turn of the current. The former phenomenon dominates in our case, causing the current to increase sharply above 1.5 V. The effect of the broadening can nevertheless be seen in the plateau around 2 V. The calculated characteristics are in good qualitative agreement with the experimental data. We think that this is not fortuitous, as the simplified molecule used in the simulation captures all critical features of the measured one. We note that the asymmetry in the experimental characteristics could be attributed to details of the bonding to gold, which might slightly differ on the two sides, or to an asymmetry in the contacts themselves, or even to torsion on the molecule as current flows. In the simulation, the symmetry of the molecule is kept in place (even when attaching it to the electrodes) and therefore no asymmetry can be found.

## Experimental

Synthetic procedures, XPS measurements and binding studies are detailed in the ESI.† Current–voltage (I–V) characteristics were taken using a Keithley 2400 source meter, controlled *via* a PC (LabView software). Prior to any electrode functionalization with molecular layers all electrode pairs of a given sample were electrically pre-characterized at  $T = 4.2$  K. Only those samples were considered for further investigation which showed clear isolating behaviour with resistances of at least 20 G $\Omega$ , at bias voltages up to a few volts. For molecular electrode functionalization the sample was cleaned with deionised water (DI) and immersed in a  $\sim 0.1$  mM OPV solution in tetrahydrofuran (THF) for 16 h. The sample was subsequently blown dry in a stream of nitrogen and, to activate molecule binding, annealed at 90° in a nitrogen atmosphere for 1 h. Following this first annealing, the sample was kept for 1 h in isopropanol at 60°, and finally immersed for 1 h in a 0.06 M solution of NH<sub>4</sub>OH in THF/isopropanol 1 : 2 w/w. After these annealing steps, the sample was cleaned from physisorbed molecules by flushing with THF, and subsequently blown dry in a stream of nitrogen. This entire procedure had been optimised before using planar Au surfaces. To investigate the molecule grafting on these samples we used single-wavelength ( $\lambda = 632.8$  nm, angle of incidence = 70°) ellipsometry, and assumed a molecular layer with refractive index  $n = 1.55$ .<sup>66</sup> The measurements yielded a mean film thickness of  $8.2 \pm 1.6$  nm which is  $68 \pm 14\%$  of the molecule contour length of 12 nm. This result can be interpreted as a full OPV monolayer on the Au surface with each molecule tilted by  $47 \pm 12^\circ$  with respect to the surface normal. NH<sub>4</sub>OH(aq) was found to be the best promoter for attaching the oligomer molecules during the nanogap functionalization.

## Conclusion

An approach to large oligomers based on phenylene vinylene with a specific length up to  $\sim 12$  nm was shown employing Horner–Wadsworth–Emmons condensation. Oligomers were prepared with different termination groups to illustrate the applicability to different types of electrodes. XPS studies confirmed that the oligomers with a thioacetate linking group reacted with the gold substrate forming a gold–thiolate bond.

Using only standard silicon process technology we prepared SOI based vertical nanogap electrode devices (VNDs) with well defined gold contacts having a  $\sim 9$  nm gap separation as analyzed by cross-sectional TEM studies. After molecular functionalization with the OPV derivatives preliminary transport measurements at  $T = 4.2$  K showed a distinct non-linear response, with a major onset of conductance around 1.4 V bias voltage. Our findings were qualitatively well supported by calculations on shorter model OPV compounds. The threshold behavior can be attributed to the transition from tunnelling across the HOMO–LUMO gap to resonant transport through LUMO states.

In summary, our preliminary electrical measurements and transport calculations indicate that suitably derivatized molecules placed on SOI VNDs may find applicability in silicon-integrated molecular electronics. Future work will focus on the synthesis of oligomers with alkyl side chains and fully conjugated thioacetates as termination groups (Ar–SAc) and of those oligomers having specific functional substitutional groups, to enable the realization of SETs, molecular switches and memory elements. Furthermore, detailed spectroscopic studies will focus on how these materials are attaching, *i.e.*, whether they form well ordered molecular monolayers, and which is their average conformation with respect to the surface (tilt angle). Parallelization of the Atomistix code will allow us in the future to calculate the transport characteristics of the synthesized molecules. Finally, methods for the specific functionalization of nanogap structures at dedicated locations in electronic circuits will have to be developed, to enable true integration of molecular devices into silicon microelectronics.

## Acknowledgements

This work was supported by EU STREP project no. 026714 with the acronym VERSATILE. Jan Alstrup is acknowledged for preparing all the substrates used for the binding studies. Dr Kim Troensegaard Nielsen is acknowledged for initial work that proved useful in this project. S. S. and M. T. acknowledge funding by the BMBF under grant 03X5513 (Junior Research Group “Nanotechnology”) and Zeiss SMT AG Oberkochen for STEM analysis. P. L. acknowledges the support of the DFG cluster of excellence Nanosystems Initiative Munich (NIM).

## References

- 1 M. A. Reed, T. Lee, *Molecular Nanoelectronics*. American Scientific Publishers: Los Angeles, CA, 2003.
- 2 N. J. Tao, *Nat. Nanotechnol.*, 2006, **1**, 173–181.
- 3 S. H. Choi, B. Kim and C. D. Frisbie, *Science*, 2008, **320**, 1482–1486.
- 4 H. B. Akkerman and B. de Boer, *J. Phys. Cond. Matt.*, 2008, **20**, 1.
- 5 N. Prokopuk and K. A. Son, *J. Phys. Cond. Matt.*, 2008, **20**, 37.
- 6 J. M. Tour, *Acc. Chem. Res.*, 2000, **33**, 791–804.
- 7 N. J. Tao, *Nature Nat.*, 2006, **1**, 173.
- 8 A. C. Spivey, D. J. Turner, M. L. Turner and S. Yeates, *Org. Lett.*, 2002, **4**, 1899.
- 9 W. Huang, G. Masuda, S. Maeda, H. Tanaka and T. Ogawa, *Chem.–Eur. J.*, 2006, **12**, 607.
- 10 Y. Liang, H. Wang, S. Yuan, Y. Lee, L. Gan and L. Yu, *J. Mater. Chem.*, 2007, **17**, 2138.
- 11 Z. Li, I. Pobelov, B. Han, T. Wandlowski, A. Blaszczyk and M. Mayer, *Nanotechnology*, 2007, **8**, 044018.
- 12 G. J. Ashwell, W. D. Tyrell, B. Urasinska, C. Wang and M. R. Bryce, *Chem. Commun.*, 2006, 1640.

- 13 C. Wang, A. S. Batsanow and M. R. Bryce, *Faraday Discuss.*, 2006, **131**, 221.
- 14 T. T. Liang, Y. Naitoh, M. Horikawa, T. Ishida and W. Mizutani, *J. Am. Chem. Soc.*, 2006, **128**, 13720–13726.
- 15 D. S. Seferos, A. S. Blum, J. G. Kushmerick and G. C. Bazan, *J. Am. Chem. Soc.*, 2006, **128**, 11260–11267.
- 16 S. Kubatkin, A. Danilov, M. Hjort, J. Cornil, J. L. Brédas, N. Stuhr-Hansen, P. Hedegård and T. Bjørnholm, *Nature*, 2003, **425**, 698–701.
- 17 H. S. J. van der Zant, Y. V. Kervennic, M. Poot, K. O'Neill, Z. de Groot, J. M. Thijssen, H. B. Heersche, N. Stuhr-Hansen, T. Bjørnholm, D. Vanmaekelbergh, C. A. van Walree and L. W. Jenneskens, *Faraday Discuss.*, 2006, **131**, 347–356.
- 18 E. A. Osorio, K. O'Neill, M. Wegewijs, N. Stuhr-Hansen, J. Paaske, T. Bjørnholm and H. S. J. van der Zant, *Nano Lett.*, 2007, **7**, 3336–3342.
- 19 A. Danilov, S. Kubatkin, S. Kafanov, P. Hedegård, N. Stuhr-Hansen, K. Moth-Poulsen and T. Bjørnholm, *Nano Lett.*, 2008, **8**, 1–5.
- 20 C. J. Brabec, N. S. Sariciftci and J. C. Hummelen, *Adv. Funct. Mater.*, 1992, **11**, 15–26.
- 21 H. Spanggaard and F. C. Krebs, *Sol. Energy Mater. Sol. Cells*, 2004, **83**, 125–146.
- 22 N. S. Sariciftci, L. Similowitz, A. J. Heeger and F. Wudl, *Science*, 1992, **258**, 1474–1476.
- 23 M. Granström, K. Petritsch, A. C. Arias, A. Lux, M. R. Andersson and R. H. Friend, *Nature*, 1998, **395**, 257–260.
- 24 S. E. Shaheen, C. J. Brabec, N. S. Sariciftci, F. Padinger, T. Fromherz and J. C. Hummelen, *Appl. Phys. Lett.*, 2001, **78**, 841–843.
- 25 H. Sirringhaus, N. Tessler and R. H. Friend, *Science*, 1998, **280**, 1741–1744.
- 26 Q. Pei, G. Yu, C. Zhang, Y. Yang and A. J. Heeger, *Science*, 1995, **269**, 1086–1088.
- 27 T. P. Nguyen, C. Stéphan, P. Le Rendu and V. H. Tran, *Optical Mater.*, 1998, **9**, 94–98.
- 28 P. Le Rendu, T. P. Nguyen and V. H. Tran, *Synth. Met.*, 1999, **101**, 649.
- 29 M. Jørgensen and F. C. Krebs, *J. Org. Chem.*, 2004, **69**, 6688–6696.
- 30 M. Jørgensen and F. C. Krebs, *J. Org. Chem.*, 2005, **70**, 6004–6017.
- 31 O. Hagemann, M. Jørgensen and F. C. Krebs, *J. Org. Chem.*, 2006, **71**, 5546–5559.
- 32 E. Peeters, P. A. van Hal, J. Knol, C. J. Brabec, N. S. Sariciftci, J. C. Hummelen and R. A. J. Janssen, *J. Phys. Chem. B*, 2000, **104**, 10174–10190.
- 33 E. Sugiono, T. Metzroth and H. Detert, *Adv. Synth. Catal.*, 2001, **343**, 351–359.
- 34 M. S. Wong and Z. H. Li, *Pure Appl. Chem.*, 2004, **76**, 1409–1419.
- 35 H. Detert and O. Sadovski, *Synth. Met.*, 2003, **138**, 185–188.
- 36 F. Giacalone, J. L. Segura, N. Martin, J. Ramey and D. M. Guldi, *Chem.–Eur. J.*, 2005, **11**, 4819–4834.
- 37 T. Jiu, Y. Li, X. Liu, H. Liu, C. Li, J. Ye and D. Zhu, *J. Polym. Sci., Part A: Polym. Chem.*, 2007, **45**, 911–924.
- 38 W. J. Li, H. B. Wang, L. P. Yu, T. L. Morkved and H. M. Jaeger, *Macromolecules*, 1999, **32**, 3034–3044.
- 39 T. Maddux, W. Li and L. Yu, *J. Am. Chem. Soc.*, 1997, **119**, 844–845.
- 40 S. P. Dudek, M. Pouderoijen, R. Abbel, A. P. H. J. Schenning and E. W. Meijer, *J. Am. Chem. Soc.*, 2005, **127**, 11763–11768.
- 41 H. Meier and D. Ickenroth, *Eur. J. Org. Chem.*, 2002, 1745–1749.
- 42 F. C. Krebs, R. B. Nyberg and M. Jørgensen, *Chem. Mater.*, 2004, **16**, 1313–1318.
- 43 K. T. Nielsen, K. Bechgaard and F. C. Krebs, *Macromolecules*, 2005, **38**, 658–659.
- 44 K. T. Nielsen, K. Bechgaard and F. C. Krebs, *Synthesis*, 2006, 1639–1644.
- 45 K. T. Nielsen, P. Harris, K. Bechgaard and F. C. Krebs, *Acta Cryst.*, 2007, **B63**, 151–156.
- 46 J. Alstrup, K. Norrman, M. Jørgensen and F. C. Krebs, *Sol. Ener. Mater. Sol. Cells*, 2006, **90**, 2777–2792.
- 47 N. Stuhr-Hansen, J. B. Christensen, N. Harrit and T. Bjørnholm, *J. Org. Chem.*, 2003, **68**, 1275–1282.
- 48 A. H. Éll, G. Csajnyik, V. F. Slagt, J.-E. Bäckvall, S. Berner, C. Puglia, G. Ledung and S. Oscarsson, *Eur. J. Org. Chem.*, 2006, 1193–1199.
- 49 D. G. Castner, K. Hinds and D. W. Grainger, *Langmuir*, 1996, **12**, 5083–5086.
- 50 R. Krahne, A. Yacoby, H. Shtrikman, I. Bar-Joseph, T. Dadosh and J. Sperling, *Appl. Phys. Lett.*, 2002, **81**, 730–732.
- 51 J. Berg, F. Che, P. Lundgren, P. Enoksson and S. Bengtsson, *Nanotechnology*, 2005, **16**, 2197–2202.
- 52 S. M. Dirk, S. W. Howell, S. Zmuda, K. Childs, M. Blain, R. J. Simonson and D. R. Wheeler, *Nanotechnology*, 2005, **16**, 1983–1985.
- 53 S. M. Luber, S. Strobel, H. P. Tranitz, W. Wegscheider, D. Schuh and M. Tornow, *Nanotechnology*, 2005, **16**, 1182–1185.
- 54 S. M. Luber, F. Zhang, S. Lingitz, A. G. Hansen, F. Scheliga, E. Thorn-Csanyi, M. Bichler and M. Tornow, *Small*, 2007, **3**, 285–289.
- 55 S. Strobel, K. Arinaga, A. G. Hansen and M. Tornow, *Nanotechnology*, 2007, **18**, 295201.
- 56 S. Strobel, R. M. Hernández, A. G. Hansen and M. Tornow, *J. Phys. Cond. Matt.*, 2008, **20**, 37.
- 57 Room temperature measurements were carried out routinely prior to all experiments to check device performance, however only for small bias to avoid device failure, since leakage currents through the semiconductor substrate generally limited the gap insulation.
- 58 Based on the lateral extensions of the OPV molecules of 1.5–2.2 nm (including side-chains) we roughly estimate of the order of 3000 molecules crossing the 5 µm wide gap in parallel when closest, one-dimensional packing is assumed.
- 59 M. Di Ventra, S. T. Pantelides and N. D. Lang, *Phys. Rev. Lett.*, 2000, **84**, 979.
- 60 J. Taylor, H. Guo and J. Wang, *Phys. Rev. B*, 2001, **63**, 245407.
- 61 A. Nitzan and M. A. Ratner, *Science*, 2003, **300**, 1384.
- 62 A. Pecchia, M. Gheorghe, L. Latessa, A. Di Carlo and P. Lugli, *IEEE Trans. Nanotechnology*, 2004, **3**, 353.
- 63 D. Sanchez-Portal, P. Ordejon, E. Artacho and J. M. Soler, *Int. J. Quantum Chem.*, 1999, **65**, 453–461.
- 64 M. Brandbyge, J. L. Mozos, P. Ordejon, J. Taylor and K. Stokbro, *Phys. Rev. B*, 2002, **65**, 165401.
- 65 S. Datta, *Electronic Transport in Mesoscopic Systems*. Cambridge, U.K.: Cambridge Univ. Press, 1995.
- 66 L. Cheng, J. P. Yang, Y. X. Yao, D. W. Price, S. M. Dirk and J. M. Tour, *Langmuir*, 2004, **20**(4), 1335–1341.

# New Low-Bandgap Materials with Good Stabilities and Efficiencies Comparable to P3HT in R2R-Coated Solar Cells

Roar Søndergaard,\* Matthieu Manceau, Mikkel Jørgensen, and Frederik C. Krebs

The field of polymer solar cells (PSCs) has progressed greatly over the last years. Many new polymers have been developed and optimized with the introduction of low-bandgap (LBG) polymers and efficiencies are now exceeding 8% for small area organic solar cells.<sup>[1]</sup> Simultaneously the field has moved from not only trying to prepare highly efficient cells on a small scale to also include large area fabrication, thus taking the first steps towards manufacture.<sup>[2–5]</sup> Unfortunately most of the high performance polymers from lab scale fabrication (a few mm<sup>2</sup>) are not compatible with processing conditions in air because of their general unstable nature under ambient conditions.<sup>[6]</sup> This makes the large area methods such as roll-to-roll (R2R) coating (1–2500 cm<sup>2</sup>) practically impossible within the scope of high throughput production of extremely cheap solar cells. Processing using R2R coating techniques can be viewed as more ‘rough’ than the laboratory techniques employed during careful optimization of a small scale devices. As a consequence of this, P3HT, which has been a leading polymer material in PSC research for around a decade, is still the best choice when it comes to compatibility with large scale processing. Efficiencies in the area of 2–3% have been reported for P3HT,<sup>[4]</sup> while virtually no other polymers have been used in publications of large area solar cell modules. If the field of PSCs is to advance further towards widespread manufacture, more polymers that can be used in large area PSCs have to be developed.

We here present two new LBG polymers, **1** and **2** (see **Figure 1**), which show good photostability, although still inferior to P3HT, and of which one also exhibits efficiencies comparable to P3HT when processed by R2R techniques.<sup>[7,8]</sup> The polymers are based on an alkoxy-substituted benzothiadiazole acceptor unit and unsubstituted benzoedithiophene donor units, with the difference being the symmetry of the benzoedithiophenes. The structural design of the polymers was chosen with the aim to prepare stable polymers. We have previously shown that side chains are generally a major contributor to photodegradation, but that degradation tends to be faster when the side chains are present at the donor unit than when they are attached to the acceptor unit.<sup>[6]</sup> In the same study it was furthermore found

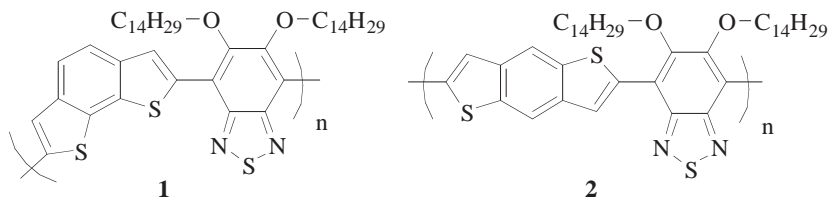


**Figure 1.** Chemical structure of the polymers **1** and **2**.

that the use of polycyclic aromatic donor units without side chains generally exhibit good photochemical stability. In order to achieve a good solubility of the polymers alkoxy side chains, which generally increases solubility considerably compared to the corresponding alkyl units,<sup>[9]</sup> were therefore chosen to be placed on the benzothiadiazole acceptor moiety, while keeping the benzoedithiophene donor units without side chains.

A common dilemma when having prepared a new polymer is which processing conditions to choose for the optimization of the final solar cell device, without spending too much time and polymer. Because of this, the actual optimization is often not very precise or complete.

We recently described a new method where the optimal relative compositions of donor (polymer) and acceptor (PCBM: [6,6]-phenyl-C<sub>61</sub>-butyric acid methyl ester) material in the active layer as well as the optimal thickness of the layer can be determined very precisely on R2R using a very limited amount of polymer.<sup>[10]</sup> By gradient application of donor, acceptor and solvent using differentially pumped slot-dye-coating, varying either the composition (polymer:PCBM; 0:100→100:0, 1% steps) or the concentration of the active materials in the ink, the use of the R2R procedure allows for much more precise optimization of the active layer buildup than is normally achieved using conventional test of spin coated devices. Generally only 2–5 different ratio compositions are tested. Here 100–200 ratio compositions can be prepared with roughly the same amount of polymer. As shown for polymer **1** in **Figure 2**, the mappings of the relative ratios gives a very precise determination of the optimal blend in the active layer.

The optimizations of solar cells with polymers **1** and **2** were performed by preparing cells with an inverted structure on PET (PET|ITO|ZnO|active layer|PEDOT:PSS|Ag) of a size of 4.2 cm<sup>2</sup> (PET: polyethylene terephthalate, ITO: Indium tin oxide, PEDOT:PSS: poly(3,4-ethylenedioxythiophene):poly(styrenesulfonate)). After optimization, which for polymer **1** showed to be a ratio of 45:55 of 1/PCBM and for polymer **2** a ratio of 41:59 of 2:PCBM, cells with optimized compositions were prepared and tested in order to fully characterize the potential of the polymers as active materials in PSCs. A total of 481 solar cells were

Dr. R. Søndergaard, Dr. M. Manceau, Dr. M. Jørgensen,  
Prof. F. C. Krebs  
Department of Energy Conversion and Storage  
Technical University of Denmark  
Frederiksborgvej 399, DK-4000 Roskilde, Denmark  
E-mail: rosq@dtu.dk



DOI: 10.1002/aenm.201100517



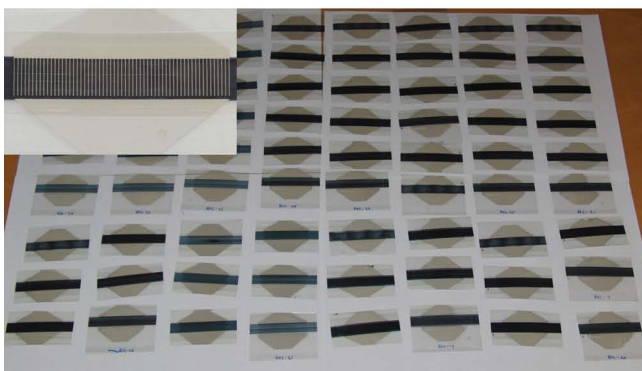
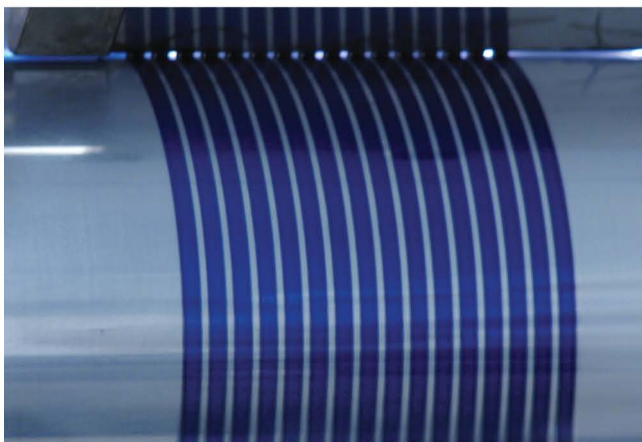
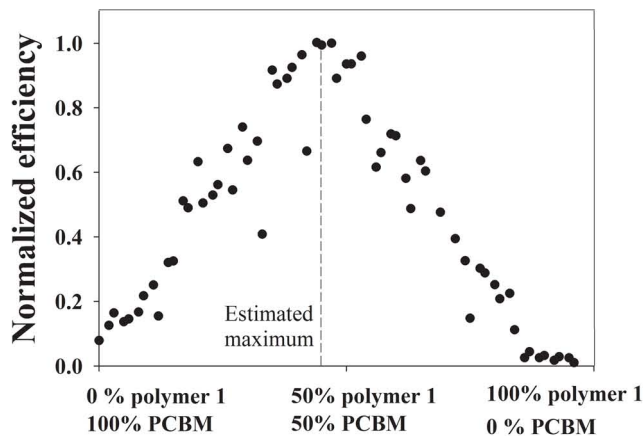


**Figure 2.** Top: Example of a ratio experiment results using differentially pumped slot-die-coating varying the relative composition of the donor and acceptor material - here shown for polymer 1. Middle: Picture of R2R processing by slot-die coating. Bottom: Examples of the final individual solar cells with an insert showing the pattern of the back electrode.

prepared during the optimization process and an additional 451 cells for the actual performance characterization. For polymer 1 the top 100 cells showed average efficiencies (PCEs) of  $1.24 \pm 0.13\%$ , open circuit voltages ( $V_{OC}$ s) of  $0.68 \pm 0.03$  V, short circuit currents ( $J_{SC}$ s) of  $5.35 \pm 0.51$  mA cm<sup>-2</sup> and fill factors (FFs) of  $33.9 \pm 1.9\%$ . Current-voltage ( $J$ - $V$ ) characteristics of a representative of the best performing cells using polymer 1 were PCE: 1.72%,  $V_{OC}$ : 0.74 V,  $J_{SC}$ : 6.40 mA cm<sup>-2</sup>, FF: 36%. These results are comparable to what has previously been

achieved in our group using P3HT under similar conditions (best P3HT cell: PCE: 2.29%,  $V_{OC}$ : 0.54 V,  $J_{SC}$ : 10.3 mA cm<sup>-2</sup>, FF: 41%).<sup>[10]</sup>

For polymer 2 the top 100 cells showed a somewhat inferior result with average efficiencies of  $0.29 \pm 0.06\%$ , open circuit voltages of  $0.42 \pm 0.06$  V, short circuit currents of  $2.33 \pm 0.29$  mA cm<sup>-2</sup> and fill factors of  $29.7 \pm 3.9\%$  and with best  $J$ - $V$  characteristics of: PCE: 0.43%,  $V_{OC}$ : 0.49 V,  $J_{SC}$ : 2.98 mA cm<sup>-2</sup>, FF: 29.8%.

In order to examine the photo stabilities of the polymers, photodegradation studies in air were performed by studying the amount of absorbed photons as a function of time (ageing) spend under AM 1.5G conditions ( $1000$  W m<sup>-2</sup>, 85 °C). The experiment is described in detail in the experimental section (UV spectra can be found in the Supporting Information). It is important to stress that these are *relative* stability studies of the polymers and bleaching times should not be mistaken for lifetimes of solar cells prepared with these. We have recently reported the photochemical stability of polymer 2,<sup>[6]</sup> but this is the first report of its use in solar cells. Both polymers show moderately good stabilities, reaching complete bleaching after approximately 55–75 h (see Figure 3). As a comparison a polymer carrying a similar alkoxy-substituted benzothiadiazole acceptor unit and the widely used cyclopentadiophene donor unit reached bleaching after approximately 7–8 h.<sup>[6]</sup> Figure 3 also demonstrates that the polymers show initial photochemical stabilities (first 20 h) that are very comparable to those of P3HT and although the long-term stability is still inferior to P3HT this is acceptable for processing in air.

When comparing to P3HT where the photochemical degradation mechanisms have been studied in great detail,<sup>[11]</sup> such knowledge is unfortunately not available for most low-band-gap polymers. In the case of P3HT photochemical degradation occurs primarily through reactions on the side chains. Although the photochemical stability has been improved a lot for the

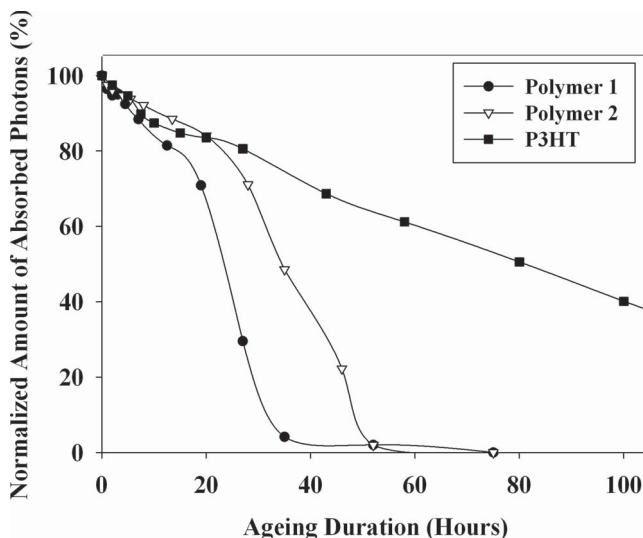


**Figure 3.** Evolution of the normalized amount of absorbed photons (see Experimental Section for details) as a function of time of photochemical ageing in ambient conditions of polymers 1 and 2 compared to P3HT (AM 1.5G,  $1000$  W m<sup>-2</sup>, 85 °C). Spline curves have been added to guide the eye.

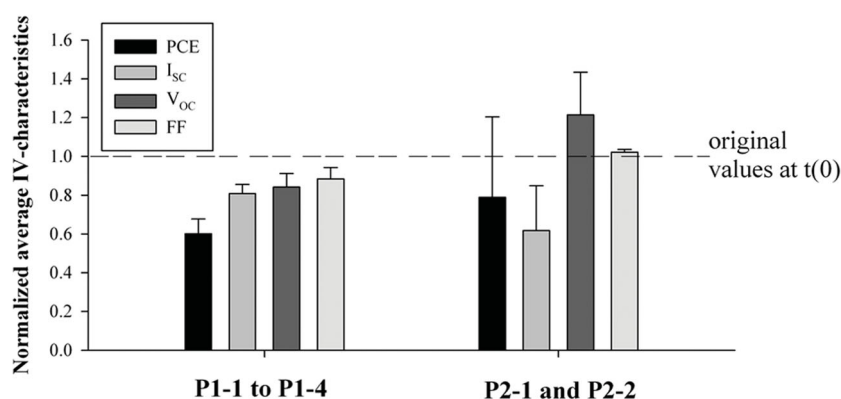


**Figure 4.** Top: Picture of the solar tracker onto which the cells were mounted for 4 months. Bottom: Normalized average  $J$ - $V$  characteristics of four cells prepared with polymer 1 (P1-1 to P1-4) and two cells prepared with polymer 2 (P2-1 and P2-2) after spending 4 months outside.

polymers 1 and 2 compared to polymers carrying side chains on the donor moiety, they still degrade faster than P3HT. One possible explanation for this could be that the molecules break down via the side chains of the dialkoxybenzothiadizole. This certainly warrants further work through a systematic investigation of the photochemical stability of the materials.

Besides the study of the photodegradation of the pure polymer in air using UV spectroscopy, a study of the  $J$ - $V$  characteristics of several cells after exposure to outdoor conditions was performed. Four cells with polymer 1 (P1-1 to P1-4) and two cells with polymer 2 (P2-1 and P2-2) were embedded in a layer of polyurethane between a hardened glass plate (front) and a polycarbonate plate (back), which was mounted on a solar tracker for maximum exposure. The  $J$ - $V$  characteristics of the cells were measured before and after outdoor exposure for four months, as shown in Figure 4, and all cells generally showed good stability. In one case (P2-2) the voltage of the device showed significant improvement after the four months.

The behavior of this cell was ascribed to originate from a contacting problem in the initial measurement. P3HT devices with the same size and geometry were not tested in this experiment so direct comparison is not possible, but compared with modules of P3HT under similar conditions the cells prepared with polymers 1 and 2 showed to be slightly inferior in terms of stability.

In summary, we have thoroughly investigated the optimal conditions for the preparation of polymer based solar cells for two new polymers by roll-to-roll processing. By use of differentially pumped slot-die coating of the donor, acceptor, and solvent, the optimal relative composition of donor and acceptor material and active layer thickness could be determined with high precision, and a series of optimized cells could hereafter be investigated. For the best performing polymer (1) the top 100 cells showed average efficiencies of  $1.24 \pm 0.13\%$ , open circuit voltages of  $0.68 \pm 0.03$  V, short circuit currents of  $5.35 \pm 0.51$  mA cm<sup>-2</sup> and fill factors of  $33.9 \pm 1.9\%$ . Representatives among the top performing cells show  $J$ - $V$  characteristics of PCE: 1.72,  $V_{oc}$  0.74 V,  $J_{sc}$  6.40 mA cm<sup>-2</sup>, FF 36%.

The polymers employed in this study were designed to have no side chains on the donor moiety in order to increase the stability. Photodegradation investigations in air showed that the polymers 1 and 2, although still inferior to P3HT in stability, are good enough for processing in air, allowing for R2R processing. Outdoor stability tests of R2R processed solar cells encapsulated in a layer of polyurethane between a hardened glass plate and a polycarbonate plate furthermore showed good long-term stability for both polymers with respect to both voltage and current over a period of 4 months. This

report describes R2R processing of low-bandgap polymers and show good photostabilities and similar efficiencies compared to P3HT. The good stability of these compounds correlate well with previously reported results, showing the benefits of polyaromatic donors bearing no solubilizing chains, and that placement of the side chains on the acceptor unit in donor-acceptor based low-bandgap polymers might be a method to increase stability in polymer based solar cells without the loss in efficiency.

## Experimental Section

**Synthesis:** The syntheses of polymers 1 and 2 are described in the Supporting Information.

**Photodegradation Studies:** Samples for photochemical testing were prepared by applying the pure polymer from chlorobenzene solution on KBr plates by spin-coating. The ageing experiment was then performed by illuminating the samples under 1 sun and ambient air using a standard solar simulator from Steuernagel Lichttechnik (KHS

575, AM 1.5G, 1000 W m<sup>-2</sup>, 85 °C). They were removed periodically and UV–vis absorbances were recorded to monitor the degradation. UV–vis absorbance spectra were recorded between 200 and 1100 nm using a UV-1700 spectrometer from Shimadzu. To quantitatively compare all the materials, the total amount of absorbed photons ( $N_{\text{Tot}}^t$ ) was monitored versus ageing time over the range  $\lambda_1$ – $\lambda_2$  by summation over the polymer absorption peaks (see SI, Table S1). This value was calculated according to the following formula:

$$N_{\text{Tot}}^t = \sum_{\lambda_1}^{\lambda_2} N_0(\lambda) \times (1 - 10^{-A^t(\lambda)})$$

where  $A^t(\lambda)$  is the absorbance at a given wavelength  $\lambda$  and time  $t$ , and  $N_0(\lambda)$  is the incident photonic flux.  $A^t(\lambda)$  was directly extracted from the UV–vis absorbance spectra of the sample at the corresponding ageing time  $t$ . The ASTM G173 standard was used as a reference for the incident photonic flux.<sup>[12]</sup> At the end of the degradation, the quantity of absorbed photons systematically reached a constant value ( $N_{\text{Tot}}^\infty$ ), after which no absorbance evolution followed. This value was always above zero due to the absorption and scattering of the KBr substrate. Finally, the normalized number of photons absorbed by the polymer was calculated by

$$N_{\text{photons}}^t = \frac{N_{\text{Tot}}^t - N_{\text{Tot}}^\infty}{N_{\text{Tot}}^0 - N_{\text{Tot}}^\infty}$$

**Device Preparation:** The ZnO films were obtained by slot-die coating a solution of Zn(OAc)<sub>2</sub>·2H<sub>2</sub>O, Al(OH)(OAc)<sub>2</sub> and Zonyl FSO-100 in water as described previously.<sup>[13]</sup> The solution was filtered immediately before coating with a 0.45 micrometer filter. The film was coated directly onto prepatterned ITO on 175 micrometer thick PET with a coating speed was 2 m min<sup>-1</sup> and the film was dried at 140 °C. The final dry thickness of the ZnO film was 25 ± 5 nm. The active layer solution was prepared by dissolving the polymer material and the PCBM (99% from Solenne BV) in separate bottles, using chlorobenzene as solvent, with a concentration of 30 mg mL<sup>-1</sup>. The solutions were filtered immediately prior to use through a 0.45 micrometer filter. The active layer solutions were differentially pumped into the slot-die coating head.<sup>[10]</sup> The coating speed was 2 m min<sup>-1</sup> and the films were dried at 140 °C. The typical wet thickness was 10 micrometers and the dry thickness was around 250 nm (depending slightly on mixing ratio due to the density differences between the polymer and PCBM). The PEDOT:PSS solution was prepared by diluting commercially available AGFA EL-P-5010 with isopropanol to a viscosity of 270 mPa s (typically 1 kg of PEDOT:PSS and 0.5 kg of isopropanol). This ink was slot-die coated directly on top of the active layer that had been previously wetted with isopropanol to enable wetting. The wet thickness was 75 micrometers and the dry thickness 20 micrometers. The coating speed was 0.9 m min<sup>-1</sup> and the drying temperature was 140 °C. The silver back electrodes were screen printed on top of the PEDOT:PSS as a grid structure with a 20% area coverage at a speed of 1 m min<sup>-1</sup> using commercially available PV 410 silver paste from Dupont. The grid consisted of 11 mm long and 0.2 mm wide silver lines with a 0.8 mm gap between the lines. The screen was a 120 mesh screen and

the final dry thickness of the silver was 10 micrometers. The drying temperature was 140 °C.

**Device Testing:** The conditions of the characterization under simulated sunlight were KHS 575 using a solar simulator from Steuernagel Lichttechnik operating at 1000 Wm<sup>-2</sup>, AM1.5G. The spectrum of the solar simulator was checked using an optical spectrum analyzer made for measuring irradiance, and its intensity was calibrated bolometrically using a precision spectral pyranometer from Eppley Laboratories. During measurements, the incident light intensity was monitored continuously using a CM4 high-temperature pyranometer from Kipp & Zonen.

## Supporting Information

Supporting Information is available from the Wiley Online Library or from the author.

## Acknowledgements

This work was supported by the Danish Strategic Research Council (2104-07-0022)

Received: September 2, 2011

Revised: November 3, 2011

Published online: March 19, 2012

- [1] Konarka Technologies Inc., www.konarka.com, accessed January, 2012.
- [2] F. C. Krebs, *Sol. Energy Mater. Sol. Cells* **2009**, *93*, 394.
- [3] F. C. Krebs, T. D. Nielsen, J. Fyenbo, M. Wadstrøm, M. S. Pedersen, *Energy Env. Sci.* **2010**, *3*, 512.
- [4] F. C. Krebs, J. Fyenbo, M. Jørgensen, *J. Mater. Chem.* **2010**, *20*, 8994.
- [5] F. C. Krebs, T. Tromholt, M. Jørgensen, *Nanoscale* **2010**, *2*, 873.
- [6] M. Manceau, E. Bundgaard, J. E. Carle, O. Hagemann, M. Helgesen, R. Søndergaard, M. Jørgensen, F. C. Krebs, *J. Mater. Chem.* **2011**, *21*, 4132.
- [7] E. Bundgaard, O. Hagemann, M. Manceau, M. Jørgensen, F. C. Krebs, *Macromolecules* **2010**, *43*, 8115.
- [8] E. Bundgaard, O. Hagemann, M. Jørgensen, F. C. Krebs, *Green* **2011**, *1*, 55.
- [9] R. Søndergaard, F. C. Krebs, *Polymers* **2011**, *3*, 545.
- [10] J. Alstrup, M. Jørgensen, A. J. Medford, F. C. Krebs, *ACS Appl. Mater. Interfaces* **2010**, *2*, 2819.
- [11] M. Manceau, A. Rivaton, J. L. Gardette, S. Guillerez, N. Lemaitre, *Polym. Degrad. Stabil.* **2009**, *94*, 898.
- [12] NREL's AM1.5 Standard Dataset: <http://rredc.nrel.gov/solar/spectra/am1.5/<math>\tau\pi/>>, accessed September, 2010.
- [13] R. Søndergaard, M. Helgesen, M. Jørgensen, F. C. Krebs, *Adv. Energy Mater.* **2011**, *1*, 68.

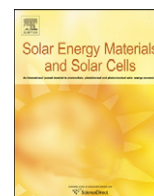




ELSEVIER

Contents lists available at [SciVerse ScienceDirect](http://www.sciencedirect.com)

# Solar Energy Materials & Solar Cells

journal homepage: [www.elsevier.com/locate/solmat](http://www.elsevier.com/locate/solmat)

## The use of polyurethane as encapsulating method for polymer solar cells—An inter laboratory study on outdoor stability in 8 countries

Roar R. Søndergaard<sup>a,\*</sup>, Theodoros Makris<sup>b</sup>, Panagiotis Lianos<sup>b</sup>, Assaf Manor<sup>c</sup>, Eugene A. Katz<sup>c,d</sup>, Wei Gong<sup>e,f</sup>, Sachetan M. Tuladhar<sup>e</sup>, Jenny Nelson<sup>e</sup>, Ralf Tuomi<sup>e</sup>, Paul Sommeling<sup>g</sup>, Sjoerd C. Veenstra<sup>g</sup>, Agnès Rivaton<sup>h,i</sup>, Aurélie Dupuis<sup>h,i</sup>, Gerardo Teran-Escobar<sup>j</sup>, Monica Lira-Cantu<sup>j</sup>, Subarna B. Sapkota<sup>k,l</sup>, Birger Zimmermann<sup>k</sup>, Uli Würfel<sup>k,l</sup>, Andreas Matzarakis<sup>m</sup>, Frederik C. Krebs<sup>a</sup>

<sup>a</sup> Department of Energy Conversion and Storage Technical University of Denmark, Frederiksborgvej 399, DK-4000 Roskilde, Denmark

<sup>b</sup> Engineering Science Department, University of Patras, 26500 Patras, Greece

<sup>c</sup> Department of Solar Energy and Environmental Physics, J. Blaustein Institutes for Desert Research, Ben-Gurion University of the Negev, Sede Boker Campus 84990, Israel

<sup>d</sup> Ilse Katz Institute for Nanoscale Science and Technology, Ben-Gurion University of the Negev, Beersheva 84105, Israel

<sup>e</sup> Department of Physics, Blakett Laboratory, Imperial College London, Prince Consort Road, London SW7 2AZ, UK

<sup>f</sup> Key Laboratory of Luminescence and Optical Information, Ministry of Education and Institute of Optoelectronic Technology, Beijing Jiaotong University, Beijing 100044, PR China

<sup>g</sup> Energy Research Centre of the Netherlands (ECN), P.O. Box 1, 1755 ZG Petten, The Netherlands

<sup>h</sup> Clermont Université, Université Blaise Pascal, LPMM, BP 10448, F-63000 Clermont-Ferrand, France

<sup>i</sup> CNRS, UMR 6505, LPMM, BP 80026, F-63171 Aubiere, France

<sup>j</sup> Centre d'Investigació en Nanociència i Nanotecnologia Laboratory of Nanostructured Materials for Photovoltaic Energy ETSE, Campus UAB, Edifici Q, 2nd Floor E-08193 Bellaterra (Barcelona), Spain

<sup>k</sup> Fraunhofer Institute for Solar Energy Systems ISE, Heidenhofstrasse 2, 79110 Freiburg, Germany

<sup>l</sup> Freiburg Materials Research Centre FMF, Stefan-Meier-Strasse 21, 79104 Freiburg, Germany

<sup>m</sup> Meteorological Institute, University of Freiburg, Germany

### ARTICLE INFO

#### Article history:

Received 2 September 2011

Received in revised form

18 December 2011

Accepted 20 December 2011

Available online 12 January 2012

#### Keywords:

Encapsulation

Polyurethane

Organic solar cells

Outdoor stability study

Round robin

Inter laboratory study (ILS)

### ABSTRACT

A new encapsulation method for organic solar cells has been tested on flexible solar modules and cells embedded in polyurethane, sandwiched between a tempered glass plate and a polycarbonate plate. Panels, each containing 10 organic solar modules/cells, were fabricated and installed for outdoor exposure in eight different countries for 4½ months. In order to minimize potential deviations in procedures and equipment, one person was responsible for the fabrication, installation and initial and final IV-measurements of the panels using the same equipment for all measurements and calibrations. The encapsulated modules/cells showed significantly reduced degradation compared with previous studies, with final average efficiencies around 40% of the original after 4½ months outdoor exposure. Photodegradation was furthermore found not to be the primary source of degradation.

© 2011 Elsevier B.V. All rights reserved.

## 1. Introduction

Organic solar cells have in recent years seen great progress in lifetimes, reaching a level in stabilities where stability studies can be carried out in the more unpredictable outdoor conditions compared to the carefully controlled laboratory environment [1–4]. This calls for the development and testing of new methods on how to encapsulate the solar cells as they are still not stable enough to be left unprotected towards oxygen and water, which can diffuse freely within the organic solar cells causing them to

degrade, if no measures are taken [5–7]. Katz et al. [2] performed an outdoor study in the Negev desert on organic solar cells on glass, sealed using glass fiber reinforced thermosetting epoxy (prepreg) by the procedure described by Krebs [8]. They found that the efficiency of P3HT/PCBM-cells dropped to approximately 10% after 32 day of outdoor exposure. An alternative approach was used by Hauch et al. [1], who used a transparent barrier film (WVTR rate of 0.03 g/(m<sup>2</sup> day) at 38 °C/100% rh) to encapsulate flexible P3HT:PCBM modules on PET. They experienced full retention and even a slight increase in efficiency after 14 months of outdoor rooftop exposure in Lowell, MA (USA), mainly due to an increase in the fill factor by 11%. Although an impressive result, changes clearly happens to the modules IV characteristics after exposing it to outdoor conditions, best illustrated by the final

\* Corresponding author. Tel.: +45 4677 4718; fax: +45 4677 4791.  
E-mail address: rosq@dtu.dk (R.R. Søndergaard).

improved fill factor and by fact that the authors show that the power density increases to approximately 140% of the initial value within a few days. Unfortunately no comparison was made of the final efficiency and the efficiency of the module after reaching maximum power density.

In a recent inter-laboratory study by Gevorgyan et al. [4], flexible modules of P3HT:PCBM on PET were encapsulated by a barrier film from Amcor Flexibles and studied at different outdoor locations. Average efficiencies of approximately 40% of original were observed after approximately 1000 h (~42 day) of outdoor exposure.

As a final example, Medford et al. prepared large panels of P3HT/PCBM flexible modules in series, testing different encapsulation methods for outside conditions. The one that showed the best preservation properties involved pre-lamination of the freshly prepared cells with a ~100 µm thick PET gas barrier layer from Amcor Flexibles with a ~50 µm pressure-sensitive acrylic adhesive, which were further laminated between a 4 mm tempered glass window and black Tetlar foil, using two sheets of 0.5 mm thick ethylene vinyl acetate (EVA), which was heated to 150 °C for 30 min causing the EVA to liquefy. The panel having an active area of 9180 cm<sup>2</sup> showed 54% of the original efficiency after 6 months outdoor exposure. Also Krebs [9] has performed 'hot lamination' in the encapsulation of indium–tin-oxide free cells using EVA, but no outdoor test was performed.

When testing an encapsulant, properties like moisture ingress from the edges, adhesion at the interfaces and diffusion temperature dependence might influence the outcome [10,11]. In order to fully test the properties of an encapsulation method it is thus desirable to perform the experiment at a multitude of locations that differs in whether condition (ambient temperature, fluctuations in ambient temperature, humidity, hours of sunlight, etc.). This can be done by round robins (RR) and inter-laboratory studies (ILS), which are important and useful methods to reach consensus of solar cells properties and establishing standard procedures for their characterization. Previously performed RR and ILS [4,12], where organic solar cells were shipped to different locations to be mounted and measured, have shown that potential problems are related to this approach. First of all different people approach an assignment in different ways, and involving many persons often results in deviations from proscribed procedures—as the old proverb goes, “too many cooks spoils the broth”. Just as important, different laboratories generally tend to have different types of equipment at their disposal, which makes it difficult to compare results afterwards. Ideally such studies should be performed by a single person to ensure that everything is done as similar as possible, using the same measuring equipment to rule out deviations.

We here present the use of polyurethane as encapsulation method in a study performed in 8 different countries, where one person has been responsible for the preparation and outdoor mounting of 8 panels, each containing 10 roll-to-roll processed polymer solar modules and solar cells encapsulated in polyurethane. The same person furthermore measured all cells after manufacturing of the panels at Risø DTU, at each test site before installing the panels, at each test site after a period of approximately 4½ months and finally again at Risø DTU after having taken down the panels and shipping them back. All measurements were done with the same equipment and the same reference for the measured light intensity was employed in all cases. In order to monitor the cells during the 4½ month period local personnel at each site performed continuous outdoor measurements of the short circuit current ( $I_{SC}$ ) and the open circuit voltage ( $V_{OC}$ ). The test site locations involved (shown in Fig. 1) were: Patras (by the Mediterranean Sea in Greece), Sede Boker (in the Negev desert of Israel), Barcelona (by the Mediterranean Sea



Fig. 1. Map showing the geographical locations of the mounted panels.

in Spain), Petten (by the North sea in the Netherlands) Clermont-Ferrand (inland in the mountainous Massif Central in France), London (inland in the southern United Kingdom), Freiburg (inland in south west of Germany) and, finally Risø DTU in Roskilde (by a fjord in Denmark). The locations were chosen for their different geographical locations and diverse local weather conditions that differ on parameters that could have an influence on the outdoor stability, such as amount of sunlight, ambient temperature, moisture and amount of salt in the air. All preparations of the panels as well as initial and final measurements were performed at Risø DTU.

## 2. Experimental procedures and methodology

### 2.1. Types of cells used

The polymer solar modules and cells used in the study consisted of four types of geometries (see Fig. 2) and four types of active material inks. All were prepared with an inverted geometry on indium tin oxide (ITO) patterned PET substrates (PET|ITO|ZnO|active layer|PEDOT|Ag) using roll-to-roll (R2R) slot die coating for all layers except for the silver, which was screen printed using UV-curable silver paste [13]. The detailed procedures of manufacture have previously been published [14,15].

Each panel contained ten modules/single cells. Module **1–3** were P3HT:PCBM modules consisting of 16 cells in series with an active area of 35.5 cm<sup>2</sup> differing only in the geometry of the silver back electrode used. For module **1** a simple busbar was used, just connecting the ITO of one cell with the PEDOT of the next to make the series connection, but leaving the main part of the PEDOT uncovered. In module **2** the connecting busbar was supplied with a silver grid, in order to facilitate charge collection, and finally in module **3** the silver fully covered the part of the PEDOT that was over the active area.

Module **4** had the same geometry as module **1** but was prepared using the commercial ink PV2000 from Plextronics. The cells **5–10** were all single cells with an active area of 4.2 cm<sup>2</sup> and a grid patterned silver back electrode. In cells **5–8** the polymer employed was polymer **A** (see Fig. 3) and in cell **9** and **10** polymer **B** was used (Additional information on polymer **A** and **B** can be found in the supporting information).

All modules were prepared during a workshop in relation with the ISOS3 conference held at Risø in October 2010. The single cells were prepared just before assembling the panels in November 2010.

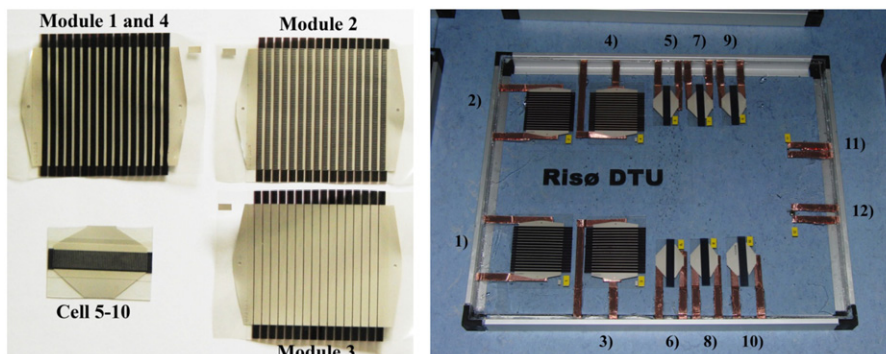


**Fig. 2.** Type of geometries used and their placement in the final panels: Modules (35.5 cm<sup>2</sup>) with just a simple busbar (module 1 and 4) connecting each cell in series in the module, a busbar with a grid (module 2), a full silver back electrode (module 3) and single cells (4.2 cm<sup>2</sup>) with a silver grid (cell 5–10).

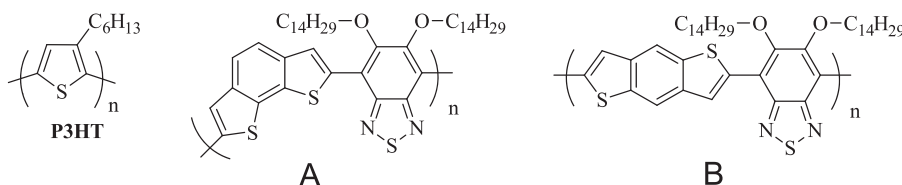


**Fig. 3.** Chemical structures of the known used polymers. Besides the commonly used P3HT, two polymers (A and B) were used. The polymers both contain an alkoxy-substituted benzothiadiazole acceptor unit and unsubstituted benzo[e]thiophene donor units, with the difference being the symmetry of the benzo[e]thiophenes. The chemical composition of the Plextronics ink is unknown.

From a total of 723 modules/cells the best of each type were selected for the preparation of nine panels each containing modules/cells 1–10 as well as two reference silicon photodiodes, cell 11 (BPW21 from Centronic, without UV filter) and cell 12 (BPW 34B from Osram, with UV-filter). Assuming a linear relation between light intensity and the corresponding current of cell 11 and 12 allows for their use as references for the light intensity.

## 2.2. Fabrication of the panels

The panels were fabricated in such a way that the final product consisted of the modules/cells embedded in polyurethane between a tempered glass front plate and a polycarbonate backside. The connection to the exterior from the embedded circuitries was made by use of copper tape. Fig. 4 illustrates the step wise procedure: (1) the cleaned tempered glass plate was covered with a layer of freshly prepared and degassed 50:50 mixture (mixed and subjected to reduced pressure, ~20 mbar, for 5 min) of a commercially available isocyanate compound and a polyol (Translux A 260 Polyol and Translux A 260 Isocyanate from Axon technologies), which upon standing transforms into the desired polyurethane. As can be seen from Fig. 4 the polyurethane is highly transparent (See the supporting information for transmission spectrum). The modules/cells 1–12 were placed in the viscous but still liquid mixture with the front side down making sure that no air was trapped underneath and that the electrodes were not covered. The isocyanate/polyol mixture was then left over night to fully polymerize to polyurethane. (2) The electrodes of each module/cell was then connected to the exterior of the panel edge by use of copper tape followed by covering the whole with another layer of 50:50 mixture of isocyanate and polyol upon which a polycarbonate plate was placed, again making sure that air was not trapped in the viscous liquid underneath the polycarbonate plate. Once more the panels were left over night to ensure full polymerization to polyurethane. (3) To every electrode was then attached the ‘male’ part of a simple snap button (used in clothes, allows for easy connection to the electrodes) before gluing the copper tape onto the polycarbonate plate with epoxy glue.

Finally an aluminum frame was mounted to give the finished panel. Of nine prepared panels eight were tested outside. In the fabrication process it should be stressed that fresh batches of the two components for the polyurethane must be used in order to get a good solid encapsulation. Fig. 5 shows an example where this was not the case, which resulted in delamination and development of bubbles within the incompletely polymerized polyurethane when the panel was exposed to higher temperatures during measurements.

## 2.3. Measuring the panels

Two types of measurements were performed in this study: (1) full *IV*-curves using a Keithley 2400 sourcemeter and a Kip & Zonen CM4 high temperature pyranometer for calibration/measurement of the light-intensity. (2) Simple measurement of the  $V_{OC}$  and the  $I_{SC}$  using an Alcron AC-9074 multimeter.

*IV*-measurements of each panel were performed

$t_0$ : at Risø DTU before shipping the panels to the location using a simulated sunlight.

$t_0'$ : at the location before mounting the panel, in order to ensure that nothing had happened during transportation. Depending on the available equipment and weather conditions this was performed indoor under simulated sunlight or/and outside under the real sun.

$t_x$ : at the location after approximately 4½ months of outdoor exposure. The measurement served to test if something had happened to the cells during shipment before the final measurement at Risø. Again depending on the available equipment and the weather these measurements were performed indoor under simulated light or outside under the real sun.

$t_x'$ : at Risø after receiving the panels from the location.

All *IV*-measurements were performed by the same person, and with the same measuring equipment.

$V_{OC}$  and  $I_{SC}$  measurements: during the 4½ month exposure time, measurements were performed directly on the mounted panels by an assigned researcher of the collaborative institutions



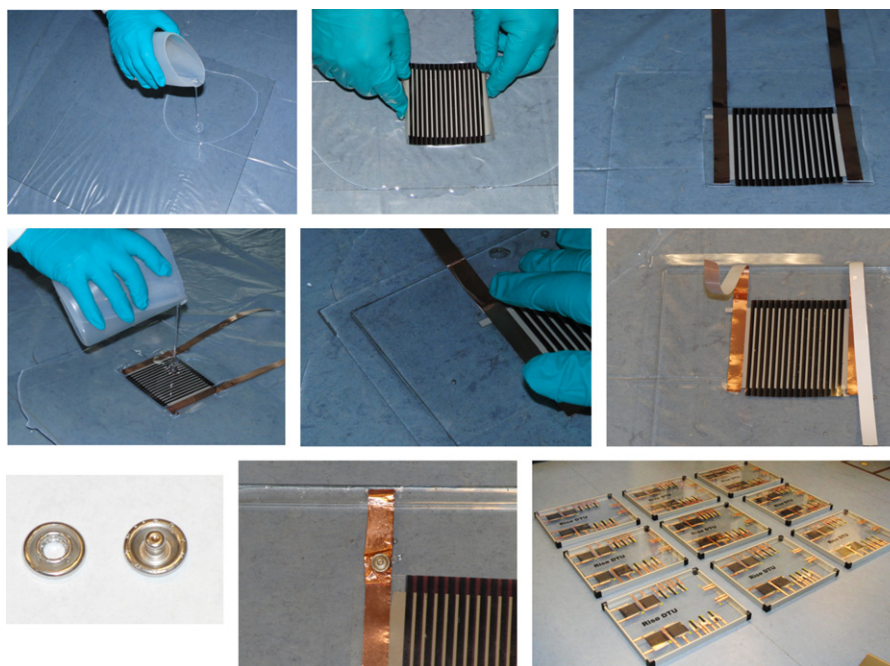


Fig. 4. Illustration of the different steps in the fabrication process of the panels.

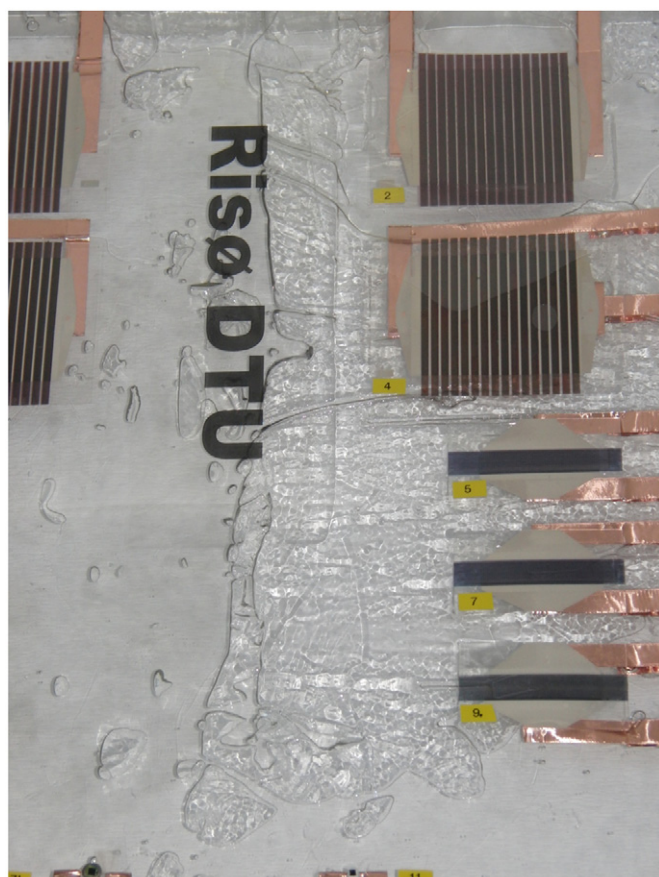


Fig. 5. Picture of a delaminated panel as a result of incomplete polymerization to polyurethane.

on each location. This was performed on days with constant light intensity, using identical multimeters, which were supplied by Risø DTU. By performing the measurements under constant light intensity, it is possible to use the build in silicon photodiodes **11**

and **12** as references for the light intensity, which allowed for a crude monitoring of the cell conditions during the whole study.

#### 2.4. Mounting the panels

When mounting the panels practical considerations, such as sufficiently solid support to attach the panel to and administrative permissions, had to be taken into account. This led to diversity in inclinations of the panels as well as the orientation. As a result of this the panels were mounted with inclination angles from 30° to 55° and facing compass directions of 130–210°. The panel at Risø was an exception as it was mounted on a solar tracker ensuring a perpendicular orientation towards the sun for maximum exposure.

### 3. Results and discussion

The panels were prepared and measured in November 2010 as described in the experimental section, and were subsequently sent by courier to the destinations. During the month of December 2010 and the beginning of January 2011 a representative from Risø DTU, then traveled between the destinations, measuring the panels again (*IV*-Curves) and mounting the panels in collaboration with staff from the local institutions. Following this was a period of approximately 4½ months where the panels were left outside at all times and where local staff measured the  $I_{SC}$  and the  $V_{OC}$  on days with stable light intensity. Finally, the same Risø DTU representative redid the whole trip, dismantling the panels and re-measuring them on site before they were sent back to Risø DTU. Because attention had to be taken towards having local personnel present at the different institutions, the traveling order of destinations was not the same on the two trips, which resulted in slight deviations in the exposure time at the different locations. An overview of exposure time and placement of the different panels is given in Table 1.

**Table 1**  
Overview of locations and outdoor placements of the individual panels.

Location	Panel elevation from horizontal	Compass direction the panel faced	Placement of the panel	Total days of outdoor exposure
Sede Boker, Israel	55°	180°	In the open attached to a pipe	144
Patras, Greece	45°	149°	In the open on a rooftop wall	150
Clermont-Ferrand, France	43°	180°	In the open on a rooftop on a preinstalled rack	140
Barcelona, Spain	47°	130°	On a railing on a building façade	138
Freiburg, Germany	48°	210°	On a scaffold mounted to a building façade	139
Petten, Holland	30°	170°	In the open on a rooftop on a preinstalled rack	105
London, UK	43°	172°	In the open onto a rail on a rooftop wall	128
Roskilde, Denmark			In the open on a solar tracker	135

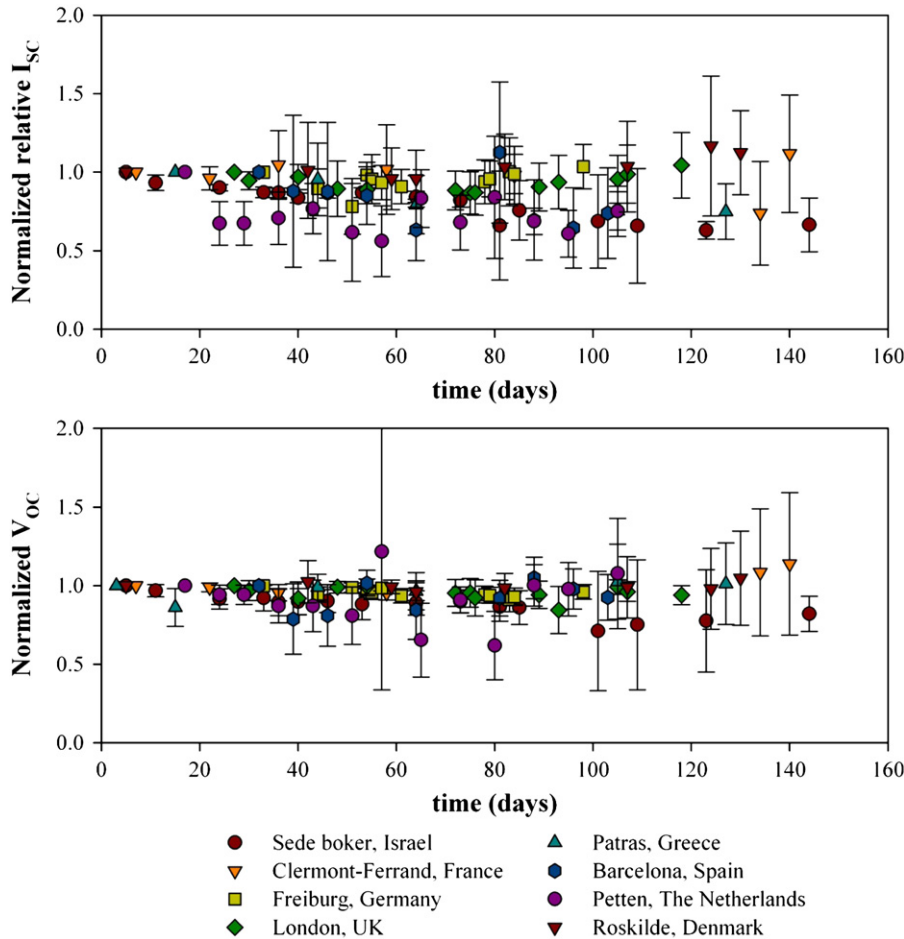


**Fig. 6.** Outdoor  $I_{SC}$  and  $V_{OC}$  measurements of the panels during the periods of outdoor exposure. **Top:** average normalized relative  $I_{SC}$  for the modules/cells 1–10 (relative to  $I_{SC}$  of the reference cell 11) for all panels. **Bottom:** average normalized  $V_{OC}$  for the modules/cells 1–10 for all panels.

### 3.1. Outdoor $V_{OC}$ and $I_{SC}$ measurements

The outdoor  $V_{OC}$  and  $I_{SC}$  measurements generally showed quite similar tendencies of slow decrease in  $I_{SC}$  while  $V_{OC}$  showed to be relatively stable, and no remarkable differences were found between the different architectures or different materials used. Fig. 6 shows the average normalized relative  $I_{SC}$  of the modules/cells 1–10 (relative to the current of cell 11 except for in London and Freiburg where the currents of cell 12 was used instead because of malfunctioning of cell 11) for each of the panels over time as well as the normalized voltage over time (Detailed illustrations of each type of cell in each panel can be found in the supporting information). It should be emphasized that the overall increase in ambient temperatures at all locations during

the study has not been taken into account, and that the results especially toward the end of the study probably would have showed lower currents if measured at the original temperatures.

Although the average trends are similar for all locations, the deviations seem to be larger on locations situated by the sea, and a number of the cells in these panels actually stopped working during the study (13% of the cell at seaside location compared to 5% of the cells at inland location). This appeared to originate from contacting problems both externally and internally in the panels. Especially in the Netherlands by the North sea, which has a higher salt concentration than the other ‘sea locations’, external corrosion of the copper electrodes appeared as illustrated in Fig. 7.

In all panels problems were encountered to some degree with the internal contact between the copper tape and the printed



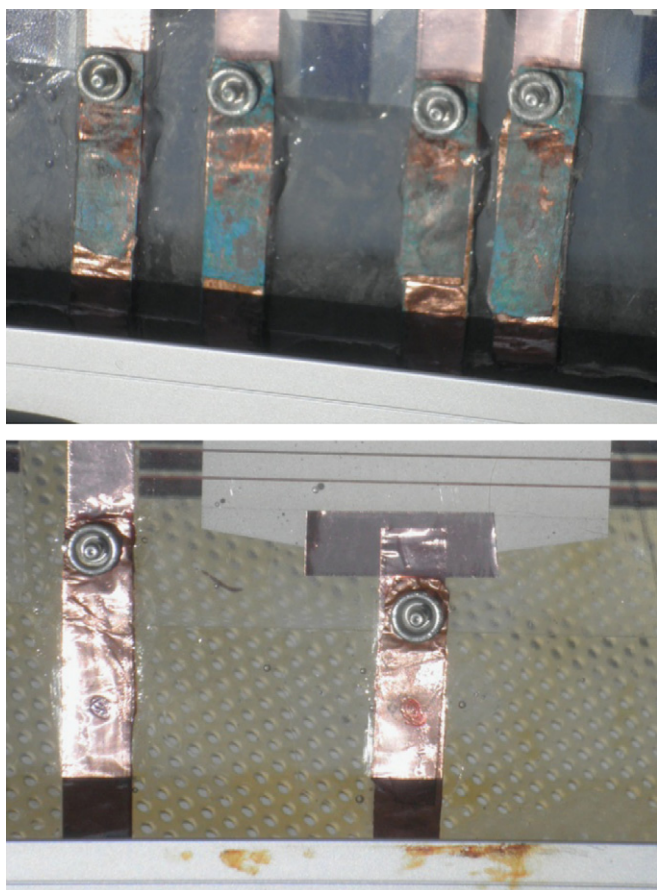


**Fig. 7.** Corrosion of the external part of the electrodes in Petten (the Netherlands) (**top**) compared to the non-corroded electrodes on the panel from Clermont-Ferrand (France) (**bottom**).

silver electrodes, which had a tendency to detach—probably caused by the temperature fluctuations, which are unavoidable in outdoor testing. This contact could in almost all cases be momentarily repaired though by appliance of pressure on the polycarbonate backside of the panel, allowing for measurements to be performed. Although it was thus possible to perform measurements, it is strongly recommended that alternative connection to the exterior is used in future projects.

### 3.2. Overall performance after outdoor exposure

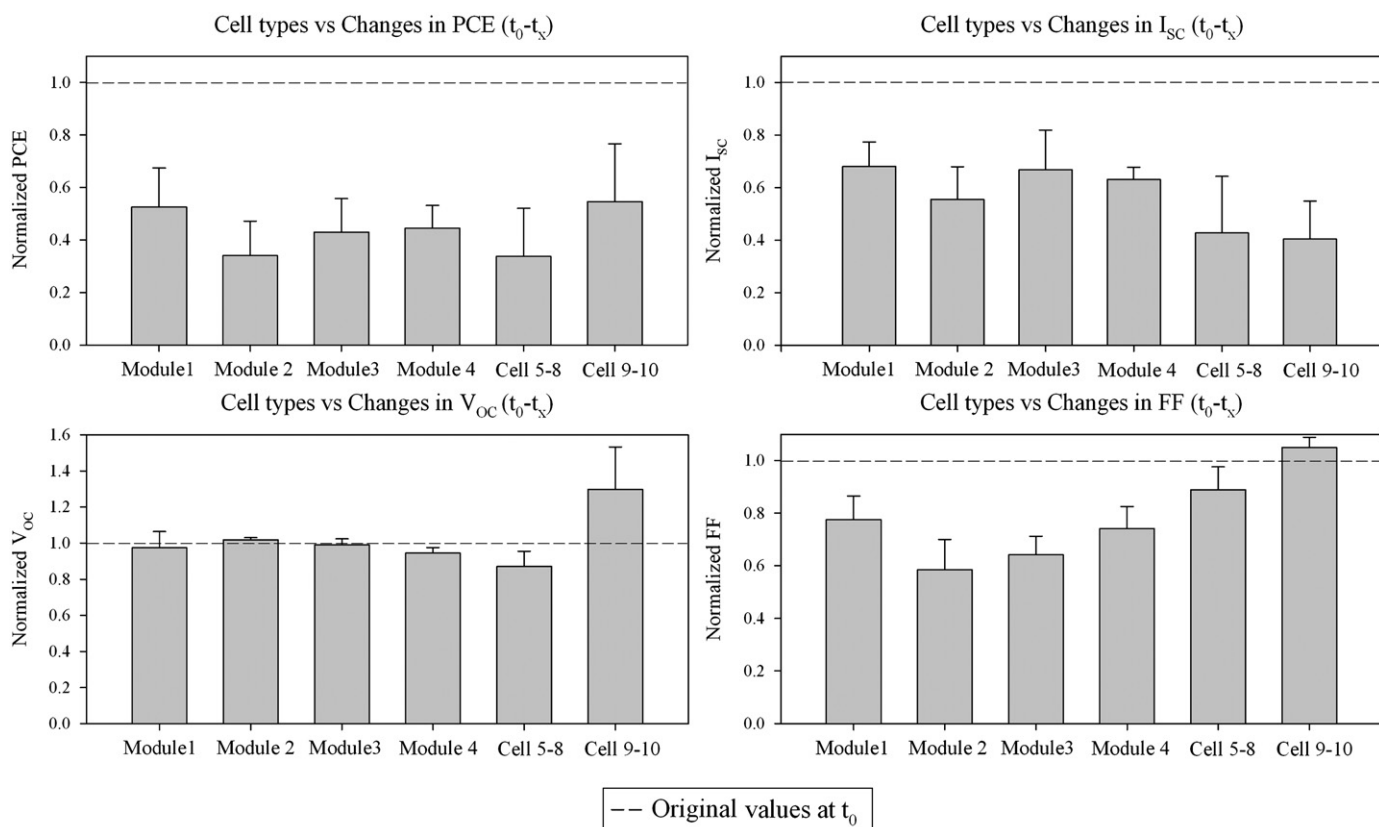
Comparison of  $IV$ -curves at  $t_0/t_0$  and  $t_x/t_x$  showed in no cases significant deviations indicating that no damage had happened to the panels during shipments between the destinations.

Fig. 8 shows the changes in  $IV$ -characteristics of the different types of cells used in the study ( $t_0-t_x$ , a more detailed version can be found in the supporting information). Table 2 furthermore shows the average values of the PCE for the different module and cell types before and after outdoor exposure.

For the P3HT modules 1–3, module 2 and module 3 shows the largest decreases in efficiency, primarily because of a larger drop in FF and for module 2 also in current. The FF for 2 and 3 were originally better ( $t_0$ ) than for module 1 and 4, but the relative gain in FF by appliance of grid or full silver structured back electrodes becomes less pronounced on a long-term basis.

The commercial polymer PV2000 used in module 4 showed to have similar stability as the P3HT module 1 having the same structure. Generally all modules show excellent preservation of the voltages and no extreme deviations are observed for the current.

For the single cells, the polymer B (9–10) is seemingly more stable than polymer A (5–8) but the difference is mainly due to an increase in voltage to a level higher than before outdoor exposure and must therefore be looked at with suspicion. The currents of



**Fig. 8.** Normalized  $IV$ -data at  $t_x$  (approximately 4½ months) showing the changes for the different types of cells used in the study.

the single cells are all reduced more than the modules, which is probably a sign of higher photodegradation of the active material.

Looking at the average IV-characteristic after outdoor exposure for the specific panels placed at the different locations, shown in Fig. 9 (Detailed presentations can be found in the supplementary

**Table 2**  
Overview of the average power conversion efficiencies before and after outdoor exposure.

	Average PCE at $t_0$ (% ( $\sigma$ ))	Average PCE at $t_x$
Module 1	1.25 (0.11)	0.65 (0.15)
Module 2	2.01 (0.22)	0.67 (0.22)
Module 3	2.14 (0.14)	0.91 (0.26)
Module 4	0.66 (0.12)	0.30 (0.10)
Cell 5–8	0.75 (0.24)	0.22 (0.1)
Cell 9+10	0.07 (0.03)	0.03 (0.01)

information), all panels have roughly experienced the same drop in efficiencies, when taking the exposure time into consideration. Although the most southern and more sunny locations seems to be slightly lower than the northern ones, the tendency is not pronounced, which indicates that other factors than photodegradation must play an important role in the degradation of the cells. This is further illustrated in Fig. 10 where the average PCE after outdoor exposure is plotted against the light energy dose received during the period of outdoor exposure (Corrections for angular mismatches are described in the supporting information). Comparing the panel mounted in the often cloudy and rainy London (128 day of outdoor exposure corresponding to an energy dose of approximately 350 kWh/m<sup>2</sup>, average PCE at  $t_x$  around 42% of original) and the panel mounted in the almost always sunny Negev desert (Sede Boker, 144 day of outdoor exposure corresponding to an energy dose of approximately 700 kWh/m<sup>2</sup>, average PCE at  $t_x$  around 35% of original), both encircled in red,

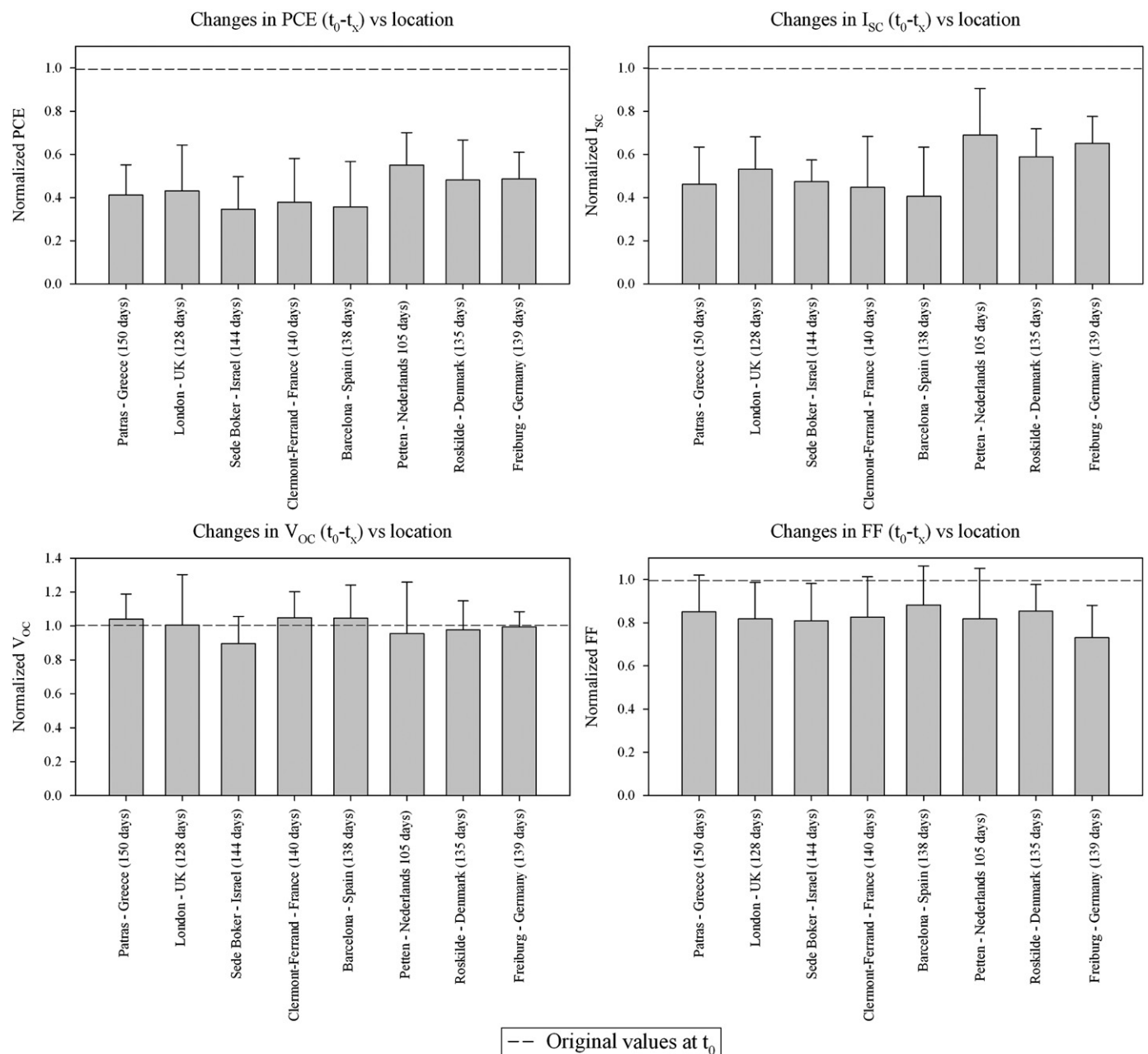


**Fig. 9.** Normalized IV-data at  $t_x$  showing the changes at the different locations used in the study. The outdoor exposure time in days is noted in parenthesis.

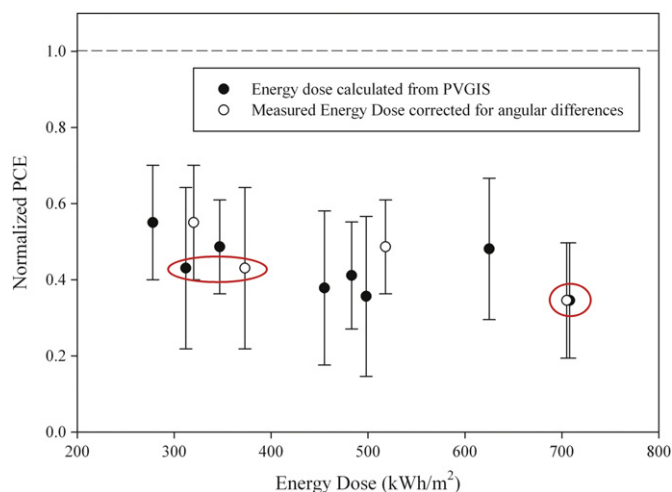


**Fig. 10.** Normalized PCE plotted against the light energy dose received during the outdoor experiment. Full dots: calculated using PVGIS estimates on the average daily solar irradiance for the given panel inclinations and compass directions [16]. Open dots: calculated on the basis of ground measurements during the exposure period. Data encircled are from London (left) and Sede Boker (right).

it is clear that photodegradation cannot be the major degradation mechanism. Had this been the case, the difference would be expected to be much more pronounced.

To evaluate the usefulness of polyurethane as encapsulation method of organic solar cells, comparison can be made with the previously mentioned results by Gevorgyan et al. [4], where P3HT modules similar to module 3 were tested outside after encapsulation with barrier foil on both back and front. Where the average PCE using barrier foil was reduced to approximately 40% after 1000 h (~42 day) of outdoor exposure, the embedding of the cells in polyurethane has prolonged this period to 4½ months, which must be considered a significant improvement.

### 3.3. Evaluation of the panel design

Besides the already mentioned contact problem (Section 3.1), between the silver electrodes of the polyurethane embedded modules/cells and the copper tape leading to the exterior, a major problem in the design was delamination at the polyurethane/glass interface caused by the different expansion coefficients of the materials when exposed to temperature fluctuations. The design originally consisted in using polycarbonate on both front and back side of the panels but due to the UV cutoff by polycarbonate this idea had to be discarded as the zinc oxide layer needs photo-doping with UV light in order to maintain good conductivity [17]. The choice of using a tempered glass plate as the front of the panel solved this problem, but the use of three different materials (glass, polyurethane and polycarbonate) caused the mentioned problems of delamination. Probably the use of two glass plates can solve the problem, but for future use of polyurethane as encapsulation, more tests needs to be performed beforehand in order to avoid this.

## 4. Conclusion

The use of polyurethane as encapsulation method for organic solar cells has been tested. A total of nine panels each containing 10 polymer solar modules/cells were fabricated using polyurethane as encapsulation sandwiched between a tempered glass plate and polycarbonate plate. Four different cell geometries and four different active materials were used in the study. Eight of the

panels were installed outside at locations in eight different countries chosen for their diversity in weather conditions in order to fully test the usefulness of the encapsulation method. In order to limit deviations caused by human factors and equipment a single person was responsible for the preparation, measurement (before and after outdoor expose), and installation of the panels at the test locations, using the same equipment for all measurements and calibrations. As a further monitoring local researchers measured  $I_{SC}$  and  $V_{OC}$  on days with stable light intensity allowing following the development of the cells during the experiment by comparison with two reference silicon photodiodes also mounted on the panel. These measurements showed a general trend of slow decrease in the current while the voltage remained more or less constant.

Examination of the *IV*-characteristic of P3HT modules with different silver back electrodes before and after outdoor exposure, showed that although an initial improvement of the fill factor can be obtained using a grid structure or a full covering of the active area compared to a simple busbar, this improvement becomes much less pronounced after outdoor exposure. In the comparison of the overall performances of the panels, it was found that although slightly lower final efficiencies were found for the panels, which had been exposed at the most southern (more sunny) locations, photodegradation showed not to be the major source of degradation of the cells.

Compared to previously published results the use of polyurethane as encapsulation method has proven to significantly reduce the degradation and average efficiencies around 40% of the original was observed after 4½ months outdoor exposure.

## Acknowledgments

Special thanks to Heinz Pakalski and Dennis Aarø from Gaia Solar A/S for supplying the tempered glass and aluminum frames. This work was supported by:

- The Danish Strategic Research Council (DSF 2104-07-0022) and EUDP (64009-0050 and 64011-0002).
- The European Commission as part of the Framework 7 ICT 2009 collaborative project HIFLEX (Grant agreement no. 248678), the Dutch Polymer Institute (DPI Project no. 678) and by Agentschap NL within the project OZOFAB (grant no. EOSLT1002).
- AM and EAK a financial support from the European Commission's Seventh Framework Program (FP7/2007-2013) under Grant Agreement no. 261936.
- The UK Big Lottery Fund/OPAL project for the London pyromometer data.

## Appendix A. Supporting information

Supplementary data associated with this article can be found in the online version at doi:10.1016/j.solmat.2011.12.013.

## Reference

- [1] J.A. Hauch, P. Schilinsky, S.A. Choulis, R. Childers, M. Biele, C.J. Brabec, Flexible organic P3HT:PCBM bulk-heterojunction modules with more than 1 year outdoor lifetime, *Solar Energy Materials and Solar Cells* 92 (2008) 727–731.
- [2] E.A. Katz, S. Gevorgyan, M.S. Orynbayev, F.C. Krebs, Out-door testing and long-term stability of plastic solar cells, *European Physical Journal—Applied Physics* 36 (2006) 307–311.

- [3] A.J. Medford, M.R. Lilliedal, M. Jørgensen, D. Aaro, H. Pakalski, J. Fyenbo, F.C. Krebs, Grid-connected polymer solar panels: initial considerations of cost, lifetime, and practicality, *Optics Express* 18 (2010) A272–A285.
- [4] S.A. Gevorgyan, A.J. Medford, E. Bundgaard, S.B. Sapkota, H.F. Schleiermacher, B. Zimmermann, U. Wurfel, A. Chafiq, M. Lira-Cantu, T. Swonke, M. Wagner, C.J. Brabec, O.O. Haillant, E. Voroshazi, T. Aernouts, R. Steim, J.A. Hauch, A. Elschner, M. Pannone, M. Xiao, A. Langzettel, D. Laird, M.T. Lloyd, T. Rath, E. Maier, G. Trimmel, M. Hermenau, T. Menke, K. Leo, R. Rosch, M. Seeland, H. Hoppe, T.J. Nagle, K.B. Burke, C.J. Fell, D. Vak, T.B. Singh, S.E. Watkins, Y. Galagan, A. Manor, E.A. Katz, T. Kim, K. Kim, P.M. Sommeling, W.J.H. Verhees, S.C. Veenstra, M. Riede, M.G. Christoforo, T. Currier, V. Shrotriya, G. Schwartz, F.C. Krebs, An inter-laboratory stability study of roll-to-roll coated flexible polymer solar modules, *Solar Energy Materials and Solar Cells* 95 (2011) 1398–1416.
- [5] F.C. Krebs, K. Norrman, Analysis of the failure mechanism for a stable organic photovoltaic during 10,000 h of testing, *Progress in Photovoltaics* 15 (2007) 697–712.
- [6] M. Lira-Cantu, K. Norrman, J.W. Andreasen, F.C. Krebs, Oxygen release and exchange in niobium oxide MEHPPV hybrid solar cells, *Chemistry of Materials* 18 (2006) 5684–5690.
- [7] M. Jørgensen, K. Norrman, F.C. Krebs, Stability/degradation of polymer solar cells, *Solar Energy Materials and Solar Cells* 92 (2008) 686–714.
- [8] F.C. Krebs, Encapsulation of polymer photovoltaic prototypes, *Solar Energy Materials and Solar Cells* 90 (2006) 3633–3643.
- [9] F.C. Krebs, Roll-to-roll fabrication of monolithic large-area polymer solar cells free from indium–tin-oxide, *Solar Energy Materials and Solar Cells* 93 (2009) 1636–1641.
- [10] G.J. Jørgensen, K.M. Terwilliger, J.A. DelCueto, S.H. Glick, M.D. Kempe, J.W. Pankow, F.J. Pern, T.J. McMahon, Moisture transport, adhesion, and corrosion protection of PV module packaging materials, *Solar Energy Materials and Solar Cells* 90 (2006) 2739–2775.
- [11] M.D. Kempe, Modeling of rates of moisture ingress into photovoltaic modules, *Solar Energy Materials and Solar Cells* 90 (2006) 2720–2738.
- [12] F.C. Krebs, S.A. Gevorgyan, B. Gholamkhash, S. Holdcroft, C. Schlenker, M.E. Thompson, B.C. Thompson, D. Olson, D.S. Ginley, S.E. Shaheen, H.N. Alshareef, J.W. Murphy, W.J. Youngblood, N.C. Heston, J.R. Reynolds, S.J. Jia, D. Laird, S.M. Tuladhar, J.G.A. Dane, P. Atienzar, J. Nelson, J.M. Kroon, M.M. Wienk, R.A.J. Janssen, K. Tvingstedt, F.L. Zhang, M. Andersson, O. Inganas, M. Lira-Cantu, R. de Bettignies, S. Guillerez, T. Aernouts, D. Cheyns, L. Lutsen, B. Zimmermann, U. Wurfel, M. Niggemann, H.F. Schleiermacher, P. Liska, M. Gratzel, P. Lianos, E.A. Katz, W. Lohwasser, B. Jannon, A round robin study of flexible large-area roll-to-roll processed polymer solar cell modules, *Solar Energy Materials and Solar Cells* 93 (2009) 1968–1977.
- [13] F.C. Krebs, T. Tromholt, M. Jørgensen, Upscaling of polymer solar cell fabrication using full roll-to-roll processing, *Nanoscale* 2 (2010) 873–886.
- [14] F.C. Krebs, J. Fyenbo, M. Jørgensen, Product integration of compact roll-to-roll processed polymer solar cell modules: methods and manufacture using flexographic printing, slot-die coating and rotary screen printing, *Journal of Materials Chemistry* 20 (2010) 8994–9001.
- [15] J. Alstrup, M. Jørgensen, A.J. Medford, F.C. Krebs, Ultra fast and parsimonious materials screening for polymer solar cells using differentially pumped slot-die coating, *ACS Applied Materials and Interfaces* 2 (2010) 2819–2827.
- [16] European Commission, <<http://re.jrc.ec.europa.eu/pvgis/apps4/pvest.php>>.
- [17] M.R. Lilliedal, A.J. Medford, M.V. Madsen, K. Norrman, F.C. Krebs, The effect of post-processing treatments on inflection points in current-voltage curves of roll-to-roll processed polymer photovoltaics, *Solar Energy Materials and Solar Cells* 94 (2010) 2018–2031.

# Low-Temperature Side-Chain Cleavage and Decarboxylation of Polythiophene Esters by Acid Catalysis

Roar R. Søndergaard, Kion Norrman, Frederik C. Krebs

Risø National Laboratory for Sustainable Energy, Technical University of Denmark, Frederiksborgvej 399, DK-4000 Roskilde, Denmark

Correspondence to: R. R. Søndergaard (E-mail: rosq@risoe.dtu.dk)

Received 23 September 2011; accepted 29 November 2011; published online 22 December 2011

DOI: 10.1002/pola.25870

**ABSTRACT:** Solubility switching of polymers is very useful in thin layer processing of conjugated polymers, as it allows for multilayer processing and increases the stability of the polymer. Acid catalyzed thermocleavage of ester groups from thiophene polymers carrying primary, secondary, and tertiary substituents have been examined by TGA-MS using different sulphonic acids. A substantial lowering of the cleavage temperature is observed, and the ester cleavage can even be performed *in situ*

on roll-to-roll-coated films on polyethylene terephthalate (PET). © 2011 Wiley Periodicals, Inc. *J Polym Sci Part A: Polym Chem* 50: 1127–1132, 2012

**KEYWORDS:** acid catalysis; conducting polymers; catalysis; decarboxylation; ester cleavage; low temperature; polythiophene ester; primary ester; secondary ester; solubility switching; tertiary ester; thermocleavage; thermogravimetric analysis (TGA)

**INTRODUCTION** One of the major challenges, within the field of polymer solar cells, has been found to be a stabilization of the active layer of the cells. Although great progress have been made with respect to boosting efficiencies for small-scale devices, which have now surpassed 9%,<sup>1</sup> a lot of work is still needed toward improving the stability of such devices as they generally have very short lifetimes. One path that in recent years has proved to be a reliable method of introducing a higher photochemical stability to the active layer is the use of thermocleavable materials.<sup>2–17</sup> Side chains are essential with respect to solubilizing the polymer thus allowing for solution processing of the active layer, but they also make the layer soft and allow for diffusion of oxygen and water to occur easily. By using thermocleavable side chains, it is possible to remove the side chains by subsequent heating after processing of the active layer. The film then becomes insoluble, much harder, and less susceptible to the reactions that lead to photo degradation. As exemplified for the polymer **1** in Scheme 1, cleavage of a tertiary ester can proceed in two steps, depending on the temperatures applied, if the ester is attached to a thiophene ring. First, the tertiary ester side chains are cleaved to the corresponding carboxylic acid (~200 °C) and further reaction by decarboxylation can be achieved by raising the temperature (~300 °C). The key problem in the process is that quite high temperatures are needed to perform the thermocleavages, and the reactions thus have to be performed on substrates that can sustain such temperatures and is in reality limited to glass.

In order for this procedure to be of any real interest for large-scale production, thermocleavage must be performed on cheap flexible substrates such as PET. This limits the temperatures to around 140 °C to avoid deformation of the substrate, and changes in the reaction conditions are, therefore, required.

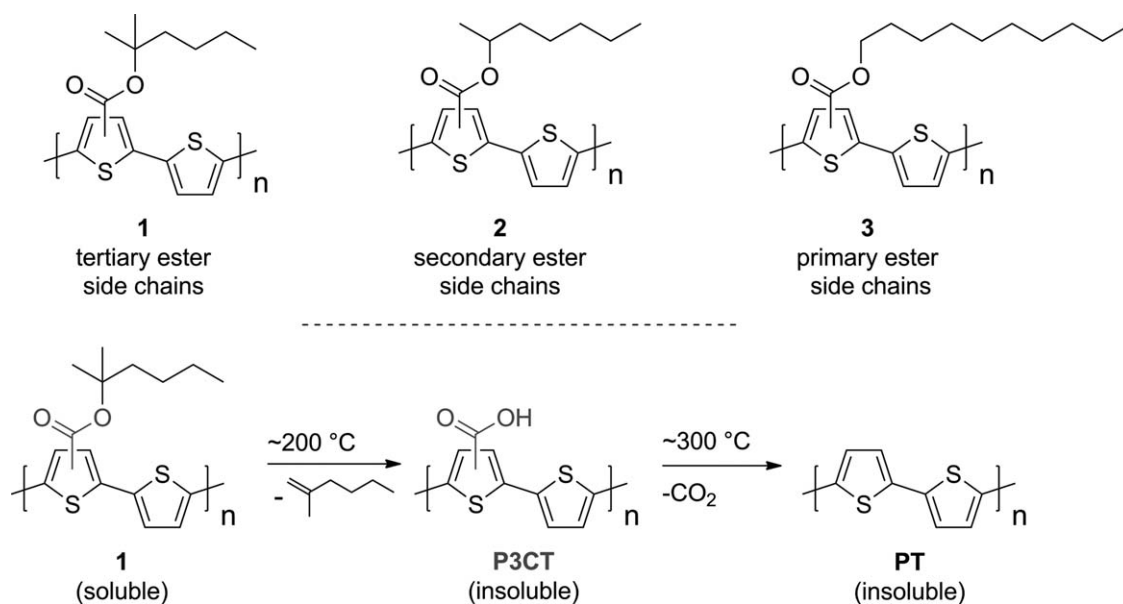
The most critical of the involved reactions is the decarboxylation step as it requires the highest temperatures. It has long been known that the analogous reaction of decarboxylation of pyrrole carboxylic acids to pyrroles can be performed by simple heating,<sup>18</sup> and it has been shown for pyrrole-2-carboxylic acid to proceed via *ipso*-displacement of CO<sub>2</sub> by hydrogen.<sup>19</sup> Because of the many similarities between pyrrole and thiophene, it is reasonable to expect that the mechanism is the same for thiophene acids and that the reaction would be catalyzed by strong acids. As it is common knowledge that ester cleavage is catalyzed by acids, the use of such opens for the potential simultaneous catalysis of the involved reactions.

We here present a series of TGA-MS experiments that show that it is possible to considerably lower the temperature of both thermocleavage reactions for thiophene polymers carrying tertiary, secondary, or primary ester side chains (polymer **1–3**, Scheme 1), by addition of different sulphonic acids in catalytic amounts. We furthermore present XPS-results that show that *in situ* cleavage of polymer **1** to P3CT is possible while processing using roll-to roll (R2R) coating on PET.

Additional Supporting Information may be found in the online version of this article.

© 2011 Wiley Periodicals, Inc.





**SCHEME 1** Top: Chemical structures of the polymers **1–3** carrying tertiary, secondary, and primary ester side chains, respectively. Bottom: Schematic illustration of the thermocleavage of the polymer **1** which carries a tertiary ester group attached to thiophene. Cleavage can proceed in consecutive steps with increasing temperature leading to either carboxysubstituted polythiophene (P3CT) or polythiophene (PT), both of which are insoluble.

## RESULTS AND DISCUSSION

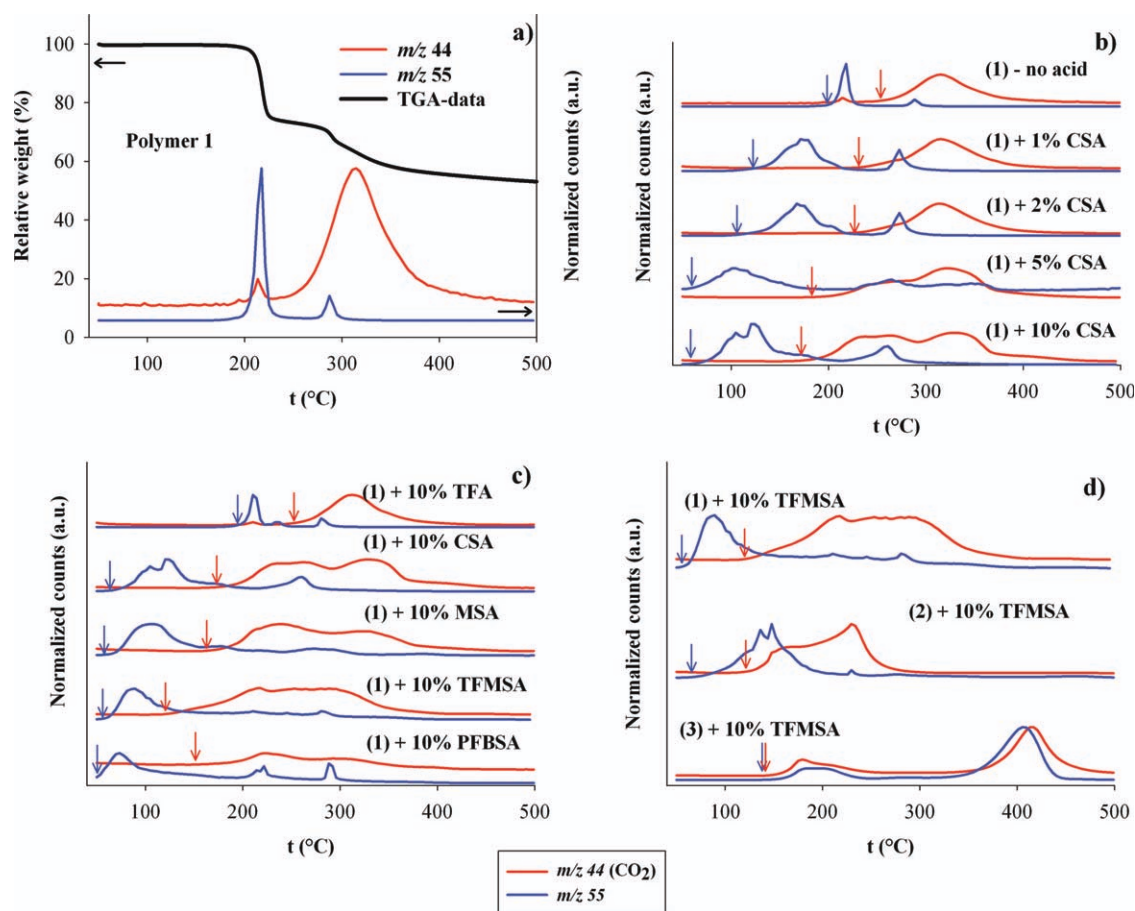
TGA-MS experiments were performed by mixing two solutions of the polymer and the acid in different ratio followed by evaporation of the solvent in air. All experiments started at 50 °C with an increase in temperature by 10 °C/min while monitoring specific masses with the MS-unit. As the added acids all evaporate to some extent during the experiment, TGA data are only reliable for the pure polymer **1**, which is shown in Figure 1(a) along with MS-data of a single representative mass ( $m/z$  55, C<sub>4</sub>H<sub>7</sub><sup>+</sup>) for the thermocleavage of the ester moiety (full representation of a range of masses can be found for all MS-experiments in the Supporting Information) and the mass of CO<sub>2</sub> ( $m/z$  44) for the monitoring of the decarboxylation process. The data show a good correlation between the observed losses in weight caused by the thermocleavage and the simultaneous raise of characteristic peaks in the MS-experiment. This shows that although the TGA-data cannot be used as a clear marker for the thermocleavage reaction when acid has been added, it is possible to monitor the characteristic mass fragmentations in the MS-experiment as shown in Figure 1(b–d) and in this way observe the acid catalyzed cleavage temperatures. The reactions were found to be very dependent on both the acid strength and the catalytic amount of acid added (the noted percentage of added acid is the relative mol % compared to the theoretical presence of ester bonds in the polymer used).

Figure 1(b) clearly shows that especially the cleavage of the ester group is easily catalyzed by even small amounts of camphor sulphonic acid, whereas the decarboxylation requires larger amounts to effectively catalyze the reaction. The importance of the acid strength is furthermore illus-

trated in Figure 1(c), where a lowering of the cleavage temperatures for both ester and acid is observed with increasing acid strength. Where trifluoroacetic acid hardly has any effect at all, CO<sub>2</sub>-evolution has an onset at temperatures as low as 110–120 °C for the much stronger acid trifluoromethanesulphonic acid (TFMSA).

Overall, an increase in the  $m/z$  55 is observed at around the same temperature where CO<sub>2</sub>-evolution starts. This is ascribed to the fact that the hardening of the polymer bulk is expected to lower the permeability towards gasses, and it is thus reasonable to assume that not all the side chains “escape” the bulk after the initial side-chain cleavage. When CO<sub>2</sub> evolution starts, CO<sub>2</sub> acts like a carrier gas and pulls some of the remaining side chains to the surface. Such retention of gasses would also explain why CO<sub>2</sub> in several cases is liberated over a rather large temperature span.

The TGA-MS experiment was furthermore performed on polymers carrying secondary (**2**) and primary (**3**) ester side chains. Also, in these cases the ester cleavage representative  $m/z$  55 (C<sub>4</sub>H<sub>7</sub><sup>+</sup>) was chosen for the illustration, as it was found to be among the most intense in the mass spectra. When comparing the thermocleavage temperatures of polymers **1–3** shown in Figure 1(d), the shift from a tertiary ester to a secondary raises the cleavage temperature of the side chain slightly (65–120 °C), but the decarboxylation reaction remains the same as expected. When going to a primary ester, the cleavage of the side chain happens at higher temperature (140–170 °C) than where decarboxylation of the free acid would commence and hence the CO<sub>2</sub>-evolution is observed immediately after (or simultaneously with) the signal from the side chain.



**FIGURE 1** TGA and MS data for acid catalyzed cleavage of thiophene polymers 1–3. The mass  $m/z$  55 is representative for the cleavage of the ester bond during formation of P3CT, and the mass  $m/z$  44 shows the evolution of CO<sub>2</sub> from the decarboxylation of P3CT to PT. The onset-temperatures for both reactions are in each case marked with arrows. (a) TGA and characteristic fragmentation ions of Polymer 1 without addition of acid. (b) Polymer 1 with different amounts of catalytic CSA. (c) Polymer 1 with addition of 10 mol % of different strong acids. (d) Polymers 1–3 carrying tertiary, secondary, and primary side chains (respectfully) with 10 mol % TFMSA. CSA, camphor sulphonic acid; TFA, trifluoroacetic acid; MSA, methanesulphonic acid; TFMSA, trifluoromethanesulphonic acid; PFBSA, perfluorobutanesulphonic acid.

On the basis of the obtained results, we suggest that the decarboxylation of 3-thiophene carboxylic acids proceeds via a similar mechanism as suggested for pyrrole-2-carboxylic acid. The fact that stronger acids leads to lower CO<sub>2</sub>-cleavage temperature, indicates that the decarboxylation mechanism without catalysis proceeds via *ipso*-substitution of the carboxylic acid as illustrated in Figure 2. The presence of strong acid can catalyze this process either by direct protonation of the thiophene ring or by stabilization of the intermediate, thus lowering the reaction barrier.

To observe whether thermocleavage of polymers can be performed on cheap flexible substrates such as PET, a R2R-experiment was performed using the two strongest acids TFMSA (0%, 1%, 5%, and 10%) and perfluorobutanesulphonic acid (PFBSA; 0%, 1%, 3%, and 5%). These acids have two advantages besides being strong. First of all, they are relatively volatile compounds, and it should thus be possible to remove them from the thin films relevant to devices which

are generally only around 100 nm thick which facilitates the exchange with the surroundings (in the bulk polymer we would expect it to be difficult to completely remove them). Second, they are easily quantifiable by XPS. As the presence of a high concentration of acid within the active layer of a solar cell could be a potential source of problems, it would be desirable to have a measure of how much acid can be removed. Solutions for processing were prepared by mixing stock solutions of polymer and acids immediately before processing by knife coating<sup>13</sup> directly onto PET. Generally, the films prepared using TFMSA showed to have small grains of precipitate in them, which is probably the result of commencing cleavage of the side chains, and at 10% TFMSA precipitation occurred to such a degree that uniform films could not be prepared. When using PFBSA, all films had an even quality without any precipitation. After roll-to-roll coating, the PET-foil was led through an oven at 140 °C for 5 min (0.2 m min<sup>-1</sup> with an oven length of 1 m), and the resulting films were subsequently analyzed by XPS. Each experiment

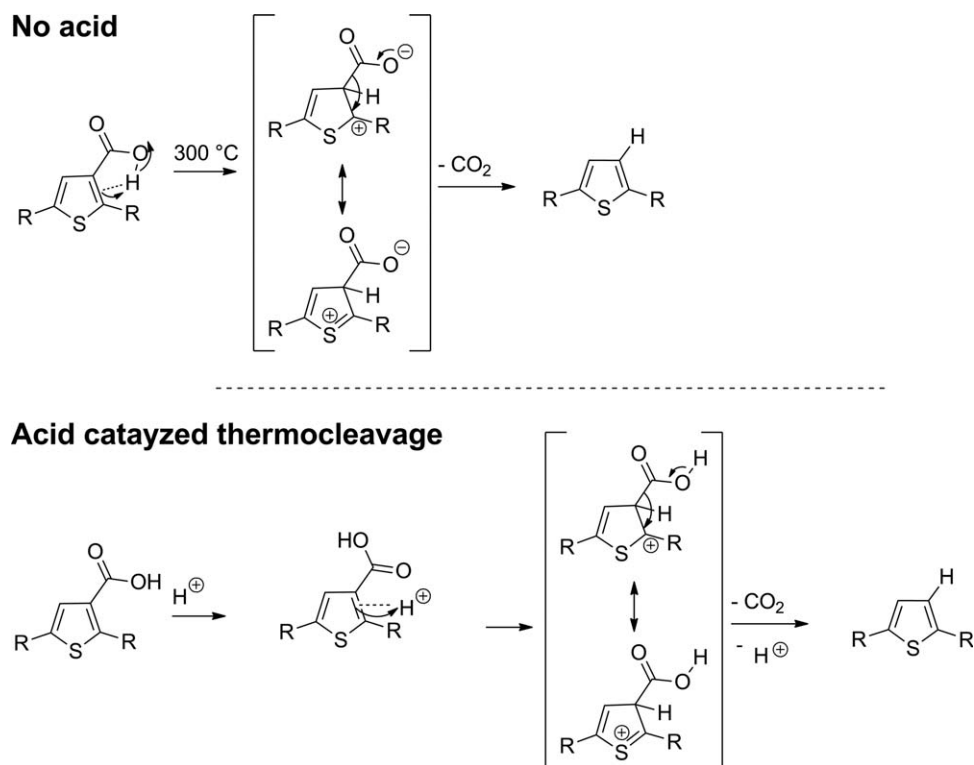


**FIGURE 2** Suggested mechanisms for the decarboxylation reaction with and without acid catalysis.

was performed twice giving a total of 16 films. Representative results are shown in Figure 3 (Collective results are given in the Supporting Information). The experiments showed that it is possible to reach an insoluble state by thermocleavage of the tertiary ester at 140 °C on PET (5 min) with usage of down to 5 mol % acid, but it also showed that under the given conditions the cleavage stops at the carboxylic acid state. This is in stark contrast to earlier work where a residence temperature of 4 h at 140 °C was required to achieve only partial thermocleavage<sup>12,13</sup> or where light induced heating to very high temperatures on heat stable substrates was used at similar web speeds.<sup>20</sup> Unfortunately, the XPS-data (see SI) also indicate that less than half of the added fluorinated acids were removed in the drying/heating process.

## EXPERIMENTAL

### Synthesis

The synthesis of polymer **1** has previously been described<sup>8</sup> using the procedure published by Liu et al.<sup>9</sup> Polymer **2** and **3** was synthesized as shown in Scheme 2.

### Heptan-2-yl 2,5-dibromothiophene-3-carboxylate (**4**)

2,5-Dibromothiophene-3-carboxylic acid (3.0 g, 10.5 mmol), DMAP (0.130 g, 1.06 mmol), and heptan-2-ol (1.644 mL, 11.6 mmol) in DCM (10 mL) were cooled to 0 °C on an ice bath. DCC (2.38 g, 11.5 mmol) was hereafter added in small portions over 5 min, left stirring while cooling for an additional 10 min and then left stirring at RT for an additional 2½ h. The mixture was filtrated, and the solid was washed thoroughly with DCM. The filtrate was then washed with

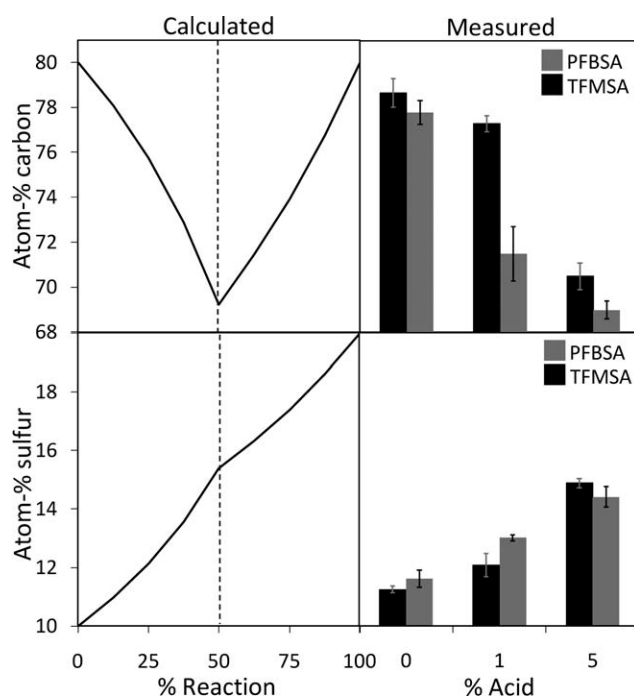
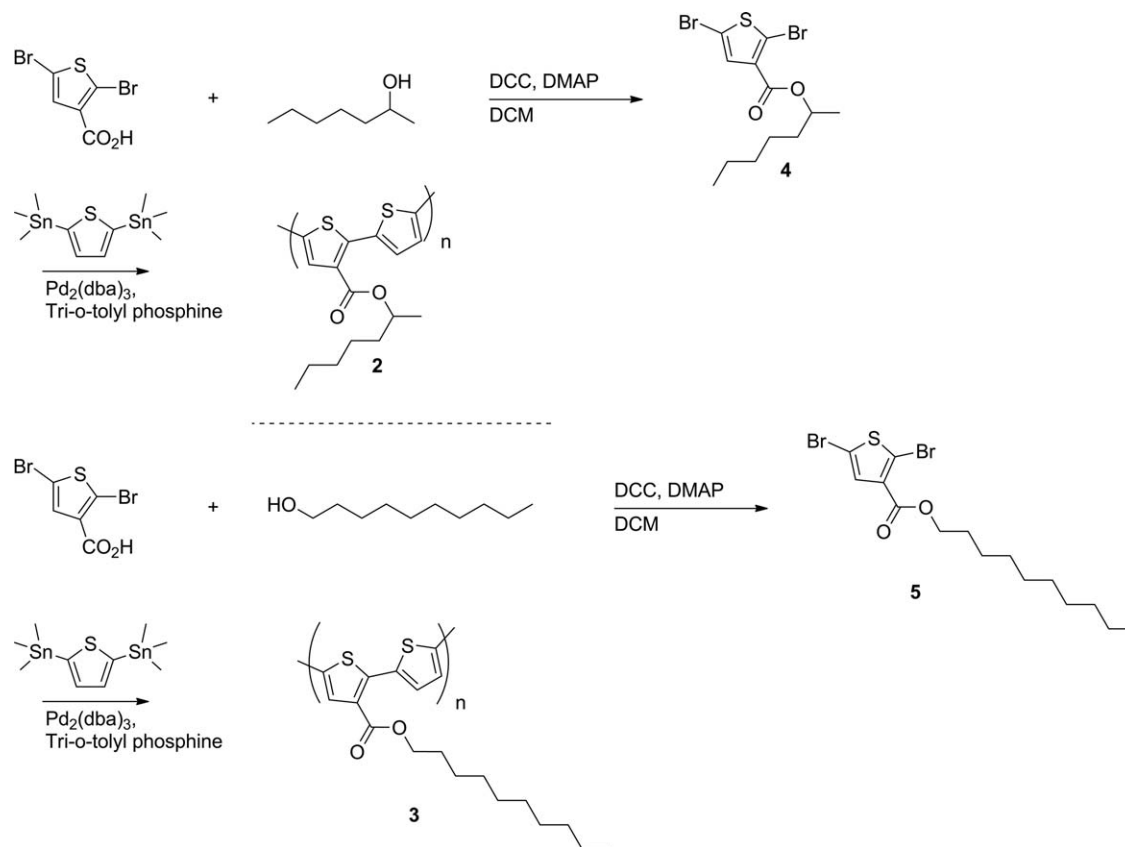


**FIGURE 3** XPS results of the analysis of films on PET prepared using polymer **1** and various amounts of catalytic acid for thermocleavage at 140 °C. The curves on the left shows graphical representation of the relative calculated atom% distribution of carbon and sulfur during a reaction where 0% reaction is polymer **1**, 50% reaction is P3CT, and 100% reaction is PT. To the right of these are shown the actual atom% measured by XPS.





**SCHEME 2** Synthetic route to the polymers **2** and **3**.

aqueous HCl (0.5 M, 2 × 25 mL), NaHCO<sub>3</sub> (2 × 25 mL), and brine (25 mL) followed by drying over MgSO<sub>4</sub>. Evaporation of the solvent yielded a crude (4.77 g), which upon gradient column chromatography (heptane/AcOEt, 1% steps) yielded the desired compound a clear colorless oil (3.9 g, 94%).

<sup>1</sup>H NMR (500 MHz, CDCl<sub>3</sub>) δ 7.33 (s, 1H), 5.09 (hex, *J* = 6.4 Hz, 1H), 1.78–1.55 (m, 2H), 1.43–1.26 (m, 9H), 0.89 (t, *J* = 6.9 Hz, 3H). <sup>13</sup>C NMR (126 MHz, CDCl<sub>3</sub>) δ 160.64, 132.52, 131.91, 118.91, 111.35, 72.70, 36.04, 31.78, 25.21, 22.68, 20.15, 14.15.

**Poly(heptane-2-yl [2,2'-bithiophene]-carboxylate 5,5'-diyl) (Polymer 2)**

**5** (504 mg, 1.31 mmol), 2,5-bis(trimethylstannyl)thiophene (538 mg, 1.31 mmol), tri-*o*-tolyl phosphine (160 mg, 0.525 mmol), and Pd<sub>2</sub>(dba)<sub>3</sub> (60.1 mg, 0.066 mmol) were mixed in degassed toluene (20 mL) under argon. The temperature was raised to 110 °C, and the mixture was left while stirring for 20 h. The polymer was precipitated by addition of the reaction mixture to methanol, and the solid was purified by soxhlet extraction with methanol for 24 h, followed by soxhlet with hexane for 6 h. The polymer was extracted with chloroform at reprecipitated from toluene in methanol after removal of the chloroform. *M*<sub>w</sub> 32269, *M*<sub>n</sub> 11179, PD 2.9

**Decyl 2,5-dibromothiophene-3-carboxylate (5)**

2,5-Dibromothiophene-3-carboxylic acid (2.0 g, 6.99 mmol), DMAP (0.085 g, 0.70 mmol), and decan-1-ol (2.48 mL, 14.0

mmol) mixed in DCM (7 mL) under argon were cooled on an ice bath. DCC (1.587 g, 7.69 mmol) was added, and the mixture was allowed to stir for 10 min after which the ice bath was removed and stirring was continued for an additional 2 h at RT. The solid in the mixture was filtered off and washed thoroughly with DCM. After removing the solvent, the crude was purified by gradient column chromatography (heptane/AcOEt, 2% steps) yielding the pure product (2.87 g, 96%). <sup>1</sup>H NMR (500 MHz, CDCl<sub>3</sub>) δ 7.34 (s, 1H), 4.27 (t, *J* = 6.7 Hz, 2H), 1.79–1.64 (m, 2H), 1.48–1.14 (m, 16H), 0.88 (t, *J* = 7.0 Hz, 3H). <sup>13</sup>C NMR (126 MHz, CDCl<sub>3</sub>) δ 161.06, 132.23, 131.91, 119.08, 111.45, 65.63, 32.04, 29.67, 29.64, 29.44, 29.36, 28.72, 26.15, 22.82, 14.25.

**Poly(decyl [2,2'-bithiophene]-carboxylate 5,5'-diyl) (Polymer 3)**

Compound **5** (0.502 g, 1.18 mmol), 2,5-bis(trimethylstannyl)thiophene (0.482 g, 1.18 mmol), tri-*o*-tolyl phosphine (0.148 g, 0.486 mmol), and Pd<sub>2</sub>(dba)<sub>3</sub> (0.055 g, 0.060 mmol) were mixed in dry degassed toluene (20 mL), and the temperature was raised to 110 °C. The mixture was left stirring for 18 h after which the mixture was precipitated by addition into methanol. The solid was purified by soxhlet extraction with methanol (1 day) and hexane (1 day) followed by extraction of the polymer with chloroform. After removing the solvent, the polymer was redissolved in toluene and precipitated in methanol. *M*<sub>w</sub> 16974, *M*<sub>n</sub> 6911, PD 2.4

**TGA-MS****General Procedure**

Stock solutions containing the respective polymers (40 mg/mL, chloroform) and the respective acids (1 mol %, 2 mol %, 5 mol %, and 10 mol % in chloroform (for PFBSA chloroform/methanol 200:1)—the concentrations were calculated from the theoretical abundance of ester groups in the polymers) were mixed in a TGA platinum pan (100  $\mu$ L), and the solvent was allowed to evaporate in air. The TGA experiment was then started at 50 °C with a subsequent increase of 10 °C/min during the experiment. MS-data for selected masses were simultaneously collected allowing for monitoring of the thermocleavage reaction. Full MS-data collected for each experiment can be found in the Supporting Information.

**CONCLUSIONS**

In summary, the influence of strong acids on the thermocleavage temperature of thiophene polymer **1** carrying tertiary side chains has been examined by means of TGA-MS and XPS. By monitoring of characteristic fragments in MS, a considerable lowering of the cleavage temperatures of both side chains (200–220 °C  $\rightarrow$  RT–50 °C) and the subsequent decarboxylation (250–300 °C  $\rightarrow$  120–150 °C) is observed when using sufficiently strong acids like trifluoromethanesulfonic acid. XPS data of roll-to-roll (R2R) processed films of polymer **1** and catalytic amounts of strong acid on PET showed that heating of the processed film to 140 °C for 5 min is sufficient to achieve cleavage to the insoluble acid stage but no indication of decarboxylation was observed. The outcome is a major improvement of previous results obtained without acid catalysis. Unfortunately, XPS-data indicate that less than half of the added catalytic acids were removed in the drying/heating process. Finally, TGA-MS experiments with polymers carrying secondary (**2**) and primary (**3**) ester side chains showed a lowering of the ester cleavage to 65–120 °C and 140–170 °C respectively, and the temperature for decarboxylation as expected was either the same as for polymer **1** or in the case of the primary ester the same as the side-chain cleavage temperature. The fact that the cleavage temperature for secondary and primary thiophene esters can be lowered so much makes these compounds potentially cheaper candidates for thermocleavable polymers in organic solar cells. Several issues still need to be resolved, such as complete removal of the catalytic acid for this procedure to be applicable in solar cell preparation on flexible substrates like PET, but a promising first step toward lowering thermo-

cleavage temperatures to acceptable levels has been achieved.

The authors thank the Danish Strategic Research Council (DSF 2104-07-0022) for financial support.

**REFERENCES AND NOTES**

- 1 Service, R. F.; *Science* **2011**, *332*, 293.
- 2 Bjerring, M.; Nielsen, J. S.; Nielsen, N. C.; Krebs, F. C. *Macromolecules* **2007**, *40*, 6012–6013.
- 3 Bjerring, M.; Nielsen, J. S.; Siu, A.; Nielsen, N. C.; Krebs, F. C. *Sol. Energy Mater. Sol. Cells* **2008**, *92*, 772–784.
- 4 Edder, C.; Armstrong, P. B.; Prado, K. B.; Frechet, J. M. *J. Chem. Commun.* **2006**, 1965–1967.
- 5 Gevorgyan, S. A.; Krebs, F. C. *Chem. Mater.* **2008**, *20*, 4386–4390.
- 6 Hagemann, O.; Bjerring, M.; Nielsen, N. C.; Krebs, F. C. *Sol. Energy Mater. Sol. Cells* **2008**, *92*, 1327–1335.
- 7 Helgesen, M.; Gevorgyan, S. A.; Krebs, F. C.; Janssen, R. A. *J. Chem. Mater.* **2009**, *21*, 4669–4675.
- 8 Krebs, F. C.; Spanggaard, H. *Chem. Mater.* **2005**, *17*, 5235–5237.
- 9 Liu, J. S.; Kadnikova, E. N.; Liu, Y. X.; McGehee, M. D.; Frechet, J. M. *J. Am. Chem. Soc.* **2004**, *126*, 9486–9487.
- 10 Manceau, M.; Helgesen, M.; Krebs, F. C. *Polym. Degrad. Stab.* **2010**, *95*, 2666–2669.
- 11 Petersen, M. H.; Gevorgyan, S. A.; Krebs, F. C. *Macromolecules* **2008**, *41*, 8986–8994.
- 12 Krebs, F. C.; Jørgensen, M.; Norrman, K.; Hagemann, O.; Alstrup, J.; Nielsen, T. D.; Fyenbo, J.; Larsen, K.; Kristensen, J. *Sol. Energy Mater. Sol. Cells* **2009**, *93*, 422–441.
- 13 Krebs, F. C. *Sol. Energy Mater. Sol. Cells* **2009**, *93*, 465–475.
- 14 Tromholt, T.; Gevorgyan, S. A.; Jørgensen, M.; Krebs, F. C.; Sylvester-Hvid, K. *ACS Appl. Mater. Interfaces* **2009**, *1*, 2768–2777.
- 15 Diliën, H.; Vandenberg, J.; Banishoeb, F.; Adriaensens, P.; Cleij, T. J.; Lutsen, L.; Vanderzande, D. J. M. *Macromolecules* **2011**, *44*, 711–718.
- 16 Diliën, H.; Palmaerts, A.; Lenes, M.; de Boer, B.; Blom, P.; Cleij, T. J.; Lutsen, L.; Vanderzande, D. *Macromolecules* **2010**, *43*, 10231–10240.
- 17 Han, X.; Chen, X.; Holdcroft, S. *Adv. Mater.* **2007**, *19*, 1697–1702.
- 18 Lancaster, R. E.; Vanderwerf, C. A. *J. Org. Chem.* **1958**, *23*, 1208–1209.
- 19 Dunn, G. E.; Lee, G. K. J. *Can. J. Chem.* **1971**, *49*, 1032–1035.
- 20 Krebs, F. C.; Norrman, K. *ACS Appl. Mater. Interfaces* **2010**, *2*, 877–887.

# 1. Introduction

**Suren A. Gevorgyan, Roar Søndergaard and Frederik C. Krebs**

## 1.1 Solar Energy

The human energy supplies are almost all related to sun, as most of the energy sources on earth are direct or indirect results of solar energy. For example fossil fuels have been slowly formed from biomaterials within millions of years using solar energy and now they are used as primary energy source by humans. Similarly, biomass through the processes of photosynthesis produces fuel that can be used for heat or electricity. Wind energy has been actively explored for decades as an energy source. It is a result of air currents that are created by solar heated air and the rotation of earth. Yet, the fastest and most efficient direct conversion of sun light into electrical energy is possible only through photovoltaic devices. The photovoltaic (PV) effect discovered by Becquerel [1,2] is the basic physical process, by which the semiconductor material converts electromagnetic radiation (sun light) into electric power.

A very small fraction of solar power (less than 0.02 %) available on earth can cover the entire energy demand of the world. By the end of year 2008, PV based sources have been providing only 0.1 % of all the energy consumed by man according to the Renewable Energy Policy Network (REN21) report [3]. While our environment is surrounded with abundant solar power, the PV technology is still too expensive to become a primary energy source. Therefore, the main task of

the solar cell field is to develop a technology, which can provide cheap PV products and make the photoconversion of sun light into electrical power cost efficient.

## 1.2 Types of Solar Cells

So far solar cells have been categorized in three generations according to the time sequence they started playing big role in the solar cell field [4].

The first generation (1G) solar cells are large scale, single junction devices. Most of the production is based on silicon wafers including single crystal and multi-crystalline silicon. About 90 % of the current photovoltaic production is based on first generation. The efficiency of the single junction cells has a theoretical limit of about 30% (the Shockley – Queisser limit) [5,6] and currently the common silicon wafer based devices show nearly 20% efficiency with the highest reported efficiencies reaching 25 [7]. Yet, the cost per produced 1 Watt of power is nearly 4 times higher than the cost of electricity produced by conventional means due to the high cost of the material (half of the cost of first generation devices is the silicon wafer) and production technology. Even though the price continuously decreases along with the progress of the technology, the 1G technology will possibly reach their price limit before achieving the competitive level in the market.

The second generation (2G) solar cells are addressing the cost issue and the primary task is to decrease the amount of expensive material used in the production process while keeping the efficiency of the device high. The foremost approach is producing thin film solar cells on low cost substrates (such as glass or copper foil). Different techniques are utilized for production process such as solution deposition, vapor deposition, electroplating and etc. and the most successful

materials for 2G are amorphous silicon, CuIn(Ga)Se<sub>2</sub> (CIGS), CdTe/CdS, which are being deposited on thin substrates. Devices based on these materials can deliver laboratory power conversion efficiencies up to 19 % while the module efficiencies are reaching 14 % due to difficulties of producing large scale uniform films [7]. Although thin film technology can significantly decrease the cost of PV, 2G solar cells will also approach a cost limit in € per watt peak ( $\text{€ W}_p^{-1}$ ) due to efficiency limits, material and processing costs.

The third generation (3G) is the alternative approach cost reduction through usage of unconventional low cost materials and by increasing the efficiency by multiple stacking of solar cells. 3G solar cells introduce the idea of multi junction solar cells, which can drastically increase the efficiency by improving the harvesting of photons and even overcome the theoretical limit of 30 %. Currently the highest efficiencies reported for multijunction solar cells are over 33 % and up to 42 % when using high concentration [7]. 3G utilizes new concepts in terms of device architectures and materials. As an example, two atypical approaches of photovoltaics are Dye – Synthesized Solar Cells (DSSCs) [8,9] and Organic Solar Cells (OSCs). DSSCs are based on combination of dyes with metal oxides and electrolyte. The efficiencies of DSSC are comparable to polycrystalline silicon with reported power conversion efficiencies up to 12 % for small lab scale devices, while the lifetime of the devices is rather low compared with inorganic solar cells.

After discovery of polymer materials with conductive properties in 1906 [10] they have been intensively studied for various electronic applications, and especially in the last decade the field of organic photovoltaics (OPVs) has been growing very quickly and showing promising potential as a low cost PV technology.

### 1.3 Organic Solar Cells

Some of the reasons for the large interest in OPVs can be summarized as: polymers allow fast, simple, low cost and large volume processing. In other words, polymers have the opportunity to be solution processed, which literally means printing or coating of solar cells using roll-to-roll (R2R) machinery similar to the way in which news papers are made. Typical organic solar cell devices have a layered structure and are commonly considered organic if the active absorbing layer comprises only organic materials, while for other layers (for example electrodes) metals and other inorganic materials can be used. The OPV field also include a category of hybrid solar cells, in which the active layer also contains an inorganic component such as quantum dots [11,12] or nanostructured inorganic metal oxides mixed with the conjugated polymer [13-15]. These types of devices will not be discussed in this book where focus is kept on fully organic active layers. The interested reader can find descriptions of hybrid solar cells in literature [16].

There have been a number of reviews discussing the development of OPVs nicely presenting the key events throughout the short history of the OPV field [17-24]. Although polymer solar cells have been developing fast, there are still three issues that are not fully unsolved: the improvement of device photoconversion efficiency (PCE) [24], extension of device lifetimes [25] and large scale production [26,27]. There are a number of loss mechanisms that result in low PCEs and currently most of the research groups in the field are struggling to overcome these mechanisms to improve the efficiency. More and more groups are addressing the stability issue and various approaches are reported for improvement of the device lifetimes. Yet, the improvements are minor and more studies are needed. Furthermore, the experiments show that when a good polymer is developed and the small model devices based on such polymer deliver

high efficiencies, it is still a large practical challenge to transfer the device structure and performance to a full R2R process for large scale production.

The objectives of this book are to present to the reader the current technologies available for producing OPV devices and discuss the current state of the art and challenges of the OPV field including some recent demonstrations of the technology. The book also presents a business analysis of OPV in the context of thin film PV devices and the economical challenges. Further company reviews for some of the companies that have targeted OPV is presented and finally the intellectual property aspects of OPV are discussed and a patent map of Europe is drawn.

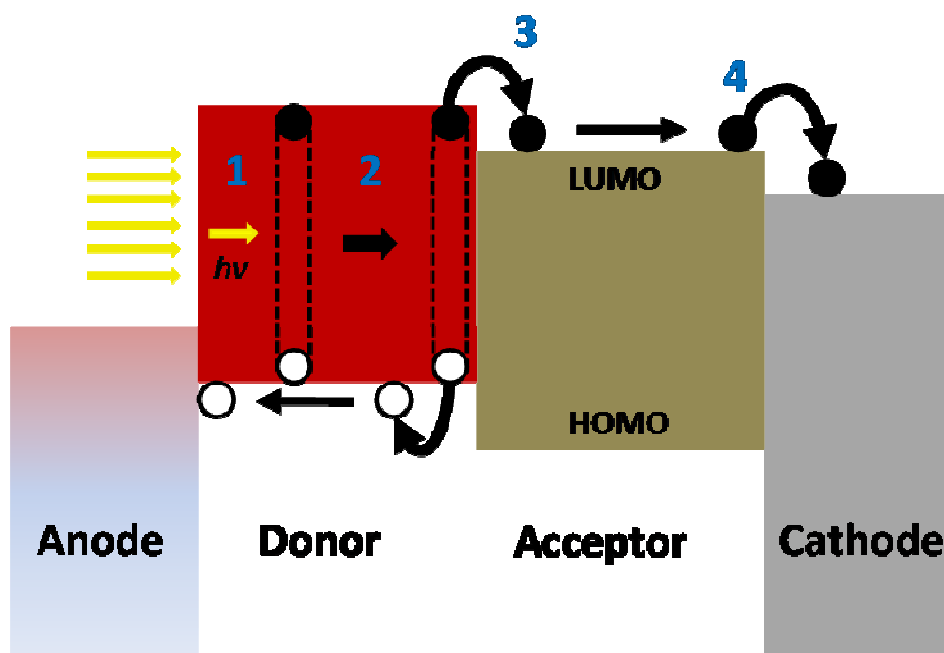


**Figure 1.1:** Schematic illustration of the photoelectric conversion mechanism

#### 1.4 Device Architecture and Operational Mechanism

The main distinction in the working principle of the organic PVs as compared to inorganic PVs is that upon absorption of a photon by an inorganic material free charge carriers are created, whereas in the case of organic materials an excited electron-hole pair or so-called “exciton” is generated, that needs to dissociate before free charge carriers are formed [28]. The exciton is a bound state of an excited electron and positive charge carrier.

The mechanism by which the light is converted to electric power in OPVs consists of 4 basic steps (Figure 1.1): 1) The photon is absorbed by the active material, which promotes the electron to the lowest unoccupied molecular orbital (LUMO), while leaving the positive charge carrier or so-called “hole” in the highest occupied molecular orbital (HOMO). The excited pair is still bound by coulomb attraction forces forming an exciton; 2) The exciton diffuses to the interface of the donor and acceptor; 3) The exciton is dissociated into free carriers at the interface between donor and acceptor and 4) Finally the free carriers are being transported and collected at the opposite electrodes. Each of the steps is crucial for efficient power generation and there are many loss mechanisms involved in this sequence. An important parameter of the absorbing material is its optical bandgap, which is defined by the difference of HOMO and LUMO. The terms donor and acceptor refer to materials with either high ionization potential (donor) or high electron affinity (acceptor). In other words a material that willingly gives electrons is brought into contact with a material with strong electron accepting properties, which forces the exciton to split into free charge carriers. The free charge collection at opposite electrodes is assured by the asymmetric ionization energy or work function of the electrodes. One of the main reasons that the efficiency of OPVs is considerably lower compared to inorganic solar cells is because the charge carriers



lose a certain amount of energy during separation of the excited pair. The common structure of the organic solar cells comprises a multilayer stack. Usually the active layer which is a combination of donor and acceptor materials is sandwiched between two electrodes.

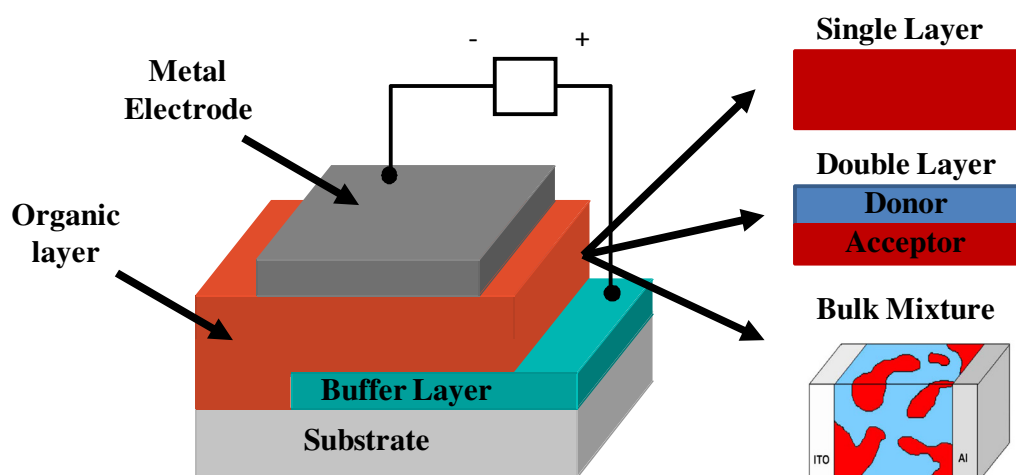


**Figure 1.2:** Device structure of a polymer solar cell. Three different designs of active layer are shown on the right hand side.

One of the electrodes needs to be transparent for illumination of the cell. In some cases certain buffer layers are being applied between the electrodes and the active layer to ensure charge selective transport. Figure 1.2 shows typical device architecture for OPVs. Excitons have a very short life time and the distance they can cross before recombination (Diffusion length) in several different conjugated polymers has subsequently been measured to be 4–20 nm [29-31]. Therefore, after the generation of an exciton it has to be separated into free charge carriers very quickly before recombination takes place. The active layer can be designed in the three different ways shown on the right hand side of the Figure 1.2. The active layer can be 1) a single layer, 2) double layer (bilayer heterojunction) or 3) bulk heterojunction (mixture of donor and acceptor in

a bulk). The first OPVs were based on a single layer structure, where the excitons are separated into free charges at the interface between the active layer and the electrode [32-34]. Since the separation of charges in this case is very inefficient the concept has not been successful. The efficiencies drastically increased after the introduction of donor/acceptor bilayer structure, where the donor and acceptor layers are brought together forming heterojunction similarly to the *pn*-junction inorganic solar cells [35]. However, only the excitons generated within the distance of the diffusion length from the interface can successfully diffuse to the interface and be separated to free carriers. Therefore, only the light absorbed by a very thin layer next to the interface can contribute to the photocurrent, while the rest is lost through recombination processes. For that reason the photocurrent delivered by these devices is quite low. The breakthrough came with the idea of the bulk heterojunction, where the donor and acceptor materials are mixed in bulk forming nanoscale morphology [36-38]. In that way the interface is extended throughout the whole active layer providing more efficient charge separation and separate paths for transport of free carriers.

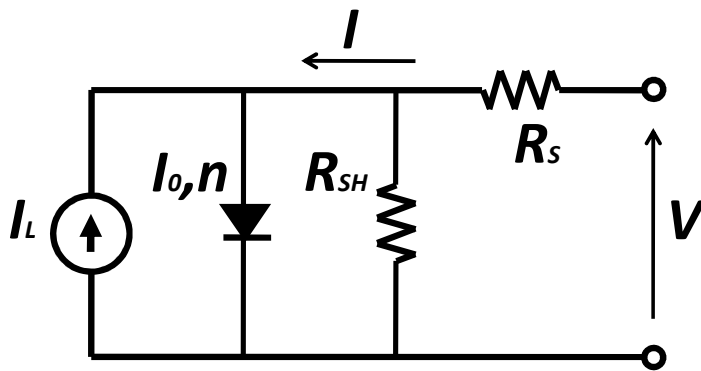


**Figure 1.3:** Electric circuit that approximates the operation principle of OPV devices.

The solar cell in the dark acts as a simple diode. The equal electric circuit that approximates the organic solar cell performance is shown in Figure 1.3. It is comprised of 1) A diode with ideality factor  $n$  and saturation current  $I_0$  (current in the dark at reverse bias), 2) A source to provide current that corresponds to photocurrent  $I_L$  generated during illumination, 3)  $R_s$  series resistance, which takes into account all the resistances at interfaces in the layers, the conductivity of the semiconductors and the electrodes, 4) Shunt resistance  $R_{sh}$ , which takes into account the leakage of the current through shunts due to the defects in the films. For good performance of the device  $R_s$  needs to be low and  $R_{sh}$  has to have high values. Figure 1.4 shows the current voltage characteristics (IV curves) for a typical solar cell. When light is shone on the device the IV curve of the cell becomes a superposition of the dark IV with the light generated current and the curve is shifted down to the 4<sup>th</sup> quadrant. The right hand side of Figure 1.4 presents the 4<sup>th</sup> quadrant of the IV curve, which shows the part where the actual power is being produced by the cell during the illumination. The figure also shows the key parameters that define the performance of the cell, which are the open circuit voltage  $V_{oc}$ , short circuit current  $I_{sc}$ , fill factor  $FF$ , the maximum power  $P_{max}$ , the voltage and the current at max power point  $V_{max}$  and  $I_{max}$ . The following expression defines the current for the circuit [39]:

$$I = I_0 \left( \exp \left[ \frac{e(V - IR_s)}{nkT} \right] - 1 \right) + \frac{V - IR_s}{R_{sh}} - I_L \quad (1)$$

where  $e$  is the elementary charge,  $kT$  the thermal energy. From this equation  $V_{oc}$  and  $I_{sc}$  can be obtained by placing a value of zero for  $I$  and  $V$  respectively (see eq. (2) and (3)). For the

approximation on right hand side of the equations below it is considered that  $R_s$  is very small and  $R_{sh}$  is very large:

$$I_{sc} = I_0 \left( \exp \left[ \frac{eI_{sc}R_s}{nkT} \right] - 1 \right) - \frac{I_{sc}R_s}{R_{sh}} - I_L \approx I_L \quad (2)$$

$$V_{oc} = \frac{nkT}{e} \ln \left[ 1 + \frac{I_L}{I_0} \left( 1 - \frac{V_{oc}}{I_L R_{sh}} \right) \right] \approx \frac{nkT}{e} \ln \left[ 1 + \frac{I_L}{I_0} \right] \quad (3)$$

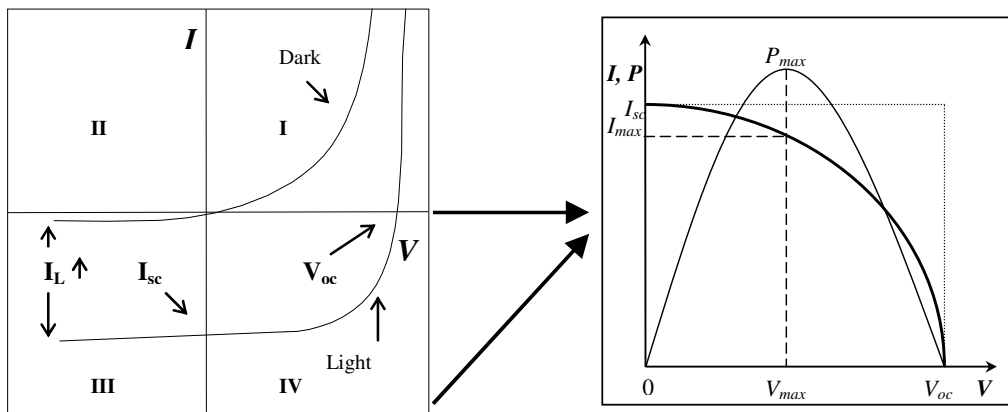


**Figure 1.4:** Dark and light IV characteristics of an OPV device (left) and the zoom in on the 4<sup>th</sup> quadrant with additional power curve (right).

The power produced by solar cell is defined as the product of the current and voltage and the maximum power will correspond to the maximum product  $\sim I_{max} \times V_{max}$ . Equation (4) below is the basic equation that defines the power conversion efficiency (PCE) of the solar cell, which shows the ratio between maximum electric power produced by the cell and the power of the incident light on the cell with a given active area  $A$ :

$$\eta = \frac{I_{max}V_{max}}{P_{in}A} = FF \frac{I_{sc}V_{oc}}{P_{in}A} \quad (4)$$

where  $FF$  is defined as:

$$FF = \frac{I_{max}V_{max}}{I_{sc}V_{oc}} \quad (5)$$

$FF$  shows how much power is produced by the cell with given  $I_{sc}$  and  $V_{oc}$  in practice compared to the theoretically possible value.  $FF$  is significantly affected by parasitic resistances  $R_s$  and  $R_{sh}$ . Typically, good operating organic solar cell delivers  $FF$  values in the range of 60 – 65 %.

Another important quantity that defines the quality of energy conversion is the quantum efficiency (QE) of a solar cell. QE defines the number of charge carriers collected at the electrodes per number of incident photons on the solar cell area at a given wavelength. If every incident photon results in one collected charge carrier then the QE is equal to unity (no recombination losses). There are two ways of defining the QE:

External Quantum Efficiency (EQE) is the ratio between number of collected carriers and number of all **incident** photons on the cell at a given wavelength.

Internal Quantum Efficiency (IQE) is the ratio between the number of collected carriers and number of all **absorbed** photons by the cell at a given wavelength (IQE does not take into consideration the light transmitted through and reflected from the cell).

### 1.5 Current State-of-the-Art and Challenges of OPVs

Currently the world record PCE report is held by newly (see chapter 5) established company called Solarmer energy, Inc and their latest reported PCE is 7.9 % for a small laboratory device (certified by NREL), while for large solar panel they have a reported power conversion efficiency of 3.9 %. Although, the numbers are modest compared to inorganic solar cells, OPVs are already applicable for different niche markets (see for example [40]). However, in order to compete with their inorganic counterparts not only in niche markets, but also in applications such as Building Integrated PVs (BIPV), OPVs have to perform at higher power conversion efficiency levels. One of the main loss mechanisms is the poor alignment of the energy levels of the donor and acceptor materials, which will be discussed in detail in chapter 2. The current challenge of the OPV field is to develop new donor and acceptor materials with better energy level alignment [24]. In addition, the improvement of the transport properties of the materials through better control of the morphology can significantly reduce the recombination losses [41].

It is a hard task to establish the current state of the art lifetimes of OPV devices, because the behavior of the devices varies from one cell type to another [42-44] and it is not an easy task to develop a standard measurement technique for evaluation of the lifetime [25]. Also OPVs are quite sensitive towards the surrounding environment (temperature, humidity, mechanical stress, light intensity) and probably the most reliable test that has been reported so far is the outdoor testing of the cells (see for example [43,45]). Konarka Technologies, inc, which is one of the leading companies in the OPV field, proved that their devices could keep almost the same performance after 1 year of exposure to real outdoor conditions and sunlight [45]. The same company claims up to 3 to 5 years of stability for their products, which has not been certified yet.

There is an intensive research going on in the direction of developing different environmental protection and encapsulation techniques for OPVs and many different encapsulation and buffer layer methods have been reported [46-50]. However, production of stable and at the same time flexible devices that will have lifetimes of a few years is still remaining a challenging task.

Although a vast number of groups have reported high efficiencies for OPVs, all the reports are based on measuring small size devices ( $\leq 1 \text{ cm}^2$  of active area). When one tries to increase the size of the cell the efficiency drastically decreases due to sheet resistance and increased amounts of defects in the films. There are a very limited number of groups/companies that are capable of producing large scale OPVs with reasonable efficiencies and even fewer groups/companies use R2R techniques for production. In order to make the OPV technology cost efficient the processing needs to be cheap, fast and in large scale. Therefore, one of the primary goals of the OPV field is to develop efficient techniques for transferring the technology from small lab scale to large R2R production without any significant loss in efficiency.

## References

1. Becquerel A.E., *Comptes Rendus De L'Académie Des Sciences*, 1839, **9**, 145.
2. Becquerel A.E., *Comptes Rendus De L'Académie Des Sciences*, 1839, **9**, 561.
3. <http://www.ren21.net/globalstatusreport/g2009.asp>
4. Darren M. Bagnall and Matt Boreland, Photovoltaic technologies, *Energy Policy*, 2008, **36**, 4390-4396.

5. W. Shockley and H. J. Queisser, Detailed Balance Limit of Efficiency of P-N Junction Solar Cells, *J.Appl.Phys.*, 1961, **32**, 510-519.
6. M. C. Hanna and A. J. Nozik, Solar conversion efficiency of photovoltaic and photoelectrolysis cells with carrier multiplication absorbers, *J.Appl.Phys.*, 2006, **100**, 074510.
7. M. A. Green, K. Emery, Y. Hishikawa, and W. Warta, Solar Cell Efficiency Tables (Version 34), *Prog.Photovolt.*, 2009, **17**, 320-326.
8. Michael Gratzel, Photoelectrochemical cells, *Nature*, 2001, **414**, 338-344.
9. M. K. Nazeeruddin, A. Kay, I. Rodicio, R. Humphry-Baker, E. Mueller, P. Liska, N. Vlachopoulos, and M. Graetzel, Conversion of light to electricity by cis-X2bis(2,2'-bipyridyl-4,4'-dicarboxylate)ruthenium(II) charge-transfer sensitizers (X = Cl-, Br-, I-, CN-, and SCN-) on nanocrystalline titanium dioxide electrodes, *J.Am.Chem.Soc.*, 2002, **115**, 6382-6390.
10. A Pochettino, *Acad.Lincei Rend.*, 1906, **15**, 355.
11. Wendy U. Huynh, Janke J. Dittmer, and A. Paul Alivisatos, Hybrid Nanorod-Polymer Solar Cells, *Science*, 29-3-2002, **295**, 2425-2427.
12. D. J. Milliron, I. Gur, and A. P. Alivisatos, Hybrid organic - Nanocrystal solar cells, *Mrs Bulletin*, 2005, **30**, 41-44.
13. A. Petrella, M. Tamborra, M. L. Curri, P. Cosma, M. Striccoli, P. D. Cozzoli, and A. Agostiano, Colloidal TiO<sub>2</sub> nanocrystals/MEH-PPV nanocomposites: Photo(electro)chemical study, *Journal of Physical Chemistry B*, 2005, **109**, 1554-1562.



14. K. M. Coakley, Y. X. Liu, M. D. McGehee, K. L. Frindell, and G. D. Stucky, Infiltrating semiconducting polymers into self-assembled mesoporous titania films for photovoltaic applications, *Adv.Func.Mater.*, 2003, **13**, 301-306.
15. A. C. Arango, L. R. Johnson, V. N. Bliznyuk, Z. Schlesinger, S. A. Carter, and H. H. Horhold, Efficient titanium oxide/conjugated polymer photovoltaics for solar energy conversion, *Adv.Mater.*, 2000, **12**, 1689-1692.
16. P. Gomez-Romero, Hybrid organic-inorganic materials - In search of synergic activity, *Adv.Mater.*, 2001, **13**, 163-174.
17. C. J. Brabec, N. S. Sariciftci, and J. C. Hummelen, Plastic solar cells, *Adv.Func.Mater.*, 2001, **11**, 15-26.
18. J. Nelson, Organic photovoltaic films, *Current Opinion in Solid State & Materials Science*, 2002, **6**, 87-95.
19. H. Spanggaard and F. C. Krebs, A brief history of the development of organic and polymeric photovoltaics, *Sol. Energy Mater. Sol. Cells*, 2004, **83**, 125-146.
20. K. M. Coakley and M. D. McGehee, Conjugated polymer photovoltaic cells, *Chem.Mater.*, 2004, **16**, 4533-4542.
21. S. Gunes, H. Neugebauer, and N. S. Sariciftci, Conjugated polymer-based organic solar cells, *Chemical Reviews*, 2007, **107**, 1324-1338.

22. B. C. Thompson and J. M. J. Frechet, Organic photovoltaics - Polymer-fullerene composite solar cells, *Angew.Chem.- Int.Ed.*, 2008, **47**, 58-77.
23. B. Kippelen and J. L. Bredas, Organic photovoltaics, *Energy & Env.Sci.*, 2009, **2**, 251-261.
24. G. Dennler, M. C. Scharber, and C. J. Brabec, Polymer-Fullerene Bulk-Heterojunction Solar Cells, *Adv.Mater.*, 2009, **21**, 1323-1338.
25. M. Jorgensen, K. Norrman, and F. C. Krebs, Stability/degradation of polymer solar cells, *Sol. Energy Mater. Sol. Cells*, 2008, **92**, 686-714.
26. F. C. Krebs, Fabrication and processing of polymer solar cells: A review of printing and coating techniques, *Sol. Energy Mater. Sol. Cells*, 2009, **93**, 394-412.
27. C. J. Brabec and J. R. Durrant, Solution-processed organic solar cells, *Mrs Bulletin*, 2008, **33**, 670-675.
28. B. A. Gregg and M. C. Hanna, Comparing organic to inorganic photovoltaic cells: Theory, experiment, and simulation, *J.Appl.Phys.*, 2003, **93**, 3605-3614.
29. J. J. M. Halls, K. Pichler, R. H. Friend, S. C. Moratti, and A. B. Holmes, Exciton diffusion and dissociation in a poly(p-phenylenevinylene)/C-60 heterojunction photovoltaic cell, *Appl.Phys.Lett.*, 1996, **68**, 3120-3122.
30. L. A. A. Pettersson, L. S. Roman, and O. Inganäs, Modeling photocurrent action spectra of photovoltaic devices based on organic thin films, *J.Appl.Phys.*, 1999, **86**, 487-496.

31. M. Theander, A. Yartsev, D. Zigmantas, V. Sundstrom, W. Mammo, M. R. Andersson, and O. Inganas, Photoluminescence quenching at a polythiophene/C-60 heterojunction, *Physical Review B*, 2000, **61**, 12957-12963.
32. G. A. Chamberlain, Organic Solar-Cells - A Review, *Solar Cells*, 1983, **8**, 47-83.
33. D. Wohrle and D. Meissner, Organic Solar-Cells, *Adv.Mater.*, 1991, **3**, 129-138.
34. R. N. Marks, J. J. M. Halls, D. D. C. Bradley, R. H. Friend, and A. B. Holmes, The Photovoltaic Response in Poly(P-Phenylene Vinylene) Thin-Film Devices, *Journal of Physics-Condensed Matter*, 1994, **6**, 1379-1394.
35. C. W. Tang, 2-Layer Organic Photovoltaic Cell, *Appl.Phys.Lett.*, 1986, **48**, 183-185.
36. J. J. M. Halls, C. A. Walsh, N. C. Greenham, E. A. Marseglia, R. H. Friend, S. C. Moratti, and A. B. Holmes, Efficient Photodiodes from Interpenetrating Polymer Networks, *Nature*, 1995, **376**, 498-500.
37. G. Yu and A. J. Heeger, Charge Separation and Photovoltaic Conversion in Polymer Composites with Internal Donor-Acceptor Heterojunctions, *J.Appl.Phys.*, 1995, **78**, 4510-4515.
38. G. Yu, J. Gao, J. C. Hummelen, F. Wudl, and A. J. Heeger, Polymer Photovoltaic Cells - Enhanced Efficiencies Via A Network of Internal Donor-Acceptor Heterojunctions, *Science*, 1995, **270**, 1789-1791.
39. C. Waldauf, M. C. Scharber, P. Schilinsky, J. A. Hauch, and C. J. Brabec, Physics of organic bulk heterojunction devices for photovoltaic applications, *J.Appl.Phys.*, 2006, **99**, 104503.

40. F. C. Krebs, M. Jørgensen, K. Norrman, O. Hagemann, J. Alstrup, T. D. Nielsen, J. Fyenbo, K. Larsen, and J. Kristensen, A complete process for production of flexible large area polymer solar cells entirely using screen printing-First public demonstration, *Sol. Energy Mater. Sol. Cells*, 2009, **93**, 422-441.
41. X. Yang and J. Loos, Toward high-performance polymer solar cells: The importance of morphology control, *Macromolecules*, 2007, **40**, 1353-1362.
42. K. Kawano, R. Pacios, D. Poplavskyy, J. Nelson, D. D. C. Bradley, and J. R. Durrant, Degradation of organic solar cells due to air exposure, *Sol. Energy Mater. Sol. Cells*, 2006, **90**, 3520-3530.
43. E. A. Katz, S. Gevorgyan, M. S. Orynbayev, and F. C. Krebs, Out-door testing and long-term stability of plastic solar cells, *European Physical Journal-Applied Physics*, 2006, **36**, 307-311.
44. S. A. Gevorgyan, M. Jørgensen, and F. C. Krebs, A setup for studying stability and degradation of polymer solar cells, *Sol. Energy Mater. Sol. Cells*, 2008, **92**, 736-745.
45. J. A. Hauch, P. Schilinsky, S. A. Choulis, R. Childers, M. Biele, and C. J. Brabec, Flexible organic P3HT : PCBM bulk-heterojunction modules with more than 1 year outdoor lifetime, *Sol. Energy Mater. Sol. Cells*, 2008, **92**, 727-731.
46. M. O. Reese, A. J. Morfa, M. S. White, N. Kopidakis, S. E. Shaheen, G. Rumbles, and D. S. Ginley, Pathways for the degradation of organic photovoltaic P3HT : PCBM based devices, *Sol. Energy Mater. Sol. Cells*, 2008, **92**, 746-752.

47. F. C. Krebs, J. E. Carle, N. Cruys-Bagger, M. Andersen, M. R. Lilliedal, M. A. Hammond, and S. Hvidt, Lifetimes of organic photovoltaics: photochemistry, atmosphere effects and barrier layers in ITO-MEHPPV: PCBM-aluminium devices, *Sol. Energy Mater. Sol. Cells*, 2005, **86**, 499-516.
48. F. C. Krebs, Encapsulation of polymer photovoltaic prototypes, *Sol. Energy Mater. Sol. Cells*, 2006, **90**, 3633-3643.
49. G. Dennler, C. Lungenschmied, H. Neugebauer, N. S. Sariciftci, M. Latreche, G. Czeremuszkin, and M. R. Wertheimer, A new encapsulation solution for flexible organic solar cells, *Thin Solid Films*, 2006, **511**, 349-353.
50. P. Vivo, J. Jukola, M. Ojala, V. Chukharev, and H. Lemmetyinen, Influence of Alq(3)/Au cathode on stability and efficiency of a layered organic solar cell in air, *Sol. Energy Mater. Sol. Cells*, 2008, **92**, 1416-1420.

## 2. Materials and Processing

**Roar Søndergaard, Suren A. Gevorgyan and Frederik C. Krebs**

### 2.1 Introduction

The typical structure of polymer solar cells comprises a number of layers, which gives plenty of choice for different materials and material combinations. One of the requirements while building a solar cell is to keep one of the faces transparent for illumination. It can be the frontface or the backface that is used for illumination depending on whether the substrate is transparent or not as shown in Figure 2.1. The frontface of the cell is usually considered to be the side of the substrate and accordingly the electrode in direct contact with the substrate is the front electrode. One has to choose the positions of the cathode and anode while building a solar cell. In case of the “normal geometry” the anode is the front electrode and in case of “inverted geometry” the anode is the back electrode. We have chosen reference device structures for each of these two geometries that will frequently be referred to throughout the context of this chapter. The reference structures are outlined in the tables below. The reader will find a detailed description of the aforementioned structures and materials in the next sections. The normal geometry reference cell will be called “the traditional device”. The traditional device has been considered as the optimal for a long period of time, since it can deliver relatively high efficiencies and is relatively easy to produce [1,2]. Yet, in the context of operational stability and large scale solution processing without vacuum coating steps the

inverted geometry has proven to be a better choice [3] and will thus be given some attention as well. The four different possibilities are shown in figure 2.1.

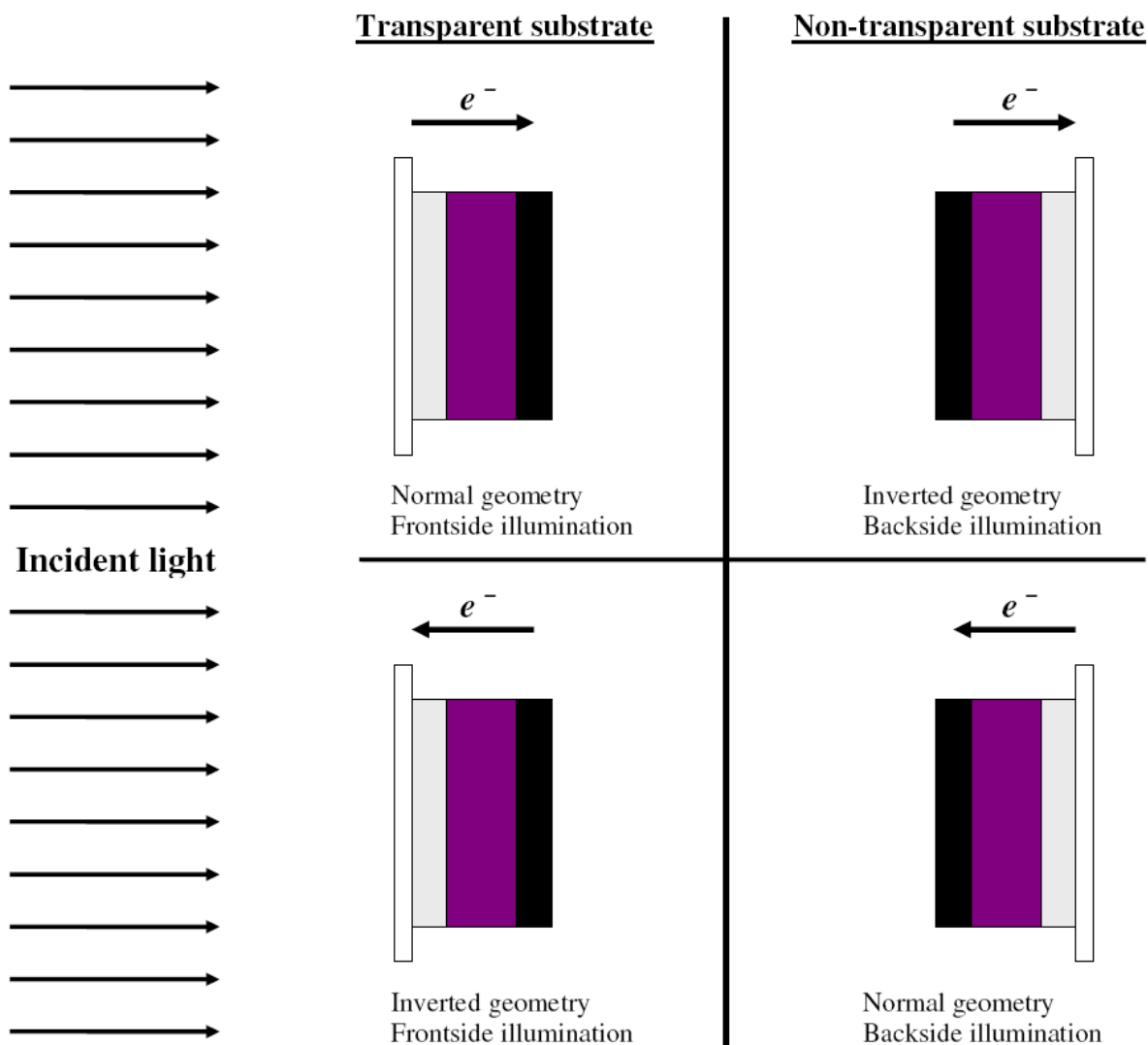


**Figure 2.1:** Different geometries of OPV devices with frontface or backface illumination. (reprinted with permission from the Royal Society of Chemistry).

The following subchapters will be a stepwise description of the different layers in solar cell devices by first giving an overview of commonly used materials for each specific layer followed by a brief introduction to how that layer can be processed.

*The Normal Geometry*

<b>Substrate</b> Glass or PET	<b>Anode</b> ITO	<b>Hole transport layer</b> PEDOT:PSS	<b>Active Layer</b> P3HT:PCBM	<b>Electron transport layer</b> LiF	<b>Cathode</b> Aluminum
----------------------------------	---------------------	--	----------------------------------	--	----------------------------

*The Inverted Geometry*

<b>Substrate</b> Glass or PET	<b>Cathode</b> ITO	<b>Electron transport layer</b> ZnO	<b>Active Layer</b> P3HT:PCBM	<b>Hole transport layer</b> PEDOT:PSS	<b>Anode</b> Silver
----------------------------------	-----------------------	--	----------------------------------	--	------------------------

PET – Polyethyleneterphthalate;

ITO – Indium Tin Oxide;

PEDOT:PSS – Poly(3,4-ethylenedioxythiophene):poly(styrenesulfonate);

P3HT – Poly(3-hexylthiophene);

PCBM – Fullerene derivative [6,6]-phenyl C61 butyric acid methyl ester;

LiF – Lithium fluoride

ZnO – Zinc oxide

**2.2 Substrate and Front Electrode**

The production of a typical device starts from the choice of the substrate, which can be transparent or non-transparent and flexible or rigid depending on the requirements for the final device. Depending on whether the front electrode is the anode (normal geometry) or the cathode (inverted geometry) the metal has to have the appropriate work function (high work function for holes and low work function for electrons).

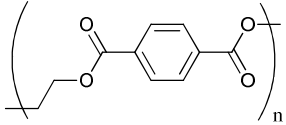
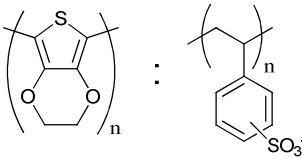
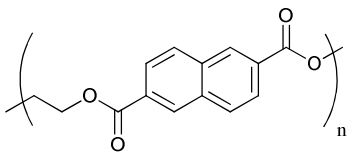
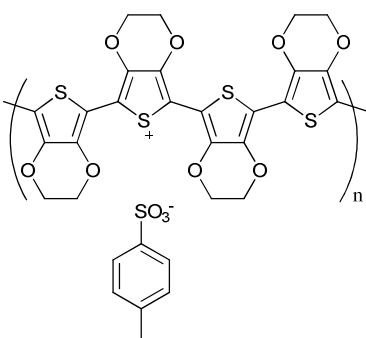
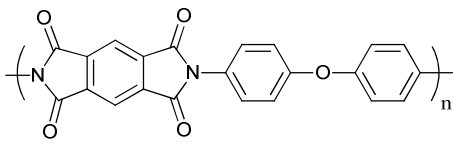
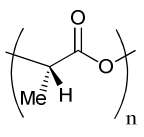
*2.2.1 Materials*

When it comes to the substrates and transparent electrodes used in the field of organic solar cells, very little deviation in choice is observed. Glass is by far the most reported substrate due to its low cost and stability towards almost any subsequent treatment (heat, chemistry etc.). The rigidity of glass though, together with the need of relative thick substrates



when increasing the size, does not really comply with the goal for plastic solar cells to be thin and flexible. This has in recent years led to more reports where the substrate instead consists of polymeric materials such as polyethyleneterphthalate (PET), poly-ethylene naphthalate (PEN), poly(4,4'-oxydiphenylene-pyromellitimide) (Kapton) which is very heat resistant, and even the biodegradable poly-L-lactide (PLLA) [3-7]. The chemical structures of these materials are shown in table 2.1.

**Table 2.1.** Chemical structures of alternatives to the glass as substrate and ITO as transparent electrode.

Substrates	Transparent Electrodes
	
PET	PEDOT:PSS
	
PEN	(VPP-PEDOT)
	
Kapton	
	
PLLA	

With respect to the transparent electrode Indium Tin Oxide (ITO) has almost exclusively been the only choice, due to its excellent properties as hole-conductor. ITO is rather expensive though, due to the scarcity of Indium which by weight is the main material in ITO. Combined with a growing demand from the expanding market of optoelectronics, which in the near future could render a steady supply of ITO problematic, this generates the need for new transparent semiconducting materials with good conductivity. One promising material which is already used extensively in combination with ITO is the highly conductive poly(3,4-ethylenedioxythiophene):poly(styrenesulfonate) (PEDOT:PSS) [8,9]. Aernouts *et al.* reported results comparable to those of ITO by using PEDOT:PSS as transparent electrode in combination with a metallic silver pattern applied to a PET substrate with at standard photographic technique in order to increase the conductivity [8]. A similar approach was reported by Tvingstedt & Inganäs that used a lithographic metal deposition method to create a silver grid on the substrate prior to deposition of diethylene glycol doped PEDOT:PSS [9]. This provided a device slightly more efficient than a corresponding ITO device.

Vapour phase polymerised PEDOT (VPP PEDOT) is an alternative approach where the PEDOT is *in situ* polymerized by evaporation of 3,4-ethylenedioxythiophene (EDOT) onto the substrate that prior to this treatment has been coated with an oxidant such as Fe(III)-tosylate [10-12]. Another approach which has already been implemented into the conventional Si-based solar cells is the use of doped zinc oxide. Doped with Al [13-16], Ga [17,18], or B [19], the ZnO is usually applied by processes like magnetron sputtering, pulsed laser deposition, spray-pyrolysis or electrodeposition.

As an example of backside illuminated devices Krebs demonstrated an inverted structure with a so called monolitical approach, where solid copper on Kapton together with a thin layer of sputtered Ti were used as substrate/electrode [6]. The electrode does not require

patterning and the cell active area is defined by the back electrode. In addition zinc can possibly be used instead of copper. Another ITO free approach is the use of solution processed silver nanoparticles on PET as substrate/electrode, which also requires backside illumination [5].

### 2.2.2 Processing

Depending on the choice of the material for the substrate/electrode the cleaning techniques might be slightly different, but the standard requirement is to treat the surface in a way that will assure good adhesion of the next. In addition, the first electrode defines the cell area in most cases and therefore requires special patterning. As an example, a patterning and cleaning of a glass/ITO plate for the traditional device is presented below. ITO can be commercially purchased either as a solid thin film or film with desired pattern applied on the substrate (Glass, PET etc.). The typical ITO thickness varies from 80 to 150 nm. The process of patterning the ITO layer is as follows: an ITO covered substrate is masked using adhesive tape or a printable etch resist, exposing the part of the ITO that should be etched. The substrate is then etched using an aqueous solution that is 20% w/w HCl(aq) and 5% w/w HNO<sub>3</sub>(aq) at a temperature of 60 °C. Typical etching times are 120 s. The substrates are then immersed in 5% NaHCO<sub>3</sub>(aq) to remove traces of acid in the adhesive before the adhesive is peeled off. As a next step, the substrate is cleaned by ultrasonication in acetone, isopropanol and Milli-q water for 15 minutes in each solution. The UV ozone treatment of ITO was found to be desirable right before the coating of the next layer (water based PEDOT:PSS solution in this case), as the treatment makes the surface more hydrophilic [20]. For patterning ITO on large scale flexible substrates (in R2R production) the reader will find a description in the chapter 4 and the literature [3]. As for inverted reference cells the final cleaning of the substrate/electrode with

Milli-q water can be omitted, since the next layer is ZnO nanoparticles dissolved in organic solvents such as chlorobenzene, o-xylene acetone, which has a lower surface tension than aqueous solutions.

## 2.3 The first intermediate layer

The insertion of intermediate layers (ILs) with the ability to selectively transport one type of charge (negative or positive) while simultaneously blocking the opposite, decreases the probability of charge recombination. Furthermore intermediate layers can sometimes be used to 'bridge' a mismatch of energy levels between the active layer and an electrode thus improving the alignment of the energy levels. In addition, electrodes have certain degree of roughness (for example ITO), which might result in shunts in the film. The intermediate layer compensates for the roughness and removes some of the shunts. The first IL is a hole or electron conductor if it correspondingly follows after either anode or cathode respectively.

### 2.3.1 Materials for the first intermediate layer

Hole conductors: As electron blocking material the most widely used is PEDOT:PSS [21,22], which, as mentioned in Section 2.1, has been used extensively in combination with ITO. However, recently the use of MoO<sub>3</sub> [23,24] or V<sub>2</sub>O<sub>5</sub> [24] as hole conducting/electron blocking layer has been progressively investigated.

Electron conductors: Implementation of a layer of TiO<sub>x</sub> [25-27] or ZnO [28-31] as first IL has been reported in inverted device structures. Li et al. reached 2.25 % device efficiency using Cs<sub>2</sub>CO<sub>3</sub> [52] as electron conducting IL.

### 2.3.2 Processing of the first intermediate layer

Figure 2.2 shows the energy levels for all the layers in the traditional device and for three possible materials, which have been often reported as hole conducting ILs. One has to take into account that the presented HOMO LUMO values are based on measurements of individual materials. In the case of buried interfaces in multilayer films the energy levels may be change somewhat in position due to the vacuum level shift and dipole effects at the interfaces. In order to efficiently block the electrons coming from the active layer the IL has to have LUMO level significantly higher than the polymer LUMO. For commonly used P3HT polymer LUMO is around 3 eV with respect to vacuum. From figure 2.2 it is clear that all three layers can efficiently block electrons in cases where P3HT is used as absorber. In terms of hole conduction it was shown that in the traditional device all three ILs could efficiently collect the holes from the polymer in the HOMO level and transport it to ITO providing good ohmic contact with the electrode. However, PEDOT:PSS has the highest conductivity among the three materials and therefore device performance is the highest compared to the other two. Since PEDOT:PSS can be dissolved or dispersed in solution, there are a number of ways it can be applied onto substrates including traditional spin coating for small substrate sizes, and printing and coating (for example slot-die coating) for large scale production. For traditional small size device an aqueous dispersion of PEDOT:PSS is spin coated on ITO forming a layer with typical thicknesses of 60 to 100 nm. The film is usually dried on a hot plate at approximately 150 °C for 5 to 10 minutes. PEDOT:PSS has by far been in the leading position among hole conducting materials in terms of processing. Most of the reports on production of  $V_2O_5$  and  $MoO_3$  metal oxide layers are based on thermal evaporation techniques, which allows for the achievement of uniform thin films, but which is an elaborate and time consuming process. Only recently solution processing of  $V_2O_5$  has been reported in inverted device

structures with efficiencies reaching 3.6 % for small devices [33]. In operation PEDOT:PSS is a source of chemical instabilities in the solar cell, which results in a decrease of device lifetime and therefore the substitution of PEDOT:PSS with more stable materials can significantly improve the device stability. In addition, it is a challenge to coat PEDOT:PSS on hydrophobic surfaces such as the active layer of P3HT:PCBM and often the solutions of such a problem requires certain sacrifices of one or more properties of the layer, such as for example conductivity of the PEDOT:PSS. Having different materials with different adhesion properties at hand can solve such hurdles.

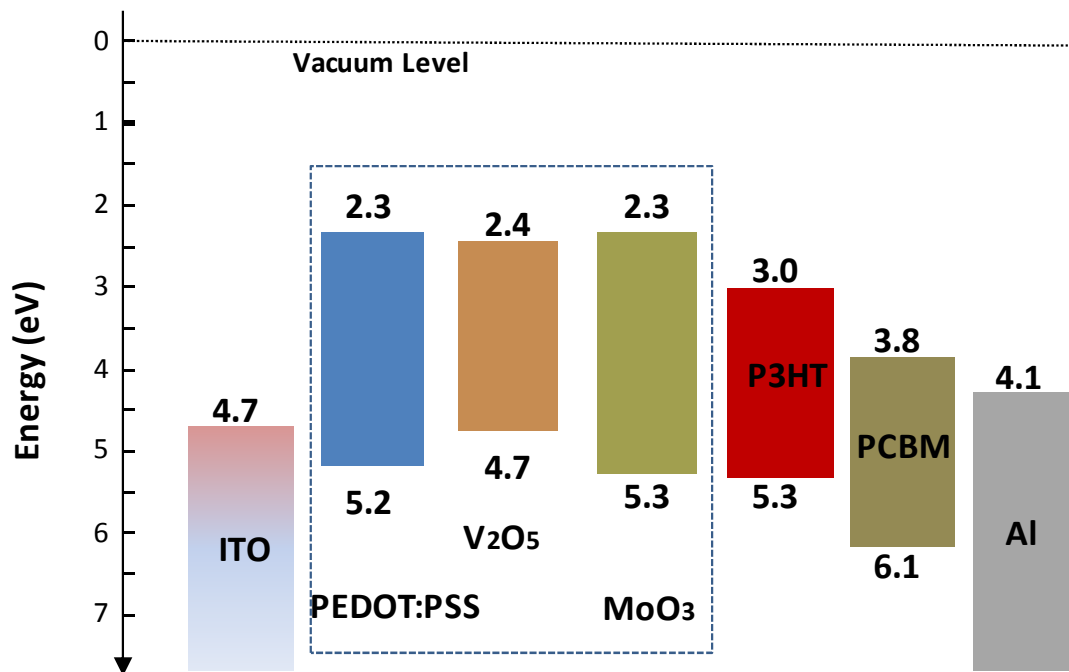


**Figure 2.2:** Energy diagram of a traditional device together with three different options of hole conducting intermediate layers (PEDOT:PSS, V<sub>2</sub>O<sub>5</sub> and MoO<sub>3</sub>)

The inverted structure based solar cells perform almost as well as the traditional device and most of the large scale R2R produced devices are based on inverted structures. In the inverted structure the first electrode is the cathode and electron conducting materials are

therefore used as the first IL. The commonly reported materials are ZnO or TiO<sub>2</sub>. Figure 2.3 shows the energy levels for both materials combined with the other layers of a typical inverted device. From the figure it is clear that both materials can efficiently block holes and can be good electron conductors. The easiest way of processing for these materials is coating using solution based nanoparticles of the metal oxides. The typical range of thickness for the hole blocking layer can vary from a few nm up to a few hundred nm.

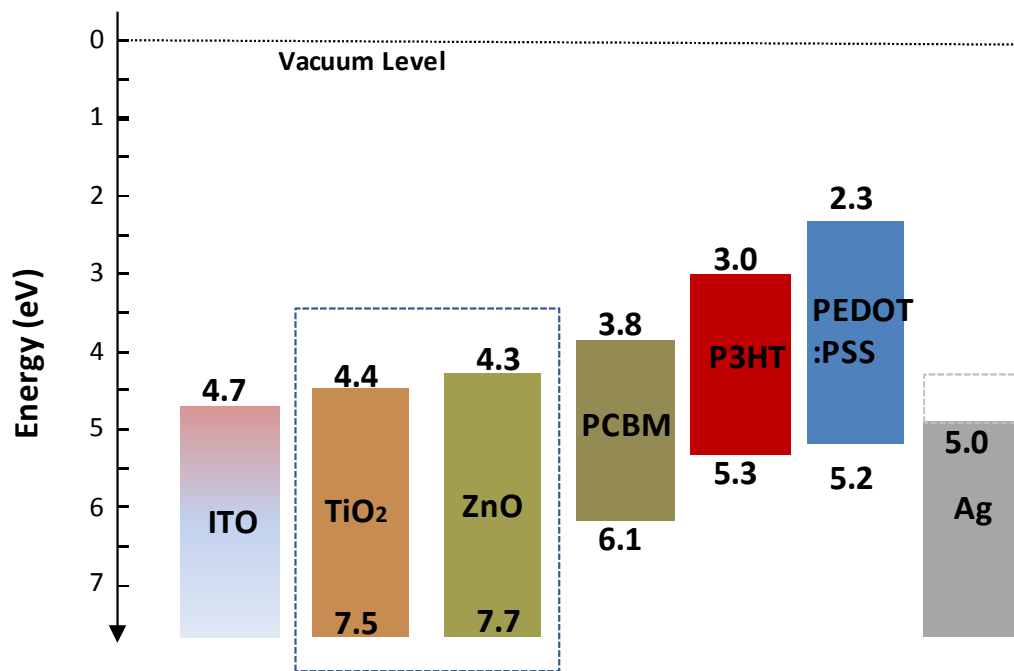


**Figure 2.3:** Energy level diagram of a typical inverted device together with the two different options of electron conduction intermediate layers (marked out in rectangular)

## 2.4 The active layer

Currently the challenge of the OPV field is to develop donor and acceptor materials that when brought together can deliver optimal device efficiencies and will have good stability under different environmental conditions. At the same time the materials have to be abundant, cost efficient and easy to process on a large scale.

While there is currently no such “full package of materials” developed yet, there are countless numbers of reports on different materials that steadily lead to progress. The following subsections outline some of the more successful materials reported so far for OPV device active layers followed by a description of different processing techniques for the active layer.

### 2.4.1 Materials for the active layer

High performance Materials: The ‘kick-off’ for polymer based solar cells happened in 1992 with the first results of photo induced charge transfer from a conjugated polymer to a buckminster fullerene ( $C_{60}$ ) reported by Sariciftci *et al.* [54] and since then the field of polymer/fullerene solar cells has been through a continuous evolution. In 1995 Yu *et al.* showed that charge separation is greatly improved when donor and acceptor materials are mixed in a bicontinuous interpenetrating network.

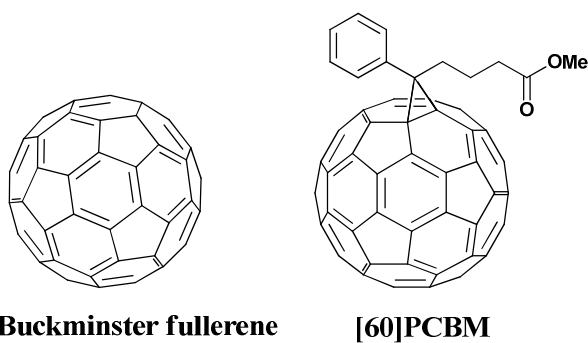


**Figure 2.5:** Molecular structures of Buckminster fullerene  $C_{60}$  and its more soluble counterpart [C60]PCBM.

This reduces the distance necessary for an exciton to travel in order to achieve charge separation at the donor/acceptor interface and thus minimizes back recombination. In their report the bulk heterojunction of the photoactive layer had 2-methoxy-5-(2-ethylhexyloxy)-



polyphenylenevinylene (MEH-PPV) as the electron donor and the soluble fullerene derivative [6,6]-phenyl C<sub>61</sub> butyric acid methyl ester (PCBM) as the electron acceptor (figure 2.5).

From an active layer materials point of view, the state of the art have long been dominated by the bulk heterojunctions prepared from poly(3-hexylthiophene) (P3HT) and the fullerenes [60]PCBM and [70]PCBM. A lot of research has been put into this and efficiencies in the range of 4-5 % have been achieved [1,2,25-27]. It should be mentioned here that the regioregularity of P3HT is quite important for the final performance [38-40]. As shown in figure 2.6 the coupling of two alkyl thiophenes can result in three different combinations.

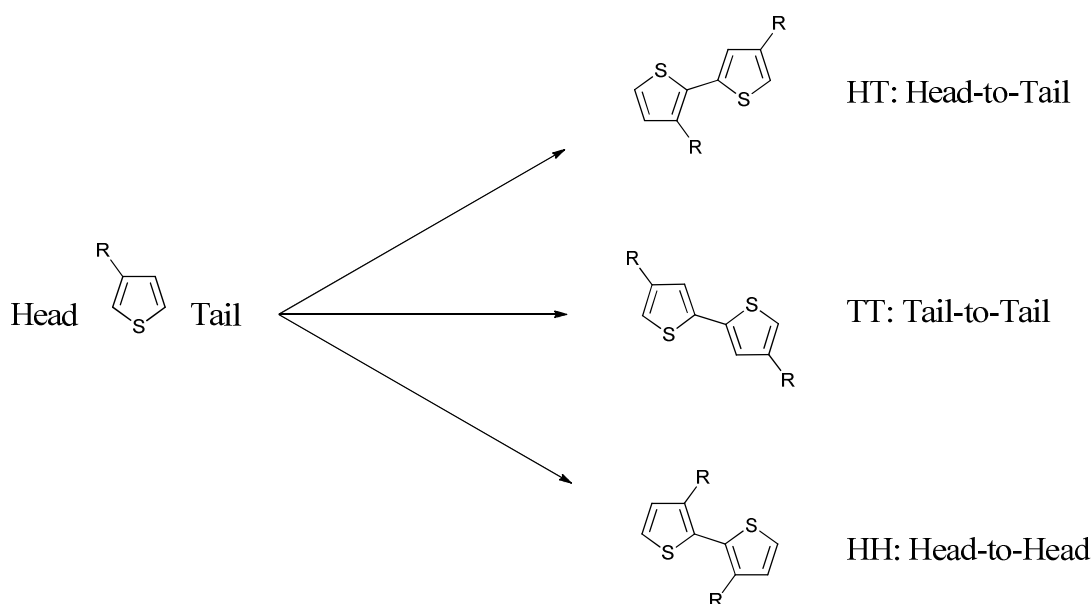


**Figure 2.6:** Regiochemistry of coupling products of two 3-alkyl-thiophenes.

By convention the more sterically hindered 2-position of the thiophene is nominated the “head” (H) of the molecule and the less hindered 5-position the “tail” (T). The regioregular head-to-tail (HT) coupled poly-3-alkylthiophene (PAT) product has a planar structure in solution and generally exhibit a lower  $\pi \rightarrow \pi^*$  transition. This is an indication of a longer conjugation length in the polymer backbone compared to regiorandom PAT (coil like

structure in solution). In contrast to the HT and TT isomer, which can easily access a planar geometry, the sterically crowded HH isomer has an unfavorable planar conformity and thus disrupts conjugation.

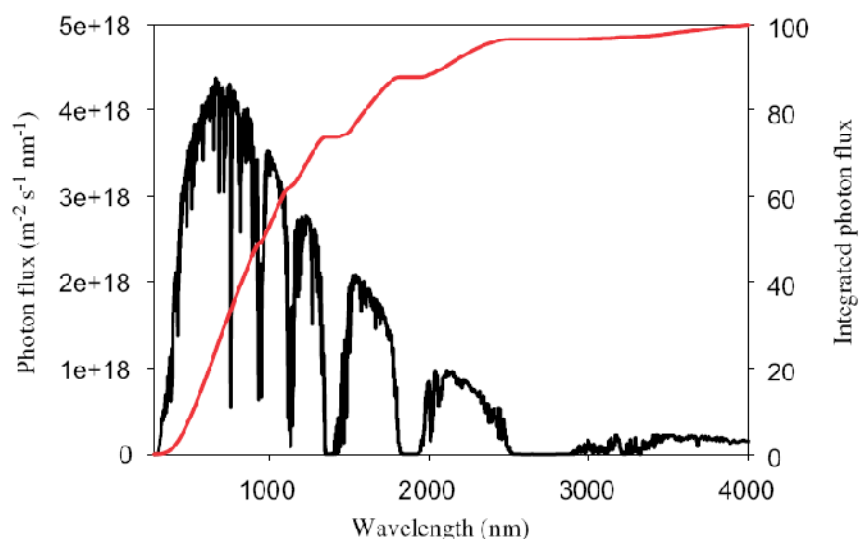


**Figure 2.7:** Photon flux from the sun at the earth's surface ( $1000 \text{ W m}^{-2}$ , AM1.5G) as a function of wavelength. The integral of the curve is shown on the right  $y$ -axis as a percentage of the total number of photons (*reprinted with permission from Elsevier*).

The main disadvantage of P3HT is the poor matching of its absorption spectrum with the solar emission spectrum. Figure 2.7 shows the solar spectrum with the curve of the integrated photon flux. The band gap of P3HT is around 1.9 eV, limiting the absorbance to wavelengths below 650 nm. Since the photon flux reaching the surface of earth from the sun has a maximum of approximately 1.8 eV (700 nm) P3HT is only able to harvest up to 22.4% of the available solar photons [41-43].

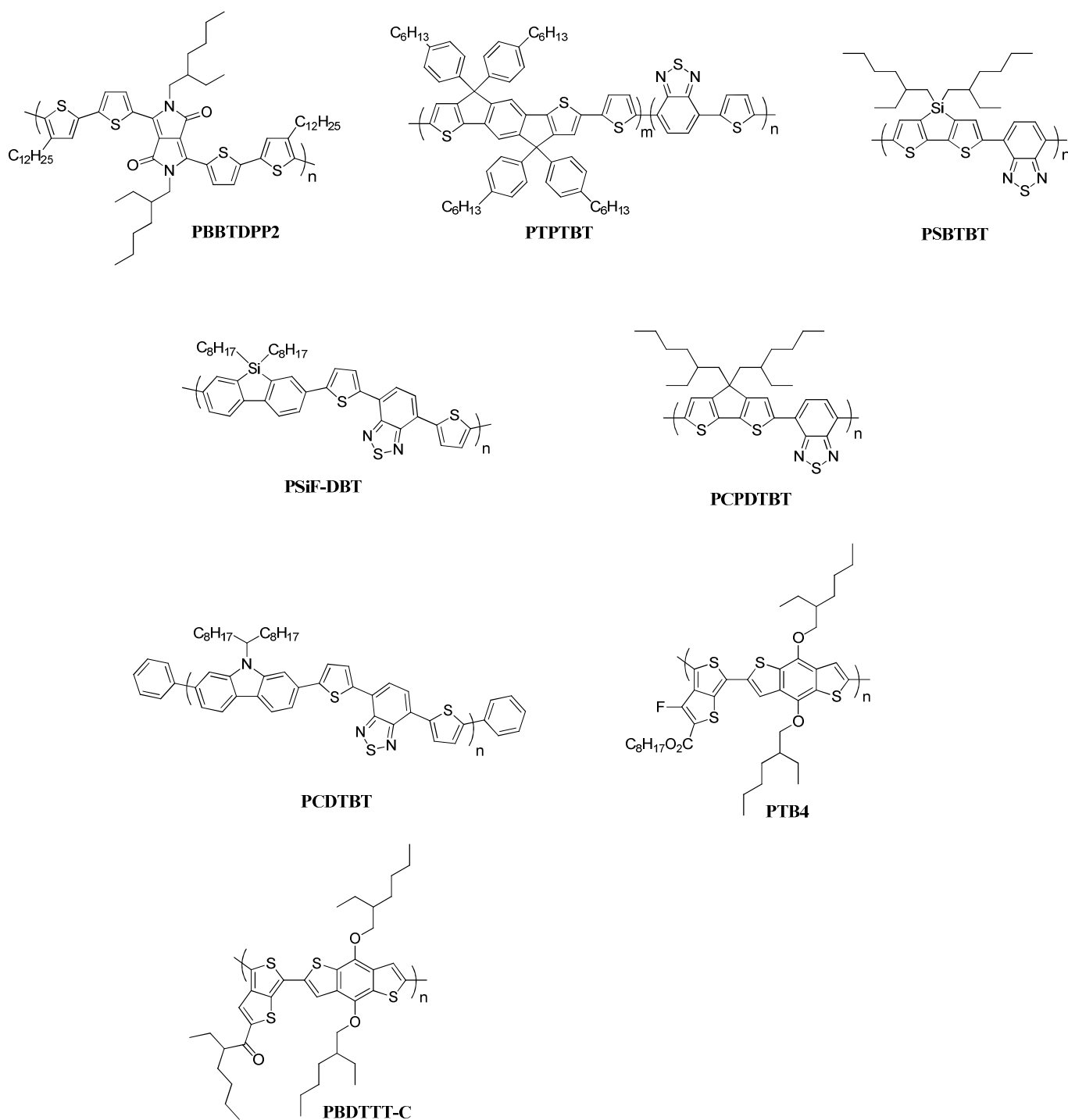
In order to increase the efficiency of OPVs to their optimal value the band gap of the polymer has to be tuned to the light spectrum in the way that it collects the highest number of photons possible. While tuning the band gap of the polymer one also has to take into account that the alignment of the bands of donor and acceptor is necessary to ensure charge separation. The offset of HOMO and LUMO levels between the two materials needs to be at least a few hundred meV in order to efficiently separate the excitons to free carriers with a minimum loss of  $V_{oc}$  [44]. Often this offset is called the exciton binding energy. The voltage of the device is defined by the difference between the energy level of the HOMO in the donor and the energy level for the LUMO in the acceptor. The number of absorbed photons and consequently also the maximum possible current is defined by the lowest band gap of two materials. If PCBM is considered as the acceptor then the optimum band gap of the polymer has been estimated to be in the range of 1.2-1.7 eV.

Decreasing the band gap of the active material allows for absorption of a larger amount of photons with potentially higher power conversion efficiencies as a benefit. The most common approach to preparing low band gap (LBG) materials is to use the donor-acceptor approach where alternating electron rich and electron poor domains are incorporated into the polymer backbone. This allows for partial charge separation of the excitons and generally results in lower band gaps [45]. The greater potential of LBG polymers has led to an increasing interest in these systems and with respect to device efficiency new LBG polymer:PCBM composites have now overtaken P3HT:PCBM with respect to the maximum achievable power conversion efficiency, seemingly with plenty of room for improvement [46-52]. Some of the most promising LBG polymers are shown in figure 2.8 and corresponding device data are listed in table 2.2.

**Table 2.2:** Photovoltaic performance of some novel polymer materials in blends with PCBM. Measurements were performed under AM1.5G conditions at 100 mW/cm<sup>2</sup> unless stated otherwise.

Polymer	Acceptor	$E_g^{\text{opt}}$ (eV)	$V_{\text{oc}}$ (V)	$J_{\text{sc}}$ (mA/cm <sup>2</sup> )	FF	$\eta$ (%)	Ref.
PBBTDPP2	[70]PCBM	1.4	0.61	11.3	0.58	4.0	[51]
PTPTBT	[70]PCBM	1.70	0.80	10.1	0.53	4.3 <sup>b</sup>	[50]
PSBTBT	[70]PCBM	1.45	0.68	12.7	0.55	4.7 <sup>b</sup>	[46]
PSiF-DBT	[60]PCBM	1.82	0.9	9.5	0.51	5.4 <sup>c</sup>	[52]
PCPDTBT	[70]PCBM	1.46	0.62	16.2	0.55	5.5 <sup>b</sup>	[48]
PCDTBT	[70]PCBM	1.88 <sup>a</sup>	0.88	10.6	0.66	6.1	[49]
PTB4	[60]PCBM	1.63	0.74	13.0	0.61	6.1 <sup>d</sup>	[47]
PBDTTT-C	[70]PCBM	1.61	0.70	14.7	0.64	6.58 (6.3 <sup>b</sup> )	[53]

<sup>a</sup> Retrieved from ref. [54]. <sup>b</sup> Average value. <sup>c</sup> Achieved under AM1.5G conditions at 80 mW/cm<sup>2</sup>. <sup>d</sup> Value after spectral correction.



**Figur 2.8:** Chemical structures of some of the promising low band gap polymers.

Among the more promising LBG polymers is the poly[2,6-(4,4-bis-(2-ethylhexyl)-4*H*-cyclopenta-[2,1-*b*;3,4-*b'*]-dithiophene)-*alt*-4,7-(2,1,3-benzothiadiazole)] (PCPDTBT, see figure 2.8) which has a structurally locked planar cyclopentanedithiophene (CPDB) as the donor unit combined with a benzothiadiazole acceptor unit. This results in a band gap of 1.46 eV [48]. Initial reports by Zhu *et al.* showed PCEs up to 3.5% for PCPDTBT/[70]PCBM bulk heterojunction solar cells and with a overall high external quantum efficiency (EQE) in the range of 400-800 nm (above 25%) with a maximum around 700 nm (38%) [55]. Optimisation of the processing conditions by adding a few volume percent of alkanethiol to the process solution of PCPDTBT:[70]PCBM improved the PCE to 5.5% through altering the heterojunction morphology [48]. A remarkably high short circuit current (16.2 mA/cm<sup>2</sup>) was furthermore achieved. A silole analogue to PCPDTBT, where the bridging aliphatic carbon in the CPDT unit has been replaced by Si (PSBTBT, see figure 2.8), has also showed promising results [46]. PCEs up to 5.1 % have been achieved for solar cells based on PSBTBT:[70]PCBM blends, and PSBTBT itself has shown hole mobility of  $3 \times 10^{-3}$  cm<sup>2</sup>/(V s) which is 3 times higher than that for PCPDTBT.

Recently there have been several claims for the lead position with respect to PCE. First Park *et al.* reported a PCE of 6.1% for a bulk heterojunction solar cell based on a blend of the polymer poly[*N*-9'-hepta-decanyl-2,7-carbazole-*alt*-5,5-(4',7'-di-2-thienyl-2',1',3'-benzothiadiazole) (PCDTBT, see figure 2.8) and [70]PCBM [49]. PCDTBT is based on a 4,7-dithienylbenzothiadiazole unit and a soluble carbazole unit that gives it a optical band gap around 1.88 eV. The high result is thus not a result of a low band gap, but instead a product of the high voltage of the device (0.88V) which is achieved through a low HOMO level of the polymer. The latter is probably due to the presence of carbazole unit which are known to have low HOMO levels. What is especially interesting by these results is that the authors achieved

close to 100% internal quantum efficiency, which shows it is possible to prepare active layers for polymer solar cells where nearly all charge carriers are collected.

Shortly after this publication the result of 6.1% (after spectral correction) was matched by Liang *et al.* using a low band gap polymer PTB4 (Figure 2.8) and [60]PCBM. PTB4 has a dialkoxy-benzodithiophene as a donor unit and a thieno[3,4-*b*]thiophene ester as an acceptor resulting in a optical band gap around 1.63 eV [47]. Fine tuning of the structure and electronic properties has been done by introducing electron-withdrawing fluorine to the thieno[3,4-*b*]thiophene unit, which reduces the HOMO energy level of the polymer.

Using a polymer with the same basic structure as Liang *et al.* but with a no flourine and a ketone instead of an ester on the thieno[3,4-*b*]thiophene unit, PBDTTT-C (Figure 2.8), a further fine tuning of the energy levels was achieved by Hou *et al.*, boosting the efficiency to 6.58% [53].

In summary, the development in photovoltaic performance for the selected novel polymer materials (table 2.2) shows that with respect to efficiency the field of organic photovoltaics have entered a new stage where a lot of energy is put in to development of new polymers opposed to the previous stage where the work was mainly focused on optimization of the P3HT:PCBM system. Nevertheless, further improvements in efficiency are required for large scale commercialization, and aside from the power conversion efficiency, processing and stability are two other important aspects that have to be addressed with equal intensity for the success of polymer solar cells. To combine all three parameters into a useful technology further research in device science and new materials are needed.

### 2.4.2 Stability by solubility switching

One way to increase the stability of organic solar cells is to render the active layer less soluble/more rigid. The softness of the active layer is causing a lot of the degradation processes that organic solar cells are prone to [56] (a description of stability issues is also described in the next chapter). Two ways of doing this by solution processable precursors is to use either thermocleavable [56-69] or cross-linkable [70-72] materials. The general principles of the two methods are shown in figure 2.9, where insolubility is induced *post* film formation either by removal of the solubilising side chains or by interconnection of the molecules in the bulk.

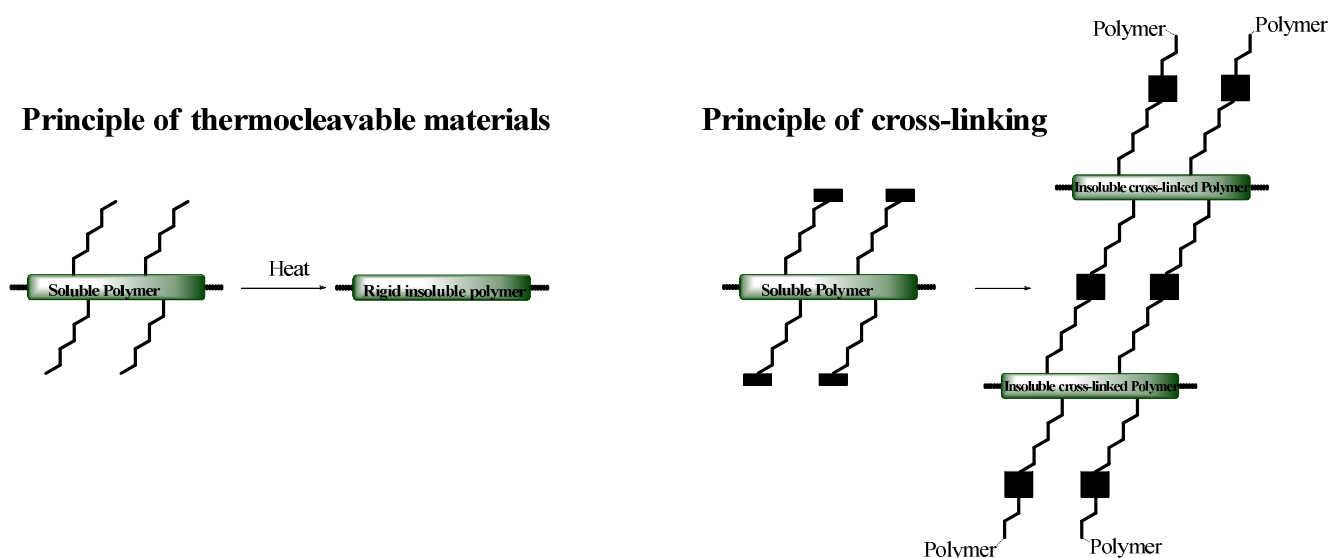


**Figure 2.9:** The general principles of thermocleavable materials where the side chains of the polymer are cleaved by thermal treatment *post* film formation resulting in an insoluble film (left). General principle of cross-linking after film preparation, where the *post* treatment causes the polymer molecules to react with each other thus increasing the ‘molecular size’ with decreased solubility as a result (right).



On important aspect to both principles is that they open up the possibility of creating multilayered structures by sequential processing. After rendering the first layer insoluble a subsequent layer can be applied as the insoluble layer is no longer influenced by the processing.

The use of thermocleavable materials addresses not only the issue of stability, but also the issue of optimisation of device performance by removal of non-absorbing material from the active layer. As most of the polymer solar cell production is based on solution processing, it requires for the materials to be soluble. Native polythiophene (PT) for example is an insoluble material and in order to achieve solubility, solubilising side chains such as alkyl groups are attached onto the conjugated polymer backbone. However, after thin film formation there is no need for side chains anymore as they make up a significant proportion of the polymer (in the case of P3HT, the hexyl groups account for 50% of the material weight) and are passive in terms of light harvesting and charge transport. In addition, the side chains make the material soft, which affects the morphological and chemical stability of the active layer [73,74]. As a consequence, devices based on materials with side chains can be rather unstable, while films that at a final stage do not have solubilising chains can form a more rigid and stable morphology, which can lead to an increase of the glass transition temperature of the material and therefore to thermally stable devices [56,58,73]. The use of thermocleavable ester groups is one possible path to achieve such properties. A route to native PT by solution processing followed by thermal cleavage was suggested by Bjerring *et al* after solid state studies on the thermal behaviour of a polythiophene with carboxylic ester groups that can be removed thermally [57]. Following this proposed route, photovoltaic devices based on PT was later prepared from the thermocleavable poly-(3-(2-methylhex-2-yl)-oxy-carbonyldithiophene) (P3MHOCT, figure 2.10) by Gevorgyan *et al*. [72]. Using solution processing to prepare the

device film and subsequent thermal cleavage to perform the chemical conversions they achieved a PCE of 1.5% for a PT:[70]PCBM device, which shows that decent efficiencies can be achieved by the method. In addition the photocurrents of the devices showed quite stable performance in time and were studied for more than 500 h. The use of thermocleavable P3MHOCT in solar cells was first reported by Liu *et al.* who showed that it converts into poly-3-carboxydithiophene (P3CT) at temperatures of  $\sim 200$  °C through elimination of 2-methylhexene (See Figure 2.10) [66].

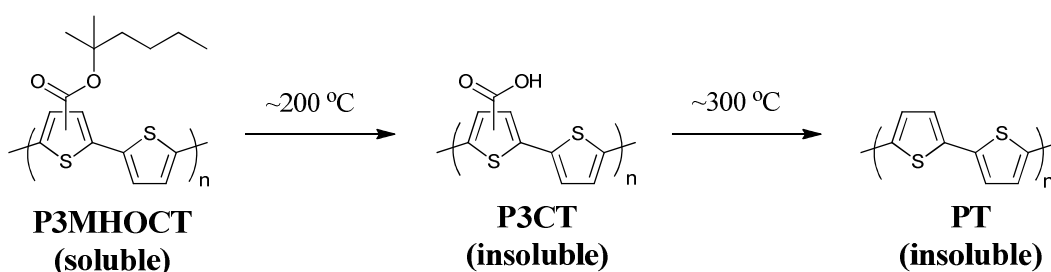


**Figure 2.10:** Preparation of native polythiophene through thermocleavage of P3MHOCT.

It was later shown by  $^{13}\text{C}$  labelling studies and solid-state NMR that P3CT could be further converted to PT at temperatures of  $\sim 300$  °C by decarboxylation (figure 2.10 and 2.11) [57]. The two distinct weight loss mechanisms are clearly visible by thermogravimetric data for P3MHOCT in the temperature range 25–475 °C (figure 2.11) showing first the weight loss from ester cleavage at 200 °C and then the second decarboxylation weight loss at 300 °C. During the annealing, it is furthermore possible to visually see the color change of the sample from red to orange (conversion from P3MHOCT to P3CT) and then from orange to purple-red (conversion from P3CT to PT) (figure 2.12-a). The UV-vis absorption spectra of P3MHOCT and [60]PCBM or [70]PCBM mixtures are shown in figure 2.12-b. It shows a significant change of

the absorption coefficient at different temperatures. In addition a small red shift of the peaks (at 500 nm) can be seen when the samples were heated up to 310 °C.

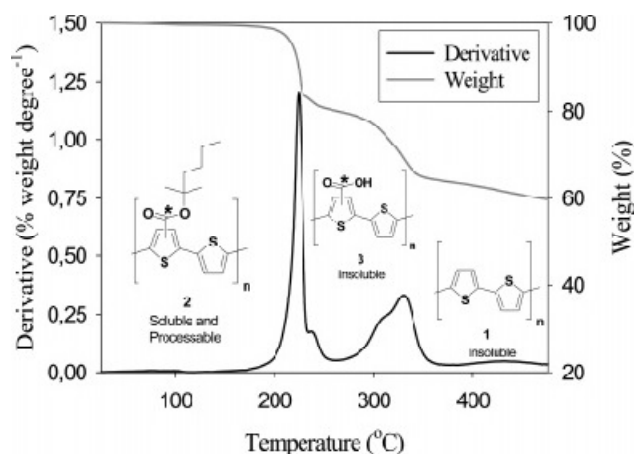


**Figure 2.11:** Thermogravimetric data for P3MHOCT in the temperature range 25-475 °C. Reprinted with permission from ref. [57] (Reprinted with permission from the American Chemical Society).

Some examples of low band gap thermocleavable polymers have been reported [60,64,67], but generally the use of thermocleavable conjugated polymers has been rather limited due to the relatively low efficiencies achieved when used in solar cell devices. It should be stated though, that even with the limited amount of research that has been invested in thermocleavable materials for OPV the efficiencies approaching 2% have been reached. Combined with the enhanced stability of thermocleaved polymer devices the technology shows a promising potential. In addition to the thermocleavable materials described above other examples have been described in the literature. These are summarized in table 2.3.

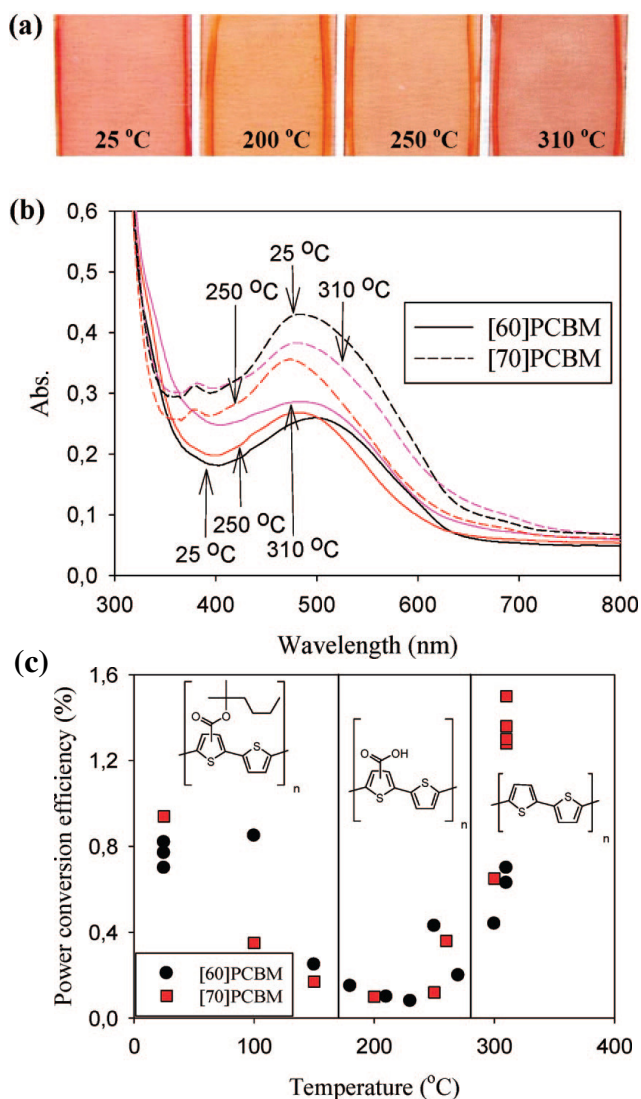
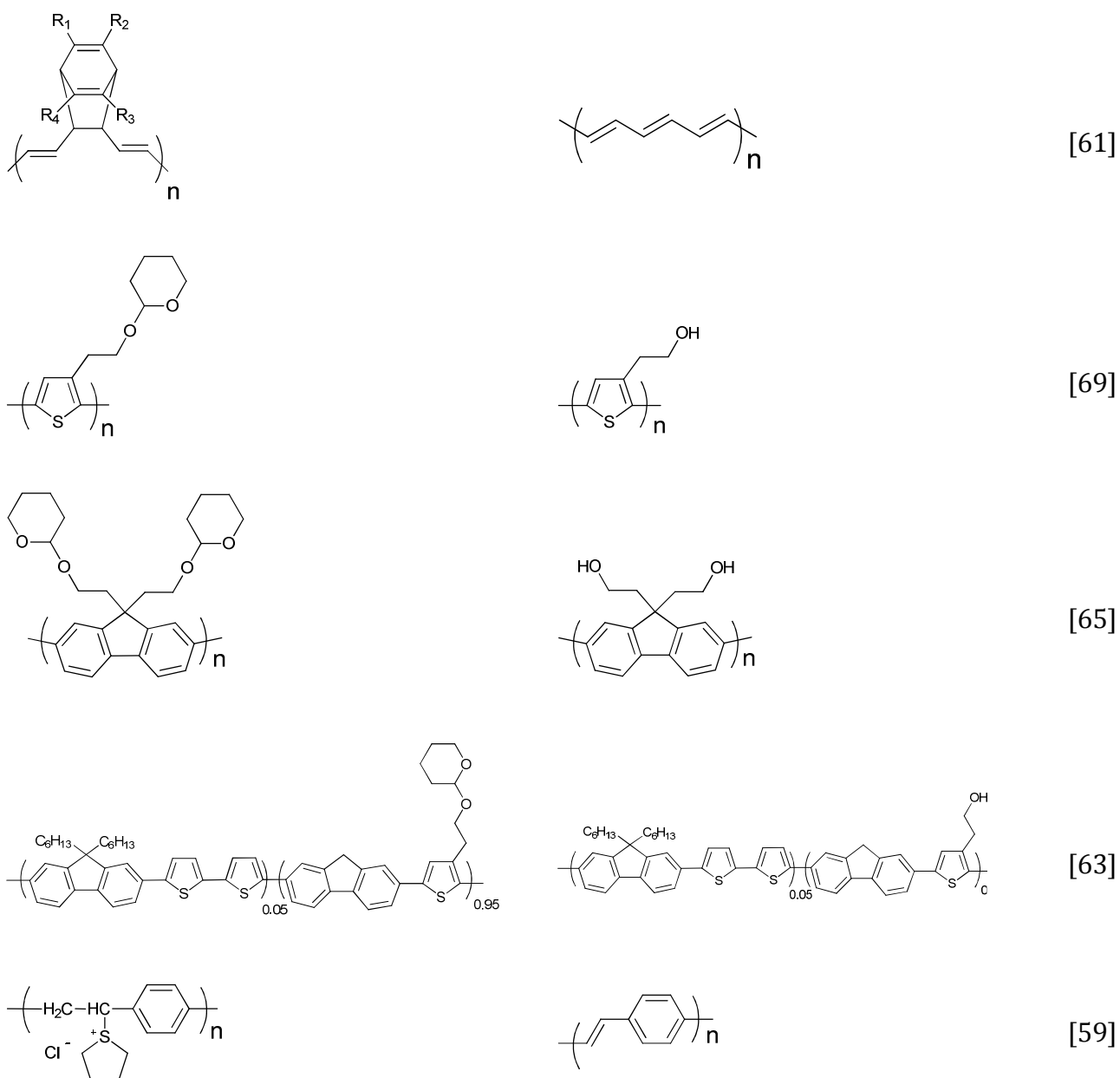


**Figure 2.12:** (a) A photograph showing the appearance of films based on P3MHOCT:[70]PCBM when heated to different temperatures. (b) UV-vis spectra of films based on P3MHOCT and [60]PCBM or [70]PCBM mixtures spincoated on glass slides and annealed at three different temperatures (25, 250, and 310 °C). (c) Efficiency versus annealing temperature for bulk heterojunctions based on P3MHOCT and [60]PCBM/[70]PCBM. Reprinted with permission from ref. [62] (Reprinted with permission from the American Chemical Society).

**Table 2.3:** List of different thermocleavable materials

Precursor	Polymer	Reference
		[64]
		[67]
R = 2-heptyl/5-nonyl/2-methyl-3-hexyl/2-methyl-2-hexyl		
		[60]
		[60]
		[68]



The approach of using cross-linkable materials to enhance stability does not have the advantage of ridding the active layer of non-absorbing material, but still approaches the issue of stabilization. Several investigations of the most widely used bulk heterojunction of P3HT/PCBM with a special focus on thermal stability have shown a drastic drop in performance due to morphological changes where large aggregations of PCBM appear in the films upon prolonged thermal treatment [75-79]. This was approached by Zhu *et al.* and Drees

*et al.* who both succeeded in suppressing PCBM aggregation by use of a fullerene derivative containing a glycidyl functionality (PCBG, figure 2.13) [70,71]. Bulk heterojunctions cross-linked by Lewis acid catalysis showed enhanced morphological stability upon heating. Unfortunately the efficiencies dropped considerably compared to similarly prepared non-cross-linked P3HT:PCBM devices.

Another approach to cross-linking of the active layer was recently published by Miyanishi *et al.* who prepared a cross-linkable analogue of P3HT, poly(3-(5-hexenyl)thiophene) (P3HNT), where the hexyl group in P3HT is substituted with a 5-hexenyl substituent [72]. Prolonged heating of the spincoated films led to cross-linking resulting in an enhanced insolubility towards chloroform. After annealing for 10 h devices prepared with P3HNT:PCBM showed a suppressed deterioration of the PCE (3.03% before annealing, 1.74% after annealing) compared to a similarly prepared P3HT:PCBM device (3.11% before annealing, 1.00% after annealing).

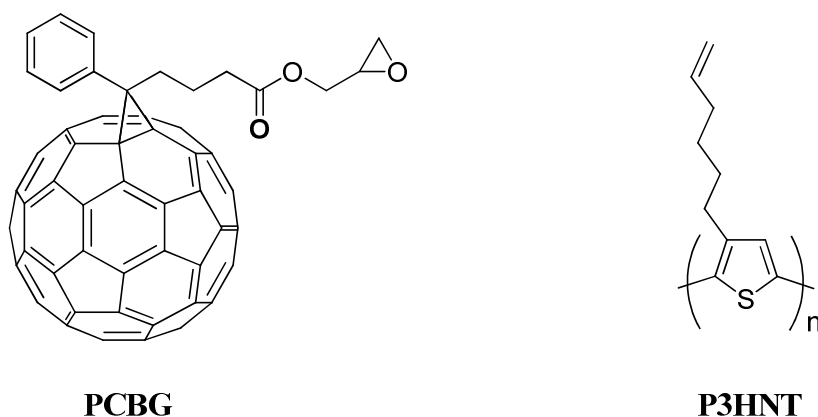


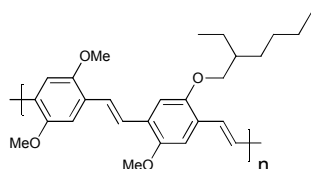
**Figure 2.13:** Chemical structures of the cross-linkable analogues of PCBM and P3HT.

#### 2.4.3 Polymer-Polymer solar cells as a potential way of fine tuning of energy levels

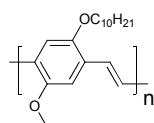
It is noteworthy that the development of new polymers seems to be a field of rising interest, their application is still bound to the use of fullerenes as the n-type component of the

heterojunction. The result of this is that polymers like PCDTBT, having close to 100 % IQE, have very little room for further optimisation. Some research has been performed in tuning the energy levels of fullerenes [80] but there is a general need for finding new n-type materials in order to be able to fine tune the donor acceptor energy levels. Potentially the 'champion' donor polymer might already exist – it just needs to be combined with the right acceptor in order to realize its full potential.

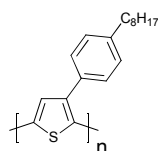
### p-type polymers



**M3EH-PPV**

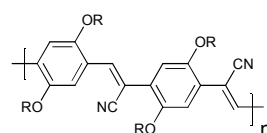


**MDMO-PPV**

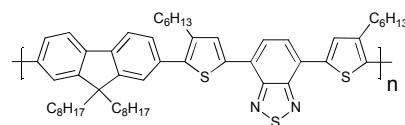


**POPT**

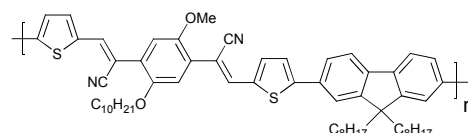
### n-type polymers



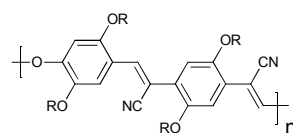
**CN-PPV**



**F8TBT**



**PF1CVTP1**



**CN-Ether-PPV**

**Figure 2.14:** Donor (p-type polymers) and acceptor (n-type polymers) materials previously reported for polymer-polymer solar cells



The use of a second conjugated polymer material as the acceptor in the photoactive layer was first reported back in the mid 1990s. The photoactive layers were prepared from blends of MEH-PPV and CN-PPV (figure 2.14), with MEH-PPV acting as the donor and CN-PPV as the acceptor material. Since these initial reports only moderate attention has been paid to polymer-polymer solar cells and only modest performance results (up to ~1.8% PCE) [81] have been achieved. This is despite the fact that polymer-polymer based donor acceptor materials potentially have several advantages to offer. While in the case of polymer:PCBM devices the polymer is the key absorber of light, since PCBM absorption has very little overlap with the solar emission spectrum. This has been partially solved by using [70]PCBM which absorbs more light [82] but [70]PCBM is still not a good absorber. On the other hand a blend of two conjugated polymers could exhibit a high optical absorption coefficient and enable absorption of solar light over a wider spectral range. In addition to this, the tuning of donor-acceptor energy levels should be fairly uncomplicated with polymers as electron acceptors because of the flexibility in design of the materials. The key issue in order to commence studies of such systems is the development of new n-type conducting polymers with acceptor properties at a level that can compete with those of fullerenes. One of the best performing polymer-polymer solar cells have been reported by McNeill *et al.* achieving a PCE of 1.8 % by using a blend of P3HT as the donor component and poly[(9,9-dioctylfluorene)-2,7-diyl-*alt*-[4,7-bis(3-hexylthien-5-yl)-2,1,3-benzothiadiazole]-2,2-diyl] (F8TBT, figure 2.14) as the n-type polymer [81]. The efficiency is somewhat lower than the state of the art polymer-fullerene solar cell by a factor of 3–4, but higher efficiencies should be reachable if the spectral overlap of the two polymers could be reduced, resulting in a wider spectral coverage. Other achievements of relatively high efficiencies have been reported for polymer-polymer

composites based on POPT:CN-PPV, MDMO-PPV:PF1CVTP1 and M3EH-PPV:CN-Ether-PPV (figure 2.14) [83-85].

#### *2.4.4 Processing of the active layer*

As was already mentioned in the introduction section the active layer can be a single layer, double layer heterojunction or bulk heterojunction. Since the latter has proven to be the most efficient one, we will focus only on bulk heterojunction.

As was shown in the previous section a broad selection of materials is used as donor and often the processing conditions vary from one material to another. As an example the carrier mobility can be different for various materials, which can affect the ratio of the bulk mixture. If the charge transport throughout the cell is not balanced (the mobilities of electrons and holes are different) then there will be an accumulation of charges during transport (the device becomes space charge limited), which leads to recombination losses [86,87]. Thus in order to avoid such accumulation the distance that separated charges need to cross to be collected at the electrodes needs to be changed in a way that it compensates the mobility difference. For example in the case of poly(phenylene vinylene) (PPV):PCBM blend the mobility of the hole is one order of magnitude lower compared to the electron mobility [86]. As a result the optimal ratio between PPV based polymers and PCBM in terms of performance is 1:4 (with higher concentration of acceptor the electrons on average have to cross longer distance to reach electrode, which compensates the mobility difference). While for the P3HT:PCBM blend in the traditional device the mobility ratio is close to unity and therefore the optimal ratio is around 1:1 [1].

Due to the growing number of materials produced for PV applications it is nearly impossible to describe the processing of each of them in detail. For that reason, this section

will focus on processing of polythiophene based materials as donor and fullerene derivatives as acceptor as a general guiding for active layer processing, while the readers interested in processing of particular materials of non polythiophene nature can use the literature provided in the materials section.

The relation of the short circuit current density  $J_{sc}$  with the number of absorbed photons is given by the following equation:

$$J_{sc} = \frac{hc}{e} \int_{\lambda_1}^{\lambda_2} \frac{P_{in}(\lambda)EQE(\lambda)}{\lambda} d\lambda \quad [6]$$

where  $h$  is Plank's constant,  $c$  is the speed of light in vacuum,  $e$  is the electric charge,  $\lambda_1$  and  $\lambda_2$  are the limits of the active spectrum of the device,  $P_{in}$  is the incident photon flux,  $EQE$  is the external quantum efficiency. In the case of absorbing layer of P3HT:PCBM with an EQE of 100 % from 280 to 650 nm the theoretical maximum value of  $J_{sc}$  will be 16.8 mA/cm<sup>2</sup> (when illuminating with 1000 W m<sup>-2</sup> and AM1.5G). However in reality the absorbing layer cannot collect all the light with 100 % efficiency, since some of the light will be reflected or absorbed by other layers. Dennler et al. reports (figure 2.15) that the number of photons absorbed by the active layer versus the thickness of the layer together with the  $J_{sc}$  (on the right axis in figure 2.15). In this case the device structure is glass (1 mm)/ITO (140 nm)/ PEDOT:PSS (50 nm)/P3HT:PCBM/Al (100 nm). In order to efficiently evaluate the amount of light being absorbed by the active layer the spatial distribution of the electromagnetic field across the device needs to be calculated. It is realized using so-called transfer-matrix formalism (TMF) [88-92]. The refractive indexes used for this calculation can be found elsewhere [93]. One can see from the figure that the number of absorbed photons generally increa with increasing layer thickness, but not monotonically. If the thickness is in the same range as the light wavelength then interference occurs, because the light is reflected by the opaque electrode.

Thus the maximum of the interference pattern needs to spatially overlap with the active layer to provide the highest absorption probability by the active layer. In the case of a 5  $\mu\text{m}$  thick active layer with an average internal quantum efficiency (*IQE*) of 100%, the maximum achievable  $J_{sc}$  value will be 15.2  $\text{mA}/\text{cm}^2$ , or approximately 20% less than in the theoretical consideration. In the case of more realistic 400 nm thickness, the maximum  $J_{sc}$  (*IQE* = 100%) is 12.8  $\text{mA}/\text{cm}^2$ . In the case of more practical average *IQE* values of 80 % (for P3HT:PCBM)  $J_{sc}$  comes down to 10.2  $\text{mA}/\text{cm}^2$ . Thus, while building an OPV device one has to bear in mind that in order to achieve the optimal current for a given device it is necessary to thoroughly design the optimal layer structure/thickness.

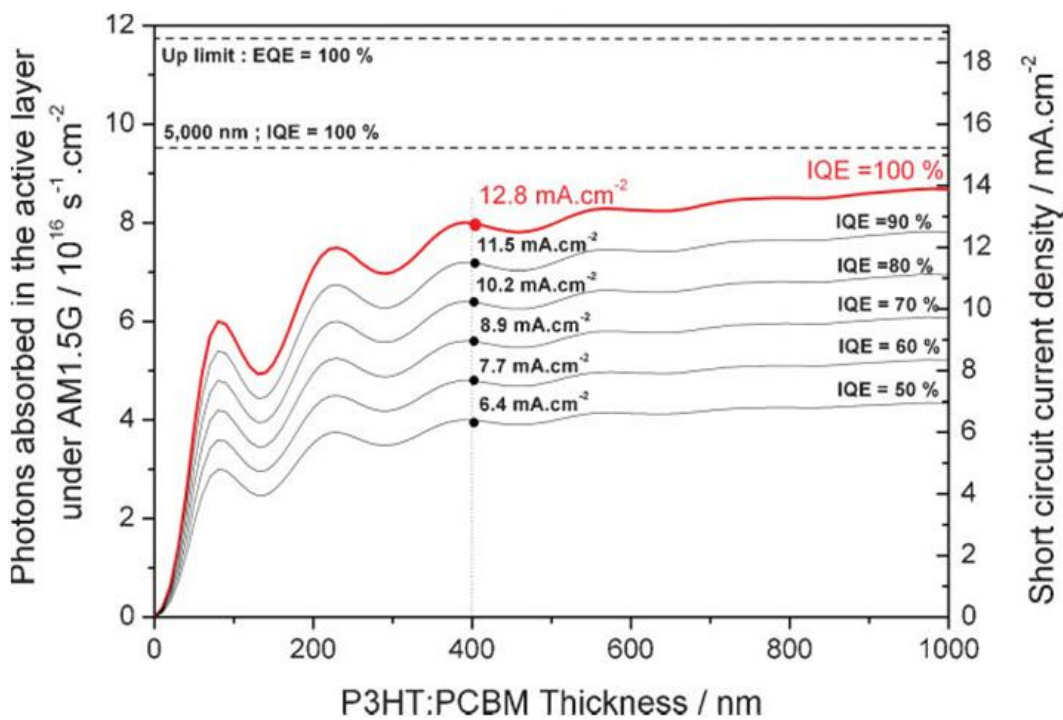


**Figure 2.15:** Number of photons absorbed in the active layer calculated by TMF, for a device having the following structure: glass (1 mm)/ITO (140 nm)/PEDOT:PSS (50 nm)/P3HT:PCBM (x nm)/Al (100 nm). The right axis represents the corresponding short-circuit current density  $J_{sc}$  at various *IQE*, indicated in the graph. Reprint from Dennler et al. (reprinted with permission from Wiley).

The photoactive blend can be coated in different ways. The most common approach for small size devices is spin coating, which can provide very good thickness and morphology. The drawbacks of spin coating is that a significant amount of material is lost while spin coating and the technique is applicable only for small size devices ( $\leq 10 \text{ cm}^2$ ) For larger scale production printing and coating (slot-die coating) techniques are applicable, which will be discussed in chapter 4. For traditional devices the general process of active layer production is as follows: a solution of P3HT:PCBM with a combined concentration of 20 to 40 mg/ml with approximately a 1:1 ratio is prepared using chlorobenzene (CLB) or dichlorobenzene (DCB) as solvent by stirring on a hot plate for few hours at 60 °C. The solution is then spin coated on top of the first intermediate layer. In some cases filtering of the solution with micro filters is beneficial. The desired thickness of the layer can be achieved by controlling the speed and the concentration of the solution. Often there is a possibility to improve the film morphology for polythiophene based materials by special treatments, which can significantly improve the film absorption and carrier conduction properties. A few such treatments are presented below:

#### *2.4.5 Thermal processing to alter the morphology*

One way to improve the performance of devices based on polythiophene is post-production thermal treatment, which can drastically change the structure and the morphology of the material [94,95]. The treatment is realized by simply annealing the complete device on a hot plate. Especially P3HT has the property to crystallize when the temperature is increased above the glass transition temperature (or melting temperature).

An example of significant improvement of the external quantum efficiency by post-production heating of the device with polythiophene based donor and fulleropyrrolidine as acceptor was shown by Camaioni et al. (figure 2.16) [96]. In addition, a remarkable red shift of the absorption of the active layer of the device is also observed after the thermal treatment (figure 2.16).

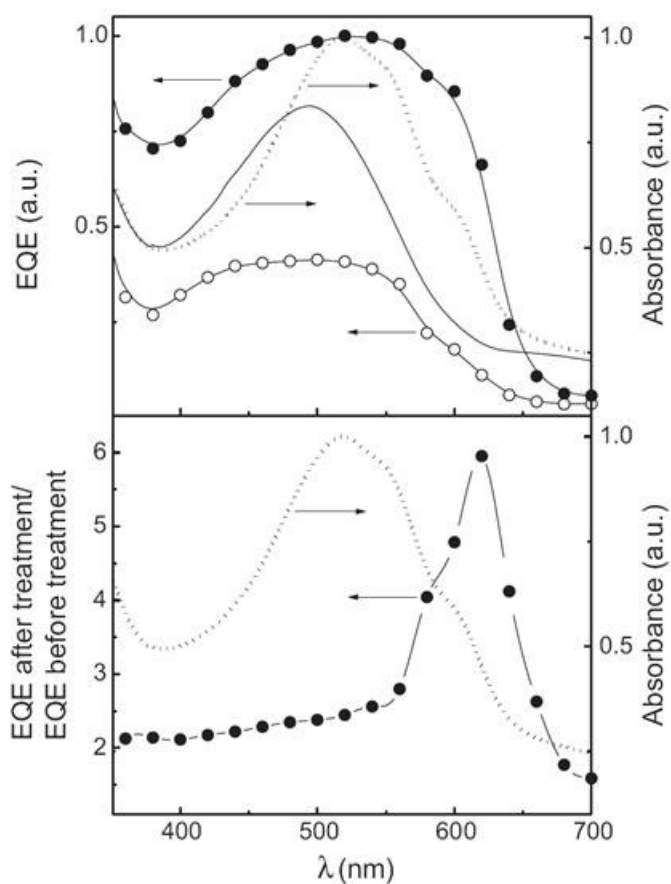


**Figure 2.16:** Absorption spectra of spin coated polymer/fulleropyrrolidine films before (solid line) and after (dotted line) the thermal treatment; EQE of spin coated polymer/fulleropyrrolidine films before (open circles) and after (solid circles) the thermal treatment (top). The ratio of the EQE after treatment to that before treatment (solid circles) and the absorption spectrum of the active layer after treatment shown again for better comparison (bottom). Reprint from Camaioni et al. [96]

It has been suggested that the heating induces slow crystallization of the polymer, giving rise to an increase in the hole mobility in the polymer, which significantly decreases the losses due to the charge recombination [97]. Heating causes a decrease in the free volume and in the density of defects at the interface due to the solvent evaporation from the layer, which could improve the morphological structure of the organic active layer [98]. Furthermore, the heating enhances the interaction between the chains in the polymer, which changes the absorption properties of the polymer and improves the morphology [99]. There have been various reports on improvement of the device efficiency by a thermal treatment (see for example [100-103]), but all the best devices reported by different groups have different annealing temperatures for the same polymer materials. It was revealed that the concentration of the acceptor material in the blend, namely the PCBM, has a large influence on the morphology upon annealing [102,104]. During the annealing process, the PCBM clusters grow. Such a phenomenon can improve the phase separation between compounds. However, the overgrowth of the PCBM cluster might lead to larger scales of phase separation, which can decrease the device performance. While being heated the average conjugation length of the polymer is increased due to ordering of the chains into more crystalline structure. This leads to creation of borders around PCBM clusters, which hampers the large-scale growth of PCBM crystals and prevents large-scale phase separation as has been confirmed by transmission electron microscopy (TEM) analyses carried out by Yang et al. (Figure 2.17) [100]. Figure 2.17 shows both the TEM image and the schematic illustration of the network. However, one has to be careful in choosing the concentration of PCBM in the mixture since in case of overweight of PCBM the polymer is not able to control the PCBM growth. As possible evidence, in some cases during the annealing of the devices “bubbles” are formed on the back electrode. The figure 2.18 presents three cells with polymer/PCBM ratios of 5/4, 5/5 and 5/6. The one with

the highest concentration of PCBM (5/6) has the strongest effect of bubble formation, while no bubbles are evident in case of lower concentration of PCBM (5/4).

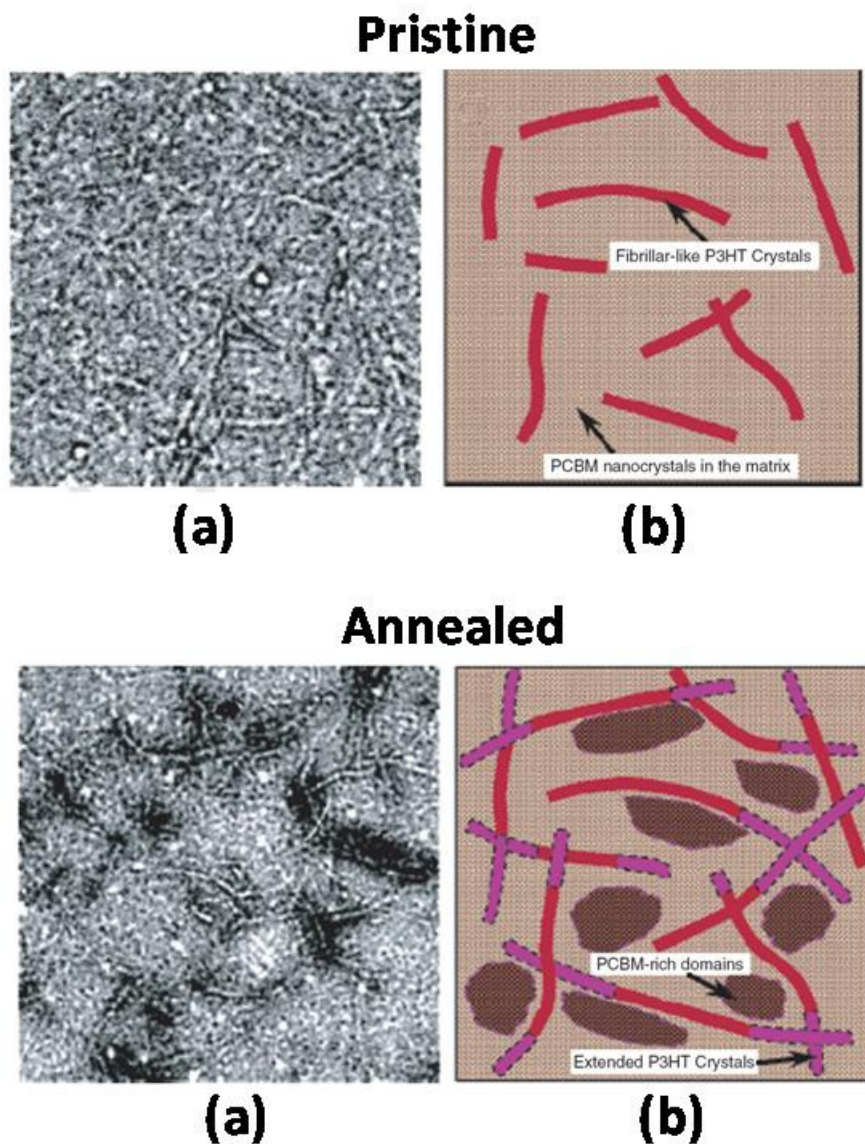


**Figure 2.17:** TEM images (a) and the corresponding schematic representation of the photoactive layer of a P3HT/PCBM polymer solar cell for pristine (top) and annealed (bottom) samples. Note: the dashed line bordered regions in the bottom right image represent the extension of existing P3HT crystals in the pristine film during the annealing step. Reprinted from Yang et al. [100].



In the same experiment the devices based on active solution that had been filtered with micro filter prior to spin coating of the film had a strong bubble formation effect independent of PCBM concentration. This indicates that during filtering certain amount of polymer is lost in the filter resulting in a significant increase of the PCBM concentration. No changes have been recorded in morphology of MDMO-PPV/PCBM films during annealing, because MDMO-PPV does not crystallize upon thermal treatment [105]. For that reason the annealing of PPV based devices generally do not show any performance improvement. The ability of polythiophene to crystallize in a particular manner as a function of temperature gives access to nanoscale control of the morphology of the donor-acceptor interpenetrating networks. As a result of such control PCE values in excess of 5% have been reported [2].

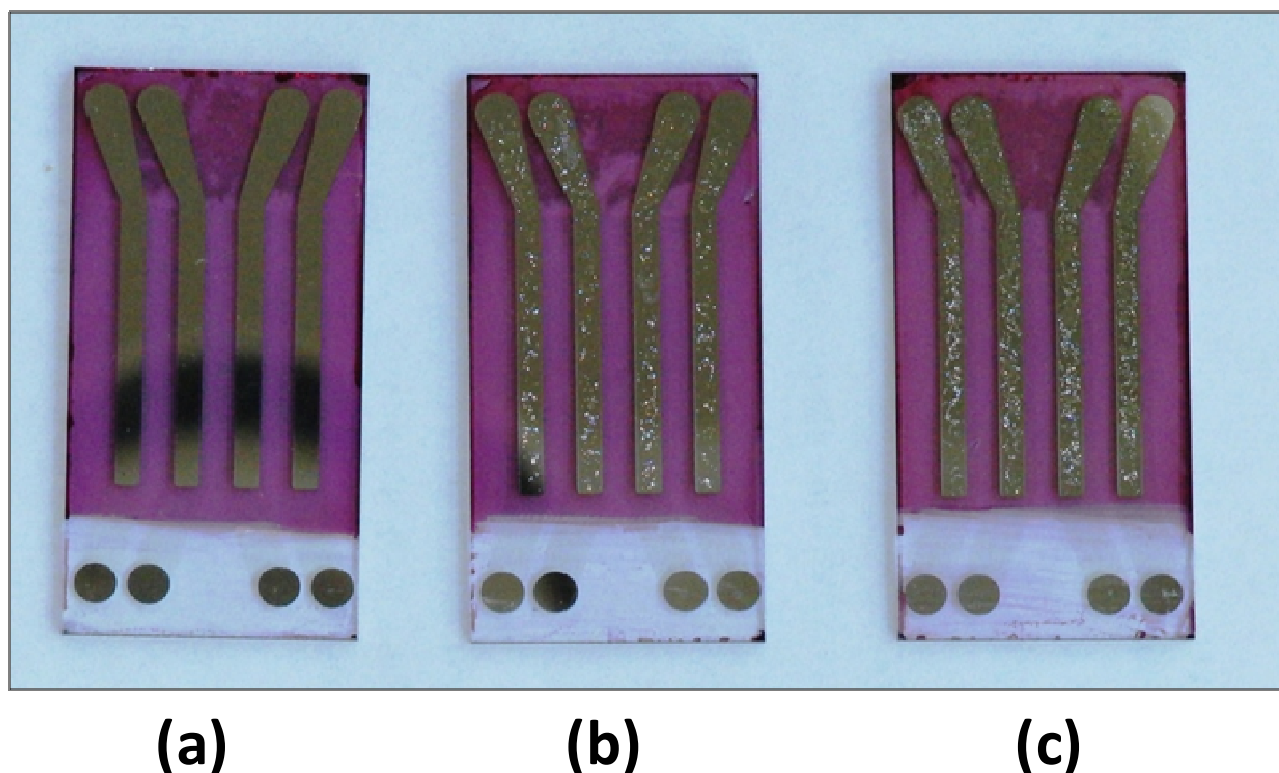


**Figure 2.18:** The image of the back side of devices with following layers: Glass/ITO/PEDOT:PSS /P3HT:PCBM/Al. The ratio of P3HT/PCBM is (a) 5/4; (b) 5/5; (c) 5/6.

Post-production annealing can also influence the interface between the active layer and the Al electrode. Studies showed that annealing improves the interfacial adhesion between the layers, which can drastically improve the charge collection at the interface [2]. Another advantage of post-production thermal treatment is that the annealing can stabilize the morphology to some extent, which improves the stability of the devices [100]. When the molecular weight ( $M_w$ ) of the polymer is considered the picture becomes slightly more complicated. The lower is the molecular weight fraction (or chain length) of the polymer the lower will be the mobility [106-108]. However, it was found that smaller  $M_w$  fractions facilitate the growth of the crystallinity, while higher  $M_w$  stay amorphous [106-108]. Too long molecular chains produce highly entangled structure and therefore make the annealing harder [109]. The optimum  $M_w$  is found to be in the range of 30 000 – 70 000 with polydispersity of around 2, which provides low  $M_w$  units for good crystal structure growth and high  $M_w$  units for interconnecting the crystalline units and creating optimal network.

As mentioned in the materials section, the regioregularity (RR) (the percentage of monomers adopting a head-to-tail configuration, rather than a head-to-head) of the polymer also has a significant impact on the device performance. A threshold of around 95% for RR seems to be necessary optimal device performance because of better transport of highly RR P3HT [110,111].

#### *2.4.6 Solvent vapour treatment to alter the morphology*

Another way to improve the photovoltaic performance of thiophene-based polymer devices is to alter the morphology of the polymer thin films by so-called solvent annealing or solvent vapor treatment. Solvent annealing is a technique for controlling the slow drying process of

freshly spin-coated films in a controlled atmosphere, which in some cases contains a certain solvent vapor. This technique has been explored generally since the 1980s for different organic material-based thin films [11,112-119]. In the case of polythiophenes, similar to thermal annealing the solvent annealing results in self-organization of the polymer chain structure into an ordered structure. The degree of such self-organization can be controlled by drying conditions of the film. Solvent annealing is realized by placing the films right after the spin coating into an environment with solvent vapour, which slows down the drying process and facilitates the crystal structure growth. Zhang et al. showed that the films of copolymers of substituted polythiophene, PEOPT, extended their absorption spectra towards longer wavelength upon treatment with chloroform vapor for 15 min [115]. The EQE for photodiodes based on the same material was also significantly increased due to the treatment. Similar absorption changes and EQE improvements were reported at a later stage on traditional P3HT:PCBM bulk heterojunction devices by different groups [1,116,117,119]. The more ordered structure of the polymer results in an enhanced conjugation length and hence a shift of the absorption spectrum to lower energies [119,120] which improves the photon absorption and therefore the generated photocurrent. However, the enhancement of optical absorption is not the only reason for the improvement in current. The hole mobility increases due to the self-organization of P3HT during the annealing processes. A time-of-flight (TOF) study conducted by Li et al. on slow and fast-grown films showed (figure 2.19) that the ratio of the mobilities of electrons to holes is close to unity for slow-grown films, whereas for fast-grown films the hole mobility is reduced by an order of magnitude due to the poor order in the structure [1]. As was already discussed above the more balanced charge collection reduces the recombination losses and thus increases the photocurrent.

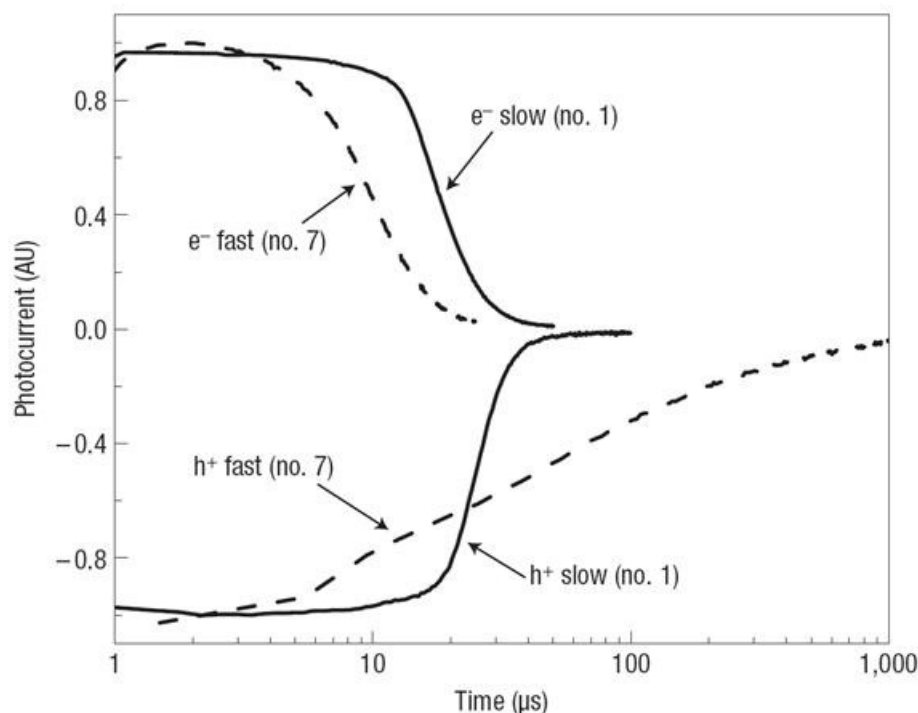


**Figure 2.19:** TOF signals of slow-grown (No. 1) and fast-grown No. 7) films plotted on a semi-logarithmic scale. Note that hole mobility in fast-grown film (No. 7) is significantly lower than electron mobility in the film, and also than the hole and electron mobilities in the slow-grown film (No. 1). Furthermore, the hole transport is dispersive in film No. 7 and the carrier transport is unbalanced. Reprinted from Li et al. [1].

Similar to a thermal treatment in the case of solvent treatment the concentration of PCBM in the bulk has significant impact on crystallinity of the polymer. The excess amount of PCBM molecules act as defect sites and destroy the ordering of P3HT by disrupting the packing of the polymer chains during the solvent removal process.

### 2.4.7 Other methods to control morphology

Often organic solar cells are fabricated on flexible substrates, such as poly(ethylene terephthalate) (PET) and due to low glass transition temperature of PET thermal annealing cannot be applied for such devices. At the same time the technique of solvent vapour annealing is a time consuming process and therefore puts constraints on production speeds and scales. For that reason a number of new approaches have been suggested for improving the morphology, which do not require any further treatment after film formation.

Berson et al. showed that by completely dissolving the P3HT polymer in p-xylene at elevated temperatures and slow cooling to room temperature, the formation of nanofibers of P3HT could be achieved [121]. By blending the nanostructured P3HT with PCBM conversion efficiencies reaching 3.6% were obtained. The nanostructure was reported to remain stable for several weeks.

The requirement for further simplification of the morphology control led to the approach of so-called additives. It was shown by a number of groups that adding certain amount of “unfriendly” solvent in the solution of photoactive blend results in strong aggregation of the polymer, which can lead to improvement of the morphology of the interface. As an example, by adding 4.25% of Nitrobenzene (NtB) in a solution of P3HT:PCBM dissolved in chlorobenzene (CLB) Moule et al. showed that strong aggregation of the polymer takes place, which significantly improves the absorption and PCEs of almost 4% were reported [122]. Li et al. achieved similar results by adding a controlled amount of pure hexane to the P3HT:PCBM blend dissolved in o-dichlorobenzene (ODCB) [123]. In both cases, the preparation of devices without the solvent mixing step and application of post-production treatment led to devices with lower PCEs. In a similar fashion the addition of different alkanethiols led to PCEs over 5 % for the devices based on PCPDTBT:PCBM[70] [48,124]. By adding 2.5% of various additives

Lee et al. achieved efficiencies of over 5.1 % for 1,8-diiodooctane and 4.5 % for 1,8-octanedithiol [124]. It was shown by field effect carrier transport measurements that the electron mobility is enhanced [125], which significantly reduces the recombination. Figure 2.20 present the mechanism of the morphology improvement with the additives according to Lee et al. [124]. The fullerene component is dissolved by the additive, while the polymer is not. As a result the fullerene is removed from the polymer mixture and fine structures of donor rich and acceptor rich domains are created.

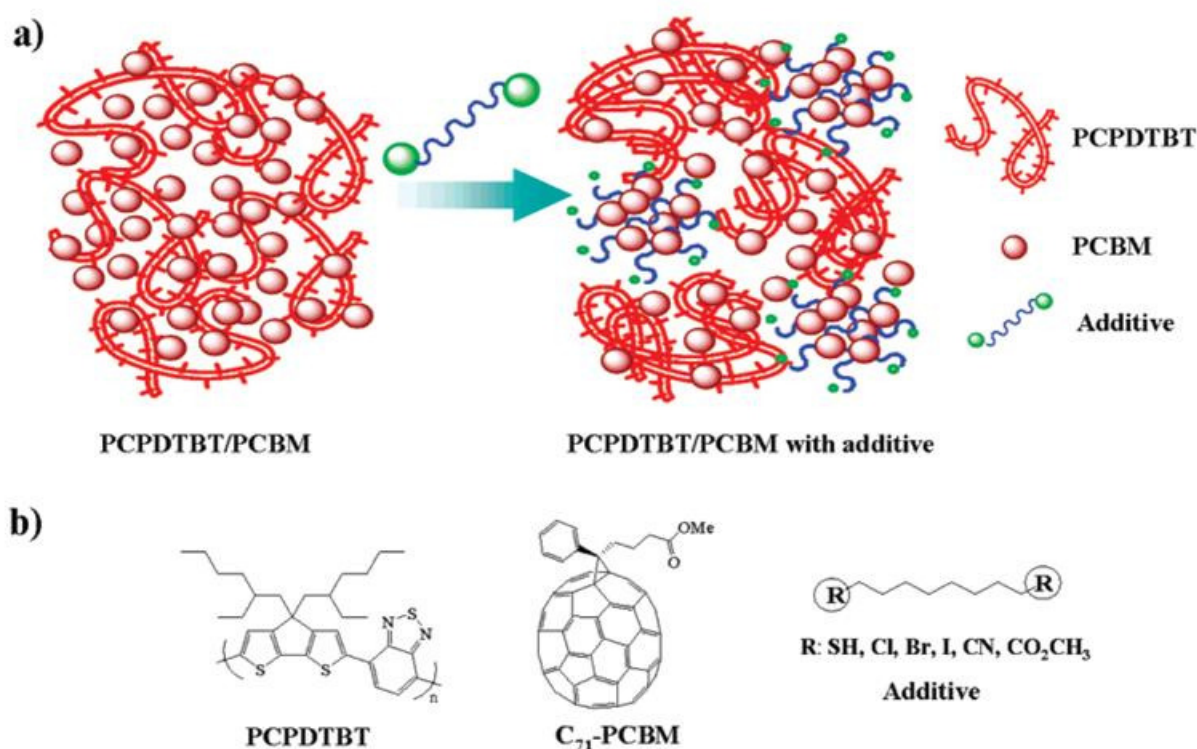


**Figure 2.20:** Schematic depiction of the role of the processing additive in the self-assembly of bulk heterojunction blend materials (a) and structures of PCPDTBT, C71-PCBM, and additives (b). Reprinted from Lee et al. [124].

The effect was confirmed by atomic force microscopy (AFM) images that show an increase of the roughness with additives [48]. In addition transmission electron microscopy (TEM)

imaging showed the formation of the aforementioned domains [124]. The improvement of the morphology with alkanethiols was shown also for P3HT polymers [126]. The additive approach proved to be a very easy and applicable method especially when other methods such as thermal annealing cannot be employed. To summarize, coating of a thin film of active layer using spin coating technique is generally a rather straight forward process, but it does not necessarily provide the optimal morphology. Therefore special pre- or post-production treatments are required to achieve the best morphology interface in the bulk of donor/acceptor.

## **2.5 The second intermediate layer**

For the same reasons as discussed in case of the first intermediate layer (IL) the implementation of the second IL between the active layer and the back electrode can be fruitful in terms of both efficiency and stability. The possible materials used are the same as described for the first IL. What is necessary to bear in mind is that if the first IL is an electron blocking layer then the second IL will be hole blocking and vice versa. However in terms of processing of the second IL there are slightly different requirements compared to the first IL, since the previous layer is the active layer with different surface properties.

### *2.5.1 Materials for the second intermediate layer*

Hole conductors: Similarly to first intermediate layer, PEDOT:PSS has been often used as hole conducting second IL in inverted devices (see for example the literature [3,25,26,29]), but also MoO<sub>3</sub> [30,127] and V<sub>2</sub>O<sub>5</sub> [32,33] have been reported.

Electron conductors: The insertion of a second intermediate layer in the form of TiO<sub>x</sub> [49,128,129] or ZnO [130] between the photoactive layer and the top electrode in the normal

geometry has been shown to improve the overall PCE of the solar cell as will be discussed in the next section. The second IL furthermore acts as a barrier between the external environment and the active layer inducing stability [131].

### *2.5.2 Processing of the second intermediate layer*

When spin coating the second IL on the active layer the wetting properties are different than for the first IL, because the surface properties are now different. For example for typical inverted structure when a PEDOT:PSS layer is to be applied on top of a hydrophobic P3HT:PCBM film it becomes nearly impossible to use water based PEDOT:PSS. As a result a special screen printing formulation of PEDOT:PSS diluted in isopropanol is used. Also the wetting of the active layer surface with isopropanol prior to PEDOT:PSS coating is beneficial. When thermal evaporation techniques are used for application of the second IL layer this is of course not a problem. Often the second intermediate layer is called an “optical spacer”. As already discussed in the active layer section, the combined layer thickness throughout the device is within the same range with the wavelength of the light, which might result in interference of the optical field. Thus, it is important to tune the thickness such that the optical field distribution in the device is such that the interference maximum of the field coincides with the active layer in order to achieve optimal absorption [132,133]. The shifting of the field distribution is realized by an optical spacer, which in most cases is a layer of  $\text{TiO}_x$  or ZnO in normal device architecture [130,132,133]. Figure 2.21 shows the optical field distribution in a traditional device with 40 nm active layer calculated by Gilot et al. using the optical modeling [130]. The group shows that by adding 39 nm ZnO optical spacer the interference maximum is shifted towards the active layer (figure 2.21). However, for certain thicknesses of the active layer the optical spacer might act negatively.



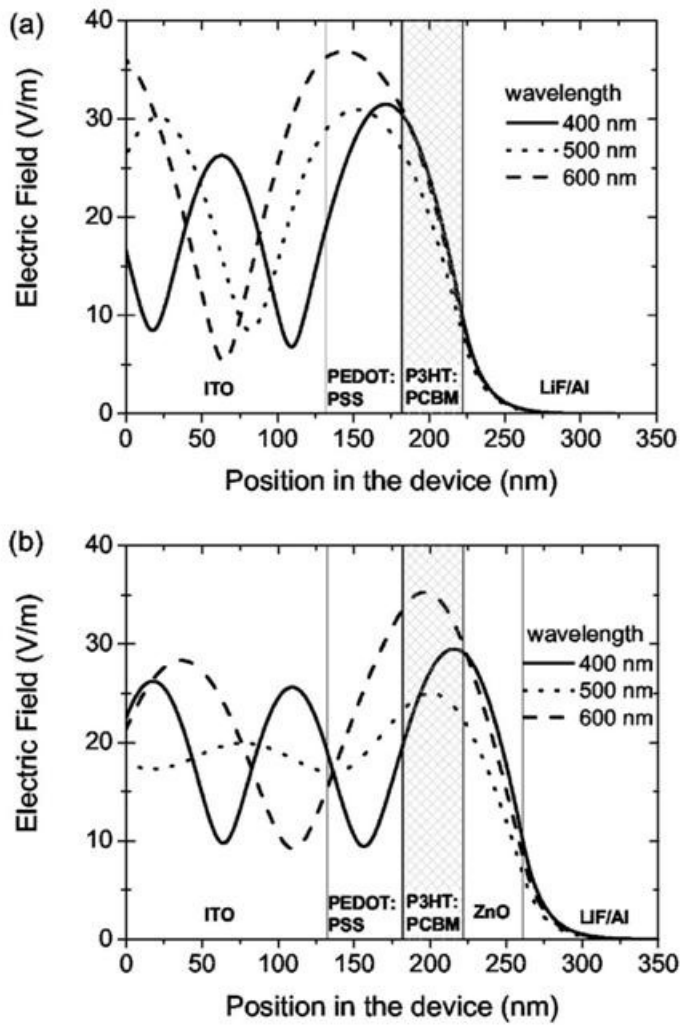


**Figure 2.21:** Calculated optical electric field for light of different wavelengths in devices with a 40 nm thick active layer, (a) without and (b) with 39 nm ZnO. Reprinted from Gilot et al.<sup>[180]</sup>

Figure 2.22 illustrates the short circuit current (100 % IQE is assumed) versus the thickness of the active layer for different ZnO thicknesses calculated by the same group [130]. From the figure it is apparent that careful choice of the optical spacer thickness is required in order to gain rather than lose in generated current.

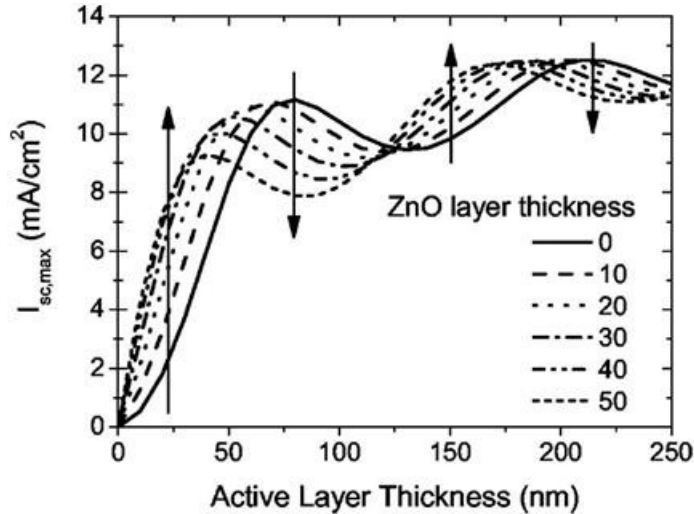


**Figure 2.22:** Calculated active layer thickness dependent short circuit current, assuming a 100% IQE for different thicknesses of the ZnO layer. Reprinted from Gilot et al. [130].

## 2.6 The back electrode

The back electrode is the final layer that completes the device structure. Similar to the front electrode the use of high or low work function metals defines the operation of the back electrode as anode or cathode respectively.

### 2.6.1 Back electrode materials

Depending on the desired work function of the back electrode different metals are used. Aluminium, silver and gold are the most commonly used but also the use of calcium electrodes has been reported. Aluminium electrodes are often applied in combination with a very thin layer of lithium fluoride (2-10 nm) [134]. The positive effect of LiF on device performance is not yet well understood, but LiF is believed to improve the ohmic contact between the electrode and the active layer. During evaporative deposition of the aluminium the LiF furthermore protects the active layer from being damaged by the heat of the evaporated metal. LiF has also been considered as an intermediate layer that blocks holes and conducts

electrons, but it is questionable whether such a thin layer can efficiently act as such. The use of LiF in combination with gold electrodes has also been reported [134]. Similar to LiF, Calcium and C<sub>60</sub>-fullerene have been utilized between the active layer and the metal electrode [74,135].

### *2.6.2 Processing of the back electrode*

Depending on whether the illumination occurs through the front or back side of the solar cell the back electrode can be non transparent, or semi transparent (often metal grids are applied). In the traditional device the back electrode is thermally evaporated Aluminum. The thickness and the rate of the Al evaporation are important for the device performance. Typical reports of Al thickness are in the range of 100 to 200 nm with a typical sheet resistance of 0.2  $\Omega$  square<sup>-1</sup>. The evaporation rate has to be low especially during the beginning of evaporation in order not to destroy the polymer surface. However, it is impossible to establish an optimal evaporation rate for aluminum, since each evaporation setup will have its own characteristics (distance between sample and source, crucibles etc.). If the back electrode is required to have a special grid pattern, a mask with desired pattern is applied during evaporation. For inverted devices, a silver (Ag) electrode is commonly used, which is commercially available as a printing paste. As a result most of the large scale produced devices are based on the Ag paste electrode. The procedure of Ag thermal evaporation is similar to Al evaporation.

## **2.7 Encapsulation**

One of the main issues of OPV field is the device stability as discussed in chapter 3. In this section we only mention that the unprotected devices that are exposed to oxygen and humidity tend to degrade within a short time. For that reason certain encapsulating

techniques are applied to prolong the device lifetime. The rate of transport across membranes is expressed in the oxygen transmission rate (OTR) and the water vapor transmission rate (WVTR). Similar to OLED devices for organic solar cell devices the following requirements were proposed for sufficient encapsulation:  $10^{-3} \text{ cm}^3\text{m}^{-2}\text{day}^{-1}\text{atm}^{-1}$  for OTR and  $10^{-4}\text{gm}^{-2}\text{day}^{-1}$  for WVTR (Figure 2.23) [136,137].

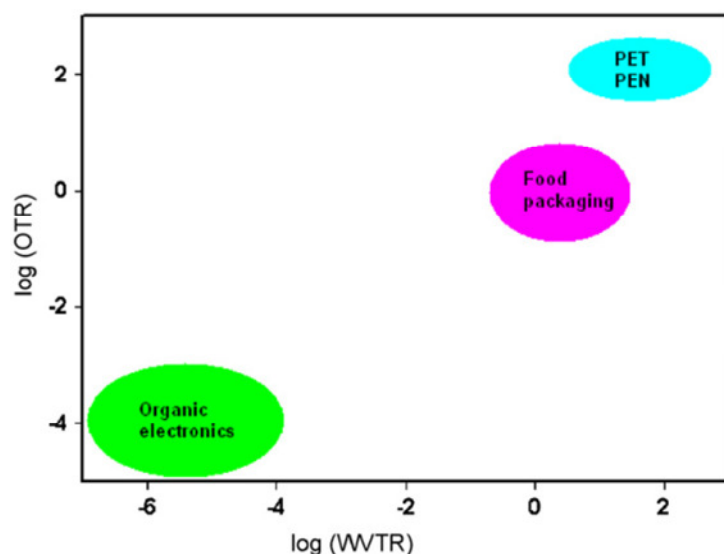


**Figure 2.23:** For commercial polymers (Poly (ethylene terephthalate) (PET) and poly (ethylene 2, 6-naphthalate) (PEN)) and the limits required for food packaging and organic electronics, respectively. Reprinted from Dennler et al. [136,137].

Commercial Poly (ethylene terephthalate) (PET) and poly (ethylene 2, 6-naphthalate) (PEN) polymer films have much higher rates of transport. Certain kinds of food and pharmaceutical packaging also require better barrier properties to avoid oxidation that has led to the development of improved polymer films with in-built barrier layers. These layers may be inorganic oxides deposited by plasma-enhanced chemical vapor deposition reaching permeation levels 1000 times lower than for the native polymer films. Multilayered barrier films consisting of alternating inorganic  $\text{SiO}_x$  and polymer PEN substrates were used to

greatly increase the lifetime of MDMO-PPV/PCBM-type solar cells. Shelf lifetimes of more than 6000 h were reported [136,137]. Commonly the small size devices, which usually are prepared on glass substrates, can for example be simply encapsulated by sealing a plate of aluminum on the glass substrate using glass fibre reinforced thermosetting epoxy (prepreg). The prepreg is knife cut to fit the size of the cell so that the active area is not covered by the sealant. The prepreg is then attached to the back plate and after heating at 80 °C the glass substrate with the solar cell layers is applied on top with mechanical force (a weight is placed on top). The sealant is allowed to thermoset for 12 h. The entire procedure is carried out inside a glove box to avoid any oxygen and water molecules being trapped inside the encapsulated area. This rigid encapsulation can assure very good protection and can possibly prolong the device lifetimes to several years. Such a technique is not flexible and is time consuming, but probably convenient for laboratory scale devices. Other encapsulation techniques include parylene coating in combination with aluminum oxide [138] and cover lids with getter materials [139]. For larger scale flexible encapsulation the reader will find more details in chapter 4.

## **2.8 Different device architectures**

As mentioned earlier there is a need for the organic solar cell society to develop new materials in order to make more efficient and stable devices, but parallel to that there is also a need for innovation and development of new device architecture if the field is to succeed. Besides roll-to-roll manufacturing which is described in chapter 4, some of the more interesting approaches are described below.

Compared to the solar cells based on inorganic semiconductors the single junction polymer devices have one major drawback which is their general narrow absorption window. A possible approach to overcome this and efficiently harvest light at both short and long wavelengths is combining more than one band gap materials/device so that each of these absorbs light from separate parts of the solar spectrum. Such devices are known as tandem cells [140-142]. The common tandem cells comprise a serial connection between two active layers, which helps in significantly increasing the voltage while keeping the current at the same level. Figure 2.23 shows a schematic illustration of the typical tandem cell architecture containing two distinct active layers placed on top of each other interconnected by an intermediate layer in order to prevent charge buildup within the cells. The intermediate layer ensures recombination of the electrons created in the first cell with the holes created in the second cell. In addition, it can act as a protective layer to support the bottom cell during deposition of the top active layer. Each active layer contains both a donor and an acceptor, and the use of materials with different band gaps enables the total absorption over wider spectral range.

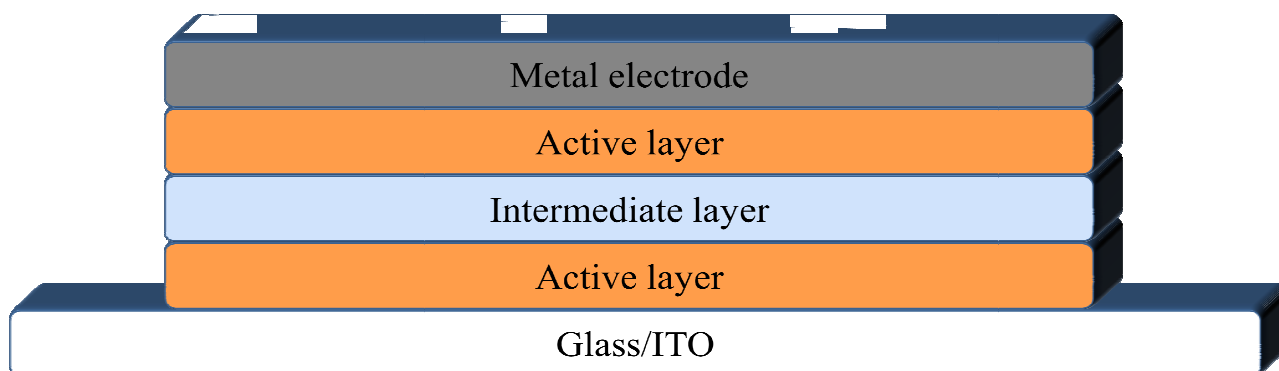


**Figure 2.23:** Typical device buildup of an organic tandem cell.

A number of different groups have reported tandem organic solar cells based on vacuum deposition of small molecules [143-146] or a combination of solution processing and vacuum deposition [147-150]. From an industrial point of view the all solution processable pathway, without the necessity of a vacuum step, is preferable because this allows for high throughput production using techniques like screen printing, ink-jet printing and roll-to-roll coating. The breakthrough in this respect was introduced by Gilot *et al.* who reported the first device where all the active layers were solutions processed (the electrodes were vacuum deposited) [151]. The authors use an approach that relies on using orthogonal solvents for the different layers, in that way that after applying a layer, the solvent used for the next step must not affect the underlying layer. This was achieved by spin-coating a n-type layer of ZnO nanoparticles from acetone on top of the first active layer followed by spin-coated layer of pH-neutralized PDOT:PSS as the hole conducting layer for the subsequent active layer. Figure 2.24 illustrates the architecture realized by Gilot *et al.*

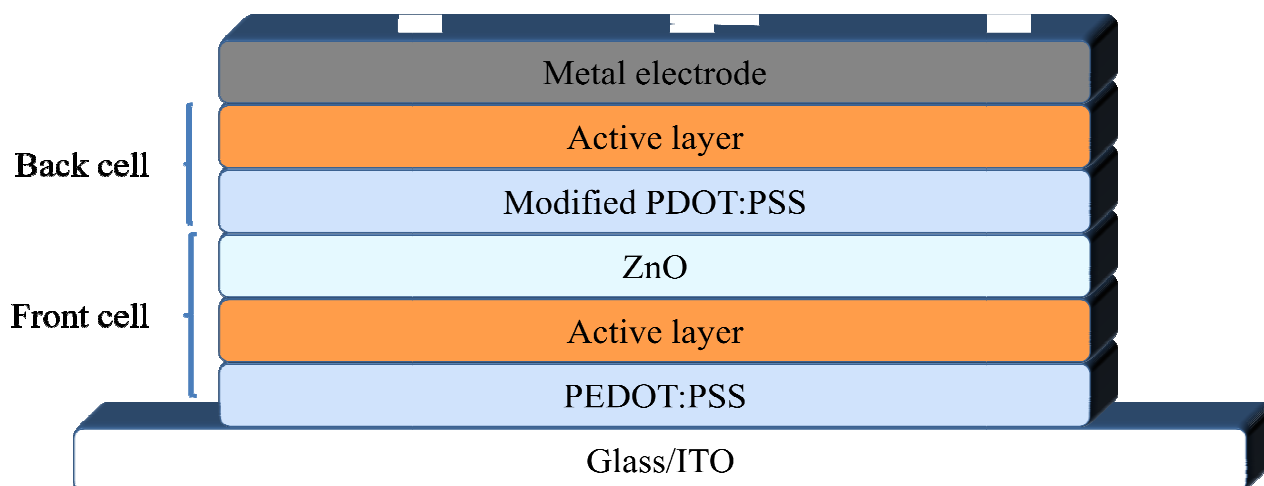


**Figure 2.24:** Device structure of the first all solution processed solar cell reported by Gilot *et al.* [151].

The highest efficiency organic tandem solar cell reported so far is based on solution processed layers and delivers 6.5 % PCE (uncertified), by Kim *et al.* [152]. The recombination layer for this cell was combination of TiO<sub>x</sub> sol-gel and PEDOT:PSS, the bottom cell active layer was PCPDTBT:[60]PCBM and the top cell active layer was P3HT: [70]PCBM. Different fullerene derivatives were used to decrease the absorption overlap between the subcells. Figure 2.25 shows the device layer sequence and the band structure. A doubling of the voltage was observed going from individual cells of PCPDTBT or P3HT to the tandem cell. An all solution based tandem cell using thermocleavable materials was reported by Hageman *et al.* [64] The authors used solution processable precursors that allow for subsequent transformation into an insoluble film by thermocleavage. The bottom cell consisted of a bulk heterojunction of P3MHOCT (see active layer materials) and ZnO, and the a blend of poly-[(3'-(2,5,9-trimethyldecan-2-yl)-oxy-carbonyl)-[2,2';5',2'']terthiophene-1,5''-diyl)-co-(2,3-diphenylthieno[3,4-b]pyrazine-5,7-diyl)] (P3TMDCTTP) and ZnO was used for the top cell. A short thermal treatment straight after film preparation resulted in elimination of the solubilising side chains converting the ester groups into the corresponding carboxylic acids. A recombination layer of PEDOT:PSS and ZnO was inserted between the two active layers. Although the final cell showed relative poor efficiency, the insoluble nature of the active materials after thermocleavage offers a non-solvent dependent route to multilayer structures which will be very advantageous in industrial utilization. The most inventive design in tandem solar cell is the utilization of folded reflective geometry where the non-absorbed light from one cell is directed towards the second one [153-156]. The most obvious advantage of the folded tandem device is that it avoids complex multilayer solution processing and other problems related to multijunction stacking while still being able to exploit the non-absorbed part of the light of one cell in the next.



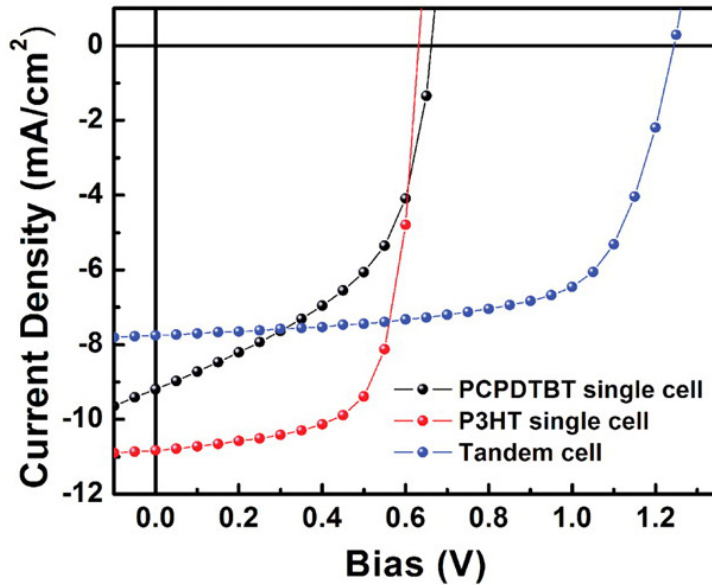
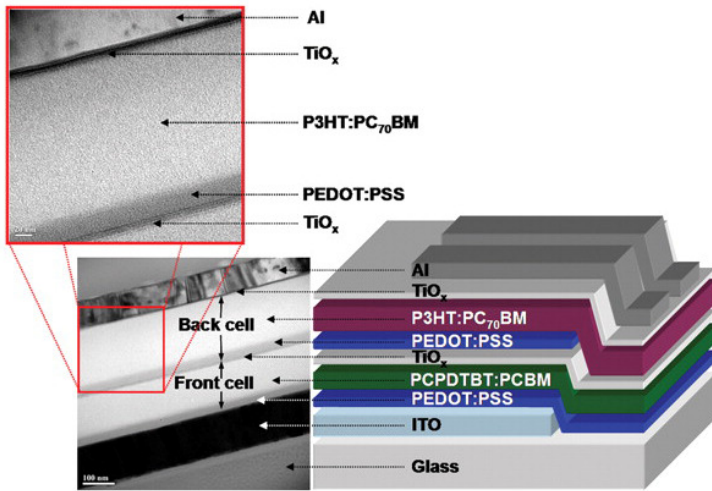


**Figure 2.25:** Device structure and IV characteristics and of the tandem cell realized by Kim *et al.* Reprinted with permission from ref. [152].

Furthermore, as the cell is not facing the light source directly but at an angle, the path of the light through the active layer increases (effectively increases the layer thickness). Finally tilting angles smaller than  $90^\circ$  can create light trapping effect, which can significantly enhance the absorption and therefore the current generation. Tvingsted *et al.* demonstrated an

increase in PCE from 2% to 3.7 upon folding two planar cells with different band gap materials from 0 to 70° (See figure 2.26).

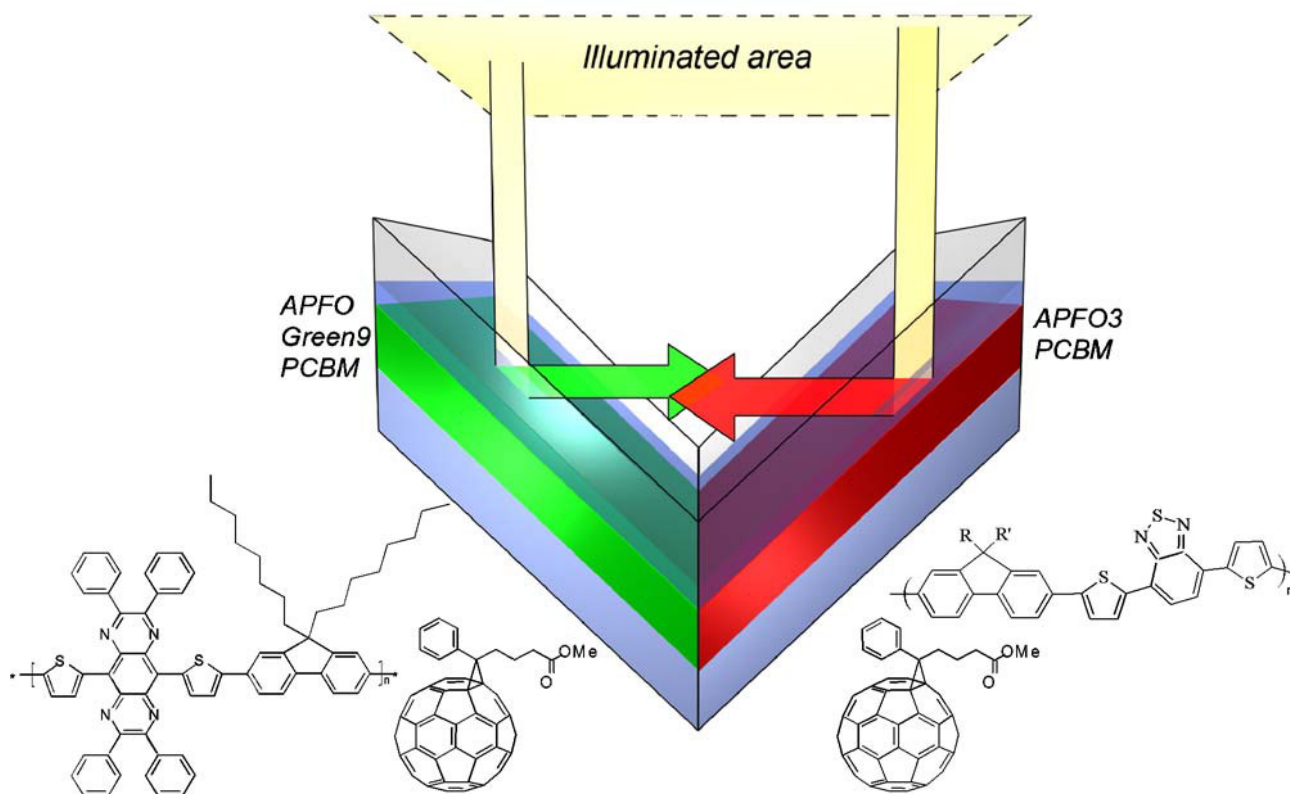


**Figure 2.26.** Folded tandem cell realized by Tvingstedt *et al.* Sketch of the folded tandem cell and the chemical structures of the exploited alternating polyfluorenes APFO3, APFO Green-9, and the acceptor molecule PCBM. Reprinted with permission from ref. [155].

An alternative approach to serially connected devices which give extremely high voltages has been introduced by Niggemann *et al.*[157], an approach that is rendered even more interesting as the device architecture avoids the use of transparent electrodes. By use of

substrates of transparent lamellar nano-structured polymer, devices of series of interconnected elementary cells (up to 1390 cells/mm) are prepared (Figure 2.27).

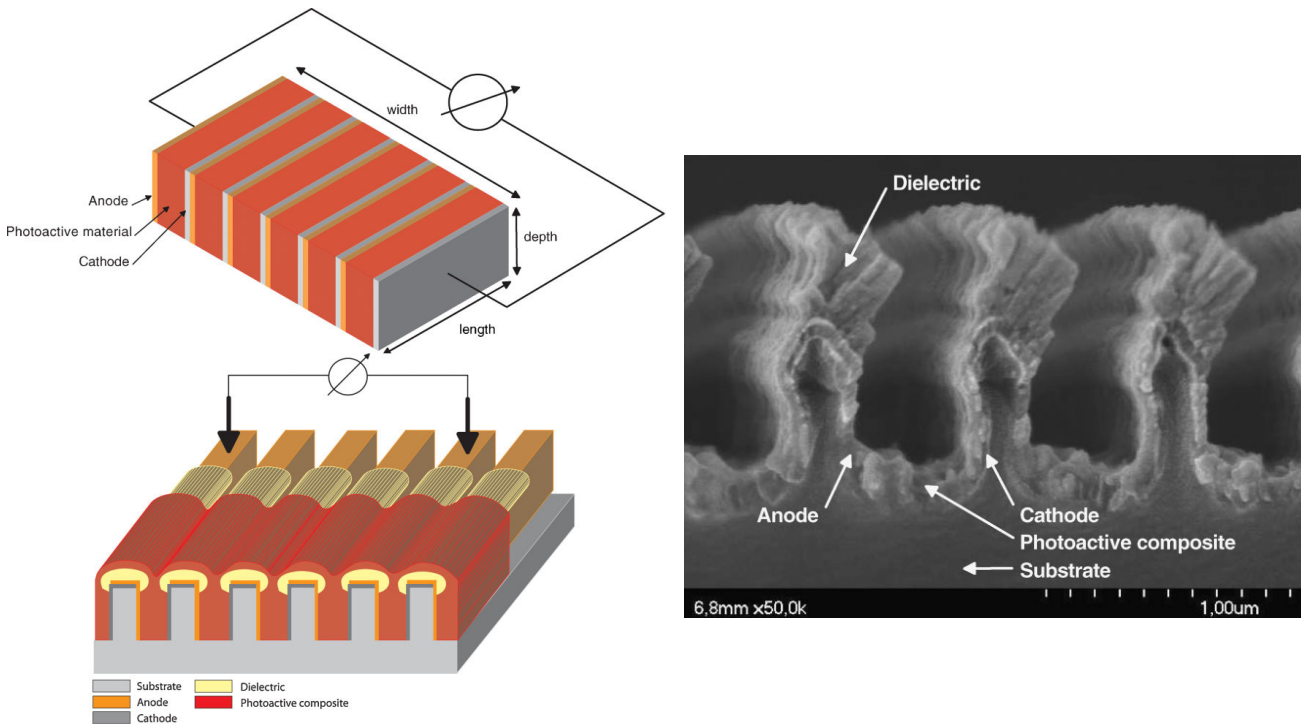


**Figure 2.27.** High voltage devices. Basic sketch of a series interconnected photovoltaic nanomodule. An elementary cell is represented by the photoactive volume sandwiched between an anode and a cathode (upper left). Schematic drawing of the series interconnected photovoltaic nanomodule. Anodes and cathodes are deposited on the walls of the nanolamellae by evaporation from an inclined incident angle. The series interconnection of adjacent elementary cells is carried out by overlapping the electrodes at the tips of the lamellae. In order to suppress charge carrier recombination, the tips of the nanolamellae are coated with a dielectric layer. The electrical contact is provided via two contact tips positioned onto the metallised nanolamellae (lower left). A SEM cross-section of a photovoltaic nanomodule. The tips of the lamellae are coated with lithium fluoride by thermal evaporation under inclined incident angles (right). Reprinted with permission from [157].

Thermal evaporation of titanium or  $\text{MoO}_3$  from inclined angles ensures deposition of the anode and cathode respectively on the vertical lamella walls. The angular deposition also insures that the anode and cathode pairs of adjacent elementary cells are interconnected at the tip of the nanolamellae. In order to suppress interconnection of adjacent cell elements by the photoactive composite, a dielectric layer of lithium fluoride was furthermore deposited at an angle on the tip of the lamellae prior to the final process step of spin-coating of the photoactive layer (P3HT/PCBM). The final devices showed very poor PCEs but an impressive open circuit voltage of 880 V was achieved.

Another approach to ITO free device architecture is the concept wrap trough, which has been known for while for silicon based solar cells [158], has been transferred to organic photovoltaics by Zimmerman *et al.* [159]. Figure 2.28 presents the structure of the device. The general idea of the wrap trough concept is to have both electrodes on the back of the devise. In order to make this possible hole/channels are created throughout the device after preparation of a traditional back electrode active layer structure. The channels are then filled with a highly conductive material connecting the upper transparent hole conductor with the back side of the substrate where a second electrode is applied. The organic solar cell by Zimmermann *et al.* is built on a thin plastic substrate with inverted layer sequence, i.e. starting with the metallic electron contact followed by the active absorber and then a layer of PEDOT:PSS. The holes/channels through the device were created by perforation with a hot needle followed by a second layer of PEDOT:PSS forming the wrap through contact. A gold contact was evaporated onto the back side of the substrate as a final step. Power conversion efficiencies of up to 2% were reached for parallel wrap through and 1.1% was reached for serial circuitry using simulated AM1.5G solar irradiation.

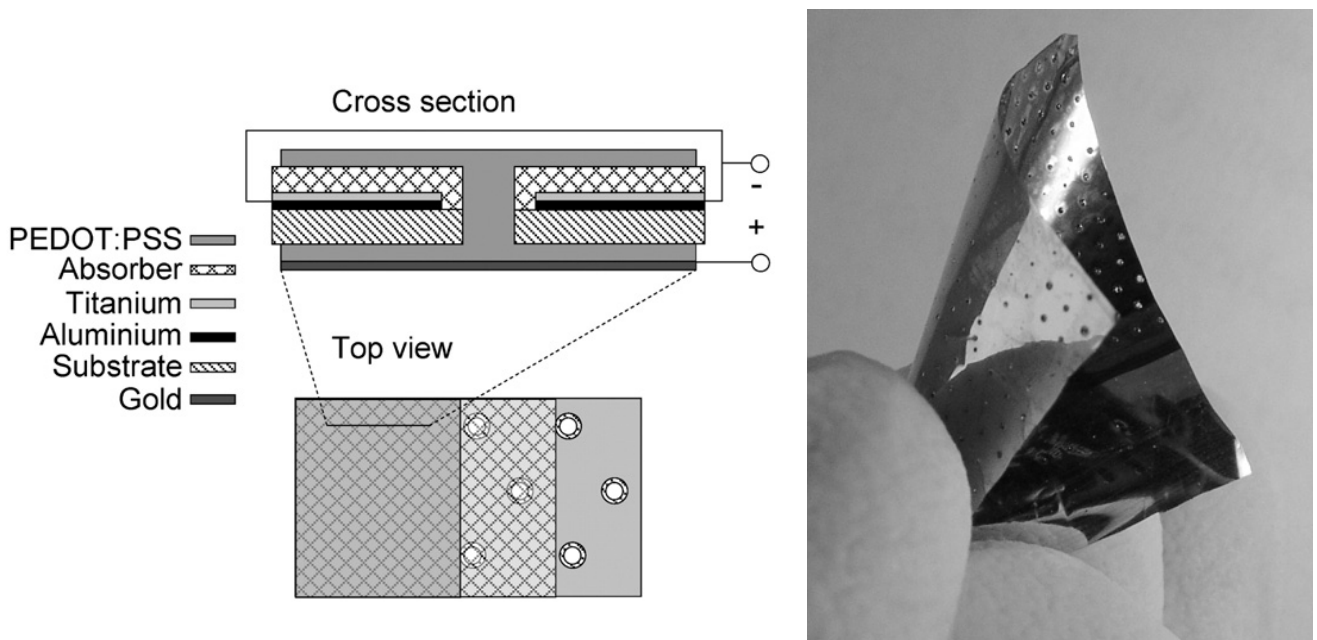
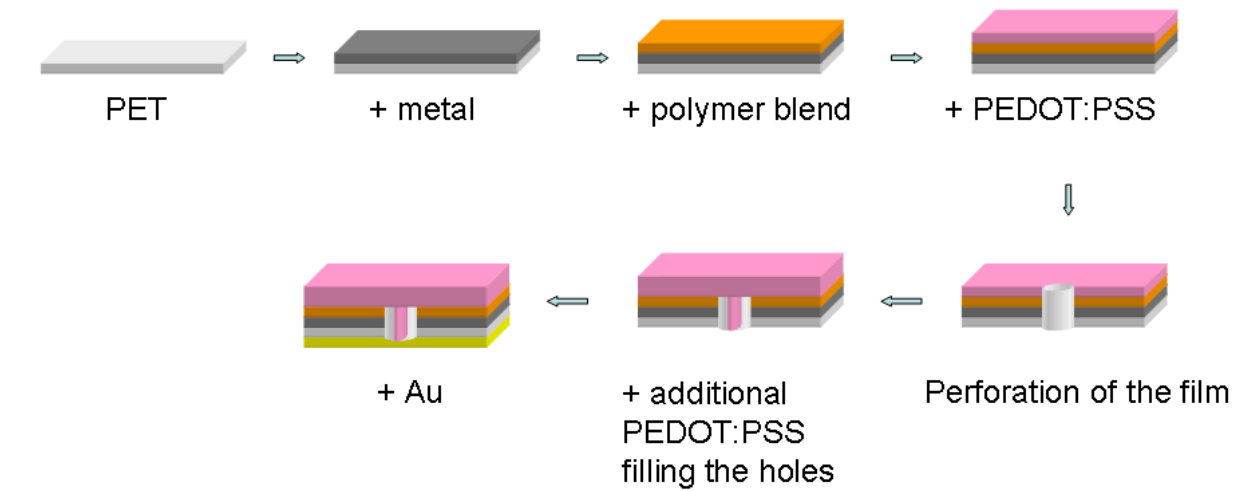


**Figure 2.28.** Wrap through cells. Schematic representation of the inverted layer sequence starting with the metallic contact on the plastic substrate followed by the active polymer blend and PEDOT:PSS. After perforation of the film a second layer of PEDOT:PSS is applied forming the wrap through contact and a gold back electrode is applied to finish the circuitry. Reprinted with permission from ref. [160] (top and lower left). photograph of a wrap through device. The two bottom representations are reprinted with permission from ref. [161].

## 2.9. Conclusions

The normal and inverted device geometry was presented and their realisation described in the context of the materials commonly used. The materials commonly explored for the electrodes, intermediate layers and electrodes were described and finally some novel materials types and device architectures were presented. It is concluded that more development of the active materials and device architectures are needed before stable polymer solar cells that can be processed at low cost can be realised.

## References

1. G. Li, V. Shrotriya, J. S. Huang, Y. Yao, T. Moriarty, K. Emery, and Y. Yang, High-efficiency solution processable polymer photovoltaic cells by self-organization of polymer blends, *Nat.Mater.*, 2005, **4**, 864-868.
2. W. L. Ma, C. Y. Yang, X. Gong, K. Lee, and A. J. Heeger, Thermally stable, efficient polymer solar cells with nanoscale control of the interpenetrating network morphology, *Adv.Func.Mater.*, 2005, **15**, 1617-1622.
3. F. C. Krebs, S. A. Gevorgyan, and J. Alstrup, A roll-to-roll process to flexible polymer solar cells: model studies, manufacture and operational stability studies, *J.Mater.Chem.*, 2009, **19**, 5442-5451.
4. M. Fonrodona, J. Escarre, F. Villar, D. Soler, J. M. Asensi, J. Bertomeu, and J. Andreu, PEN as substrate for new solar cell technologies, *Sol. Energy Mater. Sol. Cells*, 2005, **89**, 37-47.

5. F. C. Krebs, All solution roll-to-roll processed polymer solar cells free from indium-tin-oxide and vacuum coating steps, *Org.Electron.*, 2009, **10**, 761-768.
6. F. C. Krebs, Roll-to-roll fabrication of monolithic large-area polymer solar cells free from indium-tin-oxide, *Sol. Energy Mater. Sol. Cells*, 2009, **93**, 1636-1641.
7. M. Strange, D. Plackett, M. Kaasgaard, and F. C. Krebs, Biodegradable polymer solar cells, *Sol. Energy Mater. Sol. Cells*, 2008, **92**, 805-813.
8. T. Aernouts, P. Vanlaeke, W. Geens, J. Poortmans, P. Heremans, S. Borghs, R. Mertens, R. Andriessen, and L. Leenders, Printable anodes for flexible organic solar cell modules, *Thin Solid Films*, 2004, **451**, 22-25.
9. K. Tvingstedt and O. Inganas, Electrode grids for ITO-free organic photovoltaic devices, *Adv.Mater.*, 2007, **19**, 2893-2897.
10. S. Admassie, F. Zhang, A. G. Manoj, M. Svensson, M. R. Andersson, and O. Inganäs, A polymer photodiode using vapour-phase polymerized PEDOT as an anode, *Sol. Energy Mater. Sol. Cells*, 2006, **90**, 133-141.
11. A. Gadisa, K. Tvingstedt, S. Admassie, L. Lindell, X. Crispin, M. R. Andersson, W. R. Salaneck, and O. Inganas, Transparent polymer cathode for organic photovoltaic devices, *Synthetic Metals*, 2006, **156**, 1102-1107.
12. B. Winther-Jensen and F. C. Krebs, High-conductivity large-area semi-transparent electrodes for polymer photovoltaics by silk screen printing and vapour-phase deposition, *Sol. Energy Mater. Sol. Cells*, 2006, **90**, 123-132.

13. Z. Ben Ayadi, L. El Mir, K. Djessas, and S. Alaya, Electrical and optical properties of aluminum-doped zinc oxide sputtered from an aerogel nanopowder target, *Nanotechnology*, 2007, **18**, 445702.
14. D. J. Kwak, M. W. Park, and Y. M. Sung, Discharge power dependence of structural and electrical properties of Al-doped ZnO conducting film by magnetron sputtering (for PDP), *Vacuum*, 2008, **83**, 113-118.
15. S. Park, S. J. Tark, J. S. Lee, H. Lim, and D. Kim, Effects of intrinsic ZnO buffer layer based on P3HT/PCBM organic solar cells with Al-doped ZnO electrode, *Sol. Energy Mater. Sol. Cells*, 2009, **93**, 1020-1023.
16. J. S. Wellings, A. P. Samantilleke, P. Warren, S. N. Heavens, and I. M. Dharmadasa, Comparison of electrodeposited and sputtered intrinsic and aluminium-doped zinc oxide thin films, *Semiconductor Science and Technology*, 2008, **23**, 125003.
17. V. Bhosle, J. T. Prater, F. Yang, D. Burk, S. R. Forrest, and J. Narayan, Gallium-doped zinc oxide films as transparent electrodes for organic solar cell applications, *J.Appl.Phys.*, 2007, **102**, 023501.
18. H. K. Park, J. A. Jeong, Y. S. Park, S. I. Na, D. Y. Kim, and H. K. Kim, Room-Temperature Indium-Free Ga:ZnO/Ag/Ga:ZnO Multilayer Electrode for Organic Solar Cell Applications, *Electrochemical and Solid State Letters*, 2009, **12**, H309-H311.
19. B. N. Pawar, G. Cai, D. Ham, R. S. Mane, T. Ganesh, A. Ghule, R. Sharma, K. D. Jadhava, and S. H. Han, Preparation of transparent and conducting boron-doped ZnO



- electrode for its application in dye-sensitized solar cells, *Sol. Energy Mater. Sol. Cells*, 2009, **93**, 524-527.
20. P. Destruel, H. Bock, I. Seguy, P. Jolinat, M. Oukachmih, and E. Bedel-Pereira, Influence of indium tin oxide treatment using UV-ozone and argon plasma on the photovoltaic parameters of devices based on organic discotic materials, *Polymer International*, 2006, **55**, 601-607.
21. B. L. Groenendaal, F. Jonas, D. Freitag, H. Pielartzik, and J. R. Reynolds, Poly(3,4-ethylenedioxythiophene) and its derivatives: Past, present, and future, *Adv.Mater.*, 2000, **12**, 481-494.
22. Igor F.Perepichka and Dmitrii F.Perepichka, *Handbook of Thiophene-Based Materials: Applications in Organic Electronics and Photonics, 2<sup>nd</sup> Volume Set* (eds.: Igor F.Perepichka and Dmitrii F.Perepichka), Wiley, 2009.
23. L. Cattin, F. Dahou, Y. Lare, M. Morsli, R. Tricot, S. Houari, A. Mokrani, K. Jondo, A. Khelil, K. Napo, and J. C. Bernede, MoO<sub>3</sub> surface passivation of the transparent anode in organic solar cells using ultrathin films, *J.Appl.Phys.*, 2009, **105**, 034507.
24. V. Shrotriya, G. Li, Y. Yao, C. W. Chu, and Y. Yang, Transition metal oxides as the buffer layer for polymer photovoltaic cells, *Appl.Phys.Lett.*, 2006, **88**, 073508.
25. C. Waldauf, M. Morana, P. Denk, P. Schilinsky, K. Coakley, S. A. Choulis, and C. J. Brabec, Highly efficient inverted organic photovoltaics using solution based titanium oxide as electron selective contact, *Appl.Phys.Lett.*, 2006, **89**, 233517.

26. T. Ameri, G. Dennler, C. Waldauf, P. Denk, K. Forberich, M. C. Scharber, C. J. Brabec, and K. Hingerl, Realization, characterization, and optical modeling of inverted bulk-heterojunction organic solar cells, *J.Appl.Phys.*, 2008, **103**, 084506.
27. T. Kuwabara, T. Nakayama, K. Uozumi, T. Yamaguchi, and K. Takahashi, Highly durable inverted-type organic solar cell using amorphous titanium oxide as electron collection electrode inserted between ITO and organic layer, *Sol. Energy Mater. Sol. Cells*, 2008, **92**, 1476-1482.
28. M. S. White, D. C. Olson, S. E. Shaheen, N. Kopidakis, and D. S. Ginley, Inverted bulk-heterojunction organic photovoltaic device using a solution-derived ZnO underlayer, *Appl.Phys.Lett.*, 2006, **89**, 143517.
29. S. K. Hau, H. L. Yip, N. S. Baek, J. Y. Zou, K. O'Malley, and A. K. Y. Jen, Air-stable inverted flexible polymer solar cells using zinc oxide nanoparticles as an electron selective layer, *Appl.Phys.Lett.*, 2008, **92**, 253301.
30. A. K. K. Kyaw, X. W. Sun, C. Y. Jiang, G. Q. Lo, D. W. Zhao, and D. L. Kwong, An inverted organic solar cell employing a sol-gel derived ZnO electron selective layer and thermal evaporated MoO<sub>3</sub> hole selective layer, *Appl.Phys.Lett.*, 2008, **93**, 221107.
31. F. C. Krebs, Air stable polymer photovoltaics based on a process free from vacuum steps and fullerenes, *Sol. Energy Mater. Sol. Cells*, 2008, **92**, 715-726.
32. G. Li, C. W. Chu, V. Shrotriya, J. Huang, and Y. Yang, Efficient inverted polymer solar cells, *Appl.Phys.Lett.*, 2006, **88**, 253503.

33. J. S. Huang, C. Y. Chou, M. Y. Liu, K. H. Tsai, W. H. Lin, and C. F. Lin, Solution-processed vanadium oxide as an anode interlayer for inverted polymer solar cells hybridized with ZnO nanorods, *Org.Electron.*, 2009, **10**, 1060-1065.
34. N. S. Sariciftci, L. Smilowitz, A. J. Heeger, and F. Wudl, Photoinduced Electron-Transfer from A Conducting Polymer to Buckminsterfullerene, *Science*, 1992, **258**, 1474-1476.
35. C. J. Ko, Y. K. Lin, F. C. Chen, and C. W. Chu, Modified buffer layers for polymer photovoltaic devices, *Appl.Phys.Lett.*, 2007, **90**, 063509.
36. M. Reyes-Reyes, K. Kim, and D. L. Carroll, High-efficiency photovoltaic devices based on annealed poly(3-hexylthiophene) and 1-(3-methoxycarbonyl)-propyl-1-phenyl-(6,6)C-61 blends, *Appl.Phys.Lett.*, 2005, **87**, 083506-3.
37. M. Reyes-Reyes, K. Kim, J. Dewald, R. Lopez-Sandoval, A. Avadhanula, S. Curran, and D. L. Carroll, Meso-structure formation for enhanced organic photovoltaic cells, *Org.Lett.*, 2005, **7**, 5749-5752.
38. *Handbook of Conducting Polymers* (eds.: Terje A.Skotheim, Ronald L.Elsenbaumer, and John R.Reynolds), Marcel Dekker, Second edn., 1998.
39. R. D. McCullough, The chemistry of conducting polythiophenes, *Adv.Mater.*, 1998, **10**, 93-116.
40. Y. Kim, S. Cook, S. M. Tuladhar, S. A. Choulis, J. Nelson, J. R. Durrant, D. D. C. Bradley, M. Giles, I. Mcculloch, C. S. Ha, and M. Ree, A strong regioregularity effect in self-

- organizing conjugated polymer films and high-efficiency polythiophene: fullerene solar cells, *Nat.Mater.*, 2006, **5**, 197-203.
41. E. Bundgaard and F. C. Krebs, Low band gap polymers for organic photovoltaics, *Sol. Energy Mater. Sol. Cells*, 2007, **91**, 954-985.
42. R. Kroon, M. Lenes, J. C. Hummelen, P. W. M. Blom, and B. De Boer, Small bandgap polymers for organic solar cells (polymer material development in the last 5 years), *Polym.Rev.*, 2008, **48**, 531-582.
43. G. P. Smestad, F. C. Krebs, C. M. Lampert, C. G. Granqvist, K. L. Chopra, X. Mathew, and H. Takakura, Reporting solar cell efficiencies in solar energy materials and solar cells, *Sol. Energy Mater. Sol. Cells*, 2008, **92**, 371-373.
44. J. L. Bredas, D. Beljonne, V. Coropceanu, and J. Cornil, Charge-transfer and energy-transfer processes in pi-conjugated oligomers and polymers: A molecular picture, *Chemical Reviews*, 2004, **104**, 4971-5003.
45. H. A. M. van Mellekom, J. A. J. M. Vekemans, E. E. Havinga, and E. W. Meijer, Developments in the chemistry and band gap engineering of donor-acceptor substituted conjugated polymers, *Mater.Sci.& Eng., R-Reports*, 2001, **32**, 1-40.
46. J. Hou, H. Chen, S. Zhang, G. Li, and Y. Yang, Synthesis, Characterization, and Photovoltaic Properties of a Low Band Gap Polymer Based on Silole-Containing Polythiophenes and 2,1,3-Benzothiadiazole, *J.Am.Chem.Soc.*, 2008, **130**, 16144.

47. Y. Y. Liang, D. Q. Feng, Y. Wu, S. T. Tsai, G. Li, C. Ray, and L. P. Yu, Highly Efficient Solar Cell Polymers Developed via Fine-Tuning of Structural and Electronic Properties, *J.Am.Chem.Soc.*, 2009, **131**, 7792-7799.
48. J. Peet, J. Y. Kim, N. E. Coates, W. L. Ma, D. Moses, A. J. Heeger, and G. C. Bazan, Efficiency enhancement in low-bandgap polymer solar cells by processing with alkane dithiols, *Nat.Mater.*, 2007, **6**, 497-500.
49. S. H. Park, A. Roy, S. Beaupre, S. Cho, N. Coates, J. S. Moon, D. Moses, M. Leclerc, K. Lee, and A. J. Heeger, Bulk heterojunction solar cells with internal quantum efficiency approaching 100%, *Nature Photonics*, 2009, **3**, 297-2U5.
50. C. Y. Yu, C. P. Chen, S. H. Chan, G. W. Hwang, and C. Ting, Thiophene/Phenylene/Thiophene-Based Low-Bandgap Conjugated Polymers for Efficient Near-Infrared Photovoltaic Applications, *Chem.Mater.*, 2009, **21**, 3262-3269.
51. M. M. Wienk, M. Turbiez, J. Gilot, and R. A. J. Janssen, Narrow-bandgap diketo-pyrrolo-pyrrole polymer solar cells: The effect of processing on the performance, *Adv. Mater.*, 2008, **20**, 2556-2560.
52. E. G. Wang, L. Wang, L. F. Lan, C. Luo, W. L. Zhuang, J. B. Peng, and Y. Cao, High-performance polymer heterojunction solar cells of a polysilafluorene derivative, *Appl.Phys.Lett.*, 2008, **92**, 033307.

53. J. Hou, H. Chen, S. Zhang, R. I. Chen, Y. Yang, Y. Wu, and G. Li, Synthesis Of Low Band Gap Polymer and Its Application in High Effecient Polymer Solar Cells, *J.Am.Chem.Soc.*, 2009, **131**, 15586-15587.
54. N. Blouin, A. Michaud, D. Gendron, S. Wakim, E. Blair, R. Neagu-Plesu, M. Belletete, G. Durocher, Y. Tao, and M. Leclerc, Toward a rational design of poly(2,7-carbazole) derivatives for solar cells, *J.Am.Chem.Soc.*, 2008, **130**, 732-742.
55. Z. Zhu, D. Waller, R. Gaudiana, M. Morana, D. Muhlbacher, M. Scharber, and C. Brabec, Panchromatic conjugated polymers containing alternating donor/acceptor units for photovoltaic applications, *Macromolecules*, 2007, **40**, 1981-1986.
56. F. C. Krebs and H. Spanggaard, Significant improvement of polymer solar cell stability, *Chem.Mater.*, 2005, **17**, 5235-5237.
57. M. Bjerring, J. S. Nielsen, N. C. Nielsen, and F. C. Krebs, Polythiophene by solution processing, *Macromolecules*, 2007, **40**, 6012-6013.
58. M. Bjerring, J. S. Nielsen, A. Siu, N. C. Nielsen, and F. C. Krebs, An explanation for the high stability of polycarboxythiophenes in photovoltaic devices- A solid-state NMR dipolar recoupling study, *Sol. Energy Mater. Sol. Cells*, 2008, **92**, 772-784.
59. J. H. Burroughes, D. D. C. Bradley, A. R. Brown, R. N. Marks, K. Mackay, R. H. Friend, P. L. Burns, and A. B. Holmes, Light-Emitting-Diodes Based on Conjugated Polymers, *Nature*, 1990, **347**, 539-541.

60. C. Edder, P. B. Armstrong, K. B. Prado, and J. M. J. Frechet, Benzothiadiazole- and pyrrole-based polymers bearing thermally cleavable solubilizing groups as precursors for low bandgap polymers, *Chem.Comm.*, 2006, 1965-1967.
61. J. H. Edwards, W. J. Feast, and D. C. Bott, New Routes to Conjugated Polymers: 1. A 2 Step Route to Polyacetylene, *Polymer*, 1984, **25**, 395-398.
62. S. A. Gevorgyan and F. C. Krebs, Bulk heterojunctions based on native polythiophene, *Chem.Mater.*, 2008, **20**, 4386-4390.
63. T. J. Gordon, G. Vamvounis, and S. Holdcroft, Bilayer approach to laser-induced thermal patterning of pi-conjugated polymers, *Adv.Mater.*, 2008, **20**, 2486-2490.
64. O. Hagemann, M. Bjerring, N. C. Nielsen, and F. C. Krebs, All solution processed tandem polymer solar cells based on thermocleavable materials, *Sol. Energy Mater. Sol. Cells*, 2008, **92**, 1327-1335.
65. X. Han, X. W. Chen, and S. Holdcroft, Nanostructured morphologies and topologies of pi-conjugated polymers from thermally reactive polymer blends, *Adv.Mater.*, 2007, **19**, 1697-1702.
66. J. S. Liu, E. N. Kadnikova, Y. X. Liu, M. D. McGehee, and J. M. J. Frechet, Polythiophene containing thermally removable solubilizing groups enhances the interface and the performance of polymer-titania hybrid solar cells, *J.Am.Chem.Soc.*, 2004, **126**, 9486-9487.

67. M. H. Petersen, S. A. Gevorgyan, and F. C. Krebs, Thermocleavable Low Band Gap Polymers and Solar Cells Therefrom with Remarkable Stability toward Oxygen, *Macromolecules*, 2008, **41**, 8986-8994.
68. G. A. Power, P. Hodge, and N. B. McKeown, Synthesis of novel conjugated polymers containing alternating hexa-1,3,5-triene and bi-p-phenylene or ter-p-phenylene segments, *Chem.Comm.*, 1996, 655-656.
69. J. F. Yu and S. Holdcroft, Solid-state thermolytic and catalytic reactions in functionalized regioregular polythiophenes, *Macromolecules*, 2000, **33**, 5073-5079.
70. M. Drees, H. Hoppe, C. Winder, H. Neugebauer, N. S. Sariciftci, W. Schwinger, F. Schaffler, C. Topf, M. C. Scharber, Z. G. Zhu, and R. Gaudiana, Stabilization of the nanomorphology of polymer-fullerene "bulk heterojunction" blends using a novel polymerizable fullerene derivative, *J.Mater.Chem.*, 2005, **15**, 5158-5163.
71. Z. Zhu, S. Hadjikyriacou, D. Waller, and R. Gaudiana, Stabilization of film morphology in polymer-fullerene heterojunction solar cells, *J.Macromol.Sci., Chem.*, 2004, **A41**, 1467-1487.
72. S. Miyanishi, K. Tajima, and K. Hashimoto, Morphological Stabilization of Polymer Photovoltaic Cells by Using Cross-Linkable Poly(3-(5-hexenyl)thiophene), *Macromolecules*, 2009, **42**, 1610-1618.
73. F. C. Krebs and K. Norrman, Analysis of the failure mechanism for a stable organic photovoltaic during 10000 h of testing, *Prog.Photovolt.*, 2007, **15**, 697-712.



74. K. Norrman and F. C. Krebs, Lifetimes of organic photovoltaics: Using TOF-SIMS and  $^{18}\text{O}_2$  isotopic labelling to characterise chemical degradation mechanisms, *Sol. Energy Mater. Sol. Cells*, 2006, **90**, 213-227.
75. S. Bertho, I. Haeldermans, A. Swinnen, W. Moons, T. Martens, L. Lutsen, D. Vanderzande, J. Manca, A. Senes, and A. Bonfiglio, Influence of thermal ageing on the stability of polymer bulk heterojunction solar cells, *Sol. Energy Mater. Sol. Cells*, 2007, **91**, 385-389.
76. S. Bertho, G. Janssen, T. J. Cleij, B. Conings, W. Moons, A. Gadisa, J. D'Haen, E. Goovaerts, L. Lutsen, J. Manca, and D. Vanderzande, Effect of temperature on the morphological and photovoltaic stability of bulk heterojunction polymer: fullerene solar cells, *Sol. Energy Mater. Sol. Cells*, 2008, **92**, 753-760.
77. K. Sivula, C. K. Luscombe, B. C. Thompson, and J. M. J. Frechet, Enhancing the thermal stability of polythiophene: Fullerene solar cells by decreasing effective polymer regioregularity, *J.Am.Chem.Soc.*, 2006, **128**, 13988-13989.
78. K. Sivula, Z. T. Ball, N. Watanabe, and J. M. J. Frechet, Amphiphilic diblock copolymer compatibilizers and their effect on the morphology and performance of polythiophene: Fullerene solar cells, *Adv.Mater.*, 2006, **18**, 206.
79. C. H. Woo, B. C. Thompson, B. J. Kim, M. F. Toney, and M. J. Frechet, The Influence of Poly(3-hexylthiophene) Regioregularity on Fullerene-Composite Solar Cell Performance, *J.Am.Chem.Soc.*, 2008, **130**, 16324-16329.

80. F. B. Kooistra, J. Knol, F. Kastenberg, L. M. Popescu, W. J. H. Verhees, J. M. Kroon, and J. C. Hummelen, Increasing the open circuit voltage of bulk-heterojunction solar cells by raising the LUMO level of the acceptor, *Org.Lett.*, 2007, **9**, 551-554.
81. C. R. McNeill, A. Abrusci, J. Zaumseil, R. Wilson, M. J. McKiernan, J. H. Burroughes, J. J. M. Halls, N. C. Greenham, and R. H. Friend, Dual electron donor/electron acceptor character of a conjugated polymer in efficient photovoltaic diodes, *Appl.Phys.Lett.*, 2007, **90**, 193506.
82. M. M. Wienk, J. M. Kroon, W. J. H. Verhees, J. Knol, J. C. Hummelen, P. A. van Hal, and R. A. J. Janssen, Efficient methano[70]fullerene/MDMO-PPV bulk heterojunction photovoltaic cells, *Angew.Chem.- Int.Ed.*, 2003, **42**, 3371-3375.
83. M. Granstrom, K. Petritsch, A. C. Arias, A. Lux, M. R. Andersson, and R. H. Friend, Laminated fabrication of polymeric photovoltaic diodes, *Nature*, 1998, **395**, 257-260.
84. T. Kietzke, H. H. Horhold, and D. Neher, Efficient polymer solar cells based on M3EH-PPV, *Chem.Mater.*, 2005, **17**, 6532-6537.
85. M. M. Koetse, J. Sweelssen, K. T. Hoekerd, H. F. M. Schoo, S. C. Veenstra, J. M. Kroon, X. N. Yang, and J. Loos, Efficient polymer : polymer bulk heterojunction solar cells, *Appl.Phys.Lett.*, 2006, **88**, 083504.
86. C. Melzer, E. J. Koop, V. D. Mihailetschi, and P. W. M. Blom, Hole transport in poly(phenylene vinylene)/methanofullerene bulk-heterojunction solar cells, *Adv.Func.Mater.*, 2004, **14**, 865-870.

87. M. M. Mandoc, L. J. A. Koster, and P. W. M. Blom, Optimum charge carrier mobility in organic solar cells, *Appl.Phys.Lett.*, 2007, **90**, 133504.
88. Z.Knittel, *Optics of Thin Films* (eds.: Z.Knittel), Wiley, London, 1976.
89. H.A.Macleod, *Thin Film Optical Filters* (eds.: H.A.Macleod), London Adam Hilger, London,, 1986.
90. R.M.A.Azzam and N.M.Bashara, *Ellipsometry and Polarized Light* (eds.: R.M.A.Azzam and N.M.Bashara), North-Holland, New York, USA, 1977.
91. L. S. Roman, W. Mammo, L. A. A. Pettersson, M. R. Andersson, and O. Inganas, High quantum efficiency polythiophene/C-60 photodiodes, *Adv.Mater.*, 1998, **10**, 774-777.
92. H. Hoppe, N. Arnold, D. Meissner, and N. S. Sariciftci, Modeling of optical absorption in conjugated polymer/fullerene bulk-heterojunction plastic solar cells, *Thin Solid Films*, 2004, **451-52**, 589-592.
93. G. Dennler, K. Forberich, M. C. Scharber, C. J. Brabec, I. Tomis, K. Hingerl, and T. Fromherz, Angle dependence of external and internal quantum efficiencies in bulk-heterojunction organic solar cells, *J.Appl.Phys.*, 2007, **102**, 054516.
94. T. L. Benanti and D. Venkataraman, Organic solar cells: An overview focusing on active layer morphology, *Photosynthesis Research*, 2006, **87**, 73-81.
95. H. Hoppe and N. S. Sariciftci, Morphology of polymer/fullerene bulk heterojunction solar cells, *J.Mater.Chem.*, 2006, **16**, 45-61.

96. N. Camaioni, G. Ridolfi, G. Casalbore-Miceli, G. Possamai, and M. Maggini, The effect of a mild thermal treatment on the performance of poly(3-alkylthiophene)/fullerene solar cells, *Adv.Mater.*, 2002, **14**, 1735-1738.
97. J. J. Dittmer, E. A. Marseglia, and R. H. Friend, Electron trapping in dye/polymer blend photovoltaic cells, *Adv.Mater.*, 2000, **12**, 1270-1274.
98. T. Ahn, H. Lee, and S. H. Han, Effect of annealing of polythiophene derivative for polymer light-emitting diodes, *Appl.Phys.Lett.*, 2002, **80**, 392-394.
99. P. J. Brown, D. S. Thomas, A. Kohler, J. S. Wilson, J. S. Kim, C. M. Ramsdale, H. Sirringhaus, and R. H. Friend, Effect of interchain interactions on the absorption and emission of poly(3-hexylthiophene), *Physical Review B*, 2003, **67**, 064203.
100. X. N. Yang, J. Loos, S. C. Veenstra, W. J. H. Verhees, M. M. Wienk, J. M. Kroon, M. A. J. Michels, and R. A. J. Janssen, Nanoscale morphology of high-performance polymer solar cells, *Nano Letters*, 2005, **5**, 579-583.
101. F. Padinger, R. S. Rittberger, and N. S. Sariciftci, Effects of postproduction treatment on plastic solar cells, *Adv.Func.Mater.*, 2003, **13**, 85-88.
102. D. Chirvase, J. Parisi, J. C. Hummelen, and V. Dyakonov, Influence of nanomorphology on the photovoltaic action of polymer-fullerene composites, *Nanotechnology*, 2004, **15**, 1317-1323.
103. Y. Kim, S. A. Choulis, J. Nelson, D. D. C. Bradley, S. Cook, and J. R. Durrant, Device annealing effect in organic solar cells with blends of regioregular poly(3-hexylthiophene) and soluble fullerene, *Appl.Phys.Lett.*, 2005, **86**, 063502.

104. X. N. Yang, J. K. J. van Duren, M. T. Rispens, J. C. Hummelen, R. A. J. Janssen, M. A. J. Michels, and J. Loos, Crystalline organization of a methanofullerene as used for plastic solar-cell applications, *Adv.Mater.*, 2004, **16**, 802-806.
105. X. N. Yang, J. K. J. van Duren, R. A. J. Janssen, M. A. J. Michels, and J. Loos, Morphology and thermal stability of the active layer in poly(p-phenylenevinylene)/methanofullerene plastic photovoltaic devices, *Macromolecules*, 2004, **37**, 2151-2158.
106. R. J. Kline, M. D. McGehee, E. N. Kadnikova, J. S. Liu, and J. M. J. Frechet, Controlling the field-effect mobility of regioregular polythiophene by changing the molecular weight, *Adv.Mater.*, 2003, **15**, 1519-1522.
107. A. Zen, J. Pflaum, S. Hirschmann, W. Zhuang, F. Jaiser, U. Asawapirom, J. P. Rabe, U. Scherf, and D. Neher, Effect of molecular weight and annealing of poly (3-hexylthiophene)s on the performance of organic field-effect transistors, *Adv.Func.Mater.*, 2004, **14**, 757-764.
108. R. J. Kline, M. D. McGehee, E. N. Kadnikova, J. S. Liu, J. M. J. Frechet, and M. F. Toney, Dependence of regioregular poly(3-hexylthiophene) film morphology and field-effect mobility on molecular weight, *Macromolecules*, 2005, **38**, 3312-3319.
109. R. C. Hiorns, R. De Bettignies, J. Leroy, S. Bailly, M. Firon, C. Sentein, A. Khoukh, H. Preud'homme, and C. Dagron-Lartigau, High molecular weights, polydispersities, and annealing temperatures in the optimization of bulk-heterojunction photovoltaic cells based on poly(3-hexylthiophene) or poly(3-butylthiophene), *Adv.Func.Mater.*, 2006, **16**, 2263-2273.

110. H. Sirringhaus, P. J. Brown, R. H. Friend, M. M. Nielsen, K. Bechgaard, B. M. W. Langeveld-Voss, A. J. H. Spiering, R. A. J. Janssen, E. W. Meijer, P. Herwig, and D. M. de Leeuw, Two-dimensional charge transport in self-organized, high-mobility conjugated polymers, *Nature*, 1999, **401**, 685-688.
111. X. Q. Jiang, R. Patil, Y. Harima, J. Ohshita, and A. Kunai, Influences of self-assembled structure on mobilities of charge carriers in pi-conjugated polymers, *Journal of Physical Chemistry B*, 2005, **109**, 221-229.
112. F. Iwatsu, T. Kobayashi, and N. Uyeda, Solvent Effects on Crystal-Growth and Transformation of Zinc Phthalocyanine, *Journal of Physical Chemistry*, 1980, **84**, 3223-3230.
113. J. C. Conboy, E. J. C. Olson, D. M. Adams, J. Kerimo, A. Zaban, B. A. Gregg, and P. F. Barbara, Impact of solvent vapor annealing on the morphology and photophysics of molecular semiconductor thin films, *Journal of Physical Chemistry B*, 1998, **102**, 4516-4525.
114. S. H. Kim, M. J. Misner, and T. P. Russell, Solvent-induced ordering in thin film diblock copolymer/homopolymer mixtures, *Adv.Mater.*, 2004, **16**, 2119-2123.
115. F. L. Zhang, M. Svensson, M. R. Andersson, M. Maggini, S. Bucella, E. Menna, and O. Inganäs, Soluble polythiophenes with pendant fullerene groups as double cable materials for photodiodes, *Adv.Mater.*, 2001, **13**, 1871-1874.

116. Y. Zhao, Z. Y. Xie, Y. Qu, Y. H. Geng, and L. X. Wang, Solvent-vapor treatment induced performance enhancement of poly(3-hexylthiophene): methanofullerene bulk-heterojunction photovoltaic cells, *Appl.Phys.Lett.*, 2007, **90**, 043504.
117. G. Li, Y. Yao, H. Yang, V. Shrotriya, G. Yang, and Y. Yang, "Solvent annealing" effect in polymer solar cells based on poly(3-hexylthiophene) and methanofullerenes, *Adv.Func.Mater.*, 2007, **17**, 1636-1644.
118. G. H. Lu, L. G. Li, and X. N. Yang, Achieving perpendicular alignment of rigid polythiophene backbones to the substrate by using solvent-vapor treatment, *Adv.Mater.*, 2007, **19**, 3594-3598.
119. S. Miller, G. Fanchini, Y. Y. Lin, C. Li, C. W. Chen, W. F. Su, and M. Chhowalla, Investigation of nanoscale morphological changes in organic photovoltaics during solvent vapor annealing, *J.Mater.Chem.*, 2008, **18**, 306-312.
120. M. Sundberg, O. Inganas, S. Stafstrom, G. Gustafsson, and B. Sjogren, Optical-Absorption of Poly(3-Alkylthiophenes) at Low-Temperatures, *Solid State Communications*, 1989, **71**, 435-439.
121. S. Berson, R. De Bettignies, S. Bailly, and S. Guillerez, Poly (3-hexylthiophene) fibers for photovoltaic applications, *Adv.Func.Mater.*, 2007, **17**, 1377-1384.
122. A. J. Moule and K. Meerholz, Controlling morphology in polymer-fullerene mixtures, *Adv.Mater.*, 2008, **20**, 240-245.

123. L. G. Li, G. H. Lu, and X. N. Yang, Improving performance of polymer photovoltaic devices using an annealing-free approach via construction of ordered aggregates in solution, *J.Mater.Chem.*, 2008, **18**, 1984-1990.
124. J. K. Lee, W. L. Ma, C. J. Brabec, J. Yuen, J. S. Moon, J. Y. Kim, K. Lee, G. C. Bazan, and A. J. Heeger, Processing additives for improved efficiency from bulk heterojunction solar cells, *J.Am.Chem.Soc.*, 2008, **130**, 3619-3623.
125. I. W. Hwang, S. Cho, J. Y. Kim, K. Lee, N. E. Coates, D. Moses, and A. J. Heeger, Carrier generation and transport in bulk heterojunction films processed with 1,8-octanedithiol as a processing additive, *J.Appl.Phys.*, 2008, **104**, 033706.
126. Y. Yao, J. H. Hou, Z. Xu, G. Li, and Y. Yang, Effect of solvent mixture on the nanoscale phase separation in polymer solar cells, *Adv.Func.Mater.*, 2008, **18**, 1783-1789.
127. H. Schmidt, H. Flugge, T. Winkler, T. Bulow, T. Riedl, and W. Kowalsky, Efficient semitransparent inverted organic solar cells with indium tin oxide top electrode, *Appl.Phys.Lett.*, 2009, **94**, 243302.
128. A. Hayakawa, O. Yoshikawa, T. Fujieda, K. Uehara, and S. Yoshikawaa, High performance polythiophene/fullerene bulk-heterojunction solar cell with a TiOx hole blocking layer, *Appl.Phys.Lett.*, 2007, **90**, 163517.
129. A. Roy, S. H. Park, S. Cowan, M. H. Tong, S. N. Cho, K. Lee, and A. J. Heeger, Titanium suboxide as an optical spacer in polymer solar cells, *Appl.Phys.Lett.*, 2009, **95**, 013302.



130. J. Gilot, I. Barbu, M. M. Wienk, and R. A. J. Janssen, The use of ZnO as optical spacer in polymer solar cells: Theoretical and experimental study, *Appl.Phys.Lett.*, 2007, **91**, 113520.
131. K. Lee, J. Y. Kim, S. H. Park, S. H. Kim, S. Cho, and A. J. Heeger, Air-stable polymer electronic devices, *Adv.Mater.*, 2007, **19**, 2445-2449.
132. H. Hansel, H. Zettl, G. Krausch, R. Kisselev, M. Thelakkat, and H. W. Schmidt, Optical and electronic contributions in double-heterojunction organic thin-film solar cells, *Adv.Mater.*, 2003, **15**, 2056-2060.
133. J. Y. Kim, S. H. Kim, H. H. Lee, K. Lee, W. L. Ma, X. Gong, and A. J. Heeger, New architecture for high-efficiency polymer photovoltaic cells using solution-based titanium oxide as an optical spacer, *Adv.Mater.*, 2006, **18**, 572-576.
134. C. J. Brabec, S. E. Shaheen, C. Winder, N. S. Sariciftci, and P. Denk, Effect of LiF/metal electrodes on the performance of plastic solar cells, *Appl.Phys.Lett.*, 2002, **80**, 1288-1290.
135. R. De Bettignies, J. Leroy, M. Firon, and C. Sentein, Accelerated lifetime measurements of P3HT : PCBM solar cells, *Synthetic Metals*, 2006, **156**, 510-513.
136. G. Dennler, C. Lungenschmied, H. Neugebauer, N. S. Sariciftci, and A. Labouret, Flexible, conjugated polymer-fullerene-based bulk-heterojunction solar cells: Basics, encapsulation, and integration, *Journal of Materials Research*, 2005, **20**, 3224-3233.

137. C. Lungenschmied, G. Dennler, H. Neugebauer, S. N. Sariciftci, M. Glatthaar, T. Meyer, and A. Meyer, Flexible, long-lived, large-area, organic solar cells, *Sol. Energy Mater. Sol. Cells*, 2007, **91**, 379-384.
138. P. Madakasira, K. Inoue, R. Ulbricht, S. B. Lee, M. Zhou, J. P. Ferraris, and A. A. Zakhidov, Multilayer encapsulation of plastic photovoltaic devices, *Synthetic Metals*, 2005, **155**, 332-335.
139. E. A. Meulenkaamp, R. van Aar, J. J. A. M. Bastiaansen, A. J. M. van den Biggelaar, H. Borner, K Brunner, M. Buchel, A. van Dijken, N. M. M. Kikken, M. Kilitziraki, M. M. de Kok, B. M. W. Langeveld, N. M. M. Ligter, S. I. E. Vulto, P. van de Weijer, and S. H. P. M. Winter, 5464, *SPIE*, 2004.
140. T. Ameri, G. Dennler, C. Lungenschmied, and C. J. Brabec, Organic tandem solar cells: A review, *Energy & Env.Sci.*, 2009, **2**, 347-363.
141. A. Hadipour, B. De Boer, and P. W. M. Blom, Device operation of organic tandem solar cells, *Org.Electron.*, 2008, **9**, 617-624.
142. A. Hadipour, B. De Boer, and P. W. M. Blom, Organic tandem and multi-junction solar cells, *Adv.Func.Mater.*, 2008, **18**, 169-181.
143. D. Cheyns, H. Gommans, M. Odijk, J. Poortmans, and P. Heremans, Stacked organic solar cells based on pentacene and C60, *Sol. Energy Mater. Sol. Cells*, 2007, **91**, 399-404.

144. B. P. Rand, P. Peumans, and S. R. Forrest, Long-range absorption enhancement in organic tandem thin-film solar cells containing silver nanoclusters, *J.Appl.Phys.*, 2004, **96**, 7519-7526.
145. J. Xue, S. Uchida, B. P. Rand, and S. R. Forrest, Asymmetric tandem organic photovoltaic cells with hybrid planar-mixed molecular heterojunctions, *Appl.Phys.Lett.*, 2004, **85**, 5757-5759.
146. A. Yakimov and S. R. Forrest, High photovoltage multiple-heterojunction organic solar cells incorporating interfacial metallic nanoclusters, *Appl.Phys.Lett.*, 2002, **80**, 1667.
147. A. Colsmann, J. Junge, C. Kayser, and U. Lemmer, Organic tandem solar cells comprising polymer and small-molecule subcells, *Appl.Phys.Lett.*, 2006, **89**, 203506-3.
148. G. Dennler, H. J. Prall, R. Koeppe, M. Egginger, R. Autengruber, and N. S. Sariciftci, Enhanced spectral coverage in tandem organic solar cells, *Appl.Phys.Lett.*, 2006, **89**, 073502.
149. A. Hadipour, B. De Boer, J. Wildeman, F. B. Kooistra, J. C. Hummelen, M. G. R. Turbiez, M. M. Wienk, R. A. J. Janssen, and P. W. M. Blom, Solution-processed organic tandem solar cells, *Adv.Func.Mater.*, 2006, **16**, 1897-1903.
150. H. J. Prall, R. Koeppe, R. Autengruber, M. Egginger, D. Dennler, and N. S. Sariciftci, From Evaporation to Solution Processed Organic Tandem Solar Cells, 61970F, Gombert, Andreas, Strasbourg, France, 2006.

151. J. Gilot, M. M. Wienk, and R. A. J. Janssen, Double and triple junction polymer solar cells processed from solution, *Appl.Phys.Lett.*, 2007, **90**, 143512-143513.
152. J. Y. Kim, K. Lee, N. E. Coates, D. Moses, T. Q. Nguyen, M. Dante, and A. J. Heeger, Efficient Tandem Polymer Solar Cells Fabricated by All-Solution Processing *Science*, 2007, **317**, 222-225.
153. V. Andersson, K. Tvingstedt, and O. Inganas, Optical modeling of a folded organic solar cell, *J.Appl.Phys.*, 2008, **103**, 094520.
154. S. B. Rim, S. Zhao, S. R. Scully, M. D. McGehee, and P. Peumans, An effective light trapping configuration for thin-film solar cells, *Appl.Phys.Lett.*, 2007, **91**, 243501.
155. K. Tvingstedt, V. Andersson, F. Zhang, and O. Inganas, Folded reflective tandem polymer solar cell doubles efficiency, *Appl.Phys.Lett.*, 2007, **91**, 123514-3.
156. Y. H. Zhou, F. L. Zhang, K. Tvingstedt, W. J. Tian, and O. Inganas, Multifolded polymer solar cells on flexible substrates, *Appl.Phys.Lett.*, 2008, **93**, 033302.
157. M. Niggemann, W. Graf, and A. Gombert, Realization of Ultrahigh Photovoltages with Organic Photovoltaic Nanomodules, *Adv.Mater.*, 2008, **20**, 4055.
158. J. M. Gee, W. K Schubert, and P. A. Basore, Emitter wrap-through solar cell, *Photovoltaic Specialists Conference, Conference Record of the Twenty Third IEEE*, 1993, 265-270.

159. B. Zimmermann, M. Glatthaar, M. Niggemann, M. K. Riede, A. Hinsch, and A. Gombert, ITO-free wrap through organic solar cells - A module concept for cost-efficient reel-to-reel production, *Sol. Energy Mater. Sol. Cells*, 2007, **91**, 374-378.
160. M. Helgesen, R. Søndergaard, and F. C. Krebs, Advanced Materials and Processes for Polymer Solar Cell Devices, *J.Mater.Chem.*, 2010, **20**, 36-60.
161. M. Niggemann, B. Zimmermann, J. Haschke, M. Glatthaar, and A. Gombert, Organic solar cell modules for specific applications - From energy autonomous systems to large area photovoltaics, *Thin Solid Films*, 2008, **516**, 7181-7187.



Risø DTU is the National Laboratory for Sustainable Energy. Our research focuses on development of energy technologies and systems with minimal effect on climate, and contributes to innovation, education and policy. Risø has large experimental facilities and interdisciplinary research environments, and includes the national centre for nuclear technologies.

---

**Risø DTU**  
**National Laboratory for Sustainable Energy**  
**Technical University of Denmark**

Frederiksborgvej 399  
PO Box 49  
DK-4000 Roskilde  
Denmark  
Phone +45 4677 4677  
Fax +45 4677 5688

[www.risoe.dtu.dk](http://www.risoe.dtu.dk)